

PROCEEDINGS OF THE
NUCLEAR PHYSICS AND SOLID STATE PHYSICS SYMPOSIUM
1970

MADURAI, DECEMBER 27-30, 1970

Volume III-Solid State Physics

ORGANISED BY
THE PHYSICS COMMITTEE
OF THE DEPARTMENT OF ATOMIC ENERGY
GOVERNMENT OF INDIA

FOREWORD

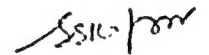
The fifteenth Nuclear Physics and Solid State Physics Symposium sponsored by the Physics Committee of the Department of Atomic Energy was held at the American College Campus of the Madurai University during December 27-30, 1970. Prof. T. Meena-kehlundaram, Vice-Chancellor, Madurai University, inaugurated the Symposium at the opening session which was presided over by Prof. B. D. Nag Chaudhuri, Chairman of the Physics Committee. About 400 physicists from all over the country participated in the Symposium.

Looking at the number of papers submitted to Nuclear Physics and Solid State Physics sections of the Symposium over the last few years, one finds that the number of contributed papers is tending to increase every year at the rate of roughly 20 papers per year. This year, 148 papers were submitted for the Nuclear Physics section and 167 papers for the Solid State Physics section. Although this trend may be taken to indicate a welcome feature of continuous growth of Nuclear Physics and Solid State Physics research in the country, the organizers of the Symposium are beginning to face the dilemma of how to programme such a large number of papers providing adequate time for an effective feed-back and discussion. We have followed this year, as in the previous ones, the practice of starring some papers in the Nuclear Physics Section and resorting to a few rapporteur sessions in Solid State Physics Section. The number of invited talks in the combined sessions of the two sections was reduced to five this year and one joint session was devoted to a discussion of "Correlations" in both the Nuclear and Solid State Physics problems.

It has been increasingly felt that the usefulness of the proceedings of an annual symposium like this can be greatly enhanced by bringing out the proceedings as fast as possible. The Symposium Committee has taken some effective steps this year to avoid delay in the publication of the proceedings. The Vols. II and III containing contributed papers have, therefore, been prepared by the direct Xerographic reproduction of the submitted papers without any correction, revision or retyping. This was made possible only with the cooperation received from most of the authors in following the instructions for preparing the papers and in strictly observing the dead-lines. If any paper was not received within the prescribed dead-line, it was assumed that the author/s did not wish to publish the full paper in the proceedings, as they might have sent it for publication elsewhere. In such cases, only the abstracts of the papers presented have been included in the proceedings. Several

persons have contributed towards our efforts to bring out the proceedings as fast as possible; but it has been possible mainly due to the untiring efforts of Dr. B. A. Dasannacharya, Secretary, Solid State Physics Section, Dr. M. G. Betlgeri, Secretary, Nuclear Physics Section, and the extreme cooperation of Dr. V. A. Kamath, Scientific Information Officer, BARC.

We would like to take this opportunity to record our thanks to the Vice-Chancellor, Madurai University, for his kind invitation to hold the symposium at Madurai. We are particularly grateful to Prof. K. S. Chandrasekaran and other members of the Physics Department of the Madurai University and the American College, Madurai, for their hospitality and the excellent arrangements made during the Symposium.



(S. S. Kapoor)

Convener,
Nuclear Physics & Solid State
Physics Symposium Committee

CONTENTS

	<u>Page</u>
LOW TEMPERATURE BEHAVIOUR OF SOLIDS AND LIQUIDS	
Variation of Transition Temperature and Superconducting State Parameters with Pressure in Tin J S Rajput	1
Dislocation Effect in the Measurement of Energy Gap in Superconductors by Ultrasonic Methods B.K Basu	5
On the Line Shape of the Josephson Radiation R Sundaram and V G Bhide	11
Onset of Turbulence in the Flow of Liquid Helium II Between Rotating Cylinders N Devaraj	17
Film Transfer of Helium II for Large Pressure Heads T S Radhakrishnan, S Rangarajan and Girish Chandra	25
Thermo-Electric Power of Dilute Magnetic Alloys at Low Temperatures M S R Chari, N S Natarajan and R G Sharma	31
Concentration-Dependence of the Electrical Resistivity Anomaly in Dilute Magnetic Alloys M S R Chari, N S Natarajan and R G Sharma	37
The Resistance Minimum of Lutetium Films U N Upadhyaya	43
Anomalous Thermoelectric Power of Dilute Magnetic Alloys Below Kondo Temperature R K. Paliwal and U N Upadhyaya	47
ELECTRONIC PROPERTIES OF SOLIDS	
A Special Case of the Saxon Hutner Theorem for Three-Dimensional Potentials K.V Bhagwat and R Subramanian	51
Generalization of the Coherent Potential Theory to Alloys with Short Range Order M M Pant and S K Joshi	57
Conduction Electron Density at the Nucleus in Dysprosium Metal D K Ray and K C Das	63
Relativistic Energy Band Structure for Crystals with Non-symmorphic Space Group A Gupta (nee Ghosh) and Santosh Kumar	67

	<u>Page</u>
Effect of Pressure on the Fermi Surface of Gold : M. G. Ramchandani	73
Electron Correlations in a Classical Plasma : K. N. Pathak and K. G. Aggarwal	77
Sum Rule, Plasma- Dispersion and Compressibility of Electron Liquid : K. N. Pathak and K. S. Singwi	81
Electron Correlations in Two Fold Degenerate Band : R. Kishore and S. K. Joshi	85
Screening of a Charged Impurity in Electron Liquid : A. P. Pathak	91
The Relation Between Kondo Effect and Hartree-Fock Theory: C. Manohar	97
Blocking of Electrons and Positrons in Crystals : A.P. Pathak and M. Yussouff	103
Corrections to the Ground State Energies of Shallow Acceptors in Ge : S. Balasubramanian	109
Minority Carrier Equivalent Lifetime in Germanium and Gallium Arsenide : A. B. Bhattacharyya and T. N. Basavraj	113
Influence of Cell Scattering due to Impurities on the Mobility in Silicon : O. P. Daga and W. S. Khokle	117
Electronic Charge Density Distribution of Lead : S. C. Roy and A. M. Ghose	121
Electrical Conductivity of Thallium Telluride : M. D. Aggarwal and J. K. D. Verma	125
Calculation of Static Dielectric Constant of 'Built-up' Barium Stearate Films : Usha Khanna, V. K. Srivastava and V. K. Agarwal	131
Thickness Dependence of the D. C. Electrical Breakdown in Thin 'Built-up' Barium Stearate Films : V. K. Agarwal and V. K. Srivastava	135
Electron Beam Induced Conductivity in As_2S_3 : B. Ghosh	139
Effect of Heat Treatment on the Electrical Resistivity of Thin Silver Films : S. Mohan and P. Jayarama Reddy	145

	<u>Page</u>
Memory Diodes from Semiconducting Chalcogenide Glasses V Subramanian	149
Switching Effects in Au-SiO ₂ -SiC System Miss T M Brindha and G Suryan	155
Recovery of High Resistance in Thin Al ₂ O ₃ Films H N K Sharma, A K Mathur, I B Bhattacharya and D L Bhattacharya	161
Electrical Conduction in Sodium Chlorate Crystals C Ramasastry, V K. Viswanatha Reddy and V S Murty	165 ^o
Electrical Conductivity of Cesium Sulphate Crystals C Ramasastry and B S V S R Acharyulu	171
Electrical Conductivity of NaI(Tl) S Muralidhara Rao and R Y Deshpande	177
Electrical Conductivity of Alpha-MnS Powered Samples Risal Singh	181
Low Temperature Electrical Conductivity of MnSe-CoSe System V N Kamat Dalal, H V Keer and A B Biswas	187
Study on the Lifetime of the Photoelectrets of ZnS P K C Pillai and K G Balakrishnan	193
Effect of Magnetic Field on the Decay Characteristics of Phosphors S H Pawar and A V Narlikar	201
Luminescence of RbCl Tl and RbBr Tl J Ramamurti	205
Optical F → M Conversion in Doped KCl Crystals E V R Sastry and T M Srinivasan	211
Electroluminescence in ZnO Electroluminophors System V B Singh and J N Nanda	217
Thermoluminescence of Quenched LaF Single Crystals S Muralidhara Rao	225
Off-Center Lead Ions in KI Crystals and Raman Scattering S Radhakrishna and K S h. Sai	231
Thermoluminescence of KBr Crystals K R N Murthy, Y V G S Murti and C Ramasastry	239

	<u>Page</u>
The Absorption and Fluorescence Spectra of Ho^{3+} in LaF_3 Crystal : Bansilal, D. Ramchandra Rao, T. M. Srinivasan and P. Venkateswarlu	245
Optical Absorption Spectrum of Ni^{2+} Doped NaF : J. P. Srivastava and P. A. Narayana	251
On the T^2 Rate of Heating for TSC Under Charge Neutrality Condition : T. C. Manchanda and V. K. Mathur	255
Lifetimes of Positrons in Alkaline Earth Halides : K. P. Singh and R. M. Singru	261
Positron Lifetimes in Some Ionic Compounds : K. P. Singh and R. M. Singru	265
On Positron Lifetimes vs. Two Gamma Angular Correlations in Real Metals : J. C. Garg and B. L. Saraf	269
Empirical Correlation Between Positron Lifetime and Electron Density in Metals : Y. S. Shishodia, B. K. Sharma, Ramesh Chandra and B. L. Saraf	273
Positron in Defects I. Estimation of Positron-Defect Binding Energy and Calculation of Two Photon Angular Correlation Curve in Metals : Y. S. Shishodia and B. L. Saraf	277
Positron in Defects II. Influence of Trapped Positron on Interpretation of Effective Mass Measurements : Y. S. Shishodia and B. L. Saraf	283
 THERMAL AND DYNAMICAL PROPERTIES OF SOLIDS AND LIQUIDS	
Critical Phenomena in the Coexistence Curve of the Binary Liquid System Carbondisulphide - Acetonitrile : K. Govindarajan, R. G. Gambhir and E. S. R. Gopal	287
Critical Phenomena in the Specific Heat of the Binary Liquid Mixture Methanol-Heptane : B. Viswanathan, K. Govindarajan and E. S. R. Gopal	293
Critical Phenomena in the Thermal Expansion of Binary Liquid System : CS_2 -Methanol : M. V. Lele, B. Viswanathan and E. S. R. Gopal	299

	<u>Page</u>
Critical Phenomena in the Coexistence Curve of the Carbonyl-sulphide-Acetic Anhydride System M V Lele S V Subramanyam and E S R Gopal	303
Temperature Dependence of Positron Life-Time in n-Octane and n-Hexadecane B V Thosar V G Kulkarni, R G Lagu and Girish Chandra	309
Temperature Dependence of Positron Life-Times in Associated and Polar Liquids B V Thosar, V G Kulkarni R G Lagu and Girish Chandra	315
Free Volume Model for the Formation and Quenching of Triplet Positronium in Simple Molecular Liquids B V Thosar V G Kulkarni R G Lagu and Girish Chandra	317
Double Resonance Study of Proton Spin - Relaxation in a Strongly Coupled Two - Spin System N R Krishna and B D Nageswara Rao	325
Proton Spin Relaxation and Molecular Motion in Liquid Thiophene Anup Kitchlew and B D Nageswara Rao	327
Heat Capacity at Constant Volume of Methyl Iodide S K Mitra Narsingh Dass and N C Varshneya	333
Debye Temperature of Water on Two State Approach S K Mitra and Narsingh Dass	337
Neutron Scattering in Liquid Argon J S Bajjal and D K Chaturvedi	341
Measurement of Self-Diffusion in Liquid Mercury S N Changdar	347
Anharmonic Contribution to Mossbauer Fraction of ^{83}Kr in Solid Krypton S S Nandwani Deo Raj and S P Furi	353
Calculation of the Mossbauer Parameters for the Disordered Lattice B P Srivastava H N K Sharma and D L Bhattacharya	359
The Mossbauer Effect Studies of 9.3 keV Transition in Krypton Solid Krishan Mahesh and N D Sharma	363
The Temperature Variation of Debye-Waller Factors of Potassium Chloride Up to the Melting Point K. Jayalakshmi and M A Viswamitra	373

Temperature Variation of the Debye-Waller Factors of NaCl and the Associated Debye Temperature Upto the Melting Point ; M. A. Viswamitra and K. Jayalakshmi	379
Debye-Waller Factor of Sodium : S. Krishna Kumar V. Valvoda and M. A. Viswamitra	385
The X-Ray Debye Waller Factor for the Mixed System $KBr_{1-x}Cl_x$: K. S. Chandrasekharan and S. K. Mohanlal	391
Additivity of Debye Characteristic Temperatures of Alloys : G. B. Mitra and T. Chottopadhyay	393
Trace Variable Forces in Alkali Halides : T. M. Haridasan and R. Revathi Raju	397
Many Body Interaction in Breathing Shell Model : A. N. Basu and Dhiranjan Roy	403
Internal Pressure in Alkali Halides and a Justification for the Breathing Shell Model : M. P. Verma	409
Effect of Electron Density Distribution of the Dynamical Behaviour of Alkali Halide Crystals : M. P. Verma and R. K. Singh	415
A Shell Model for the Ionic Molecules : A. K. Sarkar and S. Sengupta	423
Phonon Dispersion Relations in AgCl : R. Prasad and R. K. Singh	429
A Kinematic Theory of Thermal (Brillouin) Scattering of Light by Phonons in Condensed Media: N. Kumar, L. Krishnasamy and K. Srinivasa	435
Lattice Dynamics of Calcium Oxide : P. R. Vijayaraghavan and P. K. Iyengar	439
Polariton Dispersion Relations in $CaWO_4$: V. C. Sahni and G. Venkataraman	447
Proton Magnetic Resonance Studies of Some Tetramethyl Ammonium Halides : M. Mahajan and B. D. Nageswara Rao	453
Frequency Distribution and Thermodynamic Properties of Solid Ammonia : P. S. Goyal, B. A. Dasannacharya, C. L. Thaper and P. K. Iyengar	457

Anderson-Gruneissen Parameter for the Cesium Halides Miss R Revathy Raju and T M Haridasan	465
Elastic Constants of CsI Containing Impurity Ions K M Kesharwan and Bal K Agrawal	469
Group-Theoretical Study of Lattice Dynamics of KN_3 NaN_3 and NaNO_3 K R Rao and S F Trevino	473
Dispersion Relations for Phonons in KN_3 K R Rao S F Trevino H Prask and R Mical	481
Optical Phonons in Molecular Crystals of Halogens Y S Jain and H D Bist	485
Librational and Vibrational Modes in Crystal Hydrates at Liquid Nitrogen Temperature V S Tomar, H D Bist and D P Khandelwal	491
Hard-Core Potential for Rare-Gas Solids T N Agarwal and R K Gupta	499
Pseudomolecular Model for a Substitutional Impurity in a Lattice of Polarizable Atoms M Sachdev and J Mahanty	507
Theoretical Study of Vacancies and Vacancy Pairs in CaCl Type Crystals C S N Murthy and Y V G S Murti	511
Model Potential for BCC Metals S S Kushwaha and J S Rajput	515
Lattice Dynamics of Transition Metals Satya Prakash and S K Joshi	521
Electrical and Thermal Resistivities of Cesium Satya Pal	525
Variational Treatment of Ziman Limit of Thermal Resistance Due to Umklapp Processes G P Srivastava and G S Verma	531
Electron-Phonon Scattering in Te-Doped GaSb at Low Temperatures P C Sharma and G S Verma	535
Phonon Conductivity of GaAs in the Temperature Range 2 to 300°K and Guthrie's Temperature Dependences K S Dubey and G S Verma	539
The Thermal Conductivity of Nickel M S R Chavli	545

Configuration Interaction and Covalent Metal Ligand Interaction of Cu^{2+} in Dodecahedral Disposition : A. K. Roy, R. Roy and A. K. Pal	549
Magnetic Studies of Trigonal Bipyramidal Cu(II) N_5 Complex in Copper Tren Isothiocyanates : A. K. Pal, D. Pal and C. Bose	555
Crystal Field - Spin Orbit Treatment of Ligand Field Levels of Distorted Octahedral Copper (II) System : A. K. Pal, D. Pal and A. K. Ghoshal	561
Effect of the Crystalline Field on the Spin Average of Sm^{3+} in Samarium Intermetallics : S. K. Malik and R. Vijayaraghavan	567
Single Crystal EPR Studies of Planar Copper (II) Bis (N-Phynylsalicylaldimine) : Subrata Lahiry	573
Exchange Coupled Pairs in Copper Diethyl-dithiocarbamate: R. Kumari Cowsik, G. Rangarajan and R. Srinivasan	577
g-Anisotropy of O_3^- Trapped in Sodium Chlorate Crystals : C. Ramasastry and V. S. Murthy	583
A Comparative Study of the EPR of Mn^{2+} in Isostructural Single Crystals of Some Dia- and Paramagnetic Salts : R. Janakiraman and G. C. Upreti	591
Electron Paramagnetic Resonance Studies of Divalent Manganese in Ammonium Bromide Single Crystal : P. A. Narayana, G. N. Rao, M. D. Sastry, T. M. Srinivasan and Putcha Venkateswarlu	595
90° Super-Exchange Interaction in Transition Metal Phthalocyanines : S. Mitra, C. G. Barrachlough, R. L. Martin and R. C. Sherwood	599
Mossbauer and Magnetic Susceptibility Measurements on Cadmium Ferriyanide : C. R. Kanekar, V. R. Marathe, A. C. Kunwar and S. K. Date	603
Magnetic Heat Capacity of Thulium Ethylsulphate : H. V. Keer	607
Thermal and Magnetic Properties of Pr^{3+} and Er^{3+} Ions in a Crystal Field with C_{3h} Site Symmetry : Vishwamittar, S. P. Taneja and S. P. Puri	611

On Anomalous Magnetic and Thermodynamic Properties of CoF_2 , $5\text{HF} \cdot 6\text{H}_2\text{O}$, $\text{CoSiF}_6 \cdot 6\text{H}_2\text{O}$ and $\text{CoZrF}_6 \cdot 6\text{H}_2\text{O}$ B Ghosh and S K. Dutta Roy	615
Magnetic and Thermodynamic Studies of CoO(I) and CoO(II) V K. Goswami and K. S. De	623
Nature of Ligand Fields in Ferrous Ammonium Sulphate Hexahydrate and Ferrous Potassium Sulphate Hexahydrate D Pal, D Ghosh and A K Pal	629
Paramagnetic Anisotropy and Electronic Structure of Square Planar Transition Metal Compounds S Mitra C G Barraclough and R L Martin	633
Determination of the Principal Axes of the Field-Gradient Tensor from the Zeeman-Split NQR Spectra A K Saha, R Roy and S Sengupta	637
Nuclear Magnetic Resonance Studies of ^{35}Cl in $\text{K}_2\text{CuCl}_4 \cdot 2\text{H}_2\text{O}$ L C Gupta and D L Radhakrishna Setty	643
Zeeman Effect of Chlorine Nuclear Quadrupole Resonance in Mercuric Chloride and 1-Chloro-2, 4-Dinitrobenzene M. S. Vijaya and J Ramakrishna	649
On the Quadrupole Coupling Constants of ^{197}Au , ^{182}W and ^{183}W Compounds Vishwamittar and S P Puri	653
Mossbauer Electric Field Gradient Parameters in $\text{Fe}(\text{KSO}_4)_2 \cdot 6\text{H}_2\text{O}$ Single Crystals V K. Garg and S P Puri	657
Temperature Dependence of ^{35}Cl NQR Frequency in Certain Divalent Chlorates C V Ramamohan and J Sobhanadri	661
Temperature Dependence of Pure Quadrupole Resonance in Sodium Chlorate and Copper Chlorate M S Vijaya and J Ramakrishna	665
^{57}Fe Internal Fields in Nickel-Manganese Alloys Girish Chandra and T S Radhakrishnan	671
RGR in ^{57}Co Doped Mn_5Ge_3 R Nagarajan, T S Radhakrishnan and S K Date	677
The Magnetic Susceptibility and Electrical Resistivity of FeGe_2 Near its Neel Temperature U R K Rao and J V Yakhmi	683

Neutron Diffraction Studies in Some Ternary Alloys : M. R. L. N. Murthy, R. J. Begum and N. S. Satya Murthy	689
The Atomic and Magnetic Structure of Co_2TiO_4 : R. J. Begum, L. Madhav Rao and N. S. Satya Murthy	693
Exchange Integrals in Some Spinel Ferrites : R. J. Begum, L. Madhav Rao, S. K. Paranjpe and N. S. Satya Murthy	697
Effect of Micro-Structure on Mossbauer Line Shapes in Nickel-Zinc Ferrite : P. Raj and S. K. Kulshreshtha	703
Spin Relaxation of Fe^{3+} Ion in Ferrites Using Mossbauer Effect : P. K. Iyengar and S. C. Bhargava	709
Magnetic Anisotropy in $(1-x)\text{Fe}_2\text{O}_3-x\text{Al}_2\text{O}_3$ System : J. K. Srivastava and R. P. Sharma	713
Crystal Field Effects on Time Dependent Hyperfine Inter- actions : J. K. Srivastava	719
Critical Attenuation in Nickel : B. K. Basu	725
Magnon Dispersion in Magneto-Electric Antiferromagnets : R. S. Tripathi, R. P. S. Kushwaha and K. G. Srivastava	731
Thermodynamic Behaviour of a Heisenberg System of Three- Level Ions : C. M. Bhandari and Ashok Kumar Gupta	735
Phase Transition in Narrow Energy Band Hubbard Model : Ashok Kumar Gupta	741
On Dynamical Dissimilarity of Magnon Modes for Antiferro- magnets : S. P. Saxena	747
On Validity of Heisenberg - Bloch Model for Ferromagnets: S. P. Saxena	751
Antiferromagnet with Nearest Neighbour Interactions : J. Fasupathy	753
Spin-Phonon Interaction in Ferromagnetic Insulator at Low Temperatures : S. K. Ghatak	759
Nuclear Spin Phonon Interaction in Metals : A. Ramakanth	763
Contributions of the Odd-Parity Vibrational Modes to the Spin Lattice Relaxation Process : Santosh Kumar and D. K. Ray	767

LOW TEMPERATURE BEHAVIOUR OF SOLIDS AND LIQUIDS

VARIAION OF TRANSITION TEMPERATURE AND SUPER- CONDUCTING STATE PARAMETERS WITH PRESSURE IN TIN

J.S. Bajput
Department of Physics
Banaras Hindu University
Varanasi-5

I. INTRODUCTION

The transition temperature of the superconducting non-transition metals is lowered by pressure though it is not so for a number of transition metals and their alloys. The pressure dependence of the transition temperature along with the superconducting state parameters offers quite a critical and extensive test of the superconductivity theory⁽¹⁾. The three superconducting state parameters of interest are : $\langle V_{ph} \rangle$; an estimate of the phonon mediated attractive electron-electron interaction in the metal, $\langle V_C \rangle$; the Coulomb pseudopotential that measures the effectiveness of Coulomb repulsion in inhibiting superconductivity; and Z_0 , the quasiparticle mass (or energy) renormalization parameter. Several authors^(2,3) have attempted the evaluation of these parameters for non-transition metals. Here we follow an approach proposed earlier⁽⁴⁾ and characterised, firstly by the use of matrix elements between Bloch electron states instead of plane-wave matrix elements and secondly, in using for the screened electron-phonon matrix element the form suggested by Harrison for the OPW form factor and lastly in including the renormalization effects due to electron-phonon and Coulomb interactions. Here we present the results obtained for the

specific case of Sn and discuss these in the light of other available theoretical and experimental results.

II. METHOD

We calculate the spherical average of the Coulomb interaction matrix element over the Fermi surface as,

$$\bar{V}_c = \frac{4\pi}{b_F^2} \int_0^{b_F} \frac{dq}{q \epsilon(q)} \quad (1)$$

and the spherical average of the electron-phonon interaction matrix element using

$$\bar{V}_{ph} = (2 b_F^2 \theta_D^3 \bar{\Omega} M)^{-1} \int_0^{b_F} q^2 dq \frac{\left[-\frac{8\pi z^*}{q^3} + \beta \right]}{\epsilon^2(q)}. \quad (2)$$

Here $\bar{\Omega}$ is the atomic volume, $\epsilon(q)$ is the Hartree dielectric function for momentum transfer q , M is atomic mass, β is Harisson's parameter. In this formulation we introduce pressure by evaluating the Fermi wave vector $b_F = (3\pi^2 z^* / \bar{\Omega})^{1/3}$ at the compressed atomic volume of the metal. The variation of the density of states at the Fermi level is given by the electronic Gruneissen constant

$$\gamma_c = \frac{\delta \ln N_F(0)}{\delta \ln \bar{\Omega}} \quad (3)$$

The change in the phonon spectrum is accounted for by a single peak of longitudinal phonons at θ_D , the Debye frequency and the volume variations are given by the lattice Gruneissen constant

$$\gamma_g = \frac{\delta \ln \theta_D}{\delta \ln \bar{\Omega}} \quad (4)$$

The total renormalization parameter Z_0 is given by

$$Z_0 = Z_{ec} + \frac{10}{11} \left[\frac{N_F(0) \bar{V}_{ph}}{Z_{eph} + Z_{ec} - 1} \right] \quad (5)$$

Z_0C , the Coulomb contribution is taken from Rice(5). Using this, the normalized density of states

$N(0) = (0.88817 k_F^3 \gamma_c / 2^* z_0)$ is determined which gives $\langle V_{ph} \rangle = N(0) \bar{V}_{ph}$ and

$$\langle V_c \rangle = \frac{N(0) \bar{V}_c}{1 + N(0) \bar{V}_c \ln(k_F^2 / 10 \theta_D)}$$

The transition temperature is calculated using the following relationship

$$Z_0 = [\langle V_{ph} \rangle \langle V_c \rangle] \int_0^{\omega_D} \frac{d\omega}{\omega} \tanh \frac{\omega^2}{2T_c} - \langle V_{ph} \rangle \int_0^{\omega_D} \frac{d\omega}{\omega + \omega_D} \tanh \frac{\omega}{2T_c} \quad (7)$$

which can be put in the following form as well

$$Z_0 = [\langle V_{ph} \rangle \langle V_c \rangle] \ln \left(2 \gamma \frac{\omega_D}{T_c} \right) - N(0) \bar{V}_{ph} \int_0^1 \tanh \frac{1}{2} t \frac{\omega_D}{T_c} dt \quad (8)$$

III. RESULTS AND DISCUSSION

We have evaluated these parameters and the effective interaction strength which approaches zero at about $22\bar{\rho}$ volume change. The calculated transition temperature has been compared with the available experimental values (6,7) and also with the results obtained by Seiden(2) who has made calculations for two values taking $\gamma_c = 1.65$ and also $\gamma_c = 1.79$. We have however confined our calculations to a single value $\gamma_c = 1.75$.

The evaluation of these parameters for Tin using the exact OPW form factors obtained from model potential of Heine and Abarenkov at different pressures is under study using a similar method. The value of effective interaction strength as obtained in both these approaches

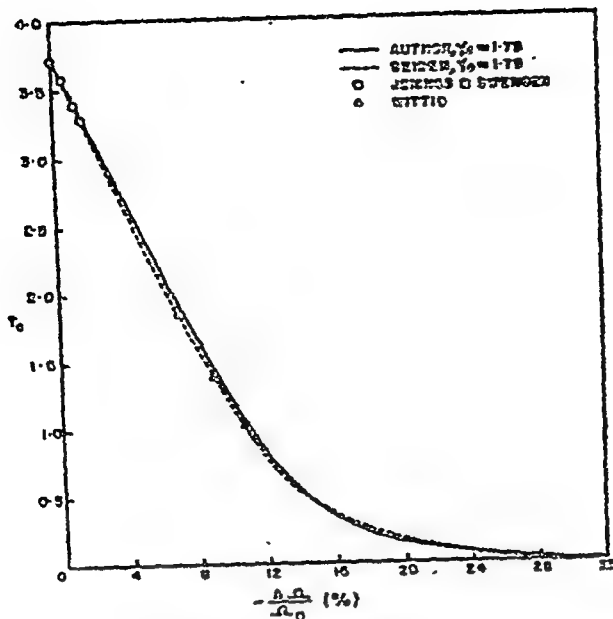


Fig. No. 1 : Variation of transition temperature of Sn with percentage volume change.

gives a rather poor agreement with the BCS relationship between transition temperature and effective interaction strength. We hope to obtain better results using more realistic pseudopotentials and phonon spectrum.

REFERENCES

1. T.F. Smith and C.W. Chu; Phys. Rev. 159, 353 (1967).
2. P.E. Seiden; Phys. Rev. 172, 452 (1969).
3. J.S. Rajput and A.K. Gupta; Phys. Stat. Solidi 40, 87 (1970).
4. J.S. Rajput and A.K. Gupta; Phys. Rev. 181, 743 (1969).
5. T.M. Rice; Ann. Phys. 31, 100 (1965).
6. L.D. Jennings and C.A. Swenson; Phys. Rev. 112, 31 (1958).
7. Jorg Wittig; Z. Physik 195, 228 (1966).

DISLOCATION EFFECT IN THE MEASUREMENT OF ENERGY GAP IN SUPERCONDUCTORS BY ULTRASONIC METHODS

B.K. Basu

Tata Institute of Fundamental Research, Bombay.

Measurements of longitudinal wave ultrasonic attenuation in superconductors, for the determination of energy gap, make use of the relation given by the BCS theory,

$$\frac{\alpha_s}{\alpha_n} = \frac{2}{e^{\Delta(T)/kT} + 1} \quad (1)$$

where α_n and α_s are the electronic attenuations in the normal and superconducting states, $\Delta(T)$ is the temperature dependent energy gap, k the Boltzmann constant and T the absolute temperature. The zero of electronic attenuation is taken as $\alpha_s(T \rightarrow 0^\circ K)$. Recent measurements^(1,2) have shown considerable deviation from this relation. In particular, the attenuation ratio α_s/α_n shows a sharp fall near the transition temperature and is in general frequency dependent. Two views have emerged to explain the above results: 1) the mean free path of electrons are not the same in the normal and superconducting states; 2) the background attenuation in particular the attenuation due to dislocations is not independent of temperature. The first of these views has been examined in detail elsewhere⁽¹⁾. We have examined here the results of Pate et al.⁽¹⁾ in high purity Pb from the second viewpoint. The results are shown in figure.1. There is a reasonable agreement of the corrected data with the BCS energy gap $\Delta(0) = 4.3kT_c$.

Ultrasonic wave causes dislocations to vibrate against the frictional or damping force B in the lattice. There are several sources of this damping and at low temperature electrons account for a part of it. In the superconducting phase a part of conduction electrons do not interact with the dislocations. This reduces the damping and hence affects the attenuation due to dislocations. If B_n and B_s are the damping constants in the normal and superconducting states due to electrons, then we have,

$$\frac{B_s}{B_n} = \frac{2}{e^{\Delta(T)/kT} + 1}$$

In addition there is damping B_1 due to impurities and imperfections in the lattice.

If one plots α/f where α is the attenuation due to dislocations against the frequency f , the curve shows a maximum at some intermediate frequency, reducing to zero at very low (as $\sim f$) and at very high (as $\sim 1/f$) frequencies. The experimental curves for high purity metal single crystals agree very well with the normalized curve calculated by Oen et al⁽³⁾. A change of the damping constant shifts the curve along the frequency axis in the ratio of the constants without altering anything else. Therefore, if we have the curve corresponding to B_1 and the ratio B_n/B_1 we can calculate the attenuation corrections due to dislocations for both normal and superconducting states.

The background attenuation data at the lowest temperature in the superconducting state was obtained from

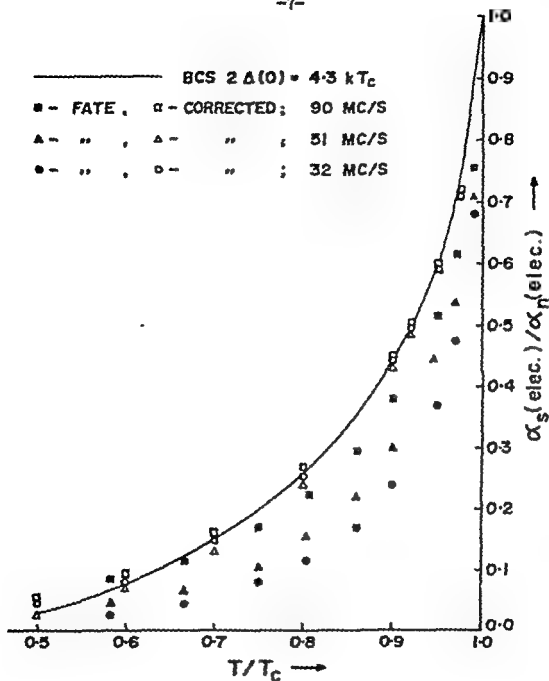


Fig.1 Plots of experimental and corrected attenuation ratio α_s/α_n in superconducting Pb against the reduced temperature T/T_c .

Ultrasonic wave causes dislocations to vibrate against the frictional or damping force B in the lattice. There are several sources of this damping and at low temperature electrons account for a part of it. In the superconducting phase a part of conduction electrons do not interact with the dislocations. This reduces the damping and hence affects the attenuation due to dislocations. If B_n and B_s are the damping constants in the normal and superconducting states due to electrons, then we have,

$$\frac{B_s}{B_n} = \frac{2}{e^{\Delta(T)/kT} + 1}$$

In addition there is damping B_1 due to impurities and imperfections in the lattice.

If one plots α/f where α is the attenuation due to dislocations against the frequency f , the curve shows a maximum at some intermediate frequency, reducing to zero at very low (as $\sim f$) and at very high (as $\sim 1/f$) frequencies. The experimental curves for high purity metal single crystals agree very well with the normalized curve calculated by Oen et al⁽³⁾. A change of the damping constant shifts the curve along the frequency axis in the ratio of the constants without altering anything else. Therefore, if we have the curve corresponding to B_1 and the ratio B_n/B_1 we can calculate the attenuation corrections due to dislocations for both normal and superconducting states.

The background attenuation data at the lowest temperature in the superconducting state was obtained from

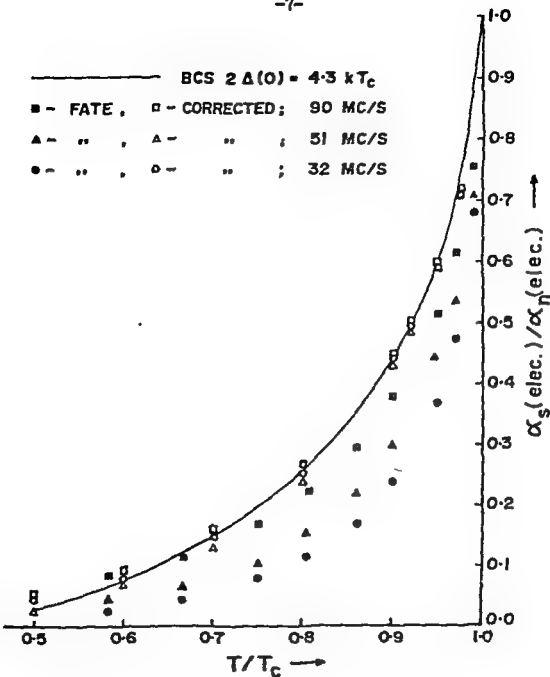


Fig.1 Plots of experimental and corrected attenuation ratios α_s/α_n in superconducting Pb against the reduced temperature T/T_c .

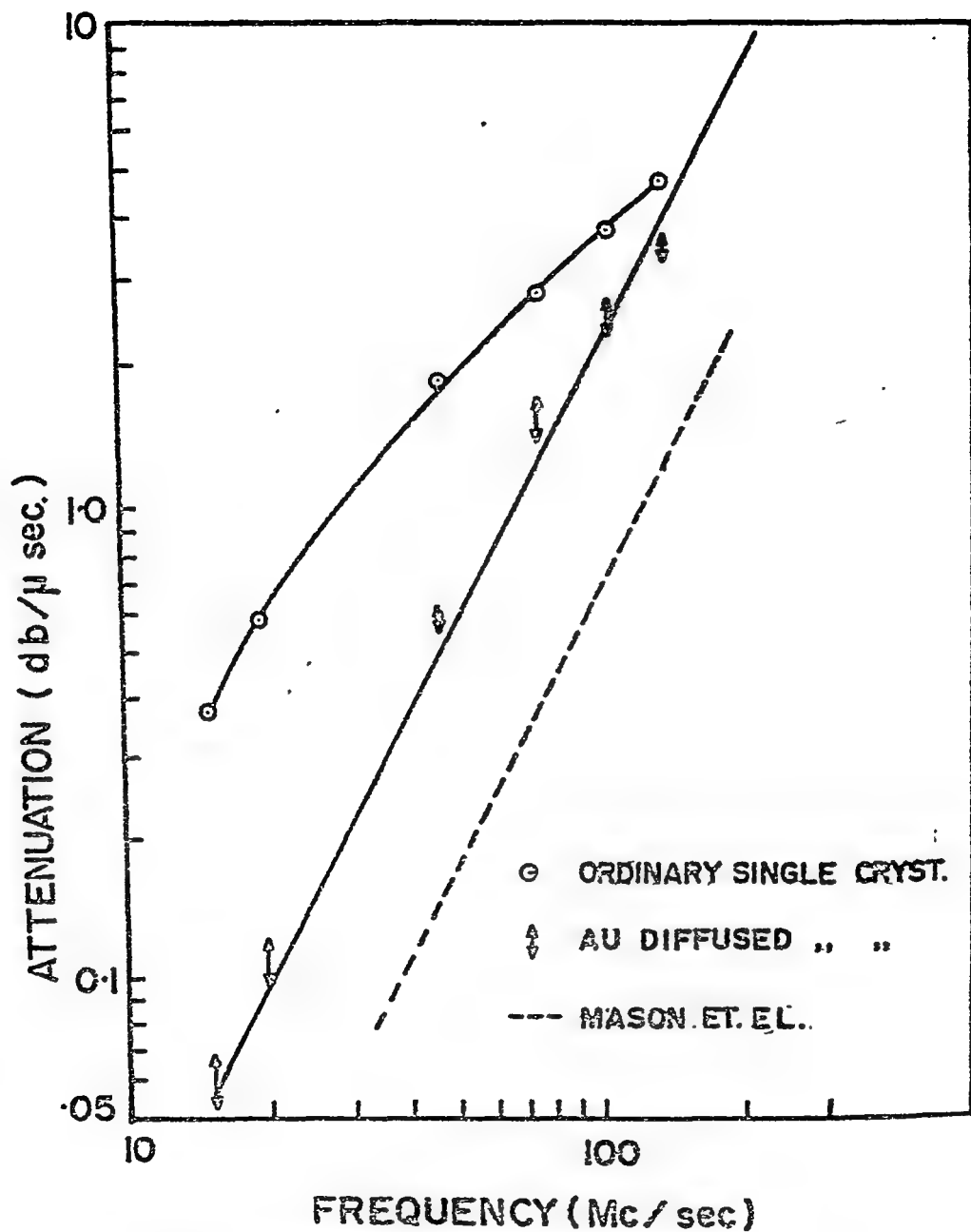


Fig.2 Ultrasonic attenuation in Pb at room temperature. The dotted curve is the expected attenuation from phonon-phonon interaction.

the authors (Pb-12: 3.30 db/cm, 7.52 db/cm and 10. db/cm for 12.8, 32 and 51 Mc/s respectively). The were fitted to the normalized curve of Oen et al. to obtain a smooth curve for all frequencies. This is dislocation attenuation curve corresponding to B_1 . Since the ratio B_n/B_1 is not known we chose a value of B_n/B_1 equal to 1.8, the same for all temperatures, to obtain good fit with the energy gap $2\Delta(0) = 4.3kT_c$ for one frequency. The data for 12.8 Mc/s has been excluded from this analysis since it involved large errors for the required corrections.

Finally, a few remarks about the evaluation.

- 1) The value of B_n which can be approximately obtained from this analysis is small. Assuming a dislocation density of 10^7 lines per sq. cm we find B_n to be approximately equal to 10^{-4} dyn sec. cm^{-2} . This agrees well with the experimental value of $B_n = 8.6 \times 10^{-5}$ dyn sec. cm^{-2} (4).
- 2) BCS theory gives $2\Delta(0) = 3.5kT_c$. The use of $4.3kT_c$ for the energy gap to 0°K is, however, supported by tunnelling experiments. 3) The use of an adjustable parameter somewhat dilutes the usefulness of this result. To prove the point beyond a reasonable doubt it will be necessary to eliminate dislocation attenuation. We find a small amount of Au diffused through dislocations reduces attenuation considerably. This is shown in figure 2. The dotted line in the figure is the expected attenuation, given by Mason (5), without dislocation loss.

REFERENCES

1. W.A. Fate, R.W. Shaw and G.L. Salinger; Phys. Rev. 172, 413 (1968).
2. R.L. Thomas, H.C. Wu and N. Tepley; Phys. Rev. Letters, 17, 22 (1966).
3. W.P. Mason; Phys. Rev. 143, 229 (1966).
4. A. Hikita and C. Elbaum; Phys. Rev. Letters, 18, 750 (1967).
5. W.P. Mason, A. Rosenberg; J. Appl. Phys. 38, 1929 (1967).

ON THE LINE SHAPE OF JOSEPHSON RADIATION

R. Sundaram and V. G. Phide
National Physical Laboratory, New Delhi-12.

I. INTRODUCTION

Since Josephson⁽¹⁾ predicted an a.c. super-current generated in a superconducting tunnel junction by a d.c. bias voltage, the electromagnetic radiation associated with the a.c. current has received considerable attention. This may be with a view to possible application of Josephson junction as a source of radiation. The linewidth has also been experimentally observed.⁽²⁾ It is the purpose of this communication to calculate the radiation linewidth. We do not introduce the concept of phase diffusion phenomenologically; phase diffusion follows explicitly from our calculation.

II. THEORETICAL

We assume that the barrier, usually an oxide layer of 20 Å thick, separating two identical superconductors, lies in the xy plane and consider variation only along x

$$\frac{\partial \phi}{\partial x} = \frac{2e d}{\hbar c} H_y x k ; \quad \frac{\partial \phi}{\partial t} = \frac{2e}{\hbar} V \equiv \omega \quad (1)$$

$$J_x = J_c \sin \phi \quad (2)$$

Here ϕ is the phase difference between the two superconductors, H is the magnetic field in the barrier, V is the voltage across the barrier and $d = 2\lambda_L + \ell$, where λ_L is the London penetration depth and ℓ is the barrier thickness. From (1), (2) and Maxwell's equations

Regarding the barrier as having a capacity C per unit area we get the field equation of Josephson.

$$\left[\frac{\partial^2}{\partial x^2} - \frac{1}{c^2} \frac{\partial^2}{\partial t^2} \right] \varphi = \frac{\sin \varphi}{\lambda_J^2}$$

$$\bar{c}^2 = c^2 / 4\pi d C ; \lambda_J^2 = \hbar c^2 / 8\pi e d J_1 \quad (3)$$

All measurements basically amount to measuring the correlation function $\langle J(t)J(t) \rangle$ where J is the a.c. supercurrent given by

$$J = R_c J_1 e^{i\varphi}$$

A general solution of the nonlinear equation (3) has not been reported so far. Applying Laplace transform, we have obtained a general solution for a linearized drive term.

$$\varphi(x, t) = \begin{cases} f(t - x/c) - \frac{x}{\lambda_J} \int_{x/c}^t \frac{J_1 \left[\frac{\bar{c}}{\lambda_J} \left(\gamma^2 - \frac{x^2}{c^2} \right)^{1/2} \right]}{\left(\gamma^2 - \frac{x^2}{c^2} \right)^{1/2}} d\tau ; & t \gg \frac{x}{c} \\ 0 ; & 0 \leq t < \frac{x}{c} \end{cases} \quad (4)$$

The integral involving the Bessel function has possibly a connection with Gauss hypergeometric function which will be reported elsewhere. For the present, we take $\varphi = \omega t - kx$.

The radiation line shape is given by the Fourier transform of the correlation function $\langle J(t)J(t) \rangle$

$$F(\omega - \omega_0) \sim \int_{-\infty}^{\infty} \exp(-i\omega t) \exp \left[\frac{2ei}{\hbar} \int_0^t V_1(t+t_1) dt_1 \right] \exp(-k^2 x^2) dt. \quad (5),$$

by Ott's theorem

$$\sim \int_{-\infty}^{\infty} \exp(-i\Omega t) \exp\left[-\frac{2e^2}{\hbar^2} \int dt dt_2 V_1(t+t_2) V_2(t+t_2)\right] \exp(-k^2 \langle x^2 \rangle) \\ = \int_{-\infty}^{\infty} \exp(-i\Omega t) \exp\left[-\frac{8e^2}{\hbar^2} \int f(\omega) \frac{\sin^2 \omega t_2}{\omega^2} \right] \exp(-k^2 \langle x^2 \rangle) dt$$

Using quasilinear techniques of Lax (3) it can be shown that both photon shot noise and the quasiparticle noise have the form $\text{Coth} \hbar \frac{eV_0}{k_B T}$. Thus it is possible to define a dynamic resistance $\frac{1}{R} = \frac{1}{R_s} + \frac{1}{R_v} + \frac{1}{R_e}$ corresponding to pair tunneling, quasiparticle tunneling and external circuit respectively and an effective temp T_e .

Using Nyquist's theorem,

$$f(\omega) = \frac{RT_e}{1 + \omega^2 R^2 C^2}$$

Calling $\frac{8e^2}{\hbar^2 R T_e}$ as D and RC , the time constant of the circuit, β , I reduces to

$$I \sim \exp(-k^2 \langle x^2 \rangle) \int_{-\infty}^{\infty} \exp(-i\Omega t) \exp\left[-\frac{D}{\beta} (\beta t - 1 + e^{-\beta t})\right] dt \quad (8)$$

The expression in parenthesis clearly demonstrates that the phase is executing a Langevin continuous diffusion (4). Perhaps this may have some relevance to the amorphous nature of the oxide layer.

The integral (8) can be readily reduced to an Incomplete Gamma function of a complex quantity

$$I \sim \exp(-k^2 \langle x^2 \rangle) \beta^{-1} \int_0^1 \exp(\alpha y) (1-y)^{s-1} dy \quad (9)$$

which is the integral representation of the confluent hypergeometric function of Kummer (5)

$$I \sim \frac{1}{\beta} \Phi(1, s+1, \alpha) \exp(-k^2 \langle x^2 \rangle)$$

where

$$\alpha = \frac{D}{\beta} ; s = \alpha + i\Omega/\beta \quad (10)$$

DISCUSSION

The first term of (10) gives a Lorentzian of

width D , which is one of the limiting cases. The other extreme case is obtained by the asymptotic behaviour of the confluent hypergeometric function for large values of α . In that case, the series (10) goes over to

$$\sim \beta^s e^{\alpha} \alpha^{-s} \Gamma(s)$$

and in this limiting case gives a Gaussian of width

$2[D\beta \ln 2]^{1/2}$. The factor $\exp(-k^2 \langle z^2 \rangle)$ enters like the Debye-Waller factor showing that the magnetic field modulates the intensity. In a finite junction a Fraunhofer term $\left[\frac{\sin(kL - n\pi)/2}{(kL - n\pi)/2} \right]^2$ will enter in the expression. Considering terms containing powers of α , it is seen that there will be narrowing of the Lorentzian line. Regarding the use of Nyquist's theorem this analysis holds very well for the region $eV_0 \leq k_B T$ and for $eV_0 > k_B T$ with limited rigour. We have not considered the coupling of the Josephson frequency with the cavity mode frequencies for which we have to make use of the general expression (4).

REFERENCES

1. B.D. Josephson, Phys. Letters 1, 251 (1962).
2. D.N. Langenberg et al., Phys. Rev. Letters 15, 294 (1965).
3. M.J. Stephen, Phys. Rev. 182, 531 (1969).
4. S. Chandrasekhar, Rev. Mod. Phys. 15, 1 (1943).
5. Higher Transcendental Functions, edited by A. Erdelyi (McGraw-Hill, New York, 1953), Vol. 1.

DISCUSSION

-15-

M.P. Verma

Your solution holds for ϕ small. You put then $\phi = (\omega t - kx)$. Thus t and x are constrained such that $(\omega t - kx)$ remains small say, nearly zero. Or, in other words, you are introducing a flow. What does this flow represent?

R. Sundaram

You could tell me if you know.

A.C. Biswas

The effect of any noise in the tunneling junction must come from the non-linear term $\sin \phi$. How do you linearise it and still expect to get some reasonable answer?

R. Sundaram

We assume that noise alone causes the broadening of the δ -function spectrum. Linearising is the first step to achieve a solution.

R. Subramanian

I did not quite follow your argument for replacing $\sin \phi$ by ϕ in your non-linear equation. I would have thought such a replacement might entirely change the nature of the solution.

Sundaram

It will not change the nature of the solution.

ONSET OF TURBULENCE IN THE FLOW OF LIQUID HELIUM BETWEEN ROTATING CYLINDERS*

N. Davaraj
Department of Physics, Central College,
Bangalore University, Bangalore-1.

I INTRODUCTION

Studies of the flow of liquid helium II between coaxial rotating cylinders at very high velocities or rotation have been made and the transition to turbulent flow has been detected. The Taylor criterion (1) has been used in the detection of the transition. Observations have been made at three temperatures 1.5150K, ^{1.7060K} and 2.117°K and the critical Reynolds numbers marking the transition are determined. It is found that the onset of turbulence occurs at all the three temperatures at Reynolds numbers around 3000. The behaviour of liquid helium II in this respect is compared with that of an ordinary liquid like carbon disulphide in the same apparatus at the room temperature.

II EXPERIMENTAL

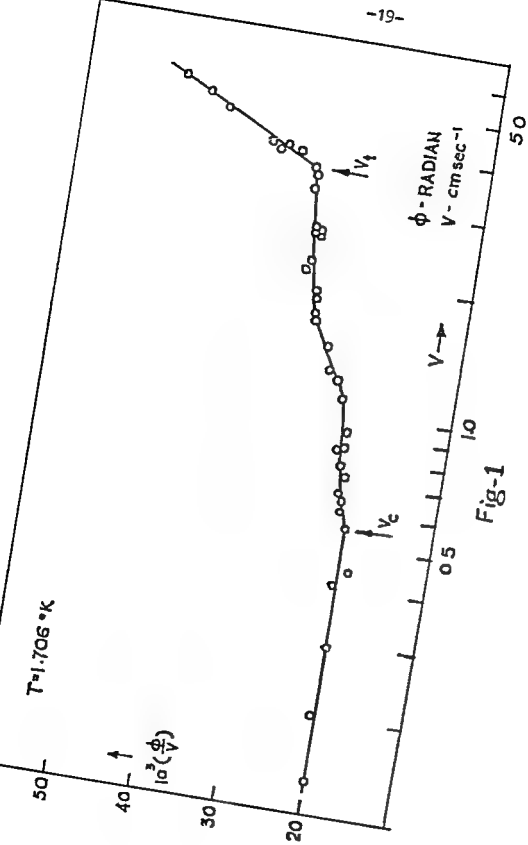
The apparatus used in this experiment is a coaxial rotating cylinder viscometer in which the outer cylinder (inner radius = 0.8380 cm.) is rotated at a constant speed and the inner cylinder (radius = 0.8126 cm.; length = 2.5390 cm.) is freely suspended by a torsion wire. The annular space (width = 0.0754 cm.) between the

Work done at the Department of Physics, University of Toronto, Toronto, Canada.

Two cylinders is filled with the fluid under investigation and the viscous torque exerted by the rotating fluid on the stationary inner cylinder is determined by measuring the resulting angular deflection of the inner cylinder. The apparatus was suitably mounted inside a liquid helium cryostat so that the flow of liquid helium II between the rotating cylinders could be studied.

In a rotating cylinder system such as this, for laminar flow of the liquid between the cylinders, the viscous torque on the inner cylinder is directly proportional to the velocity of rotation of the outer cylinder. However, Taylor has shown that at very high velocities of rotation this linear law does not hold good and at a certain velocity (V_c), known as the critical velocity, the torque begins to increase abruptly. Such a sudden change in the rate of increase of the torque marks the onset of turbulence in the flow of the liquid. The change occurs quite sharply and accurate detection of the onset of turbulence is possible. Further, the turbulent flow is characterised by the fact that the viscous torque under such a flow varies nearly as the square of the velocity of rotation. This is generally regarded as the criterion for turbulent flow between the rotating cylinders.

The viscous torque on the inner cylinder was measured as a function of the velocity of rotation of the outer cylinder at three temperatures 1.515°K , 1.706°K and 2.117°K . The temperature of liquid helium II was maintained constant.



by controlling the vapour pressure above the liquid helium bath. The vapour pressure was accurately measured and the temperature of the liquid was estimated correct to about a millidegree. Velocities as high as 7 cm sec^{-1} were employed to cover the turbulent region of the flow.

III RESULTS

The results of measurements obtained at 1.706°K are shown in Fig. 1 where $(\frac{\phi}{V})$ is plotted against V . ϕ is the angular deflection which is a quantity proportional to the torque and V is the velocity of rotation. It can be clearly seen from the figure that there are three distinct regions on the curve. In the first region (for velocities upto V_c) the flow is essentially laminar. The critical velocity V_t marks the transition to turbulent flow and in the region beyond V_t the torque is nearly proportional to the square of the velocity, being characteristic of the turbulent flow. The lower critical velocity V_c marks the onset of a secondary flow which depends on the geometry of the system as has been reported by Heikkila and Hallett (2) and also by Woods (3). The flow in the middle region consists of the laminar flow with the secondary flow superposed on it. The behaviour at the other two temperatures of investigation, 2.117°K and 1.515°K , is quite similar to the above. The values obtained for the critical velocities (V_t) marking the onset of turbulence and the corresponding Reynolds numbers (R_t) are given in Table I. This is the first time that turbulence in liquid helium II in a rotating cylinder system has been observed.

TABLE I

Critical velocities and Critical Reynolds numbers

$T^{\circ}K$	V_t cm sec ⁻¹	Re
2.117	4.5	2850 ± 150
1.706	3.5	3000 ± 100
1.515	3.6	2750 ± 250
CS_2 , $20^{\circ}C$	120	3100 ± 200

In order to make certain of the identification of V_t with the onset of turbulence in liquid helium II, the flow of a classical liquid, such as carbon disulphide, in the same apparatus was investigated and the results compared. It is found that for carbon disulphide at room temperature ($20^{\circ}C$) the critical Reynolds number marking the onset of turbulence is also about 3000 and further ~~it~~ even with this liquid the torque is found to be nearly proportional to the square of the velocity in the turbulent region. Hence, it appears that the conditions of incidence of turbulence and the flows in the turbulent region are similar both for liquid helium II and a classical liquid such as carbon disulphide.

ACKNOWLEDGEMENTS

The author is grateful to Prof. A.C. Hollis Hallett, Department of Physics, University of Toronto, Toronto, Canada, for his encouragement and useful discussions.

REFERENCES

1. Taylor G.I., Proc.Roy.Soc. A157, 546 (1936).
2. Heikkila, W.J., and Hollis Hallett, A.C., Can. Jour.Phys. 33, 420 (1955)
3. Woods, A.D.B., Ph.D Thesis, University of Toronto, Canada (1957)

DISCUSSION

C. Ambasankaran

What was the speed of rotation of the outer cylinder and how was this achieved?

N. Devaraj

With helium II experiments the speeds ranged upto about 7 cm/sec and in CS₂ at 20°C, it went upto 120 cm/sec. These speeds were obtained using Graham Variable Speed transmission together with Gear systems etc.

A.B. Biswas

Has any effect been observed on the transition temperature, due to a change in the distance (gap) between the two co-axial cylinders in view of the difference in the flow rates along this length?

N. Devaraj

All our experiments are done with a constant gap width between the cylinders. So, it is difficult to tell how exactly it depends.

A.C. Biswas

Reynold's number is not independent of temperature for $T > 0^\circ\text{K}$ since there is a normal component of the fluid at that temperature?

N. Devaraj

Critical Reynolds number, I think, is independent of temperature. The critical velocities vary with temperature but the viscosity also varies resulting in that the critical Reynolds numbers are in effect independent of temperature.

E.S.R. Gopal

1) In the liquid helium case, what is the density used for calculating the Reynolds number?

2) Is the critical Reynolds number independent of temperature of observation?

N. Devaraj

1) It is the total density that is used, because at these high velocities the superfluid part also takes part.

2) Not very much. What differences we observe may be due to experimental errors.

S.V. Subramanyam

What is the gap width between the two cylinders in the experimental set up?

N. Devaraj

0.0754 cms.

FILM TRANSFER OF HELIUM II FOR LARGE PRESSURE HEADS

T.S. Radhakrishnan, S. Rangarajan and Girish Chandra
Tata Institute of Fundamental Research, Bombay-5, India

I. INTRODUCTION

Following the original findings of Daunt and Mendelssohn⁽¹⁾ that the transfer rates of helium II film along solid surfaces were largely independent of pressure heads and the heights of the intervening barrier, there have been a large number of investigations giving widely varying results which cannot be ascribed to experimental error alone. Recently Martin and Mendelssohn⁽²⁾ have observed variation of film transfer rates with level differences upto 4 cms. This effect which is just visible at 1.3°K becomes well pronounced at temperatures below 1°K. They suggest that this level dependent transfer rates may be a general phenomenon, possibly persisting upto the lambda point and may show up provided large enough level differences are employed. Further they believe that the irreproducibility of high flow rates observed by some workers may be associated with this pattern.

II. EXPERIMENTAL

In view of this suggestion, we have measured the flow rates into and out of a beaker, employing a wide range of pressure heads upto a maximum of 29 cms in the temperature range 1.59°K to 1.07°K. The glass beaker was 45 cms. long, the inner diameter being 2.4 mm. The uniformity of bore was tested by mercury pellet method to be within 0.02%. A calibrated carbon resistance thermometer placed at the same horizontal level as the rim of the beaker showed that the rim was at a higher temperature at large heights from the bath. For this reason filling experiments were preferred, as it is necessary to keep only a small portion of the beaker outside the bath in these cas

Nevertheless a few emptying experiments were also carried out and the measurements were stopped as soon as the temperature, as indicated by the carbon resistor showed any increase. Thermal shields with reflecting surfaces were arranged at the top of the beaker. The beaker was surrounded by two glass blocks, one smaller in length covering the mouth of the beaker without touching it and the other covering the entire length of the beaker. The impurities which entered the cryostat during transfer of liquid helium from storage flask were prevented from condensing on the beaker wall by means of glass blocks which also served to isolate the beaker from the effects of jarring. A low voltage neon lamp was used as light source and the levels were followed by a catheterometer. The time intervals between two successive readings were obtained with the help of a quartz oscillator timer.

III. RESULTS

The main features of the observations are as follows:

1. In fig.1 is plotted the flow rates against the difference in levels of helium between the beaker and the bath at various temperatures in large number of runs. Some runs lasted as long as three hours. In any run at one temperature, where, both the level difference and the height of the rim of the beaker above the bath changed, the position of the meniscus in the beaker varied linearly with time giving a constant flow rate.
2. Of these, a few runs had the same range of barrier height variation and yet widely varying level differences. The same flow rates were obtained.
3. Occasionally in the same run, a constant flow rate abruptly changed into another constant rate (Fig.2). The level difference at which this change took place as well as the amount of change

were different in every such case.

4. The absolute value of flow rates changed from run to run with wide limits (from 5×10^{-5} cc/sec/cm to 10.5×10^{-5} cc/sec/cm). Values near the upper limit were less frequent while more often values around 6.5×10^{-5} cc/sec/cm were obtained.

The foregoing observations 1 and 2 seem to indicate the independence of helium II film flow rates on level differences upto 29 cms and barrier heights upto 8 cms. The large scatter in flow rates indicated by observations 3 and 4 even for the runs carried out under apparently identical conditions seems to have something in common with the discrete flow rates discussed by Turckington and Edwards (3).

IV. ACKNOWLEDGEMENTS

We thank Dr. K. Mendelssohn who was Visiting Professor at our Institute for suggesting this problem and Professor B.V. Thosar for his interest in the work.

REFERENCES

- J.G. Daunt and K. Mendelssohn, Proc. Roy. Soc. A170, 423 (1939).
- D.J. Martin and K. Mendelssohn, Phys. Letters, 30A, 107 (1959).
- R.R. Turckington and V.H. Edwards, Phys. Rev. 168, 160 (1968).

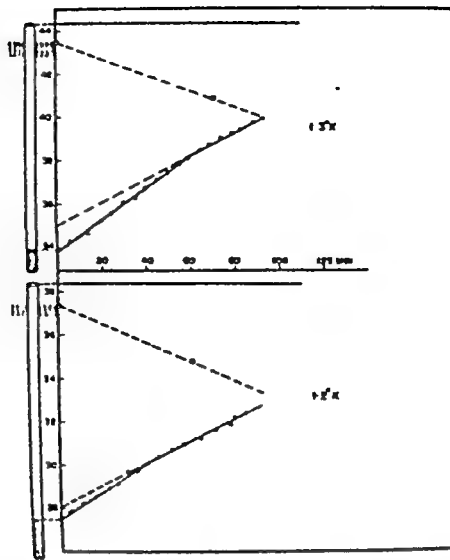


Fig.1. Flow rate against level difference at various temperatures. The vertical dotted lines connecting two horizontal lines shows the abrupt jump of flow rate in the same run to another value.

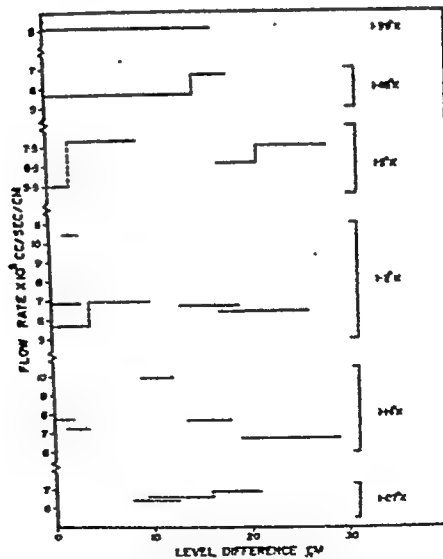


Fig.2. Beaker meniscus level against time. The points are experimental observations. Two slopes are obtained corresponding to two different rates.

A.K. Jalaluddin

1) How do you ensure the constancy of temperature of the cylinder all throughout its height?

2) Are all the runs made without warming the cylinder?

3) How reproducible are the so-called quantum jumps?

T.S. Radhakrishnan:

1) Explained in text. The carbon resistor is calibrated and one could compare the temperature as determined by the resistor with that of bath temperature, measured through vapour pressure.

2) Yes.

3) Discussed in reference 3 by Turkington and Edwards. They have made 18 runs at 1.2°K and get 7 values of flow rates, which seem to be removed from each other by a constant additive factor. To this extent it has been reproducible. We have also observed the same flow rate in more than a single run.

H.D. Bist

How does the purity of the surface of the beaker affect reproducibility of your results?

T.S. Radhakrishnan

The effects of impurities freezing on the walls of the beaker have been discussed by Brown and Mendelssohn in Proc. Phys. Soc. A53 (1950). It essen-

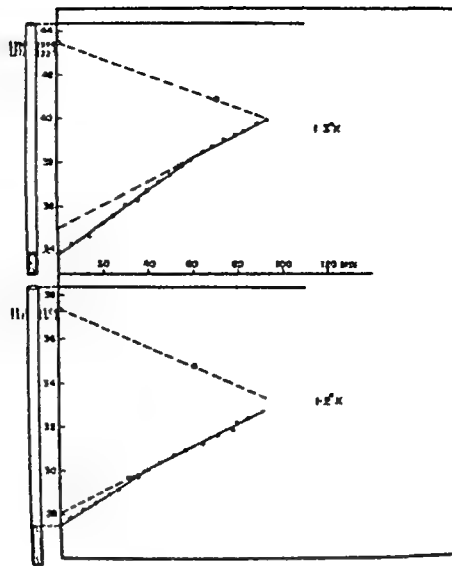


Fig.1. Flow rate against level difference at various temperatures. The vertical dotted lines connecting two horizontal lines shows the abrupt jump of flow rate in the same run to another value.

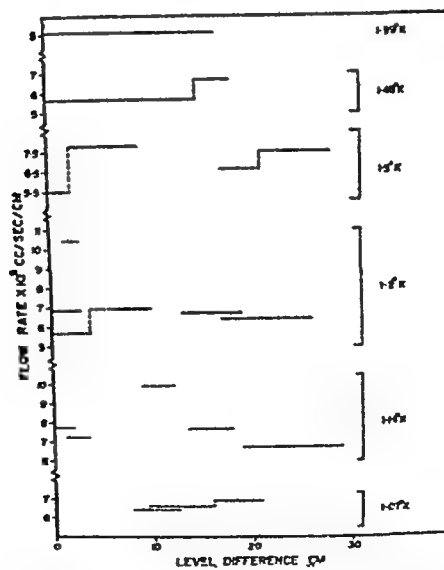


Fig.2. Beaker meniscus level against time. The points are experimental observations. Two slopes are obtained corresponding to two different rates.

A.K. Jalaluddin

1) How do you ensure the constancy of temperature of the cylinder all throughout its height?

2) Are all the runs made without warming the cylinder?

3) How reproducible are the so-called quantum jumps?

T.S. Radhakrishnan:

1) Explained in text. The carbon resistor is calibrated and one could compare the temperature as determined by the resistor with that of bath temperature, measured through vapour pressure.

2) Yes.

3) Discussed in reference 3 by Turkington and Edwards. They have made 18 runs at 1.2°K and get 7 values of flow rates, which seem to be removed from each other by a constant additive factor. To this extent it has been reproducible. We have also observed the same flow rate in more than a single run.

H.D. Bist

How does the purity of the surface of the beaker affect reproducibility of your results?

T.S. Radhakrishnan

The effects of impurities freezing on the walls of the beaker have been discussed by Brown and Mendelssohn in Proc. Phys. Soc. A53 (1950). It essen-

tially introduces additional structure to the surface of the beaker over which one does not have a control thereby changing the periphery of the beaker. The flow is proportional to the perimeter.

THERMO-ELECTRIC POWER OF DILUTE MAGNETIC ALLOYS AT LOW TEMPERATURES

M.S.R. Chari, N.S. Natarajan and R.G. Sharma,
National Physical Laboratory, New Delhi-12

I. INTRODUCTION

The thermo-electric power (TEP) of dilute magnetic alloys should be independent of the temperature T and the solute concentration c , when the localised spins are paramagnetic⁽¹⁾. For infinite dilutions, this should be⁽²⁾ roughly proportional to $J \cos^6 \eta \sin 2\eta$, where J is the (negative) exchange interaction parameter and f the function $\cos^6 \eta \cos 2\eta$ of the phase shift η for ordinary (spin-independent) scattering. Experiments show this temperature-independence only over a limited temperature range⁽³⁾.

We identify the theoretically expected temperature-independent value of the TEP with this experimentally observed extremum value S_m . From the anomalous electrical resistivity behaviour of each dilute alloy system⁽⁴⁾; as the solute content is varied, we can predict the sign and the concentration-dependence of S_m and compare these with available data.

II. DISCUSSION

The variation of the Kondo slopes d (of the ρ/c versus $\ln T$ plots) of dilute magnetic alloys systems with c , resembles that of the function f ($= \cos^6 \eta \cos 2\eta$) with η . Thus, for finite solute concentrations, one can associate a value of η (or at least set limits for it) with each value of c for a given alloy system. If this

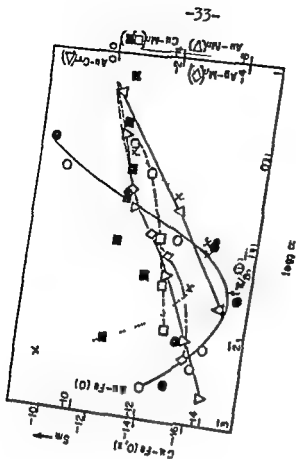
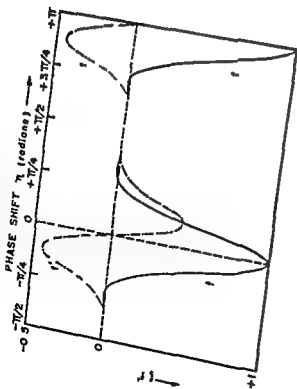
is true, S_m should vary with c in a manner similar to that of f' ($= \cos^6 \eta \sin 2\eta$) with η .

Fig. 1 shows how f and f' vary with η . Fig. 2 shows how S_m varies with the solute concentration for the various alloy systems. It can be seen that the behaviour of S_m as c is varied is compatible with that of d , presented in another paper by us at this symposium.

The negative Kondo slopes d of dilute Au-V alloys based on the data of Kume⁽⁵⁾ are shown in fig. 3(a) to have an unusual variation first steepening with increase of c , then becoming less steep. The former corresponds to $3\pi/4 < \eta < \pi$. Correspondingly f' should be negative and S_m positive for this concentration range. Experimental data⁽⁶⁾ do show a positive TEP (fig 3 b). We can expect a change of sign of S_m , beyond $c \simeq 2$.

REFERENCES

1. J. Kondo, Progr. Theor. Phys. 34, 372 (1965).
2. K. Fischer, Phys. Rev. 158, 613 (1967); J. Phys. Chem. Solids, 29, 1227 (1968).
J. Kondo, Phys. Rev. 169, 437 (1968).
3. D.K.C. MacDonald, W.B. Pearson and I.M. Templeton, Proc. Roy. Soc. A 266, 161 (1962).
A. Kjekshus and W.B. Pearson, Canad. J. Phys., 40, 98(1962).
4. Another paper by us in this section. Also M.S.R. Char, Physik. Kond. Materie 11, 317 (1970).
5. K. Kume, J. Phys. Soc.(Japan), 22, 1309 (1967), 23, 1226 (1967).
6. K. Kume, J. Phys. Soc.(Japan), 22, 1115 (1967); M.D. Daybell, D.L. Kohlstedt and W. A. Steyert, Solid State Comm. 2, 871 (1967).
7. E. Brewig, W. Kierspe, U.Schotte and D.Wagner, J. Phys. Chem. Solids, 30, 483 (1969).

[illegible]

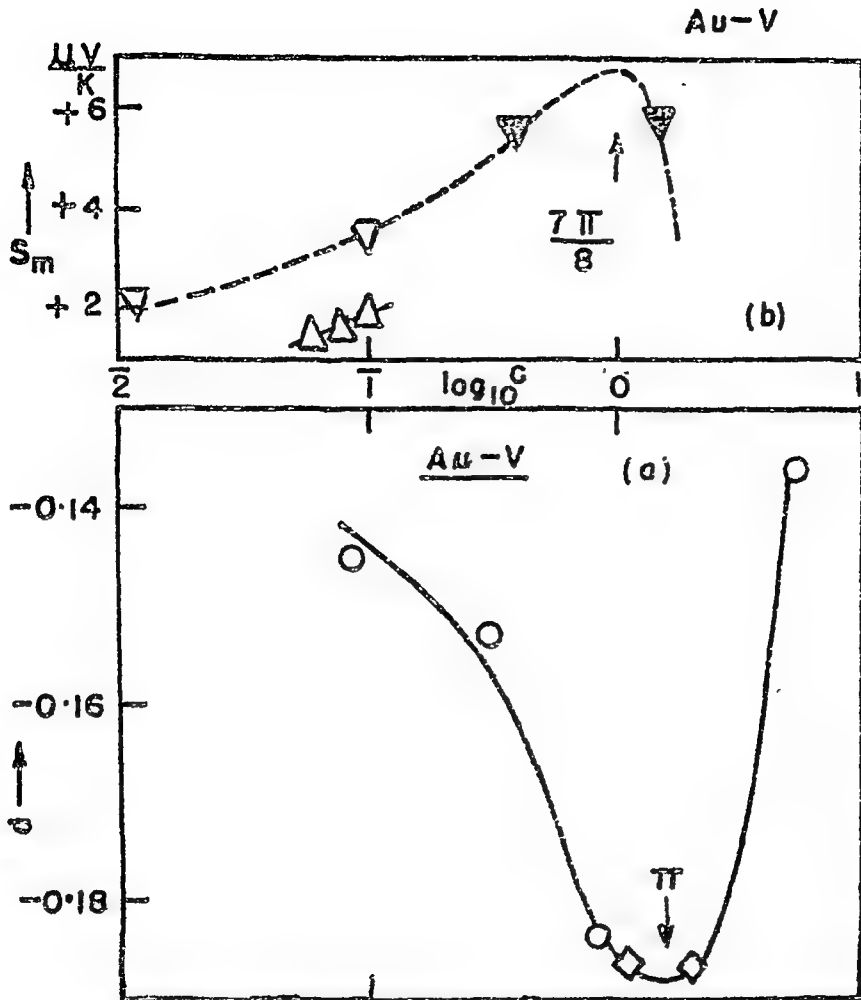


Fig. 3

Fig.3.a) Kondo slope d versus $\log_{10} c$ for the Au-V system.

b) Extremal thermoelectric power (S_m) versus $\log_{10} c$ for the Au-V system.

Markings: ∇ Extrapolated values from Kuzs, ref. 6;

∇ Daybell et al, ref. 6. For comparison, the data on Cu-V are shown (\triangle) from ref.7.

DISCUSSION

D.K. Ghosh

Do you have Hall effect data supplanting your resistivity and thermoelectric power measurements? If yes, what do they indicate as to the mechanism of resistivity change?

M.S.R. Chari

No Hall effect measurements were made by us because earlier measurements in this direction by Van Den Berg et al (at Leiden) on Ag-Mn alloys threw no new light on the subject.

CONCENTRATION DEPENDENCE OF THE RESISTIVITY ANOMALY IN DILUTE MAGNETIC ALLOYS

M.S.R.Chari, N.S.Natarajan and R.G. Sharma
National Physical Laboratory
New Delhi-12.

I. INTRODUCTION

In very dilute alloys of some of the 3d transition metals in noble metals, from the effects of the Pauli exclusion principle on the intermediate states of the higher order scattering amplitude (using the s-d exchange model), Kondo⁽¹⁾ showed that the spin-flip scattering of a conduction electron by the localised magnetic impurity (uncorrelated with its neighbours), gives a term in the electrical resistivity proportional to $cJ \ln T$ (where c is the solute concentration in atoms per cent). For a negative exchange integral J, this would increase with the fall in T and when combined with the usual T^5 -dependent intrinsic resistivity, would give the resistivity minimum.

The coupling of the ordinary, spin-independent impurity potential with J would modify this term^(2,3) to $cJ^3 \cos^6 \eta \cos 2\eta \ln T$, where η is the phase shift for ordinary scattering alone. The slope d of the ρ/c versus $\ln T$ curves of dilute rhodium-iron alloys is found⁽⁴⁾ to be positive and independent of the iron concentration. This is attributed to strong normal scattering⁽³⁾ with $\eta > \pi/4$, assuming J to be negative (anti-ferromagnetic) here also.

The theoretical treatments⁽¹⁻³⁾ presume infinitely dilute alloys so that the solute ions could be considered as isolated scattering centres for the conduction electrons. When one deals with actual alloys containing

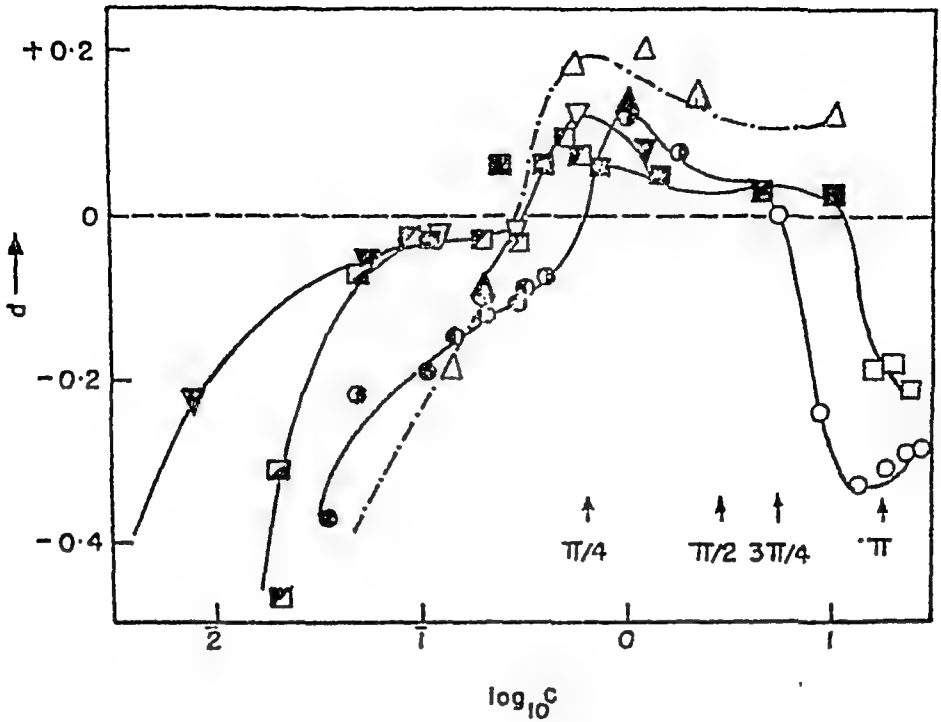


Fig. 1

1. The anomalous resistivity, parameter d ($=$ slope of ρ/c versus $\ln T$ plot for a dilute magnetic alloy of solute concentration c) plotted against $\log_{10} c$.

Markings: i) Cu-Mn (⊕, ⊙, ○, ⊗)
 ii) Ag-Mn (⊠, ⊡, ⊞)
 iii) Au-Mn (▽, ▼)
 iv) Au-Cr (△, ▲).

The phase shifts $\frac{\pi}{4}$, $\frac{\pi}{2}$ etc are marked for the Cu-Mn system.

finite solute concentrations, the variation of the Kondo slope (d) with c is suggestive of a phase shift η , itself increasing with c .

II. ANALYSIS OF EXPERIMENTAL DATA

The temperature-dependence of the electrical resistivity of the dilute magnetic alloy systems⁽⁵⁾ copper-manganese, silver-manganese, gold-manganese and others is such that i) in very dilute alloys, a resistivity minimum occurs, the resistivity below that temperature (T_m) rising steeply with the fall of T , ii) with increase of c , this steepness diminishes and a maximum appears (at T_M) and iii) on further increase of c , the minimum and maximum vanish giving place to an anomalous fall of resistivity with the fall of temperature. We have fitted the anomalous resistivity data (above T_M , if there is a resistivity maximum) to the relation $\rho/c = a \pm d \ln T$, the positive sign being used when there is no minimum but only a resistivity falling anomalously with the fall of temperature. ρ is expressed in micro-ohm-cm.

Fig. 1 shows the plot of d with c for the alloy systems Cu-Mn, Ag-Mn, Au-Mn and Au-Cr (data sources are given in ref. 6). It can be seen that these curves bear a close resemblance to the theoretical variation of the function $f(\pm \cos^6 \eta \cos 2\eta)$ with the phase shift η for ordinary scattering. Since, under conditions of isolated magnetic impurity scattering, the slope d is itself proportional to f , this means that we can adopt the theoretical infinite dilution model to that of

finite solute concentrations, provided we postulate⁽⁶⁾ a phase shift η (for spin-independent scattering) which itself increases with the increase of c .

1. THEORETICAL POSSIBILITY OF A CONCENTRATION-DEPENDENT PHASE SHIFT

It is known that an electron gas at metallic densities responds to a localised spin-dependent impurity potential in the form of RKKY (Ruderman-Kittel-Kasuya-Sida) oscillations. With an ideally pure solvent metal, these oscillations can be considered as being due to the interference of the scattered spherical wave with the incident Bloch wave. When the host metal is less pure due to the addition of a magnetic or non-magnetic impurity, the plane wave states have a finite life time (corresponding to the finite mean free path). Calculating the impurity scattering in the Born approximation and assuming the electron mean free path to be independent of energy, De Gennes⁽⁷⁾ arrives at a continuous shift of the phase of the RKKY oscillations as a consequence of impurity additions.

The inference, based on our above analysis of a concentration-dependent phase shift for ordinary scattering seems to conform to his calculation.

REFERENCES

- 1. J. Kondo; Progr. Th. Phys. 32, 37 (1964).
- 2. K. Fischer; Phys. Rev. 158, 613 (1967)
J. Phys. Chem. Solids, 29, 1227 (1968).
- 3. J. Kondo, Phys. Rev. 169, 437 (1968).
- 4. B.R. Coles; Phys. Letters, 8, 243 (1964).

5. G.J. Van den Berg; Prog. Low Temp. Physics
-Ed. C.J. Gorter (North Holland), 4, 194 (1964).
6. M.S.R.Chari; Phys. Kond. Materie, 11, 317 (1970).
7. P.G. De Gennes; J. Phys. Radium, 23, 630 (1962);
'Metallic Solid Solutions - Edited by J. Friedel
and A. Guinier' (Benjamin, 1963), paper VI.

DISCUSSION

T.V. Ramakrishnan

1) The formula quoted is valid only for $C \rightarrow 0$.
It cannot be extended ad hoc to finite C .

2) It seems unlikely that the potential scattering phase shift varies that considerably with addition of other impurity atoms.

M.S.R. Chari

1) The formula is indeed valid for infinite solute dilution. The close conformity of the variation of the Kondo slopes of dilute magnetic alloys with C , with the variation of the function $f(\eta) = \cos^2 \eta \cos 2\eta$ with η suggests to us that the formula so derived could be applied to finite C , if we could visualise a concentration-dependent phase-shift η for ordinary scattering.

2) It is certainly unlikely in normal non-magnetic dilute alloys; but De Gennes' calculation for an infinitely dilute magnetic alloy, which brings out a concentration dependent phase-shift of the RKKY oscillations, suggests that this is indeed to be expected.



THE RESISTANCE MINIMUM OF LUTETIUM FILMS.*

U.N. UPADHYAYA

Department of Physics, University of
Udaipur, Udaipur (Rajasthan)

1. INTRODUCTION :

Recently Lazerev, Kuzamento and Sudovtsov⁽¹⁾ have reported the discovery of a resistance minimum in films of the rare earth element lutetium which is a metal with a highly disorted crystal lattice. It has been found by them that the measurement of electrical resistance in a magnetic field perpendicular to the film plane showed that a field of strength up to 25 kOe does not alter the magnitude and temperature of the minimum. A similar effect is also observed in chromium⁽²⁾, though in other metals the minimum disappears in weaker fields. Lazerev et al, also find similar results for thulium films and they have suggested the possibility of some new mechanism of electron scattering at low temperatures in films of lutetium and thulium.

II. INTERACTION MECHANISM:

In the present paper a new mechanism for electron scattering is suggested which takes cognizance of the fact that the system of present interest has a highly distorted crystal lattice. This mechanism envisages local distortions around the magnetic ion site owing to disorder state or static Jahn-Teller effects. It is assumed that the local

* Supported in part by DAE, Bombay.

distortions are distributed randomly in the system such that the over all symmetry of the crystal is unchanged. This distorts a field acts as perturbation which mixes the d and s orbital states. The formulation of s - d coulomb electrostatic interaction in terms of these perturbed states gives new interaction terms in addition to the usual s - d exchange. It was been shown earlier ⁽²⁾ that such new interaction terms explain the temperature independent line width observed in ferromagnetic resonance of some transition metals.

III. FORMULATION OF HAMILTONIAN

Taking into account the additional interaction term discussed above, the Hamiltonian of the system can be written as,

$$\begin{aligned} \mathcal{H} &= \mathcal{H}_0 + \mathcal{H}_1 \\ &= \sum_{\underline{k}, \sigma} \omega_{\underline{k}} a_{\underline{k}, \sigma}^\dagger a_{\underline{k}, \sigma} - n^{-1} \sum_{\underline{k}, \underline{k}', n} \exp[i(\underline{k}' - \underline{k}) \cdot \underline{R}_n] J_0 \\ &\quad (a_{\underline{k}, \sigma}^\dagger a_{\underline{k}', \sigma} S_{n\sigma} + a_{\underline{k}, \sigma}^\dagger a_{\underline{k}', \sigma} S_{n+\sigma}) \end{aligned} \quad (1)$$

In the above the first term represent the energy of non-interacting Bloch electrons. The second term is the addition interaction term considered here. The constant J_0 involves the matrix element of the distortion field between s and d states and generalized coulomb and exchange type integrals between s and d electrons. For simplicity J_0 is assumed to be real.

Now making use of the retarded double time Greens

function and the equation of motion method, the t-matrix for conduction electrons is obtained as:

$$t(\omega) = -\frac{J_0^2}{N} \frac{\alpha(\omega)}{1 + J_0^2 \alpha(\omega) F(\omega)} \quad (2)$$

Where

$$F(\omega) = \frac{1}{N} \sum_{\underline{k}} \frac{1}{\omega - \epsilon_{\underline{k}}} \quad (3)$$

and $\alpha(\omega)$ is integral function of $t(\omega)$.

The above integral equation is simplified by considering the scattering matrix,

$$\psi(\omega + i\delta) \equiv 1 - i\pi \rho t(\omega + i\delta) \quad (4)$$

In terms of ψ the integral equation is solved self consistently and one obtains for ψ

$$\psi(z) = \frac{[|X'|^2 - (X'(z))^2]^{-1/2}}{X'(z) [|X'|^2 - (X'(\omega))^2]^{-1/2} + \exp[-(2\pi i)^{-1}] \int_{-D}^D \frac{\ln |H(\omega')|}{z - \omega'} d\omega'} \quad (5)$$

Where

$$X'(z) = 2\pi \int_{-D}^D \frac{f(\omega') - \frac{1}{2}}{z - \omega'} d\omega' \quad (6)$$

and

$$\gamma = \frac{J_0 \rho}{N} \quad (7)$$

Finally, the electrical resistivity R can be written in terms of relaxation time τ as

$$R = \frac{m}{ne^2} \frac{1}{\tau}$$

$$= \frac{m}{ne^2 \rho \pi} \operatorname{Re} [1 - \psi(\omega + i\delta)] \quad (8)$$

Thus one obtains the expression for R as,

$$R = R_0 - \alpha \ln T \quad (9)$$

Where α is a positive constant if J_0 is taken to be positive. Expression (8) indicates resistance minimum if considered in conjunction with the ideal resistance of the system. Detailed investigation of other electronic properties of the system is in progress. It may be remarked that the electron scattering interaction mechanism discussed here may be important also in the case of tunneling through barrier containing magnetic element impurities as the structure of the barrier is very similar to the highly distorted lattice structure considered in the present discussion. Such investigations are being carried out by us.

REFERENCES :

1. B.G. Lazarev, V.M. Kuz'menko and A.I. Sudovtsov, Soviet Physics 'Doklady' 14 129 (1969)
2. E.E. Semenenko, JETP Lett., 3, 291 (1966)
3. K.P. Sinha and U.N. Upadhyaya, Indian J. of pure and applied physics. 2, 273 (1964)

ANOMALOUS THERMOELECTRIC POWER OF DILUTE MAGNETIC ALLOYS BELOW KOLDO TEMPERATURE.

R.K. Palival and U.N. Upadhyaya.
Department of Physics, University of Udaipur

U D A I P U R (RAJASTHAN)

I. INTRODUCTION.

In recent years the anomalous behavior of electronic properties of dilute magnetic alloys has been studied by several workers^(1,2). In the present paper a theoretical study of the electronic properties of dilute magnetic alloys is made on the basis of Anderson's model. It is assumed that the impurity electrons are in the virtual state, and conditions for formation of localized magnetic moment are satisfied.

Following Anderson⁽³⁾ the Hamiltonian for the present system can be written as

$$H = \sum_{k,s} \epsilon_k c_{ks}^\dagger c_{ks} + \sum_j \epsilon_d c_{dj}^\dagger c_{dj} + U n_d n_v \\ + V \sum_{k,s} (c_{ks}^\dagger c_{ds} + c_{ds}^\dagger c_{ks}) \quad (1)$$

In the above, the notations used are the same as in reference 3. The Hamiltonian⁽¹⁾ has been studied earlier by Theumann⁽⁴⁾ and Oguchi⁽⁵⁾. Theumann made use of the double time Green's function and using the equation of motion method, he obtained the expression,

for the t -matrix (transition matrix). Further, Theumann studied only the behavior of anomalous resistivity. Oguchi, making use of a new Green's function method proposed by Sawada⁽⁵⁾, derived the expression for t -matrix and studied the various electronic properties of dilute alloys. However the expression obtained by Oguchi for the thermoelectric power, does not explain the available experimental results; in particular for $\text{Cu} + \frac{\text{Fe}}{\text{Cu}}$ system.

In what follows, solution for t -matrix obtained by Theumann, is used to derive the expression for thermoelectric power.

II. CALCULATION OF THERMOPOWER.

The expression for the spin independent scattering amplitude $t(\omega)$ obtained by Theumann⁽⁴⁾, can be written as

$$t(\omega) = \frac{1}{2\pi i} \left[1 - H(\omega) e^{\Delta(\omega)} \frac{\chi_+(\omega)}{\sqrt{(\chi_+(\omega))^2 + \pi^2 \Gamma^2}} \right]^{1/2} \quad (6)$$

where $H(\omega) = \frac{1 - i\pi\Gamma}{[1 - \Gamma^2]^{1/2}} |H(\omega)|^{-1} \quad (7)$

$$\Delta(\omega) = \frac{\Gamma}{2\pi i} \int_0^D \frac{dx}{\omega - x} \ln |H(x)| \quad (8)$$

and other symbols have the same meaning as in reference 4.

The relaxation time γ for conduction electrons is obtained by the following relation,

$$\gamma^{-1}(\omega) = -C R \operatorname{Im} \tau(\omega + i\delta)$$

$$= \frac{C R}{2 \pi f} \operatorname{Re} [1 - \psi^2(\omega)] \quad \dots (5)$$

In the low temperature limit ($\frac{T}{T_K} \ll 1$), the approximate expression for $\psi^R(\omega)$ turns out to be

$$\operatorname{Re} \psi^R(\omega) \approx \frac{\ln \beta(\omega)}{\sqrt{(\ln \beta(\omega))^2 + 5\pi^2}} + \frac{10\pi^4 f r}{[(\ln \beta(\omega))^2 + 5\pi^2]^{\frac{3}{2}}} + \frac{\pi^2}{2} \frac{\ln \beta(\omega)}{[(\ln \beta(\omega))^2 + 5\pi^2]^{\frac{3}{2}}}$$

where

$$\beta(\omega) = \frac{\omega^2 + \pi^2 T^2}{\pi^2 T_K^2} \quad \dots (6)$$

Finally the thermopower S is obtained, using the relation (6), using the

$$S(T) = \frac{1}{eT} \frac{K_2 - T_f K_1}{K_1} \quad \dots (8)$$

Where

$$K_n = \frac{4P}{m^*} \int T(\omega) (\omega + T_f)^n \frac{df}{d\omega} d\omega \quad \dots (9)$$

Making use of (8), (9), (6) and (5) the expression for $S(T)$, turns out to be.

$$S(T) = -\frac{\pi^2}{3|C|} \frac{K^2 T}{T_f} \left[1 + AT^5 - \frac{B}{\{[\ln(\frac{T}{T_K})^2]^2 + 5\pi^2\}^{\frac{3}{2}}} \right] \quad \dots (10)$$

where A and B are constants, which depend on the electronic and lattice properties of the system. Numerical calculations from (10), for Cu + Fe/Cu, shows that $S(T)$ is positive for $T < T_K$ and initially decreases with increasing temperature.

This is in agreement with the experimental results.
(7)
reported by Brewig et al .

REFERENCES

1. J. Kondo, Solid State Physics. (Edited by Seitz, Turnbull and Ehrenreich) 23, 184 (1969).
2. A.J. Heeger, Solid State Physics (Edited by Seitz, Turnbull and Ehrenreich). 23, 284(1969).
3. P.W. Anderson, Phys. Rev. 124, 41 (1961).
4. Alba Theumann, Phys. Rev. 178, 978(1969).
5. Akihide Oguchi, Prog. Theo. Phys. 43, 257 (1970)
6. F.J. Blatt, Solid State Physics (Edited by Seitz and Turnbull) 4, 199 (1957).
7. E. Brewig et al, J. Phys. Chem. Solids 30, 483, (1969).

.....

ELECTRONIC PROPERTIES OF SOLIDS

A SPECIAL CASE OF THE SAXON-HUTNER THEOREM FOR THREE-DIMENSIONAL POTENTIALS

K.V. Bhagwat and R. Subramanian
Tatva Atomic Research Centre, Bombay

I. INTRODUCTION

In connection with the study of electronic properties of one dimensional metals and alloys, Saxon and Hutner ⁽¹⁾ made the following conjecture which states: "Energies which are forbidden for both pure A and pure B type of metals having the same lattice constant are forbidden energies for any substitutional solid solution of A and B". This conjecture was later proved by Luttinger ⁽²⁾ for the case of a one dimensional binary alloy with one-dimensional δ -function potential between an atom and an electron. There have been attempts to generalize the result to three dimensions but these have met with little success ⁽³⁾. We have here considered the motion of an electron in a superposition of three-dimensional delta-function type potentials due to a linear infinite chain of identical atoms and also due to a periodic binary alloy and arrived at the band structure for negative energies. The expressions obtained are used to verify the Saxon-Hutner conjecture for this particular case of a binary periodic alloy.

II. THEORY

The interaction potential between the electron and an atom has been assumed to be delta-function type which can be replaced by a boundary condition ⁽⁴⁾ on the wave function.

$$\psi(y) \underset{y \rightarrow 0}{\sim} \text{constant} \cdot \left(\frac{1}{y} - \alpha \right) \dots (1)$$

The wave function for bound state of an electron in the

field of a linear infinite periodic chain of such potentials, taking into account the Bloch condition, can be readily shown to be

$$\psi(y) = A \sum_{n=-\infty}^{\infty} e^{i\alpha n} \frac{e^{-K|y-n|}}{|y-n|}, \quad \dots (2)$$

where α denotes the component of the wave vector of the electron along the chain. Without loss of generality we have set the lattice constant equal to unity. The electron energy E is related to K by the relation $E = -\hbar^2 K^2 / 2m$.

Applying the boundary condition (1) at $y = 0$ we get the following expression

$$K - \alpha = \sum'_{n=-\infty}^{\infty} e^{i\alpha n} \frac{e^{-K|n|}}{|n|}, \quad \dots (3)$$

where the prime over the summation sign means that the term $n=0$ is omitted. The sum on the r.h.s. of eq.(3) can be readily evaluated. After some simplifications we get

$$\cos \alpha = \cosh K - \frac{e^{-\alpha}}{2} \quad \dots (4)$$

α takes all the values between 0 and π . There is a band of allowed energies, $\alpha=0$ corresponds to value of K at the bottom of the band and $\alpha=\pi$ corresponds to K at the top of the band. The band may entirely lie in the negative energy region or may extend upto zero energy, depending on the value of α , the strength of the potential. There are solutions for all positive energies.

We then consider the motion of an electron in the potential due to an infinite linear chain of equidistant atoms of two types A and B situated alternately. The atoms of types A and B are characterized by strengths α and β respectively. The wave

function for a bound state of the electron can be shown to be

$$\psi(r) = A \sum_{n=-\infty}^{\infty} e^{\frac{2i\alpha n}{|r-2ni|} - K|r-2ni|} + B \sum_{n=-\infty}^{\infty} e^{\frac{2i\alpha n}{|r-(2n+1)i|} - K|r-(2n+1)i|} \dots (5)$$

where we have chosen the origin on one of the A-sites. Applying the boundary condition (1) at the positions of atoms of the two types we get a system of two linear homogeneous equations for the coefficients A and B. A nontrivial solution can be shown to exist if and only if

$$\left[\ln 2e^{-\mu/2} (\cosh K + \cos x) \right] \left[\ln 2e^{-\mu/2} (\cosh K - \cos x) \right] = \frac{\nu^2}{4}, \dots (6)$$

where $\mu = \alpha + \beta$, $\nu = \alpha - \beta$.

Depending on the values of α and β either there are two bands of allowed energies lying entirely in the negative energy region or the upper band extends upto or lies entirely in the positive energy region.

In equation (6) we set $\nu = 0$ we get back equation (4) as is to be expected. If we set $x = 0$ in eq.(6) there will be two solutions for K which will denote the lower edge of the lower band (K_{1L}) and the upper edge of the upper band (K_{2U}), for $x = \pi/2$ we get two values of K: K_{1U} , K_{2L} denoting the upper edge of the lower band and the lower edge of the upper band respectively. It can be shown that as long as $\alpha \neq \beta$ when there are two bands they are always separated by a finite gap, i.e. the two bands do not overlap, so that the identification of K_{1U} , K_{2L} poses no problem. Let $K_{U\alpha}$, $K_{L\alpha}$ be respectively the upper and lower edges of the

band for pure A metal and $K_{U\beta}$, $K_{L\beta}$ be the corresponding values for pure B-metal. Then if $\alpha > \beta$ and $K_{L\beta} < K_{U\alpha}$ (i.e. the case when the allowed band for pure B-type lattice lies entirely above that of pure A-type lattice), the following inequalities can be shown to hold.

$$K_{2U} > K_{U\beta} \quad , \quad K_{2L} < K_{L\beta} \quad ,$$

$$K_{1U} > K_{U\alpha} \quad , \quad K_{1L} < K_{L\alpha} \quad .$$

Noting that the bands are in the negative energy region these are exactly the inequalities predicted by the Saxon-Hutner theorem. Even if there is considerable overlap between bands for pure A and pure B metals (i.e. $K_{L\beta} > K_{U\alpha}$) in the alloy the bands do not overlap. The zeroth (i.e. the gap below the lower edge of the lower band) and the second (i.e. the gap above the upper edge of the upper band upto zero energy) gaps are wider in the alloy.

III. CONCLUSION

The Saxon-Hutner theorem is thus found to be true for a linear periodic binary alloy with δ -function type potential between an electron and atoms. The result may be extended to more complicated periodic binary alloys. However we have not been successful in proving the conjecture for an arbitrary substitutional alloy.

REFERENCES

1. D.S. Saxon and R.A. Hutner; Philips Res. Rep. 4, 81 (1949).
2. J.M. Luttinger; Philips Res. Rep. 6, 303 (1951).
3. I.M. Lifshitz; Advances in Physics 13, 483 (1964).
4. Yu. N. Denkov and R. Subramanian; JEMP 57, 698 (1969).

DISCUSSION

R. Sundaram

How exactly do you bring in the assumption of constancy of lattice constant in your formalism?

R. Subramanian

The constancy of the lattice constant is necessary for the sum to be evaluated exactly. Further the conjecture is true only if this assumption is made.

S.K. Joshi

Does the gap exist for any configuration for a three dimensional binary alloy?

R. Subramanian

The number of gaps depends on the actual 'strengths' of the δ -function type potentials. As far as the truth of the conjecture is concerned, we assume that the results, proved for the particular case mentioned, are true also for arbitrary configurations.

GENERALIZATION OF THE COHERENT POTENTIAL THEORY TO ALLOYS WITH SHORT RANGE ORDER

M.M. Pant and S.K. Joshi .

Physics Department, University of Roorkee, Roorkee.

The coherent potential theory seems to be the most attractive for describing electron states in disordered systems.⁽¹⁾ In this theory, the random scatterers are viewed as embedded in an effective medium whose choice is made self-consistently. This medium is chosen by requiring that a single scatterer embedded in this effective medium should produce no further scattering on the average.

For any given configuration, the single particle Green's function is given as $G(z) = (z-H)^{-1}$ where H is the one electron Hamiltonian corresponding to this configuration. The equation determining the effective Hamiltonian H_{eff} is $\langle G(z) \rangle = (z-H_{eff})^{-1}$.

If $K(z)$ is a starting approximation to H_{eff} , then we have in terms of the T matrix,

$$H_{eff} = K + \langle T \rangle [1 + R \langle T \rangle]^{-1} \quad (1)$$

where $R = (z-K)^{-1}$. The self consistent procedure for determining H_{eff} , then consists in choosing K such that $\langle T(K) \rangle = 0$ and this ensures that $H_{eff} = K$. If we express the random perturbing potential as a sum of contributions associated with each site, i.e. $H-K = \sum_n V_n$ and define a quantity Q_n by $T \equiv \sum_n Q_n$, then Q_n is given in terms of the single centre T matrix by

$$\begin{aligned} \langle T \rangle &= \sum_n \langle Q_n \rangle \\ \langle Q_n \rangle &= \langle T_n (1 + R \sum_{n' \neq n} Q_{n'}) \rangle . \end{aligned} \quad (2)$$

Then the self-consistency condition $\langle T(K) \rangle = 0$,

simplifies to $\langle T_n(K) \rangle = 0$ under the assumption of neglect of all correlations between sites m and n . Thus, this formulation is suitable for a completely randomly disordered system. If some correlation exists between the position of the scatterers e.g. short range order in a disordered binary alloy, then the above condition needs to be modified. What will be required then is that a group of ions whose positions are correlated should show no further scattering due to the difference Hamiltonian $H - H_{\text{eff}}$, on the average. We start with the following expression for the T matrix of the assembly in terms of those of the constituents.

$$T = \sum_{\alpha} t_{\alpha} + \sum_{\alpha} \sum_{\beta \neq \alpha} t_{\alpha} K t_{\beta} + \sum_{\alpha} \sum_{\beta \neq \alpha} \sum_{\gamma \neq \beta} t_{\alpha} K t_{\beta} K t_{\gamma} + \dots \quad (3)$$

where t and K correspond to H_{eff} . Because of the presence of two types of atoms, this summation splits into four sums according to

$$T = \sum_{\substack{s=1,2 \\ s'=1,2}} T^{ss'} \quad (4)$$

and s is a subscript denoting the types of atoms. It is possible⁽²⁾ to reduce the above summations, to a sum of four geometric series under an approximation which invokes simple expressions for the higher order correlations in terms of the pair correlation function i.e. the short-range-order parameter. This yields a complicated implicit equation for the effective potential, involving the short-range-order parameter, and both on-energy and off-energy shell elements of the t-matrix.

In order to make calculations feasible, we assume muffin-tin potentials for the constituents and make angular-momentum expansions of the potential and the t-matrix. The actual potentials are replaced by δ -function shell potentials of the form

$$V^s(\underline{x}, \underline{x}') = \sum_L \gamma_L(\underline{x}) \frac{\delta(\underline{x}-R)}{R^2} V_s^L \frac{\delta(\underline{x}'-R)}{R^2} \gamma_L(\underline{x}') \quad (5)$$

where R is the radius of the muffin-tin sphere and the potential amplitudes V_s^L are related to the phase shifts due to the actual potential. The condition for determining the effective potential amplitudes, then reduces to a quadratic equation.

$$A V_0^{L^2} - B V_0^L + C = 0 \quad (6)$$

where

$$\begin{aligned} A &= G^{21} + G^{22} - (G^{11} G^{22} + G^{12} G^{21}) j_L^2(xR) \\ B &= G^{11} + G^{12} + G^{12} g_e V_1^L + G^{12} g_e V_2^L + 2 V_2^L (G^{22} - G^{12} g_e \\ &\quad - G^{12} G^{22} j_L^2(xR)) + (V_1^L + V_2^L) \{ G^{21} - G^{11} g_e - G^{11} G^{22} j_L^2(xR) \} \\ C &= G^{11} V_1^L + G^{12} V_2^L + V_1^L V_2^L \{ G^{21} - G^{11} g_e - G^{11} G^{22} j_L^2(xR) \} \\ &\quad + (V_2^L)^2 \{ G^{22} - G^{12} g_e - G^{12} G^{22} j_L^2(xR) \} . \end{aligned}$$

Once V_1^L is known, determining the spectral function $\rho(E, k)$ is a straight forward matter. (3)

The chief features of the ideas presented above

- 1) Explicit account is taken of the correlation between the positions of the two types of scatterers.
- 2) The 'geometric approximation' invoked implies

that a certain class of terms in the series is still ignored.

3) It reduces to the usual criterion of $C_1t_1 + C_2t_2 = 0$ for the case of a completely random system.

4) It is capable of giving numerical results for a system like β -brass.

ACKNOWLEDGMENTS

One of us (M.P) wishes to acknowledge financial support from the Department of Atomic Energy.

REFERENCES

1. P. Soven, Phys. Rev. 156, 809 (1967).
2. J.L. Beeby, Phys. Rev. 135, A130 (1964).
3. M.M.Pant and S.K. Joshi, Phys. Letters 31A, 230(1970).

DISCUSSION

A.C. Biswas

Please explain the potential you have taken.

S.K. Joshi

The potential is a δ -function peaked at R_{mt} the radius of the muffin tin sphere. The use of such potentials in the ordered lattices has been discussed by Slater (Phys. Rev. 145, 599 (1966)) and Soven (Phys. Rev. 151, 539 (1966)) used this for disordered alloys. With such a potential the various terms of the series for T can be evaluated easily.

You mentioned that all higher order correlation functions have been expressed in terms of two-body functions. Where did you truncate and what does it mean? What is geometric approximation?

S.K. Joshi

The terms $T^{SS'}$ will involve angular integrals of the type $(S_{\alpha\beta}^{SS'})_{LL'} \sim \int Y_L(\hat{y}) g_2(\vec{y}-\vec{z}+\vec{R}_\alpha-\vec{R}_\beta) e^{-i\vec{k}\cdot(\vec{R}_\alpha-\vec{R}_\beta)} d\hat{y} d\hat{z}$ besides the radial integrals. A typical term in series $T^{SS'}$ will be of the type

$$\left(\sum_{\beta \neq \alpha} S_{\alpha\beta}^{SS'} \sum_{\gamma \neq \beta} S_{\beta\gamma}^{S'S''} \dots \sum_{\omega \neq \psi} S_{\psi\omega}^{S''S'''} \dots \right)_{LL'}$$

The approximation mentioned above is to replace $S_{\alpha\beta}^{SS'}$ by some $g^{SS'}$ which does not depend on α . The series for $T^{SS'}$ then becomes a geometric series and this is known as the "geometric approximation". For more details refer to

1. J.L. Beeby; Phys. Rev. 135, A130 (1966).
(Ref. 3 in the text)
2. M.M. Pant and S.K. Joshi; Phys. Rev. B1, 2532 (1970)

CONDUCTION ELECTRON DENSITY AT THE NUCLEUS IN DYSPROSIUM METAL

D. K. Ray
Faculte des Sciences, Universite de Paris,
91-Orsay, France

and
K. C. Das
Saha Institute of Nuclear Physics, Calcutta-9

I. INTRODUCTION

Here we shall report the result of our calculation of the conduction electron density at the nucleus in Dy metal using the non-relativistic Augmented-Plane-Wave (APW) method. Such an investigation is thought to be interesting in view of the availability of the experimental values of this quantity in different rare earth metals^(1,2). For Dy metal⁽²⁾ Mossbauer isomeric shift measurements were done with 25.7 keV γ -ray of ^{161}Dy , and the density of the conduction electrons at a nuclear site was estimated as $(1.65 \pm 0.35) \times 10^{26} \text{ cm}^{-3}$. In the present work we shall see how far the theoretical value obtained from the non-relativistic APW calculation agrees with this value.

II. THEORY

The wave function for the conduction electron, corresponding to the reduced wave vector \vec{k} and energy E , may be written as

$$\Psi_{\vec{k}, E}(\vec{r}) = \frac{1}{F_{\vec{k}, E}} \sum_n C_{\vec{k}, E, n} \phi_{\vec{k}_n}(E, \vec{r}) \quad (1)$$

CONDUCTION ELECTRON DENSITY AT THE NUCLEUS IN DYSPROSIUM METAL

D. K. Ray
Faculte des Sciences, Universite de Paris,
91-Orsay, France
and
K. C. Das
Saha Institute of Nuclear Physics, Calcutta-9

I. INTRODUCTION

Here we shall report the result of our calculation of the conduction electron density at the nucleus in Dy metal using the non-relativistic Augmented-Plane-Wave (APW) method. Such an investigation is thought to be interesting in view of the availability of the experimental values of this quantity in different rare earth metals^(1,2). For Dy metal⁽²⁾ Mössbauer isomeric shift measurements were done with 25.7 keV γ -ray of ^{161}Dy , and the density of the conduction electrons at a nuclear site was estimated as $(1.65 \pm 0.35) \times 10^{26} \text{ cm}^{-3}$. In the present work we shall see how far the theoretical value obtained from the non-relativistic APW calculation agrees with this value.

II. THEORY

The wave function for the conduction electron, corresponding to the reduced wave vector \vec{k} and the energy E , may be written as

$$\Psi_{\vec{k}, E}(\vec{r}) = \frac{1}{F_{\vec{k}, E}} \sum_n C_{\vec{k}, E; n} \Phi_{\vec{k}_n}(E, \vec{r}) \quad (1)$$

Here $\vec{k}_n = \vec{k} + \vec{k}_n$, \vec{k}_n being a reciprocal lattice vector, $F_{\vec{k},E}$ is the normalisation factor of the wave function, and, in the APW formalism, $\Phi_{\vec{k}_n}(E, \vec{r})$ is the usual APW function⁽³⁾. Using the explicit form of the APW function, the expression for the spherically averaged conduction electron charge density inside an APW sphere may be written as

$$\begin{aligned} \rho_{ce}^{(e)}(r) = & -2e \sum_{\ell=0}^{\infty} (2\ell+1) \sum_{\vec{k},E} \frac{1}{F_{\vec{k},E}^2} \frac{R_{\ell}^2(E,r)}{R_{\ell}^2(E,\sigma)} \\ & \times \left[\sum_{n,n'} C_{\vec{k},E;n} C_{\vec{k},E;n'}^* j_{\ell}(k_n \sigma) \right. \\ & \left. \times j_{\ell}(k_{n'} \sigma) P_{\ell}(\cos \theta_{\vec{k}_n, \vec{k}_{n'}}) \right] \quad (2) \end{aligned}$$

Here σ is the radius of the APW sphere and $R_{\ell}(E,r)$ is the radial solution of the Schrödinger equation containing the crystal potential in the "Muffin-tin" form. The summation over (\vec{k}, E) is extended over all the occupied states and the factor 2 takes account of both the electronic spins.

III. RESULTS

The "Muffin-tin" potential for Dy metal was constructed using the non-relativistic atomic wave functions given by Herman and Skillman⁽⁴⁾. The radius of the APW sphere was found to be 3.158 a.u. and the constant potential outside the APW spheres was calculated as -1.192 Rydberg. The energy eigenvalues were

calculated for 105 reduced wave vectors distributed uniformly within $(1/24)$ th of the Brillouin Zone; this number actually corresponds to 2100 points contained inside the whole of the Brillouin Zone⁽⁵⁾. It has been observed that except at the highest symmetry points, such as Γ and A , the differences between our results and those of Keeton and Loucks⁽⁵⁾ obtained by the relativistic APW method are not significant.

In our calculation of the spherically averaged charge density of the conduction electrons we have assumed that the conduction electrons occupy the three lowest bands, and the detailed nature of the Fermi surface has not been taken into account. Also we have considered l from 0 to 15. The conduction electron density has been found to be almost constant for r less than 0.0003 a.u. and its value at the nucleus has been found to be $0.532 \times 10^{26} \text{ cm}^{-3}$.

IV. DISCUSSION

In our calculation of the electronic density at the nucleus we have completely neglected the relativistic effects. Also, the effect of the finite nuclear size on it has not been considered. In order to take account of these two factors we can multiply our calculated value by 4⁽⁶⁾, and get $|V_{Co}(0)|^2 = 2.13 \times 10^{26} \text{ cm}^{-3}$. This

is 30% larger than the experimental value of 1.65×10^{26} cm^{-3} (2). This discrepancy is not significant in view of the fact that the experimental value itself has an error of $\pm 21\%$. It is also necessary to see how far the theoretical value changes by taking the actual Fermi surface into account.

REFERENCES

1. U. Atzmony, E. R. Bauminger, J. Hess and S. Ofer, in *Hyperfine Structure and Nuclear Radiations*, ed. E. Matthias and D. A. Shirley, North-Holland Publishing Co., Amsterdam, p. 71 (1968).
2. W. Henning, G. Kaendl, P. Kienle, H. J. Korner, H. Kulzer and K. E. Rehm; *Phys. Letters* 28A, 209 (1968).
3. T. L. Loucks; *Augmented Plane Wave Method*, W. A. Benjamin, Inc., New York (1967).
4. F. Herman and S. Skillman; *Atomic Structure Calculations*, Prentice Hall, Inc., Englewood Cliffs, New Jersey (1963).
5. S. C. Keeton and T. L. Loucks; *Phys. Rev.* 168, 672 (1968).
6. D. A. Shirley; *Rev. Mod. Phys.* 36, 339 (1964).

R10.248

RELATIVISTIC BAND STRUCTURE FOR CRYSTALS WITH NON-SYMMORPHIC SPACE GROUP

A. Gupta (nee Ghosh) and Santosh Kumar
Saha Institute of Nuclear Physics, Calcutta-9.

I. INTRODUCTION

We present here the formalism for the calculation of relativistic energy bands for crystals with nonsymmorphic space group, incorporating the technique of symmetrisation. Recently Buzano and Rasetti⁽¹⁾ have reported such calculations for crystals with symmorphic space group. The relativistic generalisation of the augmented plane wave (APW) method for the calculation of energy bands has been presented by Loucks⁽²⁾. We use the symmetrised relativistic APW (RAPW) functions, constructed from the linear combinations of four component Dirac spinors by applying projection operators of double space group, to carry out the energy band calculations.

II. FORMALISM

To calculate the relativistic band structure, we solve the Dirac equation: (units : $m = c = \hbar = 1$)

$$(\vec{\alpha} \cdot \vec{p} + \beta + \frac{1}{2} m_{ij}(\vec{r}) \gamma_i \gamma_j) \vec{\Phi}_{\vec{k}}(\vec{r}) = E \vec{\Phi}_{\vec{k}}(\vec{r}), \quad (1)$$

based on muffin-tin potential⁽³⁾. The notations are same as given by Loucks⁽²⁾. The one-electron function $\vec{\Phi}_{\vec{k}}(\vec{r})$ can be expanded in terms of symmetrised RAPW functions :

$$\vec{\Phi}_{\vec{k}}^{\nu}(\vec{r}) = \sum_{m,n,\tau} C_{n,\tau}^{m,\nu} \gamma_{\vec{k}_n,\tau\lambda}^{m,\nu}, \quad (2)$$

where $\vec{k}_n = \vec{k} + \vec{k}_n$, \vec{k}_n being a reciprocal lattice vector; ν is the irreducible representation index of double space group \tilde{G}^k , the double group of the group of \vec{k} vector G^k ; s, λ specify the particular partner of the symmetrised basis of the ν th representation and m is the projection of the spin. The functions $\gamma_{\vec{k}_n, s\lambda}^{m, \nu}$ in region I and II of the muffin-tin potential can be constructed from the corresponding unsymmetrised RAPW functions⁽²⁾ by applying full projection operator

$$P_{s\lambda, m}^{\nu} = \frac{\ell_{\nu}}{|\tilde{G}^k|} \sum_{\{\vec{T}_\nu + \vec{T}_p | R_p\} \in \tilde{G}^k} \tilde{\Gamma}_{s\lambda}^{\nu *} \{\vec{T}_\nu, \vec{T}_p | R_p\} \hat{P}_{\{\vec{T}_\nu + \vec{T}_p | R_p\}} \quad (3)$$

and can be expressed as :

$$\begin{aligned} [\gamma_{\vec{k}_n, s\lambda}^{m, \nu}]_{II} = & \frac{\ell_{\nu}}{2|P^k|} \sum_{\{0|R_p\} \in \tilde{P}^k} \tilde{\Gamma}_{s\lambda}^{\nu *} \{0|R_p\} \exp i R_p \vec{k}_n \cdot \vec{r} \exp i (\vec{k} - R_p \vec{k}_n) \cdot \vec{r}_p \\ & \times \left(\frac{k_n^0 + 1}{2k_n^0} \right)^{1/2} \left(\sum_{m'} D_{m'm}^{1/2} (R_p) \chi^{(m')} \right. \\ & \left. \times \left(\frac{\vec{r} \cdot \vec{k}_n}{1 + k_n^0} \sum_{m'} D_{m'm}^{1/2} (R_p) \chi^{(m')} \right) \right), m = \pm 1/2, \quad (4) \end{aligned}$$

and

$$\begin{aligned} [\gamma_{\vec{k}_n, s\lambda}^{m, \nu}]_I = & \frac{\ell_{\nu}}{2|P^k|} \sum_{\{0|R_p\} \in \tilde{P}^k} \tilde{\Gamma}_{s\lambda}^{\nu *} \{0|R_p\} \exp -i (R_p \vec{k}_n - \vec{k}) \cdot \vec{r}_p \\ & \times \sum_{\substack{R_p \\ k_{\mu}}}^{k_n, m} \left(\mathcal{D}_k(\hat{r}) \sum_{\mu'} D_{\mu'\mu}^{\hat{r}} (R_p) \chi_{\mu'}^{A'}(\hat{r}) \right. \\ & \left. \times \left(\mathcal{D}_k(\hat{r}) \sum_{\mu''} D_{\mu''\mu}^{\hat{r}} (R_p) \chi_{\mu''}^{A'}(\hat{r}) \right) \right) \\ & \times \exp i R_p \vec{k}_n \cdot \vec{r}_p, \quad (5) \end{aligned}$$

where $\vec{r} = \vec{r} - \vec{r}_p$, $\hat{r} = \vec{r}/|\vec{r}|$, $\hat{r}' = \hat{r} - \hat{r}'$, $k_n^0 = (1 + k_n^2)^{1/2}$

and $\hat{P}_R \chi^{(m)} = \sum_{m'} D_{m'm}^{1/2} (R) \chi^{(m')}$,

$$\hat{P}_R \chi_{\mu}^{A'}(\hat{r}) = \sum_{\mu'} D_{\mu'\mu}^{\hat{r}} (R) \chi_{\mu'}^{A'}(\hat{r}).$$

\hat{P}_R denotes group operator corresponding to the operation R . The rotation matrices $D^{\hat{r}}$ and $D^{1/2}$ are given by Rose⁽⁵⁾. $|P^k|$ is the order of the group P^k , the group formed by point group part of G^k and \tilde{P}^k is the

double group of P^k . l^* is the dimensionality of the νk irreducible representation $\tilde{\Gamma}^{\nu}$ of \mathcal{G}^k . $\tilde{\tau}_p$ is the nonprimitive translation associated with the point group operation R_p and $\vec{\tau}_p$ is a primitive translation. The radial functions f_k , g_k , the Pauli spinors $\chi^{(m)}$ and the spin angular functions $\chi_{\mu}^{k, m}$ are given by Rose⁽⁵⁾. \vec{r}_N is the position vector of the centre of the N th Slater sphere. The coefficients⁽²⁾ $A_{k, \mu}^{k, m}$ are chosen such that the upper component of the RAPT functions match at boundary of the spheres. μ takes the values from $-\frac{1}{2}$ to $\frac{1}{2}$ and

$$\left. \begin{aligned} l = k, \quad l' = k-1, \quad j = l-1/2 \quad (k > 0), \\ l = -k-1, \quad l' = -k, \quad j = l+1/2 \quad (k < 0). \end{aligned} \right\} \quad (6)$$

Using variational method⁽²⁾ and expressing $\tilde{\Phi}_K(\vec{r})$ in terms of symmetrised RAPT functions, the energy eigenvalues are obtained as the solution of the secular equation :

$$\det |M_{SS'}^{ij}(\frac{n}{m})| = 0, \quad (7)$$

$$\begin{aligned} \text{where } M_{SS'}^{ij}(\frac{n}{m}) = & \sum_{\{0|R_p\}} \frac{1}{2|P^k|} \tilde{\Gamma}_{SS'}^{\nu} \{0|R_p\} \exp \pm (K - R_p K_1) \vec{\tau}_p \\ & \times \left\{ (k_1^2 - E + mc^2) \left[\Omega_0 \delta_{K_1, K_2} K_1 K_2 - 4\pi \sum_N \sigma_N^2 \exp \pm (R_p K_2 - K_1) \vec{r}_N \right. \right. \\ & \times j_1(K_1 - R_p K_2 | \sigma_N) / (K_1 - R_p K_2) \Big] D_{mn}^{j_1}(e_p) + 4\pi \sum_N \sigma_N^2 \\ & \times \exp \pm (R_p K_2 - K_1) \vec{r}_N \sum_N \mathcal{D}_K^{ij}(\frac{n}{m}) j_2(k_1 \sigma_N) j_2(k_2 \sigma_N) \\ & \left. \times \left(\frac{c f_N(\sigma_N)}{f_N(\sigma_N)} - \frac{S_N k_2 j_2'(k_2 \sigma_N)}{j_2(k_2 \sigma_N)} \right) \right\}, \end{aligned} \quad (8)$$

where S_N is ± 1 , according to whether N is $+N$ or $-N$; Ω_0 is the volume of the unit cell, and

$$\begin{aligned}
 \mathcal{D}_k^{ij}(n) = & 4\pi \left(\frac{1 + k_i^0}{2k_i^0} \right)^{1/2} \left(\frac{1 + k_j^0}{2k_j^0} \right)^{1/2} \\
 & \times \sum_{\mu, \mu'} C(\ell \frac{1}{2} j; \mu' - n, n) C(\ell \frac{1}{2} j; \mu - m, m) \\
 & \times Y_{\ell, \mu' - n}^*(\hat{k}_j) Y_{\ell, \mu - m}(\hat{k}_i) D_{\mu', \mu}^{j'}(R_P). \quad (9)
 \end{aligned}$$

We neglect the relativistic effects in between the Slater spheres, where the electrons are much away from the nucleus and thus $k \ll c$ is a good approximation⁽²⁾.

The present method enables us to label the relativistic energy bands. This may be useful for studying the splitting of degeneracies and mixing of energy levels due to spin-orbit coupling and the time reversal symmetry.

REFERENCES

1. C. Buzano and M. Rasetti; Nuovo Cimento 67 B, 55 (1970).
2. T. L. Loucks; Phys. Rev. 139, A 1333 (1965); Augmented Plane Wave Method, (New York, W. A. Benjamin Inc., 1967).
3. J. C. Slater; Phys. Rev. 51, 151 (1937).
4. M. Tinkham; Group Theory and Quantum Mechanics, (New York, McGraw-Hill Book Co., 1964).
5. M. E. Rose; Relativistic Electron Theory, (John Wiley & Sons Inc., 1961); Elementary Theory of Angular Momentum (John Wiley & Sons Inc., 1957).

DISCUSSION

R.F. Singh

Have you studied the removal of degeneracy at certain points on the surface of the Brillouin zone?

We have observed doubling of the degeneracy at certain points on the surface of the Brillouin Zone (on the horizontal reflection plane in the k -space (ALR plane)) while investigating the non-relativistic energy band structure of lanthanum. This degeneracy is due to the time-reversal symmetry and so its removal cannot be studied until and unless some magnetic field is applied.

-73-

EFFECT OF PRESSURE ON THE FERM SURFACE OF GOLD

M.G. Ramchandani
Bhabha Atomic Research Centre, Chemistry Division, Bombay-85.

The recent study of effects of high pressure (1) on the various properties of solids has given a new dimension to the understanding of various phenomenon operative in solids. The change of the electrical resistivities and de Haas van Alphen frequencies are two such properties. Templeton (2) has recently studied the effect of pressure on the de Haas van Alphen frequencies of noble metals. Zallen (3) has observed the shift with pressure of reflectivity edge of the noble metals. These experimental results can be interpreted on the basis of band theory of solids.

The simplest free electron model for metals predicts the enlargement of Fermi surface uniformly if the metal be compressed isotropically. Ziman (4) has proposed the 8-cone model for the Fermi surface of noble metals in which the lattice parameter appears as a variable. Davis et al (5) were the first to calculate the complete band structure of copper for three different lattice parameters. Their calculations have shown that the observations of Templeton (2) and Zallen (3) can be successfully explained on the band model. In this paper we report the calculations on energy bands of gold for free lattice parameters and compare them with the experimental observations of Templeton (2) and Zallen (3).

In a previous paper (6) it has been shown that for a heavy metal like gold (atomic number 79), relativistic calculations of the energy bands are essential. For our calculations we have used Relativistic

EFFECT OF PRESSURE ON THE FERMI SURFACE OF GOLD

M.G. Ramchandani
 Bhabha Atomic Research Centre, Chemistry Division, Bombay-85.

The recent study of effects of high pressure (1) on the various properties of solids has given a new dimension to the understanding of various phenomenon operative in solids. The change of the electrical resistivities and de Hass van Alphen frequencies are two such properties. Templeton (2) has recently studied the effect of pressure on the de Hass van Alphen frequencies of noble metals. Zallen (3) has observed the shift with pressure of reflectivity edge of the noble metals. These experimental results can be interpreted on the basis of band theory of solids.

The simplest free electron model for metals predicts the enlargement of Fermi surface uniformly if the metal be compressed isotropically. Ziman (4) has proposed the 8-cons model for the Fermi surface of noble metals in which the lattice parameter appears as a variable. Davis et al (5) were the first to calculate the complete band structure of copper for three different lattice parameters. Their calculations have shown that the observations of Templeton (1) and Zallen (3) can be successfully explained on the band model. In this paper we report the calculations on energy bands of gold for three lattice parameters and compare them with the experimental observations of Templeton (2) and Zallen (3).

In a previous paper (6) it has been shown that for a heavy metal like gold (atomic number 79), relativistic calculations of the bands are essential. For our calculations we have used Relativistic

Augmented Plane Wave (APW) method of Loucks⁽⁷⁾. In a recent paper⁽⁸⁾ it has been shown that for gold, Slater exchange⁽⁹⁾ gives band structure which is in better agreement with the experimental Fermi surface data. In this calculation, we have used Slater approximation for exchange potential.

We have calculated the band structures of gold for three lattice parameters a , $0.995a$ and $0.99a$ where a is the normal lattice constant of gold.

Templeton⁽²⁾ has measured the change of the de Haas van Alphen frequencies with hydrostatic pressure for the neck and $\langle 111 \rangle$ belly orbits of the Fermi surfaces of the noble metals. The neck area increases with applied pressure for all these metals. Qualitatively our calculations also show this trend for the neck area in conformity with the results of Davis et al⁽⁵⁾ for copper. Templeton gives the value for the pressure coefficient of neck i.e. $(\Delta A/A)/\Delta P$ as $1.97 \times 10^{-6} \text{ cm}^2/\text{Kg}$. As we go from a to $0.995a$ we get the value for this quantity about seven times the experimental value. As we go from $0.995a$ to $0.99a$, we get a value which is little larger than the experimental value. The average value is $7.9 \times 10^{-6} \text{ cm}^2/\text{Kg}$. assuming the value of volume compressibility to be $5.44 \times 10^{-7} \text{ cm}^2/\text{Kg}$ as given by Neighbours and Alers⁽¹⁰⁾.

Zallen's⁽³⁾ experimental value of the shift of the reflectivity edge for gold is less than $1 \times 10^{-6} \text{ eV/bar}$. Assuming that Zallen's⁽³⁾ interpretation of transition from d band to Fermi level near L to be correct, we have estimated this shift to be about $1 \times 10^{-6} \text{ eV/bar}$. We therefore suggest that the reflectivity edge

in gold may be due to vertical transitions from d band to Fermi level as claimed by Cooper et al (11).

I thank Dr. P.G. Bhattachandani for many useful discussions I had with him while carrying out this work.

REFERENCES

1. 'Physics of Solids at High Pressures' Eds. Tomizuka C.T. and Barick R.M. (New York: Academic Press) 1965.
2. Templeton I.M. Proc. Roy. Soc, A292 413 (1966)
3. Zallen R. in 'Optical Properties and electronic structure of Metals and Alloys' Ed. Abeles P. (Amsterdam: North Holland) 1966 p. 164
4. Ziman J.M. Adv. Phys. 10 1 (1961)
5. Davis H.L., Paulkner J.S. and Joy H.W. Phys. Rev. 167 601 (1968)
6. Bhattachandani M.G. Supp. J. Phys. C(Metal Physics) 3, 81 (1970)
7. Loucks T.L. 'Augmented Plane Wave Method' (New York: Benjamin) 1967
8. Bhattachandani M.G. to be published in J. Phys. F (Metal Physics)
9. Slater J.C. Phys. Rev. 81 385 (1951)
10. Neighbours J.R. and Aiers G.A. Phys. Rev. 111 707 (1958)
11. Cooper B.R., Ehrenreich H. and Philipp H.R. Phys. Rev. 138 A 494 (1965).

DISCUSSION

- 1) What transition is responsible for the 2ev peak?
- 2) What was the variation of α in Templeton's experiments? How does it affect your comparison?

M.G. Ramachandani

1) The peak at about 2. eV is attributed to conduction band \rightarrow Fermi level.

2) Templeton has applied pressure of 25 atmospheres. This will be equivalent to a very small change in lattice constant. In going from a to $0.995a$ about 10^4 atmospheres pressure is necessary. Hence the comparison is tentative.

Santosh Kumar

When you apply pressure on the crystal and the lattice parameter changes, how is it that the symmetry of the crystal is still unchanged?

M.G. Ramachandani

The pressure is applied isotropically and hence the symmetry remains unchanged.

Satya Prakash

How do you include the pressure dependent function in your basic Hamiltonian.

M.G. Ramachandani

The pressure dependence is not included in the Hamiltonian. The band structure is calculated for different lattice constants each time.

ELECTRON CORRELATIONS IN A CLASSICAL PLASMA

K.N. Pathak and K.G. Aggarwal

Department of Physics, Panjab University, Chandigarh.

The purpose of this paper is to study the particle correlations in a system of negatively charged particles imbedded in a static uniform, neutralizing, background of positive charge. Debye and Huckel ⁽¹⁾ were the first to develop a successful theory based on the above model. Their theory gives a simple expression for the static pair correlation function:

$$g(r) = 1 - \frac{\beta e^2}{r} \exp\left\{ - (4\pi n \beta e^2)^{\frac{1}{2}} r \right\} \quad (1)$$

where n is the number density, e is the charge of the particles and $\beta = 1 / k_B T$. Debye-Huckel theory gives meaningful results only for $r > \beta e^2$. At small distances between the particles, equation (1) results in negative values of $g(r)$ which being a probability should always be positive. Nevertheless, Debye-Huckel model is useful for systems at high temperatures and low densities where coulomb correlations between the particles are of less importance. Since then there have been many attempts ⁽²⁻⁵⁾ to develop theories which could be applied to systems at lower temperatures and higher densities.

Recently Berggren ⁽⁶⁾ has used the self consistent theory of Singwi et al. ^(3, 4) to calculate the static pair correlation function of a classical plasma. Ichimaru ⁽⁵⁾ has derived an expression for the dielectric response function of a classical plasma from a solution of the Bogolubov - Born - Green - Kirkwood - Yvon equation by breaking the three particle correlation function into two particle correlation functions. We discuss here some of the results obtained on the basis of Ichimaru's theory.

The density response function, $\chi(q, \omega)$, in generalised random phase approximation (RPA) can be written as

$$\chi(q, \omega) = \chi_0(q, \omega) / [1 - \psi(q) \chi_0(q, \omega)], \quad (2)$$

where $\chi_0(q, \omega)$ is the density response function for a noninteracting gas and $\psi(q)$ is the generalised potential. In RPA, $\psi(q)$ is the Fourier transform of the bare coulomb potential. From the solution of the BBGKY equation, Ichimaru⁽⁶⁾ has obtained,

$$\psi(q) = \phi(q) [1 - G(q)], \quad (3a)$$

$$G(q) = -1/n \sum_{\underline{k}} (\underline{k} \cdot \underline{q} / k^2) S(\underline{k}) [S(\underline{k} - \underline{q}) - 1], \quad (3b)$$

where $\phi(q) = 4\pi e^2 / q^2$ and $S(\underline{k})$ is the static structure factor.

Using the fluctuation-dissipation theorem and equation (2) one obtains for the static structure factor,

$$S(q) = [1 + n\beta\psi(q)]^{-1}. \quad (4)$$

Equation (3b) can be written in a form which is more suitable for computation,

$$G(q) = -\frac{q}{4\pi^2 n} \int_0^\infty S(\underline{k}) k dk \int_{-1}^{+1} x dx \left\{ S(k+q)^2 - 2kqx - 1 \right\} \quad (5)$$

$S(q)$ can now be computed in a self consistent manner using the relations (3a), (4) and (5). In the Debye-Huckel approximation, $G(q) = 0$ and the corresponding $S(q)$ from equation (4) is

$$S(q) = q^2 / (q_D^2 + q^2), \quad q_D^2 = 4\pi n e^2 \beta \quad (6)$$

Starting with this value of $S(q)$ integration in eq. (5) can be done analytically. Therefore, substituting the Debye-Huckel $S(q)$ in equation (5) and carrying out the x integration we obtain,

$$G(q) = -\frac{q_D^2}{4\pi^2 n} \int_0^\infty \frac{k^2 dk}{k^2 + q_D^2} \left[i + \frac{k^2 + q^2 + q_D^2}{4kq} \ln \left\{ \frac{(k-q)^2 + q_D^2}{(k+q)^2 + q_D^2} \right\} \right]. \quad (7)$$

After doing the k integration by suitably choosing a contour we obtain the result of the first iteration,

$$G(q) = \frac{q^2}{16\pi} \left[\pi - 2 \tan^{-1} (2q/q) \right] \quad (8)$$

Though the calculation of self consistent $G(q)$ or $S(q)$ may require a few iterations, we can observe some important points from equation (8). It is evident from eqs. (8) and (4) that for large values of q , $G(q)$ varies as q and $\{S(q) - 1\}$ varies as $1/q$. Using this result it is not difficult to see that $G(q)$ in the second iteration diverges logarithmically. However, for small values of q , $S(q)$ goes as q^2 as expected.

We are in the process of computing $S(q)$ in a self consistent manner by truncating the k integral in eqn. (5) at some reasonable value of k . The result which we shall get for $g(r)$ will not probably be reliable for small values of r .

REFERENCES:

1. P. Debye and E. Hückel; *Z. Physik* 24, 185 (1923); 24, 305 (1925)
2. N. Rostoker and H. N. Rosenbluth; *Phys. Fluids* 3, 1 (1960).
3. K. S. Singwi, A. Sjolander, H. P. Tosi and R. H. Land; *Phys. Rev.* 176, 589 (1968).
4. K. S. Singwi and A. Sjolander; *Phys. Rev.* 1, 1044 (1970).
5. S. Ichimaru; *Phys. Rev.* 2, 494 (1970).
6. K. F. Berggren; *Phys. Rev.* 6, 1783 (1970).

DISCUSSION

T. V. Ramakrishnan

- 1) The divergence arises from large q behaviour. Does it have anything to do with Coulomb interaction

at all?

2) Is it possible to find exact large q behaviour of $S(q)$?

K.G. Aggarwal

1) I do not think so.

2) No, as far as I know.

SUM RULE, PLASMA-DISPERSION AND COMPRESSIBILITY OF ELECTRON LIQUID

K.M. Pathak

Department of Physics, Panjab University, Chandigarh-11
and

K.S. Singal

Department of Physics, Northwestern University, Evanston, ILL. USA.

In this paper we present a simple theory of electron correlations based on generalized random phase approximation. The effective mean field is determined using the third moment of the electron density correlation function. The compressibility and the plasma dispersion relation of the degenerate electron liquid are discussed.

In the linear response theory¹⁾, the dielectric function can be written in the form

$$\frac{1}{\epsilon(q, \omega)} - 1 = \phi(q) \chi(q, \omega), \quad (1)$$

where $\phi(q) = 4\pi e^2/q^2$ and $\chi(q, \omega)$ is the Fourier transform of the density response function defined as¹⁾

$$\chi(q, t) = -i \theta(t) \langle [\rho_{\vec{q}}(t), \rho_{-\vec{q}}(0)] \rangle. \quad (2)$$

It is easy to calculate the low order moments of density correlation function²⁾. The first moment is the well known f-sum rule. The third moment is explicitly given here in the form

$$-\int_{-\infty}^{\infty} \frac{d\omega}{\pi} \omega^3 \chi''(q, \omega) = \frac{n q^2}{4m} \left\{ \omega_q^2 + 4\omega_q \frac{\langle KE \rangle}{N} + \frac{1}{m} \sum_{\vec{k}} (\vec{k} \cdot \hat{q})^2 \phi(k) \times \right. \\ \left. \times [S(\vec{q} - \vec{k}) - S(k)] \right\}. \quad (3)$$

$\chi''(q, \omega)$ is here the imaginary part of $\chi(q, \omega)$, $\omega_q = \hbar q^2/2m$ and $S(k)$ is the static structure factor. It may be noted that Eq.(3) is exact.

In the generalized EPA, the density response function be

written as

$$\chi(q, \omega) = \chi_0(q, \omega) / [1 - \psi(q) \chi_0(q, \omega)], \quad (4)$$

where $\chi_0(q, \omega)$ is the density response function of a non-interacting electron gas. In RPA $\psi(q) = \phi(q)$. We calculate the first and third moments of $\chi''(q, \omega)$ from Eq.(4). The first moment is automatically satisfied and the third moment will be satisfied if

$$\psi(q) = \phi(q) [1 - G(q)], \quad (5)$$

$$G(q) = -\frac{1}{4\pi n e^2} \sum_{\vec{k}} [(\hat{q} \cdot \vec{k} + \vec{q})^2 \phi(\vec{k} + \vec{q}) - (\hat{q} \cdot \vec{k})^2 \phi(k)] [S(k) - 1], \quad (6)$$

In obtaining the above expression for $G(q)$ we have assumed that the exact kinetic energy of electron gas is not very different from the kinetic energy of free electron gas. Eq.(6) can be written in a form which is suitable for computation:

$$G(q) = -\frac{1}{4\pi^2 n} \int_0^\infty dk k^2 [S(k) - 1] \left[\frac{5}{6} - \frac{k^2}{2q^2} + \frac{(k^2 - q^2)^2}{4kq^3} \ln \frac{k+q}{k-q} \right]; \quad (7)$$

For electron liquid $S(k)$ is not known to us. However, if we use the fluctuation dissipation theorem

$$S(q) = -\frac{\hbar q^2}{4\pi^2 e^2 n} \int_0^\infty \frac{I_m[\epsilon(q, \omega)]^{-1}}{\omega} d\omega, \quad (8)$$

$S(q)$ may be determined self-consistently as was first done by Singwi et al^{3,4}).

The compressibility and the plasma dispersion relation depend on small q behaviour of $G(q)$. It can be shown from Eq.(7) that for small q

$$G(q) = -\frac{q^2}{15\pi^2 n} \int_0^\infty dk [S(k) - 1]. \quad (9)$$

On the other hand for large value of q

$$G(\infty) = \frac{2}{3} [1 - g(0)],$$

where $g(0)$ is the pair distribution function at $r=0$. The compressibility sum rule⁵⁾ can be stated as

$$\frac{C_0}{C} = 1 - (4\alpha n_s/\pi)\gamma; \quad \alpha = \left(\frac{4}{q\pi}\right)^{1/3}, \quad (11)$$

where C_0 is the compressibility of free electron gas and

$$\gamma = \lim_{q \rightarrow 0} \frac{G(q)}{(q/q_F)^2} = -\frac{1}{5q_F} \int_0^\infty dh [S(h) - 1]. \quad (12)$$

From Eq.(4) the plasma dispersion relation is given by

$$\omega_p(q) = \omega_p + \beta \hbar q^2/m, \quad (13)$$

$$\beta/\beta_{RPA} = 1 - \frac{5}{q} \left(\frac{4\alpha n_s}{\pi} \right) \gamma; \quad \beta_{RPA} = \frac{3\epsilon_F}{5\hbar\omega_p}. \quad (14)$$

In Eq.(12) if we use Hartree-Fock value of $S(k)$, we obtain $\gamma = 3/20 = 0.15$. It has been pointed out by Hedin and Lundquist⁵⁾ that energy derived compressibility corresponds to $\gamma = \frac{1}{2}$. Instead of using Hartree-Fock value of $S(k)$ in Eq.(12), if we use $S(k)$ as determined by Singwi et al^{3,4)} γ is quite close to $\frac{1}{2}$. However, we should determine $S(k)$ self-consistently to see how compressibility sum rule is satisfied and what kind of pair correlation function is obtained.

REFERENCES

1. P. Nozières, Interacting Fermi Systems (Benjamin).
2. R.D. Puff, Phys. Rev. 137, 1406 (1965).
3. K.S. Singwi, M.P. Tosi, R.N. Land and A.Sjolander, Phys. Rev. 176, 589 (1968).
4. K.S. Singwi, A.Sjolander, M.P.Tosi and R.N.Land, Phys. Rev. 21, 1044 (1970).
5. L.Nodin and S.Lundquist, Solid State Physics, ed. Seitz and Turnbull, 22, (1969).

DISCUSSION

J. Mahanty

Which is the form of $\bar{S}(k)$ that gives a better value of γ ?

K.N. Pathak

If the values of $S(k)$ calculated by Singwi et al. are used we get better result for compressibility.

ELECTRON CORRELATIONS IN TWO FOLD DEGENERATE BAND

R. Kishore and S.K. Joshi

Physics Department, University of Roorkee, Roorkee

For a long time the intraatomic exchange interaction between the electrons in the d band has been considered as one of the mechanisms responsible for the metallic ferromagnetism.¹ The model we consider here assumes a two fold degenerate band which is not realistic but is the simplest orbitally degenerate situation. It exhibits the ferromagnetism due to intraatomic exchange interaction.

The Hamiltonian for a narrow two fold degenerate band can be taken as²

$$H = \sum_{i,j} T_{ij} (a_{i\sigma}^\dagger a_{j\sigma} + d_{i\sigma}^\dagger d_{j\sigma}) + I \sum_i (n_{i-} n_{i+} + m_{i-} m_{i+}) + \sum_{i\sigma\sigma'} V n_{i\sigma} m_{i\sigma'} - V \sum_{i\sigma\sigma'} a_{i\sigma}^\dagger a_{i\sigma'} d_{i\sigma'}^\dagger d_{i\sigma} - \sum_{i\sigma} (\mu + \mu_B B) (n_{i\sigma} + m_{i\sigma}) \quad (1)$$

where I and V are the intraatomic Coulomb and exchange interactions; $a_{i\sigma}$, $d_{i\sigma}$ and $a_{i\sigma}^\dagger$, $d_{i\sigma}^\dagger$ are the annihilation and creation operators for spin σ at the lattice site i for the two orbital states which give rise to a two fold degenerate band; T_{ij} is the hopping integral, B is the applied magnetic field; μ_B is the Bohr magneton, μ is the chemical potential; and $n_{i\sigma} = a_{i\sigma}^\dagger a_{i\sigma}$, $m_{i\sigma} = d_{i\sigma}^\dagger d_{i\sigma}$. This model is based on the assumption that the interatomic interactions are unimportant in comparison to the intraatomic interactions. For simplicity the intraatomic Coulomb interaction I between electrons in the same band or in different bands is assumed to be the same. The hopping integral corresponding to hopping of the electrons from one band to another band has been considered small and is neglected in comparison to that corresponding

of electrons in the same band. The hopping integral for i to the band is required to be the same. We refer to the reader to reference (1) for detailed justification of the approximation and assumptions contained in the Hamiltonian (1).

The conditions for the existence of ferromagnetism are obtained from the condition that the onset of the ferromagnetic occurs when the paramagnetic susceptibility diverges. The paramagnetic susceptibility is given by

$$\chi = \frac{1}{k_B T} \langle M^2 \rangle - \langle M \rangle^2 / N \quad (2)$$

where $M = \sum_i (S_i^x + S_i^y)$ is the average number of electrons per site for spin \uparrow . We obtain χ from the knowledge of Fourier transforms $\langle \hat{p}^2 \rangle$ and $\langle \hat{p}^4 \rangle$ of one particle Green's functions $G_{ij}^{\uparrow\downarrow}(\omega) = \langle G_{ij}^{\uparrow\downarrow}(\omega) \rangle$ and $\tilde{G}_{ij}^{\uparrow\downarrow}(\omega) = \langle \tilde{G}_{ij}^{\uparrow\downarrow}(\omega) \rangle$ respectively. Since the Hamiltonian (1) is symmetrical in S_i^x and S_i^y we have $G_{ij}^{\uparrow\downarrow}(\omega) = \tilde{G}_{ij}^{\uparrow\downarrow}(\omega)$. And since the poles of these Green's functions give the quasi-particle bands corresponding to the degenerate orbital states, the degeneracy of the bands cannot be removed. In what follows we restrict our analysis to para or ferromagnetic states, so that we take $\langle M_{\uparrow} \rangle = \langle M_{\downarrow} \rangle$ and $\langle M_{\uparrow} \rangle = \langle M_{\downarrow} \rangle$ for all i .

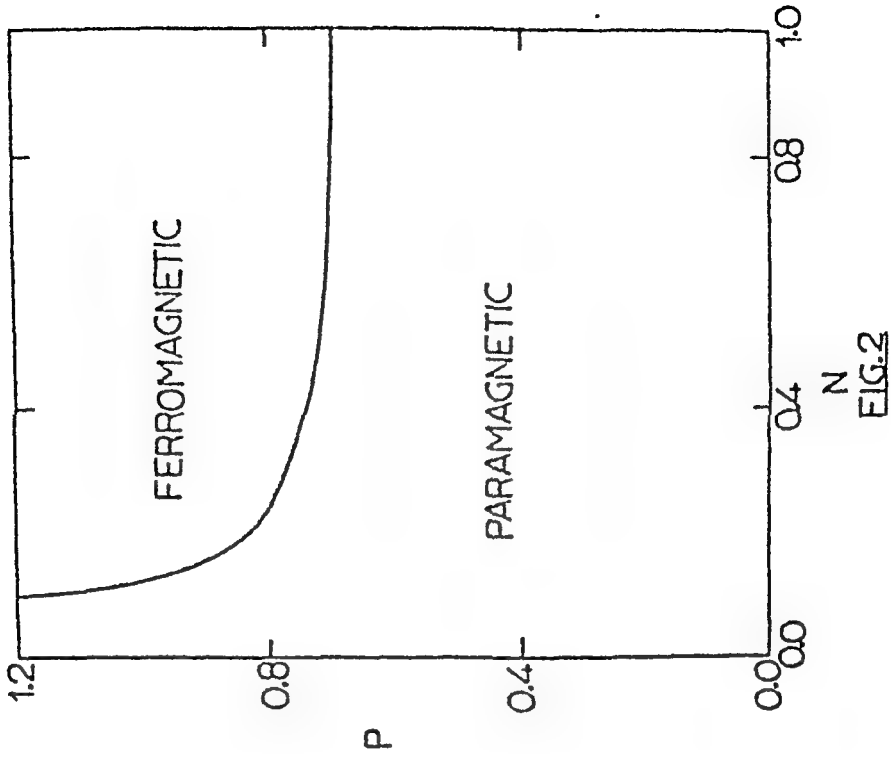
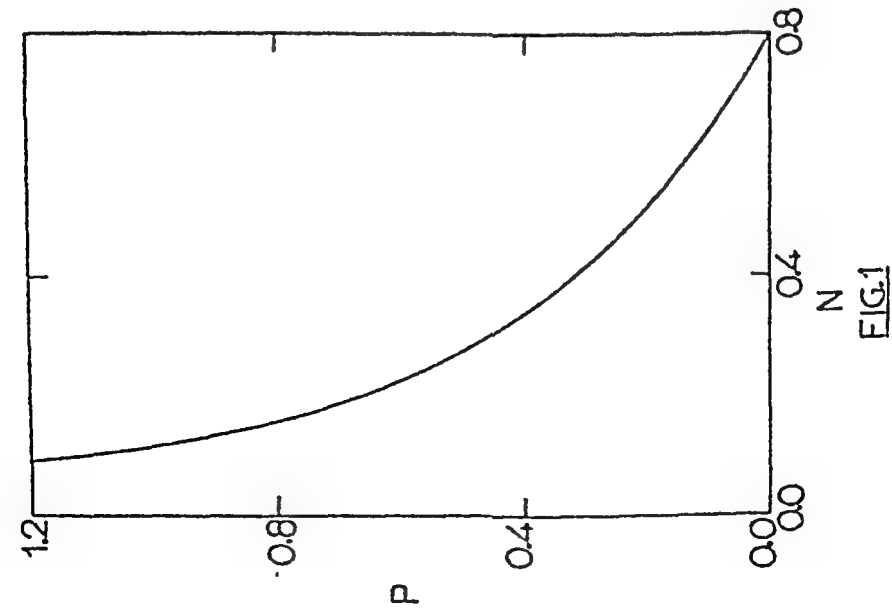
The Green's functions $G_{ij}^{\uparrow\downarrow}(\omega)$ is obtained by writing down its equation of motion. This equation of motion contains higher order Green's function involving four operators. When these higher order Green's functions are decoupled into the lower order Green's functions within the Hartree-Fock approximation, we get the usual condition for the ferromagnetism

$$(I + V) \rho(\mu - \frac{3I - V}{4} N) > 1,$$

where $N = N_+ + N_-$ is the total number of electrons per atom and $\rho(\omega)$ is the density of states per atom for the band

$$(T_1 = \frac{1}{N} \sum_{\vec{R}} \epsilon_{\vec{R}} \hat{K}^2 (\vec{R}_1 - \vec{R}_2)).$$

We study the effect of correlations by writing the equations of motion of the higher order Green's functions appearing in the equation of motion of $G_{ij}^{(n)}(\omega)$. The equations of motion contain still higher order Green's functions involving six operators plus the four operators Green's functions. We truncate the hierarchy of equations of motion by neglecting the six operators Green's functions in a manner similar to that of Hubbard⁴ assuming that the correlation between electrons at the same lattice site are stronger than that at different lattice sites. The poles of the Green's function $\tilde{G}_K(\omega)$, evaluated within the above approximations, give four quasiparticle bands. It is a tedious job to obtain the conditions for ferromagnetism from this Green's function. However the problem can easily be tackled if we take $I = \infty$. In this case we get only two bands which for nonzero intraatomic exchange interaction V are always separated by an energy gap. The total number of states in both the bands together is found to be equal to one. Thus at absolute zero for $N=1$ system behaves as a nonmetal since both the bands are completely filled. For $N < 1$, system behaves as a nonmetal when the lower band is completely filled. The density of states in the bands is a function of $P = V/\Delta$ and N , where Δ is the bandwidth of the band ϵ_K^2 . For square



density of states $\rho(\omega) = \frac{1}{\Delta}$ if $-\frac{\Delta}{2} < \omega < \frac{\Delta}{2}$ and zero otherwise. We have plotted in Fig.1 a P versus H curve for which lower band is completely filled and hence the system behaves as a nonmetal. On both sides of the curve, the system behaves as a metal: By evaluating the paramagnetic susceptibility χ_{PM} (Eq.(2)) the conditions for the existence of ferromagnetism are obtained and the results are plotted in Fig.2. This curve shows that the low density of electrons is less favorable to ferromagnetism than the higher density of electrons. A minimum value of P is required to get the ferromagnetism.

We are grateful to the Council of Scientific and Industrial Research, New Delhi for financial help.

REFERENCES

1. J.H. Van Vleck; Rev. Mod. Phys. 25, 220 (1953).
2. L.M. Roth; Phys. Rev. 149, 306 (1966).
3. D.N. Zubarev; Usp. Fiz. Nauk 71, 71 (1960) [Translation: Soviet Phys. Usp. 3, 320 (1960)].
4. J. Hubbard, Proc. Roy. Soc. A276, 238 (1963).

SCATTERING OF A CHARGED PARTICLE BY ELECTRON LIQUID

A.F. Pathak
Department of Physics
Indian Institute of Technology, Kanpur-16 (U.P.)

I. INTRODUCTION

Recently¹⁻³, lot of attention has been devoted towards the improvements over random phase approximation (RPA) and Hubbard approximation calculations of Langer and Vosko⁴ for charge distribution around a fixed charge in an electron liquid. The main difficulty with RPA and Hubbard approximation is that the pair distribution function, which is a positive definite quantity, becomes negative for very small values of r . A modification of original Hubbard formula has been shown⁵ to produce some improvements over the results for $g(r)$. We have used this modification to calculate the screening density around a fixed charged impurity and compared it with that obtained earlier by Langer and Vosko using original Hubbard approximation.

II. FORMULAE AND RESULTS

The number density fluctuation due to a static impurity of unit charge, in linear response theory, is given by⁶

$$\langle \rho(q,0) \rangle = 1 - 1/\epsilon(q,0) \quad (1)$$

where the static dielectric function $\epsilon(q,0)$, in Hubbard approximation is given by⁴

$$\epsilon(q,0) = [1 + F(q)/[1 - f(q)F(q)]] \quad (2)$$

with

$$f(q) = \frac{1}{2} \frac{q^2}{q^2 + \eta^2} \text{ and } F(q) = \frac{q_{FT}^2}{q^2} \left[\frac{1}{2} + \frac{4q_F^2 - q^2}{8q_F^2} \ln \left| \frac{1 + 2q_F}{2 - 2q_F} \right| \right] \quad (3)$$

Here q_F is radius of Fermi sphere and q_{FT} is Thomas Fermi vector. The parameter η is taken q_F in the original Hubbard approximation and in a modification suggested by Hubbard himself η^2 is taken as $q_F^2 + Q_s^2$, Q_s being screening parameter. On the other hand Brueckner⁵ has found

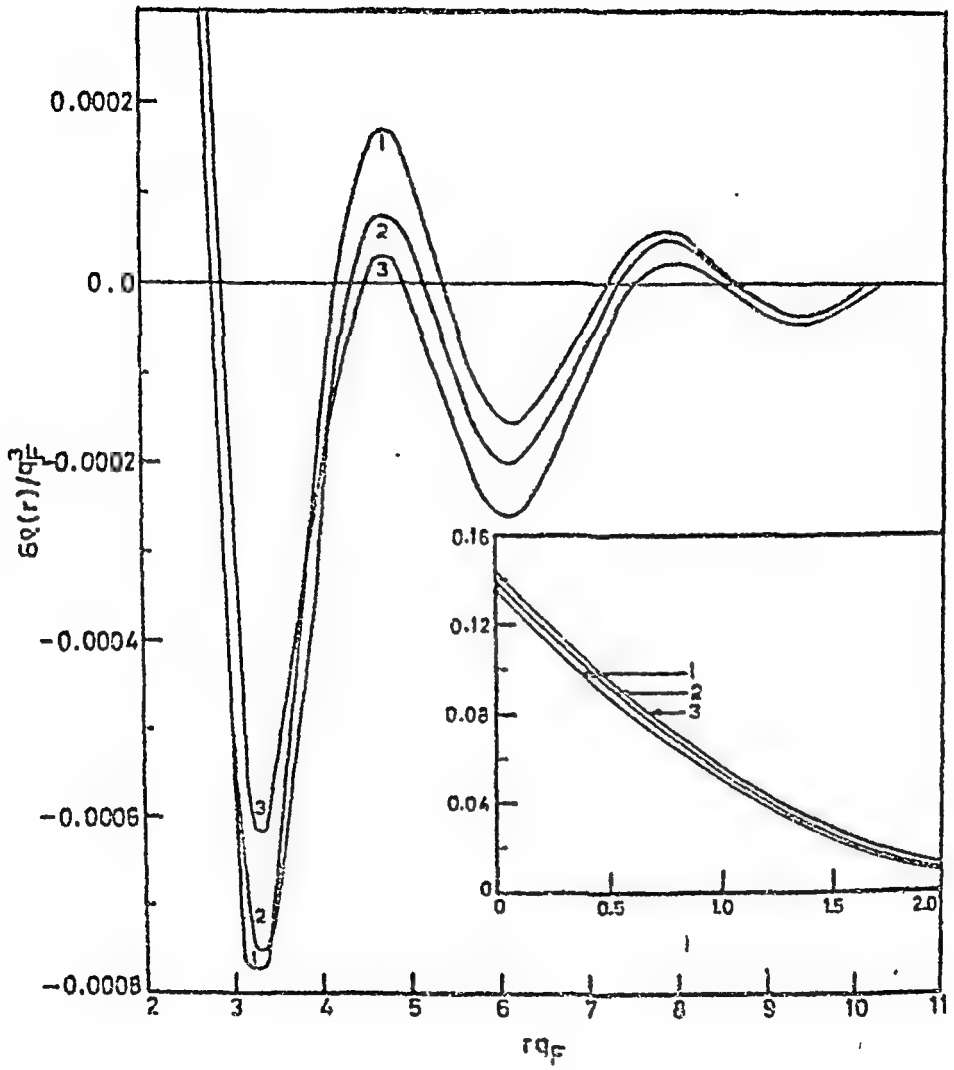


Fig-1

some improvement in pair distribution function by using $\eta = q_p/2$ and $\eta = q_p/4$. We have used these values to calculate the screening density at a distance r from a charged impurity in the electron liquid. $\delta\rho(r)$, given by⁶

$$\delta\rho(r) = \frac{1}{2\pi^2 r} \int_0^\infty dq \, q \, S(\eta(qr)) \left(1 - \frac{1}{\epsilon(q,0)}\right). \quad (4)$$

The integration has been numerically done and results for various values of η given in Tables I and II. A comparison with the results of Langer and Vosko has been made in Figure 1 for $\eta = 3$.

It is to be noted that the differences of present results with original Hubbard approximation are small compared with those obtained by Singwi et al.^{1,2} and by the author³ with different expressions for dielectric function and could not be shown on the scale of Figure 1.

REFERENCES

1. K.S. Singwi and M.P. Tosi, Phys. Rev. **181**, 784 (1969)
2. K.S. Singwi, A. Siolander, M.P. Tosi and E.H. Land, Phys. Rev. **B1**, 1044 (1970).
3. A.F. Pathak, Phys. Rev. (to be published).
4. J.S. Langer and S.H. Vosko, J. Phys. Chem. Solids **12**, 196 (1960).
5. P. Bruuers, Phys. Stat. Solidi **19**, 867 (1967)
6. See, for instance, D. Pines and P. Nozières, The Theory of Quantum Liquids

Table I. The values of $\delta\rho(r)/q_p^3$ for various values of r_s corresponding to $\eta = q_p/2$ (in units of 10^{-3})

r_{sp}	$r_s=2$	$r_s=3$	$r_s=4$	$r_s=5$	$r_s=6$
0.0	100.7	159.6	175.0	208.1	239.3
0.1	94.13	129.7	161.9	191.7	219.7
0.4	74.34	100.5	123.4	144.1	162.1
0.7	56.65	74.8	90.16	105.6	115.5
1.0	41.44	55.21	62.68	70.58	77.33
1.3	28.91	35.83	40.99	44.99	48.18
1.6	19.06	22.51	24.73	26.18	27.12
1.9	11.72	12.68	13.26	13.21	12.91
2.2	6.585	63.83	5.78	5.01	4.167
2.5	3.259	2.397	1.405	0.418	0.521
2.8	1.319	0.269	0.737	1.639	2.433

Table I contd..

3.1	0.350	-0.607	-1.428	-2.106	-2.660
3.4	-0.110	-0.744	-1.510	-1.734	-2.048
3.7	-0.049	-0.536	-0.891	-1.067	-1.191
4.0	0.029	-0.247	-0.388	-0.443	-0.445
4.3	0.104	-0.027	-0.055	-0.027	0.030
4.6	0.123	0.072	0.095	0.150	0.217
4.9	0.083	0.059	0.089	0.135	0.184
5.2	0.006	-0.019	-0.007	0.015	0.036
5.5	-0.076	-0.134	-0.123	-0.126	-0.129
5.8	-0.135	-0.183	-0.207	-0.226	-0.244
6.1	-0.157	-0.205	-0.233	-0.256	-0.276
6.4	-0.144	-0.179	-0.201	-0.213	-0.232
6.7	-0.104	-0.122	-0.130	-0.135	-0.138
7.0	-0.055	-0.053	-0.047	-0.040	-0.034
7.3	-0.011	0.005	0.022	0.038	0.051
7.6	0.018	0.041	0.062	0.008	0.095
7.9	0.027	0.049	0.069	0.084	0.096
8.2	0.019	0.036	0.048	0.057	0.064
8.5	0.002	0.009	0.014	0.015	0.016
8.8	-0.016	-0.017	-0.020	-0.025	-0.029
9.1	-0.028	-0.035	-0.043	-0.050	-0.057
9.4	-0.031	-0.039	-0.043	-0.055	-0.062
9.7	-0.025	-0.031	-0.037	-0.042	-0.046
10.0	-0.013	-0.015	-0.016	-0.016	-0.018

Table II. Values of $\delta\rho(r)/q_p^3$ for various values of r_s corresponding to $\eta = q_p/4$ (in units of 10^{-3})

ηq_p	$r_s=2$	$r_s=3$	$r_s=4$	$r_s=5$	$r_s=6$
0.0	102.4	142.1	178.3	212.1	244.0
0.1	95.84	132.2	165.2	195.7	224.4
0.4	76.00	102.9	126.6	147.9	167.5
0.7	58.20	77.09	93.1	107.1	119.6
1.0	42.84	55.26	65.28	75.68	80.87
1.3	30.14	37.59	43.19	47.58	51.10
1.6	20.11	23.96	26.51	28.23	29.41
1.9	12.58	14.03	14.63	14.76	14.60
2.2	7.265	7.254	6.784	6.103	5.327
2.5	3.778	3.025	2.094	1.137	0.210
2.8	1.693	0.696	-0.299	-1.213	-2.029
3.1	0.615	-0.337	-1.180	-1.892	-2.485
3.4	0.165	-0.592	-1.197	-1.665	-2.022
3.7	0.057	-0.468	-0.837	-1.087	-1.250
4.0	0.034	-0.236	-0.042	-0.513	-0.546
4.3	0.122	-0.052	-0.117	-0.119	-0.086
4.6	0.116	0.025	0.017	0.050	0.101
4.9	0.058	0.001	0.006	0.036	0.075
5.2	-0.030	-0.084	-0.089	-0.079	-0.064
5.5	-0.117	-0.179	-0.203	-0.213	-0.220
5.8	-0.179	-0.246	-0.281	-0.305	-0.325
6.1	-0.202	-0.264	-0.300	-0.326	-0.348
6.4	-0.187	-0.234	-0.260	-0.279	-0.293
6.7	-0.144	-0.170	-0.181	-0.186	-0.190

7.0	-0.091	-0.095	-0.083	-0.032	-0.075
7.3	-0.043	-0.029	-0.012	-0.004	0.018
7.6	-0.010	0.012	0.034	0.054	0.070
7.9	0.003	0.026	0.046	0.053	0.077
8.2	-0.001	0.016	0.030	0.041	0.049
8.5	-0.015	-0.006	-0.001	0.002	0.004
8.8	-0.031	-0.030	-0.032	-0.035	-0.039
9.1	-0.040	-0.046	-0.052	-0.059	-0.065
9.4	-0.041	-0.049	-0.056	-0.063	-0.069
9.7	-0.034	-0.039	-0.043	-0.046	-0.052
10.0	-0.020	-0.021	-0.022	-0.023	-0.023

DISCUSSION

T.V. Ramakrishnan

Very near the impurity the response of the electron gas is not linear because perturbation, is very strong. What does it mean to compare various theories in this region ?

K.N. Pathak

Could you tell which approximation is better for calculating the polarization of charge around an impurity in an electron gas?

A.P. Pathak

Out of two modifications presented here, the later (corresponding to $\eta = q_F/4$) is better, because the charge density at origin is nearer to the results of Singwi et al (Phys. Rev. B1, 1044) and that obtained by using Kleinman-Langreth forms of static dielectric functions (A.P. Pathak, Phys. Rev. 15 Sept. 1970). since later forms include interactions more correctly. However, Physical properties are to be calculated and different approximations to be tested.

THE RELATION BETWEEN KONDO EFFECT AND HARTREE FOCK THEORY

C. Manohar

Rhabha Atomic Research Centre, Chemistry Division, Trombay, Bombay 85

The attempts to understand the experiments on dilute alloys can be classified in to two types 1. Hartree - Fock theory (H - F) 2. Theory of correlations. The H - F has been extensively used by Friedel and his group to predict charge density, spin density, residual resistivity etc., and in many cases a quantitative agreement is found [1]. However this theory does not explain the temperature dependence of resistivity or susceptibility. On the other hand the theories of correlations explain the temperature dependence of resistivity and susceptibility atleast qualitatively but completely ignore the fact that H - F did have success in some cases [2]. In the present work an attempt is made to reconcile the two approaches by developing the theory of correlations in close resemblance with H - F. We use the Anderson Hamiltonian [3].

$$H = \sum_{kr} \epsilon_{kr} a_{kr}^{\dagger} a_{kr} + \sum_r \epsilon_{dr} a_{dr}^{\dagger} a_{dr} + V \sum_{kr} (a_{kr}^{\dagger} a_{dr} + a_{dr}^{\dagger} a_{kr}) + U n_{d\uparrow} n_{d\downarrow} \quad (1)$$

Now we try to construct a single particle theory by adding and subtracting a term

$$H = \sum_{kr} \epsilon_{kr} a_{kr}^{\dagger} a_{kr} + \sum_r \epsilon_{dr} a_{dr}^{\dagger} a_{dr} + V \sum_{kr} (a_{kr}^{\dagger} a_{dr} + a_{dr}^{\dagger} a_{kr}) + U_{eff} \sum_r \langle n_{dr} \rangle n_{d-r} + \left[U n_{d\uparrow} n_{d\downarrow} - U_{eff} \sum_r \langle n_{dr} \rangle n_{d-r} \right] \quad (2)$$

The idea is to define U_{eff} suitably so that effect of last two term in the square brackets can be neglected. H - P corresponds to putting $U_{\text{eff}} = U$. By doing this one classifies the impurities in to two types magnetic and non-magnetic at all temperatures. But this classification turns out to be superficial in view of the experiments [4]. The experiments on transition metal impurities seem to show that at sufficiently low temperatures all the magnetic impurities become non-magnetic. This suggests that the U_{eff} should be so defined that at $T = 0$ the impurity is always non-magnetic.

In fact such a U_{eff} has been defined by Schrieffer and Mattis [5].

Their result has been expressed in terms of Green functions.

We define

$$G_d^T(t) = 1/T \sum_{\omega} a_d e^{i\omega t}$$

The Fourier transform

) of G

form

$$G_d^T(\omega)$$

\sum

Where \sum

$N(c)$ be

- Matti

$$\text{where } U_{eff} = \lim_{\omega \rightarrow 0} \frac{U}{1 + U \phi(\omega)} \quad (6)$$

$$\text{with } \phi(\omega) \Big|_{\omega=0} = \frac{1}{2\pi} \int d\omega_1 G_d(\omega + \omega_1) G_d(-\omega_1) \Big|_{\omega=0} = \frac{1}{4\epsilon_d} \tan^{-1} \frac{\epsilon_d}{T} \quad (7)$$

Schrieffer and Mattis have proved that U_{eff} defined by eqs.(6) and (7) is so small that there will be no magnetic moment on the impurity even if $U \rightarrow \infty$. This is consistent with the experiments. There is one further interesting point. If we define the conduction electron Green function

$$G_{kh'}^{\sigma}(t) = (-i) \langle 0 | T \{ \alpha_k(t) \alpha_{k'}^{\dagger}(0) \} | 0 \rangle$$

Then its Fourier transform $G_{kh'}^{\sigma}(\omega)$ satisfies

$$G_{kh'}^{\sigma}(\omega) = \frac{\delta_{kh'}}{\omega - \epsilon_{kh'}} + \frac{V}{\omega - \epsilon_{kh'}} \left[G_d^{\sigma}(\omega) \right] \frac{V}{\omega - \epsilon_{kh'}} \quad (8)$$

From eq.(8) it follows that the t -matrix for conduction electron scattering is

$$t(\omega) = G_d^{\sigma}(\omega) \quad (9)$$

Therefore the impurity contribution to resistance at zero temperature is

$$\Delta \rho \propto - \Im \lim_{\omega \rightarrow 0} t(\omega + i\delta) \Big|_{\omega=0} = \frac{T}{(\epsilon_d + 2)^2 T^2} \quad (10)$$

In eq.10, \sum can be neglected because U_{eff} is small. Now we should expect from eq.10 that the residual resistivities of transition metal impurities in a host should have a Lorentzian form with peak in the middle of the series. This is well known in case of Al host and has recently been confirmed in Cu host alloys [4]. Therefore

this definition of U_{eff} seems promising. The next thing is to generalise the U_{eff} defined to non-zero temperatures and see if it can produce a magnetic moment at higher temperatures as has been observed experimentally. Eqs.(4)-(7) can be generalised to higher temperatures using the prescriptions given by Abrikosov et al [6]. Only modification will be in eq.7. which becomes

$$\phi(\omega) = \frac{1}{2\pi} \int_{-\infty}^{\infty} d\omega_1 G_R(\omega - \omega_1) [G_R(\omega_1) - G_A(\omega_1)] \tanh \frac{\omega_1}{2T} \quad (11)$$

where

$$G_R(\omega) = \frac{1}{\omega - \epsilon_d + iT} = [G_A(\omega)]^* \quad (12)$$

Eq.(11) can be integrated exactly giving

$$\phi(T) = \lim_{\omega \rightarrow 0} \phi(\omega) = \frac{1}{\epsilon_d \pi} \Im_m \Psi \left(\frac{1}{2} + \frac{T}{2\pi T} + i \frac{\epsilon_d}{2\pi T} \right) \quad (13)$$

where $\Psi(z)$ is the digamma function. At $T=0$, This coincides with Schrieffer-Kattis result eq.7. If T is small then for temperatures $T > T_c/2\pi$

$$\phi(T) \approx \frac{1}{2\epsilon_d} \tanh \frac{\epsilon_d}{2T} \quad (14)$$

For temperatures $T > \frac{\epsilon_d}{2}$, ϕ becomes small and from eq.6 we will have

$$U_{\text{eff}} \approx U \quad (15)$$

i.e. we retrieve H - F !! . This suggests that one can indeed classify the impurities as magnetic and non-magnetic at higher

temperatures. Only in this sense ϵ_A acts as the Kondo Temperature T_K . This looks attractive because one expects ϵ_A to be small for transition metal impurities in the middle of the series and a similar trend should be shown by T_K -as is confirmed by experiments [7].

References:

1. Articles by A.Blandin and T.Moriya in "Theory of Magnetism in transition Metals", Academic Press 1967.
2. D.R.Hamann., Phys.Rev.186, 549 (1969) and references cited therein.
3. P.W.Andersen., Phys.Rev.124, 41 (1961)
4. A.J.Esger., Solid State Phys.23, Ed.Seitz & Turnbull.
5. J.R.Schrieffer and D.C.Mattis, Phys.Rev.140, A1412 (1965)
6. A.A.Abrikosov et al., Methods of Quantum field Theory in Statistical Physics, Prentice-Hall (1963)
7. M.D.Daybell and W.A.Steyart., Rev.Mod.Phys.40, 380 (1968)

EMISSION OF ELECTRONS AND POSITRONS IN CRYSTALS

A.F. Fatkh and M. Jussouff

Department of Physics, Indian Institute of Technology, Kanpur-16 (U.P.)

I. INTRODUCTION

The classical theory of channeling and blocking effects proposed by Lindhard¹ explains satisfactorily the heavy ion channeling experiments². For light particles the quantum effects have been shown³ to be of importance and contrary to classical orbital picture the process has been shown⁴ to be dependent on the incident particle mass. In this paper we have used one phonon Debye model to calculate the electron and positron emission intensity pattern due to an emitter inside the crystal. The temperature and the energy dependence has been shown.

II. FORMULATION AND THE SCALAR WAVE EQUATION FOR PARTICLES

We consider emission of particles from a source embedded in a perfect crystal, initially in a low lying state $\{n\}$ at low temperature. Leaving aside the actual mechanism of emission, the propagation of the particle through the crystal and its subsequent escape from the crystal is considered. The Hamiltonian of the system is $H = H_0 + H_p + V$, H_0 being the crystal Hamiltonian, H_p the free particle Hamiltonian and V the interaction between the particle and the crystal. Using expansion $\Psi(x, \{S_p\}) = \sum_n |n\rangle \phi_n(x)$ in the Schrodinger E.N. $H\Psi = E\Psi$, we get⁵

$$\left[-\frac{\hbar^2 \nabla^2}{2m_p} + \langle n|V|n\rangle - E_p \right] \phi_n(x) = - \sum_{m \neq n} \langle n|V|m\rangle \phi_m(x) \quad (1)$$

where E_p is the energy with which the particle of mass m_p is emitted, x is the position of the particle and R_c is the actual position of n^{th} nucleus in the crystal. The right hand side of (1) gives renormalization of the particle wave function. The intensity at a point x outside the crystal due to emitter at R_c inside the crystal is obtained by calculating the intensity at R_c due to emitter at x , using the

reciprocity relation $\Phi_n(\underline{r}, \underline{r}_g) = \Phi_n(\underline{r}_g, \underline{r})$ which holds if the reflections at the crystal surface are neglected.

The problem of particle penetration has been treated⁵, using the expansions

$$\Phi_n(\underline{r}) = \sum_{\underline{k}} U_{\underline{k}}(n) e^{i(\underline{k}_M + \underline{k}_g) \cdot \underline{r}} \quad \text{and} \quad V_{nn}(\underline{r}) = \sum_{\underline{k}} V_{\underline{k}}(n) e^{i\underline{k}_g \cdot \underline{r}} \quad (2)$$

we can write (1) as (in first Born approximation for $\Phi_n(\underline{r})$)

$$(2\delta + \mathcal{S}_{\underline{g}}) U_{\underline{k}}(n) + \sum_{\underline{g}'} \Psi_{\underline{k}-\underline{g}'} U_{\underline{g}'}(n) = 0 \quad (3)$$

where $(\hbar^2/2m_0)(\underline{k}_g^2 + 2\underline{k}_g \cdot \underline{k}_M) = \mathcal{S}_{\underline{g}} E_p$,

$$2\delta E_p = (\hbar^2/2m_0)k_M^2 - E_p; \quad \Psi_{\underline{k}-\underline{g}'} = [V_{\underline{k}-\underline{g}'} + C_{\underline{k}\underline{g}}(n)]/E_p \quad (4)$$

$$\text{and } C_{\underline{k}\underline{g}}(n) = -(2m_0/v^2\hbar^2) \int d\underline{r} \int d\underline{r}' \exp[-i(\underline{k}_g + \underline{k}_n) \cdot \underline{r} + i(\underline{k}_g + \underline{k}_n) \cdot \underline{r}'] \\ \times \sum_{n' \neq n} V_{nn'}(\underline{r}) V_{n'n}(\underline{r}') \exp[i\underline{k}_n(\underline{r} - \underline{r}')] / 4\pi |\underline{r} - \underline{r}'| \quad (5)$$

with $k_g^2 = 2v_0/\hbar^2$ and k_g is approximately equal to k_n with a small imaginary part⁵. Using the proper boundary conditions on the wave

function at the crystal surface, we get the intensity in two beam theory³ (assuming Ψ_n'' to be small compared to Ψ_n')

$$|\Phi_n(t)|^2 = x^2 \exp[-(1 - \frac{E_g}{\sqrt{1+y^2}})t/\xi_0''] + (1-x)^2 \exp[-(1 + \frac{E_g}{\sqrt{1+y^2}})t/\xi_0''] \\ + 2x(1-x) \exp(-t/\xi_0'') \cos[\sqrt{1+y^2} t/\xi_0'] \quad (6)$$

where $x = \frac{1}{2} [1 + (y-1)/\sqrt{1+y^2}]$

$$y = \mathcal{S}_{\underline{g}}/2\Psi_{\underline{g}}', \quad (\text{Re } \Psi_{\underline{g}} = \Psi_{\underline{g}}' = [V_{\underline{g}} + \text{Re } C_{\underline{g}0}]/E_p) \\ E_g = \Psi_{\underline{g}}''/\Psi_{\underline{g}}'', \quad (\text{Im } \Psi_{\underline{g}} = \Psi_{\underline{g}}'' = \text{Im } C_{\underline{g}0}/E_p) \\ \xi_0' = (k_0 \Psi_{\underline{g}}')^{-1}, \quad \xi_0'' = -(k_0 \Psi_{\underline{g}}'')^{-1} \quad (7)$$

and t is the distance of the emitting atom from the crystal surface.

The emission pattern is conveniently described by plotting $|\Phi_n(t)|^2$ against y .

We found⁵ that in one phonon Debye model using screened Coulomb potential (for which Fourier Transforms $V_h = \frac{4\pi z_1 z_2 e^2}{(\hbar^2 + k_g^2)} \rho e^W$

27 being the usual Debye Waller factor) as interaction, in C_{ho} in

low temperature limit is given by

$$\text{Im } C_{ho} = - \frac{\pi P(z_1 z_2 e^2)^2 \bar{e}^{-2K_k^2} (2m_0)^{1/2}}{M c E_p^{1/2} (\lambda^2 + k_k^2)} \left[f_0 + 2f_1(T/\theta_D)(1 - \bar{e}^{-\theta_D/T}) \right. \\ \left. - \Lambda \left(\tan^{-1} \frac{f_2}{\Lambda} + \text{Ci} \left(\frac{\Lambda k_k c}{k_B T} \right) \sin \left(\frac{\Lambda k_k c}{k_B T} \right) - \text{Si} \left(\frac{\Lambda k_k c}{k_B T} \right) \cos \left(\frac{\Lambda k_k c}{k_B T} \right) \right] \quad (8)$$

Under the same approximations, we get⁶

$$\text{Re } C_{ho} = - \frac{\pi P(z_1 z_2 e^2)^2 \bar{e}^{-2K_k^2}}{M c E_p (\lambda^2 + k_k^2)} \left[\frac{1}{2} f_0^2 \left\{ 1 - \frac{\Lambda^2}{k_k^2} \ln \left(1 + \frac{k_k^2}{\Lambda^2} \right) \right\} + 2 f_1^2 \left\{ \left(\frac{T}{\theta_D} \right)^2 (1 - \bar{e}^{-\theta_D/T}) \right. \right. \\ \left. \left. - \frac{T}{\theta_D} \bar{e}^{-\theta_D/T} \right\} + \frac{1}{2} k_k^2 \ln \left(1 + \frac{k_k^2}{\Lambda^2} \right) + 2(\Lambda^2 - k_k^2) \left\{ \text{Ci} \left(\frac{\Lambda k_k c}{k_B T} \right) \cos \left(\frac{\Lambda k_k c}{k_B T} \right) + \text{Si} \left(\frac{\Lambda k_k c}{k_B T} \right) \sin \left(\frac{\Lambda k_k c}{k_B T} \right) \right\} \right] \quad (9)$$

Numerical evaluation with $\Lambda = 4.2 \times 10^{10} \text{ cm}^{-1}$, $k_k = 2 \times 10^{10} \text{ cm}^{-1}$, $|V_h/E_p| = 10^{-4}$ (the values taken by De Wames et al³) corresponding to copper crystal, shows that $|\text{Re } C_{ho}/V_h| \sim 10^{-5}$ and $|\text{Im } C_{ho}/V_h| \sim 10^{-5}$. Thus the attenuation is small compared to that used by De Wames et al³ (~ 0.1).

Another feature of present formalism is that $\text{Re } C_{ho}$ and $\text{Im } C_{ho}$ do not depend on the sign of the charge of the particle. However V_h is negative for electrons and positive for positrons and from Eqn. (7),

$$y \approx \frac{\sin 2\theta_B}{(V_h + \text{Re } C_{ho})/E_p} (\theta_B - \theta) \quad (10)$$

Thus $|y|$ for $\theta \rightarrow 0$ is greater for positrons and smaller for electrons.

Hence the angular width of the pattern for electrons should be smaller than that for positrons (see figs. of ref. 3).

III. CONCLUSIONS

We note that the magnitudes of $\text{Re } C_{ho}$ and $\text{Im } C_{ho}$ are small compared to V_h implying that the renormalization of the wave function does not change the intensity pattern appreciably and at higher energies the inelastic processes such as phonon emission and absorption do not participate very significantly in channeling and blocking of electrons and positrons. At low energies $\text{Re } C_{ho}$ starts increasing as $1/E_p$ and

then the correction $\text{Re } C_{ho}$ to V_h becomes significant.

We see that periodic potential field $U(r)$ of classical model used by DeTames et al^{3,4} in one particle approximation of the many particle Schrodinger Eqn. is replaced here by initial state expectation value. The attenuation is found to be small compared to what is usually taken and has dependence $(m_0/E_p)^{1/2}$. Thus attenuation will be larger at lower energy of the incident particle. Finally we see from Eqn. (10) that we get a difference in width of electron and positron emission patterns even in the two beam theory. The angular width of electrons emission pattern being small compared to that of positrons.

REFERENCES

1. J. Lindhard, Kgl. Danske Videnskab. Selskab. Mat. Fys. Medd., 34, No.14 (1965)
2. J.A. Davies, J. Denhartog and J.L. Whitton, Phys. Rev. 165, 345 (1968), see also Can J. Phys. 46, 575 (1968) and the references given therein.
3. T.E. DeTames and W.P. Hall, Acta Cryst. A24, 206 (1968).
4. T.E. DeTames, W.P. Hall and G.W. Lehman, Phys. Rev. 174, 392 (1968).
5. A.F. Pathak and M. Yussouff, Phys. Rev. (To be published, in 315 Dec. 1970 issue).
6. Details of the calculations will be published elsewhere.

DISCUSSION

T.V. Ramakrishnan

The charged particle moves with a high velocity.
Is its interaction with other charges screened?

M. Yussouff

The potential due to lattice ions at any point

has the screened Coulomb form which we use in our calculation.

Satya Prakash

What is the explicit form of the potential?

M. Yussouff

It is the usual screened Coulomb potential of the form $e^{-\lambda r}/r$.

CORRECTIONS TO THE GROUND STATE ENERGIES OF SHALLOW ACCEPTORS IN Ge

S. Balasubramanian

Dept. of Physics, Madurai University, Madurai-2.

I. INTRODUCTION

It is known (1) that the effective mass formalism does not adequately explain the ground states of shallow impurities in Ge and Si. The Coulomb potential, modified by the static dielectric constant of the host crystal, used in the effective mass equations is not valid for the immediate vicinity of the impurity atom.

The correct potential would be the difference potential given by

$$V(\vec{r}) = \pm (V_2(\vec{r}) - V_1(\vec{r})) \quad \dots\dots (1)$$

where $V_1(\vec{r})$ is the potential due to the neutral host crystal atom and $V_2(\vec{r})$ is that due to the appropriate ion, the positive sign corresponding to the hole and the negative sign corresponding to the electron. Since it is difficult to construct such a difference potential valid throughout the region of interest, one uses the coulomb potential mentioned above in the effective mass equations and then tries to find corrections to the effective mass formalism. We have reported in an earlier paper (2) the results of calculations of the corrections to the ground state energies of the donors P and As in Ge and Si. In the present work we give the results of the ground state energy corrections for the acceptors B, Al and Ga in Ge.

II. THE DIFFERENCE POTENTIAL

The difference potential given in equation (1) is constructed using the available Hartree functions for free atoms and ions (3).

The Hartree potential at \vec{r}_1 (with the origin at the impurity) due

to an electron, whose orbital function is $\psi_j(\vec{r}_2)$ given by

$$W_j(\vec{r}_1) = \int \psi_j^*(\vec{r}_2) \frac{1}{|\vec{r}_1 - \vec{r}_2|} \psi_j(\vec{r}_2) d\vec{r}_2 \quad \dots (2)$$

Therefore, the potential at the point \vec{r}_1 due to all the N electrons in the atom or ion is given by

$$W(\vec{r}_1) = \sum_{j=1}^N W_j(\vec{r}_1) \quad \dots (3)$$

A computer program for the CDC-3600 has been written for constructing $W(\vec{r}_1)$. The difference potential seen by a hole is now given by

$$V(\vec{r}) = \left[\frac{Z_I}{r} - W_I(\vec{r}) \right] - \left[\frac{Z_A}{r} - W_A(\vec{r}) \right] \dots (4)$$

where Z_I and Z_A are the atomic numbers of the impurity nucleus and the host atom respectively. We average the potential given in (4) over the angles and designate it $V(r)$. The potential so constructed has the right behaviour as $r \rightarrow 0$, namely

$$V(r) \rightarrow (Z_I - Z_A)/r$$

$V(r)$ is also found to be sufficiently slowly varying with r in the region of interest so as to be an admissible potential in the effective mass formalism.

III. ENERGY CORRECTIONS

After constructing the difference potential, we treat $V(r) - V_{o.m.}$, where $V_{o.m.}$ is the coulomb potential mentioned earlier, as a perturbation on the effective mass Hamiltonian and obtain the first order energy corrections using the familiar formula

$$E = \frac{\int F_o^*(\vec{r}) [V(r) - V_{o.m.}(r)] F_o(\vec{r}) d\tau}{\int |F_o(\vec{r})|^2 d\tau} \quad \dots (5)$$

where in the numerator the upper limit of integration w.r.t. r is R (the central cell radius). We have employed one of the envelope functions obtained by Kohn and Scheshter⁽⁴⁾ and that obtained by Suzuki, Okasaki and Hasegawa⁽⁵⁾ as zero order functions. The

energy corrections are computed with the aid of the CDC-3600 computer for various cell radii. The results are given in Table I, which also contains Casavinsky's results.⁽⁶⁾ Table II shows the experimental ground state energies and the theoretical values obtained by different workers.

TABLE I

Central cell radius in a.u.	Energy Corrections in meV for the acceptors								
	B			Al			Ga		
	CSA ^(a)	Present work		CSA ^(a)	Present work		CSA ^(a)	Present work	
	K-S	K-S _(b)	S-O-H _(c)	K-S	K-S _(b)	S-O-H _(c)	K-S	K-S _(b)	S-O-H _(c)
1.160		+0.29	+0.46		+0.14	+0.22		+0.03	+0.04
1.392		+0.06	+0.06		-0.08	-0.13		-0.02	-0.03
1.624		-0.19	-0.32		-0.28	-0.45		-0.07	-0.11
1.856	-0.92	-0.44	-0.69	-0.64	-0.47	-0.75	-0.19	-0.12	-0.19
2.088	-1.0	-0.67	-1.07	-0.73	-0.65	-1.05	-0.24	-0.17	-0.26
2.320	-1.0	-0.91	-1.45	-0.73	-0.85	-1.34	-0.25	-0.21	-0.33
2.552	-1.2	-1.15	-1.84	-0.89	-1.03	-1.64	-0.38	-0.24	-0.39
2.784	-1.3	-1.39	-2.23	-0.98	-1.22	-1.95	-0.45	-0.28	-0.44
3.016		-1.64	-2.87		-1.43	-2.28		-0.31	-0.49
3.248		-1.91	-3.03		-1.64	-2.61		-0.35	-0.55
3.480		-2.18	-3.46		-1.87	-2.97		-0.39	-0.62

(a) Casavinsky's results using Kohn-Schechter wave function

(b) Present work using Kohn-Schechter wave function

(c) Present work using Suzuki-Okasaki-Hasegawa wave function

IV. DISCUSSION

From Table I we see that the energy corrections are sensitive to the choice of the cell radius. The amount by which the ground state energy is lowered increases with increase of the cell radius chosen. This contradicts Casavinsky's earlier results⁽⁶⁾ which he obtained by using the results of the Thomas Fermi statistical model of atoms in constructing the difference potential.

From tables I and II we see that for Ga the energy correction is too small to account for the discrepancy between experimental

results and those predicted by the effective mass theory. This result is similar to that of the donor P in Si and As in Ge reported earlier⁽²⁾. In these cases, the charge numbers of the impurity ions differ by unity from those of the host crystal atoms. For B, the correction seems to be almost of the right order and it is indeed fortunate here that the Hartree functions are more accurate than for atoms of higher charge numbers.

TABLE II

Energies (Theory) in mev			Energies (Expt.) in mev for impurities ^(d)		
K-S ^(a)	M-J ^(b)	S-O-H ^(c)	B	Al	Ga
-8.8	-9.4	-10.0	-10.5	-10.8	-11.0

- (a) Kohn-Schechter approximation⁽³⁾
 (b) Mendelson-James approximation⁽⁷⁾
 (c) Suzuki-Okasaki-Hasegawa approximation⁽⁴⁾
 (d) Optical experiments⁽⁸⁾

REFERENCES

1. W. Kohn, Solid State Physics, 5, 257, Edited by F. Seitz & Turnbull (Academic Press, N.Y. 1957)
2. S. Balasubramanian, Proc. of Nuclear Phys. & Solid State Phys. Symposium, BARC, 1969.
3. E. Clementi, Tables of Atomic Functions, Sup. IEM J. Res & Dev., 2 (1965)
4. W. Kohn & D. Schechter, Phys. Rev. 99, 1903 (1955)
5. K. Suzuki, M. Okasaki & H. Hasegawa, J. Phys. Soc. Japan, 19 930 (1964)
6. P. Csavinszky, J. Phys. Soc. Japan, 20, 2027 (1965)
7. K.S. Mendelson & H.M. James, J. Phys. Chem. Solids, 25, 729 (1964)
8. R.L. Jones & P. Fisher, J. Phys. Chem. Solids, 26, 1125 (1965)

Acknowledgements:- The author is grateful to the staff of TIFR, Bombay, where the computations were done. He is also thankful to Dr. K.S. Chandrasekaran for his interest in the work.

MINORITY CARRIER EQUIVALENT LIFETIME IN GERMANIUM AND GALLIUM ARSENIIDE

A.B. Bhattacharyya and T.N. Basavaraj
Indian Institute of Technology, New Delhi - 29

I. INTRODUCTION

In diffused semiconductor devices the minority carrier lifetime is assumed a few orders of magnitude lower than the normal value which can not be explained by Shockley-Read theory of recombination of holes and electrons through trapping centers. Because of the importance of minority carrier lifetime on device characterisation a few investigations have been made on the origin of low minority carrier lifetime in diffused devices. Jan and Al-Rafai⁽¹⁾ attributed the low value of lifetime to be due to the electrostatic field gradient in a diffused layer. Later it was shown by Ho and Cho⁽²⁾ that the mobility gradient of the minority carriers in an inhomogeneous semiconductor may also be a factor contributing to low lifetime. The present paper predicts the minority carrier equivalent lifetimes in Ge and GaAs. To make an analytical study possible empirical relations for the minority carrier mobilities in these semiconductors are employed.

II. THEORETICAL

The most general continuity equation for charge carriers in a semiconductor, to be solved to characterise junction devices is given by

$$D \frac{d^2 n}{dx^2} + \left(\frac{dD}{dx} + \mu E \right) \frac{dn}{dx} + \left(E \frac{d\mu}{dx} + \mu \frac{dE}{dx} - \frac{1}{\tau_n} \right) n = 0$$

where n is the density of charge carriers, x is the position coordinate, $E(x)$ is the built-in electrostatic field, $D(x)$ is the diffusion constant, $\mu(x)$ is the mobility, $\tau(x)$ is the normal lifetime of carriers. The mobility gradient equivalent lifetime t_{μ} and the field gradient equivalent lifetime t_E are defined as

$$1/t_{\mu} = E(x) d\mu/dx \quad (3) \quad 1/t_E = \mu(x) dE/dx \quad (4)$$

The values of t_{μ} and t_E depend on the profile of impurity atoms since $E(x)$ is given by the expression

$$E(x) = \frac{kT}{q} \frac{d}{dx} [\ln N(x)] \quad (5)$$

where $N(x)$ is the impurity concentration at x . They also depend on the semiconductor since the mobility is involved. For the commonly used semiconductors like germanium, silicon and gallium arsenide and for the practical profiles like gaussian and complementary error function, the values of t_E and t_{μ} are a few orders lower compared to normal lifetime. So it becomes essential to get analytical expressions for t_E and t_{μ} for each material.

Ho and Cho⁽²⁾ have approximated the mobility data for silicon by the expression

$$\mu = a / (1 + b N^c) \quad (6)$$

where a , b and c are constants. This approximation is found to be valid for germanium also and the constants are: $a = 3.6 \times 10^3 \text{ cm}^2/\text{Volt. sec.}$; $b = 1.4 \times 10^{-12} \text{ cm.}^3\text{c}$; $c = 0.69$. The actual values⁽³⁾ and the approximated values are shown in Fig. 1. The approximation is valid for the concentration range 10^{15} to 10^{19} cm.^{-3}

The electron mobility⁽⁴⁾ in gallium arsenide can be approximated to a straight line in the concentration range

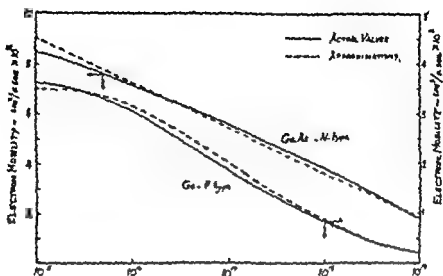


Fig. 1 Actual values and approximated values of mobility with impurity concentration.

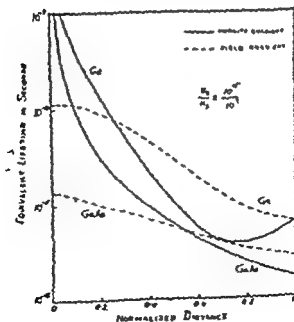


Fig. 2 Variation of equivalent lifetimes with normalized distance.

10^{15} to 10^{19} cm.⁻³ This gives the relation

$$\mu = 9 \times 10^3 - 1.9 \times 10^3 \log N(x) \quad (7)$$

Making use of Equations (3)(4)(5)(6) and (7) values of t_E

and t_μ can be found for any impurity profile.

III. RESULTS

Considering the distribution of impurity atoms to be gaussian in a diffused layer the values of t_E and t_μ are calculated and shown in Fig. 2. The values taken for other parameters are: the surface concentration $N_s = 10^{19}$ cm.⁻³; the background concentration $N_B = 10^{15}$ cm.⁻³; the thickness of nonhomogeneous layer = 1 micron.

In GaAs since the electron mobility does not change much with the impurity concentration both t_E and t_μ are effective. In Ge due to the large change of electron mobility with the impurity concentration t_μ is effective in most of the diffused region. Just at the surface t_μ becomes ∞ since the built-in field $E = 0$ for a gaussian profile at $x = 0$. This does not happen for a complementary error function profile.

REFERENCES

1. G.C. Jain and R.M.S. Al-Refai; J. Appl. Phys. 37 , 3401 (1966).
2. B.L. Ho and C.C. Cho, J. Appl. Phys. 39 , 3333 (1968).
3. A.B. Phillips, Transistor Engineering, (McGraw - Hill; New York, 1962) pp. 50.
4. C. Hilsum and A.C. Rose - Innes, semiconducting III-V compounds (Pergamon Press, Oxford 1961) pp. 140.

INFLUENCE OF CELL SCATTERING DUE TO IMPURITIES ON THE MOBILITY IN SILICON

O.P.Daga and W.S.Phokle,
Central Electronics Engineering Research Institute,
Pilani (Rajasthan)

1. Scattering due to the Change in Cell Size

When an impurity atom substitutes a host atom, the potential energy of the electron in the neighbourhood of the impurity atom is changed by an amount δV_1 from its value in the undistorted crystal. In the rigid ion approximation of Nordheim the perturbing potential δV_1 is given by^{1,2} :

$$\delta V_1 = U(\vec{r} - \vec{R}_1) - \sum_s V(\vec{r} - \vec{R}_1 - \vec{\Delta}_{1s}) \quad \dots(1)$$

where $U(\vec{r} - \vec{R}_1)$ is the potential due to an impurity and $V(\vec{r} - \vec{R}_1 - \vec{\Delta}_{1s})$ is the potential due to a host atom which is associated with the impurity bond. Here vector $\vec{\Delta}_{1s}$ represents change in bond length for the bond associated with the impurity atom. The summation over s is for all the atoms around the i^{th} impurity atom.

Since $\vec{\Delta}_{1s}$ is small, equation (1) can be expanded in a Taylors series, considering the linear term in $\vec{\Delta}_{1s}$ and summing over all the impurity atoms, we get:

$$\delta V = \sum_i (\langle U_1(\vec{r} - \vec{R}_1) - V_1(\vec{r} - \vec{R}_1) \rangle \sum_s \vec{\Delta}_{1s} \cdot \text{grad } V_1(\vec{r} - \vec{R}_1)) \quad \dots(2)$$

Using a screened Coulomb potential and $\epsilon = 4$, (For four nearest neighbour for one impurity atom) we obtain,

$$\delta V = \sum_i \left(\frac{e^2}{\epsilon} \frac{Z e^{-q(\vec{r} - \vec{R}_1)}}{(\vec{r} - \vec{R}_1)} - \frac{4 \vec{\Delta}_{1s} \cdot \text{grad } e^2 Z e^{-q(\vec{r} - \vec{R}_1)}}{\epsilon (\vec{r} - \vec{R}_1)} \right) \quad \dots(3)$$

where first term in above equation is the usual impurity potential and the second term represents additional potential due to change in bond length. The matrix element for above perturbation is given by :

10^{15} to 10^{19} cm. $^{-3}$ This gives the relation

$$\mu = 9 \times 10^3 - 1.8 \times 10^3 \log N(x) \quad (7)$$

 Making use of Equations (3)(4)(5)(6) and (7) values of t_E
 and t_μ can be found for any impurity profile.

III. RESULTS

Considering the distribution of impurity atoms to be gaussian in a diffused layer the values of t_E and t_μ are calculated and shown in Fig. 2. The values taken for other parameters are: the surface concentration $N_s = 10^{19}$ cm. $^{-3}$; the background concentration $N_B = 10^{15}$ cm. $^{-3}$; the thickness of nonhomogeneous layer = 1 micron.

In GaAs since the electron mobility does not change much with the impurity concentration both t_E and t_μ are effective. In Ge due to the large change of electron mobility with the impurity concentration t_μ is effective in most of the diffused region. Just at the surface t_μ becomes ∞ since the built-in field $E = 0$ for a gaussian profile at $x = 0$. This does not happen for a complementary error function profile.

REFERENCES

1. G.C. Jain and R.M.S. Al-Refai; J. Appl. Phys. 37 , 3401 (1966).
2. B.L. Ho and C.C. Chao, J. Appl. Phys. 39 , 3333 (1968).
3. A.B. Phillips, Transistor Engineering, (McGraw - Hill; New York, 1962) pp. 50.
4. C. Hilsum and A.C. Foso - Innes, semiconducting III-V compounds (Pergamon Press, Oxford 1961) pp. 140.

INFLUENCE OF CELL SCATTERING DUE TO IMPURITIES ON THE MOBILITY IN SILICON

G.P. Baga and W.S. Phokle,
Central Electronics Engineering Research Institute,
Pilani (Rajasthan)

1. Scattering due to the Change in Cell Size

When an impurity atom substitutes a host atom, the potential energy of the electron in the neighbourhood of the impurity atom is changed by an amount δV_1 from its value in the undistorted crystal. In the rigid ion approximation of Nordheim the perturbing potential δV_1 is given by^{1,2} :

$$\delta V_1 = U(\vec{r} - \vec{R}_1) - \sum_s V(\vec{r} - \vec{R}_1 - \vec{\Delta}_{1s}) \quad \dots(1)$$

where $U(\vec{r} - \vec{R}_1)$ is the potential due to an impurity and $V(\vec{r} - \vec{R}_1 - \vec{\Delta}_{1s})$ is the potential due to a host atom which is associated with the impurity bond. Here vector $\vec{\Delta}_{1s}$ represents change in bond length for the bond associated with the impurity atom. The summation over s is for all the atoms around the i^{th} impurity atom.

Since $\vec{\Delta}_{1s}$ is small, equation (1) can be expanded in a Taylor's series, considering the linear term in $\vec{\Delta}_{1s}$ and summing over all the impurity atoms, we get:

$$\delta V = \sum_i \left(\langle U_i(\vec{r} - \vec{R}_i) - V_i(\vec{r} - \vec{R}_i) \rangle \sum_s \vec{\Delta}_{is} \cdot \text{grad } V_i(\vec{r} - \vec{R}_i) \right) \quad \dots(2)$$

Using a screened Coulomb potential and $s = 4$, (For four nearest neighbour for one impurity atom) we obtain,

$$\delta V = \sum_i \left(\frac{e^2}{\epsilon (\vec{r} - \vec{R}_1)} \frac{-q(\vec{r} - \vec{R}_1)}{z} - \frac{4 \vec{\Delta}_{1s} \cdot \text{grad } \frac{e^2}{\epsilon (\vec{r} - \vec{R}_1)} \frac{-q(\vec{r} - \vec{R}_1)}{z}}{\epsilon (\vec{r} - \vec{R}_1)} \right) \quad \dots(3)$$

where first term in above equation is the usual impurity potential and the second term represents additional potential due to change in bond length. The matrix element for above perturbation is given by :

$$M_{kk'} = \sum_i e^{-j(\vec{k}' - \vec{k}) \cdot \vec{R}_i} \left(\int U_{k'}^* < \frac{e^2 \Delta Z e^{-q(\vec{r} - \vec{R}_i)}}{\epsilon (\vec{r} - \vec{R}_i)} - \right. \\ \left. \bar{\Delta}_{is} \cdot \text{grad} \left(\frac{4 e^2 Z e^{-q(\vec{r} - \vec{R}_i)}}{\epsilon (\vec{r} - \vec{R}_i)} \right) > U_k d\tau \right) \dots (4)$$

To evaluate above integrals we assume a uniform impurity distribution together with the earlier assumption that the positions of the two impurity atoms are uncorrelated. Under these assumptions we get:

$$(M_{kk'})^2 = \frac{1}{\epsilon^2} \left\{ \frac{4\pi \Delta Z e^2}{(k-k')^2 + q^2} \right\}^2 (1 + 16(\Delta_{is})qZ + (16(\Delta_{is})qZ)^2) \dots (5)$$

After usual Maxwellian average, relaxation time due to impurities is given by:

$$\left\langle \frac{1}{(E)} \right\rangle = \frac{\pi}{\sqrt{2}} \frac{Z^4 e^4 N_I F(E)}{\epsilon^2 E^{3/2} m^{*1/2}} \left(1 + \sqrt{\frac{2m}{\hbar^2 \pi}} (16(\Delta_{is})Zq) \right) \dots (6)$$

which leads to an expression for impurity mobility as given below:

$$\mu_I = \frac{2^{7/2} e^2 (kT)^{3/2}}{\pi^{3/2} (\Delta Z)^2 e^2 m^{*1/2}} \frac{1}{N_I} \frac{F(3kT)}{(1 + \sqrt{\frac{2m}{\hbar^2 \pi}} \sqrt{\frac{kT}{\pi}} (16Z(\Delta_{is})q))} \dots (7)$$

Above equation states that the impurity mobility is reduced by a factor

$$\frac{1}{(1 + \sqrt{\frac{2m}{\hbar^2 \pi}} \sqrt{\frac{kT}{\pi}} (16Z(\Delta_{is})q))}$$

as compared to Brooks-Herring formula.

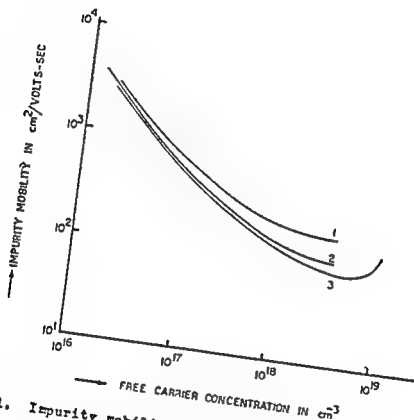


Fig. 1. Impurity mobility μ_I as a function of carrier concentration n at 78°K . Curve (1) represents the Brooks-Herring formula; Curve (2) represents corrected mobility due to cell scattering; Curve (3) represents experimental values.

2. Calculation of Δ_{is}

Δ_{is} can be estimated from the measured lattice contraction data. X-ray measurements give us average lattice contraction $\bar{\Delta}_a$, which can be easily analysed for contraction around the impurity atom. An impurity bond in Silicon lattice is given by :

$$D(\text{Si} - \text{Imp}) = 2r - \frac{\sqrt{3}}{8} \frac{\bar{\Delta}_a}{N'/N}$$

where N' and N are the impurity and host atoms concentrations and r is the covalent radius of Silicon. Therefore,

$$\Delta_{is} = \frac{\sqrt{3}}{8} \frac{\bar{\Delta}_a}{N'/N}$$

Using Cohen's data for $\bar{\Delta}_a$ the bond lengths for Si-B and Si-P bonds in Silicon are calculated as 2.242 and 2.301 Å⁰ respectively.

3. Comparison with Experiments

Mobility due to impurities is calculated from equation (7). The experimental (Granacher and Czaja)⁴ and theoretical curves are shown in fig. 1. It is clear from fig. 1 that the corrected impurity mobility agrees satisfactorily with the experimental values for various impurity concentrations. The improvement over Brooks-Herring formula is also evident.

REFERENCES

1. Horie, C. Science rep. of Tohoku, U. 34, 27 (1950).
2. Paige, E.G.S., Progress in Semiconductors, 8, (1964).
3. Cohen, B.G., Solid State Electronics, 10, 33, (1967).
4. Granacher, I. and Czaja, W., Jour. Phys. Chem. Solids, 28, 231 (1967).

ELECTRONIC CHARGE DENSITY DISTRIBUTION OF LEAD.

S.C.Roy and A.H.Ghose,

Nuclear Physics Laboratory, Bose Institute, Calcutta-9.

I. INTRODUCTION

The exact theoretical method to determine the electronic charge distribution of a high Z atom is almost impossible and one has to depend on several approximate methods. The best of these approximate methods is the Hartree¹ self consistent field model which assumes each electron to be in the field of the nucleus and an average field due to all other electrons. The only direct method to calculate the radial electronic charge distribution with only one assumption of spherical symmetry of an atom is to evaluate the integral

$$\rho(r) = \frac{1}{2\pi^2 r} \int_0^{\infty} F(Z, k) \sin kr \, k \, dk \quad \text{---(1)}$$

$k = q/t$

In this present method the atomic form factor $F(Z, q)$ which takes into account the charge distribution of an atom was determined from the coherent scattering cross-section data of gamma rays obtained experimentally. Initial attempt on this line was made by Woollan² for neon and argon using X-ray scattering data reveals that the resolution of K and L group of electrons is not possible for high Z atoms (even for Argon $Z = 18$) due to the longer wavelength of radiation in use. Therefore the scattering data of gamma rays having much smaller wavelength can be used as a successful tool to determine

the electronic charge distribution of heavy atoms like lead.

II. METHOD

The differential cross-section for the co-operative or Rayleigh scattering for a deflection of the photon through an angle θ is related with the atomic form factor $F(Z, q)$ by,

$$\sigma_R(\theta) = \frac{1}{2} r_0^2 (1 + \cos^2 \theta) |F(Z, q)|^2 \quad \dots (2)$$

where, r_0 is the classical electron radius and q is the change of the momentum of the photon and is given by $q = \frac{2E}{c} \sin \frac{\theta}{2}$; E is the energy of the incident photon. The equation (2) which is valid for non-relativistic cases made valid upto relativistic range semi-empirically³ from the observations of coherent scattering cross-section data for various values of E by introducing a new term $\varphi(E, q)$ depending on E and q in equation (2). The factor $\varphi(E, q)$ bears the following relationship

$$\begin{aligned} \varphi(E, q) &= 1 && \text{for } 0 \leq E \leq 0.4 \text{ MeV} \\ &= (13.5E - 4.4)^{-0.35q} && \text{for } E \gg 0.4 \text{ MeV} \end{aligned}$$

It has been observed that the relationship φ agrees within experimental error with experimental data upto $q = 2.5$ mc units. Thus the form factor $F(Z, q)$ is determined from the following relationship

$$F(Z, q) = \frac{1}{r_0} \left[\frac{2 \sigma_R(\theta)}{(1 + \cos^2 \theta) \varphi(E, q)} \right]^{1/2}$$

The radial electronic charge density is determined by carrying numerical integration of equation (1) using Simpson's 1/3 rule/Gauss quadrature formula for $q = 0$ to 1.5 mc units.

III. RESULTS AND CONCLUSION.

The result obtained in this way is compared with the values obtained from Hartree self-consistent field model

$$\rho(r) = \sum_{j=1}^Z \psi_j^*(r) \psi_j(r)$$

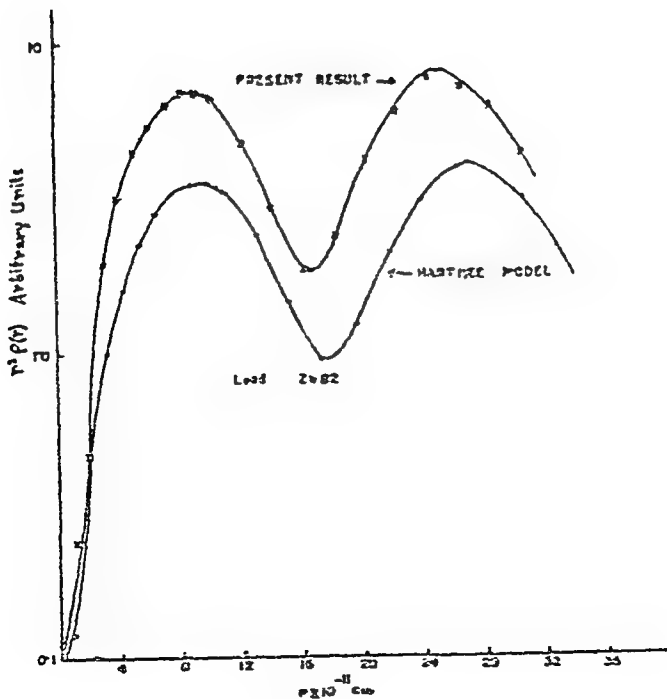
using the self-consistent wave functions tabulated by Herman and Skillman⁴. The result is in good agreement with the results obtained from Hartree model. Anomalies obtained previously⁵ using integration upto $q = 2.5$ mc unit for lead and tin indicates certain cut off to the limit of integration q is essential due to larger experimental uncertainties at higher momentum transfer region. The calculation for tin indicates that much more accurate measurement is needed for low and intermediate Z elements.

ACKNOWLEDGEMENT

Our thanks are due to Dr.S.M.Sircar, Director, Bose Institute for his kind interest in the work. One of the authors (S.C.R.) is thankful to the Department of Atomic Energy for awarding him a Senior Research Fellowship. Partial support for this work came from PL-180 project sponsored by the National Bureau of Standards, U.S.A.

REFERENCES

1. Hartree, D.R. (1928) Proc. Camb. Phil. Soc. 24,
89, 111.
2. Woollan, E.O. (1931) Phys. Rev. 38, 15.
3. Nath, A. and Ghose, A.M. (1968) NBS Technical note
No. 442.
4. Herman, F. and Skillman, S. (1963) Atomic Structure
Calculations, Prentice Hall.
5. Roy, S.C. and Ghose, A.M. (1969) Proc. Nucl. Phys.
Symposium (Roorkee) Vol.II (in press)



ELECTRICAL CONDUCTIVITY OF THALLIUM TELLURIDE

M. D. AGGARWAL and J. K. D. VERMA
Saha Institute of Nuclear Physics, Calcutta-9

I. INTRODUCTION

In recent years the thallium tellurium system has been given growing attention especially in connection with the study of the transport properties of liquid Tl-Te solutions within a wide range of compositions. Thallium-tellurium even in liquid solutions behave like a binary semiconductor. The solid state Tl-Te compounds have been studied less thoroughly. Thallium chalcogenides are of great interest because of their practical importance due to their high conductivity, large thermal emf and high photosensitivity. Studies on the electrical properties of various stoichiometric composition of thallium-tellurium system have indicated that only Tl_2Te_3 and Tl_2Te exhibit semiconducting behaviour^(1,2). While the compound Tl_2Te_3 has been extensively studied, electrical conductivity of Tl_2Te has been reported only for polycrystalline samples². This paper reports the result of some preliminary studies on the electrical conductivity of single crystals of Tl_2Te .

II. EXPERIMENTAL

The compound Tl_2Te is prepared by melting spectroscopically pure thallium and tellurium in stoichiometric proportion in sealed quartz ampoule evacuated to a

pressure of 10^{-5} Torr. The synthesis is then carried out by a method similar to that described elsewhere⁽³⁾. The ingot is then zone-refined extensively. The zone-refined ingot is then broken into pieces and loaded in another capsule with a conical tip for crystal growth by Bridgman technique. The molten charge is held for about an hour at a temperature 30°C above melting point and some amount of mechanical vibration is given to remove blow holes or voids. The ampoule is then lowered to a cold zone about 50°C below melting point. Best results are obtained when the gradient and the lowering rate have been so adjusted as to give a cooling rate of 3°C per hour. Crystals obtained in this way have been found to have room temperature resistivity of about 1.2 ohm.cm.

The measurement of conductivity, σ , is made by the conventional d.c. potentiometric method in the temperature range of 300°K to 680°K in vacuum. Measurements are made on parallelepiped single crystal specimens, the longer side being parallel to the cleavage plane. The sample is held between two silver plated copper blocks. Conductivity probes are molybdenum wires welded to the specimen by condenser discharge technique. Heating of the sample is done by a small heater placed inside the specimen holder tube and in thermal contact with the end blocks. All voltage measurements are carried out with a precision potentiometer.

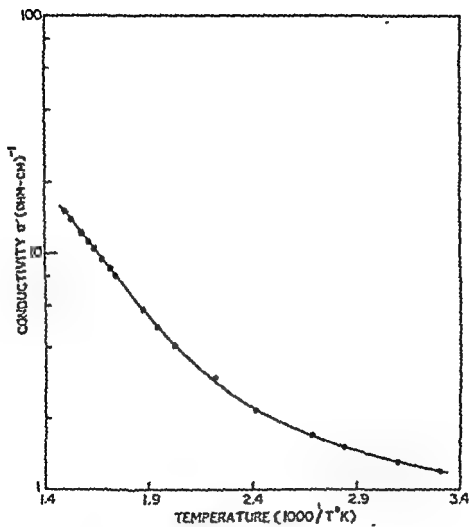


Fig. 1 Variation of electrical conductivity of Tl_2Te with temperature

III. DISCUSSION

The variation of conductivity σ with temperature for a typical crystal is shown in Figure 1. The temperature dependence of σ is used to estimate forbidden energy band gap, E_g , in the intrinsic region using the following relation³:

$$E_g = -0.397 \Delta(\log \sigma) / \Delta(1000/T)$$

The value of E_g obtained from the present investigation is estimated to be 0.6 eV. The variation of energy gap from 0.5 eV to 2.0 eV reported⁽²⁾ for different heat treatment of the compound has not been found. Thermoelectric properties are measured at all temperatures region.

REFERENCES

1. J. Choudhury, *Ind. J. Chemistry*, **20**, 261 (1962).
2. S. S. Kulkarni and S. S. Kulkarni, *Phys. Rev.*, **171**, 1021 (1968).
3. R. A. Creswell, *Phys. Rev.*, **136**, 1021 (1964).

No. The only other method by which the energy band gap can be determined is by optical method. The energy band gap determined by these two methods are, however, slightly different.

Unidentified

What is the difference between the results on polycrystalline samples and single crystals.

M.D. Aggarwal

The energy band gap (in the intrinsic region) will be the same in both the cases. However, if there is any anisotropy in conductivity or activation energy, it can be detected only in single crystals.

CALCULATION OF STATIC DIELECTRIC CONSTANT OF 'BUILT-UP' BARIUM STEARATE FILMS

Usha Khanna, V.K. Srivastava and V.K. Agrawal
Department of Physics, University of Roorkee, Roorkee

The well known 'built-up' films¹ of Barium stearate have been a subject of experimental investigations since long and a number of workers have measured their dielectric constant² (ϵ_s). However, a theoretical interpretation of these results has not been given so far. As the Barium stearate films seem to be very promising for making devices²⁻⁴, it is essential that their basic dielectric characteristic be theoretically understood. We have calculated ϵ_s of mono- and multimolecular films of Ba-stearate along the symmetry hexagonal axis along which the above measurements have been made.

The layered structure of Ba-stearate films⁵ is a simple hexagonal array with the molecules oriented with their chains normal to the supporting surface and separated by a distance 4.85\AA . The earlier attempts to calculate the Lorentz field for simple hexagonal lattices have been made by Miller⁶. His assumption that the dimensions of the molecule are much smaller than the lattice constant has no validity in the case of Ba-stearate films because the molecular size (25.75\AA)⁷ is large as compared to the lateral intermolecular distance (25\AA). Hence the Millers theory, as such, is not applicable in the present case.

Our basic approach for taking into account the size of the molecule is therefore to consider inter

actions in the presence of static electric field normal to the film. For the purpose of calculations each molecule (Molecular formula $(C_{17}H_{35}COO)_2Ba$) is thus considered to be divided into the small CH_2 groups (and of course the end $(COO)_2Ba$ group) separated by 1.27\AA along chain axis.

If all the induced dipoles are assumed to be point dipoles, parallel to each other with their axis taken to be the z axis (the external field direction), we have the field at the reference dipole, because of the others, given by

$$E_z = \sum_i \frac{3p_i z_i^2 - p_i r_i^2}{r_i^5} \quad (1)$$

where p_i is the moment of the i th dipole, r_i is the distance between the reference and the i th dipole and z_i is the z -component of r_i .

For calculating the inter molecular contribution E'_z to the local field inside the monolayer, following L. Salem,⁸ we consider two parallel linear chains of length L consisting N identical units of length λ ($N\lambda = L$). The mutual distance between them is D which must be large enough as compared to the length of basic unit λ . This assumption is obviously valid in our case. Considering the basic units as point dipoles we calculate the field between the centres of two units, one in each chain at a distance $r \gg D$.

If we number the units in the first chain $1, 2, 3, \dots, n, \dots, N$, and those in the second chain $1, 2, \dots, n', \dots, N$ the distance r between the centres of n and n' in the second chain is (assuming the centre of each chain unit to be at

its mid point) given by $\gamma = [D^2 + \lambda^2 (n-n')^2]^{1/2}$ and $Z = \lambda(n-n')$ (2)

Assuming local additivity, the total field at one molecule due to another molecule becomes

$$E'_2 = \rho \sum_{n=1}^N \sum_{n'=1}^N \frac{2\lambda^2 (n-n')^2 - D^2}{[D^2 + \lambda^2 (n-n')^2]^{3/2}} \quad (3)$$

$P = \alpha_1 E_{loc}$ where α_1 is the polarizability of the basic unit. The polarizability of unit CH_2 is assumed to be isotropic and equal to 1.84×10^{-24} c.c.

Noting that for a given value of $x = |n-n'|$, there are $2(N-x)$ terms of equal magnitudes, the only exception being the case $x = 0$ for which there are only N (equal) terms, we rewrite the above equation as

$$E'_2 = \rho \left[-\frac{N}{D^3} + 2 \sum_{\lambda=1}^N \frac{2\lambda^2 x^2 - D^2}{(D^2 + \lambda^2 x^2)^{3/2}} (N-x) \right] \quad (4)$$

The field E'_2 is calculated from (4) by considering the two chains of Ba-stearate molecule to be coincident and taking the effect of seven nearest neighbours. The intra molecular contribution E_2^2 to the local field is calculated by putting $\gamma=Z$ in eq.(1). The effect of the end $(COO)_2Ba$ group is separately calculated taking its electronic polarizability to be 6.05×10^{-24} c.c.

The local field in the multimolecular 'built-up' is calculated, following Mullers treatment ⁶ for lattices, by considering the molecules as continuously distributed in all the layers except the layer in which the reference molecule is situated. The contribution of the continuous distribution to the local field is $4\pi P$ (P = Polarization) and that of the reference is the one calculated for a monolayer by the above

The calculated E_g , 1.6 for a monolayer and 3.0, for thick multi-layer films, are in good agreement with the corresponding reported values of 1.9 (for 7 layers) and 2.5 (average)².

We (UK and VKA) acknowledge the financial assistance of CSIR.

REFERENCES

1. K.B. Blodgett and L. Langmuir, Phys. Rev., 51, 964 (1937).
2. R.H. Hardy and L.C. Scala, J. Electrochem. Soc., 113, 109, (1966).
3. P.L. Hawkes, Thin Film Integrated Circuits, 5, 304, (AEI Engineering 1965).
4. S. Horieuchi, J. Yamaguchi and K. Naito, J. Electrochem. Soc. 115, 634 (1968).
5. L.H. Gormer and K.H. Storck, J. Chem. Phys. 6, 280 (1938).
6. H. Miller, Phys. Rev. 50, 547 (1936).
7. V.K. Srivastava and A.R. Verma, Proc. Phys. Soc. 80, 222 (1962); Solid State Comm., 4, 367 (1966).
8. L. Salem, J. Chem. Phys. 37, 2100 (1962).

THICKNESS DEPENDENCE OF THE D.C. ELECTRICAL BREAKDOWN IN THIN 'BUILT-UP' BARIUM STEARATE FILMS

V.K. Agarwal and V.K. Srivastava
Department of Physics, University of Roorkee, Roorkee.

1. INTRODUCTION

As has been recently shown¹⁻⁴ the use of the 'built-up' barium stearate films seems to be very promising for making thin film devices. The breakdown strength of the films which would play a fundamental role in the development of the devices has been systematically studied in the present work. The dielectric strength varies with the nature of the electrode contacts, ambient medium, thickness of the dielectric film and the temperature etc. Specifically, the thickness dependence of d.c. electrical breakdown strength in the molecular films of barium stearate, not investigated by the previous workers,⁵⁻⁶ has been studied here. These films are ideally suited for such studies because of their easy reproducibility, homogeneity, high dielectric strength, perfect control (within 25\AA) and uniformity of their thicknesses which have already been very accurately measured.⁷

EXPERIMENTAL

Barium stearate films containing desired number of layers were 'built-up' on aluminized microscope glass by the well known technique of Blodgett and Langmuir.⁸⁻⁹ The lower Al electrode was deposited by thermal evaporation in vacuum. The d.c. measurements are made using Hg electrode contact and connecting a 90 volt

battery across the sample. The voltage is swept up from its low values by feeding it through a linear wire wound potentiometer ($\approx 100K$). The breakdown voltage shown by an abrupt rise in current was measured with a precision VTM.

111. DISCUSSION OF RESULTS

Measurements of breakdown strength (F_b) have been carried out in the thickness range ($250\text{\AA} - 1500\text{\AA}$). The dependence of breakdown strength on thickness is shown in the figure and it is found to be a power dependent function of thickness varying as $d^{-\alpha}$ where d is the film thickness and $\alpha = 0.57$. The value used for the thickness⁷ of the Ba stearate monolayer is 25.75\AA . The breakdown voltage is found to vary slightly with the size of Hg droplet. Sometimes the reproducibility of the results was not very good, apparently due to the voids and inhomogeneties in the organic insulating films.

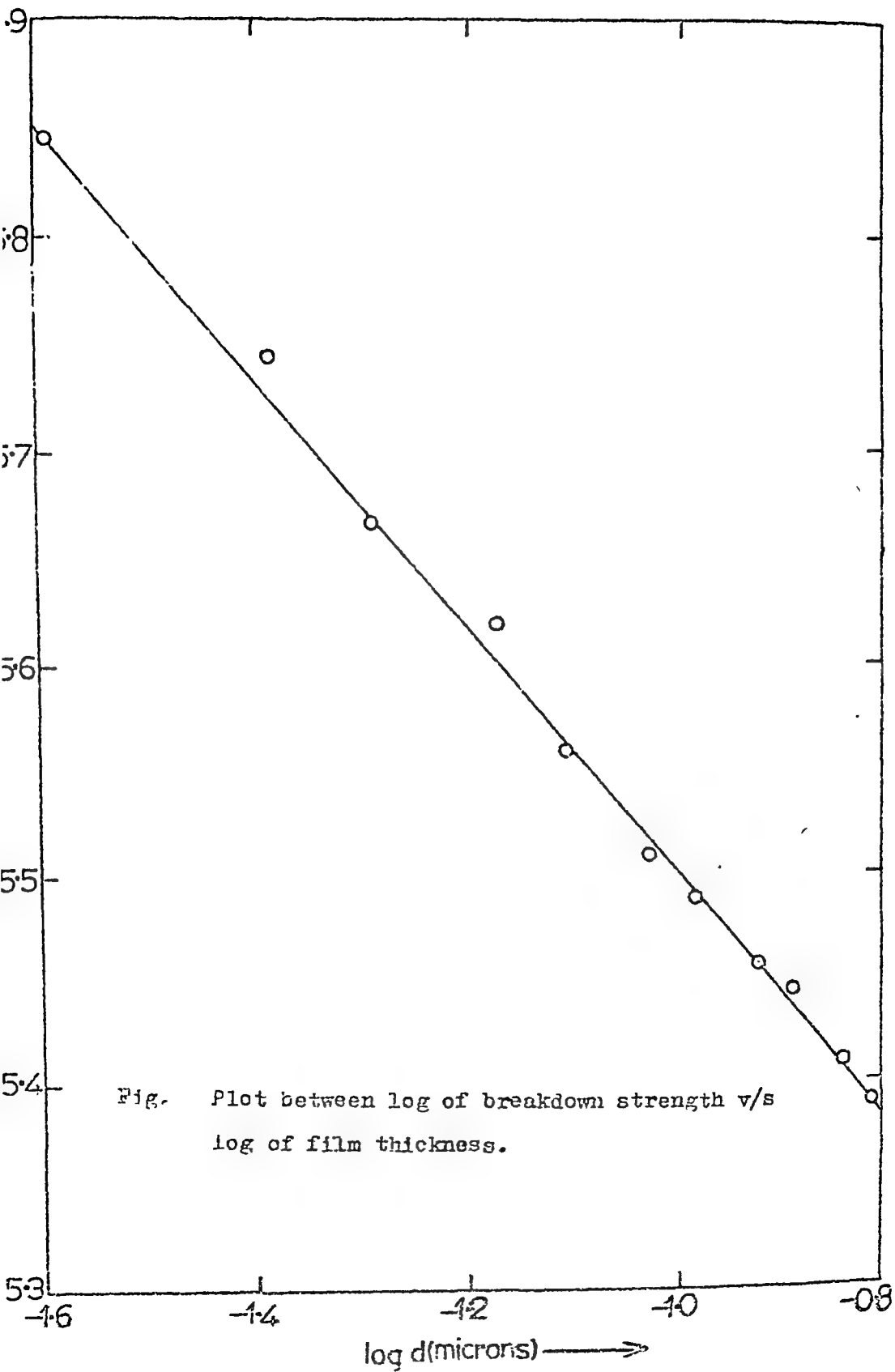
The power dependence of the breakdown strength on thickness as found by us strongly supports the theoretical approach, based on electron ionization avalanche, of Forlani and Minnaja¹⁰ who, on the basis of the electron lattice scattering mechanism in dielectric materials and the electron behaviour in the conduction band of the dielectric, derived the above kind of power dependence with ($\alpha = 0.25 - 0.5$). Also, the breakdown strength of Ba-stearate films is of the order of 10^6 V/cm. which is in close agreement with the reported values of Holt.¹¹

ACKNOWLEDGMENT

I(VKA) feel grateful to the C.S.I.R. for their financial assistance.

REFERENCES

1. J.L. Miles and H.O. McMahon, J.Appl.Phys.32,1126(1961)
2. R.W. Handy and L.C. Scala, J.Electrochem Soc., 113, No.2, 109 (1966).
3. P.L. Hawkes., Thin Film Integrated Circuit, 5, 304, (ABI Engineering 1965).
4. S. Horiuchi, J. Yamaguchi and K.Maito, J. Electrochem. Soc. 115, No.6, 634 (1968).
5. E.F. Porter and Jr. Wyman., J.Am. Chem. Soc. 60, 2853 (1938).
6. H.H. Race and S.I. Reynolds, J. Am. Chem. Soc. 61, 1425 (1939).
7. V.K. Srivastava and A.R. Verma, Proc. Phys. Soc. 80, 222 (1962); Solid State Comm.4, 367 (1966).
8. K.B. Blodgett, J. Am. Chem. Soc. 57, 1007 (1935).
9. K.B. Blodgett and I. Langmuir, Phys. Rev. 51, 964 (1937).
10. P.Forlani and N. Mirreza, Phys. Stat. Sol., 4, 311 (1964).
11. L. Ertl, Nature (GB), 214, 1103 (1967).



ELECTRON BEAM INDUCED CONDUCTIVITY IN As_2S_3

B. Ghosh
Technical Physics Division
Bhabha Atomic Research Centre
Bombay-85 AS.

I. INTRODUCTION

The electron bombardment induced conductivity has been studied on thin films of a few dielectric materials⁽¹⁻⁴⁾. The important parameter studied in most of the cases is the gain (g), being defined as the ratio of the true secondary charge transported through the film to the charge delivered to the film by the exciting beam per second. For the secondary charge transport the film is, of course, under the influence of an external bias field. Recently, it was reported⁽³⁾ that in As_2S_3 film an appreciable amount of charge might be transported during the off period for excitation by millisecond pulses. However, no systematic investigation has so far been reported on the difference between gains for d.c. and pulsed excitations. New measurements of conduction induced in arsenic trisulphide films by d.c. and pulsed excitations are presented. It is shown that the lower value of the saturation pulsed conductivity could be explained qualitatively in terms of recombination statistics of non-equilibrium carriers.

II. EXPERIMENTAL

The specimens were Au- As_2S_3 -Au sandwiches, with the As_2S_3 film thickness 2-6 micron. The dark resistivity of these films was about 10^{15} Ohm-cm. The electron beam energy was sufficient to produce uniform columnar ionisation densities⁽⁵⁾. Single pulses as well as continuous pulses with a repetition rate of 0.1 to 200 pps were used.

III. RESULTS

Shapes of induced current pulses at two temperatures are shown in Fig.1. Results reproduced here correspond to the case of the d.c. bombarding current equal to the average current (i_{pav}) for pulsed excitation. Fig. 2 shows the variation of the pulsed gain (g_M) or charge gain (g_c) with pulse repetition rate (n) for pulse width (τ) about 3 ns. For every repetition rate the average gain (g_{av}) has been plotted in the figure with the d.c. gain (g). The additional suffix m is used to indicate the values at the energy corresponding to the maximum gain. It is clear that charge gain is independent of frequency. Average gain is equal to the d.c. gain, but much larger than charge gain.

The difference between charge and average gains and the observation that the induced pulse takes a few ns (Fig.1) to attain final equilibrium value necessitated the careful study of the decay of the induced current pulse. The results of a representative specimen are shown in Fig. 3 for room temperature and 353°K. It is evident that the temperature rise has enhanced all the gains by a constant factor without narrowing down the ratio g_{av}/g_c . Hence a very small, slow decay of current between the pulses could be ruled out. The difference is traced to some other factor.

It is seen for longer pulse duration the secondary electron current build-up is complete and attains saturation when the steady state condition is reached after certain duration governed by the carrier lifetime. In this case one expects the average pulsed gain to be equal to the d.c. gain, for the simple reason that the fraction of charge which is lost during induced current build up is negligibly

small. On the other hand, for a shorter pulse duration this could be considerable fraction and could result in an effectively reduced pulsed-gain. There is a finite time for attainment of the maximum induced current. The effect of time is brought out distinctly when specifically the pulsed gain is measured. This time is relatively smaller than other time constants involved in the process. This point is further borne out by the fact that the reduction in the exciting beam width leads to further reduction in pulsed gain.

REFERENCES

1. F. Ansbacher and W. Ehrenberg; Proc. Phys. Soc. Lond. A 64, 362(1951).
2. L. Pensak; Phys. Rev. 75, 472 (1949).
3. J. Firsch; J. Phys. Chem. Solids 27, 1385 (1966)
4. S. Okabe et al; J. Appl. Phys. 40, 2894 (1969)
5. R. Ghosh; Ph.D. Thesis Lond., (1967).

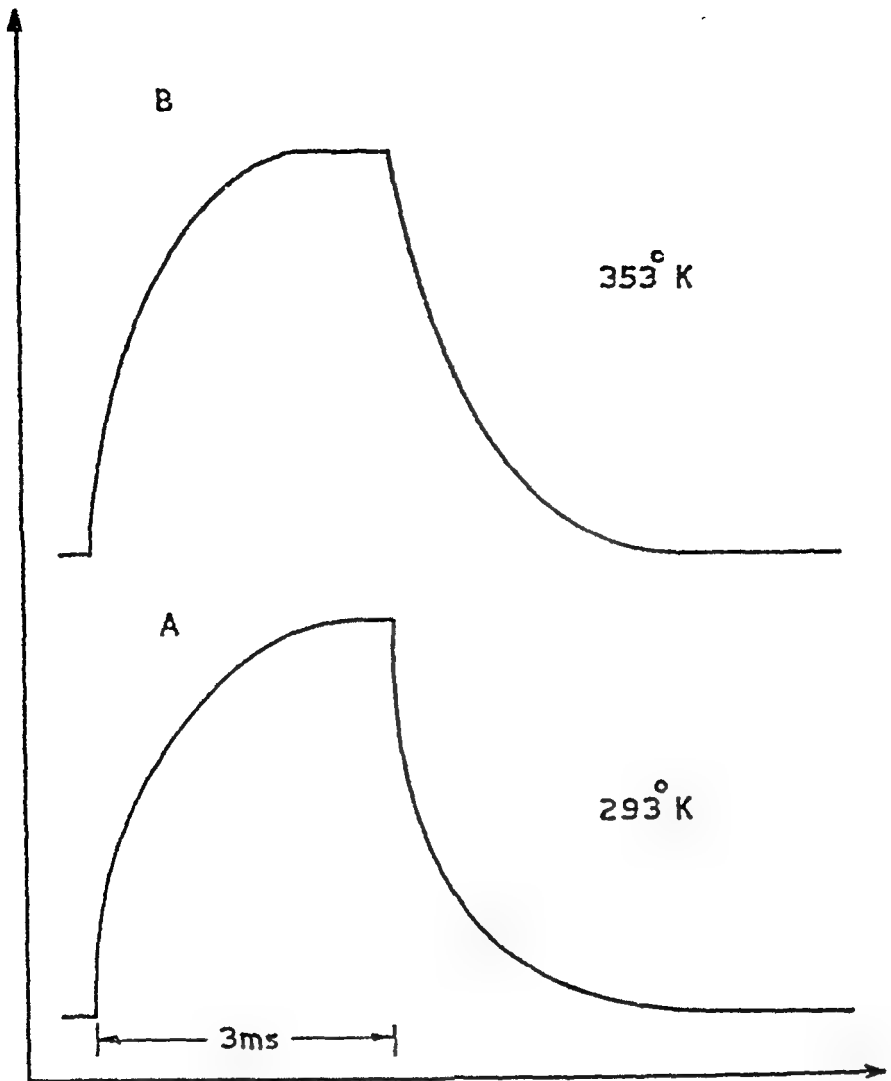


FIG.1. Induced pulse shapes at two different temperatures for primary pulse length 3 ms. Ordinate arbitrary.

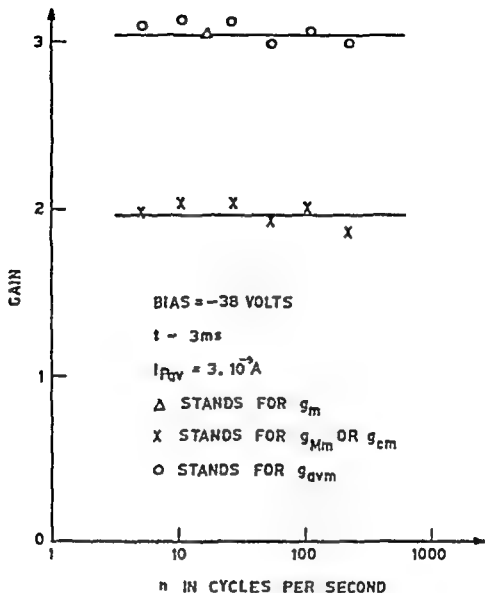


FIG. 2. Variation of gain (g) with frequency (n).
 Specimen D III, thickness 3.8 micron.

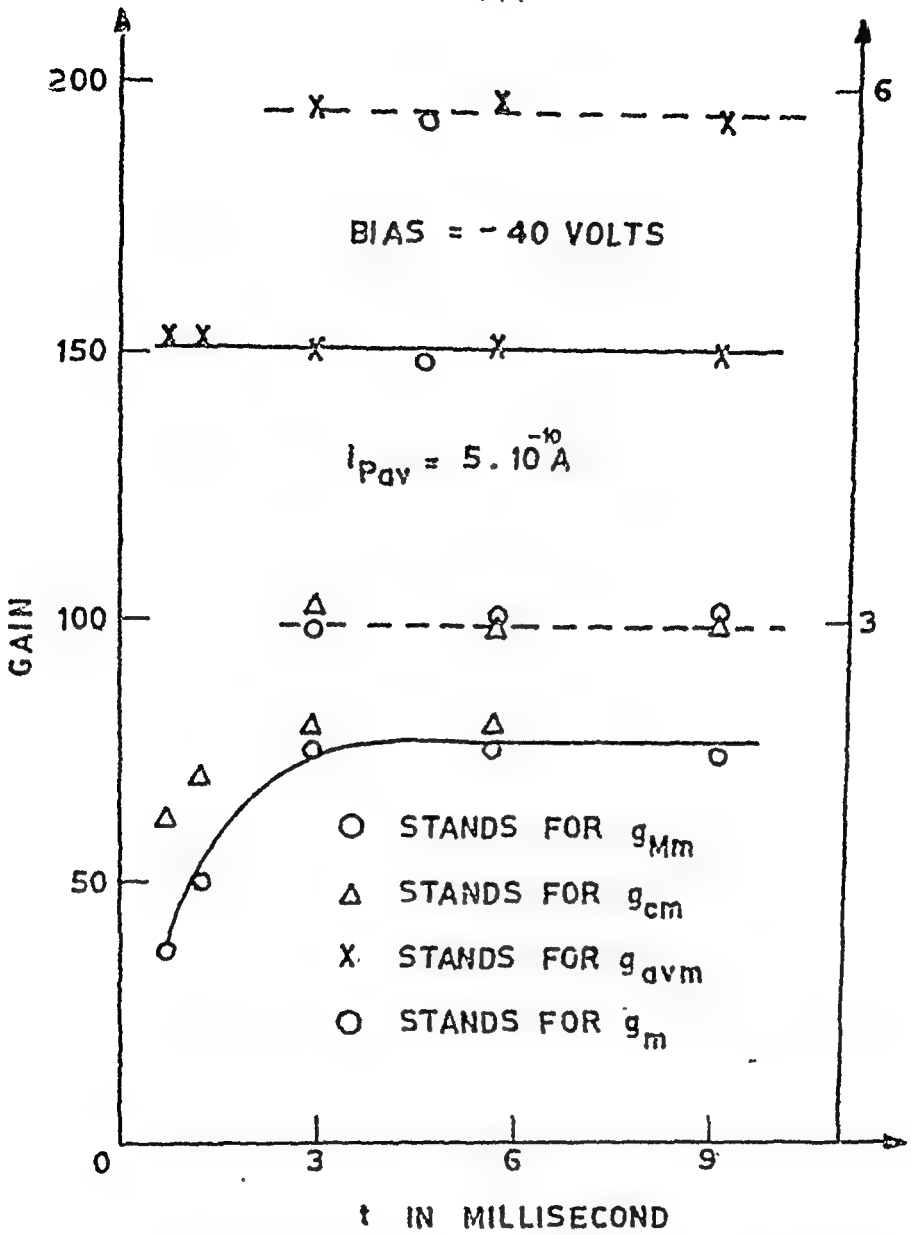


FIG. 3. Variation of gain (g) with length (t).

Specimen II, thickness

C as at 353

D, 93°K,

EFFECT OF HEAT TREATMENT ON THE ELECTRICAL RESISTIVITY OF
THIN SILVER FILMS

S. Mohan and P. Jayarama Reddy
Department of Physics,
Sri Venkateswara University, Tirupati.

I. INTRODUCTION

The dependence of resistivity (ρ) of a metallic thin film on its thickness (t), as expected from the size-effect theory^(1,2,3) has been very well established. The effect of temperature on the resistivity has also been the topic of investigation of several workers⁽⁴⁻⁸⁾. But there is a disparity in the results of these workers, probably because of different experimental environment. In this investigation, the variation of resistance of a silver film with temperature is discussed in terms of various processes that are likely to occur during the continuous heating of the freshly deposited film in vacuum.

II. EXPERIMENTAL

Thin films of silver are prepared by evaporation of pure silver metal from a tungsten filament onto 'gold seal' microscope slides. The pressure in the vacuum system has been maintained at less than 10^{-5} torr during the evaporation. The microscope slides are cleaned both by chemical methods and by ion bombardment prior to the evaporation. The resistance of the films kept in vacuum chamber are measured by standard potentiometer techniques. The thicknesses are determined by photographing the fringe system

In a multiple beam interferometer.

A heater has been designed to heat the film in vacuum upto about 300°C . The temperatures are measured using a thermistor which is placed on the substrate.

The variation of resistance of a film of thickness 390\AA with temperature is given in Table 1.

TABLE I

Resistance Vs temperature for the Silver film ($t = 390 \text{\AA}$)

Temperature ($^{\circ}\text{C}$)	Resistance (ohms)	Temperature ($^{\circ}\text{C}$)	Resistance (ohms)
32	2.69	113	2.69
44	2.71	125	2.79
53	2.73	135	2.89
59	2.74	145	2.99
64	2.73	160	3.13
73	2.71	170	3.28
80	2.69	187	4.28
90	2.65	199	9.05
95	2.64	200	11.58
99	2.63	207	18.85
105	2.64	208	32.51

III. RESULTS AND DISCUSSION

It is clear from the table that the film resistance increases slightly with temperature upto about 60°C and thereafter decreases upto about 100°C . Even though this

increase and decrease in resistance are small, they are definite and very much higher compared to experimental error. This behaviour is in agreement with the studies of Shah and Kaik⁽⁴⁾ on gold and silver films. Within this temperature, it is expected that all the imperfections in the film are annealed out. Further steady heating of the film leads to a very pronounced rise in resistance. This large increase in resistance is attributed to the agglomeration that takes place in the film. The agglomeration character has been revealed by the presence of island structure in the electron micrographs taken by Kane et al⁽⁶⁾ on their gold films heated to about 300°C. Estermann et al⁽⁷⁾ who annealed the silver films at 200°C for several hours however observed linear behaviour of resistance with temperature even upto 160°C. But they have not mentioned about the observation of any agglomeration effects in their films.

Heating of the film is stopped when the film has definite resistance and cooled to room temperature. It is found that the resistance of the film has increased to 27.9 ohms i.e. an increase by a factor of ten during the process of agglomeration compared to freshly prepared film. This increase, of course, depends on the structural changes in the film during agglomeration. The film is again heated gradually upto a temperature of about 85°C and it is found that the variation is linear. Repeated heating and cooling in this temperature range gives reproducible results, thereby showing that for an agglomerated film, the temperature variation of resistance is reversible. The temperature coefficient of resistance at 30°C is

evaluated from this data and it turns out to be 0.0026. The bulk value of temperature coefficient of resistance for silver is 0.0036. This difference is due to the size effects in the film^(5,8).

The film has been exposed to atmosphere for a few days and the resistance is measured at different intervals. A small increase in resistance is observed which may be due to chemisorption. An insulator coating may avoid this increase of resistance in the film.

IV. CONCLUSIONS

The present investigations on silver films show the existence of a critical temperature and heating of the films beyond this temperature results in agglomeration which leads to a very large increase of resistance of the films. Also, the temperature variation of resistance in agglomerated films is linear and reversible. This property helps to use these films as high resistances.

The authors thank Prof. J. Bhimasenachar, Head of the Department of Physics for his continued interest in this project of work.

V. REFERENCES

1. Fuchs, K. Proc.Camb. Phil.Soc. 34, 100 (1938)
2. Sondheimer, E.H. Phy.Rev. 80, 401 (1950)
3. Sondheimer, E.H. Advan.Phys. 1, 1 (1952)
4. Shah, V.V. and Naik, Y.G., Ind.J.Pure.Appl.Phys. 3, 20 (1964)
5. Duggal, V.P. et al Appl.Phys.Letters 13, 206 (1968)
6. Kane, W.M. et al, Jol.Appl.Phys. 37, 2085 (1966)
7. Estermann, J. et al, Jol.Appl.Phys. 41, 2802 (1970)
8. Chopra, K.L. and Bobb, L.C. Acta Metallurgica 12, 807 (1964)

V. Subramanian
Electronics Division, Bhabha Atomic Research
Centre, Trombay, Bombay-85

I. INTRODUCTION

Interest in amorphous semiconductors has grown intensely in the last two years- two special volumes (1,2) devoted to the study of semiconductor effects in amorphous solids have appeared in 1970. Many chalcogenide semiconducting glasses show switching with memory. In this paper, the electrical behaviour of diodes made from the alloy of composition $2As_2 Se_3$. $As_2 Te_3$ is described.

II. EXPERIMENTAL

1). Preparation of Diodes

The glassy material was prepared by heating the elements As, Se and Te, taken in proper weight proportions, in an evacuated and sealed quartz ampoule around $400^\circ C$ for a few hours and air-quenching the ampoule. X-ray examination of the material showed no signs of crystallinity.

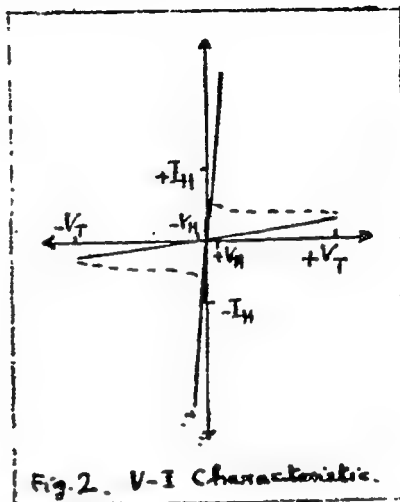
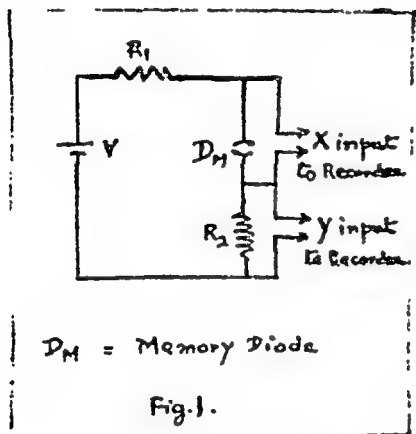
Small discs of approximately $2mm \times 4mm$ were cut with thicknesses varying from 0.5 mm to 1.5 mm. The discs were lapped to get even surfaces and cleared with trylene to remove greasy matter. With indium solder (commercial tin solder was not that good) tin-coated copper wires were soldered on to either side of the discs to get diodes in the bulk form.

Thin film diodes were prepared by sandwiching thin films of the glassy material between metal electrodes, all deposited on a glass plate by vacuum evaporation. Both the top and bottom electrodes were obtained by sandwiching a film of copper with chromium films by vacuum evaporation. Chromium has been recommended (3) as a good

electrode material. Copper was used to bring down the electrode resistance. Aluminium electrodes were also used in some of the film diodes.

ii) Electrical characteristics

The V-I characteristics of these diodes were obtained using a simple circuit as shown in Fig.1. The shape of the V-I characteristic is depicted in Fig.2.

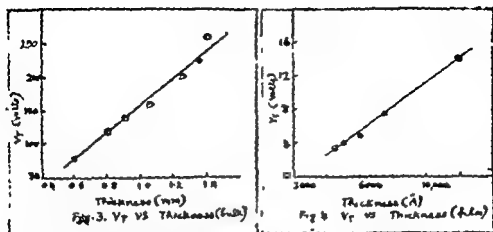


The diode (bulk as well as film) was found to switch from a high resistance state or the 'off' state to a low resistance state or the 'on' state, at a voltage V_T called the threshold voltage. Once the diode was switched into the 'on' state, it stayed in that state even after removal of applied voltage, thus possessing memory of the 'on' state. A couple of diodes were tested after a month and were found to be in the same 'on' state. To put the diode back into the 'off' state a sufficiently large current pulse with a sharp trailing edge had to be passed thro' it.

iii). Threshold voltage vs. Thickness

It was observed that V_T increased⁽⁴⁾ more or less linearly with thickness both in the bulk and film forms in the range of thicknesses considered, as seen in Fig.3 and Fig.4. However the

voltage drop V_T for a certain current I_T in the 'on' state was about the same for different thicknesses.



iv. Threshold voltage vs. temperature

The threshold voltage decreased ⁽⁵⁾ with increase of ambient temperature. The plot of V_T vs. temperature for two bulk units in Fig. 5 shows the relation to be exponential. A thin film diode (film thickness $\sim 7500 \text{ \AA}$) had $V_T = 5V$ at $25^\circ C$ whereas at liquid air temperature V_T was $30V$. V_T for a certain I_T in the 'on' state was not significantly altered by temperature.

v. Effect of temperature of preparation of glass on the electrical properties of the glass.

Samples of the glass prepared around $700^\circ C$ and $800^\circ C$ (keeping the composition, the total weight and the duration of heating the same) were found to have a resistivity of $\sim 10^7 \Omega \text{ cm}$, whereas the $900^\circ C$ sample had a resistivity of $\sim 10^6 \Omega \text{ cm}$. Bulk diodes prepared from $700^\circ C$ and $800^\circ C$ samples had a V_T of $800V$, at room temperature, for a thickness of $\sim 1.25 \text{ cm}$ whereas the $900^\circ C$ sample gave $200V$ for about the same thickness. Again, for a device thickness of 0.5 cm , the $800^\circ C$ and $700^\circ C$ samples showed a V_T of $650V$, whereas the $900^\circ C$

sample showed 80V for the same thickness. Samples prepared around 650°C and 1000°C were found to be crystalline (contained tellurium crystallites) and highly conducting electrically.

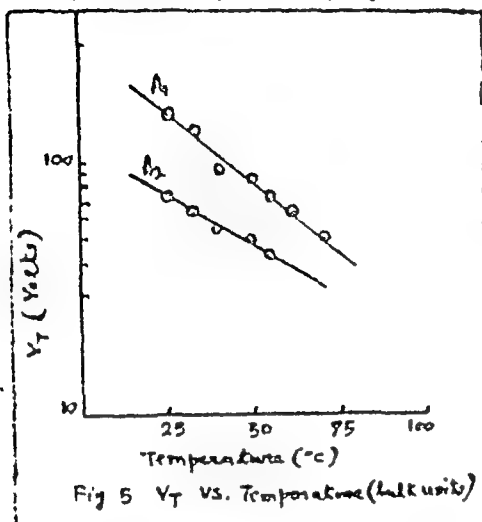
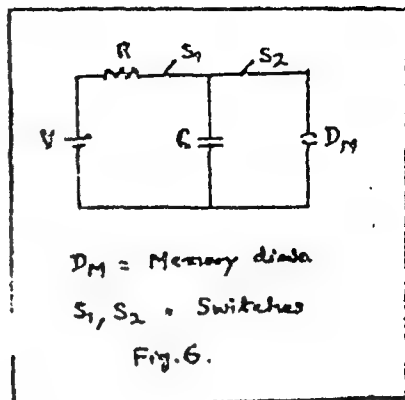


Fig 5 V_T vs. Temperature (Kelvin)



vi. 'Switching-off' is energy controlled

A simple circuit as shown in Fig. 6 was used to switch the memory diode from the 'on' state to the 'off' state. In principle a capacitor of value C was charged to a voltage V and allowed to discharge thro' the diode. Different combinations of V and C were tried. Only certain combinations which gave more than a certain amount of energy could switch the diode 'off'. For a diode of $V_T = 160V$, ('on' resistance $\sim 10k\Omega$, 'off' resistance $\sim 1M\Omega$) with a charging voltage $V = 90V$, capacitor values of about 0.022uf or more were necessary to put the diode 'off'. Again for $V = 45V$, about 0.1 uf or more was needed for switching off. Lower values of C could take the diode only to intermediate resistance ($\sim 100k\Omega$) states.

It was also observed that the energy required to switch off the diode increased with the threshold voltage of the diode. For a diode of $V_T = 55V$, with $V = 45V$, a C of 0.01 uf or more was required to effect switching off and for a diode of $V_T = 80V$,

0.05 μ f or more.

III. CONCLUSIONS

The dependance of V_T on thickness and temperature observed in memory diodes made from $2As_2Se_3.3As_2Te_3$ agrees with the earlier observations (4,5) in certain other chalcogenide semiconductors.

The effect of temperature of preparation of the glass on its resistivity is not well understood, though it may be said that in the case of 650°C sample, probably the reaction was not complete and in the case of 1000°C sample probably dissociation occurred.

A. Caillag and H. Jäger (6) have shown by pulse measurements that the switching process is energy controlled in thin film switches made from Te-As-Ge-Si. With the simple technique of discharge of a condenser thro' the diodes in the 'on' state, it is qualitatively shown that the 'switching off' is energy controlled. Moreover, very low voltages and very large condenser values were not effective, as such combinations, though energy-wise alright, meant a large time constant for the discharging process and did not allow quenching and phase change to amorphous state. Again for the same reason connecting a large resistor in the discharge path did not allow switching off, which occurred without such a resistor.

ACKNOWLEDGEMENTS

The author wishes to thank Dr. G.S. Rao, Smt. N.S. Kunte and Mr. S.V. Ranade for material preparation, Mr. R. Pinto and Mr. K.N. Jha for film deposition and Dr. P.R. Dastidar for encouragement.

REFERENCES

1. Journal of Non-Crystalline Solids, Volume 2 (1970)
2. Journal of Non-Crystalline Solids, Volume 4 (1970)
3. R.G. Keale, J. Non-Crystalline Solids 2 (1970) 558
4. S.R. Ovshinsky, Physics Rev. Letters 21 (1968) 1450
5. D.W. Deis et.al., J. Non-Crystalline Solids 2 (1970) 141
6. A. Caillag and H. Jäger, J. Non-Crystalline Solids 2 (1970) 133

DISCUSSION

T.M. Brindha

What is the mechanism of switching?

V. Subramaniam

In memory type materials, the switching is explained by a phase change mechanism. The diode material before switching is amorphous and the diode is in the high resistance state. The 'on' or the low resistance state is due to a high conductance path established by a new phase, probably crystalline, that has separated from the amorphous material as a result of the field and current at the time of switching. Because of this structural change the diode possesses a non-volatile memory of the 'on' state.

V.S. Indurkar

What is the order of switching time obtained in these chalcogenide glasses.

V. Subramaniam

The effective switching time (which includes the delay time during which the phase transformation takes place in memory diodes) is of the order of 10^{-7} sec, if the height of the switching pulse is much larger than the threshold voltage.

SWITCHING EFFECTS IN Au-SiO₂-SiC SYSTEM

Miss. Brindha, T.M and G.Suryan

Department of Physics, Indian Institute of Science,
Bangalore-12.

I. INTRODUCTION

On account of their device potential, switching phenomena of various kinds and in several materials has been a subject of active study. While in general, switching may be defined as the action of going from one impedance state to another, in the present context, we are interested in the phenomena in which there can be two or more current states for a given voltage or two or more voltage states for a given current intervened by a region of negative (incremental) resistance. Switching has been observed in a variety of substances like chalcogenides of transition metals,¹ semiconducting glasses,² pn junctions³ and in bulk semiconductors⁴. But there does not seem to be any work relating to switching in MOS structures so far. This paper reports some experimental observations on electrical switching in the Metal-Oxide-Semiconductor system formed by Au, SiO₂, SiC (p type).

II. EXPERIMENTAL

1. Device fabrication

Normal SiC crystals from the Acheson furnace have a natural oxide layer. Crystals obtained from special furnace with inert gas, are free from oxide but an oxide layer can be formed. Crystals with both the naturally grown oxide layers and specially grown oxide layers have been used for the present investigation.

11. Oxidation procedure

Mechanically and chemically polished SiC crystals were oxidised in wet oxygen ambient at 1200°C in an

as much as 100-200%.

III. DISCUSSION

From the experimental observations, it appears that any model for describing the switching should involve the pn junction caused by the inversion layer, the oxide and some mechanism for transport of carriers through the nominally insulating oxide layer. Examination of the literature shows about five models for various types of switching, involving in turn (a). Avalanche multiplication across a thin oxide layer due to tunneling⁵, (b). Change of carrier capture cross section with injection level³, (c). Intervalley transfer of electrons⁴, (d). possibility of tunnelling into the impurity states under favourable conditions⁶, (e). phase transformation in the oxide layer due to heating effects⁷. While most of the models are inadequate to explain the present observations for some reason or another, it appears likely that the model involving change of capture cross section, on account of change in injection level proposed by Berkovski and Kasymova³ for switching in Ge pn junctions with deep level impurities, comes nearest. This model relies upon the fact that rather pronounced changes in lifetime can take place with injection, with initial increase followed by a decrease, which is due to the different deep level capture centers being brought into action due to the Fermi level changes with injection. When the injection level corresponds to the increasing \mathcal{T}_p region, the voltage drop across the pn junction increases, due to which there is increased injection which in turn gives rise to further increase in \mathcal{T}_p and so on. This Avalanche type increase of carriers gives rise to negative resistance. Though most of the experimental observations are similar to that of Berkovski and Kasymova, in the present case the polarity is not favourable. Nevertheless switching

due to change of capture cross section cannot be ruled out. Further investigation is in progress.

REFERENCES

1. S.R.Ovshinsky; Phys. Rev. Letters. 21, 1450, 1968.
2. A.D.Pearson, et al; "Advances in Glass Technology", p.357, 1962.
3. P.M.Berkovski and R.S.Kasymova; Sov. Phys. Solid State. B, 1580, 1967.
4. J.B.Gunn; Solid State Commun. 1, 88, 1963.
5. K.L.Chopra; J. Appl. Phys. 36, 185, 1965.
6. T.W.Hickmott; J. Appl. Phys. 33, 2669, 1962.
7. H.Fitzsche; I.B.M. Journal of Research and Development. 13, 515, 1969.

DISCUSSION

Subrahmanyan

What is meant by negative capacitance.

T.M. Brinda

We have only said that the structure exhibits apparently negative capacitance values as obtained from the calibration formulae using the bridge dial values. We are yet to decisively interpret the behaviour. It may be that the structure shows inductive effect rather than capacitative effect in the holding voltage region.

RECOVERY OF HIGH RESISTANCE IN THIN Al_2O_3 FILMS.

H.N.K. Sharma, A.K. Mathur, I.B. Bhattacharya and
D.L. Bhattacharya. Department of Physics, Banaras
Hindu University, Varanasi - 5, U.P.

I. INTRODUCTION

Conduction in a metal-insulator-metal junction is a complicated process and can be via pinholes, metallic bridges, ionic conduction and also by other mechanisms⁽¹⁾. The current can also flow through the insulator by electron tunneling process if the thickness is $\leq 30 \text{ \AA}$.

Extensive studies on Al- Al_2O_3 -metal was made by Handy⁽²⁾ and other workers^(3, 4). Handy drew attention to the conclusion that both the electrodes interface and counter electrode interface exert a substantial influence on the tunneling characteristics. The present paper also confirms the above facts and in addition reports an observations on the delayed mechanisms of the recovery of high resistance in thin Al_2O_3 films.

II. EXPERIMENTAL.

Several Aluminium films were prepared by vacuum evaporative method. Samples of 99.99% pure aluminium were evaporated on to a cleaned glass surface at a pressure of 10^{-5} torr through a specially designed mask. The films were then oxidized by keeping it in an open furnace at 85°C for 12 hrs. Then gold counter electrodes were deposited at right angles to the oxidised aluminium films by vacuum evaporation. Indium solder was used for making ohmic contacts for the electrical connections. Experiments were performed at room temperature using the

four terminal methods.

Conduction through Al_2O_3 film starts at ~ 5 volts when the Al electrode is kept -ve. However the conduction is not found even at ~ 6.5 volts when Al electrode is kept +ve. Inelastic tunneling⁽⁵⁾ is observed as shown in fig.(1). After the conduction is established, the low voltage I - V characteristic is measured which shows a definite hysteresis effect. The I - V characteristic is found to follow Ohm's law apart from hysteresis as shown in fig. (2).

III. RESULTS

These experiments are preliminary to a long term project on electrical conduction in thin film sandwiches. From the above experiments it can be concluded that the conduction is predominantly due to tunneling as the thickness of the insulator is of the order of 20 \AA , since about $3 \times 10^7 \text{ v/cm}$ ⁽⁶⁾ is required for the conduction to be established through the oxide. The hysteresis effect observed in the I - V characteristic shows that in addition to tunneling there is a contribution to the total current by the impurities trapped in the insulator. Differences in the voltage of the establishment of conduction through the oxide may be due to work function differences of the electrodes and the inhomogeneity of the Al_2O_3 film at the electrodes contact.

The explanation of the recovery of high resistance can be given on the basis of phase transformation in the Al_2O_3 film. A.D. Pearson has already pointed out that some semipermanent phase change takes place in the amor-

phous films on heating and produces the memory phenomenon observed.

The above explanation given by him applies well in our case of delayed recovery in aluminium oxide which may be locally ordered than in his case of quick recovery in the case of semi-conducting glasses.

Further work in this aspect of tunneling is in progress.

REFERENCES

1. D. Meyerhofer and S.A. Ochs J.Appl. Phys 34, 2535 (1963).
2. R.M. Handy Phys. Rev. 126, 1966 (1962).
3. S.R. Pollack & C.E. Morris J.Appl. Phys. 35, 1503 (1964).
4. T.E. Hartman & J.S. Chivian Phys. Rev. 134A 1094 (1964).
5. R. Wolfe, C.J. Kriessman Applied Solid State Science Vol.I, Academic Press Newyork 1969, pp 365.
6. S. Paksver & K. Prathinichi J. Appl. Phys. 34, 711 (1963).
7. A.D. Pearson Proceedings of the Symposium on Semiconductor Effects in Amorphous Solids. Haliday Inn, Newyork, Newyork May 14 - 17 1969, North-Holland Publishing Company - Amsterdam 1970 pp. 9.

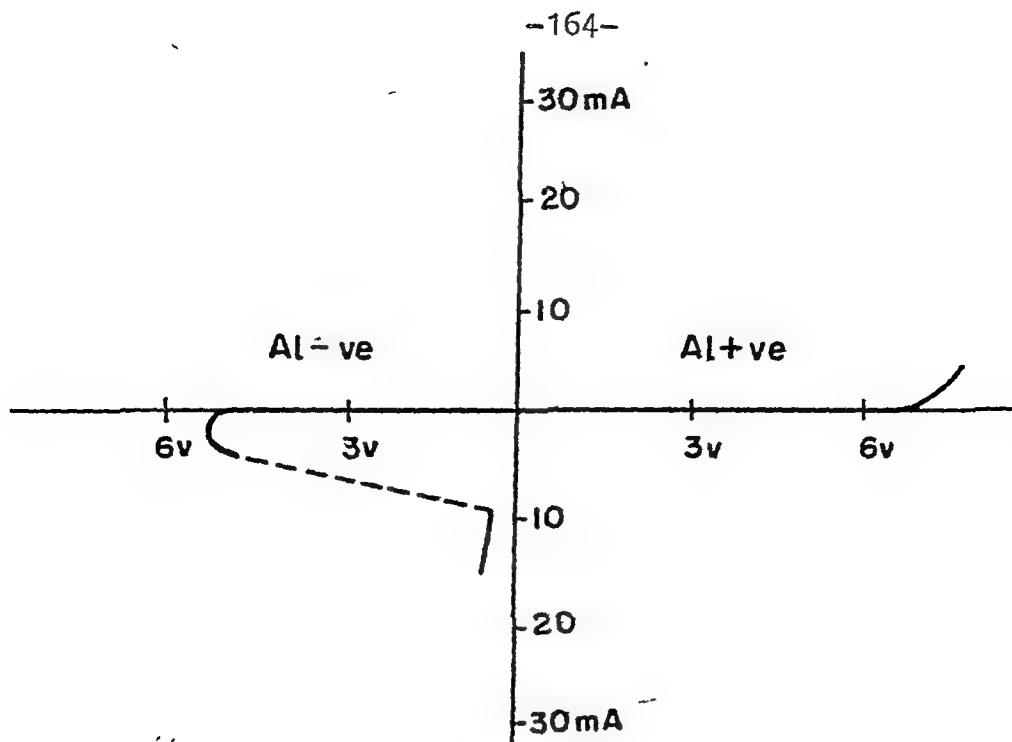


FIG.1

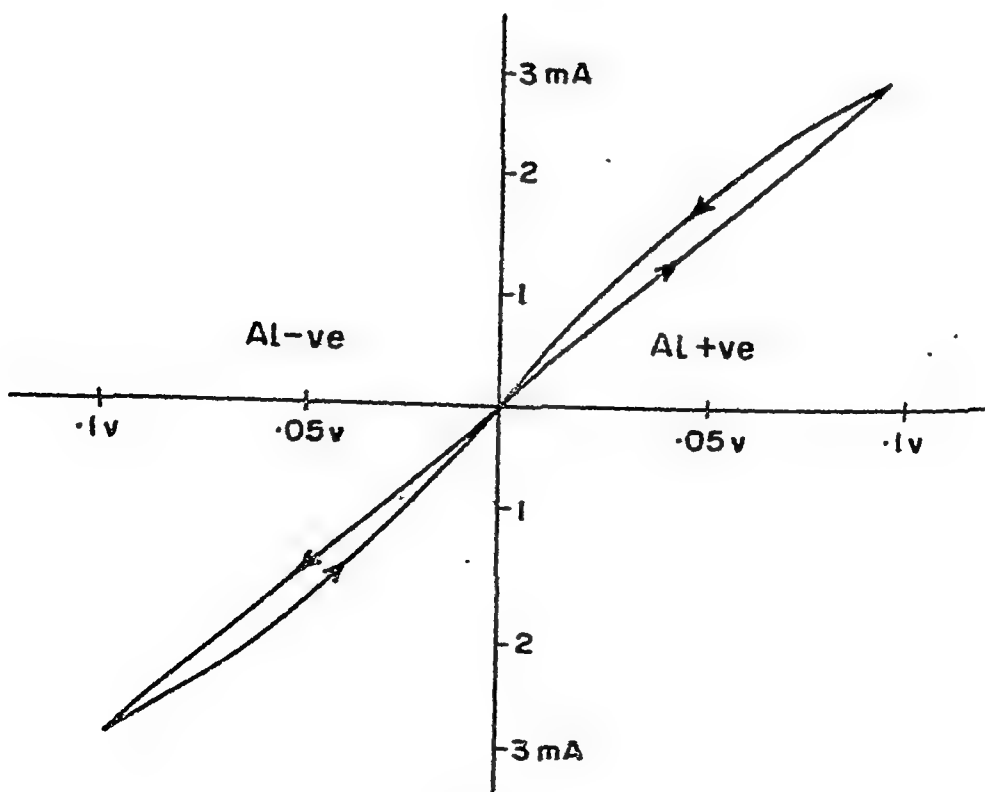


FIG.2

ELECTRICAL CONDUCTION IN SODIUM CHLORATE CRYSTALS

G. Ramasastry, K. Viswanatha Reddy and V.S. Murthy
Indian Institute of Technology, Madras-36.

I. INTRODUCTION

Sodium chlorate crystals are cubic belonging to the space group T^4 (P_{213})⁽¹⁾. The bonding between the sodium and the chlorate group is predominantly ionic.⁽²⁾ The dielectric constant,⁽³⁾ the coefficient of thermal expansion^(4,5) and the optical absorption in the long wave length edge of the fundamental electronic transition in the crystal⁽⁶⁾ all show anomalous increase above 130°C. The thermal defects that may be produced at the elevated temperatures could be responsible for such anomalous behaviour. They should also contribute to electrical transport as in other ionic crystals. A study of the variation of electrical conductivity with temperature should throw more light on the nature and the concentration of these defects.

II. EXPERIMENTAL

Single crystals of NaClO_3 are grown from solution by slow evaporation. The material was supplied by the Central Electrochemical Research Institute, Karaikudi and is labelled as extra pure. Analysis by atomic absorption spectrophotometer (Perkin-Elmer double beam instrument) gave the following cationic impurities; Ca 13.5 ppm, Fe 4 ppm, Cu 1 ppm, Pb and Mn < 1 ppm. The crystals could be doped with barium by adding a small amount of $\text{Ba}(\text{ClO}_3)_2 \cdot \text{H}_2\text{O}$ to the saturated solution at the time of crystal growing.

D.C. conductivity is measured using the G.R.1230-A D.C. voltmeter. The measured resistance of the crystal decreases with the increase of the applied D.C. voltage and reaches a nearly constant value for sufficiently large voltages (about 40V) across the crystal. The meter readings are noted within a few seconds of connecting the battery lead when the pointer comes to a temporary pause. The crystal was short-circuited in between the measurements. The effects of polarisation could be reduced considerably by this method. The crystal was kept at least for 15 minutes at each temperature which could be measured to an accuracy of $\pm 1^{\circ}\text{C}$. The thermo emfs developed between the crystal surface and the electrode foil are less than $10\mu\text{V}$.

III. RESULTS

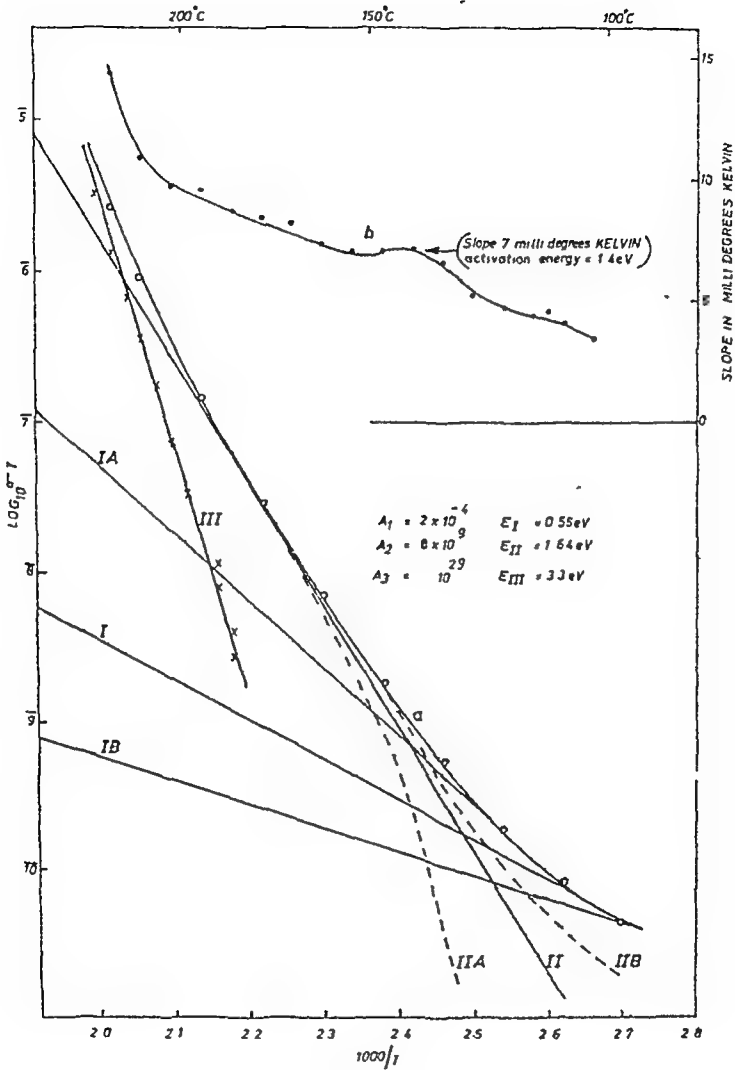
A typical $\log \sigma T$ vs $1000/T$ plot for NaClO_3 crystal is shown in figure 1 as curve 'a'. The slope of the curve varies continuously from 14 to 4 milli degrees Kelvin which is shown as curve 'b' in the same figure. It is clear that there is considerable overlapping of the contributions of the conductivity terms corresponding to the extrinsic and intrinsic regions. The experimental curve is analysed by a special graphical method to give

$$\sigma T = 2 \times 10^{-4} e^{\frac{-0.55}{KT}} + 8 \times 10^{-9} e^{\frac{-1.64}{KT}} + 10^{-29} e^{\frac{-3.5}{KT}} \quad (1)$$

The $\log \sigma$ vs T values calculated using the above equation are shown in figure 1 as open circles. Addition of divalent impurity Ba^{2+} increased the conductivity below $150^\circ C$ which may be taken as the intrinsic region. The enhancement can be due to either the increase of positive ion vacancies or negative ion interstitials formed as charge compensators for the divalent positive ion. The large size and the high polarisability precludes the interstitial motion of the chlorate ion. Hence the electrical transport is by the migration of positive ion vacancies. The activation energy of 0.55 ± 0.02 eV for the low temperature region is thus to be considered as the jump activation energy for the positive ion vacancy.

The intrinsic conduction is evident above $130^\circ C$. The slope of 1.64 ± 0.04 eV of the second line in fig. 1 can then be considered to correspond to the jump activation energy plus half the formation energy of intrinsic defects ($E_j + E_s/2$). This gives 2.18 eV for E_s , the energy for the formation of intrinsic defects which are most likely to be the Schottky type.

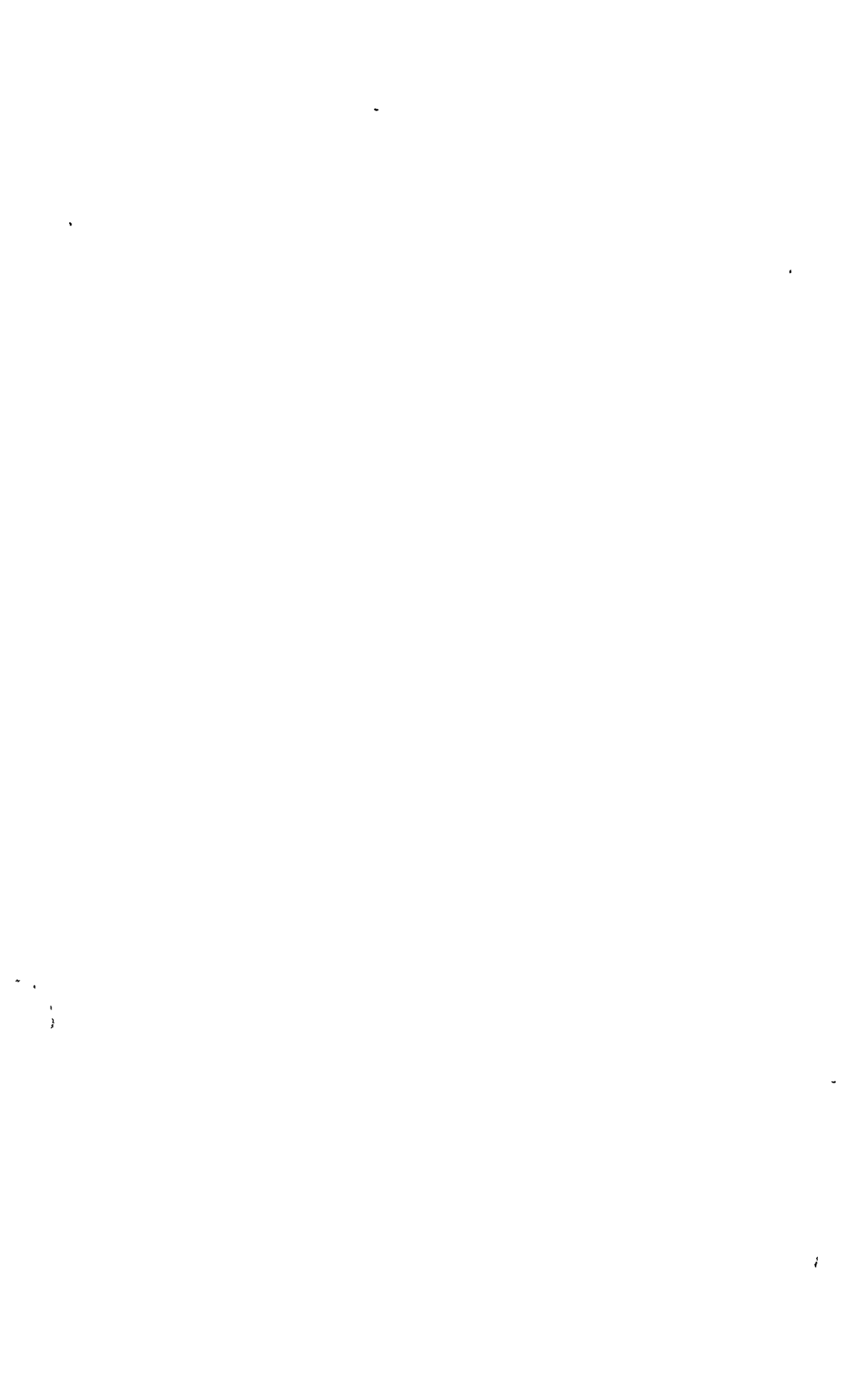
At temperatures above $200^\circ C$ there is a higher rate of rise of conductivity which necessitated the $\log \sigma$ vs $1000/T$ graph to be analysed into three straight lines with considerable overlapping effects. The cause for the excess conductivity in region III may be due to the decomposition products.



GRAPHICAL ANALYSIS OF THE EXPERIMENTAL $\log \sigma T$ VS $1000/T$ CURVE. THE CONTINUOUS CURVE 'a' REPRESENTS THE EXPERIMENTAL DATA. CURVE 'b' SHOWS THE VARIATION OF THE SLOPE AT DIFFERENT POINTS OF THE CURVE 'a'. THE OPEN CIRCLES ARE THE CALCULATED VALUES USING EQUATION 1.

REFERENCES

1. G.N. Ramachandran and K.S. Chandrasekharan; Acta. Cryst., 10, 671 (1957)
2. R. Bersehn; J. Chem. Phys. 29, 326 (1958)
3. W.P. Mason; Phys. Rev. 70, 529 (1946)
4. S.S. Sharma; Proc. Ind. Acad. Sci. 31 A, 83 (1950)
5. V.T. Deshpande and V.M. Mudholkar; Acta. Cryst., 13 483 (1960)
6. S.B.S. Sastry, R.B. Tripathi and C. Ramaswamy J.Phys Chem. Solids (to be published)



ELECTRICAL CONDUCTIVITY OF CESIUM SULPHATE
CRYSTALS

C. Ramasastry and B.S.V.S.R. Acharyulu

Solid State Physics Laboratory, Department of Physics
Indian Institute of Technology, Madras-36I. INTRODUCTION

The ionic conductivity in alkali and silver halide crystals has been extensively investigated by several authors. But non-cubic crystals have not been studied in any detail because of anisotropy of electrical conduction. However, in this laboratory a trigonal crystal, NaK_2O_3 , was studied by Ramasastry and Kurti⁽¹⁾. The sulphates of Thallium, Potassium, Caesium and Rubidium which belong to the orthorhombic system are being currently studied by the authors. The work on Thallous sulphate⁽²⁾ and Potassium sulphate⁽³⁾ has already been published and the present paper deals with the conductivity of Caesium sulphate crystals.

II. EXPERIMENTAL

The crystals were grown from solution by slow evaporation at room temperature using B.D.H. analar material. They grow in the form of tablets with large easily identifiable (010) faces. Clear crystals of about $6 \times 6 \times 2$ mm were used for the measurements after being polished on moistened chamois leather. D.C. methods were employed and the apparatus is same as the one described by Ramasastry and Kurti⁽¹⁾. The brass parts were however replaced by stainless steel ones to reduce the oxidation effects at

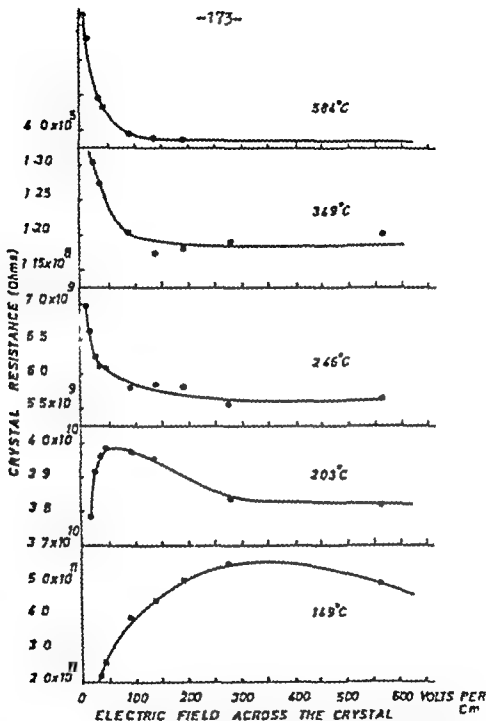
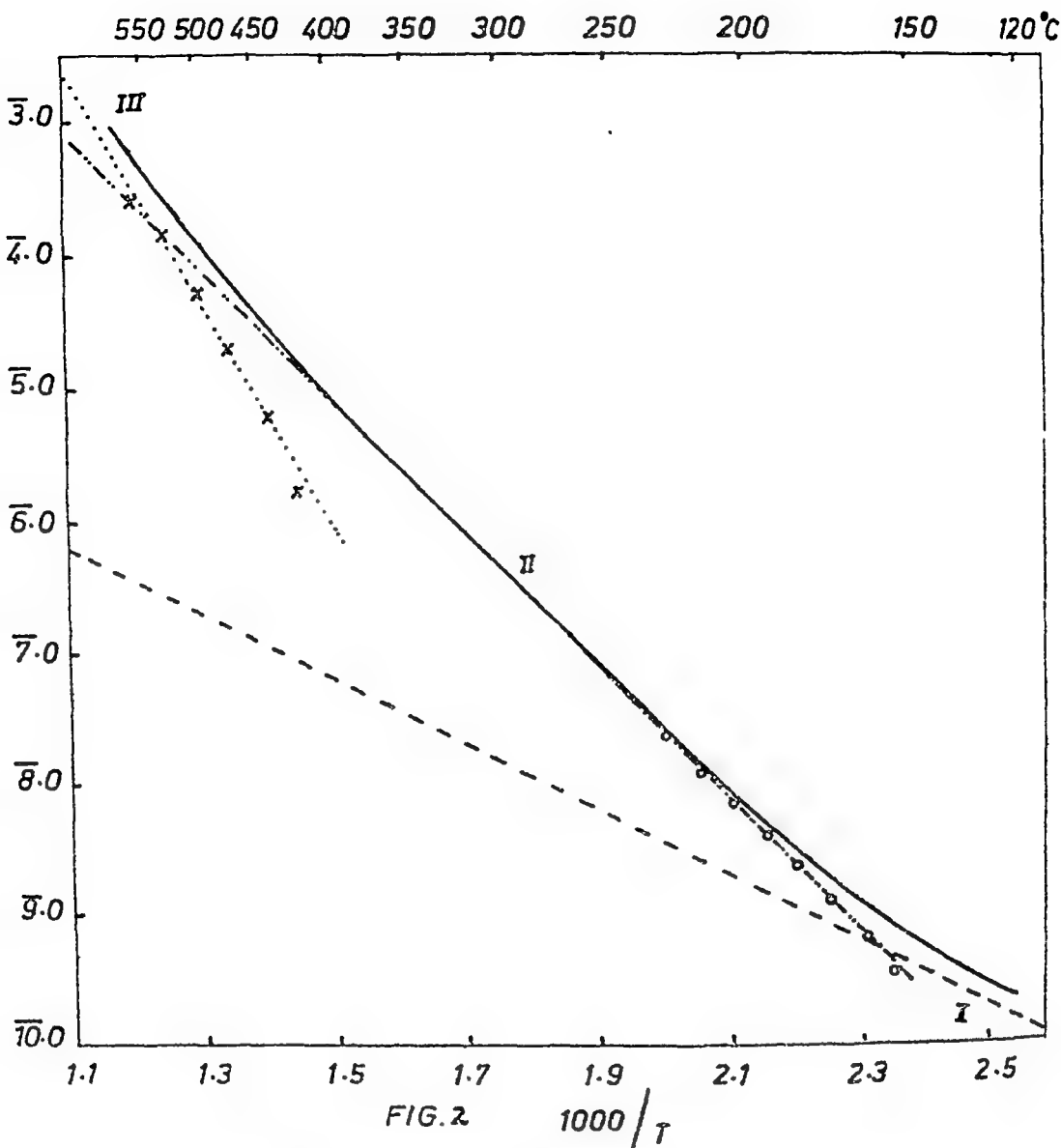


FIG 1

DEPENDENCE OF D.C. ELECTRIC RESISTANCE OF Cs_2SO_4 CRYSTAL, WITH THE ELECTRIC FIELD ACROSS THE CRYSTAL RESISTANCES CORRESPONDING TO AN ELECTRIC FIELD OF 570V/cm ARE PLOTTED IN FIG 2



ELECTRICAL CONDUCTIVITY OF Cs_2SO_4 CRYSTALS
 THE EXPERIMENTAL CURVE IS RESOLVED INTO
 THREE STRAIGHT LINES OF SLOPES .53eV (100-200°C),
 1.03eV (200-450°C) AND $\approx 2.0\text{eV}$ (450-570°C), GIVING
 A JUMP ACTIVATION ENERGY OF .53eV, AND 1.0eV
 AS THE ENERGY OF FORMATION OF A DEFECT PAIR.

V. REFERENCES

-175-

1. Ramasastry and Kurti; Proc. Roy. Soc. A 175, 441-455 (1941).
2. C. Ramasastry and B.S.J.S.R. Acharyulu, "Proceedings of the Indian Conference on Radiation Effects" Robert MacLehose and Co., Calcutta (1970) P.61-63.
3. C. Ramasastry, Y.V.G.S. Jrti and B.S.R. Acharyulu, "Modern Aspects of Soil Chemistry", Plenum Publishing Corporation, New York, (1970) P.377-390.

ELECTRICAL CONDUCTIVITY OF NaI(Tl)

S. Muralidhara Rao and R.Y. Deshpande

Technical Physics Division

Bhabha Atomic Research Centre, Bombay-85

I. INTRODUCTION

Thallium activated Sodium Iodide crystals are extensively used in γ -ray spectroscopy work. Several authors have carried out studies on the scintillation mechanism in these crystals and the scintillation response is generally related to the concentration of Tl added in the melt during the crystal growth ^(1,4). However, there is an uncertainty as regards the actual active concentration of the activator which really governs the scintillation response. In fact, even the distribution of Tl in the volume of the crystal can significantly affect the performance. In our studies we have frequently noted the effects of non-uniform distribution of Tl in the crystals. It is observed that Thallous Iodide added to the melt does not get uniformly distributed in the crystal and therefore what is seen is an average effect of many processes. As such, the correlation of scintillation response with Tl concentration leaves some ambiguity in the interpretation of the data. It is therefore felt that additional information about these crystals is necessary. One of the independent physical parameters that can provide information regarding the distribution and behaviour of the impurity in the lattice is ionic conductivity. The present work is aimed at studying the ionic conductivity of Sodium Iodide crystals—'pure' as well as doped with different concentrations of TlI.

migration of cation vacancy in the crystal.

The ratio of conductivities as measured in the extrinsic range is found to be 0.75:1.2:2.8. As against this the ratio of Tl added in the melt is 1:3:5, showing that there is no one-to-one correspondence between the added impurity concentration and observed conductivities. This could be either due to the non-uniform distribution of the impurity or a different vacancy creation mechanism (e.g. creation of multiple charge states) at higher Tl concentrations. Further experimental work is required to identify the process. It may be indicated that if the latter mechanism is true the temperature dependence of the scintillation performance could be directly related to this process.

REFERENCES

1. L.B. Murrey and A. Meyer; Phys. Rev. 122, 815 (1961)
2. R. Gilbert Kaufman et.al. I.E.E. Trans. Nucl. Science NS-17, 82 (1970)
3. J.A. Harshaw, H.C. Kramers, et.al U.S. Atomic Energy Commission Report NYO, 1577 (2952)
4. G.V. Ramamurthy and G.K. Bhide, Ind. J. Pure & Appl. Phys. 4, 24 (1966)
5. E.E. Schneider, Disc. Faraday Soc. No.31, 176 (1931)

DISCUSSION

S.K. Joshi

Will the tunneling effect due to size difference contribute to mobility of your system?

S. Muralidhara Rao

It may not be possible to talk of tunneling in the case of ionic crystals.

ELECTRICAL CONDUCTIVITY OF ALPHA-MnS POWDERED SAMPLES

Risal Singh

Solid State Physics Laboratory, DELHI-7.

I. INTRODUCTION

The electrical conductivity of some of analogous compounds was first studied qualitatively by Szwed¹ in the late thirties. However, little was known at that time about the structure of these materials and their conduction mechanism. Also, to illustrate the transport behaviour of mixed valence semiconductors, Welke² et al² reported their measurements on thermoelectric power and electrical resistivity of several compounds of the $\text{Li}_x\text{Mn}_{1-x}\text{S}$ system with rock salt structure. Although a better understanding of still vague conduction mechanism of these materials the need of extending the work on pure specimens was realized by the present author and the measurements of electrical conductivity on pure alpha-MnS pressed pellets are reported here.

II. EXPERIMENTAL

The alpha-MnS powder was prepared from anhydrous $\text{MnCl}_2 \cdot 4\text{H}_2\text{O}$ by the method adopted by Brancifort and Lindsay³. The resulting sulphide powder was dried and oxygen contamination was eliminated by passing dry H_2S over it. Finally, the powder was heated in vacuum at 1000°C to remove the excess sulphur. The powder was pressed into circular pellets using hydraulic pressure of 15 tonnes/sq.inch. The density of these pellets was found to be about 75% of the single crystal density and did not change noticeably after sintering. One pellet, designated as

sample P, was sintered in air at 1100°C for 13 hours and another one, designated as sample Q was sintered in vacuum at the same temperature. For measuring resistivity the flat surfaces of the samples were painted with conducting platinum paste and then the electrical contacts were made with spring loaded platinum electrodes. Pt_(Pt+13% Rh) thermocouples attached to the platinum electrodes were used to measure temperature. Resistivity measurements were made using Philips RCL bridge PP 9030 and Orion Ketl electrometer TR-1501.

III. RESULTS AND DISCUSSION

Curves A and B in Fig.1 show the conductivity of sample P in the air atmosphere with increasing and decreasing temperature respectively and the curves F and G are similar curves for the sample Q. The $\log \sigma$ vs. $1/T$ plots for both the samples consist of two regions separated by a knee at about 325°C. The activation energy E was calculated from each curve in the high temperature region using the relation $\sigma = A \cdot \exp(E/KT)$ and the values are given in Table I.

Table I

Sample	Curve	Activation Energy E (ev)
P	A	0.44
	B	0.34
Q	F	0.89
	G	1.53

The lower temperature region of the curves belongs to the defect-controlled region and possible sources of conductivity in this region are (a) the defect

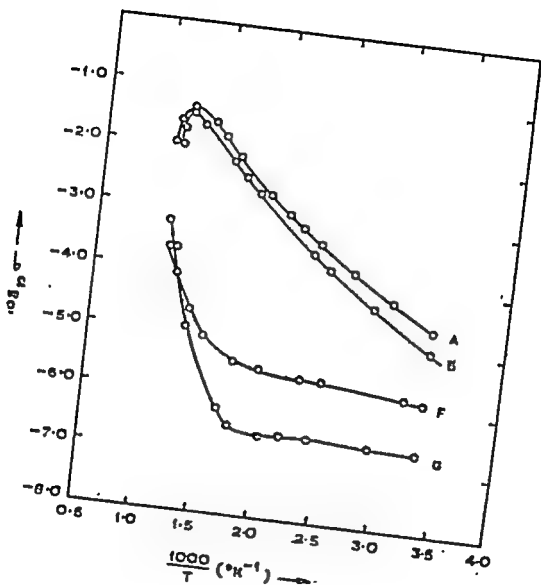


FIG. 1

structure of the host power, (b) impurities, (c) an intrinsic reaction, and (d) ionic conductivity. The temperature at the knee is sufficient to ionize some of the metal ion impurities. The activation energies calculated from the high temperature region of the curves varies considerably not only from sample to sample but also for the sample when the resistivity measurements are made with increasing and decreasing temperature. This promptly suggests that impurities still play a dominant role in the conduction mechanism. From Fig.1 it is clear that in each case the conductivity of sample P is larger than the conductivity of sample Q. This is presumably due to stoichiometric excess of oxygen ion in sample P. Each oxygen ion creates one Mn^{2+} ion vacancy. Also, as the starting material contained some monovalent metal impurities and MnS, like NiO and CoO is a mixed valence semiconductor, it causes the formation of Mn^{3+} ions. The additional positive charge on Mn^{3+} (a hole) serves as the carrier for the conduction process. The exponential dependence of resistivity on temperature and the absence of detectable Hall effect seems to indicate that it is one of the low mobility semiconductors in which 'hopping' mechanism of conduction operates. The turn off of the curves for sample P at still higher temperatures shows that at these temperatures the available acceptor sites for holes get exhausted. The present results are much of a preliminary nature and, therefore, no decisive conclusion can be taken about the way of conduction process until they are supplemented by data on other transport properties of the material.

REFERENCES

1. C.F. Squire, Phys. Rev. 56, 980 (1939).
2. R.R. Heikes, A.A. Maradudin and H.C. Miller, Ann. Phys. (Paris) 8, 733 (1963).
3. J.J. Banerwitz and R. Lindsay, Phys. Rev., 104, 318 (1956).

DISCUSSION

H.V. Keer

How far is the hopping mechanism valid in α -MnS which is expected to show a relatively considerable covalent character compared to MnO, CoO, BiO etc?

Rical Singh

I agree that α -MnS is more covalent than FeO, CoO and other similar compounds. However, from the analogy of electrical conductivity results of α -MnS with these compound and undetectable Hall effect leads us to propose that hopping mechanism is the ~~most~~ ^{most} possible. But I feel that more experimental work on transport properties of this compound is necessary before the conduction mechanism is established.

S.K. Joshi

1) Did you compare your ~~experimental results~~ ^{experimental results} with those on crystalline α -MnS?

2) What was the ~~purpose~~ ^{purpose} of this?

Risal Singh

1) Result on crystals are not yet available to my knowledge.

2) We did not make measurement of the particle size.

LOW TEMPERATURE ELECTRICAL CONDUCTIVITY OF MnSe-CoSe SYSTEM

V.N. Kamat Lalal, H.V. Kser and A.B. Biswas
Department of Chemistry, Indian Institute of
Technology, Powai, Bombay-76 (India)

I. INTRODUCTION

Electrical behaviour of transition metal oxides and chalcogenides are of considerable interest both from the theoretical and the applied point of view. It is the purpose of this paper to present results of a study on the electrical properties of the solid solutions of metallic, hexagonal (NiAs-type) CoSe and semiconducting, cubic (NaCl-type) MnSe and to show that the metal \rightarrow semiconductor transitions observed here are of different nature from those found in oxides of Ti and V.

II. EXPERIMENTAL

Samples were prepared by solid state reactions between the components at about 700°C in evacuated ($\sim 10^{-6}$ mm.Hg) sealed silica tubes. Lattice parameters were determined from an analysis of x-ray powder diffraction data (Table 1). Electrical conductivity measurements under low pressures ($\sim 10^{-6}$ mm.Hg) were made in the temperature range $80-350^{\circ}\text{K}$ (Fig.1).

TABLE - 1

Composition	Symmetry	Lattice constants Å ⁰	Metal-metal distance Å ⁰
Mn _{1.0} Co _{0.0} Se	Cubic(NaCl type)	a = 5.46	3.86
Mn _{0.8} Co _{0.2} Se	-do-	a = 5.45	3.85
Mn _{0.6} Co _{0.4} Se	-do-	a = 5.44	3.84
Mn _{0.4} Co _{0.6} Se	Hexagonal (NiAs type)	a = 3.64; c = 5.30	2.65
Mn _{0.2} Co _{0.8} Se	-do-	a = 3.63; c = 5.29	2.645
Mn _{0.0} Co _{1.0} Se	-do-	a = 3.62; c = 5.285	2.64

III. RESULTS AND DISCUSSION

It will be seen from Fig.1 that the temperature coefficient of conductivity is negative in the case of CoSe and positive in the case of MnSe. Therefore it indicates that there is a gradual transition from metallic to semiconducting behaviour as one goes from CoSe to MnSe. This may be explained on the basis of the structural data as follows:-

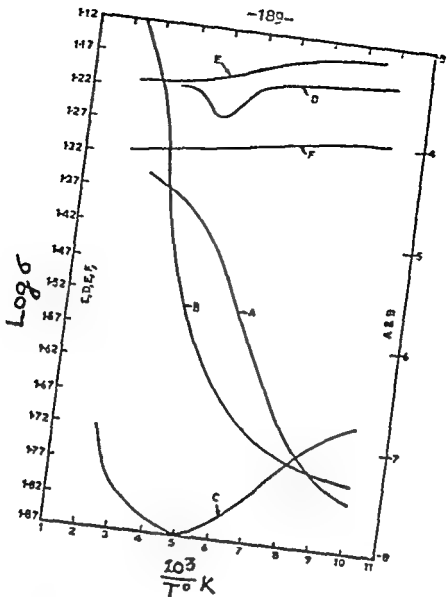


Fig.1 : electrical conductivity vs. Temperature
for the $Mn_x Co_{1-x} Se$ system.

- A - $Mn_{1.0}Co_{0.0}Se$ cubic (NaCl type)
- B - $Mn_{0.8}Co_{0.2}Se$ -do-
- C - $Mn_{0.6}Co_{0.4}Se$ -do-
- D - $Mn_{0.5}Co_{0.5}Se$ hexagonal (Kiaz type)
- E - $Mn_{0.2}Co_{0.8}Se$ -do-
- F - $Mn_{0.0}Co_{1.0}Se$ -do-

In the hexagonal CoSe, the metal-metal distance is 2.64 \AA while in cubic MnSe it is 3.86 \AA at room temperature. For the remaining solid solutions, the distances are intermediate. The shorter bond length results in metallic behaviour while the increasing separation introduces an energy gap. An analogous argument has been put forward by Dudkin⁽¹⁾ who predicted semiconductivity beyond a certain value of the ratio $\frac{[(T-T_c) - dT] \times 100}{(T - T_c)}$ where $(T-T_c)$ is the closest distance of approach of transition metal atoms and dT is the diameter of the transition metal for the coordination occurring in the compound.

For, $\text{Co}_{0.6}\text{Mn}_{0.4}\text{Se}$ and $\text{Co}_{0.4}\text{Mn}_{0.6}\text{Se}$ metal \rightarrow semiconductor transition has been observed at 208° and 202°K respectively. On lowering the temperature, presumably there is a relatively large contraction along the c-axis, which results in a direct metal-metal bond. However, low temperature x-ray studies would be required to confirm this. The above results are similar to those obtained⁽²⁾ for the MnSe-MnTe system.

At this juncture one may contrast the transition observed here with those found in oxides such as VO_2 , Ti_2O_3 , etc. These oxides, which are metallic at room temperature exhibit semiconducting nature on cooling to low temperatures. This is generally caused by magnetic

ordering which introduces an energy gap, resulting in semiconductivity.

REFERENCES

1. L.D. Dudkin, Soviet Solid State Physics 2, 371 (1961)
2. V.N. Kamat Lalal, H.V. Keer and A.B. Biswas (unpublished work).

DISCUSSION

S.K. Jothi

What is the mechanism which could explain the transition (metal - non-metal)?

H.V. Keer

On cooling semiconducting $\text{MnO}_{0.60} \text{Co}_{0.40} \text{Se}$ and $\text{Mn}_{0.40} \text{Co}_{0.60} \text{Se}$ samples to low temperatures, the metal-metal distance decreases and at the transition temperature overlap occurs, resulting in metallic conductivity. This mechanism is different from that suggested for semi-conductor-metal transitions observed in oxides of titanium and vanadium.

STUDY ON THE LIFETIME OF THE PHOTOELECTRETS OF ZnS

P.K.C. Pillai and K.G. Balakrishnan
 Indian Institute of Technology, Delhi
 New Delhi-29

I. INTRODUCTION

A "Photoelectret"⁽¹⁾ is an electrically polarised dielectric material, that has been formed by the simultaneous application of irradiation and electric field. It is found that the lifetime of these photoelectrets is very small in comparison with that of thermoelectrets. In this paper two experimental techniques have been developed which prolong this lifetime; investigations being carried out on polycrystalline ZnS (99.9% pure).

II. EXPERIMENTAL

The apparatus used for these investigations is shown in fig.1. The ZnS is prepared by the method followed by S.K. Aggarwal, R C Tyagi and H.K. Sehgal⁽²⁾. The photoelectret is prepared as follows: The sample in the form of a pellet of size 1 sq.cm. x 1 mm. is placed in between the electrodes a and b of the gadget. Care is taken to avoid air gap between the electrode and the surface of the sample. Electric field is applied across the terminals keeping the negative terminal illuminated. This procedure gives the same type of internal polarization described by Kallmann⁽³⁾ and it is found that the charge is retained for several days.

After the polarization process the sample is reilluminated with the same radiation and depolarisation current is measured with the help of an electrometer amplifier EA 511A, supplied by the Electronics Corporation of India Ltd. The depolarization current

studies have been performed with and without illuminating the sample, during polarization so as to eliminate the effects due to photo-conduction, dark polarization, etc. The difference between the two gives one an idea of the carriers responsible for the electret effect.

In order to increase the lifetime of the photoelectrets, two methods have been developed.

Method 1 : By applying a negative field.

The sample is polarized by the simultaneous application of the field and irradiation for five minutes. Then the field is switched off and the photoelectret is depolarized for ten minutes. At this moment a field equal in magnitude as that of the polarizing field, but in the reverse direction, is applied to the sample for a short time of 15 seconds.

Method 2 : Photo-dark polarization.

The sample is polarized by the simultaneous application of electric field and illumination for five minutes. Then the illumination is switched off while the field is continued for another five minutes. The experiments are repeated with different voltages (90 - 900v).

III. RESULTS

Just after the application of the reverse field, when the sample is depolarized, the current first starts flowing in the negative direction for some time (fig. 3), then becomes zero, and afterwards starts flowing in the positive direction in the case of high polarizing voltages. It can be seen from fig. 2 and table 1

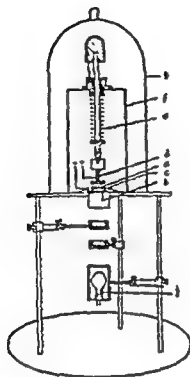


FIG. 1

Fig. 1 : Gadget used for photoelectric studies

- (a) plane electrode, (b) perforated electrode, (c) crystal,
(d) outer terminal of (a), (e) spring arrangement,
(f) metallic tube, (g) glass jar, (j) lamp.

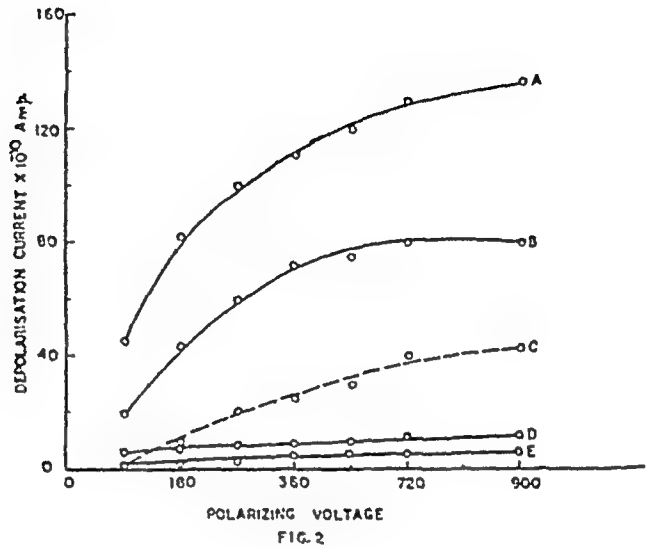


Fig. 2 : Variation of depolarization current with polarizing voltages

A and B represent measurements just after photo-dark polarization and photo-polarization respectively.

C, D and E represent measurements after 30 minutes of depolarization for reverse polarization, photo-dark polarization and photo-polarization respectively.

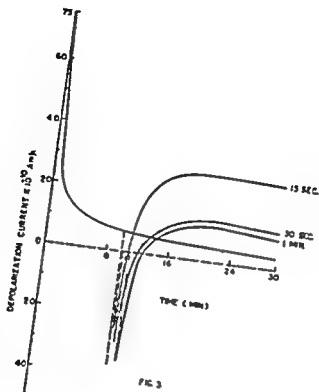


FIG. 3

Fig. 3 : Variation of depolarization current with time when the negative field is applied after 10 minutes of depolarization, along with the variation when there is no reversal of field, for the direct and reverse polarizing voltage of 540V. Also shows how the depolarization current changes for different time of reverse field application.

that this process increases the lifetime of the photoelectrets considerably. After photo-dark polarization process, it is again found that the depolarization current decays very slowly which in turn increases its lifetime (fig. 2).

When a photoconducting material is illuminated with a radiation of frequency ν , electrons and holes are produced provided the energy gap $E = h\nu$. Simultaneously if a d.c. voltage is applied across the sample these holes and electrons move to negative and positive terminals respectively and get trapped in electron and hole centres, giving rise to surface charge. In the case of higher field of 720 or 900V the number of carriers created due to direct and reverse polarization will be larger. Hence while reilluminating more number of old carriers (Na and Pb) are trying to come out, but faces a much higher repelling field of new carriers (Na and Pa). Hence Na and Pb remain trapped giving a much more stability of charge for the electrets. With lower field this stability can be achieved if the negative voltage is either applied for a longer time or is larger than the polarizing voltage. In the presence of an additional field the potential barrier is lowered and more number of carriers get trapped in deeper levels, leaving a very few carriers at the edge of the energy gap. Just after reillumination, these few carriers on the edge of band gap are ejected out to the respective bands to give rise to initial current. After one or two minutes the contribution to the current comes from carriers which are well inside the forbidden gap and it takes a longer time to come out of the trap.

TABLE I

Polarizing voltage		90V	180V	270V	360V	540V	900V
Depolarisation current (amp $\times 10^{-10}$)							
	After						
	24 hrs	0	0	1	2	3	4
Without any additional process	48 hrs	0	0	0	0	1	1
	72 hrs	0	0	0	0	0	0
	After -ve field appli- cation for 15 seconds						
	24 hrs	0	2	3.2	8	20	18
	48 hrs	4	6	7	8	12	13
	72 hrs	3	4	5	6	8	
	after photo- dark polariza- tion						
	24 hrs	0	1.5	3	5	15	10
	48 hrs	2.2	3	4.2	7	11	13
	72 hrs	2.5	4	5	6	9	10

REFERENCES

1. G. Nadjshakov: Physik 2, 226 (1938).
2. S.I. Aggarwal, R.C. Tyagi and P.K. Sehgal: Research and Industry (India) 14, 60 (1960)
3. Kallmar: Phys. Rev. 97, 1526 (1955 March).

DISCUSSION

M.R. Bhide

What is the method used for studying the dielectric polarisation.

P.K.C. Pillai

By discharging the electret.

M.R. Bhiday

Have you tried any non-destructive method for this study so that you could get a better idea of lifetime.

P.K.C. Pillai

No.

M.R. Bhiday

This non-destructive method should be developed for better understanding of the phenomena.

EFFECT OF MAGNETIC FIELD ON THE DECAY
CHARACTERISTICS OF PHOSPHORS

S.E. Pawar and A.V. Farlikar
Materials Science Laboratory, Physics Department
Shivaji University, Kolhapur-4.

I. INTRODUCTION:

The decay characteristics of phosphors are known to be influenced by several factors, such as the activator concentration, temperature, time and energy of excitation etc. However, very little attention has been given to the magnetic behaviour of phosphors. Phosphorescence is a property resulting from trapping of electrons. A change in the magnetic susceptibility χ after excitation has been observed by Rupp⁽¹⁾, and is explained⁽²⁾ as due to the difference in the magnetic character of unexcited and trapped electrons. Recently a variation of χ with magnetic field has been reported⁽³⁾, and in continuation of this work, the present investigation has been carried out to study the possible effects of the magnetic field on the decay behaviour of CaS-Bi phosphors.

II. EXPERIMENTAL:

Three different samples of CaS-Bi phosphors (see Table-I) were prepared by the method described by Bhavalkar⁽⁴⁾. The excitation was done with a Philips 125W UV Lamp and the decay was studied using RCA 931 A photo-multiplier tube and a sensitive rapid photoreter G II. Maximum D.C. field obtainable was 15000 Oe. The A.C. field was provided by the 6 KW Telecom induction heater.

III. RESULTS:

Visual observations showed that the decay was markedly affected by the presence of both D.C. and A.C. magnetic fields. In certain cases the decay time increased by approximately three times when placed in a 15000 Oe D.C. field. The plots of intensity I versus time t in both cases, that is with and without magnetic field, for all the samples shown in fig.1, are hyperbolic.

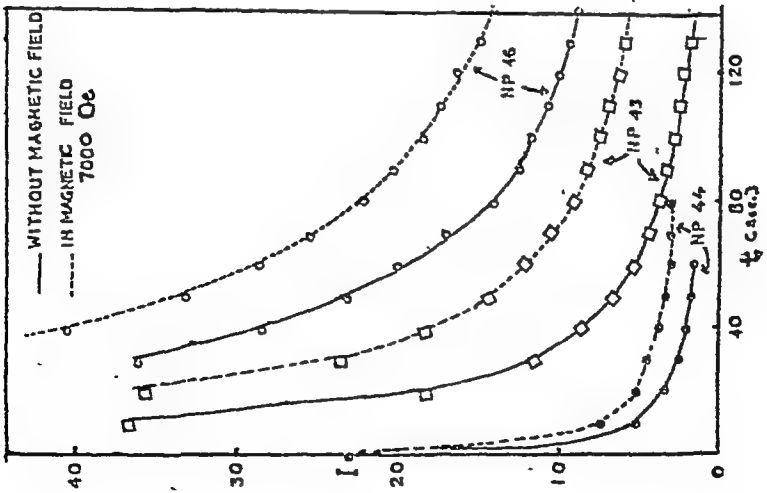


Fig. 1

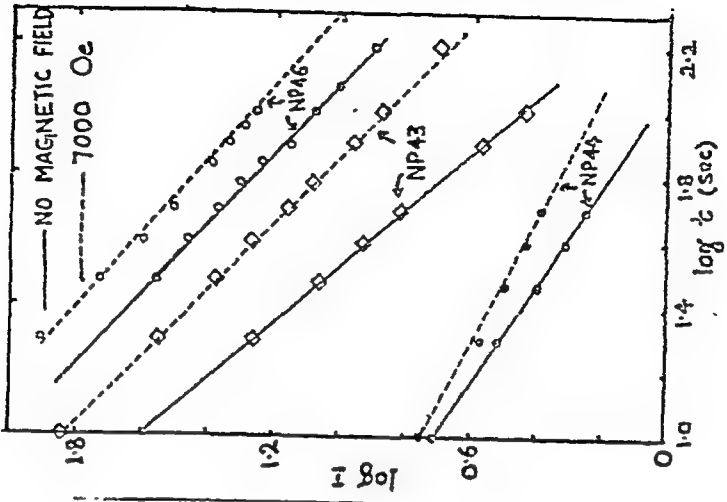


Fig. 2

The log I against log t plots are almost straight li. as shown in fig.2.

Following Randall and Wilkins⁽⁵⁾ the trap depths were calculated and are shown in Table-I. The decay constants b for each curve were determined from fig.2.

TABLE-I : DECAY CONSTANT(b) AND TRAP DEPTH E(ev)

Sr. No.	Sample No.	% of Bi in CaS	Decay constant b with-out magnetic field.	b with magnetic field.	E with-out magnetic field.	E with magnetic field.
1.	NP 44	0	0.6471	0.4864	0.6131	0.621
2.	NP 43	.0599	1.1450	0.9729	0.538	0.602
3.	NP 48	.012	0.6212	0.5121	0.614	0.619

IV. DISCUSSION:

The curves of fig.1 show that magnetic field has the effect of prolonging the phosphorescence decay. Both, the decay constant and the trap depth are affected by the magnetic field. These results are consistant with the variation of χ with the magnetic field⁽³⁾ mentioned earlier. The reason why the phosphorescence is prolonged may lie on the effect of applied field on the trap distribution.

V. ACKNOWLEDGEMENT:

The authors would like to thank their colleagues R.D.Lavangar, and C.S.Shalgaonkar for many discussions.

REFERENCES

1. E. Rupp, Ann.D. Physik 78, 505, (1925).
2. P.D.Johnson, and F.E.Williams, J.Chem.Phys., 17, 435, (1949).
3. S.H.Pavar, and A.V.Larlikar, submitted for publication.
4. D.R.Bhavalkar, Saugar University Journal, 1, 209, (1951).
5. J.T.Pandall, and P.F.W.Wilkins, Proc.Roy.Soc., A 154, 366, (1954).

DISCUSSION

V.K. Mathur

1) How did you estimate the percentage of Bi in the CaS lattice?

2) How did you eliminate the statistical variation in observing the decay of the phosphor?

S.... Pawar

1) We have prepared the phosphors by adding certain amount of solution of $\text{Bi}(\text{NO}_3)_3$ in 10 gms of CaSO_4 .

2) while observing the decay of phosphors we have kept all other things constant. To study with magnetic field, we switched magnetic field on without disturbing anything else.

K.R.N. Murthy

What is the effect of magnetic field on the decay times.

S.H. Pawar

The graphs of phosphorescence intensity versus time are given both with and without magnetic field. The decay time is larger in a magnetic field.

LUMINESCENCE OF $\text{RbCl}:\text{Tl}$ and $\text{RbBr}:\text{Tl}$

J. Banamarti

Bhabha Atomic Research Centre, Bombay-65

I. INTRODUCTION

Alkali halide crystals are transparent over a wide range. Introduction of foreign impurities gives rise to new absorption bands in this normally transparent region. One of the impurities of interest is the thallium ion. The absorption and emission spectra of thallium ion in potassium and sodium halides have been studied by several authors¹⁻³. In this paper the absorption and emission spectra of thallium ion in rubidium chloride and bromide are reported. The results are compared with those in $\text{RbI}:\text{Tl}$ ⁴.

II. EXPERIMENTAL

Single crystals were grown by Czochralski method by putting known quantity of dopant in the melt. The absorption spectra were obtained on a Cary spectrophotometer using a Cary low temperature cryostat. For measuring the emission spectra the samples were irradiated in the desired regions using a Paschen and Lomb high intensity monochromator and a vacuum ultraviolet monochromator. The emission was analysed with a monochromator photomultiplier combination. The emission spectra were obtained by scanning with the analysing monochromator for a fixed excitation wave length. The excitation spectra were obtained, at 10°K, by setting the analysing monochromator at a fixed wavelength and varying the excitation wavelength. The spectra have been corrected for the response function of the detection system and the variation of intensity of the excitation source. Further details of experimental arrangement can be found elsewhere.⁴

III. RESULTS AND DISCUSSION

Table I shows the peak positions of various absorption bands. It also shows, for three different temperatures, the peak positions of the emission bands observed by irradiation in the absorption bands

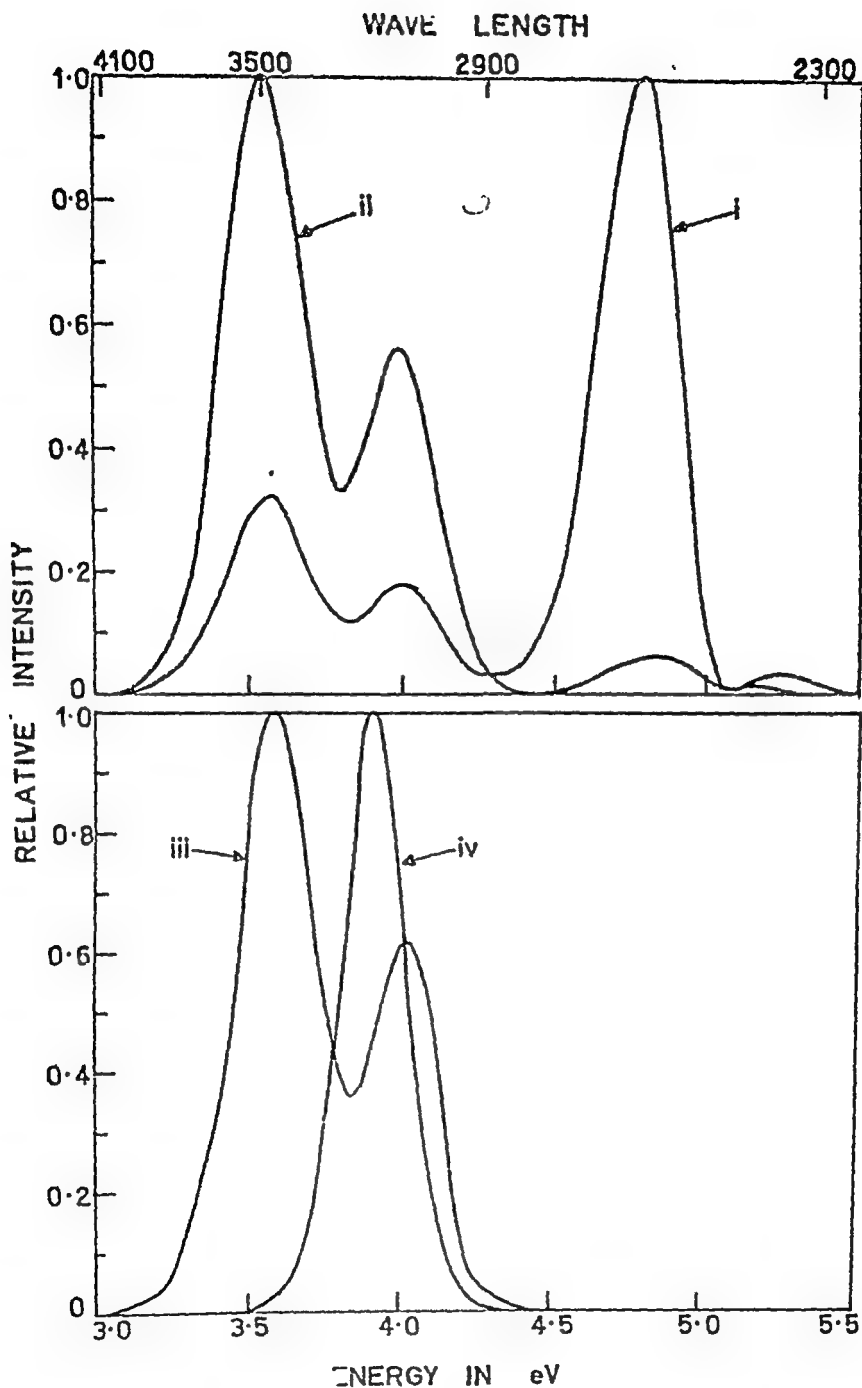


Figure 1. Emission spectra at 77° K of RbCl:Tl for excitation in (i) B band, (ii) C band and (iii) C band. (iv) Emission of RbBr:Tl at 4.2° K for A band.

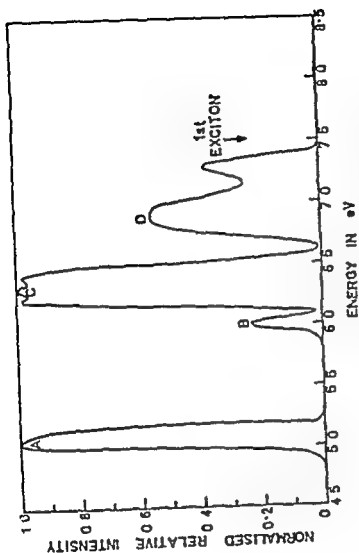


Figure 2. Excitation spectrum of the 3.58 eV emission band of KBrCl:Mn at 77°K.

and the relative intensities of emission. Fig 1 shows some of the emission spectra. The absorption bands shift to higher energies at lower temperatures. Following Seitz the peaks in the absorption spectrum are designated as A, B, C and D bands. In the case of RbCl:TL, at room temperature, the same emission spectrum is observed for irradiation in A, B and C bands. D and irradiation gives rise to an emission spectrum similar to that for C excitation. At 4.2°K, the 3.58 eV emission does not appear. In the case of RbBr:TL only one emission peak at 3.88 eV is seen prominently for irradiation in all the absorption bands. The excitation spectrum for the 3.58 eV emission at 77°K is shown in Fig.2. Excitation spectra for all other emission bands are similar to this in the case of both the crystals, RbCl:TL and RbBr:TL.

Table I.

Peak positions of emission bands, in eV, of RbCl:TL for excitation in the A, B, C and D absorption bands. The relative normalised intensity is also indicated.

Absorption Band Temp.	A		B		C		D	
	Emi. Peak	Rela. Int.	Emi. Peak	Rela. Int.	Emi. Peak	Rela. Int.	Emi. Peak	Rela. Int.
RbCl:TL 300°K 77°K 4.2°K	3.94	1.00	3.94	1.00	3.94	1.00	-	-
	3.60	0.40	3.60	0.40	3.60	0.40	-	-
	3.58	1.00	3.58	0.24	3.58	1.00	3.54	1.00
	4.03	0.60	4.03	0.18	3.98	0.56	3.98	0.43
			4.80	1.00	4.80	0.05	4.80	0.15
					5.26	0.03		
	4.03	1.00	4.03	0.21	4.03	1.00	4.03	1.00
			4.88	1.00	4.88	0.04	4.88	0.10
					5.26	0.02		
RbBr:TL 300°K 77°K 4.2°K	3.39	1.00	3.39	1.00	3.39	1.00	3.39	1.00
	3.40	0.22	3.40	0.10	3.27	0.55	-	-
	3.86	1.00	3.86	1.00	3.86	1.00	-	-
					4.60	0.10		
	3.88	1.00	3.40	0.15	3.27	0.03	3.27	0.12
			3.88	1.00	3.88	1.00	3.88	1.00
					4.60	0.06	4.60	0.05

The assignment of transitions to the absorption bands is same as those in other alkali halides¹. At 4.2°K only the 4.03 eV emission is seen in RbCl:Tl for A irradiation; it is assigned to the inverse transition corresponding to the A band i.e. ${}^3T_{1u} \rightarrow A_{1g}$. Similarly 4.26 eV emission is assigned ${}^3T_{2u} \rightarrow A_{1g}$. Since 5.26 eV emission is seen for irradiation in C band only we assign it to the inverse of the C band transition namely $T_{1u} \rightarrow A_{1g}$. The low energy emission at 3.58 eV is seen only at higher temperatures. As in the case of RbI:Tl it is attributed to the decay of perturbed exciton level. This should be observed prominently for D irradiation at 4.2°K, but it is not seen. There is an overall decrease in the intensity of emission in RbCl:Tl from 77°K to 4.2°K and this band is probably quenched by the same process. By arguments similar to above the following transitions are attributed to the emission bands of RbBr:Tl . 3.68 eV to ${}^3T_{1u} \rightarrow A_{1g}$; 3.40 eV to ${}^3T_{2u} \rightarrow A_{1g}$; 4.63 eV to $T_{1u} \rightarrow A_{1g}$ and 3.27 eV to the decay of the perturbed excitons. There is no stimulation of any of the thallium emission bands for excitation energies higher than the first exciton peak. This is unlike RbI:Tl in which two thallium emission bands are stimulated with high efficiency in the fundamental absorption region. These are attributed to the decay of the perturbed excitons⁴. The 3.54 and 3.27 eV emission bands which we have attributed to the decay of the perturbed excitons should also be stimulated in the fundamental absorption region. It is felt that this would be so if the temperature is lowered below 10°K. Lowering the temperature below 4.2°K, at which the emission spectra were taken, could increase intensity of some of the weaker emission bands; this would provide further confirmation of the transition assigned.

REFERENCES

1. F. Seitz, J. Chem. Phys. **6**, 150 (1938)
2. R. Edgerton and K.J. Tregarden, Phys. Rev. **129**, 169 (1953); **135**, 1071 (1964).
3. R. Illingworth, Phys. Rev. **136**, A 508 (1963)
4. J. Baranetti, Phys. Rev. **181**, 833 (1970)

DISCUSSION

P.A. Narayana

How do you explain the fine structure observed at low temperature?

J. Ramanurti

The fine structure in the excitation seen on the c band is due to dynamical Jahn-Teller effect and has been discussed by Toyazawa and Inoue. No fine structure is seen on the emission bands due to strong interaction of the center with the surroundings.

OPTICAL F \rightarrow H CONVERSION IN DOPED KCl CRYSTALS

K.V.R. Sastri and T.M. Srinivasan
 Department of Physics
 Indian Institute of Technology, Kanpur-16

I. INTRODUCTION

It is well known that when an alkali halide crystal containing F centers is exposed to light absorbed under the F band (F light), the concentration of F centers decreases and that of the F-aggregate centers (F₂, F₃, etc.) increases. This phenomenon of optical formation of aggregate centers has been the subject of several investigations⁽¹⁾, and various mechanisms have been proposed^(2,3). There has also been some work on the influence of impurities on the formation and decay of H centers⁽⁴⁾, which are the first products in the aggregation process. This paper describes results obtained on the room-temperature optical F \rightarrow H conversion in some doped KCl crystals. The crystals were first colored with x-rays, and then bleached with F light. The resulting growth and decay of H centers with continued F-light bleaching was studied by measuring the absorption under the H band.

II. EXPERIMENTAL

Two samples of KCl, one grown from "specture" grade material (FCl (I)) and the other from EM "Analar" grade material (KCl (II)), two samples of FCl doped with cobalt, and KCl crystals doped with barium and cadmium were studied. All crystals were grown from the melt. X-irradiation of thinly cleaved samples (thicknesses varying between 0.25 and 0.50 cm) was done with a General Electric EA-75 tube with a tungsten target operated at 60 kVp and 30 mA. Optical absorption measurements were carried out with a Cary 14⁰ spectrophotometer. Bleaching of the samples with F light was done in the sample,

compartment of the spectrophotometer, with the monochromator set at 590 nm and the slit 3mm wide. All irradiations and measurements were carried out at room temperature.

III. RESULTS AND DISCUSSION

The behaviour of the M band with increasing time of bleaching for six crystals which have all received 60 minute x-ray doses is shown in Fig. 1. Similar measurements were made on all these crystals after x-irradiation for 2 min. In addition, the KCl(I) and Co:KCl(II) crystals were studied after subjecting them to various intermediate x-ray doses. The scatter in the data is partly due to the low optical densities at the peak of the M band. In order to compare the F→M conversion efficiencies in different crystals, we define a parameter A (which might be called 'the aggregation factor') as the ratio of the change in the M-center concentration to that in the F-center concentration. The value of this parameter at the end of the first half-minute of F-light bleaching, $A_{\frac{1}{2}}$, was found to be nearly independent of the prior x-ray dose for KCl(I). In contrast, the Co- and Ba-doped crystals showed a distinctly higher $A_{\frac{1}{2}}$ for longer x-irradiation times. Values of $A_{\frac{1}{2}}$ for all the 60-min. irradiated crystals are shown in Table I. It appears that the processes involved in the F→M conversion are connected with those occurring in the F-center growth by room-temperature x-irradiation⁽⁵⁾.

Also shown in Table I are values of the ratio of the maximum to initial M-center concentration, M_{\max}/M_0 . In almost all the undoped samples studied, this ratio was less than 2, while for almost all the Co- and Ba-doped samples it was higher than 2. Similarly, the "rise time", defined as the time taken for the M band to attain its maximum value, was almost always higher in the doped crystals. The

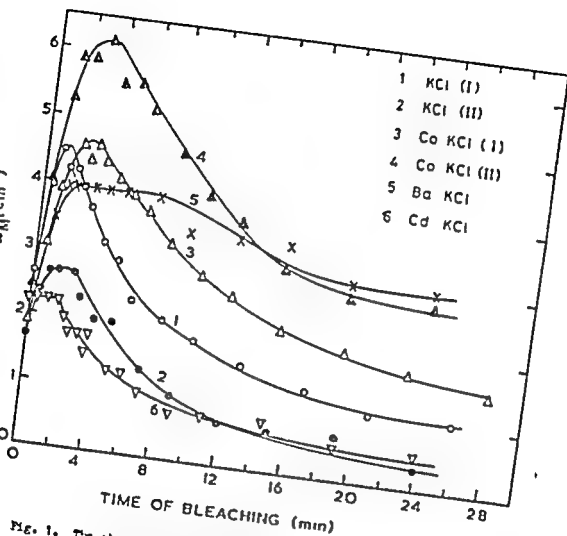


Fig. 1. The absorption coefficient at the peak of the X band, α_{λ} , plotted against the time of bleaching with P light. All crystals have been colored with x-rays for 60 min. at room temperature.

TABLE I

Sample	Dopant concentration· ppm	$A_{\frac{1}{2}}$	$\frac{M_{\max}}{M_0}$	"Rise Time" min	"Half Life" min
KCl(I)	-	0.15	1.7	1.25	5.75
KCl(II)	-	0.09	1.6	1.75	4.25
Co:KCl(I)	200	0.19	2.3	2.5	11.75
Co:KCl(II)	25	0.21	2.5	3.0	12.0
Ba:KCl	100	0.11	2.0	4.0	>20.0
Cd:KCl	50	0.00	1.0	-	-

decay in the M-center concentration, which follows the maximum as F-light bleaching proceeds, is described by a "half life", the time taken to fall to half the value at the maximum. From the tabulated values of half life, it is evident that the M centers are relatively more stable in the doped crystals. Thus, the general effect of divalent impurities appears to be to enhance the F→M conversion efficiency in crystals irradiated into the second stage of coloration, and to stabilize the M centers formed. An exception to this behaviour is the case of Cd:KCl, where the M band was found to remain at its initial height during the initial period of F-light bleaching, and then decay. Hence the parameters listed for this case are somewhat unusual compared to other cases.

The two main mechanisms proposed for optical F→M conversion involve the motion of anion vacancies to either F' centers or to F centers⁽¹⁾. Whichever mechanism is dominant, the fact that anion vacancy motion is involved in both suggests that impurities influence the mobility or concentration of such vacancies. Andrews and Kim⁽⁴⁾ propose a mechanism based on an assumed higher mobility of vacancy pairs than that of single vacancies. They suggest that excess cation vacancies present in doped crystals enhance the concentration of vacancy pairs, which then aid in the aggregation of F centers. However,

since their basic assumption is questionable⁽⁶⁾, one has to consider other possible effects of impurities. For instance, it has been suggested⁽⁷⁾, in connection with P-center growth processes, that there are certain "sources" and "traps" for anion vacancies which influence the room-temperature coloration processes. Divalent impurities might influence the concentration of these sources and/or traps⁽⁵⁾, thus altering the anion vacancy concentration. Alternatively, impurities might change the cross sections or concentrations of electron traps in the crystal. In fact, such a suggestion has been put forth by Jain et. al.⁽⁸⁾ to explain unusual behaviour of Cl:KCl.

REFERENCES

1. J.D. Compton and P. Rabin, Solid State Physics 16, 121 (1964).
2. G.Z. van Doorn, Philips Res. Rept. Suppl. 4 (1962).
3. C.J. Delbecq, Z. Physik 171, 560 (1963).
4. P.A. Andrews and Y.Y. Kin, Phys. Rev. 155, 1029 (1967); 170, 793 (1968).
5. E.V.R. Sastry and T.M. Srinivasan, Phys. Rev. B (to be published).
6. P.A. Andrews and Y.Y. Kin, J. Phys. Chem. Solids 29, 1909 (1968).
7. C. Sanchez and P. Aguillo-Lopez, Phys. Stat. Sol. 29, 217 (1968).
8. S.C. Jain, G.D. Sootha and R.K. Jain, J. Phys. C 1, 1224 (1968).

DISCUSSION

V.B. Singh

What is the depth of Cd level in KCl lattice?

E.V.R. Sastry

I do not have the data at the moment, but this is not very relevant for the vacancy processes that in general are important for P \rightarrow M conversion.

K.R.V. Murthy

1) Was the bleaching completely effective in converting all P bands to M bands?

2) What was the atmosphere in which crystals were grown?

3) If in air, the doping of Cd affects increasing of OH^- absorption band. What will be the results in such case?

E.V.R. Sastry

1) No. As shown in Table I, only a fraction of the F centers that are bleached are converted into M centres.

2) Mostly in air. Some of the doped crystals were grown by the Bridgman method after scaling the powder in vacuum.

3) Our Cd:KCl crystal was obtained from Dr. Jain's group, and did not show any OH absorption.

S. Radhakrishna

1) Does your work throw any light on why M - centers are not observed in some impurity doped crystals?

2) Is it not possible to explain all your results on the basis of the "two M-center" theory?

E.V.R. Sastry

1) Our work shows that impurities may influence the aggregation process in more than one way, and each impurity may show these effects in varying degrees. Thus, it is possible that certain impurities may completely inhibit M-center formation.

2) We don't think so. Moreover, the exact nature of the "two M center" is not clearly known.

ELECTROLUMINESCENCE IN ZnO ELECTROLUMINOPHORS SYSTEM

V.B. Singh and J.K. Kanda
Defence Research Laboratory (Materials), Kanpur-6.

I. INTRODUCTION

The nature of electroluminescent emission depends on the host base starting material and the activator incorporated in the base. $ZnS:Cu$, Cl electroluminophor is a common example to achieve blue green electroluminescent emission, and many investigators have worked with ZnS d-base material. In this communication we shall describe the phenomenon of electroluminescence in ZnO base powder where electroluminescent emission results due to A.C. and D.C. fields.

II. RESULTS AND DISCUSSIONS

Lossen⁽¹⁾ observed the luminosity in zincite crystal ($ZnO:In$), when the crystal was subjected to an electric field. Destriau⁽²⁾ doped ZnS with the activator and then used ZnO as a sensitizer in his phosphor systems. He observed that the increase of ZnO in ZnS base material lowered the threshold voltage for E.L. emission.

The variation of threshold voltage with ZnO content has been shown in fig. 1. Thus above 75% addition of ZnO in ZnS was always found suitable for efficient E.L. emission. Thus Destriau interpreted his results stating that ZnO plays a role of sensitizer so that it lowers the threshold voltage for E.L. in $ZnS:Cu$ phosphor. Vavichin⁽³⁾ observed the phenomenon of electroluminescence in a doped ZnO

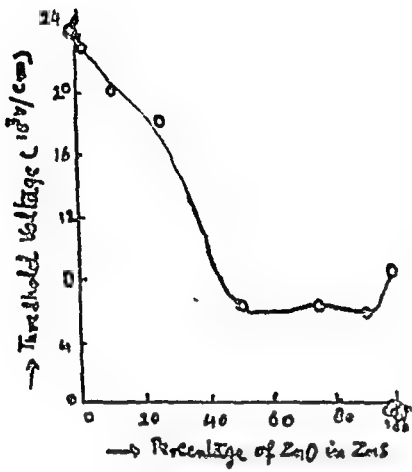


Fig. 1

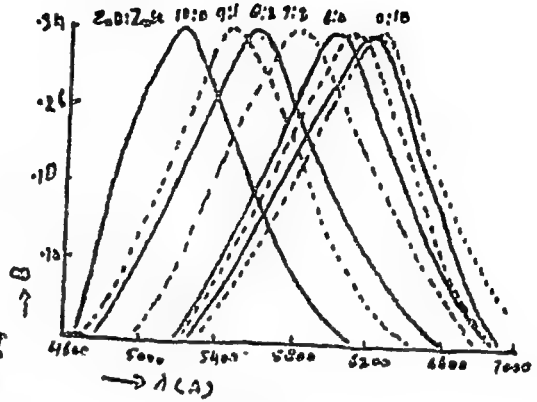


Fig. 2

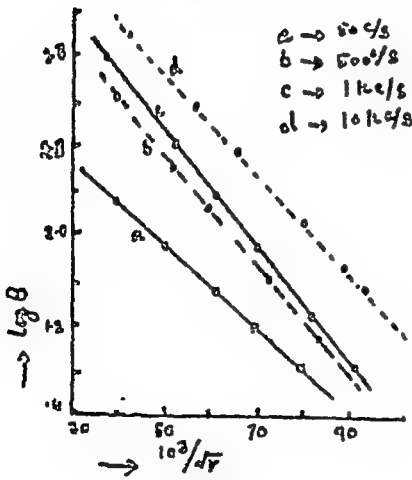


Fig. 3

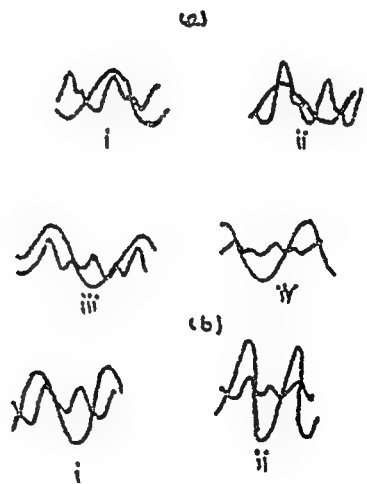


Fig. 4

crystalline powder. He explained the phenomenon of electroluminescence in ZnO as a surface phenomenon rather than volume penetration of impurity in the crystalline base. Most probably his samples of ZnO were self activated which has not been mentioned. The brightness of E.L. and the photoconductivity were increased as the sample was isolated from air and the system was evacuated. The increase of brightness was interpreted as due to desorption of oxygen from the surface of ZnO. Schwab⁽³⁾ observed the phenomenon in the mixture of ZnO and ZnS using Cu as activator and halogens and Al as coactivator, no percentage amount of ZnO and ZnS was mentioned. However, he found that E.L. intensity at higher field increases faster in ZnS phosphors rather than ZnS/ZnO.

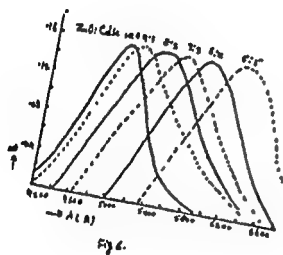
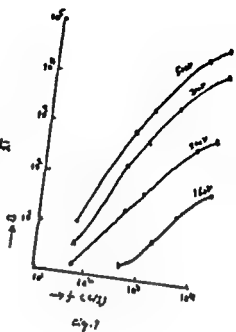
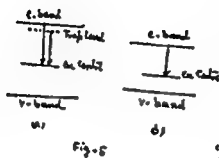
Singh et al⁽⁵⁾ prepared the ZnO electroluminescent using Cu as activator and halogens and Al as coactivators respectively. After observing the phenomenon in ZnO they prepared the alloy systems of ZnO and ZnSe electroluminescent. The percentage amount of ZnO and ZnSe were varied systematically and then the results were studied. ZnO has been taken as a base material but not as a sensitizer into ZnSe base.

The energy gap of ZnO is 3.2 eV and that of ZnSe is 2.6 eV. Then the two bases were mixed and alloyed by firing in N₂ atmosphere then the resultant energy band-gap was found to vary in between 3.2 and 2.6 eV. As a result of decrease of energy band-gap with increase of ZnSe in ZnO,

E.L. omission was found to shift towards higher wavelength side, as shown in fig. 2. The A.C. Voltage of 400V at 10K c/s, was applied on dielectric dispersed electroluminophor. Thus the energy band-gap of the alloy ZnO-ZnSe decreases as the percentage amount of ZnSe was increased. As a result of it the electroluminescent emission of (ZnO-ZnSe):Cu, Cl was found to shift from green to red region of wavelength passing over the intermediate range of the spectrum.

The mechanism of excitation and emission of E.L. in (ZnO-ZnSe):Cu, X (X denotes the halogens Cl, Br, I separately), was investigated it was found that in alloyed system the brightness varies ^{with} voltage according to following relation, $B = B_0 e^{-\frac{b}{\sqrt{V}}}$, where B is the electroluminescent average brightness at the applied voltage V, B_0 and b being the constants. The variation of brightness B with \sqrt{V} at different frequencies has been shown in fig. 4. Thus the mechanism of acceleration and Collision ⁽⁶⁾ for E.L. excitation, similar to ZnS was found to hold in this case. And the above relation also proves that the E.L. emission is coming from some specific regions, of electroluminophor, called Mott ⁽⁷⁾ and Schottkey ⁽⁸⁾ barriers.

The brightness waves ⁽⁹⁾ were studied with applied voltage for two types of electroluminophors as ZnO:Cu, X, Al and (ZnO-ZnSe):Cu, X, Al. E.L. brightness patterns at room temperature have been shown in the fig. 5. Primary and the secondary peaks of brightness are observed in the case of



ZnO samples and no secondary was observed in the case of ZnO-ZnSe system at any field frequency. It was concluded that the secondary peak due to the transition from Coactivator level to Cu centre dominates in ZnO and it vanishes in (50 ZnO-50 ZnSe) samples. Only primary peak due to transition from conduction band of resultant alloy ZnO-ZnSe, to Cu activator level survives, because of the fact that the energy band-gap decreases in alloy and thus in place of the transitions from coactivator to Cu level, the transitions start from conduction band to Cu level. The possible transitions have been shown in fig. 5.

The other system of electroluminophors possible with ZnO was ZnO-CdSe:Cu, X was prepared by Singh ⁽¹⁰⁾ et al. The energy band-gap of CdSe is 1.8 eV which is much smaller than that of ZnO. Therefore the shift of the emission towards higher wave-length was faster in this case than that of ZnO-ZnSe as the amount of CdSe was increased. The red emission was obtained even at 50% CdSe addition in ZnO as shown in fig. 6.

The variation of brightness with applied field-frequency was studied for the alloy system 50ZnO-50CdSe. It was found that the brightness attains saturation at higher frequency around 10 Kc/S as shown in fig. 7.

With the increase in A.C. frequency, the increase of the brightness was found linear. Some deviations in the variation of brightness B with frequency f were observed

from the relation $\frac{1}{B} = \frac{1}{K n_0 \omega} (1 + \frac{n_0^2 \omega}{2f})$, where K is the constant of proportionality, ω the time constant and n_0 the number of electrons initially excited from the impurity centre. Thus for large value of ω , the brightness B should vary linearly with f , but practically in this electrolumino-phor it seems that the life time of the conduction band being larger in comparison to the A.C. period, the excited electrons are unable to follow such rapid changes of voltage cycle. The transitions remain incomplete, and the saturation in the brightness results.

REFERENCES

1. O.V. Lossev; Phil. Mag. 6, 1024 (1928)
2. G.Destriaux; Phil. Mag. 38, 700 (1947)
3. I.K.Vereshagin; Optics and Spectros. 8, 219 (1960)
4. E.A.Schwager; Z. Physik 163, 44 (1961)
5. V.B.Singh and H. Mohan; Z. Physik 208, 441 (1968)
6. T.T.Piper and F.E.Williams; Brit. J. Appl. Phys. Suppl. 4, 39 (1954)
7. H.F.Katt; Proc. Roy. Soc. A 171, 27 (1939)
8. W. Schottkey; Z. Phys. 119, 539 (1942)
9. V.B.Singh and H. Mohan Z. Ang. Physik 27, 360 (1969)
10. V.B.Singh and H. Mohan Z. Ang. Physik 27, 300 (1969)

THERMOLUMINESCENCE OF QUENCHED LiF SINGLE CRYSTALS

S. Muralidhara Rao

Technical Physics Division, Bhabha Atomic Research Centre, Bombay-85

I. INTRODUCTION

Lithium Fluoride powder and single crystal phosphors are widely used in thermoluminescence dosimetry. It is found that the glow curves of LiF phosphors show spurious peaks on repeated use.¹ This limits the use of the crystal. This is however overcome by annealing the phosphor at 80°C for 50-60 hours before irradiation. The effect of pre-irradiation heat treatment thus became a topic of many investigations^{2,3,4}. The present study is made on LiF Mg Ti single crystals quenched from different temperatures to room temperature. By quenching, it is possible to freeze the equilibrium conditions existing at a high temperature and study these conditions at room temperature.

II. EXPERIMENTAL

Crystals for the present work are grown in a vacuum furnace. Commercial (I) and vacuum distilled (II) powders are used as starting materials for crystal growth. No impurities are added to the commercial powder whereas the vacuum distilled powder is doped with .1% by weight each of MgF_2 and TiO_2 . Samples of 4 mm x 4 mm x 1 mm dimensions were cleared from these crystals. About 50 of type I and 50 of type II crystals are studied. The samples are exposed to a γ -dose of 100 R from a Co^{60} source. A thermoluminescence reader unit built for this purpose is used to study the glow curves.

Initially glow curves of as cleaved samples are taken. Then the samples are kept under vacuum at 400°K for 2 hours and immediately cooled to room temperature by air cooling. These crystals are irradiated within 30 minutes of quenching and the glow curves taken immediately after irradiation. This process is repeated at higher temperatures 450° , 500° , 550° , 600° , 650° , 700° , and 750°K .

RESULTS & DISCUSSION

Fig. 1 gives the glow curves obtained from the Type I crystals quenched from different temperatures. These curves are continued in Fig. 2 to maintain clarity. The glow curve for 400°K quench is very much the same as that of the as grown crystal. When the crystal is quenched from 450°K , a low temperature peak appears at about 400°K besides the high temperature peaks at 500°K and 550°K . The peak at 550°K is not observed in the other quenches. The low temperature peak persists upto 650°K reducing in magnitude with increasing quenching temperature. Finally a single peak is obtained for quenching at 750°K .

The behaviour of the type II crystals is quite different. Fig. 3 gives the glow curves of these crystals as grown as well as quenched from different temperatures. It is observed that with increasing quenching temperature the magnitude of the low temperature peak around 400°K increases while the peak at 500°K is reduced. The reduction in the high temperature peak is consistent with earlier observations⁽⁴⁾.

It has been observed that the height of the low temperature peak is proportional to the square of the quenching temperature.

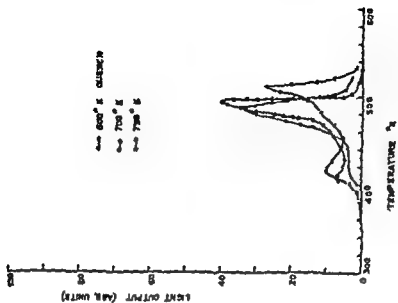


FIG. 2

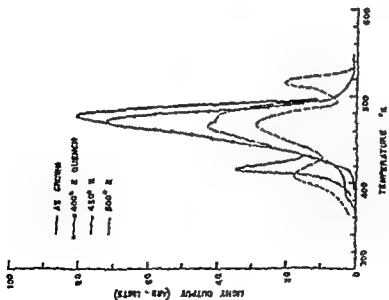


FIG. 1

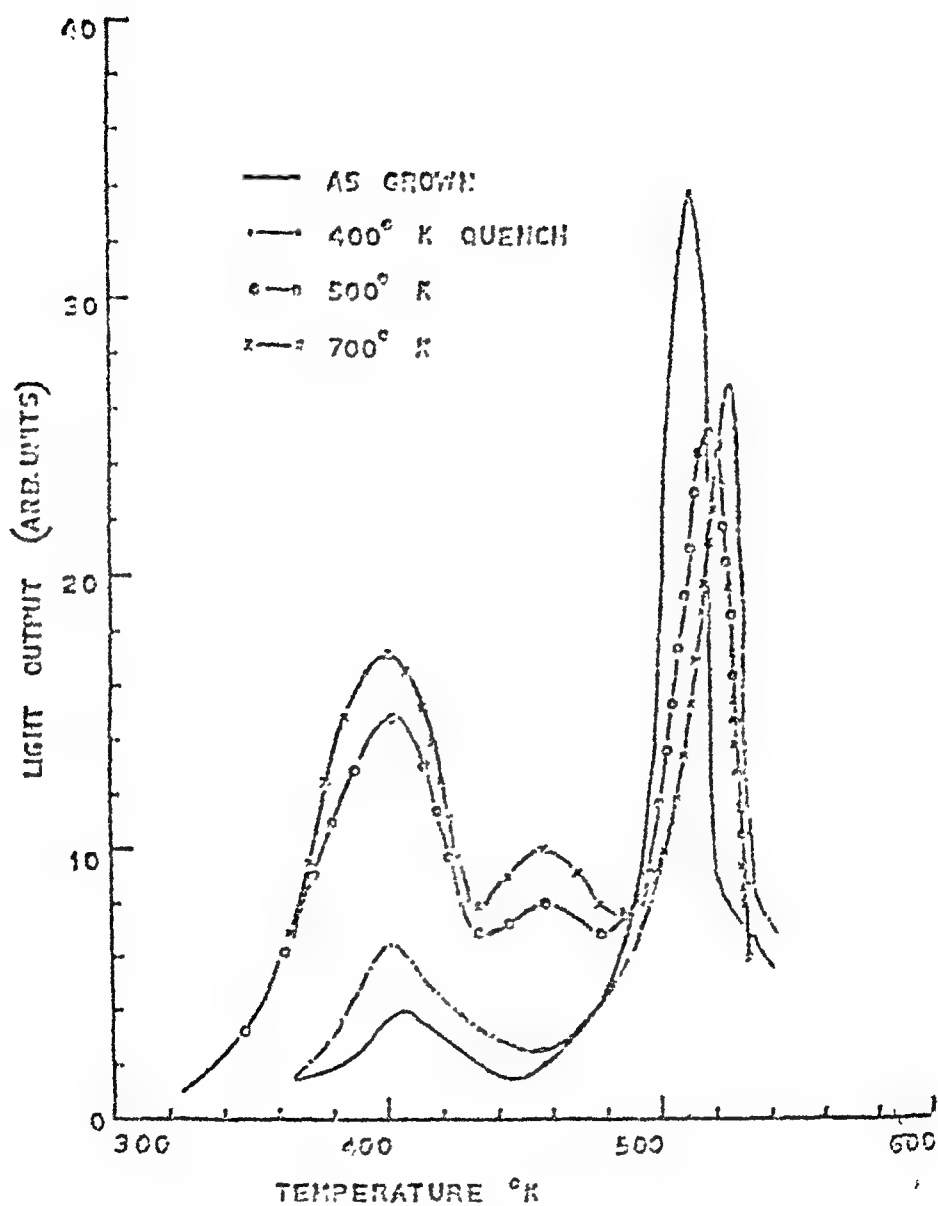


FIG. 3

complexes as estimated by dielectric loss measurements⁵. Cooling rates of about 400°K/min. are known to help impurity-vacancy associations⁶. Thus the present observation could be interpreted in terms of the dissolution of Mg^{2+} in the lattice on heating and the formation impurity-vacancy complexes on quenching. The amount of Mg^{2+} dissolved being a function of temperature and the rate of complex formation being proportional to the cooling rate. Thus with increasing quenching temperature more Mg^{2+} is dissolved and for the same cooling rate the number of complexes formed is higher for higher quenching temperature. This leads to an increase in the height of the low temperature peaks.

REFERENCES

1. J.H. Cameron et.al.
Health Physics, 20-25 (1964)
2. D.W. Zimmerman et.al.
Health Physics 12-523 (1966)
3. C.R. Watson
Washington University Thesis 1963.
4. M.M. Grube, A.Z. Grant
Phys. Tech. Zinat. Ser. No.6-40 (1968)
5. R.M. Grant Jr., J.H. Cameron.
J. Appl. Phys. 37 -3791 (1966)
6. W.J. Johnston
J. Appl. Physics 300-2060 (1962)

DISCUSSION

S.H. Pawar

- 1) What are the rates of heating.
- 2) How have you kept the rate of heating co

3) How have you saved the photomultiplier tube from heating?

S. Muralidhara Rao

1) $10^{\circ}/\text{sec}$

2) By a voltage stabilizer supplying the power to the heater.

3) By flushing the surface of the P.M. tube by cool N_2 gas.

T.M. Srinivasan

Is there any explanation for the shift in the peak position of one of the bands?

S. Muralidhara Rao

Most probably some experimental error.

V.B. Singh

Impurity is substitutionally doped or interstitially?

S. Muralidhara Rao

Because of comparatively larger ionic radii of Mg and Ti compared to Li, they go into substitutional sites only.

OFF-CENTER LEAD IONS IN KI CRYSTALS
AND RAMAN SCATTERING

S. RADHAKRISHNA AND K.S.K. SAI

DEPARTMENT OF PHYSICS

INDIAN INSTITUTE OF TECHNOLOGY

NEW DELHI-29

1. Introduction

Fukuda's work has shown¹ that alkali halides doped with lead give three major bands called the A, B and C bands. The B band arises from the forbidden $1A_{1g} \longrightarrow 3T_{2u}$ or $3E_u$ transition while the C band arises from the allowed $1A_{1g} \longrightarrow 1T_{1u}$ transitions. We report in this paper results regarding lead doped KI crystals where the forbidden band is stronger than the allowed band.

II. Experimental Techniques

Crystals of lead doped KI were prepared by diffusing lead into KI at high temperatures. The optical absorption spectra were recorded on a Cary-14 recording spectrophotometer. Room temperature and high temperature spectra were studied on a Carl-Zeiss Spectrophotometer. The Raman spectra were recorded on a CODERG Raman Spectrometer. The source of radiation was a spectra-physics He-Ne laser (6328 Å). Polarised spectra were taken by introducing a quarter wave plate in the path of the incident laser beam.

3) How have you saved the photomultiplier tube from heating?

S. Muralidhara Rao

1) $10^\circ/\text{sec}$

2) By a voltage stabilizer supplying the power to the heater.

3) By flushing the surface of the P.M. tube by cool N_2 gas.

T.M. Srinivasan

Is there any explanation for the shift in the peak position of one of the bands?

S. Muralidhara Rao

Most probably some experimental error.

V.B. Singh

Impurity is substitutionally doped or interstitially?

S. Muralidhara Rao

Because of comparatively larger ionic radii of Mg and Ti compared to Li, they go into substitutional sites only.

OFF-CENTER LEAD IONS IN KI CRYSTALS
AND RAMAN SCATTERING

S. RADHAKRISHNA AND K.S.K. SAI

DEPARTMENT OF PHYSICS

INDIAN INSTITUTE OF TECHNOLOGY

NEW DELHI-22

1. Introduction

Fukuda's work has shown¹ that alkali halides doped with lead give three major bands called the A, B and C bands. The B band arises from the forbidden $1A_{1g} \longrightarrow 3T_{2u}$ or $3E_u$ transition while the C band arises from the allowed $1A_{1g} \longrightarrow 1T_{1u}$ transitions. We report in this paper results regarding lead doped KI crystals where the forbidden band is stronger than the allowed band.

II. Experimental Techniques

Crystals of lead doped KI were prepared by diffusing lead into KI at high temperatures. The optical absorption spectra were recorded on a Cary-14 recording spectrophotometer. Room temperature and high temperature spectra were studied on a Carl-Zeiss Spectrophotometer. The Raman spectra were recorded on a CODERG Raman Spectrometer. The source of radiation was a spectra-physics He-Ne laser (6328⁰Å). Polarised spectra were taken by introducing a quarter wave plate in the path of the incident laser beam.

III. Results and Discussion

Fig.1 shows the optical absorption spectra of a lead doped KI crystal. Curve 2 is for RT and curve 1 is for LNT. Curve 3 is for the spectrum taken at 200°C. It may be seen from these curves that in lead doped KI crystals three bands at 254, 275, 354 nm are observed. In comparison with Fukuda's data¹ for NaCl, KCl and KBr crystals these bands may be designated as the C, B and A bands respectively. The quartet structure reported by Fukuda for the C band in NaCl and KCl was not observed by us even at LNT for KI crystals. This assignment however questionable since the B band which, in O_h group crystals, is forbidden as it arises from the forbidden transition ($1A_{1g} \longrightarrow 3T_{2u}$ or $3E_u$), is found to be stronger than the allowed C band. Earlier work on KI crystals doped with Tl ² where the A, B and C bands are observed, showed no such intensity reversal. In other crystals doped with similar impurities (Ga, Tl, In, and Sn)¹ also no such reversal is observed. This intensity reversal is therefore characteristic of lead doped KI crystals. It is possible that the lead impurity in KI is at an off-center position thus breaking the selection rule which forbids the transition responsible for the B band. Such off-center position being occupied by impurities has been reported³ earlier. Copper for example is at a substitutional site in NaCl and at an off-center site in KI. Li^+ is known⁴ to be at an off-center position in KCl.

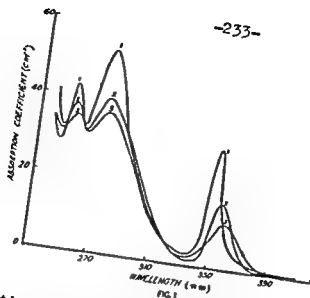


Fig.1: Optical absorption spectra of a KI: Pb Crystal. Curve 1 shows spectrum at LNT, Curve 2 at RT and Curve 3 at a high temperature of 200°C.

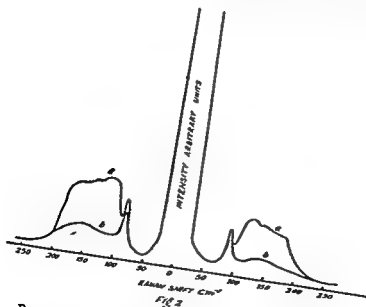


Fig.2: Raman spectra of a KI: Pb crystal. Curve 'a' shows an unpolarised spectrum and curve 'b' a polarised spectrum.

Fig.2 shows the Raman spectra of a lead doped KI crystals. It can be seen that besides a fairly strong, sharp line at 89 cm^{-1} and some weak lines beyond 180 cm^{-1} we have a broad structure between $100\text{--}170\text{ cm}^{-1}$. This is apparently a combination of three lines all of which are polarised. This structure is absent in a pure crystal. A pure crystal shows only the line at 89 cm^{-1} and the weaker lines beyond 180 cm^{-1} . This has been reported earlier⁵. The appearance of this new structure is therefore because of presence of lead impurity. Such lines were not observed in NaCl, KCl and KBr crystals. Nor do KI crystals doped with Cd and Zn give such Raman lines. The observed new lines can be interpreted as being due to the first order Raman Spectrum of KI appearing as a result of the breaking of the selection rule which forbids the first order spectrum. This would imply a break of the O_h symmetry. Curve b shows the polarised spectrum. Anti-Stokes components are also shown in order to rule out some kind of fluorescence. Thus the appearance of this new Raman spectrum lends support to the off-center position suggested for the lead ions in KI crystals.

It is therefore concluded that lead ions in KI crystals occupy off-center position.

IV. References

1. A. Fukuda Sci. of Light 13, 64 (1964).

2. F.Seitz, J.Chem.Phys. 6, 150 (1938).
3. E.Kratzig, T.Timusk and W.Martienssen Phys.Stat. Sol. 10 , 709 (1965).
4. W.D. Wilson, R.D. Hatcher, G.J. Dienes and R.Smeluchowski
Phys. Rev. 161 , 888 (1967).
5. R.S. Krishnan p. 539 "Inelastic Scattering of Neutrons"
Vol. II Int. Atomic Energy Agency Vienna
1965.

DISCUSSION

P. Venkateswarlu

Does the intensity of the first order Raman line in $KI:Pb$ depend upon the concentrations used?

S. Radhakrishna

Yes, the intensity does depend. There is not direct correlation of increase in intensity with Pb concentration, but it does increase. We have used various concentrations of lead ranging from ~ 30 ppm (.3% by weight at the time of growth) to 200 ppm (corresponding to 200 ppm (corresponding to 1% by wt. at the time of growth).

K.R.N. Murthy

What type of irradiation was used? In which atmosphere were the crystals grown?

S. Radhakrishna

Crystals were grown in argon atmosphere by Kryropolous method. A hydrogen discharge tube at high current was used for irradiation in conjunction with a monochromator.

M.A. Viswamitra

Is there any X-ray crystallographic evidence for the off-center lead position?

S. Radhakrishna

We have not attempted this but I do not think there will be any in view of the low concentration of lead in our crystals.

V.B. Singh

What is the laser assembly used in your experiment.

S. Radhakrishna

He-Ne Laser (spectra physics) - Coderg Recording equipment.

P.S. Narayanan

1) Was there any direct correlation between the intensity of the first order Raman spectrum and the concentration of Pb.

2) Was any localized mode observed in Raman effect attributable to the Pb ion?

3) Can one try to explain the activation of the first order Raman spectrum as due to the existence of a new electronic absorption at "B" rather than due to an off centre position of Pb ion.

S. Radhakrishna

1) There was a correlation in the sense that the intensity of the first order Raman line increased with lead content but there was no direct correlation.

2) No - Not with our present experiments,

3) Not with the present understanding about the B -center.

P.A. Karayana

I wonder if you can explain your results assuming that Pb^{2+} enters substitutionally with nearby charge compensation rather than as off center Pb^{2+} ions.

S. Radhakrishna

This is not possible since other impurities which are known to have near neighbour compensation do not give such a Raman Spectrum.

THERMOLUMINESCENCE OF KBr CRYSTALS

K.R.N.Murthy, Y.V.G.S.Murti AND C.Ramaswamy
Department of Physics, Indian Institute of
Technology, Madras-36.

I. INTRODUCTION

We report here the results of our studies on the thermoluminescence of KBr and KBr:Cu crystals in the temperature range $300-550^{\circ}\text{K}$ following irradiation with x-rays at room temperature. Four of the observed glow peaks are isolated and analysed.

II. EXPERIMENTAL

The crystals are grown from melt using 'Guaranteed' Reagent material. Irradiation is by X-rays from a Cu-target (32 KV, 12 ma). As the temperature of the crystal is linearly raised ($40^{\circ}\text{C}/\text{minute}$) the light output is received by an RCA 931-A photomultiplier and the glow curves are recorded on an X-Y recorder. Tempering means heating the crystal at 500°C for 2 hours and cooling to room temperature in about 10 hours.

III. RESULTS

A large number of samples have been studied. Their peak temperatures centred around 360, 377, 392, 410 and 440°K . For low irradiation doses (15 minutes) the 360°K and the 392 (or 410) $^{\circ}\text{K}$ peaks

only are produced. Heavy irradiation (2 hours) introduces an additional peak at 440°K. Tempering prior to irradiation considerably enhances the intensity of the 392(or 410)°K peak. Successive cycles of tempering and irradiation effectively isolate this peak. A new and predominant glow peak is observed in copper doped crystals when the impurity is in the cuprous state as evidenced by the characteristic optical absorption⁽¹⁾ at 4.67 eV. Figure 1 illustrates typical results.

The thermoluminescence intensity for negligible retrapping is given by⁽²⁾

$$I(\tau) = n_0 s \exp(-E/k\tau) \exp\left\{-\int_{\tau_0}^{\tau} \frac{s}{\beta} \exp(-E/k\tau) d\tau\right\} \dots\dots (1)$$

n_0 is the initial number of trapped electrons, s a frequency, E the trap depth and β the warming rate.

The glow curves at 360, 377, 392 and 410°K could be fitted to the above equation with $E = 0.86, 0.97, 1.00$ and 1.05 eV respectively. The corresponding frequencies (s) are $0.67, 3.3, 3.67$ and $3.3 \times 10^{11} \text{ sec}^{-1}$. It is evident that the kinetics is of first order.

The closeness of the activation energies suggests that the several glow peaks arise from the thermal ionization of F-Centres in different local environments. Nearest neighbour Cu^+ ions for the 377°K peak and alkaline earth impurities for the 392 and 410°K peaks are indicated. The 360°K and 440°K peaks may be related to the early and late stage F-Centres⁽³⁾.

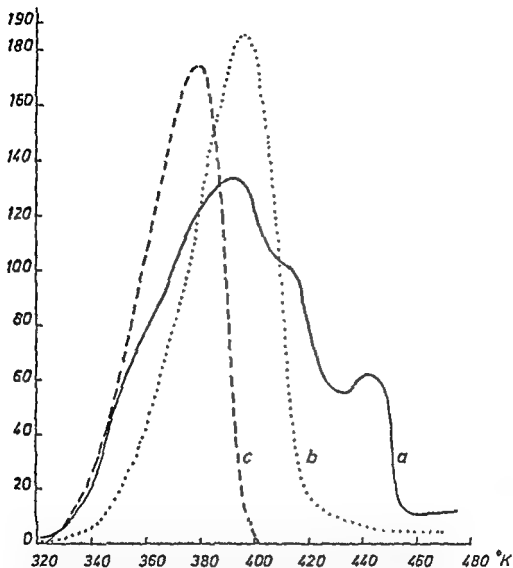


Fig.1. Glow Curves of KBr and KBr:Cu.

- a. KBr, after 2 hours of irradiation.
- b. KBr, after 3 cycles of tempering and irradiation.
(intensity reduced by 1/2 and plotted)
- c. KBr:Cu quenched from 600°C, 15 minutes irradiated
(intensity reduced by 1/2 and plotted)

The above conclusions are suggested by a comparison of the results on crystals of different purity. We have also studied the thermoluminescence of crystals from Harshaw (H) and Hilger and Watts Co.s. 'High' purity crystals ⁽³⁾ as well as those from Hilger and Watts company show the 360 and 440^oK glow peaks predominantly. The Harshaw samples on the other hand have higher divalent metallic impurity content and give a thermoluminescence like the crystals grown in this laboratory. Optical absorption and thermoluminescence studies have revealed that the undoped crystals and those from Harshaw or Hilger Watts Co.s. also contain copper as a residual impurity. It is normally present in a precipitated state but can be dissolved in the lattice by quenching from 600^oC.

REFERENCES

- (1) E. Kratzig, T. Timusk and W. Martienssen,
Phys. State. Solidi. 10, 709 (1965).
- (2) A. T. Randall and M.H.F. Wilkins,
Proc. Roy. Soc. A 184, 365 (1945).
- (3) P.C.Mehendru and S. Radhakrishna,
J. Phys. C (solid state) 2, 796 (1969).

DISCUSSION

-243-

H.D. Bist

1) Did you observe or try to observe 'glow curve' while cooling your sample?

2) Have you tried to find the spectral distribution of the glow curves?

K.R.N. Murthy

Since in the crystals thermoluminescence is due to the release of electrons from F-centres, the F-band is completely bleached after the thermoluminescence is obtained. Hence no such glow curve is observed after bleaching the F-centers.

2) Spectral distribution of glow curves is not yet done.

V.K. Mathur

How did you evaluate the integral to generate the theoretical curve? I think T^2 rate of heating may be used, which can help in the evaluation of the theoretical curve analytically.

K.R.N. Murthy

The integral was evaluated numerically by considering the small areas $dT = 2^\circ$. As regards the use of T^2 heating rate I am not very sure.

S.M. Pawar

What is time of excitation by X-rays?

K.R.N. Murthy

For low irradiation times, the time of excitation is 15 minutes, for larger irradiation times it is 2 hours.

S. Radhakrishna

What is the mechanism for four different trap depths?

K.R.N. Murthy

As regards the 377°K peak it is interpreted to be due to the dissolved Cu^+ ions from the characteristic optical absorption of Cu^+ at 4.67 since only such crystals contain 4.67 band at 377°K peak. Regarding the 359° and 440°K peaks they may correspond to the I & II stages of F-centres as observed by Mehendru & Radhakrishna (1969). Regarding the 392° & 409°K peaks, we compare the impurities in Harshaw & Hilger-Watts samples with ours. The peaks could be due to the alkaline earth impurities in the neighbourhood of F-centres, which are more in our and Harshaw samples but very less in Hilger-Watts samples, in which the peaks are not prominent.

ABSORPTION AND FLUORESCENCE SPECTRA OF Ho^{3+} IN LaF_3 CRYSTAL

Bansilal, D.Ramachandra Rao, T.M.Srinivasan,
K.V.Subbaram, and P.Venkateswarlu

Department of Physics, Indian Institute of Technology, Kanpur-

I. INTRODUCTION

The absorption and fluorescence spectra of Ho^{3+} in LaCl_3 and in some hydrated salts have been studied extensively (1,2,3) and a complete energy level scheme has been worked out. Ho^{3+} spectra show certain unusual features, 1) some lines are extremely sharp revealing hyperfine structure and ii) some are too broad without showing any structure even under high resolution. Further fluorescence experiments indicated the stable and unstable excited states¹ and the involved energy transfer processes between the excited states. Divergent opinions persist on the crystal structure of LaF_3 and the site symmetry for La^{3+} ions. In a programme of detailed work on RE ion spectra, investigations on Ho^{3+} in LaF_3 is undertaken. The results on the absorption spectrum along with polarization data photographed on Jarrell-Ash spectrograph at liquid nitrogen and liquid Helium temperatures and on fluorescence spectrum at room temperature excited by a He-Ne laser are reported in this paper.

II. EXPERIMENTAL

The absorption spectrum in the region 3300-6500 Å was photographed using a 75W. high pressure Xenon arc source on a 3.4 meter Jarrell-Ash Ebert mounting grating spectrograph at liquid nitrogen ($\sim 80^\circ\text{K}$) and at liquid helium temperatures ($\sim 15^\circ\text{K}$). The initial spectra were recorded at a dispersion of 2.5 Å/mm and the final spectra

at 0.5 Å/mm incorporating different gratings. The absorption spectrum also includes the polarization data E_H and E_I to the c axis of the single crystal using a Glan-Thompson prism. A single crystal of LaF_3 doped with 0.5 % mole Ho^{3+} obtained from Optovac, U.S.A. was used.

A He-Ne laser operating at 6328 Å has been fabricated. The laser has about 80cm plasma tube terminated by Brewster windows with a 2 meter radius of curvature on one side and a half Brewster prism on the other side. The experimental arrangement for photographing the fluorescence spectrum using the He-Ne laser is shown in Fig.1. The fluorescence spectra at room temperature were taken on a three prism Zeiss glass spectrograph with exposures of about 5 to 10 nts

III. RESULTS AND DISCUSSION

The lowest electronic configuration of $\text{Ho}^{3+} [4f^{10}]$ gives 47 multiplets (5 quintets, 22 triplets and 20 singlets) with 5I_8 as the ground state. These correspond to 107 LSJ states and each state will split into a number of levels depending upon the crystal field symmetry. The low site symmetry of the impurity ion in LaF_3 , which could be either C_{2v} , C_2 or C_s , will reveal all the $2J+1$ components. The absorption groups recorded on Jarrell-Ash spectrograph are listed below with the number of lines observed in each group indicated. The probable upper level for each group is also included.[†]

[†]A paper on "Absorption, fluorescence, and energy levels of $\text{Ho}^{3+}:\text{LaF}_3$ " has just appeared. Ref: Caspers et al, J.Chem.Phys. 52, 3208 (1970)

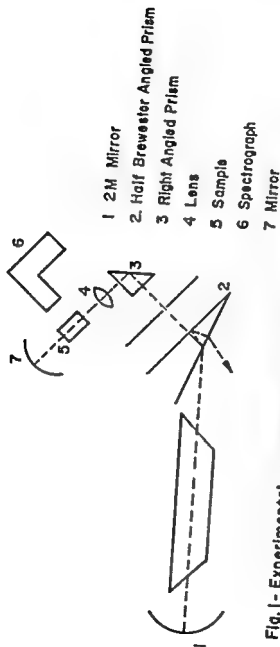


Fig.1- Experimental arrangement for photographing fluorescence spectrum

Region \AA	No. of lines	Probable upper level
6410-6350	12	5F_5
5377-5370	3	5S_2
5353-5310	9	5F_4
4820-4790	7	5F_3
4700-4650	11	3K_8
4496-4490	6	-
4480-4450	14	5G_6
4150-4120	11	5G_5
3850-3830	4	5G_4
3620-3550	11	$^3H_6, ^3H_5$
3420	1	$^5G_3, ^3L_9$
3330-3300	4	$^3K_6, ^3F_4$

As was the case in other host materials some of the lines are found to be extremely sharp while a few are very broad, the largest width being $\sim 6\text{cm}^{-1}$. In our experiments conducted at $\sim 15^\circ\text{K}$ it is expected that the Z_2 level ($\sim 5\text{cm}^{-1}$ from the Z_1 component) will be populated enough to partake in the transitions.

The fluorescence spectrum at room temperature, excited by the He-Ne laser, showed six lines at 6407, 6369, 6362, 6351, 6342 and 6337 \AA . The room temperature absorption spectrum recorded on Cary-14 spectrophotometer has low intensity at 6328 \AA (laser wavelength) as the edge of a broad band. There is, however, no absorption line at 6328 \AA at $\sim 77^\circ\text{K}$ or $\sim 15^\circ\text{K}$. We intend to take the fluorescence at low temps. to see whether it disappears.

REFERENCES

1. G.H.Dieke, and B.Pandey, J.Chem.Phys.41,1952(1964)
2. K.Rajnak, and W.P.Krupke, J.Chem.Phys.46,3532(1967)
3. I.Grohmann, K.H.Hellwege, and H.G.Kahle, Zeits. Fur Physik, 164,243(1961)

DISCUSSION

H.D. Bist

When I look into the emission spectrum excited by 6328\AA it appears to me more like a Raman spectrum. What is your objection to this explanation?

D.R. Rao

No observation of antistokes, and the far away positions of the lines rule out the observed spectrum as Raman spectrum. There is also coincidence for one line with absorption.

OPTICAL ABSORPTION SPECTRUM OF Ni^{2+} -DOPED NaF

J.P. Srivastava and F.A. Marayana
 Department of Physics
 Indian Institute of Technology, Kanpur-16

I. INTRODUCTION

The electronic absorption spectrum of Ni^{2+} in perovskite fluorides has extensively been studied by Ferguson and Guggenheim⁽¹⁾ and Ferguson, Guggenheim and Wood⁽²⁾. Earlier to these authors Knox, Shulman and Sugano⁽³⁾ have reported their studies on KNiF_3 and $\text{Ni}^{2+}:\text{KMgF}_3$, where they have concentrated mainly on the covalency effects. A comparative study of the spectrum of Ni^{2+} in KNiF_3 at room temperature and low temperature along with similar studies in $\text{Ni}^{2+}:\text{KMgF}_3$ and $\text{Ni}^{2+}:\text{KZnF}_3$ have enabled the earlier workers to understand the finer features of the spectra including the contribution of the magnetic exchange interactions. It was felt that studies on Ni^{2+} doped in a non-magnetic fluoride crystal like NaF could promote our understanding of the subject and the results obtained in such an investigation are reported here.

II. RESULTS AND ASSIGNMENTS

The absorption spectrum of NaF crystal doped with 0.1 mole per cent of Ni^{2+} has been recorded with a Cary 14 spectrophotometer at 300 and 80°K.

The sample shows characteristic absorption of Ni^{2+} in octahedral field. The spectrum observed at 300°K consists of four absorption bands located around 13,300, 7700, 6558 and 4115Å. While three of observed bands are quite intense, the fourth peak around 6558Å^{0.1} weak and appears in the form of a shoulder to the

on its higher energy side.

The ground state of Ni^{2+} in octahedral symmetry⁽⁴⁾_(O_h) is ${}^3A_{2g}(F)$ with the configuration $(t_{2g})^6(e_g)^2$. According to the energy level scheme, three spin-allowed bands should be observed which arise due to the transitions from the ground state to the excited states ${}^3T_{2g}(F)$, ${}^3T_{1g}(F)$ and ${}^3T_{1g}(P)$ arranged in the order of increasing energy. A comparison of spectra of Ni^{2+} in different fluoride crystals suggests that the three intense bands observed at 13 300, 7 700 and 4115 Å correspond to the transitions to the levels ${}^3T_{2g}(F)$, ${}^3T_{1g}(F)$ and ${}^3T_{1g}(P)$ respectively. As mentioned earlier, we have observed a weak band at 6558 Å. Knox, Shulman and Sugano⁽³⁾ have observed a similar band in $KNiF_3$. It is assigned to the spin-forbidden transition ${}^3A_{2g}(F) \longrightarrow {}^1E_g(D)$.

When the crystal is cooled to 80°K, the changes in intensity and band positions are observed. The intensity of ${}^3T_{1g}(P)$ band is found to decrease whereas that of ${}^1E_g(D)$ band increases. No noticeable change in the intensity of ${}^3T_{2g}(F)$ band could be observed. The oscillator strengths (f-values) of the bands along with details of the spectrum are given in Table I. All the bands show blue shift at low temperature. ${}^1E_g(D)$ band now appears as a double peaked band.

III. DISCUSSION

The measurements show that the intensity of the ${}^3T_{2g}(F)$ band practically does not change on cooling, which suggests that the corresponding transition is almost independent of vibrations. This transition is probably allowed through the magnetic dipole moment as established by Ferguson et al⁽⁵⁾ in $Ni^{2+}:KMgF_3$ the intensity of ${}^1E_g(D)$ band can be explained on the basis of spin-orbit mixing where it

TABLE I

Experimental data and analysis of the absorption spectrum of Ei^{2+} -doped NaF at 80°K

Transition	Observed		Calculated (cm^{-1})	$f \times 10^6$
	λ (\AA)	(cm^{-1})		
${}^3\text{A}_{2g}(\text{P})$				
${}^3\text{T}_{2g}(\text{P})$	13 072	7 650	7 700	3.4
${}^3\text{T}_{1g}(\text{P})$	7 600	13 158	12 959	8.0
${}^1\text{E}_g(\text{D})$	6 500	15 385	15 382	
	6 324	15 873		
${}^3\text{T}_{1g}(\text{P})$	4 105	24 361	24 391	11.4

$B = 950 \text{ cm}^{-1}$, $C = 4210 \text{ cm}^{-1}$ and $Dq = 770 \text{ cm}^{-1}$

borrow intensity from ${}^3\text{T}_{2g}(\text{P})$ through its interaction with the Γ_3 component of ${}^3\text{P}_{2g}(\text{P})$. The shift observed in the different bands is contributed partly to the lattice contraction and partly to the thermal depopulation of the ground state vibrational levels.

Another point, which deserves a more careful discussion, is the structure of ${}^1\text{E}_g(\text{D})$ band at 80°K . As pointed out earlier an additional line appears on the higher energy side of the original line. The origin of this satellite at 6324 \AA (Table I) has been discussed by several workers in other crystals. Sugano and Tanabe⁽⁶⁾ have suggested that this line could appear as a result of the excitation at an ion-pair. Balkanski, Koch and Shulman⁽⁷⁾ have attributed it to the stabilisation of ground state due to exchange effects in KLiF_3 and NaF_2 . More recently, Zannarichi and Bongers⁽⁸⁾ have identified two similar lines (a^* , b^*) as magnon sidebands corresponding to the two magnetically inequivalent sites in HbNiF_3 . But these sources, which are mainly magnetic in nature, are out of question in Ei^{2+} .

because LaF_3 is diamagnetic and the concentration of Ni^{2+} is very small (0.1% per mole). But according to Ferguson and Guggenheim⁽¹⁾, the energy surfaces of $^1E_g(D)$ state are displaced with respect to ground state in such a way that the minimum lies at relatively larger values of the internuclear distances. This occurs because of the spin-orbit interaction discussed above. Therefore a convincing reason for the appearance of the additional line at $6324\overset{0}{\text{\AA}}$ seems to be the excitation of a mode involving more than one phonon, known more commonly as a multiphonon mode.

REFERENCES

1. J. Ferguson and H.J. Guggenheim, J. Chem. Phys., 44, 1095 (1966).
2. J. Ferguson, H.J. Guggenheim and D.L. Wood, J. Chem. Phys., 40, 322 (1964).
3. J. Knox, R.G. Shulman and S. Sugano, Phys. Rev., 130, 512 (1963).
4. Y. Tanabe and S. Sugano, J. Phys. Soc. Japan, 9, 766 (1954).
5. J. Ferguson, J.J. Guggenheim, L.F. Johnson and H. Kamimura, J. Chem. Phys., 38, 2579 (1963).
6. S. Sugano and Y. Tanabe, Tech. Rep. Inst. Solid State Phys., Univ. Tokyo Ser., A71, 1 (1963).
7. W. Balkanski, P. Moch and R.G. Shulman, J. Chem. Phys., 40, 1597 (1964).
8. A. Zanmarchi and P.F. Bongers, Solid State Commun., 6, 27 (1968).

ON THE T^2 RATE OF HEATING FOR TSC UNDER CHARGE NEUTRALITY CONDITION

T.C. Manchanda and V.V. Mathur
Department of Physics, Kurukshetra University, Kurukshetra.

I. INTRODUCTION

Saunders⁽¹⁾ has pointed out that in the 2nd order kinetics of TSC based on Garlick and Gibson⁽²⁾ model, the mean life time τ of carriers is not constant and under charge neutrality condition

$$f = n + h \approx h \quad \dots\dots(1)$$

it is inversely proportional to h , where f is the number of vacant recombination centres and h that of filled traps.

Chen⁽³⁾ has investigated the effect of non-constancy of τ on TSC curves for Garlick and Gibson model for linear rate of heating and has shown that under charge neutrality condition of eqn. (1) the TSC curve rises and after attaining a maximum falls rather very slowly.

Kelly and Laubitz⁽⁴⁾ have suggested a rate of heating proportional to T^2 with certain advantages. Here we have investigated, therefore, the effect of such a rate of heating on the TSC under charge neutrality condition.

II. THEORETICAL

The rate equations for the present are

$$\frac{dn}{dt} = \alpha n - \beta n(h-n) - \gamma n \quad \dots\dots(2)$$

$$\frac{dh}{dt} = -\alpha h + \beta n(h-n) \quad \dots\dots(3)$$

where α is probability for an electron to escape from the trap, β for retrapping and γ is the probability of recombination of an electron with a hole.

the total number of traps.

Under the usual condition $\frac{dn}{dt} \ll \frac{dh}{dt}$ and for $\beta = \gamma$, the equation (2) gives

$$n = \frac{\alpha h}{\beta H} \quad \dots\dots\dots(4)$$

Substituting this value of n in (3) we get

$$\frac{dh}{dt} = \alpha - \frac{\alpha h^2}{H} \quad \dots\dots\dots(5)$$

which yields on integration

$$h = \frac{h_0}{1 + \frac{\alpha_0 h_0}{H} \int_{T_0}^T \frac{e^{-E/KT}}{q} dT} \quad \dots\dots\dots(6)$$

q being the rate of heating and T_0 the initial temperature.

The TSC is given by

$$\sigma = e \mu n = e \mu \frac{\alpha_0 h_0}{\beta H} \frac{e^{-E/KT}}{1 + \frac{\alpha_0 h_0}{H} \int_{T_0}^T \frac{e^{-E/KT}}{q} dT} \quad \dots\dots\dots(7)$$

For $q = AT^2$, we have

$$\sigma = e \mu \frac{\alpha_0 h_0}{\beta H} \frac{e^{-E/KT}}{1 + \frac{\alpha_0 h_0 k}{H A E} e^{-E/KT}}$$

~~The condition for maximum TSC~~

The condition for maximum i.e. $\left. \frac{d\sigma}{dT} \right|_{T=T^*} = 0$, where T^* is the temperature at the maximum, gives

$$\frac{\frac{\alpha_0 h_0 k}{H A E} e^{-E/KT^*}}{1 + \frac{\alpha_0 h_0 k}{H A E} e^{-E/KT^*}} = 1 \quad \dots\dots\dots(8)$$

which cannot be satisfied for any value of T^* , indicating thereby that the TSC curve exhibits no maximum.

For $q = C$, σ to a good approximation is given by

$$\sigma = e \mu \frac{\alpha_0 h_0}{\beta H} \frac{e^{-E/KT}}{1 + \frac{\alpha_0 h_0 k}{H C E} T^2 e^{-E/KT} \left(1 - \frac{2KT}{E}\right)}$$

which leads to the following result

$$\frac{e^{E/KT^*}}{T^{*3}} \approx 2 \frac{\alpha_0 h_0 k^2}{H C E^2} \quad \dots\dots\dots(9)$$

This condition is always satisfied for some value of T^*

so that TSC curve would exhibit a maximum in this case.

III. RESULTS AND DISCUSSION

The results of eqns.(8) and (9) have been verified by plotting the values of $\frac{\sigma}{e\mu}$ for the two cases. To account for the behaviour of σ , neglecting temp. dependence of μ , consider the expression

$$\sigma = - e\mu\tau \frac{dh}{dt}$$

so that $\log \frac{\sigma}{e\mu} = \log \tau + \log(-\frac{dh}{dt}) = \log(\frac{1}{\beta h}) + \log(\frac{dh}{dt})$
 For T^2 rate of heating, initially τ does not vary much but at higher temperatures the increase in $\log \tau$ compensates the decrease in $\log(-\frac{dh}{dt})$. Consequently σ initially rises in the same manner as $(-\frac{dh}{dt})$ but at higher temps^{erature}, it tends to asymptotic value of $\frac{e\mu AE}{\beta k}$. For linear rate of heating, the rise in $\log \tau$ at higher temperatures is considerably less than the fall in $\log(-\frac{dh}{dt})$. σ , therefore, after an initial rise falls down and approximately tends to $\frac{e\mu CE}{\beta k T}$ within the range of the ^{exptl} ~~exptl~~. Thus σ would continuously decrease with temperature at higher temperatures after having a maximum value.

Generally the experimentally observed TSC curves fall much more rapidly than the theoretical curves under charge neutrality condition. Above considerations shown that with the linear rate of heating the TSC curve analysis by the methods utilizing half intensity temperatures, particularly the higher one, are of doubtful utility and further T^2 rate of heating is not desirable under the charge neutrality condition as the maximum does not occur and hence no method (except the method of initial rise of Garlick and Gibson) of analysis can be applied.

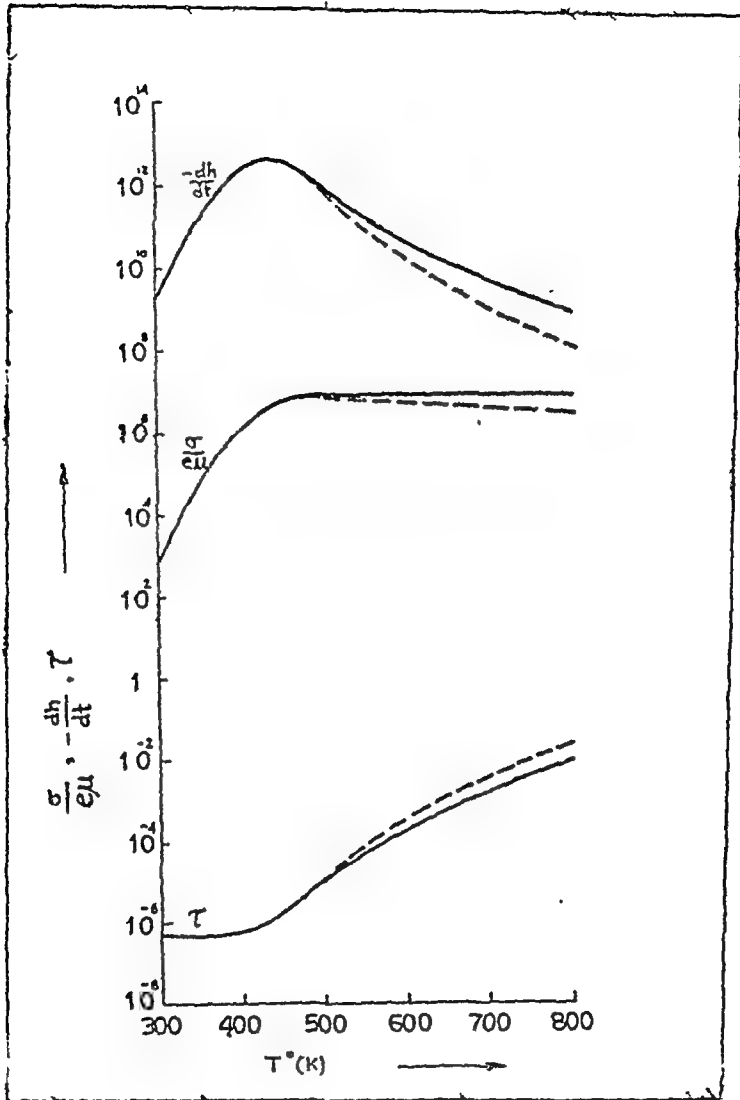


Fig -1

Variation of $-\frac{dh}{dt}$ and τ with temperature. Solid curves are for $q = A T^2$ rate of heating ($A = 10^{-5} \text{ deg}^{-1} \text{ sec}^{-1}$). Broken curves are for linear rate of heating ($q = 2 \text{ deg. K sec}^{-1}$)

Thus we summarize the behaviour of TSC curve under charge neutrality condition as follows

(a) linear rate of heating

(1) first order process-no TSC peak⁽⁵⁾

(2) second order process- a TSC peak is observed such that the rise of the TSC is much faster than decay⁽³⁾

(b) Non-linear rate of heating ($q = At^2$)

(1) first order process---- no TSC peak⁽⁵⁾

(2) second order process--- no TSC peak(present investigation).

Authors feel that the above properties may indicate whether the charge neutrality condition in a system is valid or is not valid. In case the charge neutrality condition holds, which is considered normally to be the case, the above model is rather inadequate to explain the observed physical processes.

REFERENCES

- (1) I.J.Saunders; Brit. J.Appl. Phys., 18, 1219 (1967)
- (2) G.F.J.Garlick and A.F.Gibson; Proc.Phys.Soc., 60, 574 (1948).
- (3) R.Chen; Brit.J.Appl. Phys.(JPhys. D.), Ser.2,2, 371 (1969).
- (4) P.J.Kelly and M.J.Laubitz; Can. J. Phys., 45, 311, (1967).
- (5) P.Bräudlich and A.Scharmann; phys. stat.sol., 18, 307,(1966).

LIFETIMES OF POSITRONS IN ALKALINE EARTH HALIDES

K.P. Singh and R.M. Singru
Indian Institute of Technology, Kanpur

I. INTRODUCTION

Recently Garg and Saraf⁽¹⁾ have tried to explain the positron lifetime data of Bisi et al.⁽²⁾ on alkali halides by assuming that the longer lifetime τ_2 ($\sim 0.3 - 0.8$ nsec) arises out of an interaction of positrons with electron plasma surrounding the halogen atom. They write $\lambda_2 = \frac{1}{\tau_2}$ as

$$\lambda_2 = \lambda_0 + \lambda_p \quad \text{-- (1)}$$

where λ_0 is the annihilation rate of the $(e^+-\text{anion})$ complex and λ_p is the pick-off rate. They assume $\lambda_p = N \tau_0^+ C \rho$ where ρ is effective electron density for each halogen atom and $\lambda_0 = 0.8 \times 10^9 \text{ sec}^{-1}$ for chlorides. Eq.(1) has been extended to other halides (I) by writing it as

$$\lambda_2 = \lambda_0 \left(r_{cl}/r_x \right) + \lambda_p \left(r_x/r_{cl} \right)^3 \quad \text{-- (2)}$$

where r_{cl} and r_x are respectively the chloride and other ionic radii. In the expression for λ_p , ρ has been taken as seven times the molecular density of the halide. The values obtained from this model for alkali halides are in very good agreement with the experimental values of Bisi et al.

We have tried to extend the model of Garg et al to the positron lifetime data on alkaline earth halides reported by Garbarini and Zappa⁽³⁾.

II. PRESENT CALCULATIONS

In our modification of eq (2), we have replaced λ_0 by $2\lambda_0$, since for each molecule of alkaline earth halide there are now two halogen ions which can form complex of the type $(e^+-\text{anion})$. Further, for calculating λ_p we take the effective electron density ρ as equal

to fourteen times the molecular density (n) because in alkaline earth halides we can expect fourteen electrons to contribute to the electron plasma in a molecule. After putting the values of λ_0 and λ_p the expression for λ_2 is as follows:

$$\lambda_2 = \left[1.6 \left(\gamma_{ce} / \gamma_x \right) + 1.05 n \left(\gamma_x / \gamma_{ce} \right)^3 \times 10^{-22} \right] \times 10^9 \gamma_{ce}^{-1} \quad \text{--- (3)}$$

Using this formula we have calculated $\tau_2 = \frac{1}{\lambda_2}$ values for the alkaline earth halides studied by Gambarini et al.

TABLE I

Sample	Expt (+) τ_2 (10^{-10} sec)	Expt (+) I_2 (%)	Calc. τ_2 (10^{-10} sec)	V_i (%)
1. MgF_2 (S.C)*	3.06 ± 0.09	37.0 ± 1.9	3.00	38.4
2. CaF_2 (S.C)*	3.28 ± 0.10	43.5 ± 2.2	3.16	41.5
3. SrF_2 (S.C)*	3.47 ± 0.10	51.1 ± 2.6	3.34	45.7
4. BaF_2 (S.C)*	3.78 ± 0.11	62.6 ± 3.1	3.52	50.5
5. $BaCl_2$	5.73 ± 0.17	17.1 ± 0.9	3.62	33.1
6. $CaBr_2$	6.23 ± 0.19	38.5 ± 1.9	3.68	32.3
7. $SrBr_2$	5.39 ± 0.16	41.5 ± 2.1	3.65	28.6
8. SrI_2	7.41 ± 0.22	28.8 ± 1.1	3.52	23.5

(S.C)* = Single Crystal; + Data from Ref. 3

III. RESULTS

The results of our calculations of τ_2 values are summarized in Table I. We find that in case of fluorides, which were studied in the form of single crystals, the agreement between the calculated and the reported values of τ_2 is excellent. However, such an agreement for other four halides (which have been studied in the form of multicrystalline samples) is rather poor. It is important to mention here that even the measured τ_2 - values in these four

halides are larger by a factor of two as compared to the fluorides. The reason for this disagreement is not clear to us but it seems likely that the multicrystalline nature of these samples could give rise to some unresolved longer lifetime components⁽⁴⁾ thus increasing the τ_2 - values. In any case, single crystal data should be more reliable for any model application of this kind.

In the present case of four alkaline earth fluorides we wish to point out that I_2 and τ_2 values increase with the interstitial volume, V_i (Table I). Such a dependence of τ_2 on V_i has already been observed⁽⁵⁾ in the case of alkali halides. Such a dependence on V_i seems to support the possibility of (e^- -anion) complex. Larger values of V_i should provide larger room for the formation of the complex leading to higher I_2 and larger V_i should decrease the pick-off rate leading to an increased τ_2 .

REFERENCES

1. J.C. Carg and B.L. Saraf, Chem. Phys. Letts. 2, 591 (1970).
2. A. Bisi, A. Fiorentini and L. Zappa, Phys. Rev. 134A, 328 (1964).
3. G. Gamberini and L. Zappa, Phys. Letts. 27A, 498 (1968).
4. R. Paulin and G. Ambrosino, Journ. Phys. 29, 263 (1968).
5. K.P. Singh, R.M. Singru and C.N.R. Rao, Chem. Phys. Letts. 3, 247 (1969).

POSITRON LIFETIMES IN SOME IONIC COMPOUNDS*

K. P. Singh and R. M. Singru
Indian Institute of Technology, Kanpur

I. INTRODUCTION

Among ionic solids positron lifetimes have been studied in alkali halides^(1,2) and several oxides⁽³⁾. The long-lived τ_2 (~ 0.5 nsec) component in alkali halides has been attributed⁽²⁻⁴⁾ to three major processes (i) annihilation from a complex compound (e^+ -anion) (ii) annihilation with vacancy or interstitial centres (crystal defects) and (iii) annihilation of positrons trapped in polaronic states. To understand these processes it is necessary to study positron annihilation in ionic solids other than alkali halides.

Recently Colombino and Fiesella⁽⁵⁾ have measured angular correlation of two photons resulting from positron annihilation in some ionic compounds such as sulphates, hydroxides, etc. From the observed intensities of the narrow components of the angular correlation curves, they conclude that positronium is formed in these compounds. We have measured positron lifetimes in some of the sulphates and hydroxides studied by Colombino and Fiesella with an aim to verify their results.

II. EXPERIMENTAL

Measurements were carried out with a time spectrometer (described elsewhere⁽⁶⁾) having a time resolution of 0.6 nsec with ^{60}Co prompt gamma rays. The positron source consisted of a $5\text{ }\mu\text{Ci } ^{22}\text{NaCl}$ deposited and sandwiched between two 0.1 mil thick nickel foils. All the samples were studied in air in the form of pellets prepared at a pressure of 8000 lb/in².

* Work supported by Department of Atomic Energy, Government of India.

III. RESULTS

The results of the present study are summarised in Table I. We could fit the lifetime spectra with two components. A search for a possible third component with lifetime $\tau_3 \gg 10$ nsec put an upper limit on its intensity $I_3 < 0.5$ %. A survey of Table I indicates that the relatively large lifetimes in these compounds are similar to those found in molecular systems (where positronium is formed) rather than alkali halides or oxides. This is not surprising since compounds such as sulphates and hydroxides containing oxyanions are not as highly ionic as alkali halides.

We find from our results that a plot of I_2 versus the interstitial volume V_1 has considerable scatter, perhaps due to the larger statistical errors in I_2 . We also find that our $\tau_2 - I_2$ data for sulphates and hydroxides is satisfactorily described by the 'free-volume model' equation⁽⁷⁾

$$\frac{4}{3} I_2 = a [1 + \ln(\tau_2/\tau_1)] / [b + \ln(\tau_2/\tau_1)] \quad \text{---(1)}$$

with $a = 4.0$ and $b = 0.01$. We, therefore, feel that our results support the possibility of positronium formation in these ionic compounds.

REFERENCES

1. A. Bisi, A. Fiorentini, and L. Zappa, *Phys. Rev.* 134A, 323 (1964).
2. C. Sussolati, A. Dupasquier and L. Zappa, *Nuovo Cimento* 52B, 529 (1967).
3. P. Sen and A.P. Patro, *Nuovo Cimento* 64B, 324 (1969).
4. V.I. Goldanski and E.P. Prokopen, *Sov. Phys. Solid State* 6, 264 (1965); *ibid* 8, 409 (1966).
5. P. Colombino and B. Fiscella, *Nuovo Cimento* 58B, 413 (1968).
6. K.P. Singh, R.M. Singru and C.N.R. Rao, *J. Phys. B* (Proc. Phys. Soc. (1970) To be published.
7. B.V. Thosar, V.G. Kulkarni, R.T. Lagu and G. Chandra, *Phys. Letts.* 28A, 760 (1969); also R.G. Lagu, V.G. Kulkarni, B.V. Thosar and G. Chandra, *Proc. Ind. Acad. Sci.* 69A, 760 (1969).

TABLE I

results of life-time measurements. In all compounds τ_1 was about 0.3 nsec. Values of interstitial volume v_i are taken from Ref.5.

S.No.	Compound	τ_2 (nsec)	I_2 (%)	v_i (%)
1.	Na_2SO_4	1.89 ± 0.32	3.9 ± 1.6	51.73
2.	K_2SO_4	1.71 ± 0.12	5.3 ± 0.9	46.30
3.	$\text{MgSO}_4 \cdot 7\text{H}_2\text{O}$	1.45 ± 0.15	6.7 ± 2.4	55.94
4.	$\text{Na}_2\text{SO}_4 \cdot 10\text{H}_2\text{O}$	1.82 ± 0.13	3.2 ± 0.6	60.96
5.	LiOH	2.23 ± 0.40	2.4 ± 0.9	55.79
6.	$\text{Ca}(\text{OH})_2$	1.61 ± 0.20	4.8 ± 1.8	57.50
7.	$\text{Al}(\text{OH})_3$	1.94 ± 0.30	3.4 ± 1.3	44.93
8.	$\text{LiOH} \cdot \text{H}_2\text{O}$	1.14 ± 0.10	6.7 ± 1.7	55.38
9.	Li_2CO_3	1.51 ± 0.15	4.4 ± 1.4	50.00
10.	H_3BO_3	1.36 ± 0.10	13.5 ± 2.3	59.53

DISCUSSION

K. Rama Reddy

Search for the positronium formation in condensed nuclei by the angular correlation measurements is difficult. However the magnetic field quenching using high fields (~ 25 k G) will be positive test of the positronium formation. Further this should give the effect of the solid state environment on the positronium if one evaluates carefully, the hyperfine interaction. This interaction is proportional to the $|\psi(0)|^2$ and hence the solid state effects should shown up in careful measurements.

How do the lifetimes of positron vary in simple alkali metals or, in other words, with \hbar^2 ?

R. M. Singru

The lifetime τ is almost same for the alkali metals K, Rb, Cs but it is slightly lower for Na and Li, in that order.

M. P. Verma

You are saying that electrons collect around positron giving a density of 7, the molecular density. I feel most of the electrons in ionic crystals are tightly bound to the core and in your scheme, therefore, you have probably to say that the density is enhanced many more times than by a factor of 7 around a positron. This point needs perhaps a more critical examination and physical explanation.

R. M. Singru

Yes. A more physical explanation of this scheme is necessary.

M. Yussouff

In view of the volume requirements for the formalism of positronium, is it possible to perform positron annihilation experiments to study the mechanism of capture of positrons by defects?

R. M. Singru

Such experiments could always be tried.

ON POSITRON LIFETIMES VS. TWO GAMMA ANGULAR CORRELATIONS IN REAL METALS

J. C. Garg and B. L. Saraf

Department of Physics, University of Rajasthan, Jaipur

Calculations of core and valence enhancement factors due to positron electron interaction in metals are useful in understanding the results of two photon angular correlation experiments and the lifetime measurements simultaneously. The theoretical angular distribution of 2-gamma annihilation radiation calculated in the one-electron approximation are often in good agreement with experiment. The area under the theoretical angular distribution gives directly the annihilation rates; this rate is, however, smaller than the experimental rate by an order of magnitude. It is thus of interest to attempt a reconciliation of these two aspects of positron annihilation in metals.

The total annihilation rate of a positron in metals in one electron theory is given by^(1,2)

$$\lambda_t = \frac{c r_0^3}{8\pi^2} (A_v + A_c) = \lambda_v + \lambda_c \quad (1)$$

where A_v and A_c are the angular distributions of two photon annihilation radiation due to valence and core electrons respectively; r_0 is the classical electron radius and c is the velocity of light. The valence electrons are treated in the Wigner-Seitz approximation and the core electrons in the Bloch-tight binding approximation.

Following Ferrell et al.⁽¹⁾ the one electron rates can be enhanced by introducing angle independent enhancement factors K_v

and E_0 where ⁽⁷⁾

$$E_v = \frac{\lambda_{Pos}}{R_0} + \left(2 - \frac{\gamma_s^3}{\chi^3}\right) \quad (2)$$

and

$$E_c = \frac{8\pi^2}{c\gamma_0^2} \frac{(\lambda_{exp} - \lambda_v)}{A_c} \quad (3)$$

The calculated E_v/E_c values using Eqs. (2) and (3) for metals Na and Cu are given in Table I. The values of λ_{exp} are those obtained by Weisberg and Serke.⁽³⁾

To obtain the enhanced angular distribution the ~~enhanced~~ valence parts of angular distribution are enhanced by making E_v/E_0 as given in Table I. The positron wavefunctions and the angular distributions, resulting from valence and core electrons for Na and Cu have been computed in reference (1) and (4). The experimental and theoretical curves are then normalized to have the same areas. The curves for sodium is presented in fig. 1 together with the experimental curve from reference (5). The theoretical curve for the $[1\bar{1}0]$ direction in copper is presented in fig. 2. The experimental curve is from reference (6).

~~Theoretical curve for the~~

The agreement between the theory and experiment is fairly good. It may be mentioned here that to reproduce the angular correlations we have not used any adjustable parameter. Had we taken E_v/E_0 as variable, we should have obtained a ~~much~~ closer fit to experiments.

Table I

Metal	E_v	E_c	E_v/E_c
Cu ($r_B = 2.66$)	5.05	1.01	5.00
Na ($r_B = 3.96$)	12.28	5.3	5.72

REFERENCES

1. J.H. Terrell, H.L. Weisberg and S. Berko, *Positron Annihilation* (Academic Press, New York, 1967) p. 269.
2. J.C. Garg and B.L. Saraf, *J. Phys. Soc. Japan*, 27, 1895 (1969).
3. H. Weisberg and S. Berko; *Phys. Rev.* 154 249 (1967).
4. S. Berko and J.S. Flaskett, *Phys. Rev.* 112, 1877 (1958).
5. A.T. Stewart, *Can. J. Phys.* 35, 914 (1957).
6. K. Fujiwara and O. Suseoka, *J. Phys. Soc. Japan* 21, 1947 (1966).
7. J.C. Garg and B.L. Saraf^a, *Phys. Letters*, 30A, 369 (1969)

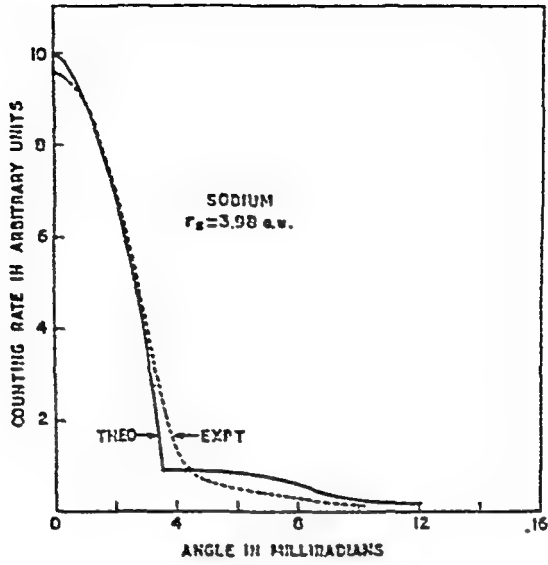


FIG. 1

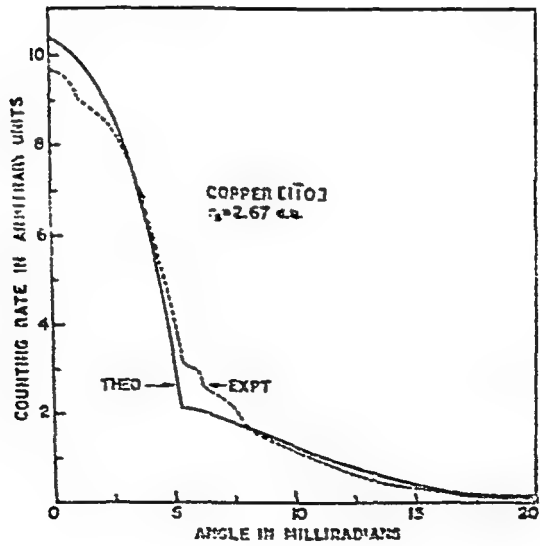


FIG. 2

EMPIRICAL CORRELATION BETWEEN POSITRON LIFETIME AND ELECTRON DENSITY IN METALS

Y S. Shishodia, B K. Sharma, Kamesh Chandra and B L. Saraf

Department of Physics, University of Rajasthan,
Jaipur

The lifetime of positron in an electron gas is governed by the density of electrons at the site of positron. The electron density at positron site is considerably enhanced. Compared to that in normal metal due to strong polarization effects of the positron. Perkins and Woll Jr⁽¹⁾ have given an empirical method of estimating the lifetime in transition metals. A generalization of their approach has been given by Shishodia and Saraf⁽²⁾ to include the rare earth metals.

The annihilation rate (inverse lifetime) is given by

$$\frac{1}{\tau_A} = \epsilon \pi r_0^2 c [\eta_c + \eta_d + \eta_f] \quad (1)$$

where r_0 is the classical electron radius, c is velocity of light, ϵ is density enhancement factor, η_c is density of conduction electrons and η_d , η_f are the densities of slightly deeper bound d and f shell electrons. The factors η and η_f have been included to account for the physically plausible fact that the positron has little coagulating effect on bound electron compared to conduction electrons.

The core contribution to two photon ^{annihilation} \angle in alkali metals, Mg and Si is known to be small. Assuming that the core contribution is small for lead also, we have chosen Cs, Rb, Y, Li, Na, Ag, Si and Pb, and using the results of Weisberg and Perko⁽³⁾

for positron mean lifetime, have calculated ϵ for each of them. A least square fit between ϵ and n_c has been found to be

$$= (2.30 \pm 0.13) + (53.71 \pm 0.67) \frac{1}{n_c} - (3.39 \pm 2.40) \frac{1}{n_c^2} \quad (2)$$

The constant factor K has been chosen as 0.04 to account for positron mean lifetime in copper and is assumed to be same for all d shell electrons while the constant η has been fixed at 0.010 to account for positron mean lifetime in a rare earth metals.

We have calculated the position mean lifetime in all the metals using Eq. (2) for the enhancement factor and the results are shown in figure 1. The calculated lifetimes agree within 10% with the measured lifetimes. The ~~rather~~ experimental values have not been shown for sake of clarity. The reliability of above approach in estimating the position mean lifetime in alkali metals under pressure and cerium phase transition will be published elsewhere (2).

Rare Earth Metals: The lifetimes in these metals have been calculated by assuming that they are trivalent except Eu and Yb which are bivalent. The agreement with measured values of Rodda and Stewart⁽⁴⁾ is good.

Transition Metals: The lifetimes of this class of ~~xx~~ metals have been calculated and indicate a large core contribution. It is known from bound structure calculations that the ~~3d~~ configuration $3d^{n+1}4s$ gives better agreement with experimental results than the

(5)

configuration $3d^x 4s^2$. Slater has discussed the possibility of occurrence of non integral number of electrons of the form $3d^{n+x} 4s^{2-x}$ in the two band. The parameter x which leads to minimum energy of the configuration has been found to be 0.46 for Cobalt and 0.51 for Ni.

We have calculated the mean lifetime in Cobalt configuration $3d^7 4s^2$, $3d^{7.5} 4s^{1.5}$ and $3d^8 4s^1$ and configurations $3d^8 4s^2$, $3d^{8.5} 4s^{1.5}$ and $3d^9 4s^1$ for Nickel. The results are given in Table I, along with measured lifetimes by Weisberg and Berko.

The calculated lifetime differs by about 20% for the two configurations and an intermediate configuration having non-integral number of electrons in the two bands might be really existing in these metals.

Conclusions: The calculated lifetimes for all metals are good agreement with measured lifetimes in general. This formation can be used to estimate lifetimes in metals and metallic alloys. With the availability of more accurate experimental values, the positron might serve as a tool for determining electron density.

References:

1. A. Perkins and E.J. Woll Jr., Phys. Rev. 178, 530 (1969).
2. Y.S. Shishodia and B.L. Saraf (to be published).
3. H. Weisberg and S. Berko, Phys. Rev. 154, 249 (1967).
4. J.L. Rodda and M.G. Stewart, Phys. Rev. 131, 255 (1963).
5. J.C. Ox Slater, J.B. Mann, T.M. Wilson and J.H. Wood, Phys. Rev. 184, 672-694 (1969).

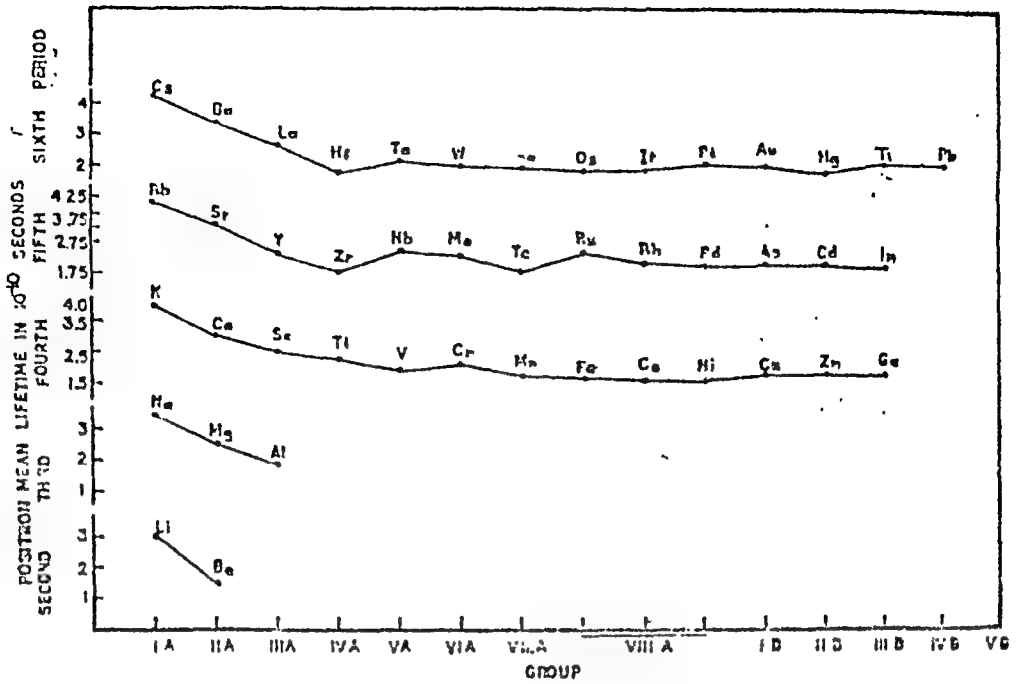


Table I. Positron mean lifetime in Cobalt and Nickel for various configurations. τ_{expt} are from Weisberg and Berko.

Element	Configuration	ϵ	τ_{est} (ns)	τ_{expt} (ns)
Cobalt	$3d^7 4s^2$	4.15	0.155	
	$3d^{7.5} 4s^{1.5}$	4.76	0.172	0.162
	$3d^8 4s^1$	5.97	0.186	
Nickel	$3d^8 4s^2$	4.14	0.152	
	$3d^{8.5} 4s^{1.5}$	4.76	0.167	0.175
	$3d^9 4s^1$	5.95	0.181	

POSITRON IN DEFECTS I. ESTIMATION OF POSITRON-DEFECT BINDING ENERGY AND CALCULATION OF TWO PHOTON ANGULAR CORRELATION CURVE IN METALS

I.S. Shishodia and B.L. Saraf

Department of Physics, University of Rajasthan, Jaipur, India

A simple model of 'trapping' of positron (1) by defects in metals has been successful in explaining the strong temperature dependence of positron mean life time in them. The angular correlation curves arising out of the annihilation of positrons in metals which are either at temperatures near in neighbourhood of their melting point or which have been plastically deformed to create defects (2, 3, 4) have marked differences from the annihilation curves in metals in which the defect number is practically zero. The localization of positron at the defect site would give it an increased kinetic energy. The purpose of this paper is to calculate the expected angular correlation curve arising out of annihilation of the trapped positron with a conduction electron, and estimate the energy with which the positron is bound to the defect.

We take the ground state wavefunction of the trapped positron to be (we use atomic system of units)

$$\psi_+(r) = \left(\frac{2^3}{\pi}\right)^{1/2} \exp(-2r)$$

where $\frac{1}{2}$, the "size" of the wave function is related to the binding energy W in the usual manner $\frac{1}{2} = \sqrt{2W}$

The distribution of p -ability $P(k_+)$ that this positron has momentum between k_+ and $k_+ + dk_+$ is

$$P(\vec{k}_+) \propto \left| \int e^{-i\vec{k}_+ \cdot \vec{r}} \cdot e^{-\gamma r} d^3\vec{r} \right|^2$$

$$\propto \frac{1}{(\gamma^2 + k_+^2)^4} \quad (2)$$

The electron momentum distribution $P(k_-)$ is given by the Fermi function at temperature T , but since the electron gas degeneracy is not lifted at temperatures at which experiments are done, we follow Brandt et al. (5) and take the electron momentum density to be that at absolute zero. Thus

$$\begin{aligned} P(\vec{k}_-) &= 1 & \text{for } k_- < k_F \\ &= 0 & \text{for } k_- > k_F \end{aligned} \quad (3)$$

To calculate the probability $P(k_-)$ that the annihilating γ -rays have momentum K_z in the z direction, we fold the momentum distribution of electrons given by Eq. (3) with that of the positron given by Eq. (2) and integrate over E_x, K_y .

$$P(K_z) \propto \int_{-\infty}^{\infty} \int_{-\infty}^{\infty} dk_x dk_y \int_{-k_F}^{+k_F} \int \frac{1}{(\gamma^2 + k_+^2)^4} \cdot \delta(\vec{k}, \vec{k}_- + \vec{k}_+) \quad (4)$$

$dk_x dk_y dk_z$

On integration this yields

$$\begin{aligned} P(x) \propto \frac{1}{2} (3x^2 - 3a^2 + 1) & \left\{ \tan^{-1}(x-a) - \tan^{-1}(x+a) \right. \\ & + \frac{x-a}{(x-a)^2+1} - \frac{x+a}{(x+a)^2+1} \left. \right\} + 2\chi \left[\frac{1}{\{(x-a)^2+1\}^2} - \frac{1}{\{(x+a)^2+1\}^2} \right] \\ & + (\chi^2 - a^2 - 1) \left[\frac{x-a}{\{(x-a)^2+1\}^2} - \frac{x+a}{\{(x+a)^2+1\}^2} \right] \quad (5) \end{aligned}$$

where $\chi = \frac{k_z}{\gamma}$ and $a = \frac{k_F}{\gamma}$ are dimensionless quantities

We have calculated the correlation curve from the expression (5) for various values of parameter 'a' and the variation of with a is shown in the figure. It is obvious from the figure that the localization increases the intensity of the correlation curve near the Fermi momentum. A careful measurement of temperature variation of the quantity $\frac{P(k_F)}{P(0)}$, will yield information about the energy of formation of vacancy and from the maximum value of this ratio where all positrons are trapped one can deduce the binding energy of the positron to the defect. We have estimated binding energies for a few metals namely Bi, Hg, Li, Na, K, Rb and Cs. In estimating the binding energies in Bi and Hg we have used experimental data of (3) and (4), and the energies are 1.17 eV, 0.84 eV. The alkali metal data are presented in slope form and in calculating the ratio the method suggested by Brandt (5) was followed. The intensity of two photon correlation curve near Fermi momentum was calculated at melting temperature using the effective mass values of Stewart. Assuming that this smearing is due to defects we have calculated the binding energies. The estimated values are 0.12, 0.10, 0.10, 0.12, 0.11 eV respectively for Li to Cs. However, because of the roundabout procedure followed in calculating the smearing these values may contain an error as large as 25%. The experiment of Brandt and Wang in Sodium indicate a mean lifetime change only after melting and thus one may conclude that these values are lower limits of binding energies. The calculated values agree satisfactorily with theoretically computed values of Hodges(6).

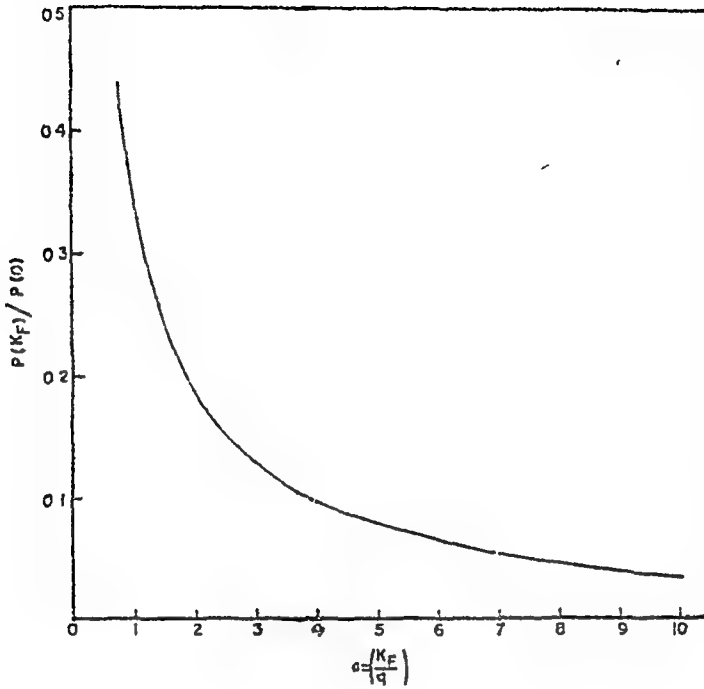


Figure 1. The variation of ratio of two photon intensity at Fermi momentum compared to that at zero momentum with positron localization.

References:

- (1) D.Q. Connors and R.H. West, Phys. Letters 30A, (1969) 24.
- (2) S. Berko and J.C. Erskine, Phys. Rev. Letters 19 (1967) 307.
- (3) D.R. Gustafson, A.R. Mackintosh and D.J. Zaffarano, Phys. Rev. 150 (1963) 1455.
- (4) R.H. West and H.E. Gussack, Positron Annihilation, Academic Press (1967).
- (5) W. Brandt, L. Eder and S. Lundqvist, Phys. Rev. 142 (1966) 165.
- (6) G.E. Hodges, Phys. Rev. Letters 25 (1970) 284.

DISCUSSION

K. Rama Reddy (Comment)

Since the authors are not present let me make some remark. If the wave function of the trapped positron is like s -state wave function then it is unlikely that one obtains pronounced changes at or around the Fermi momentum. The matrix element for the annihilation clearly rules out the possibility of having this increased intensity near the Fermi momentum.

POSITRON IN DEFECTS II.-INFLUENCE OF TRAPPED POSITRON ON INTERPRETATION OF EFFECTIVE MASS MEASUREMENTS

Y.S. Shishodia and B.L. Saraf

Department of Physics, University of Rajasthan, Jaipur

The temperature dependence of 2γ - angular correlation from positrons annihilating in alkali metals has been studied experimentally by Stewart and co-workers(1,2). Employing a model described by Kim (2) in detail they have used their data to determine the ratio m^* of the effective and bare masses and found the values 1.8 ± 0.3 , 1.8 ± 0.2 , 2.1 ± 0.3 , 2.3 ± 0.3 , $2.5(7)$ respectively in Li, Na, K, Rb and Cs. However, calculations of the electron positron, positron phonon, and in case of Na, the band effective mass (3) all tend to give values of m^* close to unity. This discrepancy makes it desirable to re-examine whether the experiment can be expected to give positron effective mass.

Majumdar (4) and Brandt et al. (5) have calculated the expected correlation curve arising out of annihilation of a thermalized positron, whose momentum distribution can be taken to be a Maxwellian, characteristic of temperature T of solid, with conduction electron gas. Since the influence of temperature is maximum near the Fermi momentum, Majumdar suggests a measurement of quantity $\frac{P(K_F)}{P(0)}$, where $P(K_F)$ is the probability that γ -rays have momentum K_F in Z direction and $P(0)$ is the probability of zero momentum in Z direction.

Majumdar has also considered extraneous effects of mean free path and thermal expansion but these terms are expected to be small at low temperatures.

However, these and all other workers have not taken account of the influence of vacancies which are created at higher temperatures. A vacancy represents an attractive potential for the positron and if the increase in kinetic energy is ~~minimized~~ outweighed by the potential energy the positron will be trapped and it will have a momentum distribution corresponding to that of a bound particle. Experiments on temperature variation of positron mean lifetime in sodium (6) and theoretical estimate of positron binding energy to defects (7) are two independent evidences which compel us to include the vacancy effects.

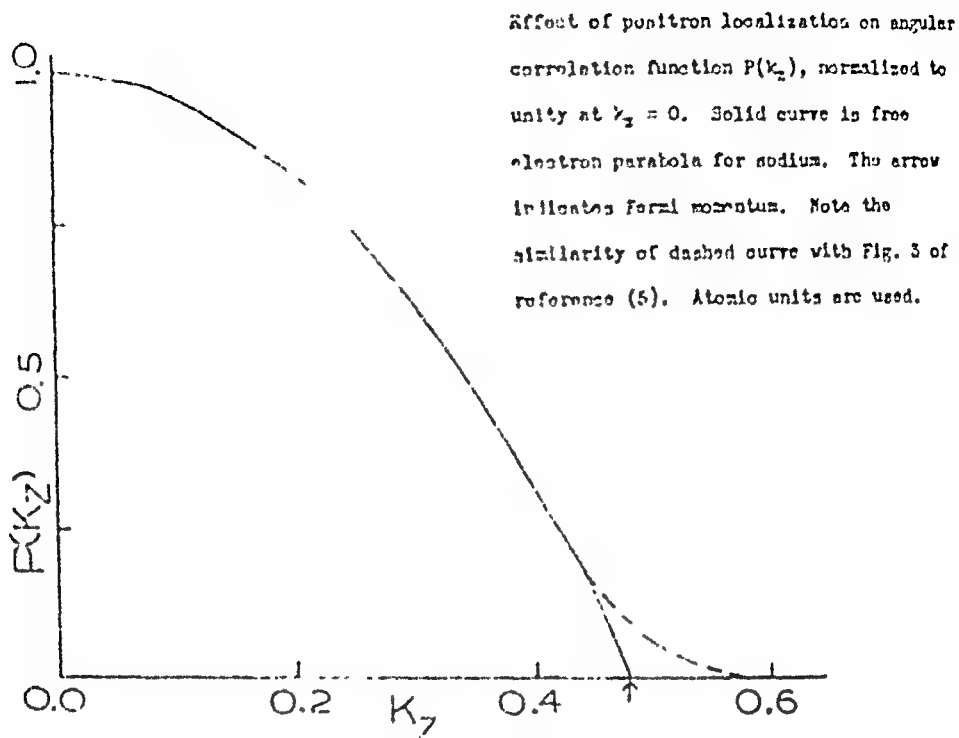
Describing the trapped positron by a wave function of the form

$$\psi_+(r) = \left(\frac{2}{\pi}\right)^{1/2} \exp(-qr)$$

where q is related to binding energy W by the relation $q = \sqrt{-2W}$ we have calculated the expected correlation curve arising due to annihilation of this trapped positron with a conduction electron gas, shown in fig. 1 along with the free electron parabola for a typical case of sodium metal (8). The curve for sodium and all other metals have the common feature of increased two photon intensity near the Fermi momentum. The ratio of two photon intensity at the Fermi momentum to that at zero momentum has been calculated using the binding energies given by Hodges (7). Although the positron-defect binding energies for alkali metals are ~ 0.01 Rydberg, owing to the variation of Fermi momentum the ratio is maximum for Cs and minimum for Li, the actual values being 0.068, 0.032, 0.101, 0.107 and 0.115 for Li, Na, K, Rb and Cs. This variation is similar to that of the effective masses.

A measurement of ratio $\frac{P(K_F)}{P(\sigma)}$ at any temperature will contain contribution from positrons which are annihilating as free particles and from trapped positrons. At temperatures below and near the melting point where the mean lifetime is independent of temperature, all the positrons are annihilating as free particles, and it is this region which should be investigated to look for the effective mass. However, only at two points 110°K and 300°K, experiments have been performed, and even here the positrons do not appear to be thermalized at 110°K. Thus there is lack of experimental data for a correct estimation of effective mass. The positron mean lifetime undergoes appreciable change on melting in Na thus implying that the positrons are trapped and then annihilated (6). The data analysis of Stewart and his group implies that they have assumed the positrons as thermalized and have Maxwellian momentum distribution at all temperatures, an assumption of doubtful validity for liquid metals, in which positrons are trapped.

Thus we are of the opinion that a careful measurement of temperature variation of ratio $\frac{P(K_F)}{P(\sigma)}$ is needed to correctly estimate the vacancy contribution to the smearing of the correlation curve, which in addition to measurement of effective mass can also be used to estimate the energy of formation of vacancy. Till such measurements are performed, the effective mass values given by Stewart can serve only as upper limits.



References:

1. A.T. Stewart and J.B. Shand, Phys. Rev. Letters 16, 261 (1966); S.M. Kim, A.T. Stewart and J.P. Carbotte, Phys. Rev. Letters 18, 385 (1967).
2. S.M. Kim and A.T. Stewart, Bull. Amer. Phys. Soc. 12, 532 (1967).
3. C.K. Majumdar, Positron Annihilation in Liquids and Solids in Theory of Condensed Matter, I.A.E.A., Vienna (1968).
4. C.K. Majumdar, Phys. Rev. ~~142A~~ 140, A237 (1965).
5. W. Brandt, L. Eder and S. Lundqvist, Phys. Rev. 142, 165 (1966).
6. W. Brandt and H.F. Waune, Phys. Letters 27A, 700 (1968).
7. C.H. Hodges, Phys. Rev. Letters 25, 284 (1970).
8. Y.S. Shishodia and B.L. Saraf, Proc. Nucl. Phys. and Solid State Phys. Symposium, Madurai 1970 (Preceding paper).

THERMAL AND DYNAMICAL PROPERTIES OF SOLIDS AND LIQUIDS

CRITICAL PHENOMENA IN THE BINARY LIQUID SYSTEM CARBONDISULPHIDE - ACETONITRILE COEXISTENCE CURVE

K.Govindarajan, R.D.Gambhir and E.S.R. Gopal
Department of Physics, Indian Institute of Science,
Bangalore-12.

I. INTRODUCTION

Partially miscible binary liquid mixtures offer some interesting features for study. Historically, the study of the coexistence curves of these mixtures was important in settling the then vital question whether the top of the coexistence curve is rounded or flat⁽¹⁾. But, nowadays, it is well established that the coexistence curve has a rounded top, and the interest, naturally, lies in the precise values of B_x and β , which govern the shape of the coexistence curve, close to T_c . If x' and x'' are the two mole fractions of the first component which have the same separation temperature T , then B_x and β are defined by $|x' - x''| = B_x(1 - T/T_c)^\beta$. In this paper, the results of the coexistence curve measurements on the system CS_2 - CH_3CN close to its UCST are given, and taking CS_2 as the first component, all mole fractions will be referred to mole % CS_2 .

II. EXPERIMENTAL ARRANGEMENT

The analar grade samples of CS_2 and CH_3CN supplied by the manufacturer (Merck Co., Germany) were used straightaway, without any further purification. The samples were contained in pyrex glass cells of about 8 ml capacity. Each cell had a vertical height of about 2 cms and had a capillary joined to it. Liquid samples to give the mixture of known composition were weighed and filled in each previously cleaned cell and small teflon seals were forcefitted into the capillary leaving very little dead space in the cells. The composition of each mixture is accurate to $\pm 0.02\%$.

The thermostat employed in the present measurement consists of a copper container of about 15 litres capacity, filled with paraffin oil and fitted with

While horizontal mixing of the thermostat fluid was ensured by the stirrer, vertical mixing was achieved by bubbling air through the fluid. Two perspex slits, cemented to the thermostat, were used for visual observation. The sample cells were contained in a beaker, also filled with paraffin oil and the latter was immersed in the thermostat. The temperature of the outer bath was electronically controlled to ± 20 millidegs. while the temperature in the glass beaker had a short time stability of ± 5 millideg. Temperature differentials and absolute temperatures were measured by a thermistor ($227^{\circ}\text{C} \sim 5\text{K}\Omega$) in conjunction with a high sensitivity 20 Hz a.c. bridge coupled with a p.s.d. While the differential temperatures were precise to ± 2 millidegree, absolute temperatures were accurate only to ± 50 millidegrees.

The samples were all raised to the one phase region and after allowing them to stand at this temperature for about an hour, gradual cooling was started. Preliminary experiments in which the cooling was done more rapidly gave an idea of the variations in the actual cooling in, the actual cooling in, ment was at about 100 milli in steps of 10 time for equilibrium after each step brown colors appeared near x viewed through light, and was very strong • large refractive index (2) phenomena and reproducible in

III. RESULTS AND

The phase different compositions from about 40 mol temperature of T

also apparent from Fig. I(a), the compositions having $x_1^1 = 58.23$ mole % and $x_1^2 = 59.20$ mole % separated at the same temperature. In other words, the difference in separation temperatures between them seems to be less than 1 millideg. and thus could not be resolved in the present experiment. Finer measurements, such as those done by Thomson and Rice⁴ or Vims et al.⁵ may perhaps reveal the difference. But observations clearly indicated that for the composition $x_1^1 = 58.23$ mole %, after the intense fogging was cleared, the meniscus appeared a little away from the middle and from the bottom, whereas for $x_1^2 = 59.20$ mole % the meniscus appeared almost from the middle. In view of all these, and also in view of the fact that the $(T_c - T)^{1/3}$ vs x plot, Fig. I(a), also indicates the same, the value $x_c = 59.20$ mole % CS_2 was chosen. The choice $T_c = 60.21 \pm 0.03$ is the direct experimental observation and the Fig. I(a) indicates the correctness of this choice.

This set of x_c , T_c values were used to analyse the top of the coexistence curve and to get the β and B_x values. The analysis is shown in Fig. I(b), where $\log_{10}|x-x_c|$ vs $\log(1-T/T_c)$ is plotted over the region $1.10^{-5} < (1-T/T_c) < 10^{-2}$. This plot indicates good linearity over the three decades of $(1-T/T_c)$ and gives $\beta = 0.36 \pm 0.02$ and $B_x = 1.90 \pm 0.1$. For comparison, the values of B_x and β obtained by other workers is as follows: Vims et al.⁵ for the system 3 methyl pentane-nitromethane have obtained $\beta = 0.33-0.34$ and $B_x = 2.01$; Thomson and Rice⁴ for the system perfluoromethyl cyclohexane - carbontetrachloride get $\beta = 0.35-0.37$ and $B_x = 1.68$; Rowden and Rice³ obtain $\beta = 0.340-0.347$ for the system aniline-cyclohexane; and Viswanathan et al.⁶ report $\beta = 0.35$ and $B_x = 2.1$ for the system carbon-disulfide-methanol. For a number of other liquid gas critical points and magnetic transitions also similar values $\beta \sim 0.34$, $B \sim 1.9$ have been reported⁷.

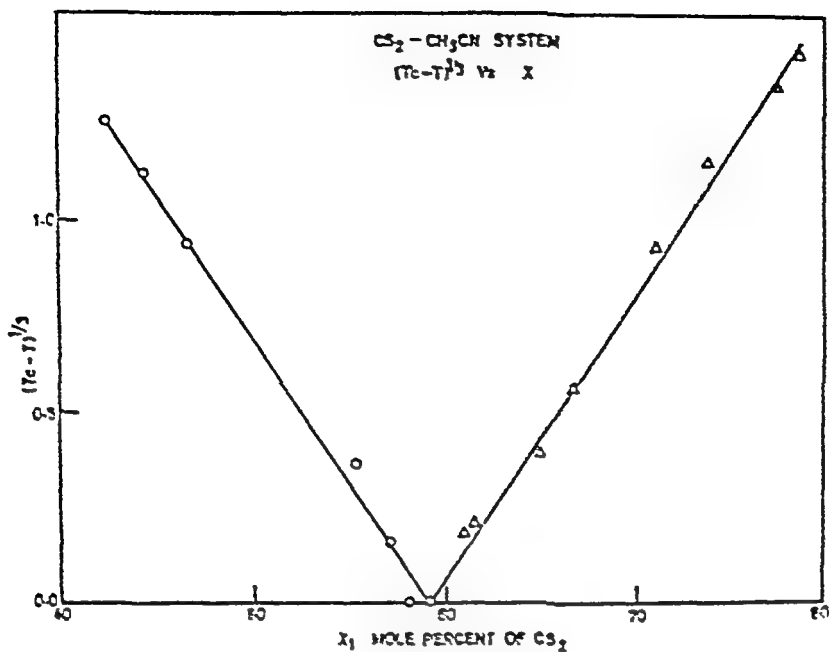
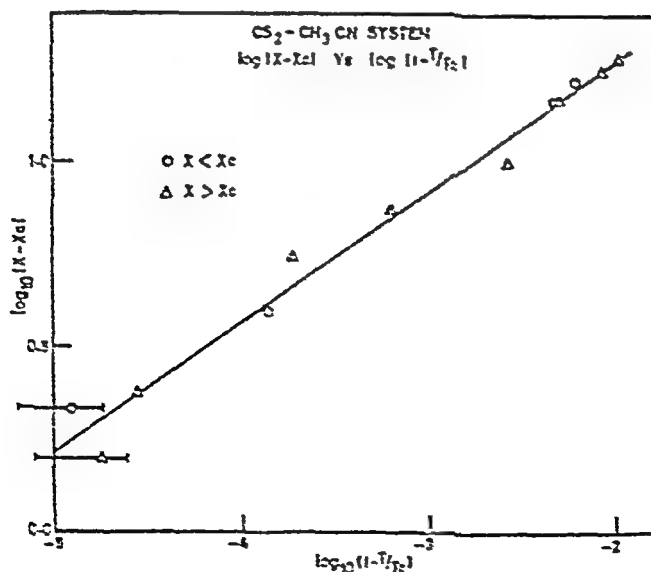


FIG. 1(a). Plot of $(T_c - T)^{1/3}$ against mole % of CS_2 in the binary liquid system $\text{CS}_2 - \text{CH}_3\text{CN}$.

FIG. 1a.



(b). Plot of $|X - X_c|$ against $(1 - T/T_c)$ for the system $\text{CS}_2 - \text{CH}_3\text{CN}$.

FIG. 1b.

Two earlier measurements⁴ of the coexistence curve are much flatter than the present curve. There is also some scatter in x_c , T_c . As is well known, such differences, may arise from chemical purity and lack of thermal equilibrium in some of the earlier studies.

REFERENCES

1. O.K. Rice; Chem. Rev. 44, 69 (1949).
A.P. Kudchadkar, G.H. Alani and B.J. Zwolinski;
Chem. Rev. 68, 659 (1968).
2. P. Mondain-Monval and J. Quiquerez;
Jour. Bull. Soc. Chim. 7, 914 (1940).
3. E.W. Rowden and O.K. Rice; J. Chem. Phys. 19,
1423, (1951).
4. D.R. Thomson and O.K. Rice; J. Amer. Chem. Soc.
86, 3547, (1964).
5. A.H. Wims, D. McIntyre and F. Hynne; J. Chem. Phys.
50, 616, 1969.
6. B. Viswanathan, R.D. Gambhir and E.S.R. Gopal;
J. Chem. Phys. (to be published).
7. P. Heller; Rept. Prog. Phys. 30, 731, (1967).
8. Landolt-Bornstein Tables II, edited by K.H. Hellwege
(Springer, Berlin 1962), Vol.2, pp. 3-550.

ACKNOWLEDGEMENT

It is a pleasure to thank Prof. R.S. Krishnan and Prof. P.S. Narayanan for much encouragement, Dr. S.V. Subramanyam and Mr. B. Viswanathan for considerable assistance during the experiments, the DAE and the CSIR for financial assistance and fellowships.

DISCUSSION

A.K. Jalaluddin

Is there any possibility of having the metastability of the system affecting your observations?

E.S.R. Gopal

Metastable states are avoided by two techniques- firstly waiting for a sufficient length of time at a fixed temperature but with gentle mechanical agitation. Secondly by cycling the temperature up and down between one phase and two phase regions.

CRITICAL PHENOMENA IN THE SPECIFIC HEAT OF THE BINARY LIQUID MIXTURE METHANOL-HEPTANE

B. Viswanathan, K. Govindarajan and E.S.R. Gopal
Department of Physics, Indian Institute of Science, Bangalore-12.

Following the work of Bagatskii et al.⁽¹⁾ on the C_p of argon, measured at the critical density, considerable interest has grown in the behaviour of specific heat near gas-liquid critical points for a number of substances and in the binary liquid systems close to their critical solution temperature (C.S.T.). In the case of binary liquid systems, the specific heat of interest is C_p , measured at the critical composition. There have been very few measurements on C_p near CST in binary liquid systems⁽²⁻⁵⁾. The existing data are not precise enough to make a quantitative study of the behaviour close to T_c . In the present paper we report the measurements on specific heat of the system methanol-heptane, measured at the critical composition and its immediate neighbourhood.

An adiabatic vacuum calorimeter constructed for the present study, has been used. The calorimeter vessel containing the sample is of silver. To facilitate uniformity of temperature in the liquid specimen and reduce the equilibrium time, a number of thin silver foils has been spot-welded inside the silver vessel. The calorimeter vessel is surrounded by an adiabatic shield, a floating shield and a vacuum jacket. The calorimeter vessel is filled with the required amounts of the liquids leaving minimum dead space and is sealed carefully at the top. Compositions are known correct to $\pm 0.02\%$ by weight.

The specific heat of $\text{C}_2\text{H}_5\text{OH}-\text{C}_7\text{H}_{16}$ mixture has been measured in the temperature interval $45-60^\circ\text{C}$ over the entire composition range, with special attention to the critical region. A very pronounced anomaly has been observed at the critical temperature $T_c = 51.82 \pm 0.05$ for the sample with composition $X_c = 61.40$ mole % of MeOH (Fig. I(a)). Anomalies have also been observed for samples with compositions in the close neighbourhood of X_c and they are less pronounced than that at X_c , as is clearly shown in Figure I(a). The L.H.S. corresponds to $X = 0.988 X_c$ and the R.H.S. corresponds to $X = 1.016 X_c$. This perhaps suggests the view that the magnitude of the singular contri-

bution to specific heat reduces as one moves away from X_c, T_c . Such anomalies at the critical density and its neighbourhood have been observed earlier by Moldover and Little⁽⁶⁾ in C_v on He^3 and He^4 . Our earlier work on CS_2 -methanol system⁽⁵⁾ also shows a similar behaviour.

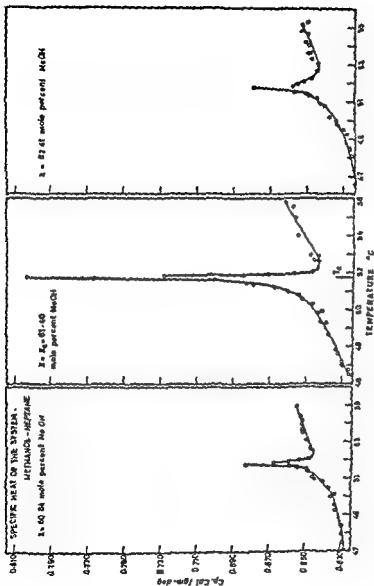
The anomaly in C_p at X_c has been analysed in terms of the logarithmic singularity given by $C_p^\pm = A_\pm + B_\pm \log_0 \left[1 - T/T_c \right]$ where the plus sign refers to $T > T_c$ and the minus sign $T < T_c$. The analysis is shown in Fig. 1(b). The two branches are represented with the coefficients $B_- = -0.0333$; $A_- = 0.455$ for $T < T_c$ and $B_+ = -0.03274$; $A_+ = 0.416$ for $T > T_c$. Nearly equal values of B_+ and B_- suggest a symmetric logarithmic singularity. Close to T_c the calorimetric step-width has been only 26-30 m.deg. and a small asymmetry in the coefficients B_+ and B_- cannot be ruled out with a slightly different choice of T_c . Within the experimental limits, $T > T_c$ branch appears to fit a weak power law also with $\alpha \approx 0.07$ where α is defined by

$$C_p^\pm = A_\pm' + B_\pm' \left[1 - T/T_c \right]^{-\alpha}$$

Voronel and Ovadova⁽⁴⁾ have recently measured and analysed the specific heat in methanol-cyclohexane near T_c and observe an asymmetric logarithmic singularity. However there is a small uncertainty in X_c in their measurements. A recent analysis⁽⁷⁾ on the specific heat data of triethylamine-water system shows that logarithmic and power-law singularities are equally acceptable. The same ambiguity persists in the present work also. Higher resolution experiments are needed to clarify the situation.

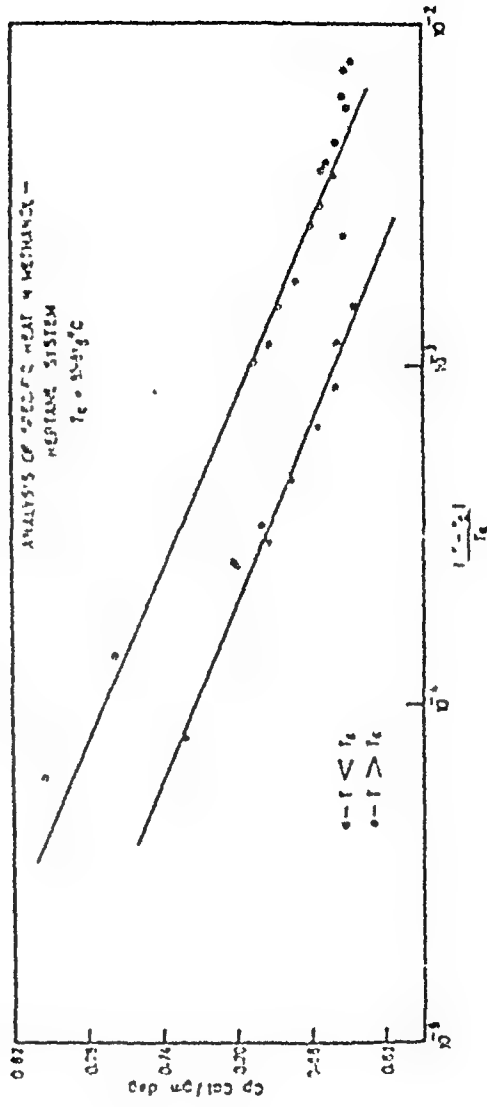
ACKNOWLEDGEMENTS:

The authors thank Prof. R.S. Krishnan and Prof. P.S. Narayanan for their encouragement, Mr. R.D. Gambhir and Dr. S.V. Subramanyam for their assistance in the early stages of the work, U.G.C. and DAE for their financial assistance and fellowships.



no 1a

Figure 1. (a) Specific heat of methanol-*n*-heptane system as a function of critical composition and its immediate neighbourhood.



(b) Analysis of the specific heat at X_{c1} C_p plotted against $\log [1 - T/T_c]$.

REFERENCES:

1. M.I. Bagatskii, A.V. Voronel and V.G. Gusak; Sovt. Fyz. JETP, 16, 517 (1963).
2. V.K. Serebrenko and Ya. V. Egupov; Zhur. Fiz. Khim. 32, 121 (1958).
3. H. Schmidt, G. Jura and J. Hildebrand; J. Fyz. Chem. 63, 297 (1959).
4. A.V. Voronel and T.M. Ovodova; Sovt. Phys. JETP Letters, 2, 169 (1969).
5. P.D. Gambhir, B. Viswanathan and E.S.P. Gopal; to be published. See also Proc. Nucl. Phys. and Solid State Phys. Symp., Roorkee, 1969 (under publication).
6. M.R. Moldover and W.A. Little; Proc. Conf. on Critical Point Phenomena NBS Misc. Publication, 1966.
7. Yu.F. Blagoi and V.G. Gusak; Sovt. Fyz. JETP, 29, 326 (1969).

DISCUSSION

J. Pasupathy

Is the Ising model used here in a similar way as it is for binary alloys?

E.S.R. Gopal

Yes. The only extension is that there are three variables - temperatures, pressure and composition.

A.K. Jalaluddin

In the case of liquid gas system the logarithmic nature of the critical specific heat dependence on temperature is not universally accepted. Is it possible that in the case of the binary mixture the objections are valid.

S.R. Gopal

The situation in binary liquids is the same as regards the α exponent. A logarithmic fit or a power law with $\alpha \sim 1/10$ is equally acceptable. The same ambiguity exists in many studies of liquid gas transitions.

CRITICAL PHENOMENA IN THE THERMAL EXPANSION OF THE BINARY LIQUID SYSTEM

 CS_2 -METHANOL

M V Iele (Central Instruments and Services Laboratory),
 B Viswanathan and E S P. Gopal (Department of Physics),
 Indian Institute of Science, Bangalore 12.

There have been very few measurements⁽¹⁻³⁾ made on the thermal expansion of the binary liquid mixtures, especially in the critical region. Although a lambda type anomaly has been suggested in thermal expansion close to the critical solution temperature⁽⁵⁾ (CST), the nature of the anomaly has not been resolved in any of the earlier data. The thermal expansion behaviour in CS_2 - CH_3OH system has an additional interest in that the specific heats of the system have been studied earlier⁽⁴⁾. The knowledge of both thermal expansion and specific heat close to CST enables one to discuss various aspects of the Pippard relations. In binary liquid systems, two quantities $\partial T_c / \partial P$ and $\partial X_c / \partial P$ are involved.

A dilatometer has been constructed for the present study. The dilatometer is of glass and volume change ΔV have been measured in the conventional way, by following small changes in the level of the liquid in a capillary attached to the dilatometer vessel. The capillary tube was of ~ 0.15 cm diameter so that it would be possible to detect small changes in volume without any breaking of the liquid column. The glass dilatometer was built with the view of studying the phase separation phenomena in the opalescent region near CS^* , as the measurements are carried out. Small changes in temperature were measured using a thermistor in an a.c. bridge. A small magnet, enclosed in a glass capsule, was placed inside the vessel and a rotation of the magnet ensured homogeneity of temperature in the liquid specimen. A dilatometer, with a metal bellows as the container for the liquid samples, was also built to study the thermal expansion over a wider range of temperature. This was made possible by adjusting the volume of the bellows. Both the dilatometers were calibrated by measuring the thermal expansion of the pure liquid components for which data were available. The data with the two dilatometers agreed to within one per cent.

The thermal expansion of CS_2 - CH_3OH mixture has been measured in the temperature interval 30 - 40°C over a wide range of compositions. Special attention was paid to the critical region as determined from

our earlier coexistence curve measurements on this system⁽⁵⁾:

$x_c = 80.5 \pm 0.5$ wt. % CS_2 and $T_c = 36.31^\circ C$. A very pronounced anomaly in thermal expansion has been observed close to T_c for the sample with the composition $x = 80.3 \pm 0.3$ wt.% CS_2 (Fig. I(a)). It might be recalled⁽⁴⁾ that an anomaly was observed in specific heat on the same system for the sample with the composition $x = 80.14$ wt. % CS_2 . The anomaly in α is more pronounced than that in C_p . The thermal expansion data near T_c has been analysed in terms of a logarithmic singularity on given by

$$\alpha = C^{\pm} + D^{\pm} \ln |1 - (T/T_c)|.$$

The analysis is shown in Figure I(b). There is a considerable scatter in the values of α in both branches. The temperature step-width in the present study has been only of the order of 50-100 m.deg close to T_c and much weightage cannot be given to values of α close to T_c . Further there was a possibility of some concentration gradients in the unstirred part of the liquid in the capillary. However the analysis suggests a more or less symmetric logarithmic singularity in α . In fact the two branches in Figure I(b) are characterised by the parameters

$$\begin{aligned} C^- &= 0.875 \times 10^{-3} & ; & & D^- &= -8.58 \times 10^{-5} & \text{for } T < T_c \\ C^+ &= 0.811 \times 10^{-3} & ; & & D^+ &= -8.27 \times 10^{-5} & \text{for } T > T_c \end{aligned}$$

This is interesting in the light of the fact that a symmetric logarithmic singularity was observed in specific heat near T_c in the same system⁽⁴⁾. This suggests the possibility of correlation, the asymptotic behaviour in α and C_p in terms of Pippard's scheme. More careful measurements of α are in progress to make a more quantitative study. The earlier experimental suggestion of a logarithmic singularity in thermal expansion was made by Atkins and Edwards in He^4 near the λ point and has been discussed by Buckingham and Fairbank⁽⁶⁾.

ACKNOWLEDGEMENT:

The authors thank Dr. S.V. Subramanyam for much assistance during the experiments, the DAE, UGC and CSIR for financial assistance.

REFERENCES:

1. I.P. Krichevskii, N.E. Khazanova and L.R. Linshits;
Zhur. Fiz. Khim. 29, 547 (1955).
 2. I.P. Krichevskii, N.E. Khazanova and L.R. Linshits;
Zhur. Fiz. Khim. 33, 1484 (1959).
 3. G. Jura, D. Praga, G. Inki and J.E. Hildebrand
Proc. Nat. Acad. Sci. USA, 39, 19 (1953).
 4. R.D. Gambhir, B. Viswanathan and E.S.R. Gopal.
Proc. Nucl. & Solid State Symposium, DAE, Roorkee (1969),
(under publication)
 5. B. Viswanathan, R.D. Gambhir and E.S.R. Gopal
Proc. Nucl. & Solid State Symposium, DAE, Roorkee (1969)
(under publication).
 6. M.J. Buckingham and W.M. Fairbank; Prog. in Low Temp.
Phys. Volume 3, p. 80 (1961), Ed. C.J. Gorter.
-

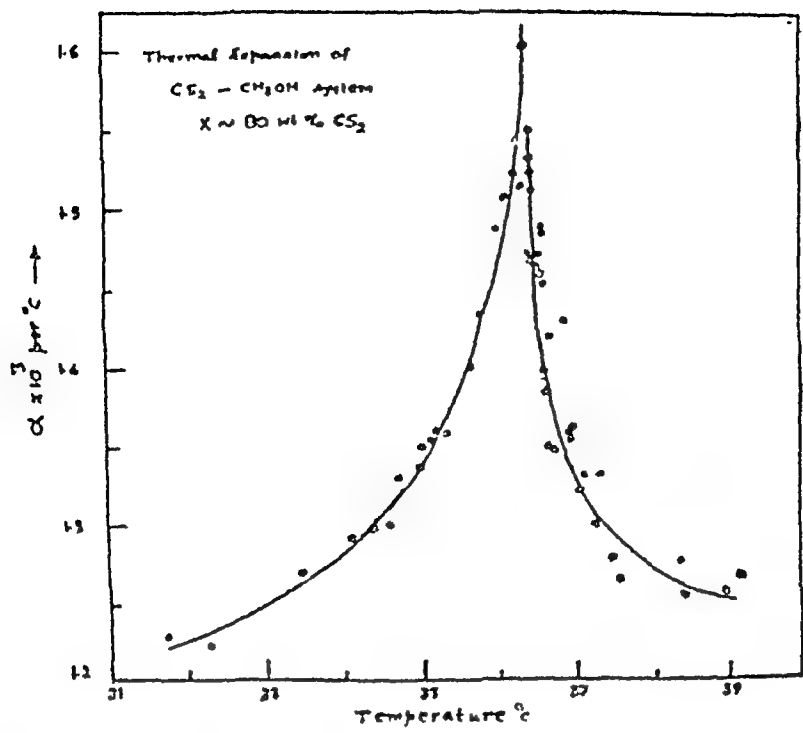
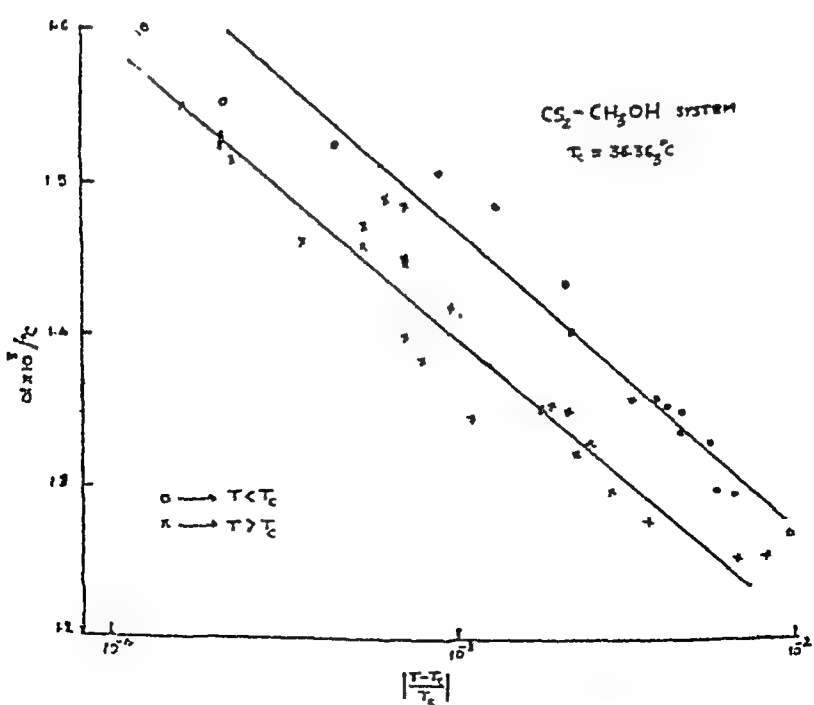


Figure I(a) Thermal expansion of $\text{CS}_2 - \text{CH}_3\text{OH}$ system at x_c, T_0 .



(b) Analysis of thermal expansion coefficient near T_0 shown on a semi-logarithmic scale.

CRITICAL PHENOMENA IN THE COEXISTENCE CURVE OF THE CARBON DISULPHIDE - ACETIC ANHYDRIDE SYSTEM

I.V. Lele, Central Instruments and Services Laboratory,
S.V. Subramanyam and E.S.R. Gopal
Department of Physics, Indian Institute of Science,
Bangalore-12

I. INTRODUCTION

The study of critical point phenomena in binary liquid mixtures gives valuable information on the general phase transformation processes. Several of the physical properties like heat capacity, thermal expansion etc., show anomalous behaviour in the vicinity of critical solution temperature. These measurements require an accurate determination of the coexistence curve of the binary system under consideration, which has also some interest in its own right in connection with the critical indices. In the present paper, we report the results obtained for the coexistence curve of carbondisulphide-acetic anhydride system. This is a typical polar-non-polar system exhibiting an upper critical solution temperature of about 30.56°C at a critical composition of 63.9% by weight of CS_2 . The results of earlier investigators⁽¹⁻⁴⁾ show much scatter in these data (T_c varying from 29.6 to 30.6°C , x_c varying from 63 to 68 wt.% of CS_2).

II. EXPERIMENTAL DETAILS

In the present work, samples of the liquids were taken from a large stock of analytical reagent grade chemicals and a large number of observations were made. The results were reproducible indicating that the effect of impurities, if any, is common to all measurements. The coexistence measurements were done in a new thermostat constructed for this purpose. A solid state proportional temperature controller was used and a constancy of temperature to about ± 2 millidegrees was obtained over a period of many hours. During some runs of exceptional stability, temperature constancy to within a millidegree was achieved near the critical temperature. ~~See~~

Temperatures were measured using a thermistor ($R_{25^{\circ}\text{C}} = 10\text{K}\Omega$) in a low frequency a.c. bridge giving a resolution of 0.5 millidegree. The absolute values of temperatures may possibly be off by as much as ± 30 mdeg but the differential temperatures, which are needed in the analysis of the coexistence curve, are accurate to a millidegree.

The mixing and demixing of phases in the binary system were observed in small glass bulbs of about 9 ml capacity. The height of the bulb was kept less than 2 cm to avoid gravity effects. Close fitting teflon plugs were used to seal the bulb capillary, leaving very little dead space. The compositions of two liquids were determined accurately by weight and are correct to $\pm 0.02\%$. The phase separation temperatures were found both while heating the system from two phase to one phase and while cooling the system from one phase to two phase. The appearance and disappearance of menses as well as the intensity of opalescence in transmitted light were used as the criteria to find phase separation temperature.

III.. RESULTS AND DISCUSSIONS

The coexistence curve obtained in the present investigation is shown in Fig.1(a) along with the curves of earlier workers. The exact location of critical point is done by using the law of rectilinear diameters. The critical values are found to be 30.56°C for T_c and 63.9 wt.% of CS_2 for x_c . In fact the bulb filled with the concentration showed the maximum opalescence and the interface appeared or disappeared just at the centre, as is to be expected for a critical system. The differences between the T_c , x_c values of the various studies arise probably from the differences in chemical purity and thermal instrumentation.

The coexistence curve can be fitted to an exponential law $(x' - x'') = B_x \left| (T_c - T)/T_c \right|^{\beta}$ where x' and x''

are the two compositions having the same phase separation temperature T . The exponent β is very important and it describes the mechanism of the phase transformation. For magnetic and gas-liquid transitions, it has a value $1/3$ and theoretical calculations for 3 dimensional lattice gas Ising model also give a value of about $1/3$. In order to determine β and B_x for this binary system, a log-log plot of $|x_c - x|$ vs $|(T_c - T)/T_c|$ is drawn and is shown in the Fig. I(b). The linearity is found to be valid over a large temperature range of $10^{-6} < |(T_c - T)/T_c| < 10^{-2}$. The slope of the straight line fit gives $\beta = 0.34 \pm 0.01$ and the constant $B_x = 1.68 \pm 0.1$. These values of β and B_x are in agreement with other estimates like those of Thomson and Rice⁵ for the binary liquid system perfluoromethylcyclohexane-carbon tetrachloride ($\beta = 0.36 \pm 0.01$; $B_x = 1.68$), Wins et al.⁶ for the binary liquid system 3-methyl pentanitroethane ($\beta = 0.33 \pm 0.01$, $B_x = 2.01$), Viswanathan et al.⁷ for carbondisulphide-methanol ($\beta = 0.35 \pm 0.03$, $B_x = 2.1$), Govindarajan et. al.⁸ for carbondisulphide-acetonitrile ($\beta = 0.36 \pm 0.02$; $B_x = 1.9 \pm 0.1$) and values like $\beta \sim 0.34$, $B_x \sim 1.8$ for a number of liquid-gas critical points and magnetic transitions⁹.

ACKNOWLEDGEMENT

The authors thank the authorities of the Institute of Science for allowing the use of facilities, Messrs B. Viswanathan and K. Govindarajan for considerable assistance and the DAE for financial support.

REFERENCES

1. D.C. Jones and H.F. Metts, J. Chem. Soc. London, p.1177 (1928).
2. G. Poppe, Chem. Abst. 30, 2826 (1936).
3. K.L. Hochalov, Chem. Abst. 32, 7333 (1938).
4. A.N. Campbell and E.M. Kartzmark, Can. J. Chem. 45, 2433 (1967).
5. D.R. Thomson and O.K. Rice, J. Amer. Chem. Soc. 86, 3547 (1964).
6. A.M. Wins, D. McIntyre and F. Hynes, J. Chem. Phys. 50, 616 (1969).
7. B. Viswanathan, R.D. Gambhir and E.S.R. Gopal, J. Chem. Phys. (in press).
8. K. Govindarajan, R.D. Gambhir and E.S.R. Gopal (This Proceedings)¹
9. P. Heller, Rept. Progr. Phys. 30, 731 (1967).

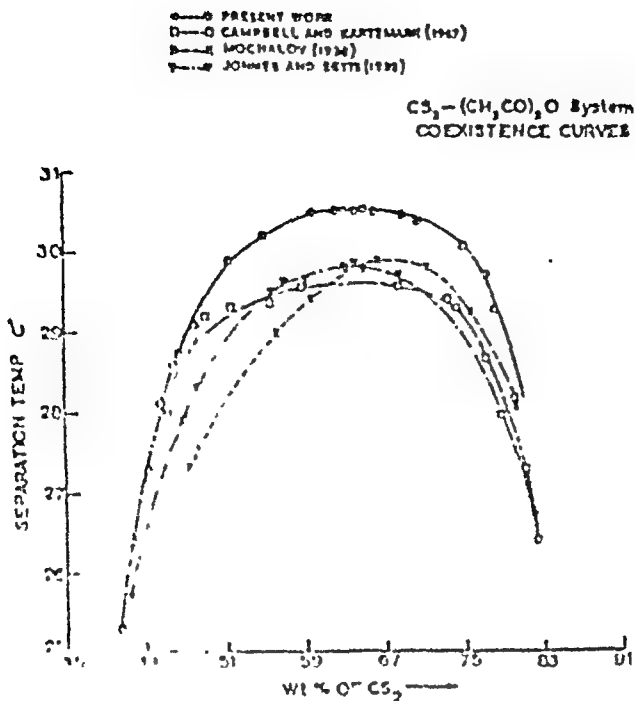
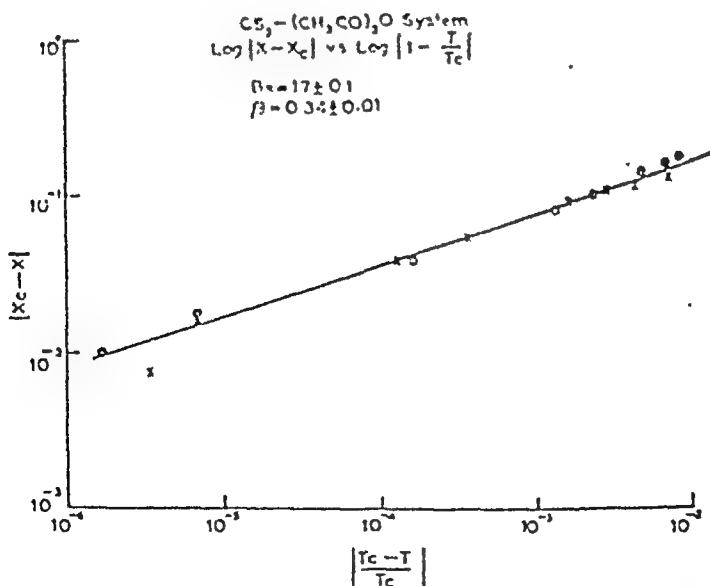


Fig. 1(a). Coexistence curves of $\text{CS}_2 - (\text{CH}_3\text{CO})_2\text{O}$ system;



(b). Variation of $|x - x_c|$ with $|1 - T/T_c|$ for the $\text{CS}_2 - (\text{CH}_3\text{CO})_2\text{O}$ system on a logarithmic scale.

DISCUSSION

H.D. Bist

You are trying to achieve temperature accuracy of the order of 10^{-6}°C ; What about the effect of the chemical composition and impurities on the value of α and β ?

E.S.R. Gopal

The temperature resolution is 10^{-3}°C , giving a fractional resolution $(T - T_c)/T_c$ of $1 \text{ in } 10^6$. The chemical impurities affect the critical composition and temperature but not the exponents α and β . We perform all the experiments on the same liquid samples thereby keeping the impurities common to all the measurements.

A.B. Biswas

The temperature has been measured to an accuracy of a millidegree. What is the difference between the heating and cooling curves?

E.S.R. Gopal

In coexistence curve there is no hysteresis measurable to this order. In the specific heats we have measured only during the heating rates. During cooling we have only observed the long time taken to cool across the critical temperature.

TEMPERATURE DEPENDENCE OF POSITRON LIFE-TIMES IN n-OCTANE AND n-HEXADECANE

B.V. Thossar, V. G. Kulkarni, R.G. Lagu and Girish Chandra
Tata Institute of Fundamental Research, Bombay 5

I. INTRODUCTION

It is well known that the lifetime spectra of positrons annihilating in molecular materials exhibit a delayed component, τ_2 , which has been attributed mainly to orthopositronium atoms decaying by the pick-off process. A free volume model for the formation and decay of ortho- Ps atoms in molecular materials has been reported earlier⁽¹⁾. The relative stability of the Ps atoms of near-thermal energy, diffusing through the medium is enhanced if the material has a number of regions of low electron density, called sites or cavities, where the Ps atom preferentially stops. Thus the free volume and its distribution into order govern the pick-off rate of ortho- Ps atoms in a given molecular material.

It has been shown empirically⁽²⁾ that for molecularly simple liquids like n-alkanes, the viscosity, η , is related to v_f/v_m where v_f is the average free volume per molecule. It is, therefore, interesting to look for a correlation between viscosity, η , and the lifetime, τ_2 , in simple liquids like n-alkanes. In this paper, the measurements of τ_2 at various temperatures in n-octane and n-hexadecane, two members of the n-alkane series, are reported.

II. EXPERIMENTAL

The liquids were degassed in order to eliminate the effect of dissolved oxygen on τ_2 . The liquid in a very thin wet film was at a fixed time and was pumped to high vacuum. It was then allowed to fill a vacuum and frozen again and the gases liberated in the vacuum

gases evolved. The degassed liquid was transferred in vacuum to the glass chamber containing the scaled positron source, Na^{22} , and a thermocouple for measuring temperatures. This glass chamber sealed under vacuum was sandwiched between two scintillation detectors, and the lifetime spectra were obtained by the standard technique of slow-fast coincidence using a multichannel analyser.

III. RESULTS

The value (τ_2) of the delayed component in the lifetime spectra of positrons annihilating in pure, degassed n-octane and n-hexadecane under vacuum are given in Table 1. Several spectra were taken to obtain consistent results. The values of viscosity, η , for these liquids, shown in Table 1, are obtained by interpolating the data on viscosity at different temperatures available in literature⁽²⁾. It is seen from Table 1 that τ_2 increases and η decreases with increasing temperature.

TABLE 1

n-OCTANE			n-HEXADECANE		
Temperature (°C)	τ_2 (n-sec) (± 0.1)	Viscosity (η) (millipoise)	Temperature (°C)	τ_2 (n-sec) (± 0.1)	Viscosity (η) (millipoise)
- 20	3.1	8.6	25	3.2	32
25	3.6	5.1	55	3.3	18
35	3.8	4.6	65	3.5	15.5
45	3.0	4.1	85	3.6	11.4
55	4.1	3.7	95	3.7	10
			115	4.0	7.8
			175	4.2	4.2

IV. DISCUSSION

According to the free volume model⁽¹⁾ for the formation and

annihilation of Ps atoms in condensed molecular media, the free volume is distributed into sites of average volume ' v ' and the lifetime τ_2 is related to ' v ' by $\tau_2 = \tau_1 \exp\left(\frac{v - v_0}{v_0 - v}\right)$, or

$$\frac{v_1}{v} = \frac{b \left(1 + \ln \frac{\tau_1}{\tau_2}\right)}{b + \ln \frac{\tau_1}{\tau_2}} \quad \text{----- (1)}$$

where v_1 and v_0 are respectively the lower and the upper limit of v . The constants $\tau_1 = 0.7$ nsec. and $v_0/v_1 = b = 0.01$ were set empirically to obtain best fit for the $I_2 - \tau_2$ correlation curves.

fig.1 shows a plot of $\frac{v_1}{v}$ versus $\ln \eta$ (η in millipoise) for n-octane and n-hexadecane. v/v_1 was computed by using eqn.(1) from the observed values of τ_2 at different temperatures. The linear nature of the plot suggests that η is related to $\frac{v_1}{v}$ by a relation of the type, $\eta = P \exp\left(Q \frac{v_1}{v}\right)$ where P and Q are constants for a given liquid.

For n-alkanes, Doolittle⁽²⁾ has experimentally verified the relation $\eta = A \exp\left(B \frac{v_m}{v_f}\right)$ where A and B are constants for a given liquid, v_m is the molecular volume and v_f the average free volume per molecule. Thus $\frac{v_1}{v}$ in eqn.(1) is seen to be analogous to $\frac{v_m}{v_f}$ in the expression for viscosity.

A correlation of lifetimes, τ_2 with the density, ρ , is also worth noting for these liquids. If M is the gram-molecular weight,

$$v_f = \frac{M}{\rho N} - v_m$$

where N is Avogadro's number. Assuming that v_f , the average free volume per molecule is proportional to the average site volume ' v ' in simple liquids, i.e. $v_f = K_2 v$

$$v = \frac{M}{\rho N K_2} - \frac{v_m}{K_2}$$

Substituting for v from eqn.(1) and rearranging,

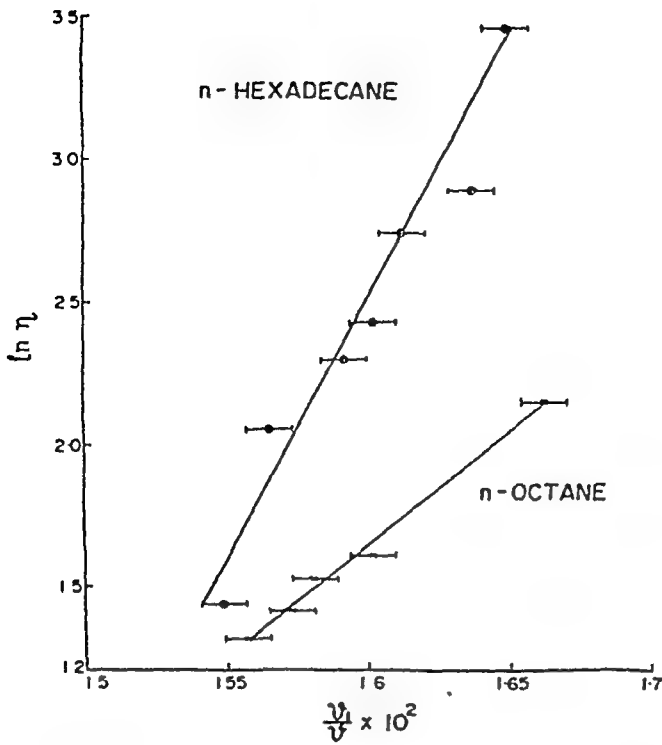
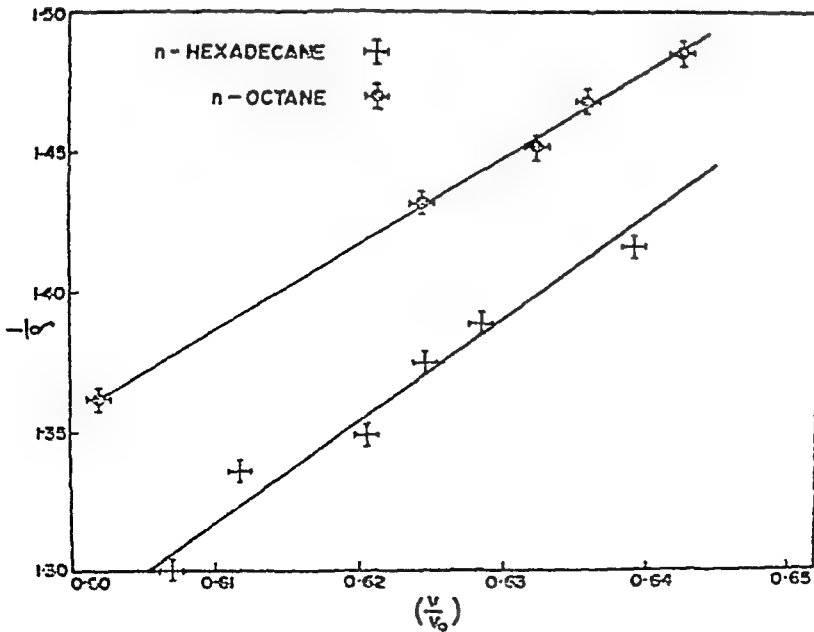


Fig.1 : Plot of $\ln \eta$ (η in millipoise) versus $\frac{v}{v_0}$ for n-octane and n-hexadecane.



Plot of $\frac{1}{\rho}$ versus $\frac{v}{v_0}$ for n-octane and n-hexadecane.

$$\frac{1}{\rho} = \frac{K_2 N U_1}{b M} \left[\frac{b + \ln \frac{T_2}{T_1}}{1 + \ln \frac{T_2}{T_1}} \right] + \frac{N U_m}{M}$$

$$\text{i.e. } \frac{1}{\rho} = \frac{K_2 N U_1}{b M} \left[\frac{U}{U_0} \right] + \frac{N U_m}{M} \dots \dots \dots (2)$$

Fig.2 shows the plots of $\frac{1}{\rho}$ versus $\frac{U}{U_0}$ for n-octane and n-hexadecane. The values of ρ for both these liquids at different temperatures were obtained by interpolating the data given by Doolittle. The plots in Fig.2 are linear since all other quantities except $\frac{U}{U_0}$ and $\frac{1}{\rho}$ are independent of temperature for a given simple liquid.

The intensity I_2 is $30 \pm 2\%$ at all the temperatures for both these liquids. This is consistent with the observation of Wilson et al⁽³⁾ for liquids subjected to pressure.

REFERENCES

1. R.G. Lagu, V.G. Kulkarni, B.V. Thosar and Girish Chandra; Proc. Ind. Acad. Sci. 69A, 48 (1969).
2. A.K. Doolittle; Jour. Appl. Phys. 22, 1031 and 1471 (1951) and 23, 236 (1952).
3. E.E. Wilson, P.O. Johnson and R. Stump; Phys. Rev. 129, 2091 (1963).

TEMPERATURE DEPENDENCE OF POSITRON LIFETIMES
IN ASSOCIATED AND POLAR LIQUIDS

B.V. Thosar, V.G. Kulkarni, R.G. Lagu and Girish Chandra
Tata Institute of Fundamental Research, Bombay-5

It has been shown⁽¹⁾ that in simple, unassociated liquids like n-octane and n-hexadecane, the delayed component, T_2 , of the lifetime of positrons increases with increasing temperature. It is also known that the viscosity of these simple liquids decreases with increasing temperature. It is interesting to look for a similar variation of T_2 with temperature in associated and polar liquids.

The lifetime, T_2 , was measured at various temperatures in glycerol, aniline, phenol and iodobenzene. Glycerol is a hydrogen-bonded liquid, aniline and phenol are polar and associated liquids while iodobenzene is polar but unassociated. All these liquids were degassed before the measurements of T_2 by a technique described elsewhere in these proceedings.

In glycerol, T_2 varies only slightly from 1.8 ± 0.1 nsec. at -15°C to 2.0 ± 0.1 nsec. at 120°C even though its viscosity changes by three orders of magnitude. Likewise, aniline gives a very little increase in T_2 with temperature, i.e. 2.35 ± 0.1 nsec. at 25°C to 2.55 ± 0.1 nsec. at 80°C . The viscosity of aniline varies from about 40 millipoise at 25°C to about 10 millipoise at 80°C .

Table 1 shows the results of T_2 and I_2 for phenol and iodobenzene.

It is seen that T_2 increases and I_2 decreases during the change of phase from solid to liquid in phenol. Melting point of phenol is about 42°C . This result is consistent with the observation of Goldanskii⁽²⁾ et al in phenol and by de Zafra⁽³⁾ et al in water.

TABLE 1

PHENOL			IODOBENZENE		
Temperature (°C)	τ_2 (nsec) (± 0.05)	I_2 (%)	Temperature (°C)	τ_2 (nsec) (± 0.2)	I_2 (%)
- 25	1.25	22	25	3.0	1.6
25	1.50	17	40	3.4	1.6
30	1.55	17	62	-	-
35	1.75	13	80	4.0	1.6 (?)
42	1.85	12	95	-	-
47	1.90	12			
67	1.90	12			

Iodobenzene which is polar but unassociated exhibits a relatively large change in τ_2 with temperature as seen from Table 1.

The results for iodobenzene are preliminary. It is seen, however, that τ_2 changes appreciably with temperature in iodobenzene which is an unassociated liquid.

REFERENCES

1. B.V. Thosar, V.G. Kulkarni, R.G. Lagu and Girish Chandra; Phys. Lett. 33A, 129 (1970).
2. B.G. Hogg, G.M. Laidlaw, V.I. Goldanskii and V.P. Shantarovich; Atomic Energy Review 6 No.1, 186 (1968).
3. R.L. de Zafra and W.T. Joyner; Phys. Rev. 112, 19 (1958).

FREE VOLUME MODEL FOR THE FORMATION AND QUENCHING OF TRIPLET POSITRONIUM IN SIMPLE MOLECULAR LIQUIDS

B.V. Thosar, V.G. Kulkarni, R.G. Lagn and Girish Chandra
Tata Institute of Fundamental Research, Bombay-5

According to the free volume model reported earlier⁽¹⁾, the specific free volume, V_f , of a molecular material is distributed into the regions of low electron density, called sites or cavities, with an average volume v per site. The positronium atom of near thermal energy, diffusing through the medium, is preferentially confined to these sites. The pick-off rate λ_2 is related to ' v ' by

$$\lambda_2 = \lambda_1 \exp - \left(\frac{v - v_1}{v_0 - v_1} \right),$$

where v_1 and v_0 are respectively the lower and upper limits of v .

If the three photon events from triplet positronium atoms are neglected in a condensed medium where there is a considerable quenching of triplet positronium atoms, i.e. if λ_3 is neglected in comparison to λ_2 , we can write

$$\tau_2 = \tau_1 \exp \left(\frac{v - v_1}{v_0 - v_1} \right), \dots \dots \dots (1)$$

where $\tau_1 = \frac{1}{\lambda_1} = 0.7$ nsec.

Setting $v/v_0 = b$, eqn.(1) can be written as

$$\frac{v}{v_1} = \frac{1}{b} \left[\frac{b + \ln \frac{\tau_2}{\tau_1}}{1 + \ln \frac{\tau_2}{\tau_1}} \right] \dots \dots \dots (2)$$

The value of b was set at 0.01 to get the parametric fit of the correlation curves for the observed data of I_2 and τ_2 .

In a condensed molecular medium the cavities are surrounded by the molecules of molecular volume v_m . The Ps atom in a cavity of volume v interacts with the excluded volume enclosing it, resulting in the pick-off lifetime τ_2 . The excluded volume per cavity depends upon the molecular volume v_m and the co-ordination number. Thus

τ_2 depends upon v and v_m . Assuming $\psi_1 = k_1 \psi_m$ in simple molecular liquids, where k_1 involves the co-ordination number, eqn. (2) can be written as,

$$\frac{\psi}{\psi_m} = \frac{k_1}{b} \left[\frac{b + \ln \frac{T_2}{T_1}}{1 + \ln \frac{T_2}{T_1}} \right] \dots \dots \dots (3)$$

Since τ_2 depends upon ψ/ψ_m , it is interesting to compare the positron annihilation data with those transport properties of the liquids that depend upon the ratio of free volume to molecular volume, for example viscosity, η .

Doolittle⁽²⁾ measured the viscosities of n-alkanes as a function of temperature and has suggested and verified for pure un-associated liquids an empirical relation, $\eta = A \exp \left(B \frac{\psi_m}{\psi_f} \right)$, where ψ_f is the average free volume per molecule, A and B are constants for a given n-alkane. Cohen and Turnbull have provided a theoretical justification for the empirical relation of Doolittle.

Assuming that the average site volume v in simple liquids is proportional to ψ_f , the average free volume per molecule, i.e.,

$\psi_f = k_2 \psi$ eqn. (3) can be written as

$$\frac{\psi_f}{\psi_m} = \frac{k_1 k_2}{b} \left[\frac{b + \ln \frac{T_2}{T_1}}{1 + \ln \frac{T_2}{T_1}} \right]$$

which can be combined with the expression for η to get

$$\left. \begin{aligned} \ln \eta &= \ln A + \frac{b}{k_1 k_2} \left[B \frac{1 + \ln \frac{T_2}{T_1}}{b + \ln \frac{T_2}{T_1}} \right] \\ \text{or } \ln \eta &= \ln A + \frac{b}{k_1 k_2} \left(B \frac{\psi_o}{\psi} \right) \end{aligned} \right\} \dots \dots \dots (4)$$

Fig.1 shows a plot of $\ln \eta$ versus $B \frac{\psi_o}{\psi}$ for n-alkanes from n-pentane to n-hexadecane at room temperature. The data for τ_2 is taken from Gray et al⁽³⁾, and the values of B tabulated by Doolittle⁽²⁾ are used to compute $B \frac{\psi_o}{\psi}$. The plot shows a monotonic increase as implied in eqn. (4). The deviation from linearity for

higher members of the series and the discrepancy in the value of the intercept may be due to over-simplification in the assumptions τ is. A monotonic dependence of v_1 on v_2 and of v_f on v was simplified into a relation of proportionality. Also τ_1 which involves co-ordination number was assumed to be constant over the series.

A correlation of T_2 with density ρ for n-alkane series is also interesting. If M is molecular weight and f is Avogadro's number,

$$U_f = \frac{M}{fN} - U_m$$

$$\text{assuming } U_f = K_2 U$$

$$\frac{U}{U_m} = \frac{M}{fN K_2 U_m} - \frac{1}{K_2}$$

Using eqn.(3),

$$\frac{1}{f} = \frac{K_1 K_2 N U_m}{b M} \left[\frac{U}{U_0} \right] + \frac{N U_m}{M}$$

For the homologous series, v_3 may be assumed to be proportional to the molecular weight M , i.e. $v_3 = K_3 M$

$$\frac{1}{f} = \frac{K_1 K_2 K_3 N}{b} \left[\frac{U}{U_0} \right] + K_3 N \quad (5)$$

Fig.2 shows a plot of $\frac{1}{f}$ versus $\frac{U}{U_0}$ for n-alkanes, from n-pentane to n-hexadecane, showing a linear relation between the two quantities. The correlation of T_2 with density in simple liquids becomes meaningful when interpreted on the basis of free volume.

REFERENCES

1. R.G. Laga, V.G. Kulkarni, S.V. Thosar and Girish Chandra; Proc. Ind. Acad. Sci. 69A, 49 (1969).
2. A.V. Doolittle; Jour. Appl. Phys. 22, 1031 and 1471 (1951) and 23, 236 (1952).
3. P.R. Gray, C.F. Cook and G.P. Sturm Jr.; Jour. Chem. Phys. 48, 1145 (1968).

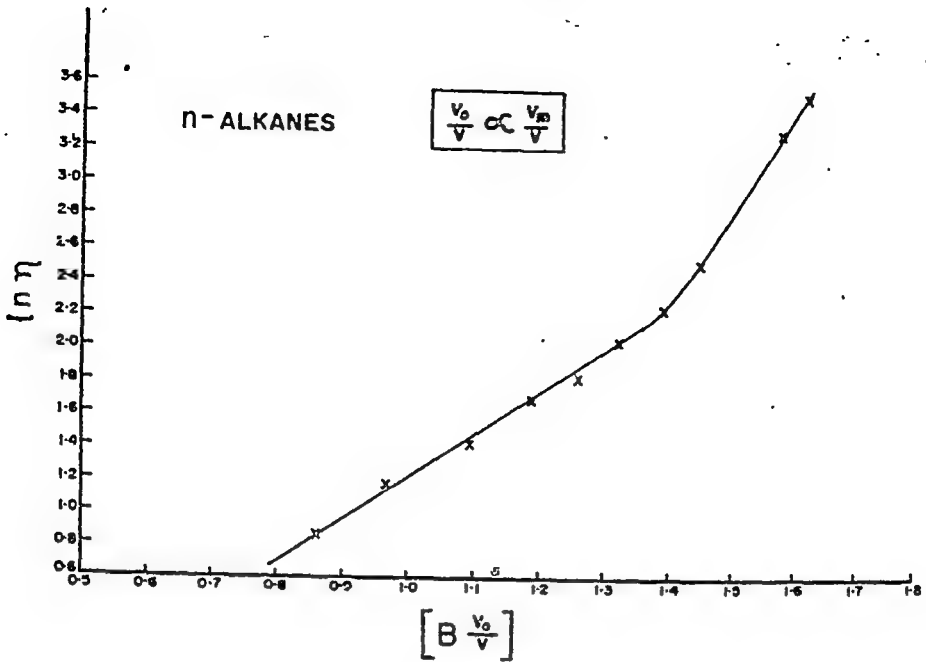


Fig.1 : Plot of $\ln \eta$ (η in millipoise) versus $B \frac{V_0}{V}$ for the series of n-alkanes at room temperature.

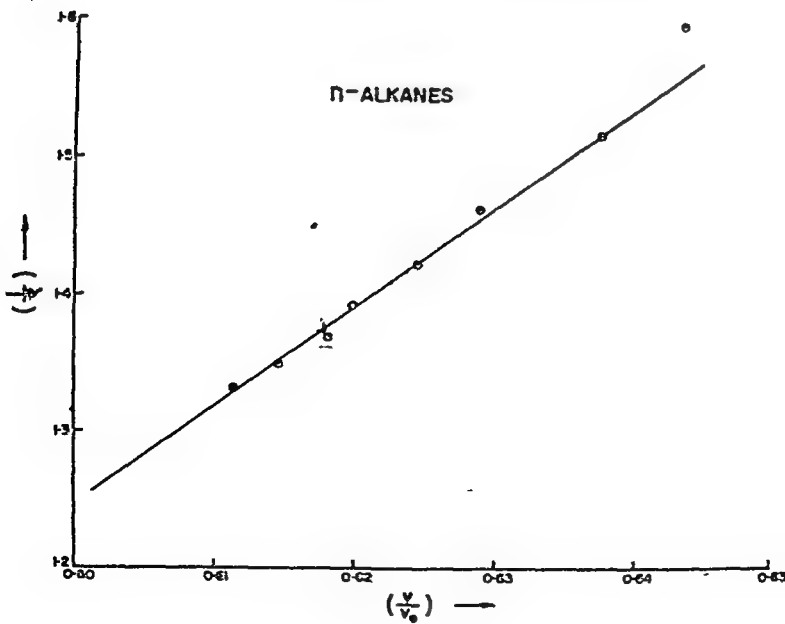


Fig.2 : Plot of $\frac{1}{\phi}$ versus $\frac{V}{V_0}$ for the series of n-alkanes at room temperature.

DISCUSSION

A.B. Biswas

- 1) Has any work been reported to detect phase changes (structural) in solids.
- 2) What is the concept of free volume , available volume or nonavailable volume? How is the molecular volume calculated for non-spherical molecules?

V.G. Kulkarni

- 1) Yes. The work on liquid crystals is an example where different life-times are recorded for the three phases.
- 2) The total free volume V_f is considered to be made of many sites of average volume ' v '. The results show that the role played by free volume in determining the viscosity and positron life-times in molecular materials is analogous. The actual calculation of the free volume is not intended.

R.M. Singru

Positrons annihilate with electrons and therefore besides free volume electron density should affect positron life-times and intensities. How would you take this effect into account?

V.G. Kulkarni

Positron life-times are affected by electron density only. The free volume model takes the variation in elec-

tron density into account by considering the changes in the volume.

S.K. Joshi

Why in your free volume you do not care for correlations with neighbours? You apparently treat your system as random.

V.G. Kulkarni

These correlations are too fast for positron life-times which are of the order of a few nano-seconds.

DOUBLE RESONANCE STUDY OF PROTON SPIN RELAXATION IN A STRONGLY COUPLED TWO SPIN SYSTEM

H.R. Krishna and B.D. Nageswara Rao

Department of Physics

Indian Institute of Technology, Kanpur-16 (U.P.)

I. INTRODUCTION

In this paper a study of proton spin relaxation processes in the two spin system (AB) in 2-chloroacrylonitrile is presented (1). The relaxation parameters (at room temperature) were obtained by analyzing the double resonance spectra obtained by irradiating each of the four transitions with strength varying from 0.015 Hz to about 2.35 Hz using density matrix formalism (2,3,4). Frequency-sweep double resonance experiments were performed on a well-degassed sample of 2-chloroacrylonitrile using a Varian HR-100 NMR spectrometer modified to include a field-frequency control loop (5).

II. RESULTS AND DISCUSSION

The single resonance spectrum of the molecule is shown in Fig. 1a. The chemical shift between the two protons is given by $|v_A - v_B| = 9.85 \pm 0.1$ Hz and the coupling constant $|J_{AB}| = 2.8 \pm 0.1$ Hz. Assuming that J_{AB} is positive, the transitions from left to right are labelled as (1-3), (2-4), (1-2) and (3-4) (6). Fig. 1b shows a typical 'low' irradiation double resonance spectrum corresponding to irradiation of (2-4).

The mechanisms of relaxation considered for the analysis are (i) external isotropic random fields with mean square amplitudes $f(A)$ and $f(B)$, correlation C_{AB} between protons A and B and correlation time τ_c and (ii) internal dipole-dipole interaction with correlation time τ_r .

Low irradiation spectra

These spectra are dependent upon the absolute values of various relaxation elements. Using density matrix formalism with "Simple-line approximation" it has been shown that for an AB system if the transition (2-4) is irradiated the following rules obtain (1,7):

- (a) If the mechanism of relaxation is internal dipole-dipole interaction between the protons,

$$R_{2-4}^{2-4} = 3 \frac{S_{13}^d}{S_{13}^o} + \frac{S_{34}^d}{S_{34}^o} = 4.0 \quad (1)$$

where S_{ij}^d and S_{ij}^o are double and single resonance intensities respectively of a transition (i — j). R_{2-4}^{2-4} is independent of the parameters of relaxation and irradiation. For any other mechanism, the functions R_{2-4}^{2-4} will be different from 4.0 and are dependent upon the parameters of irradiation and relaxation.

- (b) If the relaxation is through isotropic random fields with $f(A)/f(B) = 1.0$ and $C_{AB} = 0.0$,

$$R_{2-4}^{2-4} = \frac{S_{13}^d}{S_{13}^o} + \frac{S_{12}^d}{S_{12}^o} = 2.0 \quad (2)$$

independent of the parameters of relaxation and irradiation. For other mechanisms this function is dependent on both parameters.

- (c) If relaxation is through isotropic random fields with $f(A)/f(B) = 1.0$ and $C_{AB} = 1.0$, then

$$R_{2-4}^{2-4} = \frac{S_{13}^d}{S_{34}^d} = 1.0 \quad (3)$$

Similar functions of intensities can be calculated for irradiation of other transitions.

Figure 2 shows theoretical curves and experimental points of R_{2-4}^{2-4} and R_{2-4}^{2-4} . Mechanism (ii) does not agree with experimental points while mechanism (i) (with $f(A) = f(B)$) in general shows a better

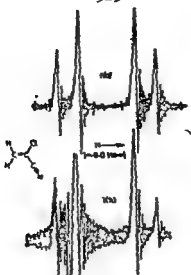


Fig. 1. (a) Simple resonance spectrum of 2-chloroacrylonitrile.

$$[\nu_A - \nu_B] = 9.85 \text{ Hz and } J_{AB} = 2.8 \text{ Hz}$$

(b) Irradiation of line 2(2-4) with a strength of 0.047 Hz.

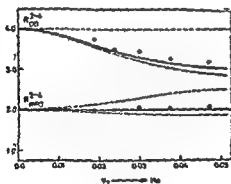


Fig. 2. Theoretical plots of R_{MD}^{2-4} and R_{RFO}^{2-4} (corresponding to the irradiation of (2-4)) calculated for (i) internal dipole-dipole interaction with $T_r = 2.7 \times 10^{-11}$ Sec. (dashed line) (ii) external isotropic random fields with $f(A) = f(B)$, $C_{AB} = 0.0$, and $2 f(A) T_c = 0.14$ rad/sec (solid line) and (iii) - 2 - with $f(A) = f(B)$, $C_{AB} = 1.0$ and $2 f(A) T_c = 0.13$ rad/sec. (chain line). The experimental for are denoted by \odot while for R_{RFO}^{2-4} by \square .

agreement. Further, since the outer lines in Fig. 1b do not have same intensity, the correlation C_{AB} is different from 1.0.

An analysis of the spectra obtained for 'high' irradiation strengths where additional transitions are present, also shows good agreement with mechanism (i) with $f(A)=f(B)$ (and $C_{AB}=0.0$) and does not agree with mechanism (ii).

The relaxation for protons in 2-chloroacrylonitrile at room temperature can therefore be described by the interaction with external isotropic random fields with equal mean square amplitudes at the site of the protons with no appreciable correlation between them.

REFERENCES

- (1). Krishna, N.R., and Nageswara Rao, B.D., Molec. Phys. (1971) in press.
- (2). Nageswara Rao, B.D., 1970, "Advances in Magnetic Resonance", Vol. 4., edited by J.S. Waugh (London and New York, Academic press, p. 271.
- (3). Bloch, F., 1956, Phys. Rev., 102, 104.
- (4). Redfield, A.G., IFT J. Res. Develop 1, 19 (1957).
- (5). Anil Kumar and Nageswara Rao, B.D., 1968, Molec. Phys., 15, 377.
- (6). Pople, J.A., Schneider, V.G., and Bernstein, H.J., 1959, "High Resolution Nuclear Magnetic Resonance", (New York: McGraw-Hill Book Company, Inc.), Chap. VI.
- (7). Abragam, A., 1961, "Principles of Nuclear Magnetism" (Oxford University Press), Chap. XII, p 522.

PROTON SPIN RELAXATION AND MOLECULAR MOTION IN LIQUID THIOPHENE

Anup Kitchlew and B.D. Nagaswara Rao

Department of Physics, Indian Institute of Technology, Kanpur-16

I. INTRODUCTION

Nuclear magnetic relaxation techniques can be used to study molecular motion in liquid systems by determining the correlation times for the molecular motion which can be related to appropriate macroscopic transport coefficients⁽¹⁾. This paper presents an experimental study of spin-lattice relaxation time, T_1 , and coefficient of self-diffusion, D , in liquid thiophene in the temperature range 300°K to 550°K.

The measurements were made using spin-echo techniques. A spectrometer equipped with a variable temperature cryostat was fabricated⁽²⁾. The results are shown in Fig. 1. The errors in these measurements are about $\pm 5\%$. Dissolved oxygen was removed from the sample by first flushing with nitrogen gas, then subjecting to freeze-pump-thaw cycles and finally by 'gattering'.

II. ANALYSIS AND DISCUSSION

The significant relaxation mechanisms in thiophene are the inter- and intramolecular dipolar interactions and spin-rotation interactions. The interproton distances in thiophene are such that I_1 and I_2 experience much weaker intramolecular dipolar interactions compared to S_1 and S_2 . The equations of motion for $I_x = I_{1x} + I_{2x}$ and $S_x = S_{1x} + S_{2x}$ are coupled so that the relaxation decay is a sum of two exponentials. The observed relaxation, however, is a single exponential since the amplitude of one is much smaller than the other. The observed relaxation rate is given by

$$k_{obs} = (T_1)_{obs}^{-1} = [5(6T_1^{inter})^{-1}] + [(T_1^{SR})^{-1}] + [\gamma^4 \hbar^2 (\frac{3}{4} \tau_s \chi_s^{-6} + \tau_{IS} \chi_{IS}^{-6}) + \frac{1}{2} \{ (\frac{3}{2} \gamma^4 \hbar^2 \tau_s \chi_s^{-6})^2 + ((3T_1^{inter})^{-1} + \gamma^4 \hbar^2 \tau_{IS} \chi_{IS}^{-6})^2 \}^{1/2}] \quad (1)$$

$$= k_{inter} + k_{SR} + k_{DD} \quad (2)$$

where γ is the gyromagnetic ratio of the protons, r_s and r_{IS} are the distances and τ_s and τ_{IS} are the correlation times appropriate for the dipolar interactions ($S_1; S_2$) and (I_1, S_1) (or (I_2, S_2)) respectively. $(T_1^{inter})^{-1}$ and $(T_1^{SR})^{-1}$ are the respective relaxation rates if the intermolecular dipolar interaction and the spin-rotation interaction were individually responsible for relaxation. k_{inter} , k_{SR} and k_{DD} refer to the three terms in heavy parentheses in Eq. (1). An estimate of k_{inter} as a function of temperature is made using a 'hard-sphere' model translational diffusion theory⁽³⁾. A hard-sphere radius $a=1.54$ Å was estimated for thiophene. k_{inter} vs temperature is shown in Fig. 2. The contribution from reorientational motion $k_{intra} = k_{SR} + k_{DD}$ can be separated from k_{obs} by subtracting k_{inter} from it. This is plotted in Fig. 2. k_{SR} is given by⁽⁴⁾

$$k_{SR} = C'D \quad (3)$$

$$\text{where} \quad C' = \frac{2}{3} I_1 \sum_{i=x,y,z} [C_{ii}^2 - 2C_t(C_{ii} - C_t)] I_i,$$

where C_{ii} are the diagonal elements of the spin-rotation tensor, $C_t = \frac{1}{3} \sum_i C_{ii}$, I_i are the principal moments of inertia and D_\perp refers to the rotational diffusion constant along an axis perpendicular to the plane of the molecule. In writing Eq. (3), an approximation that τ_j is the same for the three principal axes is made. The rotational diffusion constants are then related in the inverse ratios of the corresponding moments of inertia. Using Huntress⁽⁴⁾ expression k_{intra} becomes

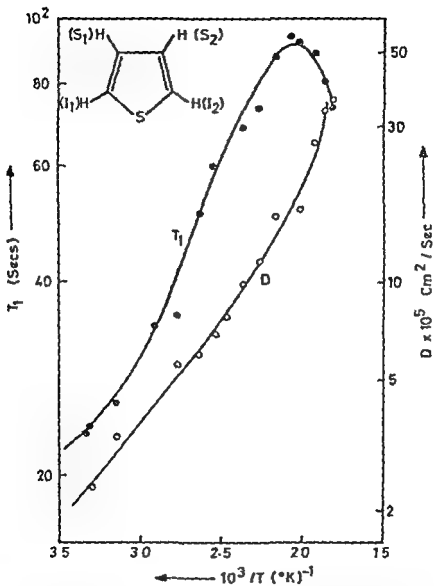


Fig. 1. Spin-lattice relaxation time, T_1 , and coefficient of self-diffusion, D , in thiophene as a function of temperature.

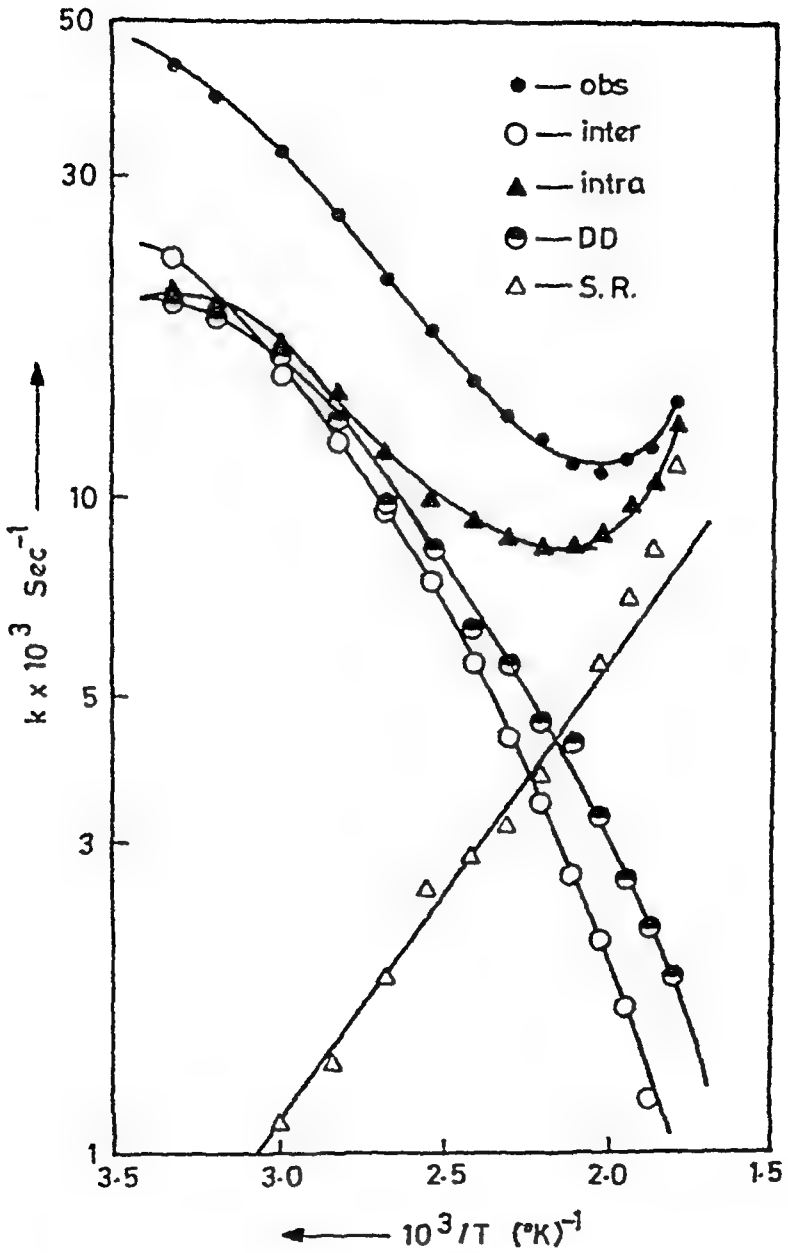


Fig. 2. Various contributions to the observed relaxation rates in thiophene vs $(10^3/T)$.

$$k_{\text{untra}} = C'D_1 + \frac{3.301 \times 10^8}{D_1} + \frac{1.015 \times 10^8}{D_1} \left[1.586 + (1 + 1.086 \times 10^{-15} \times \frac{C}{D_1})^2 \right]^{1/2} \quad (4)$$

The condition for a minimum in $k_{\text{ir-ra}} \pm 16. \pm 7\%$ (Fig. 3) gives $C = 3.16 \times 10^{-14}$ and hence a value of $C_1 \leq 1.01 \text{ wt.}$ From this and from known values of C/D_1 , D_1 as a function of temperature can be determined whence k_{DD} and k_{GR} as a function of temperature can be obtained. These are also plotted in Fig. 2.

D_1 is seen to obey an Arrhenius equation upto 160°C with an activation energy of 3.2 kcal/mole. The reorientational motion of thiophene molecules is found to be diffusional upto 140°C . The determination of various contributions and D_1 is done by (a) a hard-sphere translational diffusion theory and (b) T_g using the same for all three axes. (a) is found to be satisfactory for C/D_1 in liquid and may not be a serious assumption. The results obtained from D_1 and T_g show that (b) is also a satisfactory assumption for this case.

REFERENCES

1. E. Kubo, J. Phys. Soc. Japan, 12, 570 (1957);
2. Anup Kitchlew and B.D. Peggawara Rao, Technical Report No.1/70, Department of Physics, Indian Institute of Technology, Kanpur, (U.P.) India (1970).
3. H.C. Torrey, Phys. Rev. 92, 962 (1953).
4. T.J. Huntress, Jr., J. Chem. Phys. 48, 3524 (1968).

DISCUSSION

B. Venkataraman

Having found out the different contributions to the relaxation and their dependence on temperature, have you attempted fitting the overall curve for temperature dependence of T , with these contributions.

B.D.N. Rao

The contributions of the mechanisms are obtained from the experimental data itself and therefore they must add up to reproduce the observed dependence of T_1 on temperature.

G. Venkataraman

What is the physical difference between τ_r and τ_J , both of which appear to be correlation times characterising molecular rotations?

B.D.N. Rao

τ_r is the correlation time of fluctuation in molecular orientation (θ, ϕ) whereas τ_J is the correlation time for fluctuations in molecular angular velocity ω . These two quantities have opposite temperature dependences.

HEAT CAPACITY AT CONSTANT VOLUME OF METHYL IODIDE

S.K.Mitra, Narsingh Dass and N.C.Varshneva
Physics Department, University of Roorkee, Roorkee.

I. INTRODUCTION

A study of the volume dependence* of heat capacity of a liquid has relevance to the understanding of state of molecular motion in it^(1,2). In the interpretation of liquids from significant structure theory (S-S-theory) the total energy will be composed of (i) external energy (rotational and translational), and (ii) internal energy (vibrational and librational), corresponding to the gas-like and the solid-like structures, respectively. Consequently, the specific heat at constant volume, C_v can be expressed as a sum of the external energy part, C_v , and internal energy part C' .

$$C_v = C_v + C'$$

C_v can be obtained from the total partition function f , which, in its turn, will be built-up from those coming from the solid-like structure, f_s , and from the gas-like structure, f_g .

$$f = (f_s)^{NV_s/V} (f_g)^{N(V-V_s)/V}$$

where N is the Avogadro's no and V and V_s are the volume of the liquid and the volume of the solid-like structure in it respectively.

The purpose of the present paper is to deduce C_v and compute its values at various volumes and temperatures for methyl iodide from the S-S theory on the one hand, and from thermodynamical expressions on the other hand.

*From the experimental point of view, the pressure dependence

A fairly good agreement between these values reassures the validity of the assumption of S-S theory in the first place and also leads to information regarding molecular motion. These are discussed in the conclusion.

II. THEORY

Computation of C_v on thermodynamical consideration has been done from two independent expressions. One due to Harrison, Low and Molwyn-Hughes^(3,4).

$$C_v - C_{v^0} = \left[T(V - V^0)/(C k_T^0) \right] \left[-2x^2 + \gamma \right] - \left[(TV^0)/(C-1) k_T^0 \right] \times \\ \left[C\alpha^0 - 2\alpha^0 x + \alpha^0 dT + 2x^2/C - \gamma/C \right] \left[(V^0/V)^{C-1} - 1 \right] \dots (4)$$

where $x = \frac{1}{k_T^0} \left(\frac{dk_T^0}{dT} \right)$, $\gamma = \frac{1}{k_T^0} \left(\frac{d^2 k_T^0}{dT^2} \right)$ and $C = \frac{2}{3} \left(\frac{1}{k_T} \right)$

and other due to Narsingh Dass and Varshneya⁽⁵⁾.

$$C_v - C_{v^0} = \left[T\alpha^0/k_T^0 \right] \left[\frac{1}{\alpha^0} \frac{d\alpha^0}{dT} - \frac{1}{k_T^0} \frac{dk_T^0}{dT} \right] (V - V^0) \quad (2)$$

The symbols have their usual meanings. Superscript zero refers to the value at a reference pressure taken as one atmosphere.

To compute C_v from S-S. theory we take the partition function given by Lu et al⁽⁷⁾:

$$f = \left\{ \left[\exp(-E_s/RT) / (1 - \exp(-\theta/RT)) \right]^6 \right\} \left[1 + (x-1)n \exp(-aE_s/(x-1)RT) \right] \\ \times \prod_{i=1}^5 \left[1 / (1 - \exp(-h\nu_i/RT)) \right]^{N/x} \left[(2\pi m kT)^{3/2} / \rho^3 \right] (eV/N) \\ \times (8\pi^2 (8\pi^2 ABC)^{1/2} / 2\rho^3) \cdot \prod_{i=1}^5 \left[\exp(-h\nu_i/kT) \right]^{N(1-\frac{1}{x})} \quad (3)$$

and deduce from it the expression for C_v

$$C_v = 2kT \left(\frac{\partial \ln f}{\partial T} \right) + kT^2 \left(\frac{\partial^2 \ln f}{\partial T^2} \right) \quad (4)$$

where a is a characteristic parameter, $x = \frac{V}{V_s}$, E_s = sublimation energy of crystal, n = number of nearest neighbours in liquid phase, θ = Einstein temperature. Other symbols have their usual meanings.

minizing the free energy at the melting point:

$$A = -kT \ln f, \quad \left(\frac{dA}{dT}\right)_{m, f} = 0$$

The parameters have the values:

$$10^6 K_T^U = 32.7 - 0.0186T + 1.50 \times 10^{-3} T^2 \quad (\text{ref. } \dots)$$

$$10^3 \sigma^0 = 0.814 + 1.241 \times 10^{-3} + 0.605 \times 10^{-6} \varepsilon^2 \quad (\text{---} \varepsilon, \text{---})$$

$E_a = 8615.0 \text{ cal/gm.}$ $V_8 = 5.20$ $\rho = 0.92$

and $\alpha = 0.0015$.

III. CONCLUSION IS

The results given in Table 2-3 - ~~Table 2-3~~ ^{Table 2-3} are in good agreement among them. The results ~~are in good agreement~~ ^{are in good agreement} among the expressions should be acceptable at ~~the~~ ^{these} ~~the~~ ^{these} values. The results from 5-5 ~~are in good agreement~~ ^{are in good agreement} with the increase of C_v with increasing ~~the~~ ^{the} volume). This should be ~~the~~ ^{the} 5-5 theory calculations, (if ~~the~~ ^{the} to $V = 58.12$) where the ~~the~~ ^{the} solid-like structure, ~~the~~ ^{the} energy has been under

REFERENCES

1. J.D. Bernal;
2. Staveley, Tupman
3. D. Harrison
4. D.I.R. Low
5. Narsingh Dutt
6. Narsingh Dutt
7. W.C. Liu, M.C.

Table I. Cv (Cal's deg⁻¹ mole⁻¹) of CH₃I by different methods.

V	253.2°K			263.2°K			273.2°K		
	I	II	III	I	II	III	I	II	III
58.47	12.72	12.72	13.50	12.99	12.98	13.67	13.20	13.22	13.84
59.15	12.26	12.30	13.41	12.57	12.58	13.58	12.84	12.84	13.75
59.85	11.78	11.88	13.326	12.14	12.17	13.49	12.45	12.45	13.66
60.56	11.28	11.44	13.25	11.69	11.74	13.42	10.04	12.07	13.59
61.29	10.75	10.98	13.17	11.22	11.32	13.34	11.61	11.63	13.51
62.81	9.93	10.29	13.027	10.45	10.65	13.37	10.92	11.00	13.37

V	283.2°K			293.2°K			308.2°K		
	I	II	III	I	II	III	I	II	III
58.47	13.55	13.65	14.01	13.90	14.14	14.18	14.54	15.09	14.45
59.15	13.23	13.28	13.92	13.64	13.80	14.09	14.35	14.77	14.36
59.85	12.89	12.91	13.84	13.35	13.44	14.02	14.14	14.43	14.28
60.56	12.53	12.53	13.76	13.03	13.07	13.94	13.90	14.10	14.21
61.29	12.15	12.13	13.69	12.70	12.70	13.87	13.64	13.75	14.13
62.81	11.53	11.53	13.54	12.16	12.12	13.73	13.21	13.39	13.99

DEBYE TEMPERATURE OF WATER ON TWO-STATE APPROACH

S.K. Mitra and Narsingh Dass

Physics Department, University of Roorkhee, Roorkhee

I. INTRODUCTION

The cold neutron scattering technique has recently been applied successfully to study the dynamics of atomic motion in liquid. From the studies of inelastic scattering of cold neutron which takes place in a time scale of 10^{-13} sec. it comes out that water shows solid-like properties, whereas the fluid-like properties are observed on a time-scale larger than 10^{-13} sec. Recently, Singwi and Sjolander¹ and Larsson¹ were able to explain the general trend of both the quasi-elastic and inelastic scattering of cold neutrons and the magnitude of the diffusive broadening in case of solid like water by assigning a Debye frequency spectrum with a Debye temperature $\Theta = 135$ K.

II. THEORY

To calculate Θ in solids, the expression² generally employed

$$\Theta = \frac{h}{k} \left[\left(9N/4\pi V \right) / \left(\frac{1}{C_L^3} + \frac{2}{C_T^3} \right) \right]^{1/3} \quad (1)$$

where the symbols have their usual meanings. Considering water as isotropic monatomic solid³, the Θ temperature can be computed from Eq.(1). The velocities C_L and C_T may be given in terms of density, ρ , adiabatic compressibility, β_s , and Poisson's ratio, σ , corresponding to water exhibiting solid-like properties:

$$\left[\frac{1}{C_L^2} + \frac{2}{C_T^2} \right] = (\rho \beta_{s,\infty})^{3/2} \left[2 \left\{ \frac{2(1+\sigma)/3(1-2\sigma)}{1} \right\}^{3/2} + \left\{ \frac{(1+\sigma)/3(1-\sigma)}{1} \right\}^{3/2} \right] \quad (2)$$

In the above equation σ and $\beta_{s,\infty}$ are not directly known. We calculate these in the following way. Neglecting the relaxation components of various involved parameters in the two state approaches we may write:

$$\beta_{s,\infty} = \beta_{T,\infty} - \frac{V \gamma (\alpha_{\infty})^2}{C_{p,\infty}} \quad (3)$$

where $\beta_{T,\infty}$, $C_{p,\infty}$, V and α_{∞} , respectively, the isothermal compressibility, heat capacity at constant pressure, volume and coefficient

of thermal expansion for the solid-like character of water.

Further, Poisson's ratio can be given^{3,4} as:

$$\sigma = (3A-2)/(6A+2) \text{ where } A = K_{T,\infty}/G_{T,\infty} \quad (4)$$

In eq.(4), $K_{T,\infty}$ and $G_{T,\infty}$ are bulk modulus and modulus of rigidity, respectively, corresponding to the solid-like character of water.

Herzfeld and Litovitz⁴ has shown that

$$\eta_V = K_{T,h} \tau_V \text{ and } \eta_A = G_{T,h} \tau_A \quad (5)$$

where η_V and η_A are volume and shear viscosity, τ_V and τ_A are volume and shear relaxation time and $K_{T,h}$ is relaxational part of the bulk modulus. Thus from eqs. (4) and (5) we get

$$A = (K_{T,\infty}/K_{T,h}) \cdot (\eta_V/\eta_A) \quad (6)$$

In eq.(6), τ_V and τ_A are taken of the same order. In doing so, we⁴ have been guided by the fact as remarked by Herzfeld and Litovitz⁴ and also by Piccerelli and Litovitz¹³ that within the experimental error, the volume and shear relaxation times in associated liquids are of the same order of magnitude.

Thus it is clear from the above discussions that σ is model dependent whereas earlier workers^{5,6} have taken it model independent. The values of σ from eqs. (4) and (6) are reported in the fifth column of given table.

III. CALCULATIONS

Since the value of θ obtained from neutron diffraction experiments differ from the calculated values, we think it worth while to calculate θ using more reasonable values for coefficient of thermal expansion and that too on the various two-state approaches available in the literature. Thus, we have used

$$(i) \alpha_\infty = \alpha_{ice} = 5.6 \times 10^{-6} / ^\circ\text{C} \quad (7a)$$

$$(ii) \alpha_\infty = \alpha - \alpha_h \text{ where experimental value}^7 \text{ of } \alpha = -0.031 \times 10^{-3} / ^\circ\text{C} \quad (7b)$$

$$(iii) \alpha_\infty = \alpha - \alpha_h \text{ where calculated value}^8 \text{ of } \alpha = -0.0581 \times 10^{-3} / ^\circ\text{C} \quad (7c)$$

Now, the various two-state parameters of water required at 0°C in

calculating the Debye temperature on the basis of two-state approaches are taken from reference 7. The values so obtained are reported in the given table. Further, using the value of $\alpha_{ps} = \alpha_{cs} = 5.6 \times 10^{-6}/^{\circ}\text{C}$ and $\sigma = \sigma_{cs} = 0.33$ (at $\sim 1.5^{\circ}\text{C}$), we have also calculated θ which is reported in the below table.

Two state approaches given by	Values θ			Calc. from eq. (4)	*Value of θ using ice parameters
	From eq. 7(a)	From eq. 7(b)	From eq. 7(c)		
	θ	θ	θ		
Davis and Litovitz	133.52	-	-	0.3322	150.8
Nemethy and Scheraga	241.37	262.19	260.39	-0.1619	107.2
Ducken	200.20	216.26	216.73	0.0106	112.2
Smith and Lawson	114.48	-	-	-0.4374	204.2
Frank and Quist	112.04	130.13	112.65	0.45	132.7
Litovitz and Carnevale	119.13	-	-	0.4148	131.2
Grjotheim and Krogh-Moe	250.00	-	-	-0.1825	103.9
Hall	119.13	-	-	0.4148	165.6

IV. CONCLUSIONS:

Calculated values of θ on basis of different two state approaches do not show much sensitivity with respect to the approach chosen for water and most of the values lie near the standard value 135°K . Nevertheless, the calculations do indicate that:

- (1) Frank and Quist approach is most satisfactory in this regard.
- (ii) Approach of Davis and Litovitz, and that of Smith and Lawson seem to have something basically wrong in this respect because making use of eqs. 7(b) and 7(c), these models give imaginary values of θ which is meaningless whereas making use of eq. 7(a) these models also

give an admissible value of Debye temperature.

(iii) Namethy and Scheraga¹¹ and Eucken model¹² give high value of θ . This may be due to the fact that Namethy and Scheraga have estimated β_{TA} quite small. Eucken's estimate based on the assumption that water behaves normally at high pressure also leads to high value of Debye temperature.

ACKNOWLEDGEMENT

The authors are thankful to Dr. N.C. Varshneya for his suggestions. They are also thankful to University Grants Commission and Department of Atomic Energy of India for financial support.

REFERENCES

1. Thermal Neutron Scattering, Ed. P.A. Egelstaff. (Academic Press, New York 1965).
2. S.S. Mitra, J.Sci. Industr. Res.(India)21A, (1962), 76
3. S.C. Jain and R.C. Bhandari, J. Phys. Soc. Japan, 23 (1967), 476.
4. K.F. Herzfeld and T.A. Litovitz, Absorption and Dispersion of Ultrasonic Waves. (Academic Press, New York, 1959).
5. S.K. Joshi, J. Chem. Phys., 35, (1961) 1141.
6. S.C. Jain and R.C. Bhandari, Chem. Phys. Letters, 2, (1968), 33.
7. G.M. Davis and T.A. Litovitz, J. Chem. Phys. 42, (1965), 2563.
8. Harrington Duce and N.C. Varshneya, J. Phys. Soc. Japan, 25, (1968), 1452.
9. Northwood, Canadian, J. Res., 25A (Phys) (1947). 68.
10. Smith and A. Lowson, J. Chem. Phys. 22, (1954), 451.
11. G. Namethy and H.A. Scheraga, J. Chem. Phys., 36, (1962), 3382.
12. A. Eucken, Z. Electrochem. 52 (1948), 255.
13. R. Fiescicelli and T.A. Litovitz, J. Acoust. Soc. Am. 29 (1957), 1009.

NEUTRON SCATTERING IN LIQUID ARGON

J.S. Bajjal and D.K. Chaturvedi

Department of Physics & Astrophysics, Delhi University,
Delhi-7.I. INTRODUCTION

In the present paper we have calculated $G_2(\underline{r}, t)$, or its space-time transform $S_2(\underline{k}, \omega)$ in the Non-Gaussian approximation by taking the solid state behaviour into account, according to the model of Rahman, Singwi and Sjolander⁽¹⁾ (RS3). Similar calculations for $G_2(\underline{r}, t)$ in the Non-Gaussian approximation were previously done by Gibb's and Ferziger⁽²⁾ (GF). But in their model these authors did not incorporate the oscillatory motion characteristic of liquids. The various parameters occurring in our model have been obtained by having a best fit of the velocity autocorrelation function with the computer experiments of Nijboer and Rahman⁽³⁾. The Non-Gaussian corrections have been obtained by the best fit of the calculated Non-Gaussian $S_2(\underline{k}, \omega)$ for different values of $\alpha / (\alpha + \beta)$ with the computer experimental Non-Gaussian $S_2(\underline{k}, \omega)$ of Nijboer and Rahman at $K = 2 \text{ \AA}^{-1}$. Here α and β are the binary collision rate and the Langevin friction coefficient respectively.

II MATHEMATICAL FORMULATION

For a combined binary collision Langevin diffusion model, GF⁽²⁾ have obtained an integrodifferential equation for the self correlation function $G_2(\underline{r}, t)$ as

$$G_2(\underline{r}, t) = H(\underline{r}, t) + \alpha \int_0^t d^3r' \int_0^{t'} dt' G_2(\underline{r}-\underline{r}', t-t') \quad (1)$$

Where $H(\underline{r}, t)$ represents the probability per unit volume that a molecule initially at the origin with a Maxwellian distribution of velocity will be found at \underline{r} at time t without having made a hard collision. The second term represents the probability that the molecule had a hard collision at \underline{r}' at time t' and then reached at \underline{r} at time t . Though GF have calculated $H(\underline{r}, t)$ for a simple Langevin diffusion, eq(1) is equally valid for more complex models. Therefore, in this paper we have taken the model of RSS to calculate $H(\underline{r}, t)$ and introduced thereby some degree of solid like behaviour into the model.

Following GF we introduce the Fourier transforms

$$Q(\underline{k}, \omega) = \int_0^\infty dt \int d^3r e^{i(\underline{k} \cdot \underline{r} - \omega t)} G_s(\underline{r}, t) \quad (2)$$

$$I(\underline{k}, \omega) = \int_0^\infty dt \int d^3r e^{i(\underline{k} \cdot \underline{r} - \omega t)} H(\underline{r}, t) \quad (3)$$

To proceed further, we now consider the model of RSS to calculate $H(\underline{r}, t)$. We write

$$H(\underline{r}, t) = P(t) H_0(\underline{r}, t) \quad (4)$$

where $P(t) = e^{-\alpha t}$ is the probability that no hard collision will occur prior to t . $H_0(\underline{r}, t)$ represents the motion of the molecule in the absence of hard collision. So we have according to the model of RSS.

$$H_0(\underline{r}, t) = \frac{1}{\pi^{3/2} b^3(t)} e^{-r^2/b^2(t)} \quad (5)$$

where

$$b^2(t) = \frac{4k_B T}{m} \left\{ \left(\frac{\omega'}{\omega_D} \right)^3 \frac{e^{-\beta t} - 1 + \beta t}{\beta^2} + \frac{3}{\omega_D^3} [\phi(\omega_D t) - \phi(\omega' t)] \right\} \quad (6)$$

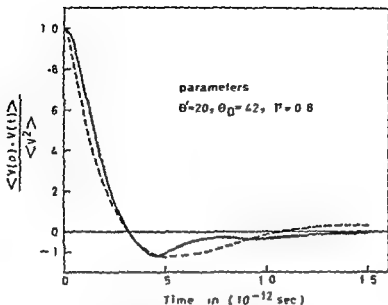


Fig. 1. Velocity autocorrelation in liquid argon at 87.5°K. Computer experiments (Solid line), best fit of the present model to the computer experiment (dashed line).

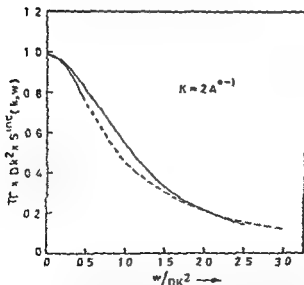


Fig. 2. $\pi \times Dk^2 \times S^{inc}(k, w)$ as a function of w/DK^2 under non-Gaussian approximation model (Solid line), computer experiment (dashed line).

where $\phi(\omega, t)$ is given by

$$\phi(\omega, t) = \omega - \frac{1}{t(1+\tau^2)^{1/2}} \left\{ e^{\frac{\tau\omega t}{(1+\tau^2)^{1/2}}} \left[(1-\tau^2) \sin\left(\frac{\omega t}{(1+\tau^2)^{1/2}}\right) - 2\tau \cos\left(\frac{\omega t}{(1+\tau^2)^{1/2}}\right) \right] \right\}$$

Since $H_0(\underline{r}, t)$ is Gaussian, the Fourier transform of $H(\underline{r}, t)$ is easily found to be

$$\begin{aligned} Y(\underline{k}, t) &= \int \underline{k} \cdot \underline{r} H(\underline{r}, t) d^3r \\ &= i\gamma p - \left[\frac{k_0 T}{m} k^2 \left\{ \left(\frac{\omega'}{\omega_D} \right)^3 \frac{e^{-1+\beta t}}{\beta^2} + \frac{3}{\omega_D^3} [\phi(\omega_D, t) - \phi(\omega', t)] \right\} + \alpha t \right] \end{aligned} \quad (7)$$

whence

$$I(\underline{k}, \omega) = \int_0^\infty i\gamma p \left[-\frac{k_0 T}{m} k^2 \left\{ \left(\frac{\omega'}{\omega_D} \right)^3 \frac{e^{-1+\beta t}}{\beta^2} + \frac{3}{\omega_D^3} [\phi(\omega_D, t) - \phi(\omega', t)] \right\} - (\alpha + i\omega)t \right] dt \quad (8)$$

and following GF, we can express the scattering cross section $S_s(k, \omega)$ in the form

$$S_s(k, \omega) = \frac{1}{\pi \alpha} \frac{U(1-U) - V^2}{(1-U)^2 + V^2} \quad (9)$$

where U and V are the real and imaginary parts of $I(\underline{k}, \omega)$. Since it was found difficult to evaluate U and V in an analytical form, these were calculated numerically with the help of IBM computer 1620.

III RESULTS

First of all the parameters occurring in the velocity autocorrelation function⁽⁴⁾ were fixed by calculating the best fit with the Nijboer and Rahman's result as shown in Fig.(1). To estimate the Non-Gaussian correction in the model, we have calculated $S_s(k, \omega)$ in the Non-Gaussian approximation from eq(9) for different values of $\alpha / (\alpha + \beta)$ and then compared it with the computer

results of Nijboer and Rahman in the Non-Gaussian approximation so as to give the best fit with the predetermined parameters θ' , θ_D , T and $(\alpha + \beta)$ as shown in Fig.(2). The value of $\alpha / (\alpha + \beta)$ obtained from our model (0.85) is in agreement with the value calculated earlier by Gibbs's⁽⁵⁾ (0.875). These results show that in real fluids (to the extent that they are described by this model) the magnitude of 'hard core' interactions, is about four times the 'soft core' interactions.

REFERENCES

1. A. Rahman, K.S. Singwi, and A. Sjolander, *Phy. Rev.* 126, 997 (1962).
2. A.G. Gibbs and J.H. Ferziger, *Phy. Rev.* 136, 701 (1965).
3. B.R.A. Nijboer and A. Rahman, *Physica* 32, 415 (1966).
4. For the detail of velocity autocorrelation function see J.S.Bajjal and D.K. Chaturvedi, *Physica* (Under publication).
5. A.G. Gibbs, Symposium on Inelastic scattering of neutrons by condensed systems, Brookhaven National Laboratory, 1965.

DISCUSSION

Om Singh

You have calculated the scattering cross section using the non-Gaussian approximation. What is the percentage contribution for this corrections?

There is a very big difference

$\frac{1}{2} \times \frac{1}{2} = \frac{1}{4}$

[illegible]

$\frac{1}{2} \times \frac{1}{2} = \frac{1}{4}$

THESE

$\frac{d}{dt} \left(\frac{\partial L}{\partial \dot{x}} \right) = \frac{\partial L}{\partial x}$

THE UNITED STATES OF AMERICA
DEPARTMENT OF THE INTERIOR
BUREAU OF LAND MANAGEMENT
WASHINGTON, D. C. 20250

$$\frac{1}{2} \left(\frac{1}{2} + \frac{1}{2} \right) = \frac{1}{2}$$

1. 凡在本行工作的员工，均须遵守本行各项规章制度。
 2. 凡在本行工作的员工，均须遵守本行各项规章制度。
 3. 凡在本行工作的员工，均须遵守本行各项规章制度。
 4. 凡在本行工作的员工，均须遵守本行各项规章制度。

Abstract

[illegible]

results of Nijboer and Rahman in the Non-Gaussian approximation so as to give the best fit with the predetermined parameters θ' , θ_p , T and $(\alpha + \beta)$ as shown in Fig.(2). The value of $\alpha / (\alpha + \beta)$ obtained from our model (0.85) is in agreement with the value calculated earlier by Gibbs⁽⁵⁾ (0.875). These results show that in real fluids (to the extent that they are described by this model) the magnitude of 'hard core' interactions, is about four times the 'soft core' interactions.

REFERENCES

1. A. Rahman, K.S. Singwi, and A. Sjolander, *Phy. Rev.* **126**, 997 (1962).
2. A.G. Gibbs and J.H. Ferziger, *Phy. Rev.* **136**, 701 (1965).
3. B.R.A. Nijboer and A. Rahman, *Physica* **32**, 415 (1966).
4. For the detail of velocity autocorrelation function see J.S. Baljal and D.K. Chaturvedi, *Physica* (Under publication).
5. A.G. Gibbs, Symposium on Inelastic scattering of neutrons by condensed systems, Brookhaven National Laboratory, 1965.

DISCUSSION

Om Singh

You have calculated the scattering cross section using the non-Gaussian approximation. percentage contribution for this ..

D.K. Chaturvedi

It is about 20% at $k = 2\text{\AA}^{-1}$.

S.K. Joshi

In what way does your model give information about the potential in or near the core region.

D.K. Chaturvedi

In our model the estimation of the hard collision probability α gives the strength of the hard core potential, whereas β gives the strength of the soft core interactions respectively.

MEASUREMENT OF SELF-DIFFUSION OF LIQUID MERCURY.

S.N.Changdar,

Bose Institute, Calcutta-9.

I. INTRODUCTION

Self-diffusion coefficients of liquid mercury have been measured in the temperature range 5° - 40°C by a simple method based on radioactive tracer technique^{1,2}. The experimental geometry consists of solute and solvent columns of equal lengths with the radiation detector placed vertically over the diffusion cell. For the above experimental conditions, when $kt > 0.5$ where $k = \frac{\pi^2 D}{4L^2}$, D the diffusion coefficient and $2L$ the total length of the diffusion column, in the Fourier expansion solution of Fick's second law of diffusion

$$\frac{\partial c(x,t)}{\partial t} = D \frac{\partial^2 c(x,t)}{\partial x^2} \quad (1)$$

all even order terms vanish and it is adequately represented by the first term

$$N_0 - N_t = A \exp(-kt) \quad (2)$$

where N_t is the count rate at time t and N_0 the count rate when solute and solvent columns are completely mixed up. A is a constant depending on geometry which is eliminated when the ratios of $(N_0 - N_t)$ at different values of t are taken. Thus D can be measured by noting the variation of $N_0 - N_t$ with time.

II. EXPERIMENTAL

The diffusion cell is constructed on the principle of sliding cell technique. It consists essentially of two stainless steel slabs of dimensions 2.5" x 2" x 1" . They are placed in a brass vessel of dimensions 5"x2"x1", the lower steel slab was kept fixed with respect to the brass vessel.. The upper slab could be slowly moved with respect to the lower one by means of a sliding screw arrangement. There is a central hole in the lower slab, and two in the upper slab, one of which together with the hole in the lower slab constituted the diffusion column. The vessel was placed on a shock proof mounting which was made as vibration free as possible under existing circumstances. For temperature control we used a thermostat where the temperature could be made constant within $\pm 0.02^{\circ}\text{C}$. The anthracene counter was placed vertically over the diffusion column. The counter was connected to a highly stable electronic circuit which consisted of amplifier, analyser, scaler etc. The long term stability of the system was checked to within $\pm 0.1\%$ for a period of 24 hours.

The depth of the lower cavity of the cells was 1 cm and 1.5 cm, and the diameter of the cavity was 0.6 cm. Initially the lower cavity was completely filled up with the radioactive solute having H_2^{203} as the tracer. Then the amount of mercury required to fill the lower cavity was calculated and the requisite amount was weighed by

means of a sensitive balance. It was then poured into the hole of the upper slab. A very thin layer of light grease between the two carefully ground interfaces of the two plates served as precautions against leakage of liquid. The open hole was covered with a thin aluminium foil. Readings were taken after the elapse of one hour after the solvent column was superposed on the solute column. The measurements were made in the temperature range 5-40°C.

We solved Fick's second equation for a unidirectional flow and we found out the diffusion coefficient assuming that diffusion took place in one direction only. But in our arrangement the diameter of the diffusion column was finite. To test the effect of radius on diffusion measurements we measured the diffusion coefficients of mercury at 40°C by using cells of 1.5 cms length and of diameters 0.6 cm, 0.8 cm, 1.0 cm. The results at different diameters did not differ widely and they were within experimental error.

III. RESULTS

In the following table we give the results obtained in our laboratory and for comparison we also give some of the results obtained by Hoffman³ and Nachtrieb and Petit⁴. The measurements were taken at normal atmospheric pressure. Fig. 1. gives a typical plot of $\log_e (N_0 - N_t)$ vs. time and fig.2 gives the variation of diffusion coefficient of mercury with temperature.

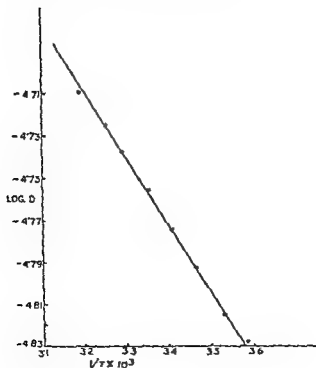
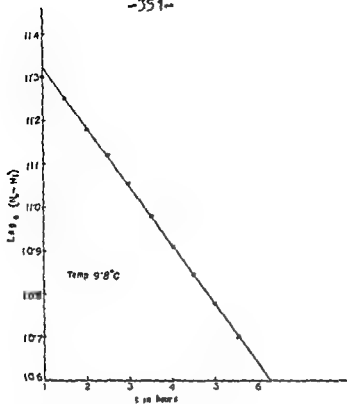
Table I.

Temperature °K	$D \times 10^5$ cm sec ⁻¹	Investigator
273.2	1.39	Nachtrieb and Petit.
275.7	1.52	Hoffman.
278.2	1.48	Present worker.
283.0	1.53	Present worker.
288.6	1.61	Present worker.
289.6	1.68	Hoffman.
293.7	1.68	Present worker.
296.2	1.79	Hoffman.
298.2	1.76	Present worker.
303.5	1.63	Nachtrieb and Petit.
308.2	1.87	Present worker.
313.2	1.92	Present worker.
314.7	1.98	Hoffman.

The Stokes-Einstein radius of mercury atoms was calculated by using Stokes-Einstein equation $r = \frac{RT}{6\pi\eta} \cdot \eta$, the viscosity coefficient was taken from Bingham and Thomson's⁵ data and the radius was found to be $0.32 \pm 0.01 \text{ \AA}$. The disagreement with the experimentally found radius 1.5 \AA is obvious because the assumption of continuous medium valid for the Stokes-Einstein equation is not valid for mercury.

ACKNOWLEDGEMENT

The author expresses his grateful thanks to Prof. A.M. Ghose, Head of the Dept. of Physics, Bose Institute for helpful discussions. He also expresses his thanks to Prof. S.M. Sircar, Director and Dr. D.M. Bose, former Director, Bose Institute for their interest in the work.



VARIATION OF D WITH TEMPERATURE IN MERCURY

REFERENCES

1. A. Nath. - Proc. Nucl. Phys. Symp., Bombay,
Part II 157 (1966).
2. Changdar S.N., Nath A. - Sci. and Cult. 36,183(1970)
3. Hoffman R.E. - J. Chem. Phys. 20, 1567 (1952).
4. Nachtrieb N.H. and Petit J. - J. Chem. Phys. 24,
746 (1956).
- *5. Bingham E.C., Thompson T.R. - J. Am. Chem. Soc.
50, 2878 (1928).

ANHARMONIC CONTRIBUTION TO MOSSBAUER FRACTION OF ⁸³Kr IN SOLID KRYPTON

S.S.Nandwani, Deo Raj and S.P.Puri
Department of Physics, University of Roorkee, Roorkee.

I. INTRODUCTION

Gilbert and Violet⁽¹⁾ (GV) measured the Mössbauer fraction 'f' in solid Krypton between 5 and 85°K. The observed values were considered to be significantly lower than predicted by them using the Kr phonon spectra of Brown and Horton⁽²⁾ based on Mie-Lennard Jones (4-6) potentials. These calculations were based on harmonic approximation and no account was taken of anharmonicity. But an adequate treatment must include anharmonic effects in all rare gas solids because of their small binding energies. Particularly, in the case of Kr, it has been shown⁽³⁾ that the anharmonic contribution to the vibrational properties are appreciable for $T > \theta_D/10$. Subsequently, a number of workers⁽⁴⁻⁷⁾ have incorporated the anharmonicity and have claimed good agreement.

Normally the effect of anharmonic terms in the interatomic potentials on normal mode frequencies are accounted for either in quasi-harmonic approximation given by⁽⁸⁾

$$\omega_k^{qh}(T) = \omega_k^h(T_0) \exp \left\{ -3 \int_{T_0}^T \alpha(\tau') Y(\tau') d\tau' \right\} \quad \text{--- (I-a)}$$

or through their explicit temperature dependence given by^(9,10)

$$\omega_k^a = \omega_k^h \left(1 + \frac{A E_v h}{3 N k_B} \right) \quad \text{--- (I-b)}$$

But a proper calculation of temperature dependent properties should include both^(11,12), the change in the volume due to thermal expansion (Eq.I-a) as well as the explicit anharmonic effects

Eq.I-b) leading to

$$\omega_k^a(T) = \omega_k^h(T_0) \left[1 + \frac{A E_v h}{3 N k_B} + \exp \left\{ -3 \int_{T_0}^T \alpha(\tau') Y(\tau') d\tau' \right\} \right] \quad \text{--- (I-c)}$$

Calculations have been carried out on these lines and the results are compared with the experiment and discussed in the light of earlier calculations.

II. CALCULATIONS

Krypton has f.c.c. lattice and in the harmonic approximation the Mössbauer fraction is given by the expression :

$$f = \exp \left[- \frac{E_r^2}{2Mc^2k} \frac{1}{3N} \int_0^{\omega_{\max}} \frac{g(\omega)}{\omega} \coth \left(\frac{\hbar\omega}{2k_B T} \right) d\omega \right] \dots \quad (II)$$

The 'f' values at various temperatures ranging from 5-100°K have been calculated using Eq.(II) after applying the mass correction⁽¹³⁾ to the frequency and then modifying according to the Eqs. I(a)-I(c) for the quasiharmonicity, explicit temperature dependent anharmonicity, and the total anharmonicity respectively. Any change in $g(\omega)$ consequently upon the change in ω is unimportant as it is a normalized function. We have also used the $g(\omega)$ function derived from MLJ (m-6) potential. The input data of $\gamma(T)$ and $3\mathcal{L}(T)$ at various temperatures studied were taken from the latest experimental work of Losee and Simmons⁽¹²⁾ and the value of $A \approx 1 \times 10^{-3}/^\circ\text{K}$ from that of Feldman & Horton⁽¹⁴⁾.

III. RESULTS AND DISCUSSION

The results of calculations of f vs T for the harmonic, quasiharmonic, the explicit temperature dependent anharmonic and the complete anharmonic cases are compared with experimental results⁽¹⁾ in Fig.1.

Brown⁽⁴⁾ using explicit anharmonic approximation and $g(\omega)$ derived from MLJ(m-6) potentials, tried to fit the experimental observations by parametrizing A. It appears that due to a mistake in the change of variable, (Eq(6) in Ref.4), the resultant curve went down contrary to expectations. Further more he accounts only partie-

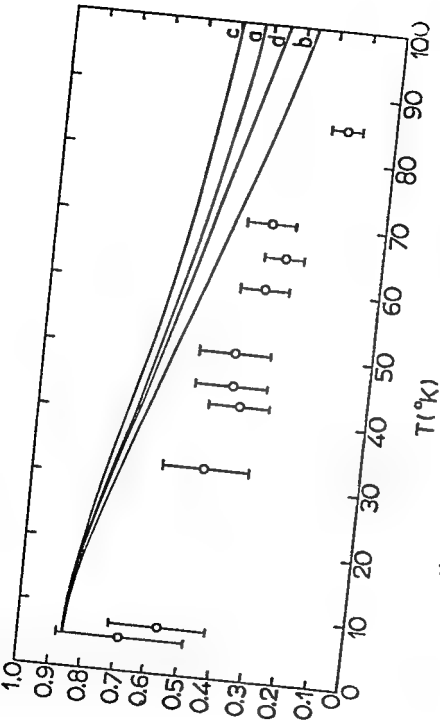
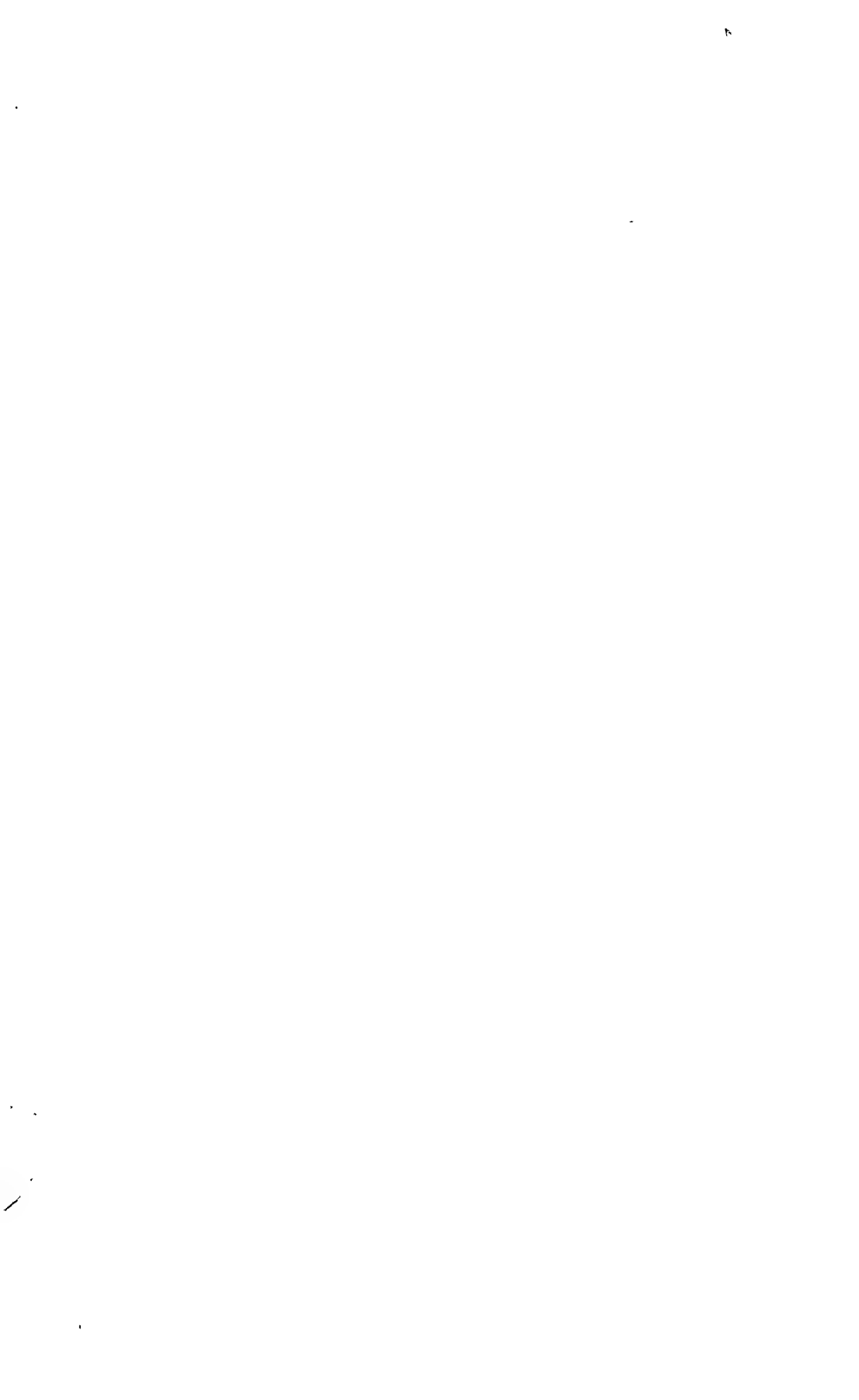


fig.1 A plot of f' vs temperature using (a-6) potential⁽²⁾ for : (a) harmonic (b) quasi-harmonic (c) explicit temperature dependent anharmonicity & (d) total anharmonicity. The circles denotes the experimental values (GV).

lly for the anharmonicity by considering just the explicit temperature dependence. Mahesh⁽⁶⁾ using Debye theory and quasi-harmonic approximation, claimed the agreement with the experiment. This is open to serious objection since Debye approximation is at best a first approximation & an experimentally measured $g(\omega)$ should be preferable. However, in the event of lack of measured $g(\omega)$, the next best recourse is to adopt some model dependent calculation of $g(\omega)$ which has been successful in explaining some other physical measurements such as specific heat, $\Theta_D(T)$ curve etc. Moreover, he assumed the temperature independence of $\gamma(T)$ and $3\alpha(T)$ which is not at all tenable in view of recent investigations⁽¹²⁾. Further he has also accounted for anharmonicity only partially. Vashishta and Pathak⁽⁵⁾ used quasi-harmonic approach in Debye approximation and fitted the experiment with calculations by parameterizing Θ_D . They concluded that Θ_D lies between 45-50°K. It may also be commented that γ and α values at different temperatures used by them, have been modified by recent experiments⁽¹²⁾. Furthermore, parametrization is an arbitrary procedure which takes the onus out of job. Of course, they also account for anharmonicity only partially. In the case of present calculations, Fig.1, we see that the harmonic curve (a) is far removed from the experimental results indicating the necessity of incorporation of anharmonic contribution. Incorporation of explicit temperature dependent anharmonicity (curve c) further aggravates the trend whereas the quasi-harmonic approximation (curve b) displaces it towards the experimental points. This latter trend is also borne out by the calculations of Vashishta & Pathak⁽⁵⁾ as well as of Goldman⁽⁷⁾. The complete anharmonicity (curve d), although not reproducing the experimental observations faithfully, does represent the experiment more closely than Brown⁽⁴⁾.

References

1. K.Gilbert and C.E.Violet, Phys. Letters 28 A, 285 (1968).
2. J.S.Brown and G.K.Horton, Phys.Rev. Letters 18 , 647(1967).
3. R.H.Beaumont, H.Chihara and J.Morrison, Proc. Phys.Soc. (London) 38 , 1462 (1961).
4. J.S.Brown, Phys. Rev. 187, 401 (1969).
5. P.Vashishta and K.N.Pathak, Physica 10 Apr.(1970), pp 587.
6. K.Mahesh, J.Phys.Soc. Japan 28 , 818 (1970).
7. V.V.Goldman, Phys. Rev. 174, 1041 (1968).
8. K.N.Pathak and B.Deo, Physica 35, 167 (1967).
9. T.H.K.Barron, Lattice Dynamics edited by R.F.Wallis, pp.247 pergamon press, New York (1965).
10. W.G.Overton, Jr., J.Phys.Chem.Solids, 29, 711 (1968).
11. A.J.Leadbetter, J.Phys.C.(Proc.Phys.Soc.) 1 , 1481 (1968);
ibid 1 , 1489 (1968).
12. D.L.Losee and R.G.Simmons, Phys.Rev. 172, 944 (1968).
13. R.Glaiss, Phys. Stat. Sol. 17, 761 (1966).
14. J.L.Feldman and G.K.Horton, Proc. Phys. Soc.(London), 92, 227 (1967).



CALCULATION OF THE MOSSBAUER PARAMETERS FOR THE DISORDERED LATTICE

B.P. Srivastava, H.N.K. Sharma and D.L. Bhattacharya
Department of Physics, B.H.U. Varanasi-5.

We have considered the crystal lattice in which a vacancy interstitial pair has been formed by nuclear irradiation. Considering only the nearest neighbour interactions of these point defects we have calculated the Lamb-Mossbauer fraction, with the double-time Green's function technique, for the disordered lattice. Assuming the vacancy interstitial pair as a perturbation, and taking vacancy as the origin and following Maradudin et al. ⁽¹⁾

We can write the total Hamiltonian as

$$H = \sum_{l\alpha} \frac{p_{l\alpha}^2(l)}{2M} + \frac{1}{2} \sum_{l\alpha} \sum_{l'\beta} \phi_{l\alpha}(l) u_{l'\beta}(l') - \sum_{\alpha} \frac{p_{\alpha}^2(0)}{2M} \\ + \sum_{\alpha} \frac{p_{\alpha}^2(\alpha)}{2M} + \frac{1}{2} \sum_{\alpha} \sum_{l\beta} f(\alpha^2) \frac{R_{\alpha}^0(l) R_{\beta}^0(l)}{R_{\alpha}^2} f'(\alpha(l)) \\ [u_{\alpha}(l) - u_{\alpha}(0)] [u_{\beta}(l) - u_{\beta}(0)] \quad (1)$$

where $f(X^2)$ is the function of X which is the distance between the vacancy and interstitial, the rest are same as Maradudin ⁽¹⁾. Substituting the value of $p_{\alpha}(l)$ and $u_{\alpha}(l)$ we can write the unperturbed Hamiltonian from (1) as

$$H_0 = \sum_{hs} \hbar \omega(\vec{k}_s) a_{\vec{k}_s}^{\dagger} a_{\vec{k}_s} \quad (2)$$

where $a_{\vec{k}_s}^{\dagger}$ and $a_{\vec{k}_s}$ are the creation and destruction operators.

The perturbed Hamiltonian becomes

$$H_1 = -\hbar \sum_{\vec{k}_1} \sum_{\vec{k}_1'} U(\vec{k}_1, \vec{k}_1') B_{\vec{k}_1} B_{\vec{k}_1'} \\ + \hbar \sum_{\vec{k}_1} \sum_{\vec{k}_1'} V(\vec{k}_1, \vec{k}_1') A_{\vec{k}_1} A_{\vec{k}_1'} \quad (3)$$

where $U(\vec{R}_i, \vec{R}'_{j'}) = u_\alpha(\vec{R}_i) u_\alpha(\vec{R}'_{j'})$;

$$\text{and } u_\alpha(\vec{R}_j) = \left[\frac{\omega(\vec{R}_j) q(x)}{4N} \right]^{1/2} e_\alpha(\vec{R}_j) \quad (4)$$

$$\text{and } f(kx) = \left[\frac{\omega_1(\vec{R}_i) q(x)}{\omega(\vec{R}_i)} \right]^{1/2} \frac{[f(\vec{R}_x) f(\vec{R}'_x) - 1]}{e^{2\pi i \vec{R} \cdot x}} \quad (5)$$

here $\omega_1(k_j)$ is the localized frequency of (k_j) th mode due to the interstitial atom.

$$\text{and } V(\vec{R}_i, \vec{R}'_{j'}) = \sum_r U_r(\vec{R}_i) U_r(\vec{R}'_{j'})$$

$$\text{where } U_r(\vec{R}_i) = \left[\frac{F_r(x^2) F''(R(r))}{4MN \omega_1(\vec{R}_i) R_0^2} \right]^{1/2} R(r) \left[e^{2\pi i \vec{R} \cdot R(r)} - 1 \right] \quad (6)$$

The above Hamiltonian (1) is of the same form as given by Maradudin et al. ⁽¹⁾ So proceeding as in ref. (1) we

get the final expression for the Green's function as

$$G(\vec{R}_i, \vec{R}'_{j'}; E) = G_U(\vec{R}_i, \vec{R}'_{j'}; E) + 4\pi \sum_{\vec{R}_s} \sum_{\vec{R}'_{s'}} G_U(\vec{R}_i, \vec{R}_s; E) U_r(\vec{R}_s) [I - 4M_U(E)]_{r, r'}^{-1} U_{r'}(\vec{R}'_{s'}) G_U(\vec{R}'_{s'}, \vec{R}'_{j'}; E) \quad (7)$$

where $G_U(\vec{R}_i, \vec{R}'_{j'}; E)$ is the Green's function for a Bravais crystal containing a single point defect.

and

$$G_U(\vec{R}_i, \vec{R}'_{j'}; E) = \frac{\omega(\vec{R}_i)}{\pi} \frac{\Delta(\vec{R} + \vec{R}') \delta_{ij'}}{E^2 - \omega^2(\vec{R}_i)} + \frac{4E^2}{\pi} \frac{1}{E^2 \omega^2(\vec{R}_i)} \frac{[\omega(\vec{R}_i) \omega(\vec{R}'_{j'})]^{1/2}}{E^2 \omega^2(\vec{R}'_{j'})} \sum_r \frac{e_\alpha(\vec{R}_i) e_\alpha(\vec{R}'_{j'})}{4N} \left[1 - \frac{E^2}{N} \sum_{\vec{R}_s} \frac{e_\alpha^2(\vec{R}_s)}{E^2 \omega^2(\vec{R}_s)} \right]^{-1} \quad (8)$$

The matrix $M_U(E)$ has the elements

$$[M_U(E)]_{r, r'} = \pi \sum_{\vec{R}_i} \sum_{\vec{R}'_{j'}} U_r(\vec{R}_i) G_U(\vec{R}_i, \vec{R}'_{j'}; E) U_{r'}(\vec{R}'_{j'}) \quad (9)$$

and

$$\epsilon = \frac{q(x)}{1 + q(x)}$$

The Green's function is now written as

$$G(\vec{R}_1, \vec{R}_2, E) = \frac{\omega(\vec{R}_2) \Delta(N+N') \delta_{12}}{\pi E^2 \omega^2(\vec{R}_1)} + \frac{\epsilon E^2 [\omega(\vec{R}_1) \omega(\vec{R}_2)]^{1/2}}{\pi N \left[E^2 \omega^2(\vec{R}_1) \right] [E^2 \omega^2(\vec{R}_2)]^{1/2}} \\ \sum_{\vec{R}_3} e_{\alpha}(\vec{R}_1) e_{\alpha}(\vec{R}_2) \left[1 - \frac{\epsilon E^2}{N} \sum_{\vec{R}_4} \frac{e_{\alpha}^2(\vec{R}_4)}{E^2 \omega^2(\vec{R}_4)} \right]^{-1} \\ + 4\pi \sum_{\vec{R}_3, \vec{R}_4} \sum_{\alpha, \beta} G_{\alpha\beta}(\vec{R}_1, \vec{R}_2, E) U_{\alpha}(\vec{R}_3) [I - 4\pi M(E)]_{\alpha\beta}^{-1} U_{\beta}(\vec{R}_4) \quad (10)$$

The exponent of the Debye-Waller is expressed⁽¹⁾ as

$$2M = -\frac{4\pi^2}{2NM} \sum_{\vec{R}_1, \vec{R}_2} \frac{(\vec{R}_1 \cdot \vec{e}(\vec{R}_1)) (\vec{R}_2 \cdot \vec{e}(\vec{R}_2))}{(\omega(\vec{R}_1) \omega(\vec{R}_2))^{1/2}} \quad (11) \\ \times \frac{2\pi}{\beta N} \sum_{n=-\infty}^{\infty} G_{\alpha}(\vec{R}_1, \vec{R}_2, i\omega_n)$$

We can express

$$2M = 2M_0 + 2M_1 + 2M_2 \quad (12)$$

where $2M_0$, $2M_1$ are already known for crystals with cubic symmetry⁽¹⁾. The matrix $M_{ij}(E)$ in the expression (10) can be shown to be diagonal matrix⁽²⁾. So using this fact and solving the last component of the Green's function in the expression (10) and then substituting this simplified value in the expression (12) we get, after considerable algebra, the following expression for $2M_2$ for lattice with cubic symmetry.

$$2M_2 = \frac{2}{9} \frac{\pi}{NM} (2\pi k)^2 \sum_{\vec{R}_1} \frac{2\hbar n_1 + 1}{\omega(\vec{R}_1)} \left[\frac{\sum_{n=0}^{\infty} G(n)}{1 - \frac{2}{3} \epsilon \omega_n^2 G(n)} \right] \quad (13)$$

where

$$\Gamma_{1n} = \left[\frac{4\pi^2 f \alpha^2}{m a^2} \frac{\rho^2(R(R))}{\sin^2 \pi \vec{R} \cdot \vec{R}(R)} \right] \frac{\omega(\vec{R}_1)}{\omega_1(\vec{R}_1)}$$

where we have neglected the higher order terms of Γ_{1n} and have considered the small change in the localized frequency mode due to the impurity i.e.

$$W_1(k_j) \rightarrow W(k_j) \text{ so that } \epsilon \rightarrow 0 \quad (14)$$

The total exponent of the Debye Waller factor is

$$2M = 2M_0 \left(1 + \frac{2M_1}{2M_0} + \frac{2M_2}{2M_0} \right)$$

Substituting the value and considering the condition (14), we get,

$$\frac{2M}{2M_0} = \left[1 + \frac{8}{3} \Gamma_k \sum_{n=0}^{\infty} G(n) \right] \quad (15)$$

where $G(n) = G_x(n) + G_y(n) + G_z(n)$

So for N vacancies-interstitial pairs, neglecting the point defect pair- point defect pair interaction, we get the exponent of the Debye-Waller factor as

$$2\mathcal{M} = \frac{2M}{2M_0} = \left[1 + \frac{8}{3} N \Gamma_k \sum_{n=0}^{\infty} G(n) \right] \quad (16)$$

This expression gives the change in the Debye Waller factor due to the point defect pairs for the cubic crystals. The change is possibly detectable experimentally and is now the subject of investigation.

ACKNOWLEDGEMENT

Two of the authors (BPS) and (HNK) are thankful to the C.S.I.R., New Delhi for granting the financial help.

REFERENCES

1. Maradudin, Flinn and Redcliffe, Annals of Phys., 26, 81 (1964).
2. Maradudin, A.A., Annals of Physics, 30, 371 (1964)

The Mössbauer effect studies of 9.3 KeV transition in Krypton solid.

Krishan Mahesh and N.J.Sarma

Department of Physics, Kurukshetra University, Kurukshetra.

I. Introduction

Recently a direct observation of the Mössbauer effect for the 9.3 KeV transition of $\text{Kr}^{83\text{m}}$ ($7/2^+ \rightarrow 3/2^+$) in frozen Krypton between the temperatures 5-95°K has been reported by Gilbert and Violet[1] . The source and the absorber were obtained by flowing the Kr gas into the source and absorber cells, both placed within the same cryostat. The experimental f_E -T variation when compared with the theoretical f_{BH} -T variation as predicted from the phonon frequency distribution (pfd) of solid Krypton of Brown and Horton [2] , however, revealed a large disagreement.

The Debye model calculations by Mahesh [3] of the temperature dependence of the recoilless fraction (f_A -T) which included also the anharmonicity corrections of the lattice thermal expansion type, yielded, however, a better agreement with the experiment at low ($T < 40^\circ\text{K}$) and, to some extent, at high temperatures ($T > 80^\circ\text{K}$). In these calculations the characteristic Mössbauer temperature $\theta_M(0^\circ\text{K}) = 42^\circ\text{K}$, obtained by extrapolation [4] from Pasternak et al's [5] value of 37°K at 50°K was used. The corresponding Debye temperature θ_D^C of the Krypton solid obtained from the heat capacity data is $\approx 65^\circ\text{K}$ [6] . Furthermore, using the Debye model the temperature dependence of the Mössbauer energy shift (second order relativis-

shift) S was also studied and was found to be of the expected form.

Frozen Krypton being an ideal monoatomic solid and the agreement between experiment and the theory still being unsatisfactory, it was considered worthwhile to make a detailed cubic structure calculations of the temperature dependence of the recoilless fraction f_G -T and also of the energy shift S using the pfd of Kr-lattice vibrations computed by Gupta [7] who used the quasi-harmonic rigid atom model which includes the fourth nearest neighbour central force interactions.

II. Theoretical

The recoilless fraction f and the energy shift S, can be expressed as the integral quantities in the phonon frequency spectra. For a monoatomic lattice of cubic symmetry the expressions for f and S are given as [8] :

$$f = \exp \left[- \frac{E_R}{h} \frac{1}{3N} \int_0^{\omega_m} \frac{g(\omega)}{\omega} \coth \left(\frac{\hbar\omega}{2kT} \right) d\omega \right] \quad (1)$$

and
$$S = \frac{3\hbar}{4Mc} \frac{1}{3N} \int_0^{\omega_m} g(\omega) \omega \coth (\hbar\omega / 2kT) d\omega \quad (2)$$

with
$$3N = \int_0^{\omega_m} g(\omega) d\omega \quad (3)$$

as the normalizing factor and the various symbols have the usual meaning.

The integrals in equations (1), (2) and (3) are evaluated by numerical integration over the pfd [7]. To do this the whole frequency spectrum [7] was divided into 60 equal intervals of $0.025 \times 10^{12} \text{ sec}^{-1}$ width each. The midpoint of each step was taken as the one representing

that interval and the corresponding ordinate gave for instance the value $g(\nu_i)$ at ν_i at the i th midpoint. The alternative forms of eqs (1) and (2) which become directly usable for numerical evaluation, are expressed as, using $\omega_i = 2\pi\nu_i$

$$f_G(T) = \exp - \frac{\lambda}{\phi(\nu_i)} \sum_{i=1}^{60} \frac{g(\nu_i)}{\nu_i} \operatorname{cth} \left(\frac{\omega_i}{T} \right) \quad 4$$

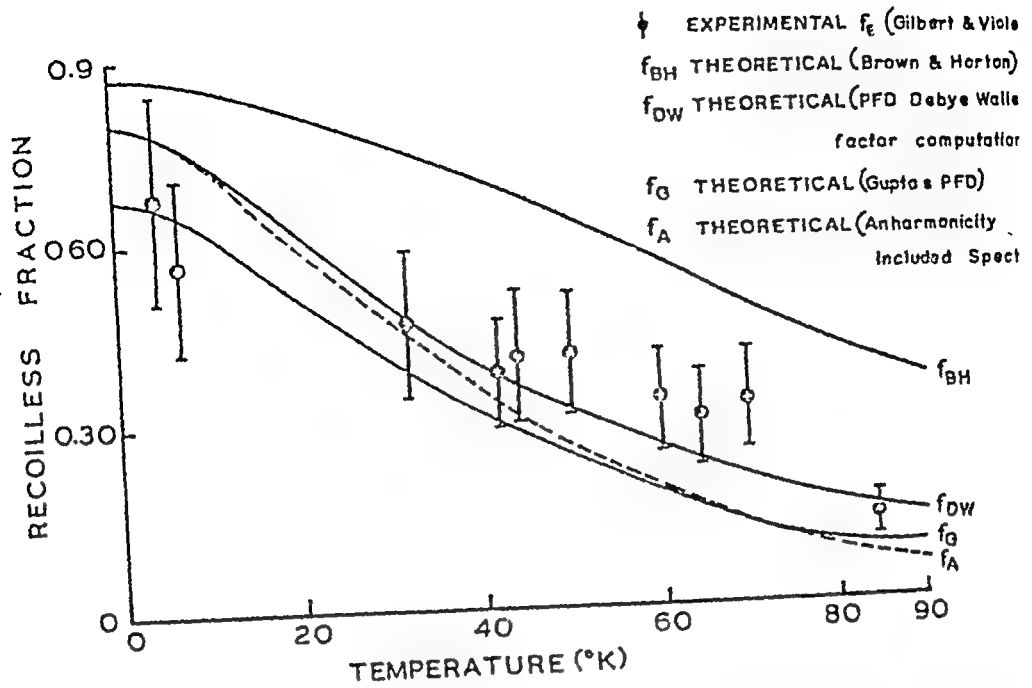
and
$$S_G(T) = \frac{B}{\phi(\nu_i)} \sum_{i=1}^{60} g(\nu_i) \operatorname{cth} \left(\frac{\omega_i}{T} \right) \quad 5$$

with
$$\phi(\nu_i) = \sum_{i=1}^{60} g(\nu_i) \quad 6$$

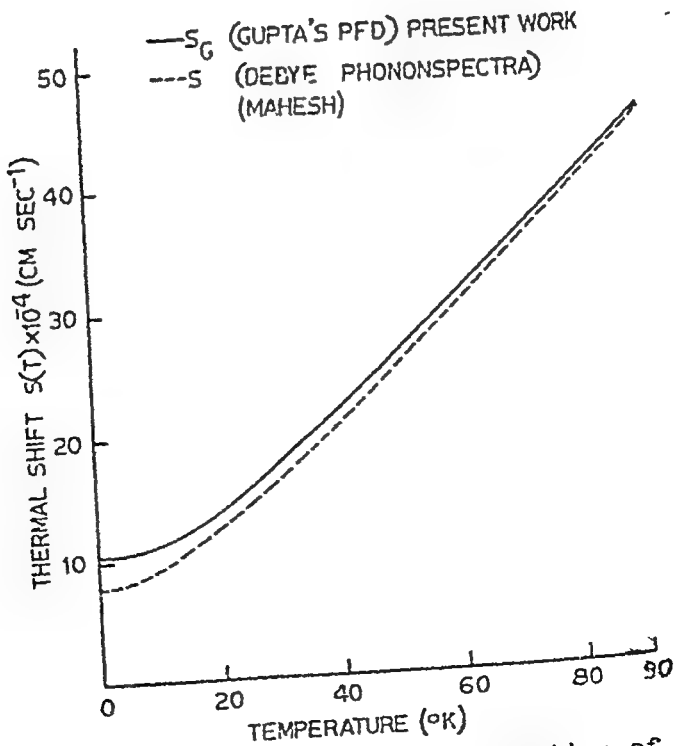
III. Results and Discussion

The computer-calculated values of $f_G(T)$ and $S_G(T)$ are plotted as functions of temperature and are shown in fig.1. and 2 respectively. The $f_G(T)$ variation is compared with (i) the experimental f_G-T variation of Gilbert and Violet [1] (ii) the theoretical $f_{BA}-T$ variation predicted from Brown and Horton's [2] phonon frequency spectra, (iii) the theoretical f_A-T variation — dashed curve, in fig.1, obtained by Mahesh [3] using the Debye frequency spectra with a cut-off defined by $\frac{\hbar\omega_{\max}}{k} = \theta_M = 42^\circ K$ which also includes the effect of lattice anharmonicity, and (iv) the theoretical $f_{DW}-T$ variation obtained using the Tables prepared by Muir Jr [9] for computing Debye — Waller factors in Mössbauer effect studies. The f_{DW} values however do not incorporate any anharmonicity corrections but represent more accurate calculations at $T > 1/5 \theta_M$.

The temperature dependence of S_G based on the quasiharmonic pfd model is compared with the corresponding Debye model calculations by Mahesh [3]. This is shown in fig.2.



1. Recoilless fraction as a function of the the temperature.



2. Mössbauer energy shift as a function of the temperature.

A careful observation of the "f-T" variation in fig.1 reveals, at least qualitatively, the detailed model dependence of the recoilless fraction. Quasiharmonic central force interaction model yields a close agreement with the experiment of Gilbert and Violet [1] in the region of low temperatures. This, using $f(T=0) = \exp - 3E_R / 2k\theta_M(0)$, corresponds to the characteristic temperature $\theta_M(0) \approx 25^\circ\text{K}$. It, however, exhibits an evident departure, at low temperatures, as compared to the f_A^- and f_{DW}^- values - the latter two values in fact coinciding, and indicates the possibility of the low frequency Kr-spectrum not being Debye-like which rather lends support to the contention of Gilbert and Violet [1]. Almost similar situation is observed in case of the temperature dependence study of the Mössbauer energy shift in fig.2. The reason for large deviations in the f_{BH}^- values as compared to f_E^- , f_A^- , f_{DW}^- or f_G^- values are not, however, obvious to us. It might perhaps be in the method of calculations. Furthermore, at intermediate temperatures ($45^\circ < T < 80^\circ$) the different 'f' - values show marked deviations from the experiment although, again at $T > 80^\circ\text{K}$ all the 'f'-values appear to show, in general, an improved agreement. It is possible, that at intermediate temperatures some kind of "Vacancy readjustment" in the source might be responsible for the deviations. This, of course, is rather speculative.

Of all, the f_{DW}^- values, unaccounted for anharmonicity corrections also, show the best agreement with the

experiment. Comparison, particularly at $T=85^{\circ}\text{K}$, between the f_{E} - values on one hand and f_{A} -, f_{G} -, and f_{D} - on the other, rather indicates the negligible effect of anharmonicity in Kr-solid which possibility appears to bear agreement with the findings recently reported by Gupta ^{etal} [10]. The slight difference between the f_{G} - and f_{A} - values at 85°K is more or less due to the less accurate[†] [9] evaluation of the latter.

IV. Acknowledgement

The authors thank Dr.H.P.Gupta, Prof.B.Dyal, Prof.S.K. Joshi, Dr.A.K.Rajgopal and Dr.R.J.Bezum for helping us in many ways in this work . For providing facilities and help in computation work the authors sincerely thank Drs.S.C.Mathur and P.Avtar and are grateful to Dr.K.K.Nagpaul and Prof.N.Nath for their keen interest in the work and providing^{the} facilities.

[†]The usual expression [3] used for evaluating f at $T>1/5 \theta_{\text{M}}$ in the Debye model gives values which are smaller [9] than those obtained using almost exact numerical evaluation of the Debye integral.

References

1. G.Gilbert and C.E.Violet: Phys. Letters 23A, 285(1968)
2. J.S.Brown and G.K.Morton: Phys. Rev.Letters 18, 647 (1967)
3. Krishan Mahesh: J.Phys.Soc.Japan, 23, 818 (1970)
4. Krishan Mahesh: Nucl.Instrum and Methods 65,349(1968)
5. M.Pasternak, A.Simonculous, S.Buksman and T.Sonnino: Phys.Letters 22, 52 (1966)
6. N.Bernardes: Phys.Rev. 112, 1539 (1958)
7. N.P.Gupta: Aust.J.Phys., 22, 47 (1969)
8. D.Raj.and S.P.Puri: Phys.Stat.Solidi.34,K13 (1967)
9. A.d.Luir Jr.: "Tables and Graphs for computing Debye - Waller factors in Mössbauer effect studies". Atomic International report No.A1-6693 (1962).(Circulated).
10. N.P.Gupta and R.A.Gupta: J.Phys. C (Solid State Phys.) 2, 190 (1969).

DISCUSSION

Unidentified

I guess in krypton anharmonicity must be rather strong and it is difficult to say that a model without anharmonicity consideration can really be applied to any study on this substance at temperature even about 10-15°K.
K. Mahesh

In the potential expansion cubic and quartic terms would contribute. The cubic contribution is positive. The quartic value may be +ve or -ve depending upon the substance. It is just possible that in the case of an

Krypton it is negative so that the net contribution may be quite small. Furthermore, without the inclusion of lattice anharmonicity, an improved agreement with the experiment is revealed.

S.C. Bhargava

The uncertainty in value of recoilless fraction is large at lower temperature. What is reason for that?

K. Mahesh

As reported by Gilbert and Violet, the Mossbauer source and absorber are prepared by flowing the Krypton gas into cryogenic cells, the former being irradiated with high neutron flux to produce $\text{Kr}^{83\text{m}}$ (9.3 keV) isomer. Although I cannot comment precisely but the reason may be in the method of preparation of the source and absorber.

Satya Prakash

How do you justify the Debye model for the phonon spectrum?

K. Mahesh

It is not useful to view everything in lattice dynamics from the stand point of heat capacity. θ_D^C in many materials shows a large temperature variation from zero to moderately low temperatures (Blackman, Handbuch der Physik VII/I (1955)) whereas there is very little temperature variation of the Mossbauer characteristic



THE TEMPERATURE VARIATION OF DEBYE-WALLER FACTORS OF POTASSIUM CHLORIDE UP TO THE MELTING POINT.

K. Jayalakshmi and M.A. Viswamitra

Department of Physics, Indian Institute of Science, Bangalore-12, India.

Recently, Kashiwase⁽¹⁾ and Willis⁽²⁾ have analysed the X-ray data of James and Brindley⁽³⁾ up to 936°K on KCl for the influence of anharmonicity on the Debye-Waller factors determined with X-rays. We have now carried out X-ray studies on both NaCl and KCl single crystals over a range of temperature close to their melting points. The results of KCl are presented here.

Intensity data of twelve (hk0) reflections were collected upto 1028°K from four, spectroscopically pure, single crystals of KCl (less than 0.15 mm thick), using balance-filtered MoK α radiation and ω -scan, on a Hilger and Watts Y190 linear diffractometer. Six (hkl) reflections were also measured at some lower temperatures. The recording, refinement and analysis of these data are similar to those described in the NaCl study⁽⁴⁾. The Debye-Waller B factors for K⁺ and Cl⁻ ions were found to be same within estimated standard deviations.

Fig.1 shows the temperature dependence of the experimental B-factors. Fig.2 shows the plot of $(\lambda/\sin\theta)^2 \log_e(\rho_T/\rho_0)$, vs temperature. The symbols have the same meaning as mentioned before⁽⁴⁾. The line A corresponds to the harmonic theory of Debye and Waller, with a constant $\Theta = 235^\circ\text{K}$ quoted by Barron et al⁽⁵⁾.

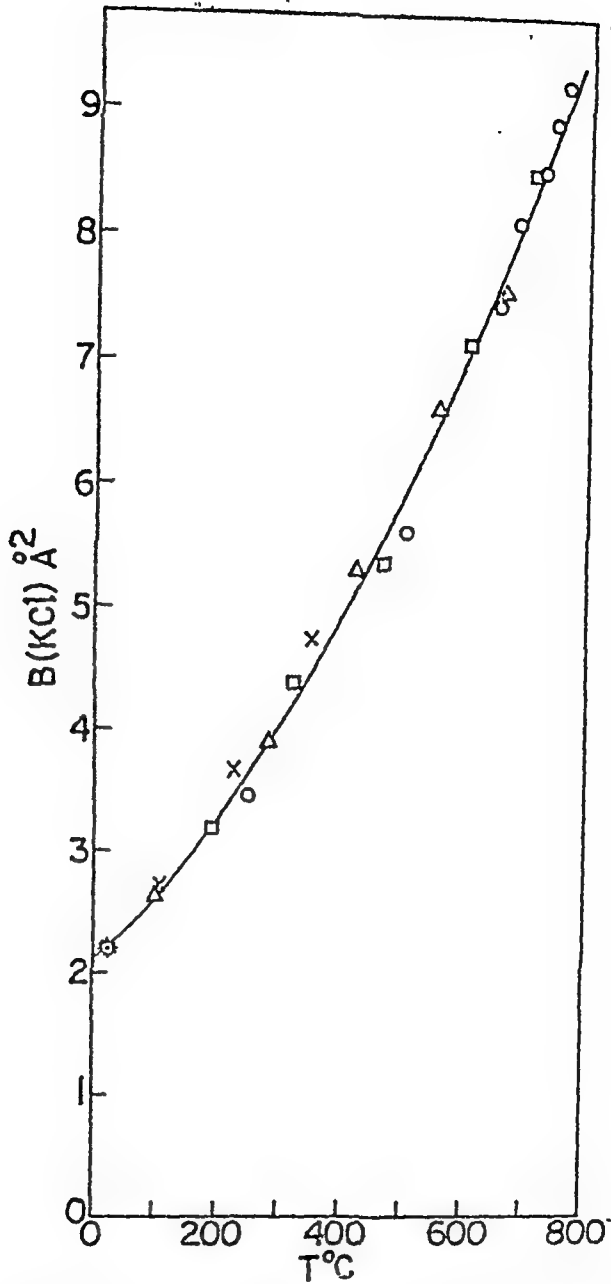
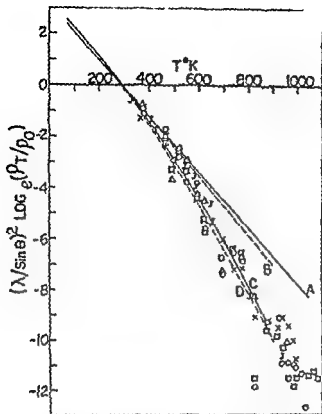
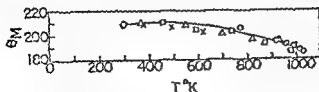


Fig.1. B(KCl) vs temperature, for four crystals (different symbols). represents the average value at room temperature. The least square fitted (smooth) curve is given by

$$B(KCl) = 2.12 + 4.66 \times 10^{-3} \times T + \dots \\ 5.95 \times 10^{-6} \times T^2 \text{ (T in } ^\circ\text{C)}.$$



g.2. Variation of $(\lambda/\sin\theta)^2 \log_e(\rho_T/\rho_0)$ with temperature in $^{\circ}\text{K}$, for reflections, 0 - (600); \square - (620); \times - (640); Δ - (800) and \circ - Experimental values of James and Brindley. A - Harmonic theory of Debye and Waller with $\Theta = 235^{\circ}\text{K}$. B - Harmonic plot based on Buyers and Smith's calculations. C - Zener and Bilinsky's correction, with $\Theta(0) = 235^{\circ}\text{K}$. D - Quasiharmonic correction of Willis applied on Buyers and Smith's theoretical values.



g.3 Variation of Debye characteristic temperature Θ with temperature.

Curve C corresponds to the phenomenological theory given by Zener and Bilinsky⁽⁶⁾ taking account of the temperature dependence of Θ , with $\Theta(0) = 235^\circ\text{K}$. Curve B corresponds to the harmonic plot, based on Buyers and Smith's calculations⁽⁷⁾. Curve D has been drawn using quasiharmonic correction due to Willis⁽²⁾, applied on the harmonic B values of Buyers and Smith. From the close agreement of C and D with experimental points, it is seen that the anharmonic contribution to the Debye-Waller factors comes essentially from thermal expansion up to the highest temperature. It may be mentioned that, in NaCl, the coincidence between the quasiharmonic plot obtained from Buyers and Smith's harmonic B-factors and the experimental points is not good.

Fig.3 shows the Debye temperature Θ_D calculated⁽⁸⁾ from experimental B-factors as a function of temperature. The ratio of the r.m.s. displacement of atoms to the nearest neighbour distance⁽⁹⁾, reaches a critical value of 0.18 at fusion. Other significant parameters at 25°C and melting are: $B_K = B_{Cl} = 2.16$ and 9.50\AA^2 ; $\Theta_M = 210$ and 184°K and $(\overline{u^2})^{1/2} = 0.28_6$ and 0.60_1\AA .

We thank Prof. D.C.Hodgkin, F.R.S., and Prof. D.C. Phillips, F.R.S., for the experimental facilities provided to one of us (MAV). We thank Prof. R.S. Krishnan and Prof. P.S. Narayanan for their interest.

REFERENCES

1. Y.Kashiwase; J. Phys. Soc. Japan; 20, 320 (1965).
2. B.T.M. Willis; Acta Cryst. A25, 277 (1969).
3. R.W. James and G.W. Brindley; Proc. Roy. Soc. A121, 155 (1928).
4. M.A.Viswamitra and K.Jayalakshmi; (previous paper)
5. T.H.K.Barron, W.T. Berg and J.A. Morrison; Proc. Roy. Soc. A242, 478, (1957).
6. C.Zener and S.Bilinsky; Phys. Rev. 50, 101 (1936).
7. W.J.L. Buyers and T.Smith; J. Phys. Chem. Solids, 29, 1051 (1968).
8. R.W.James; Optical Principles of Diffraction of X-rays, London: Bell (1948).
9. P.D.Pathak; (Private communication, 1970).

REFERENCES

1. Y.Kashiwase; J. Phys. Soc. Japan; 20, 320 (1965).
2. B.T.M. Willis; Acta Cryst. A25, 277 (1969).
3. R.W. James and G.W. Brindley; Proc. Roy. Soc. A121, 155 (1928).
4. M.A.Viswamitra and K.Jayalakshmi; (previous paper)
5. T.H.E.Barron, W.T. Berg and J.A. Morrison; Proc. Roy. Soc. A242, 478, (1957).
6. C.Zener and S.Bilinsky; Phys. Rev. 50, 101 (1936).
7. W.J.L. Buyers and T.Smith; J. Phys. Chem. Solids, 29, 1051 (1968).
8. R.W.James; Optical Principles of Diffraction of X-rays, London: Bell (1948).
9. P.D.Pathak; (Private communication, 1970).

TEMPERATURE VARIATION OF THE DEBYE-WALLER FACTORS OF NaCl AND THE ASSOCIATED DEBYE TEMPERATURE UP TO THE MELTING POINT

M. J. Viswanitra and K. Jayalakshmi

Department of Physics, Indian Institute of Science, Bangalore-12.

Experimental determination of Debye-Waller factors up to fusion are necessary for a critical appraisal of the anharmonic theories of these factors and also for checking the validity of the theories of melting relating thermal vibrations of atoms to their melting temperatures. Such investigations, up to fusion, have not been carried out so far for alkali halides. We have now obtained experimental Debye-Waller factors and the associated Θ_D values up to close to the melting temperatures for NaCl and KCl.

X-ray intensity data were collected, on a high temperature furnace⁽¹⁾, from six spectroscopically pure, single crystals of NaCl (≤ 0.15 mm thick), using balance-filtered $MoK\alpha$ radiation and ω -scan, on a Hilger and Watts K190 linear diffractometer. The data on any one crystal were collected in a single experimental run, involving only the heating of the crystal, as alternate heating and cooling was found to produce permanent changes in the reflecting power of the crystal. The final set of intensities, which consisted of 17 independent reflections of both odd and even indices ranging upto (20) and (731), were in general, the averages of 4 to 8 equivalent reflections in the upper half of the reciprocal lattice. The intensities were corrected for L_p factors and also for first order thermal diffuse scattering, using the method of Cooper and Rouse⁽²⁾. The observed structure factors were compared with the values calculated using form factors⁽³⁾ corrected for dispersion, and the B -values in the exponent of the Debye-Waller factor were obtained after several

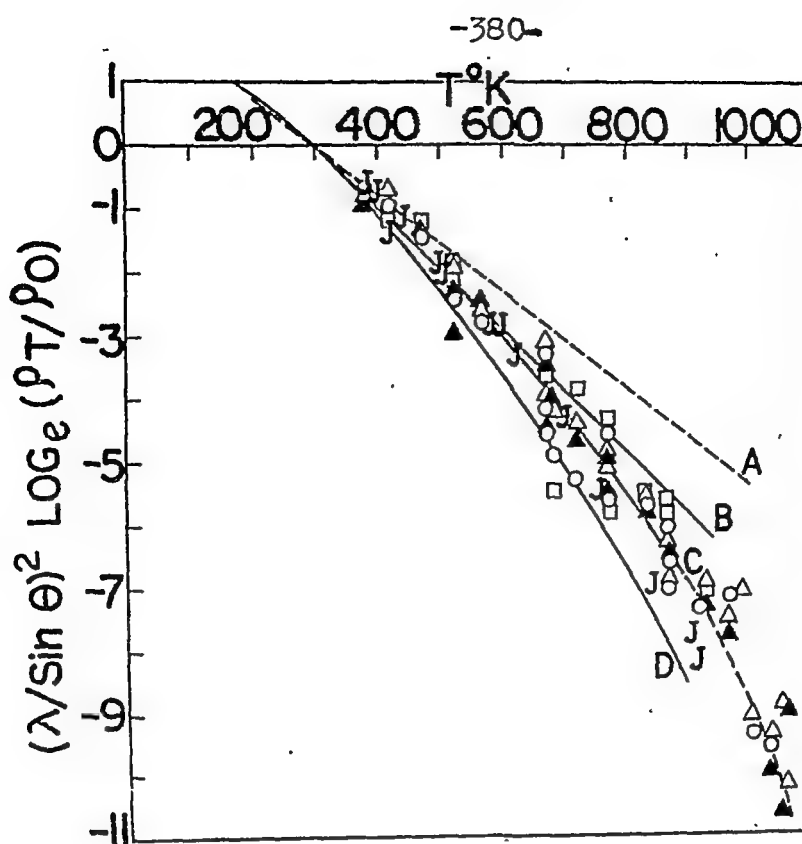


Fig. 1. Variation of $(\lambda/\sin\theta)^2 \log_e (P_T/P_0)$ with temperature for reflections; Δ - (600), \blacktriangle - (620), O - (640), \square - (800); J - James' values⁽¹⁰⁾. A - Harmonic theory of Debye and Waller; B - Harmonic plot, based on the values of Buyers and Smith (computed from the DD model of Karo and Hardy⁽¹¹⁾); C - Zener and Bilinsky's correction, with $\Theta(0) = 321^\circ\text{K}$; D - Quasiharmonic correction of Willis applied to $B^h(T)$ factors of Buyers and Smith.

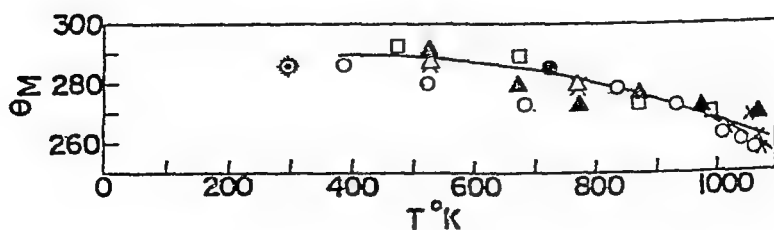


Fig. 2 Variation of Debye characteristic temperature Θ_D with temperature.

cycles of structure factor least squares refinement at each temperature. The temperature dependence of these values for the two ions are given by the least square fitted polynomials

$$B_{Na} = 1.56 + 3.32 \times 10^{-3} T + 3.27 \times 10^{-6} T^2 \text{ (}^\circ\text{C)}$$

$$B_{Cl} = 1.28 + 3.76 \times 10^{-3} T + 2.53 \times 10^{-6} T^2$$

Fig. 1 shows the plot of $(\lambda/\sin\theta)^2 \log_e(\rho_T/\rho_0)$ as a function of temperature where ρ_T and ρ_0 are the intensities at $T^\circ\text{K}$ and at room temperature. Curve A corresponds to the harmonic Debye-Waller theory, using a constant $\Theta = 321^\circ\text{K}$, taken from specific heat measurements⁽⁴⁾. Curve C is calculated from Zener and Bilinsky's phenomenological theory⁽⁵⁾, which takes account of the temperature dependence of Θ , using $\Theta(0) = 321^\circ\text{K}$. There is excellent agreement between this and the experimental points up to 900°K . Beyond this, the experimental points exhibit a steeper fall (indicated by dotted line) showing thereby that the contributions of quartic and higher order anharmonic terms in the interaction potential of the crystal to the Debye-Waller factors are significant. Curve B corresponds to theoretical harmonic $B^h(T)$ factors given by Buyers and Smith⁽⁶⁾. Curve D is obtained from curve B after applying quasiharmonic correction⁽⁷⁾. These quasiharmonic values show a steeper fall than the experimental points contrary to the situation in KCl , where agreement was found up to 700°K by Willis⁽⁷⁾, with the experimental data of James and Brindley⁽⁸⁾.

Fig. 2 shows the temperature variation of Θ_M calculated⁽⁹⁾ from the experimental B-values.

Some of the significant parameters obtained in the present measurement at 25°C and 800°C (taken from best-fitted curves) are:

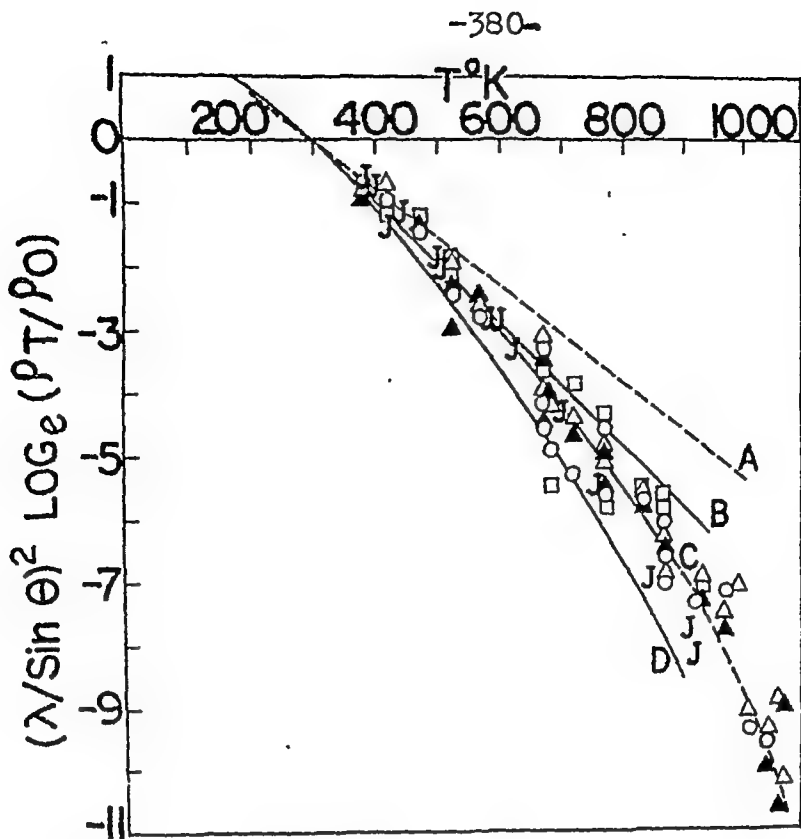


Fig. 1. Variation of $(\lambda/\sin\theta)^2 \log_e (P_T/P_0)$ with temperature for reflections; Δ - (600), \blacktriangle - (620), O - (640), \square - (800); J - James' values⁽¹⁰⁾. A - Harmonic theory of Debye and Waller; B - Harmonic plot, based on the values of Buyers and Smith (computed from the DD model of Karo and Hardy⁽¹¹⁾); C - Zener and Bilinsky's correction, with $\Theta(0) = 321^\circ\text{K}$; D - Quasiharmonic correction of Willis applied to $B^h(T)$ factors of Buyers and Smith.

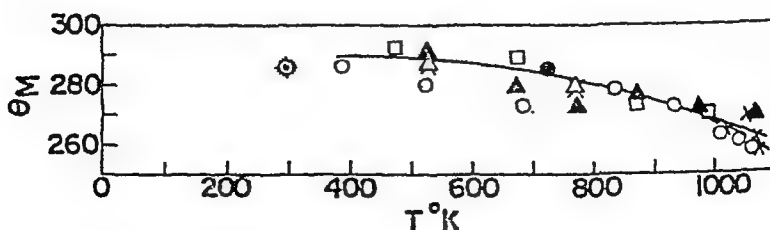


Fig. 2 Variation of Debye characteristic temperature Θ_D with temperature.

cycles of structure factor least squares refinement at each temperature. The temperature dependence of these values for the two ions are given by the least square fitted polynomials

$$B_{Na} = 1.56 + 3.32 \times 10^{-3} T + 3.27 \times 10^{-6} T^2 \quad (T^\circ C)$$

$$B_{Cl} = 1.28 + 3.76 \times 10^{-3} T + 2.53 \times 10^{-6} T^2$$

Fig. 1 shows the plot of $(\lambda/\sin\theta)^2 \log_e(\rho_T/\rho_0)$ as a function of temperature where ρ_T and ρ_0 are the intensities at $T^\circ K$ and at room temperature. Curve A corresponds to the harmonic Debye-Waller theory, using a constant $\Theta = 321^\circ K$, taken from specific heat measurements⁽⁴⁾. Curve C is calculated from Zener and Bilinsky's phenomenological theory⁽⁵⁾, which takes account of the temperature dependence of Θ , using $\Theta(0) = 321^\circ K$. There is excellent agreement between this and the experimental points up to $900^\circ K$. Beyond this, the experimental points exhibit a steeper fall (indicated by dotted line) showing thereby that the contributions of quartic and higher order anharmonic terms in the interaction potential of the crystal to the Debye-Waller factors are significant. Curve B corresponds to theoretical harmonic $B^h(T)$ factors given by Buyers and Smith⁽⁶⁾. Curve D is obtained from curve B after applying quasiharmonic correction⁽⁷⁾. These quasiharmonic values show a steeper fall than the experimental points contrary to the situation in KCl , where agreement was found up to $700^\circ K$ by Willis⁽⁷⁾, with the experimental data of James and Brindley⁽⁸⁾.

Fig. 2 shows the temperature variation of Θ_A calculated⁽⁹⁾ from the experimental B-values.

Some of the significant parameters	pres
measurement at $25^\circ C$ and $800^\circ C$ (taken from	1

$a = 5.640$ and 5.892 \AA ; $\alpha = 38.65$ and $74.0 \times 10^{-6}/^{\circ}\text{C}$; $B_{\text{Na}} = 1.59$ and 6.60 \AA^2 ; $B_{\text{Cl}} = 1.37$ and 6.15 \AA^2 ; $(\overline{u^2})_{\text{Na}}^{\frac{1}{2}} = 0.25$ and 0.50 \AA ; $(\overline{u^2})_{\text{Cl}}^{\frac{1}{2}} = 0.23$ and 0.48 \AA ; $(\overline{u^2})_{\text{Mean}}^{\frac{1}{2}}/r_{\text{Na-Cl}} = 0.083$ and 0.167 ; $\Theta_M = 286$ and 258°K .

We thank Prof. D.C. Hodgkin, F.R.S. and Prof. D.C. Phillips, F.R.S., for the experimental facilities given, and Prof. P.S. Narayan for discussions. We thank Prof. R.S. Krishnan for his kind interest.

REFERENCES:

1. M.A. Viswamitra and K. Jayalakshmi; J. Sci. Instr. 3, 656 (1970).
2. M.J. Cooper and K.D. Rouse; Acta Cryst. A24, 405 (1968).
3. D.T. Cromer and J.T. Waber; Acta Cryst. 18, 104 (1965).
4. J.A. Morrison, D. Patterson and J.S. Dugdale; Canad. J. Chem. 33, 375 (1955).
5. C. Zener and S. Bilinsky; Phys. Rev. 50, 101 (1936).
6. W.J.L. Buyers and T. Smith; J. Phys. Chem. Solids 29, 1051 (1968).
7. B.T.M. Willis; Acta Cryst. A25, 277 (1969).
8. R.W. James and G.W. Brindley; Proc. Roy. Soc. A121, 155 (1928).
9. R.W. James; Optical Principles of the Diffraction of X-rays, London: Bell (1948).
10. R.W. James; Phil. Mag. 49, 585 (1925).
11. A.M. Karo and J.R. Hardy; Phys. Rev. 129, 2024 (1963).

DISCUSSION

M.P. Verma

Comparison of Debye temperatures upto the melting point should involve theoretical frequency distribution

function at high temperatures which can be done as a parallel calculation in a study of equation of state of substances. It will be good if such a comparison is brought about. I am afraid any comparison based on low temperature estimates of Θ_D may be very wrong because anharmonic corrections will be serious at high temperatures. One can probably refer to the work of G.C. Fletcher on NaCl; the probable references are Austr. J. Phys. 1958, '59 & '63. In the last paper he considers both the 3rd and 4th order terms in the potential energy expansion.

M.A. Vishwanitra

We have not compared the present Θ_M values with any other Θ values upto the melting point. We would like to do this if, as you suggest, other Θ values are available from Fletchers' work. As far as higher order anharmonic-term contributions are concerned, the present Θ_M values do show that they are important particularly beyond 900°K in NaCl, because of the steeper fall of experimental points in the region 900°K to fusion.

DEBYE-WALLER FACTOR OF SODIUM

S. Krishna Kumar, V. Valvoda* and M.A. Viewamitra
 Department of Physics, Indian Institute of Science, Bangalore-12.

Recently the temperature dependence of Debye-Waller factors of Na and several other metals has been investigated theoretically using the Krebs' model, by Singh and Sharma⁽¹⁾. The only experimental X-ray determination of Debye-Waller factor of Na has been the early work of Dawton⁽²⁾, who investigated the variation of X-ray intensities with temperature. We have now determined the Debye-Waller factor of Na at room temperature from accurate X-ray intensity data from 3 single crystals. Several single crystal samples about 1 cm in length and 0.3 to 1 mm in diameter were grown from melt in quartz and Lindemann capillaries. The bulk material was a Schering and Kahlbann product stored in the Department for several years. Sample 1, 10 mm x 0.9 mm, was prepared by cooling a molten wire sample (in a sealed quartz capillary from 120°C to room temperature over 1 hour in a paraffin oil bath, previously freed of moisture by exposure to freshly cut Na shavings. Samples 2 and 3 were grown directly from the bulk metal as follows: tiny pieces of Na were melted in paraffin oil, and small globules were pushed into Lindemann capillaries (≈ 0.3 mm dia). The capillaries containing Na globules, were then heated in a paraffin oil bath to 120°C, and cooled to room temperature in an oven over 5 hours, and then sealed. Single crystals prepared in both ways were found to be oriented along $[1\ 1\ 1]$ direction.

Preliminary X-ray photographs indicated that the crystals which were best suited for diffraction work, were those which were fast

* Present address: Charles University, Faculty of Mathematics and Physics, Department of Solid State Physics, Prague-2, Czechoslovakia.

cooled and not annealed slowly. Slowly cooled crystals invariably gave much lower intensities for low angle reflections than the calculated values, indicating that the thermal history and mode of preparation of the samples influenced the X-ray intensities considerably.

Bragg intensities of 12 independent reflections, from these 3 samples, were collected on multiple films, using $\text{CuK}\alpha$ radiation, in the equinclination Weissenberg setting. The integrated intensities were measured on a microdensitometer and the final intensity values used, were the averages of a large number of measurements as indicated in Table I. The intensity data were corrected for Lorentz-polarisation factor, spot shape, and absorption. Cromer and Waber⁽³⁾ form factors, f_{Na} , corrected for anomalous dispersion⁽⁴⁾ were used.

A starting value for the Debye-Waller B factor was obtained by a plot of $\log_e I/f_{\text{Na}}^2$ vs $\sin^2\theta/\lambda^2$ (Fig. 1), which clearly indicated the presence of extinction effects in the observed intensities. The B value was then refined by several structure factor least square cycles, initially omitting extinction-affected reflections. In the final cycles, however, secondary-extinction-corrected intensities, with g factors⁽⁵⁾ of 0.0022, 0.0048 and 0.0061 for samples 1, 2 and 3 respectively were used.

Table I gives the results of the present study. B_{TDS} refers to B value corrected for thermal diffuse scattering, by Lucas method⁽⁶⁾, the required elastic constants having been taken from Daniels⁽⁷⁾.

The authors thank Prof. R.S. Krishnan and Prof. P.S. Narayanan for their kind interest. The help given by the Metallurgy Department in using their microdensitometer is acknowledged.

TABLE I

Observed and calculated structure factor data (given for Sample 1 only).
E, Debye characteristic temperature Θ , and $\langle u^2 \rangle^{\frac{1}{2}}$ values are the
averages over the three samples.

h k l	No. of measure- ments.	P_o	P_c	Authors	B \AA^2	(H) $^\circ K$	$(u^2)^{\frac{1}{2}}$ \AA
2 0 0	4	11.10	11.17	Present	6.81 ± 0.08	147.5	0.51
1 1 2	26	8.51	8.56	Present (R_{TDS})	7.64 ± 0.08	140.1	0.54
2 0 2	18	6.40	6.35				
3 1 0	24	4.64	4.82	Dawton (Calcu- lated)	$6.87^{(2)}$		
2 2 2	2	3.91	3.59				
1 2 3	40	2.88	2.84	Others		149.9 ⁽⁸⁾	
4 0 0	4	2.73	2.20			150.0 ⁽⁹⁾	0.50 ⁽⁹⁾
3 0 3	6	1.72	1.73			131.0 ⁽¹⁰⁾	
4 1 1	12	1.61	1.70				
4 2 0	5	1.12	1.33				
3 3 2	4	0.93	1.04				
2 2 4	2	0.81	0.82				

R-factor: 2.55%; $B = 6.94 \text{ \AA}^2$
(E.S.D. = 0.08).
in B

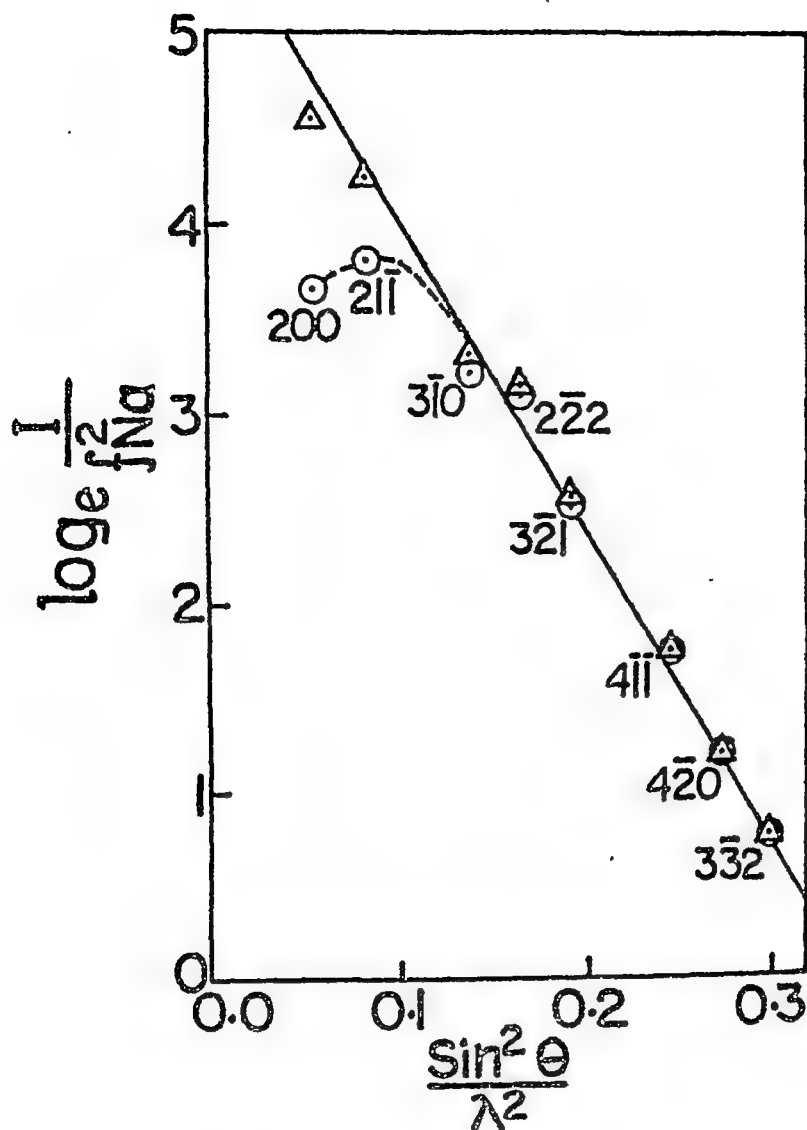


Fig. 1. Plot of $\log_e I / f_{Na}^2$ -vs- $\frac{\sin^2 \theta}{\lambda^2}$ for Na given for sample 1, I layer with rotation axis being $[111]$.

- \circ Intensities not corrected for extinction
- \triangle Intensities corrected for secondary extinction.

REFERENCES:

1. A.K. Singh and P.K. Sharma; *J. Phys. Soc. Japan* 26, 425 (1969).
2. R.H.V.M. Dawton; *Proc. Phys. Soc. (Lond)* 49, 294 (1937).
3. D.T. Cromer and J.T. Weber; *Acta Cryst.* 18, 104 (1965).
4. *International Tables for X-ray Crystallography*; Vol. III, p. 214, Birmingham: Kynoch Press (1962).
5. G.H. Stout and L.H. Jansen; *X-ray Structure Determination*, The Macmillan Company, New York (1968).
6. B.W. Lucas; *Acta Cryst.* A25, 627 (1969).
7. W.B. Daniels; *Phys. Rev.* 119, 1246 (1960).
8. D.L. Martin; *Phys. Rev.* 139, A150 (1965).
9. K. Lonsdale; *Acta Cryst.* 1, 142 (1948).
10. E. Tøners; *Arkiv f. Fysik* 11, 247 (1957).

-----oOo-----

THE X-RAY DEBYE WALLER FACTOR FOR THE MIXED SYSTEM $\text{KBr}_x.\text{Cl}_{1-x}$.

K.S. Chandrasekaran and S.K. Mohanlal
Department of Physics, Madurai University, Madurai-2

Optical phonons in mixed systems exhibit 'one mode' or 'two mode' behaviour, depending on several criteria which have been recently proposed and checked by their lattice spectra. In this work, the X-ray Debye Waller factor has been examined for one such mixed system, $\text{KBr}_x.\text{Cl}_{1-x}$.

The integrated intensities were measured by a Geiger counter spectrometer, fabricated for this purpose. For a check on the measurements, the end member crystals, KCl and KBr were used. For the scanning range and geometry employed the contribution of diffuse intensity was negligible. The measured Debye Waller factors for KCl and KBr were in good agreement with other recent work.

The same set up was then used for the mixed system, $\text{KBr}_x.\text{Cl}_{1-x}$, for which single crystals were prepared with different values of x from aqueous solutions. Lattice distortion contribution, enhancing the X-ray Debye Waller factor, reported for certain mixed systems, is found to be not appreciable in the present case. Attempts are in progress to fit the observed Debye Waller factors to a 'virtual crystal model'.

ADDITIVITY OF DEBYE CHARACTERISTIC TEMPERATURE OF ALLOYS

G. B. Litra and T. Chattopadhyay
Department of Physics, Indian Institute of Technology,
Kharagpur-2

I. INTRODUCTION

From the stand point of the experimentalist it would be highly desirable to obtain an expression for the Debye characteristic temperature of an alloy in terms of the Debye characteristic temperatures of the component metals. So far, such expressions have been limited to the one derived from the Neumann-Kopp⁽¹⁾ relation and the other being due to Simarska⁽²⁾. The former model effectively assumes the alloy to be built of independent blocks of the mother materials while the latter assumes the vibrations of the atoms of the two types to be independent of one another. So far, there has been no such relationship on the basis of lattice dynamics of the alloy as a whole.

This paper aims at presenting such an expression and to compare this theory with the two previous theories in the light of experimental data for Copper-Nickel and Copper-Aluminium binary alloys.

II. THEORETICAL

The Debye Characteristic Temperature Θ of a crystal is given by

$$\Theta = C \frac{k^{\frac{1}{2}}}{M^{\frac{1}{2}} \rho^{\frac{1}{6}} v_L^{\frac{2}{3}}(\sigma)} \quad (1)$$

where $C = \frac{h}{k} \left(\frac{10/4\pi}{} \right)^{\frac{1}{3}}$ for $\Theta = \Theta_{\text{Debye}}$ and $\frac{h\sqrt{5}}{k}$ for $\Theta = \Theta_M$ where the symbols are as given by James

Now,
$$K = \frac{C_{11} + 2C_{12}}{3} \quad (2)$$

According to the De Launay⁽⁴⁾ model of lattice vibrations

$$\begin{aligned} \alpha C_{44} &= \alpha_1 + 3\beta \\ \alpha(C_{11} - C_{44}) &= \alpha_1 + 4\alpha_2 - \beta \\ \alpha(C_{12} + C_{44}) &= 2(\alpha_1 - \beta) \end{aligned} \quad (3)$$

where α is the lattice constant and $\alpha_1, \alpha_2, \beta$ different force constants. Niu and Shimizu⁽⁵⁾ have recently given expressions for force constants of an alloy $AB(pq)$ composed of two metals A and B in the atomic proportions p and q respectively which are

$$\begin{aligned} \alpha_1^{AB(pq)} &= (\alpha_1^{AA} + \alpha_1^{BB} - 2\alpha_1^{AB}) p^2 + 2(\alpha_1^{AA} - \alpha_1^{BB}) p + \alpha_1^{BB} \\ \alpha_2^{AB(pq)} &= (\alpha_2^{AA} + \alpha_2^{BB} - 2\alpha_2^{AB}) p^2 + 2(\alpha_2^{AA} - \alpha_2^{BB}) p + \alpha_2^{BB} \\ \beta^{AB(pq)} &= (\beta^{AA} + \beta^{BB} - 2\beta^{AB}) p^2 + 2(\beta^{AA} - \beta^{BB}) p + \beta^{BB} \end{aligned} \quad (4)$$

Assuming σ to be same for the alloy as for its component metals and the Cauchy relationship to be approximately valid, we have, combining equations (1), (2), (3) and (4) -

$$\begin{aligned} (H)_{AB(pq)}^2 &= \left[\frac{M_{AA}}{M_{AB(pq)}} (H)_{AA}^2 + \frac{M_{BB}}{M_{AB(pq)}} (H)_{BB}^2 - \frac{2M_f}{M_{AB(pq)}} (H)_f^2 \right] p^2 \\ &+ 2 \left(\frac{M_f}{M_{AB(pq)}} (H)_f^2 - \frac{N_{BA}}{M_{AB(pq)}} (H)_{BB}^2 \right) p + \frac{M_{BB}}{M_{AB(pq)}} (H)_{BB}^2 \end{aligned} \quad (5)$$

III. EXPERIMENTAL

Using X-ray powder diffraction technique as described by Litra and Chattopadhyay⁽⁶⁾, the Debye characteristic temperatures of specpure Aluminium, Copper, Nickel and some of their alloys have been measured and

shown in Table I.

Table I

Material	Experimental	from Neumann- Kopp Model	from Simerka model	from eqn. (5)
Al	400	-	-	-
Cu	303	-	-	-
Ni	381	-	-	-
80% Ni in Cu	353	364	362	354
60% Ni in Cu	334	349	345	333
40% Ni in Cu	325	334	330	322
.08% Cu in Al	368	399	399	399
5.87% Al in Cu	324	-	-	-

IV. RESULTS AND DISCUSSIONS

Table I also shows the results of calculation of the Debye Characteristic Temperatures of the alloys in terms of the experimentally determined values of the parent metals on the basis of equation (5) as well as the Neumann-Kopp⁽¹⁾ and Simerka⁽²⁾ models. It is obvious that the Neumann-Kopp rule gives the poorest agreement and that the present model the best. The discrepancies between the theoretically calculated and experimentally observed values may largely be attributed to the anharmonicity of lattice vibrations which has not been taken care of in the De launsey model. Weiss⁽⁷⁾ has shown that anharmonicity results in a considerable dependance on temperature of the Debye temperature factor. That such temperature

dependence exists has been shown by Mitra⁽⁸⁾.

REFERENCES

1. Mentioned in (2).
2. Simerska, M. - Czech. J. Phys. B. 13, 737 (1963).
3. James, R. W. - The Optical principles of the Diffraction of X-rays. Bell. London, p.223 (1950).
4. De Launay, C. - Solid State Physics Vol. 2
Scitz F. Turnbull, D. Academic Press Inc. Publishers,
New York (1956).
5. Niu, H and Shimizu, M. - J. Phys. Soc. Jap. 22,
437 (1967).
6. Mitra, G. B. and Chattopadhyay, T. - Proc. National
Science Academy 36A, 77 (1970).
7. Weiss, R. J. - X-ray Determination of Electron
Distributions, North Holland, Publishing Co.
Amsterdam p.56 (1966).
8. Mitra, G. B. - Proc. Nuclear Physics and Solid State
Physics, Symposium, Bombay, Dec. 28-31, 1968).

TRACE VARIABLE FORCES IN ALKALIHALIDES

T.M. Harijagan and R. Revathy Raju
Physics Department, Madurai University, Madurai-2.

I. INTRODUCTION

The purpose of this paper is to make an investigation on the trace variable forces in nine alkali halides on the basis of the Brout sum rule as modified by Rosenstock and his co-workers(1). A unified analysis is now possible for alkali halides because of the availability of adequate and fairly accurate experimental data on the phonon dispersion.

II. THE SUMRULE AND TRACE VARIABLE FORCES

The deviation from constancy of the trace of the dynamical matrix, for the different phonon wavevectors arise from the existence of interactions of 'non electromagnetic' type between any two atoms or from interactions due to overlap of different sets of "like" neighbours. These forces are called the trace variable forces. In crystals the trace variable force is almost from the second category. In order to account for the existence of trace variable forces, Rosenstock modified the Brout sum rule as

$$\sum_{\lambda=1}^{3n} \omega_{\lambda}^2(q) = \sum_{\lambda=1}^{3n} \omega_{\lambda}^2(0) + \sum_m \psi^{(m)}(q) P_m \quad (1)$$

where $\omega_{\lambda}(q)$ is the frequency of the phonon belonging to the λ th branch and wavevector q . $\omega_{\lambda}(0)$ is the phonon frequency of λ th branch for zero wavevector. $\psi^{(m)}(q)$ is contribution to the trace from the m th trace variable force, which is the overlap interaction of the m th set of

"like" neighbours. P_m is a constant which is a measure of the strength of the overlap interaction from the m^{th} "like" neighbours and n is the number of atoms in the unitcell. Knowing $\omega_i(q)$ for all the $3n$ branches and $\psi_m^{(\eta)}(q)$ one gets information on the P_m .

III. APPLICATION TO THE ALKALIHALIDES

The unit cell of dimension $2r_0$ consists of one alkali atom and one halogen. Each atom is surrounded by six atoms of the other kind at $(100)r_0$ and they constitute the first set of "unlike" neighbours. Each atom is surrounded by 12 atoms of the same kind at $(110)r_0$ and they belong to the first set of "like" neighbours and the overlap arising from them constitute the lion share to the trace variable force. The second set of "like" neighbours, 8 in number, situated at $(200)r_0$ and the third set consisting of 24 atoms and lying at $(210)r_0$ are also considered in our present analysis to obtain some semi quantitative information of their relative importance, in the overlap interactions.

From the geometry of the atomic positions the $\psi^{(m)}(q)$ for the three sets of "like" neighbours labelled as $m=1, 2$ and 3 can be written as follows.

$$\psi^{(1)}(q) = 3 - (\cos \pi q_1, \cos \pi q_2 + \cos \pi q_2 \cos \pi q_3 + \cos \pi q_3 \cos \pi q_1) \quad (2)$$

$$\psi^{(2)}(q) = 3 - (\cos^2 \pi q_1 + \cos^2 \pi q_2 + \cos^2 \pi q_3) \dots \dots \dots (3)$$

$$\psi^{(3)}(q) = 3 - (\cos 2\pi q_1, \cos \pi q_2 \cos \pi q_3 + \cos \pi q_1 \cos 2\pi q_2 \cos \pi q_3 + \cos \pi q_1 \cos \pi q_2 \cos 2\pi q_3) \dots \dots \dots (4)$$

Following Rosenstock we define

$$\sum(q) = \left[\sum_{\lambda=1}^{3n} \omega_{\lambda}^2(q) - \sum_{\lambda=1}^{3n} \omega_{\lambda}^2(0) \right] / \left[\sum_{\lambda=1}^{3n} \omega_{\lambda}^2(0) \right] \dots \dots \dots (5)$$

Then Eq(1) becomes

$$\Sigma(q) = [P_1 \psi^{(1)}(q) + P_2 \psi^{(2)}(q) + P_3 \psi^{(3)}(q)] / [\sum_{i=1}^3 \omega_i^2(q)] \quad (6)$$

One can compute $\Sigma(q)$ for various q values lying along (100) (110) and (111) directions from experimentally available phonon frequencies. The $\psi^{(i)}(q)$ are obtained from Eqs 2, 3 and 4. Thus one gets a system of equations in P_1, P_2 and P_3 , the number of equations being the number of phonon wave vectors for which all the phonon frequencies are known. Then from a least square analysis of these equations, best fit values of P_1, P_2 and P_3 can be found.

IV. RESULTS AND DISCUSSION

The $\Sigma(q)$ values were evaluated for the nine alkali halides from the experimental dispersion relations (2 to 10) and the P_1, P_2 and P_3 evaluated are given in the following table.

Table 1. Values of P_m in alkali halides

Alkali halides	(2) LiD	(3) LiF	(4) NaF	(5) NaCl	(6) NaBr	(7) NaI	(8) KCl	(9) KBr	(10) KI
P_m in units of $[\sum_{i=1}^3 \omega_i^2(q)]$									
P_1	.13	.04	.06	.02	0	0	0	0	0
P_2	.07	.04	.01	.04	.07	.03	0	0	0
P_3	-.05	.01	-.03	-.01	0	0	0	0	0

In LiD, P_1 is around twice P_2 and P_3 is very small as one expects. But in LiF, P_2 is comparable with P_1 and P_3 is still very small. One finds that as one goes from NaF to NaI, P_1 goes on falling whereas P_2 goes on increasing with

a fairly insignificant P_3 . The larger values of P_2 in them are contrary to one's expectations. Within the accuracy of the presently available data the trace variable forces are found to be virtually absent in potassium halides. One also does not find a simple homologous rule for the forces in the alkali halides as in the germanium type crystals. Analysis is in progress with the recent experimental data on RbF and RbCl(11).

We thank Prof.K.S. Chandrasekaran and colleagues for discussions.

REFERENCES

1. H.B. Rosenstock; Lattice Dynamics (Edited by R.F. Wallis) H.B. Rosenstock and G. Blaken; Phys. Rev.129,1959(1963); Phys. Rev.145,546(1966).
2. J.L. Verble, J.L. Warren and J.L. Yarnel; Phys. Rev.168, 980 (1968).
3. G. Bolling, H.G. Smith, R.N. Nicklaw, P.R. Vijaya Raghavan and M.K. Walkinson; Phys. Rev.168, 970 (1968).
4. W.J.L. Buyers; Phys. Rev.153,923 (1967).
5. G.Raunio, L. Almqvist and R. Stedman; Phys. Rev.178, 1496 (1969).
6. J.S. Reid, T. Smith and W.J.L. Buyers; Phys. Rev.1, 1833 (1970).
7. A.D.B. Woods, B.N. Brockhouse and W.Cochran; Phys.Rev.119, 980 (1960).
8. J.R.D. Copley, R.W. Macpherson and T. Timusk; Phys.Rev.182, 965 (1969).
G. Raunio and L. Almqvist; Phys.Stat.Solidi,33,209(1969)
9. R.A. Cowley, A.D.B. Woods, B.N. Brockhouse and W.Cochran Phys.Rev.131, 1030 (1963).
10. G. Dolling, R.A. Cowley, C. Schittenhelm and I.M.Thorson Phys.Rev.147,577 (1966).
11. G. Raunio and S. Rolandson; J.Phys.C(Solid state Phys.). 3, 1013 (1970).

DISCUSSION

M.P. Verma

Trace variable forces in (q, c, c) and (q, q, q) differ very much in magnitudes and sign also. It seems the difference in the scheme presented by the authors appears to be small as they take it as a percentage.

$\sum D_{\alpha\alpha}(\frac{q}{k}) - \sum \omega_j^2(q)$ shows a definite difference otherwise.

P.S. Narayanan

1) May I ask as to what will be the form of the sum rule for the trace variable forces in more complicated crystals where the $\omega_j(0)$'s may belong to different irreducible representations.

2) Can this method be combined with the product rule of Cochran for ferroelectrics in order to guess the nature and influence of overlap forces on ferroelectric behaviour.

T.M. Haridasan

For all crystals, irrespective of the number of atoms and irreducible representation, the sum rule remains the same since it is the trace of the dynamical matrix which one analyses for the trace variability. So when all the phonon frequencies are available at the same time for different wave vectors, this analysis can be applied.

MANY BODY INTERACTION IN BREATHING SHELL MODEL:

A. N. Basu, Jadavpur University, Calcutta-32

and

Dhir-njrn Roy, Indian Association for the Cultivation of Science, Calcutta-32.

INTRODUCTION :- Recently various models have been proposed to explain the lattice dynamics of ionic crystals. Of these the breathing shell model^(1,2) of Schroder, which is an improvement of the shell model⁽³⁾ and takes account of the breakdown of the Cauchy relation, is now widely used. The purpose of the present paper is to critically analyse the breathing motion. It is found that the breathing effectively introduces three and four-body interactions in the crystal. Expressions for elastic constants including the breathing motion of the ions interpreted as a change in the ionic radii are derived from the homogeneous deformation theory.

THEORY :- To account for the breathing motion we assume that ionic shell radii undergo change during lattice vibrations. Then the energy density of the crystal will be given by

$$\Phi = \frac{1}{2V_0} \left[\sum_{kk'} \phi(r_{kk'}) + \sum_k y_k (d_k - d_k^0)^2 \right] + U_{\text{Coulomb}} \dots (1)$$

where V_0 is the volume per unit cell and the overlap energy ϕ is taken in the usual form

$$\phi(r_{kk'}) = b\beta_{kk'} \exp \left\{ (d_k + d_{k'} - r)/\rho \right\} \dots (2)$$

(d_k = radius of the k th ion). In the second term ν_k is the spring constant which controls the breathing motion, d_k^0 is the free ion radius. We shall confine overlap energy to nearest neighbours only. Let us now consider a homogeneous deformation such that the (i, k) ion is displaced by $u(k)$ from the equilibrium position and the radius of the k -th ion changes by ξ_k from its equilibrium value in the crystal. We can now expand $\bar{\Phi}$ in powers of $u(k)$ and ξ_k . The linear terms will vanish and that part of the quadratic terms which depends on breathing is given by

$$\Delta \bar{\Phi}^B = \frac{1}{2} \nu_0 \left[-\frac{1}{2} \sum_i D \phi'(r_i) (\bar{u}_1^2 \bar{r}_1) (\xi_1 + \xi_2) + \frac{1}{2} \sum_i \phi''(r_i) (\xi_1 + \xi_2)^2 + \nu_1 \xi_1^2 + \nu_2 \xi_2^2 \right] \dots (3)$$

where $\phi(r_i) = \frac{d\phi(r)}{dr}$, $\bar{r} = \frac{1}{N} \sum_i r_i$, $r = r(\frac{1}{2} \bar{r}_k)$ and \bar{r} is the Lagrangian strain tensor and summations have the same significance as in (1). For arbitrary homogeneous deformation, values of ξ_k can be found from the condition

$\frac{\partial}{\partial \xi_k} (\Delta \bar{\Phi}^B) = 0$. These equations can be used to eliminate ξ_k in (3). After elimination the expression becomes

$$\Delta \bar{\Phi}^B = -\frac{1}{4\nu_0} A(\nu_1, \nu_2) \sum_{k_1, k_2} \sum_{k'_1, k'_2} (D_1 \phi'_1)(D_2 \phi'_2) (\bar{r}_1, \bar{r}_1) (\bar{r}_2, \bar{r}_2) \dots (4)$$

where

$$\bar{r}_1 = r(\frac{1}{2} \bar{r}_{k_1}) ; \bar{r}_2 = r(\frac{1}{2} \bar{r}_{k_2}) ; A(\nu_1, \nu_2) = \frac{\nu_1 + \nu_2}{(\sum 2\phi''(r_i)(\nu_1 + \nu_2) + 2\nu_1\nu_2)} \dots (5)$$

The contribution of breathing to the elastic constants are given by

$$C_{\alpha\beta\gamma\delta}^{(B)} = -\frac{1}{2\nu_0} A(\nu_1, \nu_2) \sum_i \sum_j (\bar{r}_i \phi'_i) (\bar{r}_j \phi'_j) (\bar{r}_1)_\alpha (\bar{r}_1)_\beta (\bar{r}_2)_\gamma (\bar{r}_2)_\delta \dots (6)$$

For NaCl structure, the specific contributions are

$$C_{11}^{(B)} = C_{12}^{(B)} = -\frac{2\phi''(r_0)^2(\nu_1 + \nu_2)}{r_0 \{ 5\phi''(r_0)(\nu_1 + \nu_2) + \nu_1\nu_2 \}} ; C_{44}^{(B)} = 0 \dots (7)$$

These expressions agree with those obtained from the long wave theory of the breathing shell model.

Many body interactions:

We rewrite the energy density (4) in two parts. Terms for which $k=k'$ are separated from terms for which $k \neq k'$.

Using displacements $u(l, k)$ we write

$$\Delta \Phi^B = -\frac{1}{4V_0} A(l_1, l_2) \left[\sum_{k \neq k'} \sum_{l_1, l_2} \frac{\partial \Phi_1}{\partial u_{k_1}(l_1, k)} \frac{\partial \Phi_2}{\partial u_{k_2}(l_2, k)} u_{k_1}(l_1, k) u_{k_2}(l_2, k) \right. \\ \left. + \sum_{k \neq k'} \sum_{l_1, l_2} \frac{\partial \Phi_1}{\partial u_{k_1}(l_1, k)} \frac{\partial \Phi_2}{\partial u_{k_2}(l_2, k)} u_{k_1}(l_1, k) u_{k_2}(l_2, k) \right] \quad (7)$$

where

$$\Phi_1 = \Phi(l_1, k_1), \quad \Phi_2 = \Phi(l_2, k_2), \quad \Phi_3 = \Phi(l_3, k_3), \quad k \neq k'.$$

In obtaining equation (8) we have used the result that every ion position is a centre of symmetry. The first term in (8) shows that the contribution to energy due to displacements of (l_1, k_1) and (l_2, k_2) particles depends on the third particle (l_3, k_3) . Hence it indicates the presence of an effectively three body interaction. Similarly the second term indicates the presence of an effectively ^{four} ~~from~~ body interaction. It should, however, be noted that two body interaction terms are also present which are obtained if we put $(l_1, k_1) = (l_2, k_2)$ in the first summation. Similarly in the second summation if we put $(l_1, k_1) = (l_2, k_2)$ we get terms which are again due to three body interactions. Thus we conclude that the introduction of breathing motion implies the introduction of additional two body, three body and four body interaction between the ions.

In the deformable shell model introduced by Basu and Sengupta⁴, a three body interaction resulting from the deformability of the ion shell has been discussed. Sarker

and Sengupta⁵ was able to represent this interaction in an analytic form. Comparison of their expression for many body energy density of the crystal with equation (4) shows that the three body interaction in breathing shell model is not exactly the same as in the deformable shell model. Whether expressions for a static, three and four body interactions can be given which are effectively the same as those implied in the breathing shell model is being investigated.

ACKNOWLEDGEMENT :- The authors express their sincerest thanks to Prof. S. Sengupta for his guidance during the course of the work.

References :-

1. U. Schroder, Solid State Commun. 4, 347 (1966)
2. V. Nusslein and U. Schroder, Phys. Stat Sol. 21, 309 (1967)
3. A.D.B.Woods, W. Cochran and B.N.Brockhouse,
Phys. Rev. 119, 980 (1960)
4. A. N. Basu and S. Sengupta, Phys. Stat. Sol.
29, 367 (1968)
5. A. K. Sarker and S. Sengupta, Solid, State Commun.
7, 135 (1969)

DISCUSSION

R. Srinivasan

1) The elastic constants calculated in the harmonic approximation should be properly compared by extrapolation of the linear part of the plot of c_{ij} vs T to absolute zero. In the alkali halides the magnitude of the Cauchy discrepancy may be considerably changed by this process.

2) We have computed the photoelastic constants of several alkali halides on the shell model. It is well known that the anisotropies of the Lorentz and Coulomb forces yield too high values for the photoelastic constants, and changes in short range polarisability are important. In our calculations these changes are taken into account by including the anharmonicity of the short range interaction. While this reduces the discrepancy between calculated and observed values there is still some disagreement indicating a further contribution arising from the deformation of the shell. The use of the breathing shell model may perhaps improve the agreement.

3) One knows that a transfer of charge from the cation to the anion during lattice vibrations gives rise to a second order dipole moment which plays a role in determining the intensity of second order infrared absorption. Neither the shell model or the breathing shell model appear to provide for the appearance of a second order dipole moment. One could perhaps consider a shell

model in which the charges on the shell depend on the distance between adjacent ions and vary during lattice vibrations such a model also will give rise to three and four body forces and will resolve the Cauchy discrepancy.

M.P. Verma

Regarding the comment of Prof. Singh that minimisation of the breathing energy independently is not quite valid I have to say that the breathing has been introduced in the shell model as an independent normal coordinate and as there is no intermixing of the coordinates in the energy expression for the translational and breathing motions the two energies will automatically satisfy the minimisation requirement independently. This is also obvious from my calculations on internal pressure (paper S49).

INTERNAL PRESSURE IN ALKALI HALIDES AND A JUSTIFICATION FOR THE BREATHING SHELL MODEL.

K.P. Varna

Department of Physics, Agra College, Agra-2.

I INTRODUCTION

In a study of pressure dependence of compressibilities of various solids Borelius ⁽¹⁾ has observed that for relatively low pressures the experimental data can be represented sufficiently well by the equation

$$\frac{\delta v}{pv_0} \cdot \alpha + \frac{\delta v}{v_0} = -\frac{\beta}{\alpha} \quad (1)$$

where v_0 and v are the volumes at zero pressure and at p , δv is the compression $v - v_0$ and α, β are two parameters. The parameter α obviously behaves like a pressure which tends to expand the solid and has been named the internal pressure. The present study shows that the internal pressure in ionic crystals can be caused by the fluctuations in the energies of the clouds loosely bound to the cores.

In the conventional shell model of ionic solids each ion is assumed to be divided in two parts: the core consisting of the nucleus and the tightly bound electrons and the shell consisting of the loosely bound electrons. Both the core and the shell have been introduced as rigid entities and the only freedom permitted is a relative displacement. While the core could well be approximated by a rigid sphere the assumption that the loosely bound electrons form a rigid structure seems to be a very crude approximation of their behaviour and if possible must be replaced by a more realistic one. Taking a hint from the experimental electron density maps we can assume the shell to consist of a uniform distribution of a fluid electron cloud bounded on the inside by the rigid core and on the outside by a thin film over which the density of the cloud continu-

ously falls from the constant value inside to zero at the ion surface. Such a structure is characteristic of every fluid surface and is responsible for the existence of a tension in the surface film. The electron cloud film assumed here will have a negative value for this tension because of mutual repulsion between the elemental portions and will tend to get a maximum area for the surface. The stabilization is provided by the attractive field of the core which binds the film together.

The coulomb energy of the shell in the field of its core can approximately be expressed as a function of the ion radius and in all treatments in which the ion is not considered as rigid we must include this shell energy in the expression of the crystal potential. In particular the equilibrium of the crystal lattice will be achieved by a simultaneous minimization of the interatomic potential and the shell potential. This is necessary because if the shells are supposed to retain their spherical symmetry any fluctuations in the energies of the shells will not affect the interatomic potential significantly.

The expression of these ideas in mathematical form on classical lines directly leads to an equation identical in form with equation (1) with values of the parameters α and β surprisingly near to the values empirically obtained by Borrelus.

II MATHEMATICAL FORMULATION

Let the core be a sphere of radius b and charge Xe and the shell a uniform cloud of total charge Ye distributed over $b < r < a$. The ion radius is a and the ion charge $Ze = (X+Y)e$. We can now consider every element of the shell cloud to be revolving round the nucleus in a circular orbit and obtain the total energy of the cloud under a uniform pressure P in the form

$$\frac{3XY(\bar{a}^2 - \bar{b}^2)}{4(\bar{a}^3 - \bar{b}^3)} + \frac{3Y^2}{2(\bar{a} - \bar{b})} \left\{ \frac{\bar{a}^2 - \bar{b}^2}{5} - \frac{\bar{b}^3(\bar{a}^2 - \bar{b}^2)}{2} \right\} + \frac{4\pi}{3} P(\bar{a}^3 - \bar{b}^3). \quad (2)$$

If we note that the shells must contain more than a few electrons we shall find from the experimental electron density maps that $b \ll a$. We can therefore use the simplifying assumption $b^2 \ll a^2$. To the expression (2) we must add the surface energy $4\pi\bar{a}^2 S$ of the film and if p is the external pressure P must be equal to $p + \frac{2S}{a}$. In a crystal like NaCl the shell energy per unit cell can therefore be expressed as

$$\psi_s = \sum_{\kappa} \frac{3Y_{\kappa}}{4a_{\kappa}} \left(Z_{\kappa} - \frac{3Y_{\kappa}}{5} \right) + \frac{20\pi}{3} a_{\kappa}^2 S_{\kappa} + \frac{4\pi}{3} p a_{\kappa}^3. \quad (3)$$

where $\kappa = 1$ and 2 for Na^+ and Cl^- respectively. In the equilibrium configuration this energy will be minimised independently of the intratomic potential with the restriction $a_1 + a_2 = r = \text{constant}$ leading to

$$\frac{3Y_{\kappa}}{4a_{\kappa}} \left(Z_{\kappa} - \frac{3Y_{\kappa}}{5} \right) + \frac{40\pi}{3} a_{\kappa} S_{\kappa} + 4\pi p a_{\kappa}^2 = k(r); \quad \kappa = 1, 2. \quad (4)$$

The total crystal potential is obtained by adding to ψ_s the intratomic potential ϕ and the applied pressure p can be expressed as

$$p = - \frac{\partial \phi}{\partial v} + \frac{k(r)}{6r^2} + \frac{4\pi}{3} (a_1^3 + a_2^3) \frac{\partial k}{\partial v}. \quad (5)$$

If we increase the pressure from zero to a small value p we shall be able to write $\frac{\partial k}{\partial v} = \frac{k}{\delta v}$ where δv is the corresponding compression.

We can now put equation (5) after a little simplification as

$$\frac{\left(\frac{\delta v}{\partial v} \right) \left[- \frac{\partial \phi}{\partial v} + \frac{1}{12r^2} \sum_{\kappa} \left\{ - \frac{3Y_{\kappa}}{4a_{\kappa}^2} \left(Z_{\kappa} - \frac{3Y_{\kappa}}{5} \right) + \frac{20\pi}{3} a_{\kappa} S_{\kappa} \right\} \right]}{\left\{ (\pi/3 r^2) (a_1^2 + a_2^2) + 1 \right\}} + \frac{k}{v_e} = - \frac{4\pi}{3v_e} \frac{(a_1^3 + a_2^3)}{\left\{ (\pi/3 r^2) (a_1^2 + a_2^2) + 1 \right\}}. \quad (6)$$

which is identical in form with equation (1) having

$$\frac{\beta}{v_e} = \frac{4\pi}{3v_e} \frac{(a_1^3 + a_2^3)}{\left\{ (\pi/3 r^2) (a_1^2 + a_2^2) + 1 \right\}}. \quad (7)$$

In fitting the experimental data Borelius observes that β/v_e is equal to .35 for the alkali halides with the NaCl structure he has studied. It is therefore encouraging to find that equation (7) gives

for β/v_0 values ranging from .34 to .44 for the ratio of ionic radii a_2/a_1 going from 1 to 2. The values for lithium halides with large a_2/a_1 range between .41 and .57 so that a similar study on these salts might check on the validity of the theory presented in this paper.

III DISCUSSION

The approximate theory given above agrees with the empirical equation of Borélius surprisingly well and expresses the internal pressure in terms of quantities which could be connected to electrical properties of the ions. A study of such connections is currently in hand. The theory can also find application in studies relating the compressibility and its derivative. Further the fulfilment of equation (4) for every ion separation demands that the shells breathe when thermal waves propagate through the solid and provides a justification for the breathing shell model of Schroder.⁽²⁾

IV REFERENCES

1. G. Borélius, Ark. Fys. 29 499 (1965)
2. V. Schroder, Solid. Stat. Commun. 4 347 (1966)

DISCUSSION

M.P. Verma

Regarding comment of Prof. R.P. Singh about the consideration of a surface structure in the ions I can only say that the electron density maps directly indicate that it is so. The density variation is very much like in a liquid surface and wherever there is a continuous fall in density over a small distance a parallel tension must arise (as, for example, explained in the text book

on Properties of Matter by Noakes). However it is true that the electrons mainly interact with long range forces and hence the situation has to be analysed more critically.



EFFECT OF ELECTRON DENSITY DISTRIBUTION ON THE DYNAMICAL BEHAVIOUR OF ALKALI HALIDE CRYSTALS

M.P. Verma
Department of Physics, Agra College, Agra-2.

and

R.K. Singh
Department of Physics, Banaras Hindu University, Varanasi-5.

I INTRODUCTION

(1) (2)
Verma and Singh (see also Singh and Verma) have developed a lattice dynamical model of ionic crystals which takes account of three-body overlap forces in almost an exact way. This has been achieved by evaluating the lattice sums in the expression of such forces given by Lindqvist (3) and by injecting the force constants thus obtained into the shell model of Woods et al (4). An application of this model to the potassium and sodium halides (Singh and Verma (2,5,6)) has shown that this 8-parameter theory presents excellent agreements with experimental dispersion curves. The model finds a strong support in the derivation of the shell model from fundamental considerations as given by Sinha (7). When parametrised, Sinha's equations go over into ours with only minor differences. We can, therefore, claim that our model, although developed on intuitive considerations, is a convenient representation of an essentially fundamental theory of lattice dynamics.

The importance of the inclusion of three body forces in our consideration becomes evident when we note that earlier modifications of the shell model like those given by Cowley et al (8) and Dolling et al (9) employing ten to fourteen parameters obtain the best agreements with experiments only when some of the parameters take values which can not be understood physically. It is possible that the unrealistic values of these parameters result from a replacement of an operative force like the three-body overlap by other interactions

the constraint imposed on these interactions by the application of the method of least squares, invariably employed to obtain the best fit between the theoretical and experimental dispersion curves.

While the model gives excellent results with the sodium and potassium halides its application to lithium salts does not give as good results. It is obvious that the lithium salts behave somewhat differently and if our model has to be applicable to them it must be so modified as to distinguish between the lithium salts and those of the heavier alkali metals. A modification that immediately suggests itself is the inclusion of anharmonic terms in the crystal potential. Since, however, our model refers to the atomic configuration at 0°K and the experimental dispersion curves available for comparison have also mostly been obtained at low temperatures the effect of anharmonicity of vibrations may not be really significant. We can see in this connection that even though the zero point energy in LiF is the largest in the alkali halide family it constitutes only 1.7 per cent of the total crystal energy.

A modification of our model in another direction is suggested by the study of the electron density maps in the family of crystals under consideration. A good discussion of such maps has been recently given by Brill⁽¹⁰⁾ who observes that while in the halides of heavier alkali metals the charge transfer ranges between .98e and 1.02e in LiF the charge transfer is only about .88 electrons. The spherical symmetry of the charge density distribution, characteristic of the alkali halide crystals, is found in this case also to the same approximation suggesting that the lithium halides are purely ionic with a modified valence Z viz. $Z = .88e$. This is an important observation indicating a significant difference between lithium halides and the later members of the family and may well be the distinguishing feature we are looking for. It is obviously pertinent to use in a

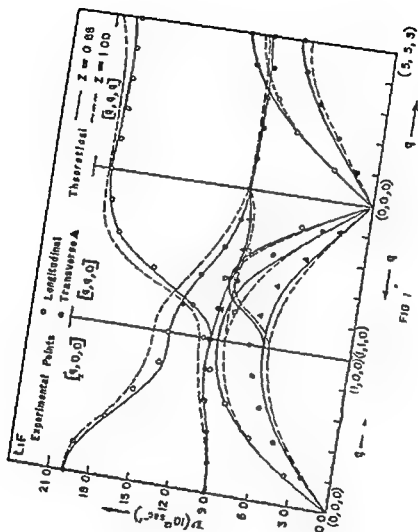
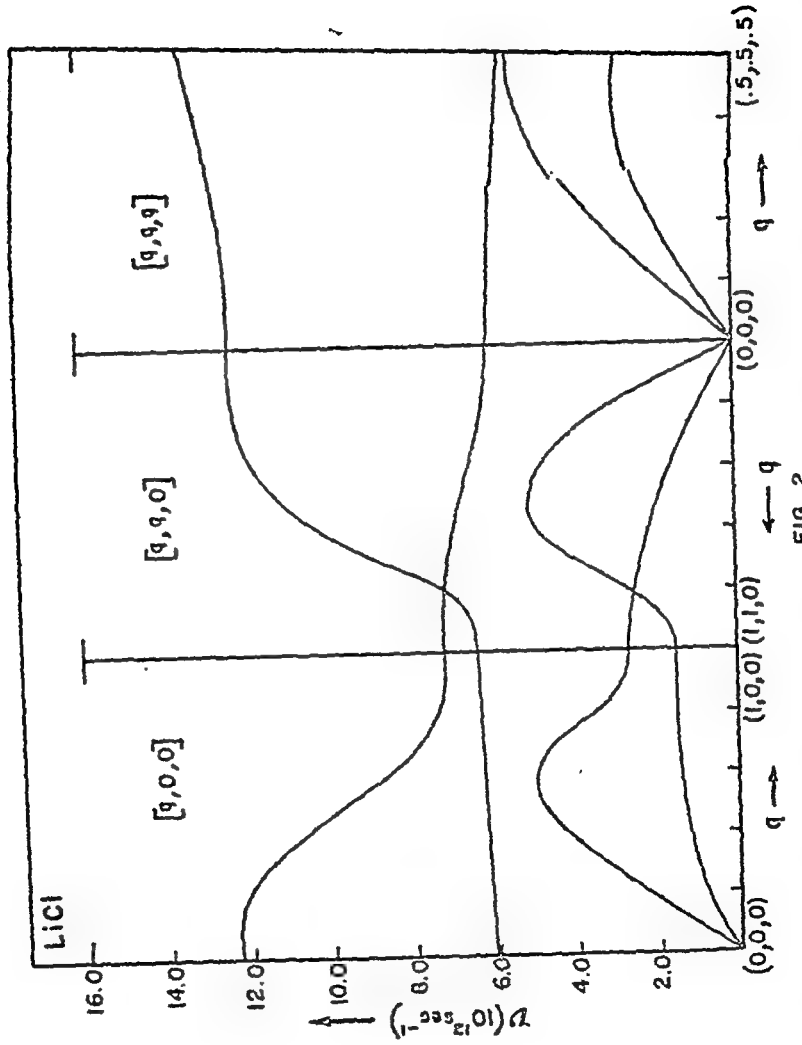


FIG 1



study of lithium salts a value .88e for the valence Z rather than the value e .

We are presenting here the results of a lattice dynamical study of LiF and LiCl based on the model described in references 1 and 2 both for $Z = e$ and $Z = .88e$. The dispersion curves thus obtained show a significant improvement for $Z = .88e$. The next section describes the main results and conclusions.

II RESULTS AND CONCLUSIONS

The input data for calculating the parameters of the theory are listed in table I. The accompanying numbers in parentheses refer to the original references.

Table I Input data

Substance	LiF	LiCl	Scale
Property			
C_{11}	12.460(11)	6.074(14)	} $10^{11} \frac{\text{dyn}}{\text{cm}^2}$
C_{12}	4.240(11)	2.270(14)	
C_{44}	6.490(11)	2.692(14)	
L	19.700(9)	12.857(14)	} 10^{12}Sec^{-1}
T	9.150(9)	6.112(14)	
1	0.029(12)	0.029(12)	} 10^{-24}cm^3
2	0.880(12)	2.947(12)	
a	2.000(13)	2.554(13)	10^{-8}cm

The parameters of the theory were calculated by using these values, both for $Z = .88e$ and $Z = e$, which were then used to compute the dispersion curves in the symmetry directions. These curves are shown in Figs. 1 and 2. The curves show that $Z = .88e$ is a more appropriate choice for the system considered here.

This ionic charge $Z = .88e$ is not an effective result.

can probably get good agreement with these data by suitably choosing the model with $Z = .88e$ also. In our model the values of the parameters are used from the experimental dielectric constants together with other constants. As regards cohesive energy we have not checked but it should not be very different. Further I do not know if the calculations you are referring to are from fundamental principles.

A SHELL MODEL FOR IONIC MOLECULES

A. K. Sarkar, Physics Department, Krishnagar College,
W. Bengal, & S. Sengupta, Maulana Azad College, Calcutta

I. INTRODUCTION

Several semiclassical models have recently been used to calculate the properties of ionic molecules. Rittner⁽¹⁾ and Varshni⁽²⁾ used classical expression for energy of interaction between ions having electrical polarisabilities and added an overlap interaction between the ions. Toshi and Doyama⁽³⁾ in addition to the above assumed the negative ions to be polarisable by the overlap interaction (deformation dipole model). In the present paper we have obtained equations corresponding to a shell model for the ions. The equations are compared with those of other models and the quantum mechanical interpretation of different terms is discussed.

II. SHELL MODEL EQUATIONS

The given picture is a diagrammatic representation of an ionic molecule in the shell model. Here $Z_{1c}e$, $-Z_{1s}e$, $Z_{2c}e$ and $-Z_{2s}e$ are the electrical charges of positive ion core, positive ion shell, negative ion core and negative ion shell respectively. For alkali halide type molecules,

$$Z_{1c} - Z_{1s} = 1 \quad \text{and} \quad Z_{2c} - Z_{2s} = -1$$

Equilibrium condition gives for

$$\text{positive ion core : } -\frac{Z_{1c} Z_{2c} e^2}{r^2} + \frac{Z_{1c} Z_{2s} e^2}{(r-d_1)^2} - k_1 d_1 = 0 \quad \dots (1)$$

$$\text{negative ion core : } \frac{Z_{1c} Z_{2c} e^2}{r^2} - \frac{Z_{1c} Z_{2s} e^2}{(r+d_1)^2} - k_2 d_1 = 0 \quad \dots (2)$$

$$\text{positive ion shell : } -\frac{Z_{1s} Z_{2s} e^2}{(r+d_1-d_2)^2} + \frac{Z_{1s} Z_{2c} e^2}{(r+d_1)^2} + k_1 d_1 + \phi'(r+d_1-d_2) = 0 \quad (3)$$

Three

negative ion shell: $\frac{z_{1s} z_{1s} e^2}{(r+d_1-d_2)^2} - \frac{z_{2s} z_{2s} e^2}{(r-d_2)^2} + k_2 d_2 - \phi'(r+d_1-d_2) = 0$ (4)

Three of these four equations are independent. Here k_1 and k_2 are the spring factor for the positive and negative ion shell respectively and $\phi(r) = a \exp(-\frac{r}{\rho})$... (5)
 a and ρ being the overlap force parameters.

Free ion polarisabilities are given by

$$\alpha_+ = \frac{z_{1s}^2 e^2}{k_1} \quad \& \quad \alpha_- = \frac{z_{2s}^2 e^2}{k_2} \quad \dots \quad \dots \quad (6)$$

Assuming $\alpha_+, \alpha_- \ll r^3$ and retaining up to terms first order in $\frac{e^2 \alpha_{\pm}}{r^4}$ we get the cohesive energy $u(r)$ and dipole moment $\mu(r)$

as $u(r) = -\frac{e^2}{r} + \phi(r) - \frac{e^2}{2r^4} \left\{ (\alpha_+ + \alpha_-) - \left(\frac{\alpha_+}{z_{1s}^2} + \frac{\alpha_-}{z_{2s}^2} \right) \right\} + \frac{\phi'(r)}{r^2} \left(\frac{\alpha_+}{z_{1s}^2} - \frac{\alpha_-}{z_{2s}^2} \right)$... (7)

$$\mu(r) = er - \frac{e}{r^2} \left\{ (\alpha_+ + \alpha_-) + \left(\frac{\alpha_+}{z_{1s}^2} - \frac{\alpha_-}{z_{2s}^2} \right) \right\} \quad \dots \quad \dots \quad (8)$$

Assuming adiabatic condition the vibrational frequency

is given by

$$\omega^2 = \frac{1}{m} \frac{d^2 u}{dr^2} = \frac{1}{m} \left[\left(\frac{\partial^2 u}{\partial r^2} \right)_{d_1, d_2} + \left(\frac{\partial u}{\partial d_1 \partial r} \right)_{d_2} \cdot \frac{dd_1}{dr} + \left(\frac{\partial u}{\partial d_2 \partial r} \right)_{d_1} \cdot \frac{dd_2}{dr} \right] \quad \dots \quad (9)$$

III. COMPARISON WITH OTHER MODELS

If terms of the form $\frac{\alpha_{\pm}}{z_{1s}^2}$ etc are neglected, expressions for u and μ become the same as those used by Rittner⁽¹⁾ and Varshni⁽²⁾ up to terms first order in $\frac{e^2 \alpha_{\pm}}{r^4}$. Toshi and Doyama⁽³⁾ somewhat arbitrarily assume that the deformation dipole is centered in the negative ion and add energy of interaction between this dipole moment with the electrical field due to the positive ion. Up to first order in $\frac{\alpha_{\pm}}{r^4}$ their expression for energy and dipole moment becomes

$$u(r) = -\frac{e^2}{r} + \phi(r) - \frac{e^2}{r^4} \frac{\alpha_+ + \alpha_-}{2} + \frac{e}{r^2} \mu_d(r) \quad \dots \quad (10)$$

$$\& \quad \mu(r) = er - \frac{e}{r^2} (\alpha_+ + \alpha_-) + \mu_d(r) \quad \dots \quad (11)$$

where $\mu_d(r)$ is the empirically introduced deformation dipole moment.

Assuming that $\mu_d(r) \propto \phi(r)$ Toshi et al express $\mu_d(r)$ in terms of $\phi(r)$ and the Sziget charge defect observed in the corresponding ionic crystal.

The above equations are different from those of the shell model. If we remember that for equilibrium separation r_0 , $\frac{e^2}{r_0^2} + \phi'(r_0) \approx 0 \left(\frac{a_0}{r_0} \right)$, then the two sets of equations become comparable for $r=r_0$ if we put

$$\mu_d(r_0) = -\frac{e}{r_0^2} \left(\frac{a_0}{Z_{10}} - \frac{a_0}{Z_{20}} \right) \quad (12)$$

The shell model energy expression will then differ by the second term in the coefficient of $\frac{e^2}{r^4}$. This comparison is, however, artificial as the above $\mu_d(r_0)$ will lead to zero charge defect. The difference between the shell model and the deformation dipole model is fundamental because $\mu_d(r)$ is essentially a first order exchange effect while the term $\mu_d(r)$ in the shell model is a second order exchange effect.

IV. QUANTUM MECHANICAL ANALYSIS

We use a simplified model. Two ions a and b are separated by a distance r , $Z_a e$ and $Z_b e$ are the nuclear charges and we consider only one electron states for each ion. Electrons are in parallel spin state. The interaction energy V and the dipole moment operator D_z are given by, with negative ion as origin and \vec{r} as the Z direction,

$$V = -\frac{Z_a e}{r_{a1}} - \frac{Z_b e}{r_{b1}} + \frac{e^2}{r_{12}} \quad \& \quad D_z = -e(r_1)_z - e(r_2)_z + Z_b e r$$

Where we assume electrons 1 and 2 to be associated with ion a and b respectively. Neglecting exchange effect and using perturbation theory we get up to second order perturbation

$$u(r) = \frac{Z_a Z_b e^2}{r} + \langle v \rangle \simeq -\frac{e^2}{r} - \frac{e^2}{r^4} \cdot \frac{\alpha_+ + \alpha_-}{2} \dots \dots (13)$$

$$\& \quad \mu(r) = \langle D_z \rangle \simeq e r - \frac{e}{r^2} (\alpha_+ + \alpha_-) \dots \dots (14)$$

To consider the exchange effects, we construct the antisymmetrised zero order wave function and calculating the average values of v and D_z up to first order, we get

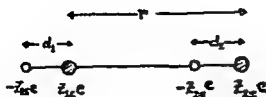
$$u_{ex}(r) = S^2 \langle \phi_o(1,2) | v | \phi_o(1,2) \rangle - \langle \phi_o(1,2) | v | \phi_o(2,1) \rangle \simeq S^2 \frac{e^2}{r} \equiv \phi(r) \dots (15)$$

$$\begin{aligned} \text{and } \mu_{ex}(r) &= S^2 \langle \phi_o(1,2) | D_z | \phi_o(1,2) \rangle - \langle \phi_o(1,2) | D_z | \phi_o(2,1) \rangle \\ &= 2e \langle \phi_o(1,2) | (r_1)_z | \phi_o(2,1) \rangle - e S^2 r \simeq A r^2 \phi(r) \dots (16) \end{aligned}$$

Where S is the overlap integral and $A = \frac{1}{2e} \frac{r_- - r_+}{r_- + r_+}$; r_+ , r_- are the ionic radii. In the evaluation of the last integral we have used exchange charge model of Dick and Overhauser⁽⁴⁾. Comparing the above results with equations (10) & (11) we find that if we put $\mu_d = \mu_{ex}$, then in Toshi's model the energy term $\frac{e}{r^2} \mu_d(r)$ must be a second order exchange effect. The corresponding correction in

$\mu_d(r)$ is, however, absent. Moreover, $\mu_d(r) \propto r^2 \phi(r)$ rather than $\phi(r)$ as Toshi et al assume. Similarly in the self model expressions (7) and (8) extra terms are present both in $u(r)$ and $\mu(r)$ which are contributions from the second order exchange effects. But surprisingly the first order exchange effect is absent in the expression for $\mu(r)$.

It is, therefore, concluded that neither the shell model nor the deformation dipole model is quantum mechanically consistent up to the second order exchange effects. A consistent quantum mechanical model is being developed and the results will be reported soon.



REFERENCES

1. E. S. Rittner, J. Chem. Phys., 19, 1030 (1951)
2. Y. P. Varshni, Trans. Faraday Soc., 53, 132 (1957)
3. H. P. Toshi & M. Doyama, Phys. Rev., 160, 716 (1967)
4. B. J. Dick & A. W. Overhauser, Phys. Rev., 112,
90 (1958)

PHONON DISPERSION RELATIONS IN AgCl

R. Prasad and R.K. Singh
Physics Department, B.H.U., Varanasi-5

I. INTRODUCTION

Silver chloride is one of the noble-metal halides crystallising in the same crystal structure (f.c.c.) as the alkali halides. This is an interesting substance for the study as it differs in electronic configuration from the simplest ionic crystals - the alkali halides. In the case of alkali halides the outer most electrons occupy closed shells while the outer electrons of the cations do not occupy the closed shell in the noble metal halides. This leads to the failure of the rigid-ion approximation used by Born⁽¹⁾ and Kellermann⁽²⁾ and the Cauchy relation. Thus, the rigid ion model which fails to account for the Cauchy discrepancy can not describe the correct behaviour of this solid. The shell model developed by Woods et.al.⁽³⁾ on the other hand successfully accounts for the electrical and mechanical polarizations but suffers from the same limitation as the rigid ion model to describe the elastic behaviour. These limitations involved in the above models reveal a poor agreement between theoretical and experimental⁽⁴⁾ dispersion curve as shown by Joshi and Gupta⁽⁵⁾. The serious discrepancy in acoustic branches obtained by these authors clearly indicates the necessity of a more sophisticated theory to take proper account of elastic

as well as dielectric behaviour of the ionic solids.

Recently a new model developed by Singh and Verma⁽⁶⁾ herein after referred to as Singh and Verma model (SVM) which is capable of describing the correct elastic and dielectric properties of ionic solids has been applied to study the lattice dynamics of alkali halides⁽⁷⁾ with great success. In the present paper we have applied the SVM to study the crystal dynamics of silver chloride. The computed dispersion curves (Θ_D -T) curves and combined density of states (C.D.S.) curves show an excellent agreement with experimental results whenever available.

II. CALCULATION AND RESULTS

The parameters Z ($= 1$), A , B , $f(a)$, $\left(a \frac{df}{da}\right)$, γ_1, γ_2 , d_1 and d_2 which appear in SVM were fixed from the knowledge of infrared absorption frequency dielectric constants $\epsilon_0/\epsilon_\infty$, the elastic constants C_{11} , C_{12} and C_{44} the atomic polarizabilities α_1 and α_2 for the positive and negative ions respectively, and the equilibrium condition,

$$B = -1.165p, \text{ where } p \text{ is } [1 + 12 f(a)]$$

The input data used for the calculation of parameters are given in Table 1 along with the corresponding references. The parameters obtained are also given in the same Table.

TABLE 1 - INPUT DATA AND PARAMETERS OF AgCl

INPUT DATA	REF	PARAMETERS *
$C_{11} = 7.590 \times 10^{11}$ dyms/cm ²	8	$f(a) = -0.041$ (-0.025)
$C_{12} = 3.908$ "	8	$\left(a \frac{df}{da}\right) = 0.358$ (0.407)
$C_{44} = 0.689$ "	8	$A = 7.149$ (7.149)
$\epsilon_1 = 0.783 \times 10^{-24}$ cm ³	9	$B = -0.598$ (-0.598)
$\epsilon_2 = 4.557$ "	9	$d_1 = 0.107$ (0.139)
$\nu_T = 3.089 \times 10^{12}$ sec ⁻¹	1	$d_2 = 0.299$ (0.211)
$\nu_L = 5.221$ "	1	$\gamma_1 = -1.019$ (-0.783)
$a = 2.780 \times 10^{-8}$ cm	5	$\gamma_2 = -2.114$ (-2.993)

*The values without and within the paranthesis correspond to the ionic charge $Z = 1.0$ and $Z = 0.88$ respectively.

The phonon spectra of silver chloride has been computed using the parameters given in Table 1 obtained from SVM. The calculated dispersion curves for the three symmetry directions are shown in Fig.1 together with the experimental data⁽⁴⁾ for the acoustic branches.

III. DISCUSSION

It is found that the agreement between our calculations and experimental results from the dispersion curves is excellent. Joshi and Gupta's calculations⁽⁵⁾, however, show very large deviation from the experimental results especially at high wave vectors. The good agreement obtained here, however, shows that the SVM developed by including the effect of three-

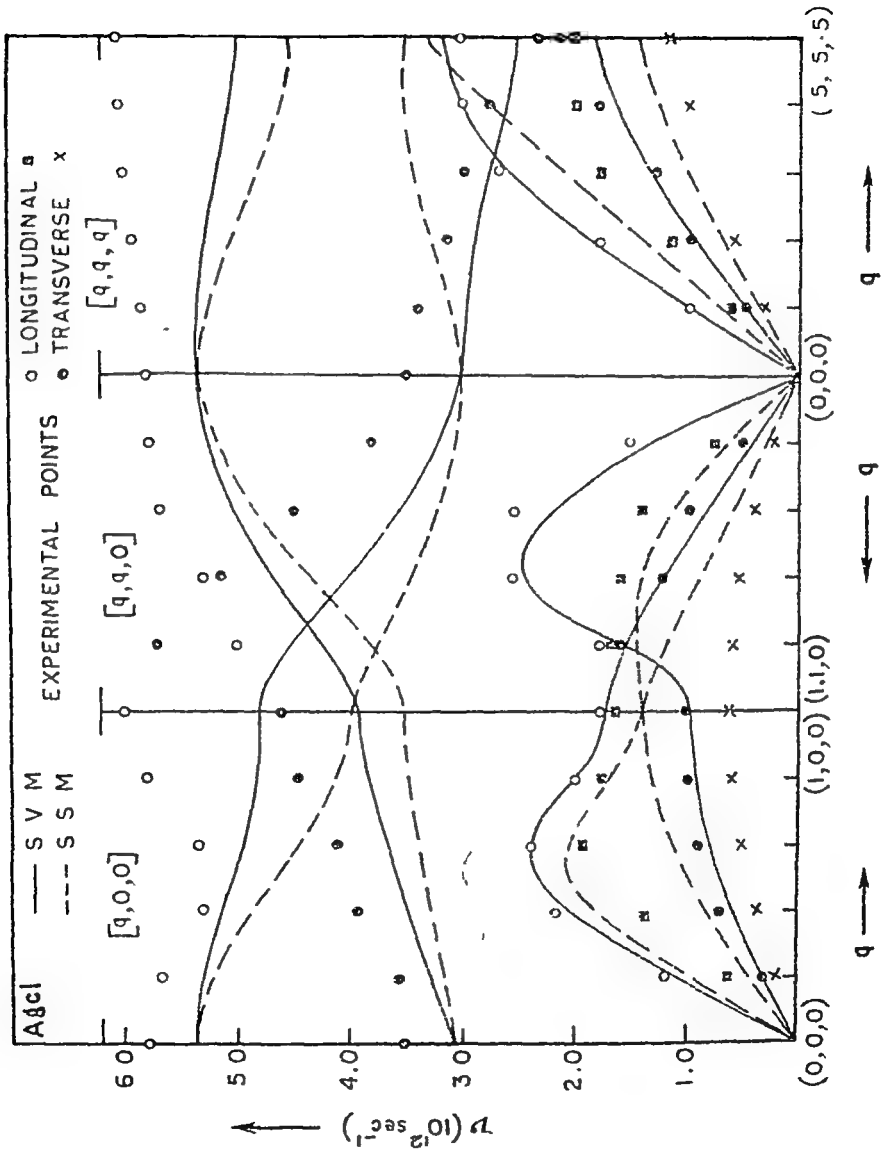


FIG. 1

actions quite satisfactory results in the case of noble-metal halides also.

It is worth mentioning here that this phenomenological model based on ~~simpler~~ considerations is almost equivalent to the shell model regarously derived by Sinha based on quantum mechanical considerations.

REFERENCES

1. M. Born and K. Huang; Dynamical Theory of Crystal Lattices (Clarendon Press, Oxford, England, 1954).
2. E.W. Kellermann; Phil. Trans. Roy. Soc. (London) A238, 513 (1940)
3. A.D.B. Woods, W. Cochran, and B.N. Brockhouse; Phys. Rev. 119, 980 (1960)
4. H. Cole; J. Appl. Phys. 24, 482 (1953)
5. S.K. Joshi and R. Gupta; Phys. Rev. 126, 933 (1962)
6. R.K. Singh and M.P. Verma; Phys. Stat. Sol. 36, 335 (1969)
7. R.K. Singh and M.P. Verma; Phys., Stat., Sol., 38, 851 (1970)
8. W. Hildshaw, J.T. Lewis and C.V. Briscoe; FI Rev., 163, 876 (1967)
9. K.G. Bausiger and K.S. Iyengar; Acta Cryst. 14, 727 (1961)
10. S.K. Sinha; Phys. Rev. 177, 1256 (1969)

A KINEMATIC THEORY OF THERMAL(BRILLOUIN)SCATTERING OF LIGHT

BY PHONONS IN CONDENSED MEDIA

N.KUMAR,(MRS.)L.KRISHNASAMY AND K.SRINIVASA

Department of Physics, Indian Institute of Science, Bangalore-12

I. INTRODUCTION

The scattering of light from spatially correlated fluctuations of the thermodynamical variables, such as density, temperature or entropy, concentration and order-parameter, propagating in condensed media, is referred to as the thermal or Brillouin-Mandelstam scattering. In the thermodynamical theories of the light scattering (1-5) the above statistical fluctuations are assumed to amplitude-modulate the optical dielectric constant of the medium and thus scatter light. The Brillouin components appear as the acoustic side-bands. In crystals, in particular, the spatially correlated density fluctuations are produced by phonons. The latter are often likened to moving diffraction gratings and, therefore, the Brillouin doublet appears naturally enough as a result of the Doppler effect. In the present paper the latter purely kinematic argument is developed from the atomistic viewpoint in that we take due cognizance of the motional frequency modulation of the incident radiation due to the Doppler effect involving the kinematics of the polarisable centres individually. The presence of the central component (non-zero Landau-Placzek ratio⁽⁶⁾) is explained in terms of certain non-propagating local modes.

II. FORMULATION

We shall consider the scattering of a monochromatic plane polarised coherent light by the acoustic phonons in a crystal containing one (polarisable) atom per unit cell. Also, without any essential loss of generality, we shall take the electric field

vector of the incident light to be normal (\perp) to the plane containing the incident and the scattered directions. With this parametrisation we describe the incident light by the field vector $\vec{E}_I(\vec{r}, t)$

$$\vec{E}_I(\vec{r}, t) = \hat{e}_\perp E_{0\perp} \cos(\omega_0(\vec{k})t - \vec{k} \cdot \vec{r}), \quad \dots \quad (1)$$

with $\omega_0(k) = ck$, where c is the velocity of light in the medium.

Here \hat{e}_\perp is a unit vector normal to the reference plane chosen above, and all other symbols are self-explanatory.

The lattice displacement at the j^{th} site due to the acoustic phonon of wavevector \vec{q} is given by

$$\vec{u}_j(\vec{r}_j, t) = \hat{e}_q u_q \sin(\omega_q(\vec{q})t - \vec{q} \cdot \vec{r}_j), \quad \dots \quad (2)$$

with $\hat{e}_q = \vec{q}/q$, and $\omega_q(\vec{q}) = c_s q$, where c_s is the speed of sound.

The dipolar electric polarisation $\vec{P}(\vec{r}_i, t)$ induced on the moving site at the i^{th} site as seen by the detector in the scattered direction

is given by

$$\vec{P}(\vec{r}_i, t) = \hat{e}_\perp \alpha E_{0\perp} \cos \left[\int dt \left\{ \omega_0(\vec{k}) \left(1 - \frac{\vec{u}(\vec{r}_i, t) \cdot (\vec{e}_{\vec{k}'} - \vec{e}_{\vec{k}})}{c} \right) \right\} - \vec{k} \cdot \vec{r}_i \right] \dots \quad (3)$$

where primes denote the corresponding scattered quantities.

Here we have taken into account the motional frequency modulation (Doppler effect) during absorption and re-radiation by the atoms.

Thus we have a phased array of frequency modulated electric dipoles and the resultant electric field intensity $\vec{E}_I'(\vec{r}, t)$ can at \vec{r}_0 be written down from the antenna theory as

$$\vec{E}_I'(\vec{r}, t) = \frac{\pi \epsilon_0 E_{0\perp} \hat{e}_\perp}{\Omega \lambda^2 R} \int_{\Omega} d\vec{k} \cos \left[\omega_0(\vec{k})t - \frac{\omega_0(\vec{k})}{c} \vec{r}_0 \cdot \hat{e}_q \cdot (\hat{e}_{\vec{k}} - \hat{e}_{\vec{k}'}) \sin(\omega_0(\vec{k})t - \vec{q} \cdot \vec{r}) - (\vec{k} - \vec{k}') \cdot \vec{r} \right], \quad \dots \quad (4)$$

with $\lambda = 2\pi/k$, and the overhead dot indicating time differentiation.

The right-hand side can now be expressed in terms of the Bessel functions of integral order. We get after some reduction

$$\vec{E}_I'(\vec{r}, t) = \pm \hat{e}_\perp \left(\frac{\pi \epsilon_0 N E_{0\perp}}{2 \lambda^2 R} \right) \delta_{\vec{r} - \vec{r}_0, \vec{q} + \vec{q}} J_1 \left(\frac{u_q}{c} \omega_0(\vec{k}) \vec{r}_0 \cdot (\hat{e}_{\vec{k}} - \hat{e}_{\vec{k}'}) \right) \sin \{ (\omega_0(\vec{k}) \pm \omega_q(\vec{q}))t - \vec{k} \cdot \vec{r} \} + O\left(\frac{1}{\lambda}\right) \quad \dots \quad (5)$$

where g is some reciprocal lattice vector. Ignoring the "Umklapp" processes that correspond to the higher order diffraction peaks,

we get the usual Bragg condition of momentum conservation

$$\vec{q} = \vec{k} - \vec{k}', \quad k \sim k' \quad \text{and} \quad q \cong 2k \sin \theta/2, \quad \text{where } \theta \text{ is the scattering angle} \quad \dots \quad (6)$$

from (5) and (6) that the spectrum of the scattered

light consists of a doublet spaced $\Delta\omega = 4Kc_2 \sin \frac{\theta}{2}$ apart and placed symmetrically about the central component that has zero intensity.

The relative intensity of each of the Brillouin components can at

once be written down as

$$\left| \frac{\vec{E}'_1(\vec{R}, t)}{E_{0L}} \right|^2 = \left(\frac{\pi^2 N^2 \alpha^2}{8 \lambda^4 R^2} \right) J_1^2 \left(2 \mathcal{U}_{\vec{q}} \frac{\omega_0(\vec{R})}{c} \sin \theta/2 \right) \dots \quad (7)$$

Recalling that $\mathcal{U}_{\vec{q}} \sim \Omega$ (Brillouin approximation), we can write

$$J_1^2 \left(2 \mathcal{U}_{\vec{q}} \frac{\omega_0(\vec{R})}{c} \sin \theta/2 \right) \approx \mathcal{U}_{\vec{q}}^2 \frac{\omega_0^2(\vec{R})}{c^2} \sin^2 \frac{\theta}{2} \dots \quad (8)$$

Also, we have from lattice dynamics

$$\langle \mathcal{U}_{\vec{q}}^2 \rangle = \left(\frac{k}{\rho \Omega \omega_{\vec{q}}(\vec{q})} \right) \left(\langle n_{\vec{q}} \rangle + \frac{1}{2} \right) \dots \quad (9)$$

where $\langle n_{\vec{q}} \rangle$ is the average occupation number of the phonon mode \vec{q} .

Combining (7), (8) and (9), we get after some reduction

$$\left| \frac{\vec{E}'_1(\vec{R}, t)}{E_{0L}} \right|^2 = \left(\frac{\pi^2}{8 \lambda^4} \right) \left(\frac{k N^2 \alpha^2}{\rho \Omega c_s} \right) \frac{1}{R^2} \sin^2 \frac{\theta}{2} \quad \text{for } k_B T \ll \hbar \omega_{\vec{q}}(\vec{q}), \quad (10)$$

and

$$= \left(\frac{\pi^2}{8 \lambda^4} \right) \left(\frac{N^2 \alpha^2}{\rho \Omega c_s} \right) \frac{k_B T}{R^2} \quad \dots \quad (11)$$

for $k_B T \gg \hbar \omega_{\vec{q}}(\vec{q})$.

Here k_B is Boltzmann's constant.

As noted earlier there is, however, a central frequency component of non-zero intensity in the scattered light. In the present formulation such a component arises naturally if we take into account any spatially uncorrelated local modes that may well be present in the crystal. We can have, for instance, a radial (s-like) vibrational

mode localised at the site \vec{r}_0 represented by the displacement field

$$\vec{u}(\vec{r} - \vec{r}_0) = \mathcal{U}_0 \exp(-\beta/2 (|\vec{r} - \vec{r}_0|^2)) \sin \omega_0 t \hat{e}_{\vec{r} - \vec{r}_0} \quad (12)$$

Under the assumption of the random spatial distribution of the centres (Random Phase Approximation) the intensities can be added. Proceeding, therefore, as before we get the following expression for

the intensity of the central component

$$\left| \frac{\vec{E}'_1(\vec{R}, t)}{E_{0L}} \right|^2 = \left(\frac{\pi^2 N_0 \alpha^2}{8 \lambda^4 R^2 c^2} \right) \cdot \frac{(k_B T)^2}{\omega_0^4 m^2} \quad \dots \quad (13)$$

and

$$= \left(\frac{N_0 \alpha^2}{4 \pi^2 R^2 c^2} \right) \cdot \frac{(k_B T)^2}{(\omega_0^4 m^2)} \left(\frac{\beta}{\sin \frac{\theta}{2}} \right)^6 \quad \dots \quad (14)$$

for $2k \sin \frac{\theta}{2} \ll \beta$.

III. DISCUSSION

In the foregoing sections we have established an atomistic justification of the purely kinematic viewpoint of Brillouin scattering according to which the spatially-correlated density fluctuations propagating in condensed media(phonons) are entirely equivalent to moving diffraction gratings. In the thermodynamic treatment the above corresponds to adiabatic density fluctuations that are assumed to modulate the optical dielectric constant of the medium. (11) gives the scattering by the zero-point phonons and is purely a quantum effect. It is seen to be anisotropic. In practice, however, it is negligibly small as compared with the contribution due to the thermal scattering(12). The latter is rightly seen to be isotropic for the chosen parametrisation. The apparently wrong temperature dependence is due entirely to the neglect of the phonon damping effects(finite life time). (13,14) give the intensity of the central component owing to the presence of the randomly distributed local modes. The latter correspond to the isobaric density fluctuations and give rise to a non-zero Landau-Placzek ratio. Conceptually speaking it will be of interest to apply this approach to Brillouin scattering off spin-waves where the translatory motion of the particles has no classical analogue. This is being attempted.

REFERENCES

1. M. Smoluchowski, Ann. Physik 25, 205(1908).
2. A. Einstein, Ann. Physik 33, 1274(1910).
3. L. Brillouin, Ann. Phys. (Paris) 88, 17(1922).
4. Immanuel L. Fabelinski, Molecular Scattering of Light (Plenum, New York, 1968).
5. R. W. Mountain, Rev. Mod. Phys. 38, 205(1966).
6. Landau and Placzek, Phys. Z. Soviet Union 5, 172(1938).

LATTICE DYNAMICS OF CALCIUM OXIDE

P.R. Vijayaraghavan and P.K. Iyengar.
Nuclear Physics Division, Bhabha Atomic Research Centre,
Trombay, Bombay 85

I. INTRODUCTION

The lattice dynamics of crystalline solids have been studied extensively using the technique of inelastic scattering of thermal neutrons. For ionic crystals, particularly for those having the sodium chloride structure, a shell model⁽¹⁾ theory has been found to be reasonably adequate to formulate the dynamics of the lattice. In this paper we report our measurements at room temperature on the phonon dispersion relation of calcium oxide - a solid having the sodium chloride structure - along the three principal high symmetry directions. The results together with the available data on elastic constants,⁽²⁾ dielectric constants⁽³⁾ and optical measurements⁽⁴⁾ have been analysed using the point ion and shell model approaches.

II. EXPERIMENTS AND RESULTS

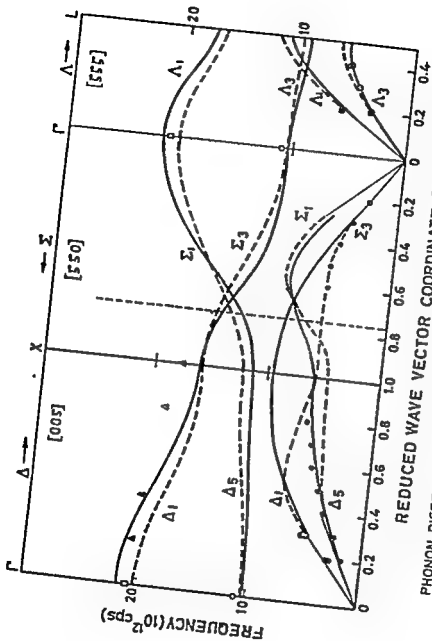
A single crystal of CaO weighing approximately 13.6 gms was aligned with the $[1\bar{1}0]$ axis vertical. Measurements were done using the constant Q mode of operation, (TAS mode). The high frequency longitudinal optical phonons were observed using the Beryllium detector spectrometer⁽⁵⁾ (BDS mode) technique.

The measured dispersion relation for phonons propagating along the $[100]$, $[110]$ and $[111]$ directions is

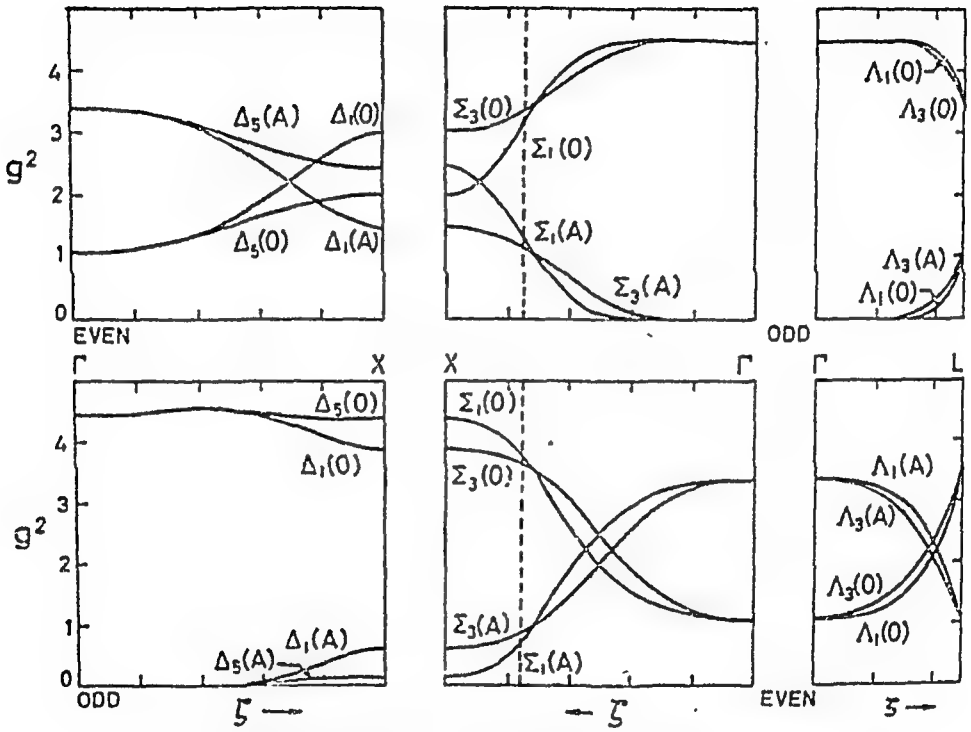
shown in Fig. 1. The closed circles correspond to data obtained by using the TAS mode while the closed triangles are due to the BDS mode. The open circles at $q = 0$ corresponds to the infrared absorption frequency, while the open square, also at $q = 0$, corresponds to the frequency of the longitudinal optic mode calculated using the Lyddane-Sachs-Teller relation. The continuous lines are a three parameter (point ion model) fit to the data while the dashed lines are those obtained by the addition of two more parameters - viz. the electronic and short range polarisabilities of the oxygen ion. The initial slopes of the acoustic branches are based on the elastic constant data at 270°K.

III. THEORETICAL MODELS

The values of the various parameters, obtained by a least square analysis of the data, are given in Table I. The point ion model itself gives a reasonably good fit to the data. An alternate model which includes the oxygen ion polarisabilities seems to improve the overall fit. This assumption that the oxygen ion is more polarisable than the calcium ion is based on the data of Pauling and Tessman⁽⁶⁾ et al. This model also sets equal the short range ion-ion, ion-shell and shell-shell interactions. The least square fitted value for the electronic polarisability of the O^{2-} ion ($1.88 \times 10^{-24} \text{ cm}^3$) agrees closely with value due to Tessman ($1.3 \times 10^{-24} \text{ cm}^3$ for oxygen in CaO), whereas Pauling's value is $3.86 \times 10^{-24} \text{ cm}^3$. Addition of two more parameters to include the polarisabilities of



PHONON DISPERSION CURVES FOR CALCIUM OXIDE AT ROOM TEMPERATURE



STRUCTURE FACTORS FOR CALCIUM OXIDE

the Ca^{++} ion did not improve the fit any significantly. The five parameter model was also used to calculate the inelastic scattering structure factor shown in Fig. 2.

REFERENCES

1. A.D.B. Woods, W. Cochran and B.H. Brockhouse, Phys. Rev. 119, 980 (1960).
2. H.E. Hite and R.J. Kearney, J. Appl. Phys. 38, 5424 (1967).
3. K. Hojendahl, K. Danske Vidensk, Selkab, 16, No. 2 (1938).
4. B. Szigeti, Trans. Faraday Soc. 45, 155 (1949).
5. P.K. Iyengar in Thermal Neutron Scattering, Ed. P.A. Egelstaff, Academic Press (1965) p. 132.
6. J.R. Tessman, A.H. Kahn and W. Shockely, Phys. Rev. 92, 890 (1953).

TABLE I

Parameters for the two models for calcium oxide discussed in text. (v is the volume of the primitive unit cell)

Parameter	Unit	Point ion model	Shell model	definition
A	$(e^2/2v)$	25.52	29.84	near neighbour short range radial force constant.
B	$(e^2/2v)$	-2.62	-2.886	near neighbour short range tangential force constant
Z	(e)	1.60	1.70	ionic charge
α	$(1/v)$	—	0.0679	electronic polarisability for oxygen ion
d	(e)	—	0.1616	short range (mechanical) polarisability for oxygen ion.

DISCUSSION

G. Venkataraman

I would like to make the general observation that care is required in comparing the elastic constants of crystals obtained from neutron scattering experiments with those deduced from ultrasonic measurements. This has been pointed by Cowley (Proc. Phys. Soc. 90, 1127 (1967)) who shows that if anharmonic effects are present then the elastic wave propagates in a collision-dominated manner in the ultrasonic region, and in a collision-free manner in the neutron experiments. In other words, $\omega\tau \ll 1$ in one case and $\omega\tau \gg 1$ in the other, where τ is the life-time of the phonon. Owing to this difference, the elastic constants obtained from the two sources need not agree.

E.S.R. Gopal

Regarding the question raised by Dr. Venkataraman, namely an expected difference in sound velocity in the thermal region, $\omega\tau \gg 1$, and hydrodynamic region, $\omega\tau \ll 1$ a difference was suggested in liquid helium but experiments showed no such differences. What is the situation in solids.

G. Venkataraman

The experimental situation is that in many cases

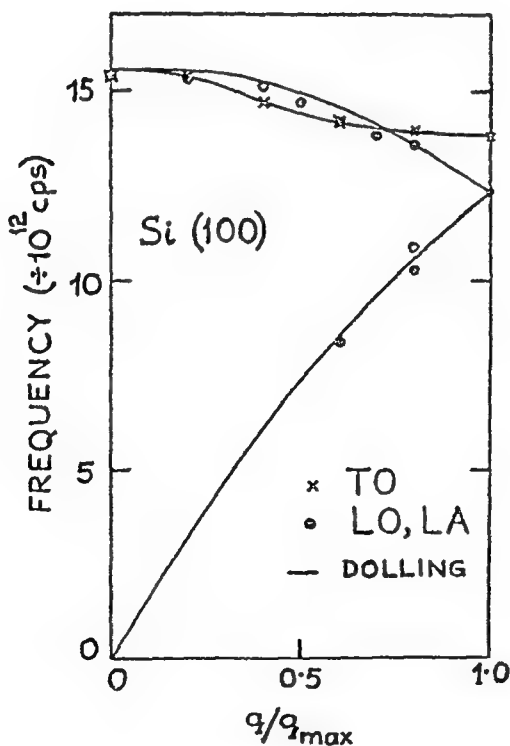
a measurable difference can be detected in solids. See Cowley et al. in Neutron Inelastic Scattering (IAEA, Vienna, 1968), Vol. I, p.281.

C.L. Thaper

The question of the use of the inverted filter spectrometer for measuring phonon dispersion relations is a controversial one. It is often believed that one cannot fix the magnitude and the direction of the phonon wave vector, q , as a result of the uncertainty in the outgoing wave vector, k' , which can, in principle, vary from 0 to the cut off value determined by the inverted filter. We, at Trombay, have made measurements of phonon dispersion relations in silicon, in the Γ -X direction, at constant-E modes of operation, with a view to seeing whether a suitable k' can be chosen to give a unique dispersion relation. Our observations, taken with a Debye-Scherrer camera, in the Γ -X direction in Silicon, showing a constant energy of 10 meV, are shown in the accompanying figure. The figure shows a series of points indicating Dolling's Γ -X dispersion relation. Solids and Liquids, in the Γ -X direction, are shown in agreement on a triple-axis spectrometer. The figure also shows the dispersion of acoustic phonons. [111] direction in Silicon. The figure shows a series of points indicating Dolling's Γ -X dispersion relation. Solids and Liquids, in the Γ -X direction, are shown in agreement on a triple-axis spectrometer. The figure also shows the dispersion of acoustic phonons. this question

A computer programme on the lines of Cooper and Nathans with a modified analyser function has been written to calculate the phonon line shapes. A detailed report on this alongwith measurements on Beryllium will be published elsewhere.

It may be mentioned that with this technique one can quite easily observe the optical phonons which are rather hard to see on a triple-axis spectrometer.



POLARITON DISPERSION RELATIONS IN CaWO_4

V.C. Sahni and G. Venkataraman

Nuclear Physics Division, Bhabha Atomic Research Centre,
Trombay, Bombay-85.I. INTRODUCTION

In this paper we present a calculation of the polariton dispersion curves in CaWO_4 (space group I_4/a) - a substance whose dynamics is of considerable interest.¹ Polaritons are coupled phonon-photon modes whose existence was first predicted by Huang².

II. THEORETICAL BASIS OF CALCULATION

Recently Pick³ has shown that the dispersion curves for the polaritons can be obtained from the secular equation:

$$\det \begin{vmatrix} \underline{G}(\vec{k}) - \underline{M} \omega^2 & \underline{\Xi}^\dagger(\vec{k}) \\ \underline{\Xi}(\vec{k}) & \frac{1}{4\pi} (\nabla^2 \underline{\Xi}(\vec{k}) - \underline{\Xi} \nabla^2) \end{vmatrix} = 0$$

$\xleftarrow{3n} \quad \xleftarrow{3} \quad$

In (1) $\underline{G}(\vec{k})$ is the dynamical matrix, \underline{M} is the mass matrix, $\underline{\Xi}^\dagger(\vec{k})$ is the tensor representing the short-range part of electrical interaction, $\underline{\Xi}(\vec{k})$ is the tensor representing the long-range part of electrical interaction, \underline{Q} is a matrix with elements $Q_{ij} = \frac{1}{4\pi} (\nabla^2 \delta_{ij} - \delta_{ij} \nabla^2)$, ∇^2 is the Laplacian operator, \vec{k} and ω are the wave vector and frequency respectively.

and frequency and $n^2 = k^2 c^2 / \omega^2$.

If one assumes a model for the crystal, one can calculate ϵ_∞ , $\bar{\epsilon}$, and ϵ_∞^∞ and hence the dispersion curves. In practice it is very difficult to do so. However, it is possible to transform (1) such that it involves parameters that occur in the infrared dispersion formula and these being experimentally measurable, e.g., using IR reflection studies, one can calculate the dispersion curves for polaritons using experimental data. The actual transformation is involved and will be discussed elsewhere. Here we note that for a uniaxial crystal, e.g., CaWO_4 , the following formulae apply for polaritons propagating along and at right angles to unique axis (c-axis).

Propagation along c-axis:

Transverse modes (doubly degenerate) $\frac{k^2 c^2}{\omega^2} = \epsilon_\perp$;

Longitudinal modes: $\epsilon_\parallel = 0$.

Propagation at right angles to c-axis:

Transverse modes: $\frac{k^2 c^2}{\omega^2} = \epsilon_\parallel$ and $\frac{k^2 c^2}{\omega^2} = \epsilon_\perp$;

Longitudinal modes $\epsilon_\perp = 0$. (2)

Here

$$\epsilon_\perp = \epsilon_\perp^\infty + \sum_i S_{i,\perp} \omega_{i,\perp}^2 / (\omega_{i,\perp}^2 - \omega^2) , \quad (3a)$$

$$\epsilon_\parallel = \epsilon_\parallel^\infty + \sum_i S_{i,\parallel} \omega_{i,\parallel}^2 / (\omega_{i,\parallel}^2 - \omega^2) . \quad (3b)$$

The summation in (3a) runs over IR active modes which appear in reflection spectra observed with light incident along c-axis; the summation in (3b) pertains to IR active

modes which appear when light is incident normal to the c-axis and has polarization parallel to it. The oscillator strengths $S_{1,1}$ and $S_{1,n}$ and the dispersion frequencies $\omega_{1,1}$, $\omega_{1,n}$ though related to lattice dynamical quantities, are more conveniently obtained from IR experiments. In (3) we have ignored the damping factor usually used in the interpretation of IR data.

III. RESULTS AND CONCLUSIONS

Taking the parameters occurring in equations (2) and (3) from Barker's analysis¹, dispersion curves were calculated, and are displayed in Fig.1. An interesting feature is that even modes which correspond predominantly to internal vibrations of the WO_4^{--} ion show considerable dispersion (cf mode $\geq 200 \text{ cm}^{-1}$). This shows the need for care while discussing the internal vibrations of molecular groups in complex crystals, particularly using the picture of an isolated molecule interacting with its environments.

Unfortunately, the polariton spectrum in CaWO_4 cannot be studied by using standard Laser Raman Spectroscopy as has been done in other cases⁴ since CaWO_4 has inversion symmetry which makes these modes Raman inactive. However, as has been demonstrated recently⁵, a breakdown of the usual selection rules can be achieved by the application of an external electric field, and one can thus study modes which were previously Raman inactive. This method called electric-field-induced Raman scattering can be exploited to study experimentally the

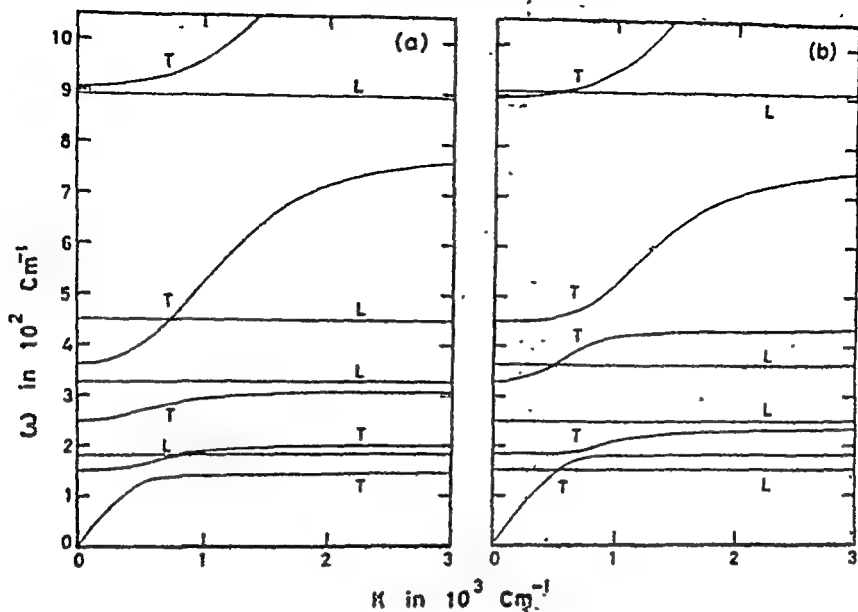
POLARITON DISPERSION RELATIONS IN CaWO_4 

Fig.1. Curves in (a) and (b) refer to polaritons propagating along and perpendicular to c-axis respectively. (L - longitudinal, T - transverse). In (a) the T-branches are doubly degenerate. In (b) of the two transverse branches we have not shown the dispersion curves for the branch the polarisation of which is perpendicular to c-axis, since these are same as the ones labelled T in (a).

polariton dispersion in CaWO_4 .

REFERENCES

1. A.S. Barker; Phys. Rev. 135, A742 (1964).
2. K. Huang; Proc. Roy. Soc. A208, 352 (1951).
3. R.M. Pick; Advances Phys. 19, 269 (1970) and references therein.
4. See Light Scattering Spectra of Solids, edited by G.B. Wright, Springer-Verlag, New York (1969) for references.
5. P.A. Fleury and J.M. Worlock; Phys. Rev. 174, 613 (1968).

DISCUSSION

Satya Prakash

1) How do you distinguish between phonon like and photon like modes?

2) Is photon like mode equivalent to the optical mode?

V.C. Sahni

1) The distinction between phonon like and photon like modes is that the energy of the former is dominantly mechanical, while that of the latter is dominantly electromagnetic.

2) No.

H.D. Bist

How do you distinguish between ordinary and extraordinary polaritons?

V.C. Sahni

The polarisation vector of the former is perpendicular to unique axis (c-axis), while that of the latter is parallel to the unique axis.

PROTON MAGNETIC RESONANCE STUDIES OF SOME POLYCRYSTALLINE AMMONIUM HALIDES

M. Mahajan and S.D. Nagsewara Rao
Department of Physics
Indian Institute of Technology, Kanpur (U.P.)

I. INTRODUCTION

Proton magnetic resonance studies have been made in three polycrystalline tetramethyl ammonium halides $[(CH_3)_4N]^+ X^-$ ($X = Cl, Br, I$; referred to below as TXM) in the temperature range 120°K to 350°K. All the three compounds are known to contain two molecules per unit cell which is tetragonal in structure⁽¹⁾. The C-H and C-N distances and the relative orientations of different CH_3 groups are not known. This study provides information about the internal motions that take place in these compounds and allows an estimate of the C-H and C-N distances.

The experiments were performed on a Varian-4200 wide-line NMR spectrometer operating at 8.0 Mc and provided with a V-4257 variable temperature accessory.

II. RESULTS AND DISCUSSION

The experimental linewidths (ΔH) and second moments (S) for the typical case of TXCl are shown in Fig. 1. The other two compounds exhibit rather similar behaviour. It can be seen from Fig. 1 that with increase of temperature line narrowing takes place in two distinct steps. (See ranges I, II and III in Fig. 1). A second moment analysis (see below) shows that the line narrowing from I to II is due to the methyl group rotation about the C_2 axis and that from II to III to the general reorientation of the TXM ion.

Second moments are calculated for all the three regions and are summarized in Table I. They are obtained on the basis of the following considerations: (1) The contribution to S from nitrogen and halogen nuclei is expected to be small⁽²⁾ (~ 0.1 G²) and, therefore, only

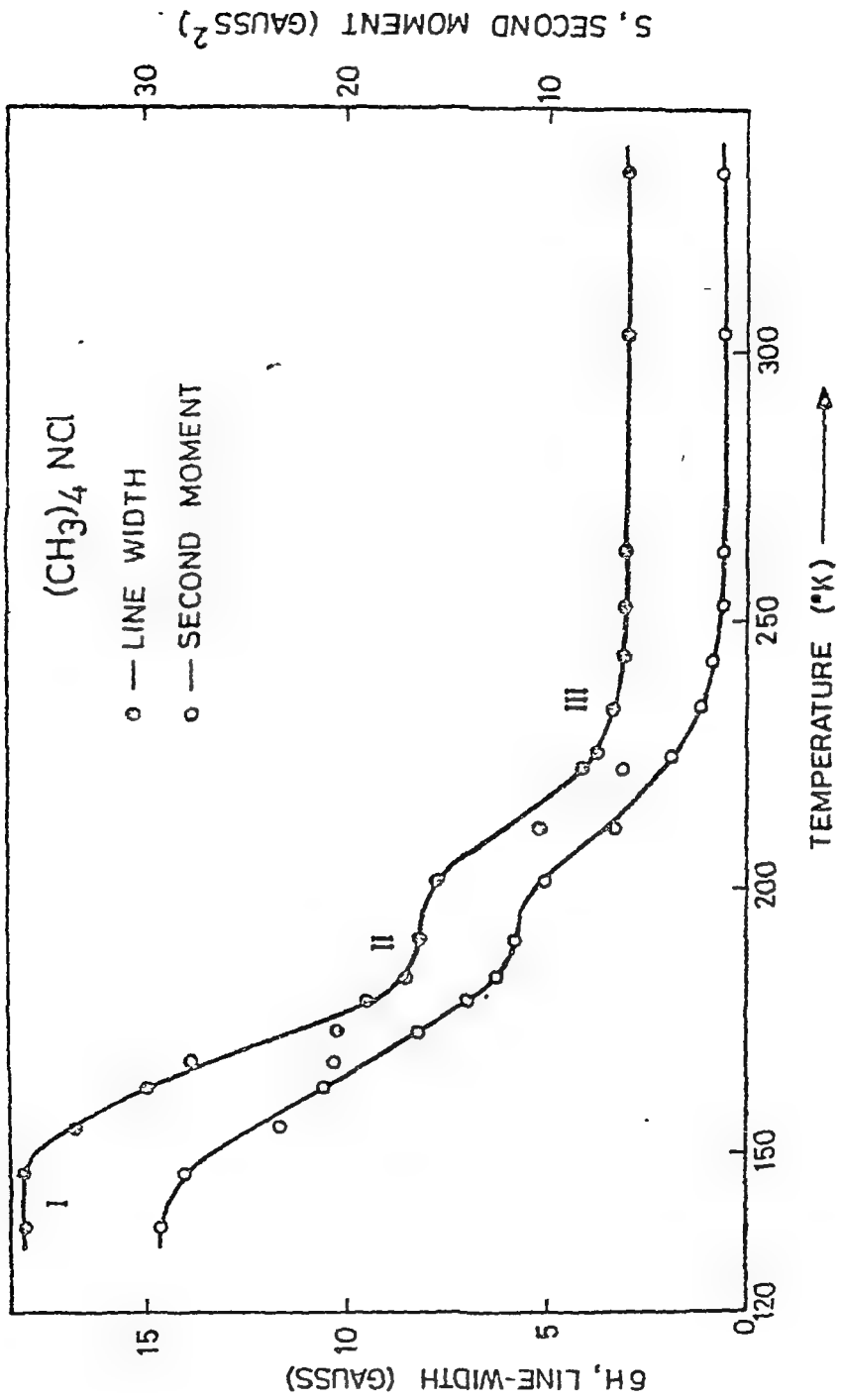


Fig. 1. Linewidth δH and second moment S versus temperature

proton-proton interactions are considered.

(2) This contribution is then divided into two parts S_{CH_3} and $S_{\text{CH}_3-\text{CH}_3}$ representing respectively the contribution from within a methyl group and that from interactions between protons on different methyl groups.

Table I. Calculated and experimental values of second moments for TiCl_3 , TiBr_3 and TiI_3 in regions I, II and III. For further explanation of the values see text.

Compound	Region	S_{obs} (G^2)	S_{CH_3} (G^2)	$S_{\text{CH}_3-\text{CH}_3}$ (G^2)	S_{cal} (G^2)
TiCl_3	I	30 ± 2.0	22.4	8.0	30.4
	II	11.6 ± 1.0	5.6	7.36	12.96
	III	1.2 ± 0.1	0	1.15	1.15
TiBr_3	I	31 ± 2.0	22.4	8.0	30.4
	II	11.2 ± 1.0	5.6	7.35	12.95
	III	1.2 ± 0.1	0	1.15	1.15
TiI_3	I	31 ± 2.0	22.4	8.0	30.4
	II	11.1 ± 1.0	5.6	6.4	12.0
	III	0.98 ± 0.1	0	0.97	0.97

3) In region I, which is taken to be the rigid lattice case, $S_{\text{CH}_3-\text{CH}_3}$ is taken to be 8.0 G^2 based on the work of Smith⁽³⁾. A C-H distance of $1.09 \pm 0.01 \text{ \AA}$ gives S_{CH_3} equal to $22.4 \pm 1.0 \text{ G}^2$ which taken along with $S_{\text{CH}_3-\text{CH}_3}$ shows good agreement for all three compounds.

4) In region II S_{CH_3} is taken to be $\frac{1}{2}$ th of its rigid lattice value whereas in region III intramolecular contribution to S averages out to zero. $S_{\text{CH}_3-\text{CH}_3}$ for the regions II and III are calculated using Van Vleck's⁽⁴⁾ formula assuming that the magnetic moments of the three protons in CH_3 group (in region II) and the twelve protons in TiI_3 (in region III) to be concentrated at the center of their rotation. Calculated values of S in regions II are somewhat higher than S_{obs} and it is noted that the C-H distances should be chosen from the two of

the form given by Tycko(1).

Activation energies for the two motions calculated from the line-shape data using the modified RD formula⁽⁵⁾ are tabulated below:

Molecule	Activation Energy (kcal/mole)	
	$\tau_{1/2}$ group rotation	$\tau_{1/2}$ ion rotation
TMCl	6.5 ± 0.5	3.3 ± 0.9
TMBr	7.5 ± 0.7	12.3 ± 0.7
TMF	6.5 ± 0.5	11.6 ± 0.4

REFERENCES

1. Tycko R.T.G., In Crystal Structures (Edited by R.T.G. Tycko) Vol. 1, p. 107, Wiley, New York (1963).
2. Gutowsky H.S., Luke G.E. and Pataczin R., J. Chem. Phys. 22, 643 (1954).
3. Smith G.T., J. Chem. Phys. 23, 422 (1955).
4. Van Vleck J.H., Phys. Rev. 74, 1169 (1949).
5. Gutowsky H.S. and Luke G.E., J. Chem. Phys. 18, 162 (1950).

FREQUENCY DISTRIBUTION AND THERMODYNAMIC PROPERTIES OF SOLID AMMONIA.

P.S. Goyal, B.A. Dasannacharya, J.L. Tnaper and
P.K. Iyengar

Nuclear Physics Division, Bhabha Atomic Research Centre,
Trombay, Bombay 85.

The one phonon incoherent scattering cross section of neutrons by a molecular solid is given by,⁽¹⁾

$$\left(\frac{d^2\sigma}{d\Omega d\omega} \right)_{inc} \sim \left[\frac{k}{k_0} \frac{\kappa^2}{2m\omega} \eta(\omega, T) \right] g_{eff}(\omega) e^{-2W} \quad (1)$$

if one assumes that the internal modes are well separated from the external modes and the translation-rotation coupling in the external modes can be neglected. Here the symbols have their usual⁽¹⁾ meanings; in particular, e^{-2W} is the well known Debye-Waller factor and $g_{eff}(\omega)$, an effective frequency distribution function (fdf), is a weighted sum of the translational phonon fdf, $g_T(\omega)$, and the rotational fdf, $g_R(\omega)$:

$$g_{eff}(\omega) = g_T(\omega) + \frac{m}{m_R} g_R(\omega) \quad (2)$$

m_R is an effective rotational mass and is less than M , the mass of the molecule. Thus, the rotational scattering appears with an enhanced intensity.

In this paper we report the measurement of $g_{eff}(\omega)$ for solid ammonia at 105°K, and the calculation of some thermodynamic quantities from this. In order to obtain good resolution, energy gain experiments with rotating crystal spectrometer were used for low energy transfers (i.e. low ω) and energy loss experiments with an inverted filter spectrometer were used for energy

transfers larger than $17.5 \text{ meV} [140 \text{ cm}^{-1}]$. The combined data after correction for some instrumental effects and for terms in the square bracket are shown in Fig. (1). The Debye-Waller factor e^{-2W} was corrected for by an iterative procedure.⁽¹⁾ The contribution from multiphonon processes was removed by extending the formulae of Sjolander⁽²⁾ for our case and is shown by the dashed curve in Fig. (1). The final $g_{eff}(\omega)$, derived after these corrections is shown in Fig. (2).

The regions of various peaks show an overall qualitative agreement with the infrared and Raman data.⁽³⁾ On the basis of this comparison, we believe, that the first two peaks arise due to translational motions and the latter ones due to librations. This is also consistent with the fact that the rotational peaks should appear with enhanced intensity. A separation of $g_T(\omega)$ and $\frac{m}{M_R} g_R(\omega)$ on this basis is shown by the dashed line in Fig. (2).

The rotational and translational motions should contribute equal degrees of freedom to the phonon spectrum. One can determine $g_T(\omega)$ and $g_R(\omega)$ on this basis and then proceed to calculate the thermal capacity, C_V , using standard expressions. A comparison of our calculation with measured⁽⁴⁾ thermal capacity is shown in Fig. (3). The agreement is within 2% upto 130°K . Above this temperature the anharmonic effects start becoming important.

In order to make a more sensitive comparison a

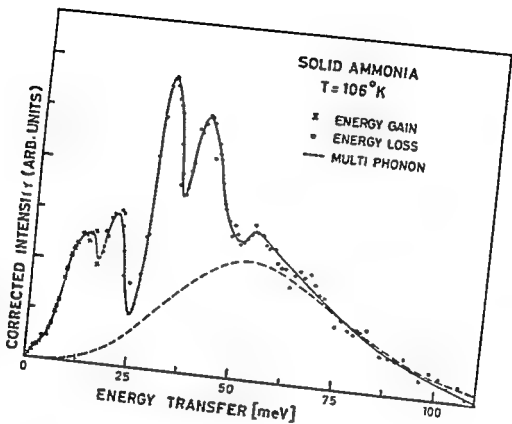


Fig.1. Corrected scattered neutron intensity as function of energy transfer.

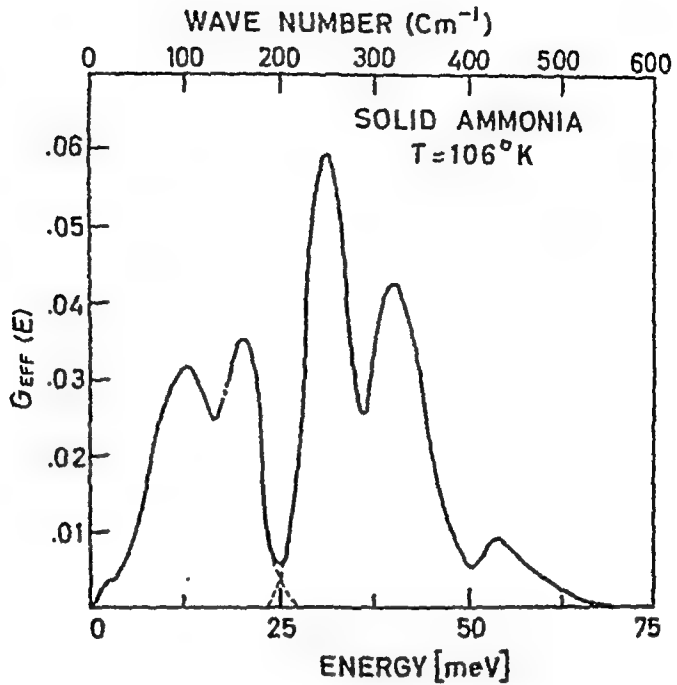


Fig.2. The effective phonon frequency distribution function.

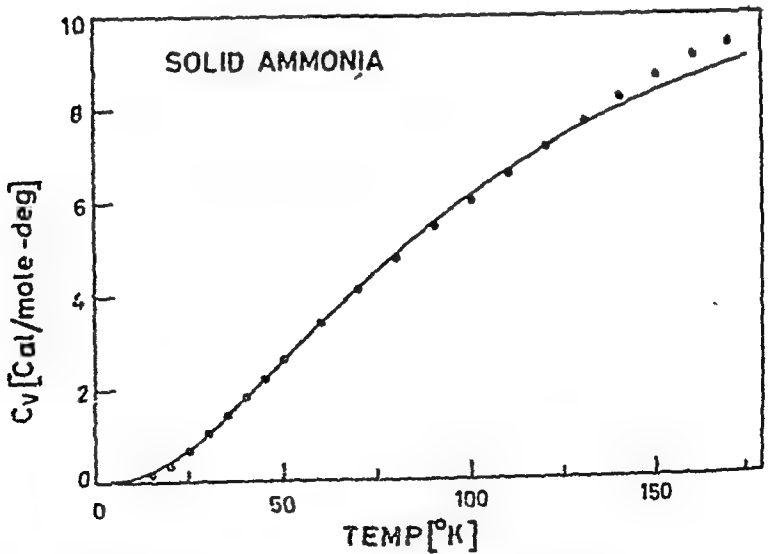


Fig.3. Thermal capacity of solid ammonia. (•) measured — calculated.

moments-analysis of the thermal capacity was performed using a method similar to that used by Leadbetter⁽⁵⁾ for ice. The moments calculated from C_v and fdf are compared in Table I. The agreement is reasonable. The

TABLE I

	TRANSLATIONAL		ROTATIONAL	
	From fdf (cm^{-1})	From C_v (cm^{-1})	From fdf (cm^{-1})	From C_v (cm^{-1})
$(u_{-1})'$	99	114	259	251
$(u_{-2})^{1/2}$	129	120	280	300
$(u_{-4})^{1/4}$	140	127	296	298
$(u_{-6})^{1/6}$	148	131	312	300

cause of the difference in moments could be anharmonicity. This is being examined in greater detail.

The root mean square amplitude, $(\overline{u^2})^{1/2}$, of the vibration of the hydrogen atom in solid ammonia, using our fdf comes to 0.214 Å. This agrees well with that calculated from thermal capacity⁽⁵⁾ data, which gives $(\overline{u^2})^{1/2} = 0.202$ Å.

REFERENCES

1. H. Prask, H. Boutin and S. Yip, J. Chem. Phys. **48**, 3367 (1968).
2. A. Sjölander, Ark. Fys. **14**, 315 (1958).
3. A. Anderson and S.H. Walmsley, Mol. Phys. **9**, 1 (1965)
4. V.G. Manzhelii and A.M. Jolkachev, Soviet Physics - Solid State **8**, 827 (1966).
5. A.J. Leadbetter, Proc. Roy. Soc. (London) **287A**, 403 (1965).

DISCUSSION

M.P. Verma

1) What kind of an agreement is obtained when one compares Θ_D rather than C_V ?

2) What kind of rotational transmissions (parallel to lattice waves) are assumed?

P.S. Goyal

1) The agreement between Θ_D calculated from C_V and from our frequency distribution function is within 2%.

2) The librational waves propagate in a way similar to the translational ones. The problem can be formulated in a similar fashion with suitable force constants for this case.

ANDERSON-GRUNEISEN PARAMETER FOR THE CAESIUM HALIDES

Miss Revathy Raju and T.N. Haridasan
Dept. of Physics, Madurai University, Madurai-2.

1. INTRODUCTION

Anderson(1) when interpreting Watchman's experimental observations of the temperature dependence of the Young's modulus in crystals(2) derived a relationship involving the temperature dependence of adiabatic bulk modulus B_s , the specific heat C_p , atomic volume V and the Gruneisen parameter γ , as

$$\frac{dB_s}{dT} = -\delta \gamma (C_p/V) \dots \dots \dots (1)$$

where δ is called Anderson-Gruneisen parameter, following Chang (3) and is found to be an equally important crystal parameter as γ itself. From the Mie-Gruneisen equation of state, Anderson derived that

$$\delta = \frac{1}{\alpha K_s} \left(\frac{dK_s}{dT} \right) \dots \dots \dots (2)$$

where α is the coefficient of volume expansion and K_s , the adiabatic compressibility. He showed that δ is temperature independent. He(4) also related δ to the pressure derivative of adiabatic compressibility as

$$\delta = -\frac{1}{K_s^2} \left(\frac{dK_s}{dP} \right)_T - (1-q) \dots \dots \dots (3)$$

where q is given by

$$\gamma = \gamma(0) \left(\frac{V}{V_0} \right)^q$$

That is q measures the volume or temperature dependence of γ . Thus it is possible now to unify the temperature and pressure derivatives of compressibility through relations (2) and (3).

The purpose of the present paper is to evaluate δ and q from the recent experimental information on pressure and temperature dependence of elastic constants^(5,6) for the caesiumhalides. The motivation for this is the experimental observation of White⁽⁷⁾ and Bailey and Yates⁽⁸⁾ on the thermal expansion and temperature dependence of γ , of the caesiumhalides, which indicate that γ is temperature independent for these crystals. Hence one expects q to be zero for the caesiumhalides.

II. METHODS OF CALCULATION

The parameter δ is calculated using Eqs (2) and (3) with q put equal to zero. Chang from thermodynamical reasoning has deduced that

$$\delta = 2\gamma \dots \dots \dots (5)$$

This result is found to be more realistic for caesium halides than for the rocksalt type crystals since both γ and δ are known to be temperature independent.

Mathur et al.^(9,10) have computed δ for NaCl type crystals, apart from the above mentioned equations, by using a Born-Mayer potential with nearest neighbour overlap interaction. In fact they derived an expression for δ with a general potential of the type

$$\Phi(V) = -\frac{A}{V^m} + Bf(V) \dots \dots \dots (6)$$

For an interatomic potential of the type

$$\Phi = -A/V^{m/3} + B/V^{n/3} \dots \dots \dots (7)$$

one finds

$$\delta = \frac{m+n}{3} + 2 - \gamma \dots \dots \dots (8)$$

In the present calculation the values $m=1$ and $n=12$ have been used.

For a Born-Mayer potential

$$\phi = \lambda e^{-V/\rho} \dots \quad (9)$$

following Mathur et al.⁽⁹⁾ one can show that

$$\delta = \frac{R}{3\rho} \left[\frac{R}{\rho} - 3 \right] / \left[\frac{R}{\rho} - 2 \right] \quad (10)$$

Where $R = \frac{r}{\sqrt{3}} 4^{\frac{1}{3}} \dots (11)$

r being the nearest neighbour distance. $\frac{R}{\rho}$ has been evaluated from Madlung constant and compressibility, with (1) ionic charge taken to be unity. (2) ionic charge taken to be equal to Sziget's effective charge z^* deduced from infrared data⁽¹¹⁾. Finally δ is evaluated from Eq (5).

III. RESULTS AND CONCLUSIONS

The values of δ evaluated from equations (2), (3), (8), (10) and (5) are given in the table below for the three caesiumhalides.

TABLE I

Crystal	Values of δ computed from Eqs.						q
	(2)	(3) ($q=0$)	(8)	(10) ($z=1$)	(10) ($z=z^*$)	(5)	
CsCl	4.64	4.76	4.27	3.58	4.81	4.12	-.12
CsBr	4.51	4.71	4.33	3.63	5.92	4.00	-.20
CsI	4.44	4.65	4.32	3.76	8.06	4.02	-.21

The values of δ obtained by various means show reasonable agreement. But it is to be noted that δ for Born-Mayer potential with ionic charge 1 is very small, compared to the value obtained from experimental data whereas δ evaluated with Sziget's effective charge is extremely large. This shows that a Born-Mayer potential with only nearest neighbour overlap interaction is not adequate to

explain the values of δ in caesiumhalides. The values of q deduced from Eqs (2) and (3) are negative for caesium halides and are very nearly equal to zero. This is consistent with the experimental observation of Bailey and Yates on the temperature dependence of γ .

We thank Prof. K.S. Chandrasekaran for his keen interest in this work.

REFERENCES

1. O.L. Anderson; Phys. Rev. 144, 553 (1966)..
2. J.B. Watchman, Jr.W.E.Tofft, Jr.D.G. Lam and C.S. Apstein; Phys. Rev. 122, 1754 (1961).
3. Y.A. Chang; J. Phys. Chem. Solids 28, 697 (1967).
4. O.L. Anderson; J.Geophys. Res. 72, 3661 (1967).
5. Y.A. Chang and G.R. Barsh; Phys. Rev. Lett. 19, 1381 (1967).
6. O.D. Slagle and H.A. McKinstry; J.Appl. Phys. 38, 2, 45 (1967).
7. G.K. White; Proc. Roy Soc.(Lon) A286, 204 (1965)
8. A.C. Bailey and B. Yates; Phil. Mag. 16, 1241 (1967).
9. V.K. Mathur and S.P. Singh; J. Phys.Chem.Solids 29, 959 (1968).
10. V.K. Mathur, S.P. Singh and D.R. Vij; J. Chem.Phys. 48, 4784 (1969).
11. G.O. Jones, D.H. Martin, P.A. Hawer and C.H. Perry; Proc. Roy. Soc.(Lon) A261, 10 (1961).

DISCUSSION

Satya Prakash

Did you try to calculate γ from the first principle approach?

2) γ is dependentat on phonon wave-vector. How do you average for this dependence?

T.M. Haridashan

1) I did not.

2) I have deduced the q dependence from the ex-

perimentally available results on temperature and pressure dependence of elastic constants (and hence compressibility) and compared it with the experimentally deduced γ values from thermal expansion measurements.

M.P. Verma

1) Have you studied the temperature and pressure dependence of γ ? If so how does it depend?

2) The n values result in a change in the γ value (ref. Srinivasan and Ganesan). How does your γ value compare with theirs? If there is difference how do you explain?

3) Different physical properties will involve different effective γ and it is difficult to compare one with the other.

T.M. Haridashan

1) I have not studied the temperature and pressure dependence of γ .

2) The change in value of n will definitely alter the value of δ . I was not interested in the dependence of n on γ but on the temperature dependence of γ . The n value which is consistent with the Born Mayer potential must be such that $n \approx \frac{B}{P} - 1$ (see Born and Huang). Thus we have just taken n to be 12.

3) Again it is not the γ_{eff} deduced from different experimental methods that we compared, but it is rather the volume dependence of γ (viz. q) that is compared.

ELASTIC CONSTANTS OF CsI CONTAINING IMPURITY IONS^a

K.M. Kesharvani and Bal K. Agrawal

Physics Department, Allahabad University, Allahabad-2

I. THEORY

The changes in the elastic properties of a crystal of CsCl-structure having substitutional point defects are determined by using a T-matrix method.⁽¹⁻³⁾ For a small concentration p of defects, the perturbed phonon frequencies are

$$\tilde{\omega}_{\vec{k},s}^2 = \omega_{\vec{k},s}^2 + p \operatorname{Re} \langle \vec{k},s | \underline{t}_1(z) | \vec{k},s \rangle, \quad \dots(1)$$

where the notations are those of reference (3), and the impure crystal properties are represented by a tilde. \underline{t}_1 , the T-matrix for a single defect is given by

$$\underline{t}_1(z) = \underline{P}_1(\omega^2) [\underline{I} + \underline{g}^0(z) \underline{P}_1(\omega^2)]^{-1}, \quad \dots(2)$$

The symmetry properties of this T-matrix are discussed in reference (3) in detail. From the knowledge of phonon frequencies $\tilde{\omega}_{\vec{k},s}$ and their group velocities, we determine the elastic constants of the impure crystal. Up to the first order in concentration, the perturbed elastic constants are

$$\begin{aligned} \tilde{C}_{11} &= C_{11}^0 + \frac{2p}{3a} \left[\frac{\lambda}{1+\lambda/v_{1E}} + \frac{2\lambda'}{1+\lambda'/v_E} \right] \\ \tilde{C}_{12} &= C_{12}^0 + \frac{2p}{3a} \left[\frac{\lambda}{1+\lambda/v_{1E}} - \frac{\lambda'}{1+\lambda'/v_E} \right] \quad \dots(3) \\ \tilde{C}_{44} &= C_{44}^0 + \frac{p}{3a} \frac{2\lambda\lambda' + (3\lambda\lambda'/v_{2E}^2)}{1+\lambda/v_{2E}^2} \end{aligned}$$

and the change in the bulk modulus is

$$\Delta K = \frac{2p}{a} \frac{\lambda}{1+\lambda/f_{1g}}, \quad \dots(4)$$

where a is the interatomic distance. λ and λ' are the central force constant and noncentral force constant changes (hereafter CFC and NCFC) in the units of squared frequency. C^0 's are elastic constants of the perfect crystal, f 's are the effective force constants and are determined by different combinations of the various Green's function matrix elements. f_{1g} , f_g and f_{2g} denote the contributions made by A_{1g} , E_g and F_{2g} irreducible representations, respectively. The contributions of all other irreducible representations either vanish or are $O(k^4)$ which are neglected.

II. CALCULATIONS AND RESULTS

Using Eqs. (3) and (4), the bulk elastic constants and the bulk modulus are calculated for a CsI crystal containing impurity ions Rb^+ , K^+ and Tl^+ . The CFCs due to the impurities are taken from the infrared lattice absorption experiments. These experiments have successfully been explained recently by our group⁽⁴⁾ after using a central force constant model for the defect. These changes for different impurity ions are presented in Table I. We assume that NCFC's are less than the CFC's. Both positive or negative changes have been considered for determining the modified elastic constants. For the sake of comparison, results are also computed for CFC only. The Green function matrix elements $g(z)$ for CsI have been computed by Ram and Agrawal⁽⁴⁾ in the Breathing Shell

model. The values $g(0)$ are utilised for calculating the parameters f 's. The results for the three host impurity systems for a fractional concentration 0.05 of impurities are presented in Tables II-IV. The elastic constants for the pure CsI are taken from Marshall and Kunkel.⁽⁵⁾ The experimental measurements of the elastic constants for CsI containing impurity ions are not available. In order to have an idea of the observed changes in the elastic constants due to impurities, we present the results of the experimental measurements of these effects in the case of dilute alloys of Nickel i.e. Ni-Fe(10.8%)⁽⁶⁾ and Ni-Co (10%)⁽⁷⁾ in Table-V. From these tables we may conclude that the calculated changes are in reasonable agreement with experimental results. The detailed calculations and results will be published elsewhere.

REFERENCES

1. R.J. Elliott, J.A. Krumhansl and T.H. Merrett in Proceedings of the International Conference on Localized Excitation in Solids 1967, Plenum Press p. 709 (1968).
2. G. Benedek and G.F. Kardelli, Phys. Rev. 167, 837(1968).
3. Bal K. Agrawal, Phys. Rev. 186, 712(1969).
4. P.N. Ram and Bal K. Agrawal, to be communicated for publication.
5. B.J. Marshall and J.R. Kunkel, J. Appl. Phys. 40, 5191 (1969).
6. D.I. Bower, E. Claridge and I.S.T. Tsong, Phys. Status Solidi 29, 617(1968).
7. H.J. Leaty and H. Warlimont, Phys. Status Solidi, 37, 623(1970).

Table-I Changes in central force constant deduced from Infrared Lattice Absorption data.⁽⁴⁾

System	$\Delta f/M^+ (10^{25} \text{ sec}^{-1})$	$\Delta f (10^4 \text{ g sec}^{-1})$
CsI:Rb ⁺	-0.07	-0.154
CsI:K ⁺	-0.11	-0.243
CsI:Tl ⁺	-0.33	-0.728

Table-II Percentage changes in the elastic constants of CsI containing a fractional concentration .05 of Rb⁺

$\Delta f'/\Delta f$	$\bar{C}_{11} - C_{11}^0$	$\bar{C}_{12} - C_{12}^0$	$\bar{C}_{44} - C_{44}^0$	ΔK
-0.125	-0.4	-2.1	-1.6	-1.0
0.0	-0.6	-1.9	-1.7	-1.0
0.125	-0.7	-1.7	-1.8	-1.0

Table-III percentage changes in the elastic constants of CsI containing a fractional concentration .05 of K⁺

$\Delta f'/\Delta f$	$\bar{C}_{11} - C_{11}^0$	$\bar{C}_{12} - C_{12}^0$	$\bar{C}_{44} - C_{44}^0$	ΔK
-0.125	-0.7	-3.6	-2.8	-1.7
0.0	-0.9	-3.2	-2.9	-1.7
0.125	-1.1	-2.9	-3.1	-1.7

Table-IV percentage changes in the elastic constants of CsI containing a fractional concentration .05 of Tl⁺

$\Delta f'/\Delta f$	$\bar{C}_{11} - C_{11}^0$	$\bar{C}_{12} - C_{12}^0$	$\bar{C}_{44} - C_{44}^0$	ΔK
-0.125	-4.1	-17.4	-16.9	-8.9
0.0	-4.6	-16.5	-17.5	-8.9
0.125	-5.2	-15.4	-18.2	-8.9

$C_{11}^0 = 2.725 \times 10^{11}$, $C_{12}^0 = 0.767 \times 10^{11}$, $C_{44}^0 = 0.873 \times 10^{11}$ in dynes/cm²

Table-V Percentage changes in the experimentally measured elastic constants for Ni-Fe⁽⁶⁾ and Ni-Co⁽⁷⁾ alloys.

System	$\bar{C}_{11} - C_{11}^0$	$\bar{C}_{12} - C_{12}^0$	$\bar{C}_{44} - C_{44}^0$	ΔK
Ni-Fe	-2.6	-1.3	-0.7	-1.9
Ni-Co	-3.6	1.5	-4.2	-0.9

$C_{11}^0 = 2.612 \times 10^{12}$, $C_{12}^0 = 1.508 \times 10^{12}$, $C_{44}^0 = 1.317 \times 10^{12}$ in dynes/cm²

*Work supported by C.S.I.R., INDIA.

GROUP THEORETICAL STUDY OF LATTICE DYNAMICS OF KN_3 , NaN_3 AND NaNO_3

K.R. Rao

Nuclear Physics Division, Bhabha Atomic Research Centre,
Trombay, Bombay 85
and S.F. Trevino
Picatinny Arsenal, Dover, New Jersey, U.S.A.

I. INTRODUCTION

The application of group theory to the study of molecular vibrations and of little groups technique to lattice vibrations are well known. Recently Maradudin and Vosko¹ developed a procedure, wherein the irreducible multiplier representations of groups are used to study symmetry properties of lattice vibrations in crystals. This method is quite general and powerful to study crystals of any complex structure containing large number of atoms and 'molecules' in the unit cell.

II. THEORY

Let $\{S\}$ denote the set of space group operations of a crystal, the operation S being denoted by

$\{ \underline{S} | \underline{u}(S) + \underline{x}(\mathbf{r}) \}$ in Seitz's notation.

$G(\mathbf{q})$, the space group of \mathbf{q} , a wavevector of the lattice, consists of those operations $\{R\}$ of $\{S\}$ which have the property that

$$\underline{R} \mathbf{q} = \mathbf{q} - \underline{G}' \quad (1)$$

\underline{G}' being a reciprocal lattice vector. One can associate a matrix representation $\{T(\mathbf{q}, \underline{R})\}$ with the point group of the wavevector $G_0(\mathbf{q})$, underlying the space group $G(\mathbf{q})$.

The multiplication rule for this representation is

$$\underline{T}(\underline{q}, \underline{R}_i) \underline{T}(\underline{q}, \underline{R}_j) = \phi(\underline{q}, \underline{R}_i, \underline{R}_j) \underline{T}(\underline{q}, \underline{R}_i, \underline{R}_j) \quad (2)$$

where $\phi(\underline{q}, \underline{R}_i, \underline{R}_j)$ is a multiplier. This representation is known as a Multiplier Representation. The associated Irreducible Multiplier Representations (IMR) are given in books by Kovalev² and Slater.³ Recently Sahni and Venkataraman⁴ have outlined a method to deduce these IMRs.

If there are r atoms and r' 'molecules' in the primitive unit cell one can define a $3r + 6r'$ dimensional dynamical space (Each of the atoms and 'molecules' have three degrees of freedom of translations and in addition each of the 'molecules' have three more degrees of freedom associated with the rotations in general. Hence the $(3r+6r')$ dimension). The matrix representation $\underline{T}(\underline{q}, \underline{R})$ is defined in this $(3r + 6r')$ dimensional space by the elements

$$T_{\alpha\beta}(\underline{q}, k, k', \underline{R}) = \exp\{i\underline{q} \cdot [\underline{x}(k) - \underline{R}\underline{x}(k')]\} \delta(k, K) \det |\underline{R}|_{(3)}$$

α and β are components of motion of k^{th} and k'^{th} constituents (atoms or 'molecules') in the unit cell. α and β go over the cartesian components (x, y, z) if k or k' are atoms and over $(x, y, z, \theta_x, \theta_y, \theta_z)$ if k or k' are 'molecules', $\theta_x, \theta_y, \theta_z$ denoting rotations about x, y or z axis. K is the label of the sublattice reached as a result of the operation R or k' . The factor $\det |\underline{R}|$ does not enter if α and β are translational

components. $\det [\underline{R}] = +1$ for proper rotations and -1 for improper rotations.

The $\underline{T}(\underline{q}, \underline{R})$ matrices have a central role in Maradudin and Vosko's formalism. These matrices have the properties:

- (a) They are unitary
- (b) They commute with the dynamical matrix $\underline{D}(\underline{q})$
i.e. $\underline{T}^{-1}(\underline{q}, \underline{R}) \underline{D}(\underline{q}) \underline{T}(\underline{q}, \underline{R}) = \underline{D}(\underline{q})$
Hence $\underline{D}(\underline{q})$ can be 'reduced'.
- (c) $\underline{T}(\underline{q}, \underline{R})$ s are reducible. c_s , the number of times s^{th} IMR is contained in $\underline{T}(\underline{q}, \underline{R})$ is given by

$$c_s = \frac{1}{h} \sum_{R \in G_0(\underline{q})} \chi(R) \{ \chi^s(R) \}^*$$

Here h is order of group $G_0(\underline{q})$, $\chi(R)$ the character of $\underline{T}(\underline{q}, \underline{R})$ and $\chi^s(R)$ is character of Matrix representation of R in the s^{th} IMR.

- (d) Projection operator techniques can be used to construct a matrix $\underline{\Xi}(\underline{q})$ of the wavevector adapted symmetry vectors. $\underline{\Xi}(\underline{q})$ can be used to diagonalize the 'reduced' $\underline{D}(\underline{q})$ by the relation

$$\underline{\mathcal{D}}(\underline{q}) = \underline{\Xi}^+(\underline{q}) \underline{D}(\underline{q}) \underline{\Xi}(\underline{q})$$

$\underline{\mathcal{D}}(\underline{q})$ is block diagonalised form of $\underline{D}(\underline{q})$.

III. RESULTS

We have used the approach given in section II to study three crystals characterised by Table I.

The multiplication rule for this representation is

$$\underline{T}(\underline{q}, \underline{R}_i) \underline{T}(\underline{q}, \underline{R}_j) = \phi(\underline{q}, \underline{R}_i, \underline{R}_j) \underline{T}(\underline{q}, \underline{R}_i, \underline{R}_j) \quad (2)$$

where $\phi(\underline{q}, \underline{R}_i, \underline{R}_j)$ is a multiplier. This representation is known as a Multiplier Representation. The associated Irreducible Multiplier Representations (IMR) are given in books by Kovalev² and Slater.³ Recently Sahni and Venkataraman⁴ have outlined a method to deduce these IMRs.

If there are r atoms and r' 'molecules' in the primitive unit cell one can define a $3r + 6r'$ dimensional dynamical space (Each of the atoms and 'molecules' have three degrees of freedom of translations and in addition each of the 'molecules' have three more degrees of freedom associated with the rotations in general. Hence the $(3r+6r')$ dimension). The matrix representation $\underline{T}(\underline{q}, \underline{R})$ is defined in this $(3r + 6r')$ dimensional space by the elements

$$T_{\alpha\beta}(\underline{q}, k, k', \underline{R}) = \exp\{i\underline{q} \cdot [\underline{x}(k) - \underline{R}\underline{x}(k')]\} \delta(k, K) \det |\underline{R}| \quad (3)$$

α and β are components of motion of k^{th} and k'^{th} constituents (atoms or 'molecules') in the unit cell. α and β go over the cartesian components (x, y, z) if k or k' are atoms and over $(x, y, z, \theta_x, \theta_y, \theta_z)$ if k or k' are 'molecules', $\theta_x, \theta_y, \theta_z$ denoting rotations about x, y or z axis. K is the label of the sublattice reached as a result of the operation R or k' . The factor $\det |\underline{R}|$ does not enter if α and β are translational

components. $\det |\underline{R}| = +1$ for proper rotations and -1 for improper rotations.

The $\underline{T}(\underline{q}, \underline{R})$ matrices have a central role in Maradudin and Vosko's formalism. These matrices have the properties:

(a) They are unitary

(b) They commute with the dynamical matrix $\underline{D}(\underline{q})$

$$\text{i.e. } \underline{T}^{-1}(\underline{q}, \underline{R}) \underline{D}(\underline{q}) \underline{T}(\underline{q}, \underline{R}) = \underline{D}(\underline{q})$$

Hence $\underline{D}(\underline{q})$ can be 'reduced'.

(c) $\underline{T}(\underline{q}, \underline{R})$ s are reducible. c_s , the number of times s^{th} IMR is contained in $\underline{T}(\underline{q}, \underline{R})$ is given by

$$c_s = \frac{1}{h} \sum_{R \in G_0(\underline{q})} \chi(R) \{ \chi^s(R) \}^*$$

Here h is order of group $G_0(\underline{q})$, $\chi(R)$ the character of $\underline{T}(\underline{q}, \underline{R})$ and $\chi^s(R)$ is character of Matrix representation of R in the s^{th} IMR.

(d) Projection operator techniques can be used to construct a matrix $\underline{\Xi}(\underline{q})$ of the wavevector adapted symmetry vectors. $\underline{\Xi}(\underline{q})$ can be used to diagonalize the 'reduced' $\underline{D}(\underline{q})$ by the relation

$$\underline{\mathcal{D}}(\underline{q}) = \underline{\Xi}^+(\underline{q}) \underline{D}(\underline{q}) \underline{\Xi}(\underline{q})$$

$\underline{\mathcal{D}}(\underline{q})$ is block diagonalised form of $\underline{D}(\underline{q})$.

III. RESULTS

We have used the approach given in section II to study three crystals characterized by Table I.

TABLE I

Crystal	Space Group	Crystal Class	Model	3r+6r'
NaN ₃	D _{3d} ⁵	Rhombohedral	Atomic	12
			Molecular	9
KN ₃	D _{4h} ¹⁸	Tetragonal	Molecular	18
NaNO ₃	D _{3d} ⁶	Rhombohedral	Molecular	18

We have (i) labelled the branches of $\mathcal{D}(\mathbf{q})$ according to various IHR's; determined the degeneracies if any

(ii) reduced $\underline{\underline{D}}(\mathbf{q})$

(iii) determined the symmetry vectors;

(iv) block diagonalised $\underline{\underline{D}}(\mathbf{q})$ to obtain $\underline{\underline{\mathcal{D}}}(\mathbf{q})$

for several wavevectors in the Brillouin zone. The most important aspect of our work has been the 'computerisation' of the problem including determination of the algebraic relations connecting different elements of $\underline{\underline{D}}(\mathbf{q})$ that 'reduce' $\underline{\underline{D}}(\mathbf{q})$. A generalisation of the program is underway.

REFERENCES

1. A.A. Maradudin and S.H. Vosko Revs. Mod. Phys. 40, 1 (1968).
2. O.V. Kovalev Irreducible Representations of the Space Groups, Gordon and Breach Science Publishers, New York (1964).
3. J.C. Slater Quantum Theory of Molecules and Solids II, McGraw Hill Book Co., New York (1965).
4. V.C. Sahni and G. Venkataraman. Phys. Kond. Materie 11, 199 (1970).
Ibid 11, 211 (1970).

DISCUSSION

G. Venkatraman

I would like to make the general observation that spectroscopists often tend to think that a factor group analysis done, say, a la Bhagawantam and Venkatarayudu, constitutes a complete group theoretic classification of the vibrational modes. It does not. The B-V method does the job only for the $q = 0$ modes. For the other regions of the Brillouin cone (and these have become interesting now owing to the availability of extensive data), one must use the little-group approach or the multiplier-representation approach as discussed in this paper.

P.S. Narayanan

In the analysis of 1st order Raman and Infrared spectra the factor group analysis method of Bhagawantam and Venkatarayudu is adequate since only the frequencies corresponding to $q \sim 0$ are observed. But it was recognised even by B-V that this method has to be extended by space group analysis for explaining 2nd order processes. Therefore the development of little group is useful.

G. Venkataraman

In making my comment it was certainly not my intention to imply that B-V themselves were not aware

of the limitations of the factor-group approach. Only that many others who use the B-V method do not seem to appreciate its restricted validity. I do, however, readily concede that the factor-group method is quite adequate in the context of first order infrared and Raman spectra. I claim, nevertheless, that it is not adequate for classifying polariton branches even though in this case also $q \sim 0$.

R. Srinivasan

Spectroscopic investigations deal with phonons with q close to zero. Ordinary group theoretical analysis deals with $q = 0$. Will the little group analysis give significantly different results from the conventional one as regards polarisation and activity?

K.R. Rao

Conventional group theoretical results (of say the factor group method) pertain to exactly $q = 0$. The point group associated with $q = 0$, $G_0(0)$, is isomorphic with the point group of the lattice itself. On the other hand when we consider finite \underline{q} , however small they may be, the corresponding groups of the wave vectors $G_0(\underline{q}$'s) differ from $G_0(0)$ and also from each other depending on the direction of \underline{q} . Hence the results obtained by little group technique or by using

the irreducible multiplier techniques should yield different results. For example any of the degeneracies at $q = 0$ will be lifted at q -finite in many examples. So also the polarisation vectors will be different with respect to the wave vector. Off-hand I am unable to say about the infrared activity;



DISPERSION RELATIONS FOR PHONONS IN KN_3

K.R. Rao

Nuclear Physics Division, Bhabha Atomic Research Centre,
Trombay, Bombay 85.

S.F. Trevino and H. Prask

Picatinny Arsenal, Dover, New Jersey, U.S.A.
and

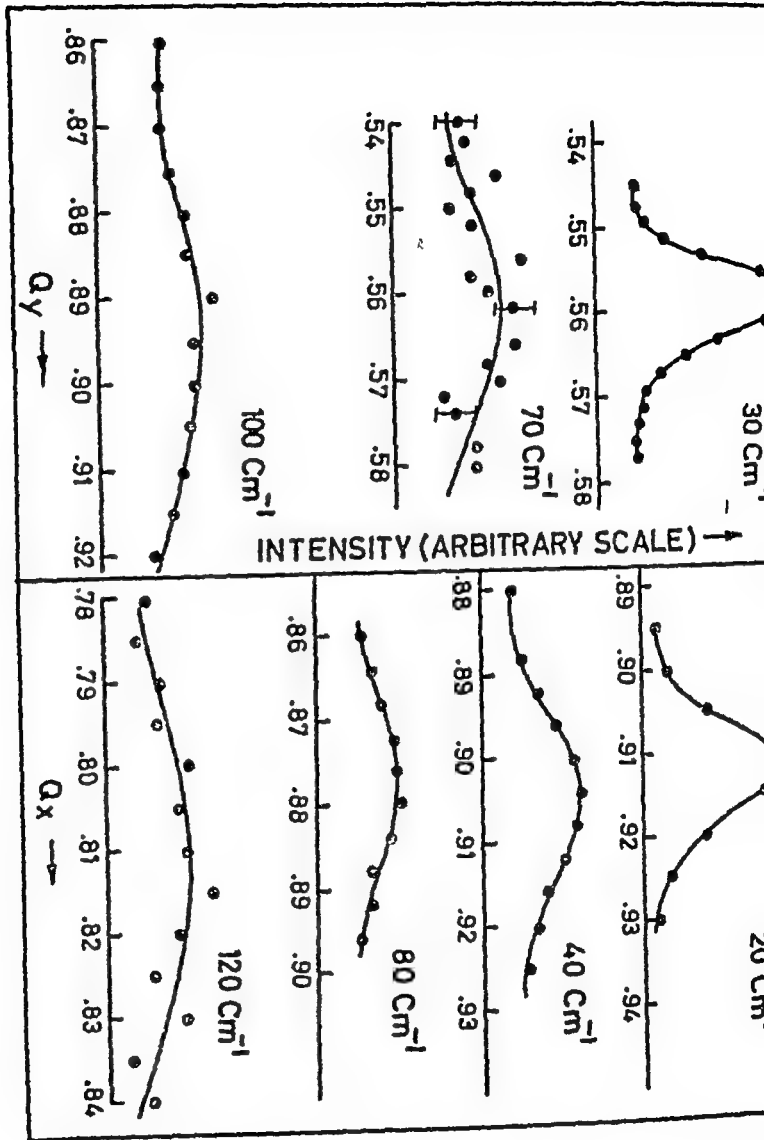
R. Mical

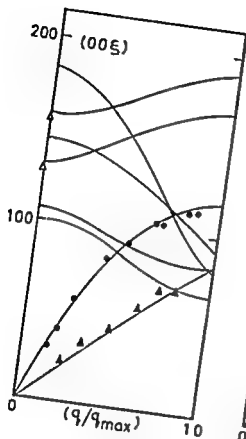
Massachusetts Institute of Technology,
Cambridge, Mass. U.S.A.I. INTRODUCTION

The Inorganic azides form a family of compounds exhibiting various degrees of stability. $\alpha\text{-PbN}_3$ and $\text{Ba(N}_3)_2$ have complex structures and differ markedly in their explosive behaviour. In contrast, several of the stable alkali metal azides possess, very nearly the same relatively simple crystal structure as AgN_3 , a sensitive primary explosive. A knowledge of lattice dynamics of the alkali azides may, therefore help in understanding this behaviour of varying degrees of stability in azides. In this paper we report results of coherent inelastic neutron scattering studies from KN_3 at room temperature. This is the first of such studies in any azide.

II. EXPERIMENTAL

No single crystal of sufficiently large size was available for the experiments. A pseudo-single crystal, composed of 25 solution-grown KN_3 "crystalites" (each of $\sim 1.5 \times 1.5 \times 0.2$ cm), was built up. The measurements were carried out on the Picatinny Arsenal triple axis spectrometer at the 5 MW AMMRC - Reactor at Watertown, Mass.





Rocking curve of the sample crystal had a FWHM of $\sim 1.5^\circ$. Longitudinal and transverse acoustic phonons were measured along $(0\ 0\ \xi)$ and $(\xi\ \xi\ 0)$ directions. Typical phonons are shown in Fig. 1. Most of the measurements were carried out in the 'constant E' mode of scans as peak intensities in the 'Constant Q' scans were rather weak. Focussing effects were extensively employed in these studies. The progressive increase in the width of phonons as we reach the zone boundary phonons may be due to a combination of focussing and life time effects. Optical phonons have not been observed so far.

III. DISCUSSION

A rigid ion model is employed to analyse the experimental data. The following assumptions are made

- (1) only external mode analysis is adequate
- (2) there is no rotation - translation coupling
- (3) Huggins-Mayer type potential describes the repulsive interaction in the system. Only two parameters - the effective charge and a parameter b in the repulsive potential - were treated as adjustable. By successive adjustments to the branches in the $(0\ 0\ \xi)$ direction, these parameters were derived. The dispersion relations calculated are shown in Fig. 2. Experimental points are shown by closed circles. A more detailed model is being developed and details of this study will be published elsewhere.

OPTICAL PHONONS IN MOLECULAR CRYSTALS OF HALOGENS

Y.S. Jais and H.D. Bist

Department of Physics

Indian Institute of Technology, Kanpur-16

I. INTRODUCTION

In this paper we suggest a model to explain the observed infrared (ir) absorption and Raman scattering by the optical phonons in halogen crystals which can not be understood satisfactorily considering only two coplanar molecules in a unit cell⁽¹⁻³⁾.

II. DISCUSSION

X-ray diffraction studies in the polycrystalline films of halogens indicate that all of them exhibit a molecular layer structure and belong to γ_h^{18} space group with four molecules per unit cell⁽⁴⁻⁶⁾. This structure in which each molecule is located at the site C_{2h} is shown schematically in the left half of Fig. 1 and is hereafter referred to as model I. An analysis based on this model does not explain the invariably observed internal modes of halogens in the ir spectra of all these crystals. A better comprehension of the optical phonons could be achieved if our suggestion regarding a model having 4 molecules in a unit cell and belonging to space group γ_h^{16} is valid for the crystal structure. A schematic diagram for the suggested model (referred to as model II) is shown in the right half of Fig. 1.

In model II the halogen molecules are constrained to have C_s site symmetry by displacing them with respect to their positions in model I by a small but finite amount in the bc plane; thus destroying the centre of inversion falling on their inter atomic axis. Model II maintains close consistency with the structure assigned from X-ray techniques in the sense that the dimensions of the unit cell and the separations between molecular layers have been maintained. The displacements are fixed

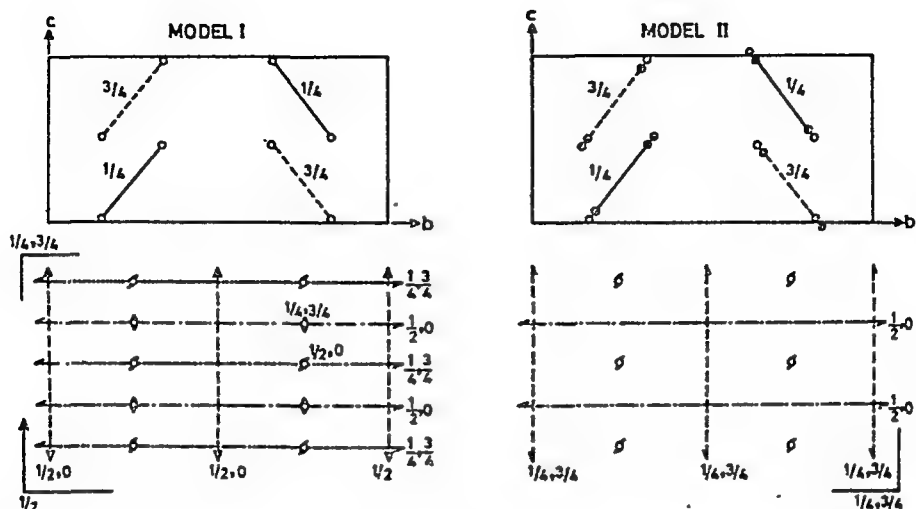


FIG. 1. Projection of crystal structure of halogens in bc plane in models I and II with existing symmetries shown underneath. The original halogen positions denoted by open circles (\circ) have been displaced to take positions of filled circles (\bullet) in model II. Standard notations are used to denote: the mirror (—) the glide (---), the diagonal glide (---) planes; the two fold (\rightarrow , $\frac{1}{2}$), the two fold screw (\rightarrow , $\frac{1}{2}$) axes and inversion centres (O). The fractional numbers denote the height in terms of lattice constant a .

to convert model I to model II may possibly be undetectable by X-ray techniques.

Taking 4 molecules per unit cell, the spectral activity and polarizations of fundamental optical phonons and acoustic modes have been summarized in Table 1 for both model I (column 4) and model II (column 6).

Table 1: Symmetry species of fundamental phonons in halogen crystals

Types of motion	Iso- lated $D_{\infty h}$	Symmetry			
		Crystalline state			
		Model I		Model II	
		Site C_{2h}	Crystal D_{2h}^*	Site C_s	Crystal D_{2h}
Translation	Σ_u^+	B_u	$2B_{2u} + B_{1u} + B_{3u}^*$	A'	$A_g + B_{1g} + B_{2g} + B_{3g}^*$
	Π_u	A_u	$2A_u + B_{3u} + B_{2u}^*$	A''	$B_{1g} + B_{2g} + A_u + B_{3g}^*$
		B_u	$2B_{1u} + B_{2u} + B_{3u}^*$	A'	$A_g + B_{1g} + B_{2g} + B_{3g}^*$
Rotation		A_g	$2A_g + 2B_{3g}$	A'	$A_g + B_{1g} + B_{2g} + B_{3g}^*$
	Π_g	B_g	$2B_{1g} + 2B_{2g}$	A''	$B_{1g} + B_{2g} + A_u + B_{3g}^*$
Vibration	Σ_g^+	A_g	$2A_g + 2B_{3g}$	A'	$A_g + B_{1g} + B_{2g} + B_{3g}^*$

† In these columns B_{1u} , B_{2u} and B_{3u} denote the infrared (ir) active modes polarized along x, y and z-axis, respectively. All the modes with g subscript are Raman active. The u species (except A_u) are ir active.

* Indicates the acoustic modes.

The available ir and Raman data have been summarized in Table II where our tentative assignments (column 5) based on model II have been given along with those of earlier workers⁽²⁻⁵⁾ (column 4).

Model II explains the occurrence of the internal modes in the ir spectra of all these crystals (cf. Table II). The intensity distribution in the Raman spectra also supports the model in the sense that the two most intense bands could be attributed to the librational modes⁽⁷⁾. The splittings observed in Raman scattering in the internal phonon region and the occurrence of only two prominent bands in ir in the translatory phonon region also support model II.

Table II : Observed optical phonons and their assignments in halogen crystals

Band positions [†] (in cm ⁻¹)			Suggested Assignments [‡]	
Cl ₂	Br ₂	I ₂	Earlier [†]	Model II
Raman				
533 (s)	294 (s)		A _g (Im)	A _g (Im)
529 (w)	296 (w)		Iso(Im)	Iso (Im)
522(vv)			Iso(Im)	Iso (Im)
	301(vv)		B _{3g} (Im)	B _{3g} (Im)
138(vv)	110(vv)		B _{3g} (L)	B _{1g} +B _{2g} (T)
113 (s)	96 (s)		A _g (L)	A _g +B _{3g} (L)
94 (s)	92 (s)		B _{2g} (L)	B _{1g} +B _{2g} (L)
77(vv)	70(vv)		B _{1g} (L)	A _g +B _{3g} (T)
	53(vv)		B _{1g} ?	A _g +B _{3g} (T)
Infrared				
	203 (w)	211(v) 210**	?	B _{1u} +B _{2u} (Im)
50 (s)	74 (s)	65(s) 61**	B _{2u} (T)	B _{2u} (T)
62 (s)	48 (s)	41(s) 41**	B _{3u} (T)	B _{3u} (T)
?	?	?		B _{1u} +B _{2u} (L) +B _{3u}

[†]The Raman data are from references (2) and (3); and ir data are from reference (1) (our ir absorption data for solid iodine taken at RT using nujol mull technique have been shown in the table with double asterisk. Symbols (s), (v) and (vv) have been used to denote strong, weak and very weak intensities.

[‡]The translational, librational, and internal modes have been denoted by (T), (L) and (Im) respectively. 'Iso' represents A_g type mode corresponding to the isotopic species.

[†]Assignments of Raman lines are from references (2) and (3) and those of ir bands are from reference (1).

The absence of a few additional expected librational bands in the ir spectra for model II may be due to very small change in dipole moment for these modes. Single crystal work on iodine would be necessary to unequivocally support the above model.

The authors are grateful to Professor P. Venkateswarlu for helpful discussions during the course of work. Thanks are due to the CSIR

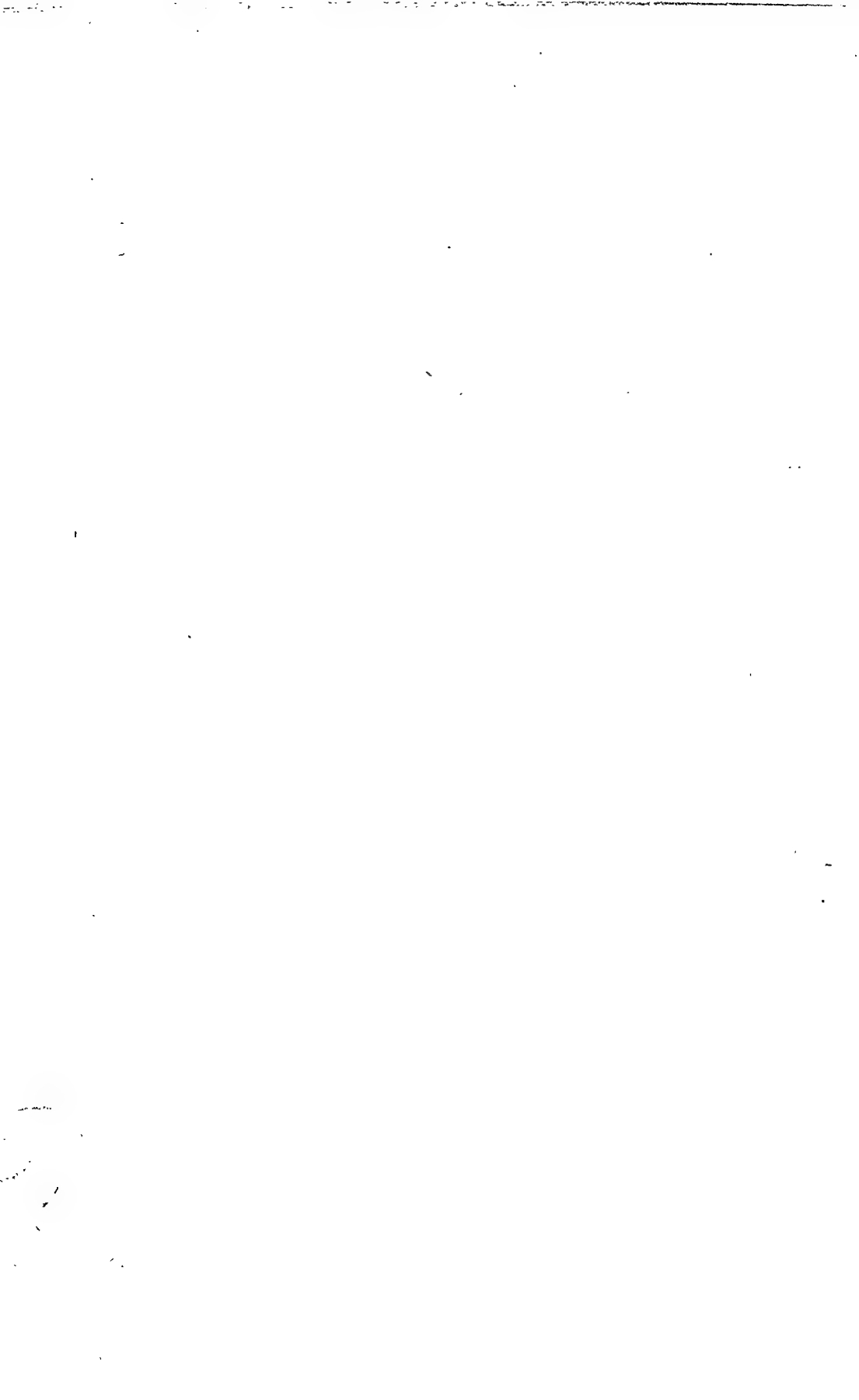
REFERENCES

1. S.H. Walmsley, and A. Anderson, Mol. Phys. 7, 411 (1964).
2. K. Suzuki, T. Yokoyama and K. Ito, J. Chem. Phys. 50, 3392 (1969).
3. K. Suzuki, T. Yokoyama and K. Ito, J. Chem. Phys. 51, 1929 (1969).
4. R.L. Collin, Acta, Cryst., 2 431 (1952); 9, 537 (1956).
5. B. Vonnegut, and B.J. Warren, J. Amer. Chem. Soc. 58, 2459 (1936).
6. A.I. Kitaigirovski, G.L. Khetsyanova, and Y.T. Struchov, J. Phys. Chem., Moscow, 27, 720 (1951).
7. S. Bhagavantam, and T. Venkataramu, Proc. Ind. Acad. Sci. A9, 224 (1939).

DISCUSSION

K.S. Chandrasekaran

X-ray diffraction gives straight forward information about the symmetry elements of the unit cell. Centre of symmetry is also unambiguously found by statistical methods as well as by anomalous scattering techniques for non-centrosymmetric cases. After finding the structure (i.e., the positions of the atoms in the unit cell) by comparing calculated and observed diffraction intensities, information on local symmetry is also obtained.



LIBRATIONAL AND VIBRATIONAL STRETCHING IN BARIUM CHLORATE MONOHYDRATE AT LIQUID NITROGEN TEMPERATURE

Y.S. Talar and H.D. Bist
Indian Institute of Technology, Kanpur-16
and

D.P. Khandelwal
R.B. Technological Institute, Kanpur-2

I. INTRODUCTION

Several examples of the complementary aspects of infrared (ir) and neutron inelastic scattering (nis) studies have been discussed in literature⁽¹⁾. Here we present a detailed analysis of the ir spectra of barium chlorate monohydrate (hereinafter called BCM) in the range 250-4000 cm^{-1} in conjunction with the available nis data.

II. EXPERIMENTAL

The salt BCM was obtained from Fluka (Switzerland). The deuterate was prepared with D_2O (99.4% pure) obtained from BAPC, Tromba, Borba. The ir spectra of the salt in KBr pellets were recorded with Perkin-Elmer 521 spectrophotometer using Tagnor-Hornig type cell in the temperature range -193° to $+190^\circ\text{C}$ keeping the optical geometry unchanged.

III. RESULTS

The observed positions of the bands and their assignments are given in Table I. The bands in the regions 3300-3600 cm^{-1} and 1500-1630 cm^{-1} obviously correspond to the stretching (ν_a and ν_s) and bending (ν_b) modes of H_2O . The translational modes of both H_2O and ClO_3^- , as well as the librational modes of ClO_3^- would fall below 250 cm^{-1} . Among the internal modes of ClO_3^- the ν_1 , ν_2 and ν_3 modes could be identified by comparing with the corresponding bands in BaClO_3 ⁽²⁾. The ν_4 bands, expected in the librational region⁽³⁾ of water, were identified on the basis of their differential behaviour with respect to other bands on controlled variation of temperature.

Table I: Vibrational frequencies of barium chlorate monohydrate at 300°K

Frequency (cm^{-1})	Absorbance (arb.)	Half-width (cm^{-1})	Assignment	Frequency (cm^{-1})	Absorbance (arb.)	Half-width (cm^{-1})	Assignment
392	.09	32	T	939	.78	6	ν_1
457	.26	13	R	963	1.48	20	ν_3
489	.45	4	ν_4	983	1.27	20	ν_3
489	.50	4	ν_4	1002	.77	13	ν_3
500	.17	3	ν_4	1593	.29	9	ν_b
504	.18	4	ν_4	1614	.31	14	ν_b
570	.41	36	w(?)	3380	.55	30	ν_B
613	.34	15	ν_2	3430	.29	30	ν_A
918	.29	22	ν_1	3510	.15	20	ν_B
932	.37	4	$1\nu_1$	3570	.13	35	ν_A

(ii) H_2O content (partial dehydration), and (iii) D_2O substitution.

Crystalline BCT belongs to C_{2h}^6 space group with four molecules per unit cell⁽⁴⁻⁵⁾. The site symmetries of ClO_3^- and H_2O in the unit cell may be shown to be C_1 and C_2 respectively. The deduced site- and factor-group-splittings for both ClO_3^- and H_2O in BCT are given in Table II. Since there are 4 water molecules per unit cell each mode of isolated H_2O will split into four, out of which two will be active in ir. This is corroborated in the spectrum where each of the internal modes of H_2O exhibits a doublet.

In the case of ClO_3^- we expect site symmetry splitting (in ν_3 and ν_4 bands only), factor group splitting (e.g. $2A_u + 2B_u$), and isotopic splitting (due to $^{35,37}\text{Cl}$). The magnitude of site splitting is expected to be the largest. In factor group splittings the separation between the two A_u or between two B_u species may be too small, so that A_u to E_u separation alone may be observed. For isotopic splitting the expected magnitudes⁽²⁾ in cm^{-1} are close to 8 (ν_1), 4.5 (ν_2), 11.3 (ν_3) and 1.2 (ν_4) with relative intensities 3:1 for ^{35}Cl and ^{37}Cl species. These considerations form the basis of identifying the ν_4 mode and for assignments of the components of ClO_3^- bands.

In the ν_1 mode the assigned A_u to B_u splitting ($939-918 \text{ cm}^{-1}$) is

Table II: Site band factor group splittings in Larium chlorate crystals

Symmetry of ClO_4^-			Symmetry of H_2O		
Isolated	Site	Crystal	Isolated	Site	Crystal
C_{3v}	C_1	C_{2h}	C_{2v}	C_{2v}	C_{2h}
(T_2, ν_1, ν_2) (R_2) $(\nu_{xy}, \nu_{xy}, \nu_3, \nu_4)$	A_1 A_2 E	A_g A_u B_g B_u	(T_2, ν_a, ν_b) (R_2) (ν_x, ν_y) (ν_y, ν_x, ν_a)	A_1 A_2 B_1 B_2	A_g A_u B_g B_u

21 cm^{-1} . The 932 cm^{-1} band has been assigned as the isotopic counterpart of 939 cm^{-1} band on the basis of its observed separation (7 cm^{-1}) and intensity. In the ν_4 mode the larger interval of $\sim 15 \text{ cm}^{-1}$ ($504-489$) may be attributed to the site splitting and the $\sim 5 \text{ cm}^{-1}$ separations to the factor group splitting (A_u-B_u), the expected isotopic splitting (1.2 cm^{-1}) being too small to show up. The ν_3 and ν_4 modes were expected to show 3 and 4 components respectively. But apparently due to overlapping ν_3 shows only 3 broad components and ν_4 hardly shows a structure as shown in Fig. 1.

The bands at 392 , 457 and 570 cm^{-1} disappear on deuteration and also at higher temperatures. These may therefore be assigned as librational modes of P_2O . In agreement with his work on single crystals⁽³⁾ the bands 392 and 457 cm^{-1} are attributed to twisting (T) and rocking (R) modes respectively. Calculations based on u-bond and electrostatic interactions give⁽³⁾ the wagging (W) mode of H_2O in PCl_4 at 576 cm^{-1} which is very close to the band observed at 570 cm^{-1} . However this band shows many other variations which could be comprehended only after single crystal work. It is interesting to note that under conditions in which the librational bands of P_2O disappear the bands belonging to the internal modes show little distortion.

Thanks are due to the Council of Scientific and Industrial Research (India) for financial assistance.

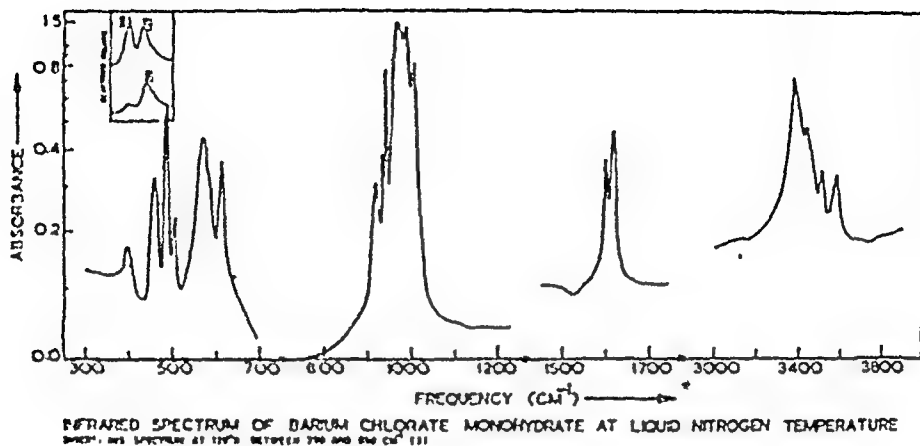


Figure 1

REFERENCES

1. H. Dautin and S. Yip; Molecular Spectroscopy with Neutrons, The MIT press, Cambridge, Mass. (1968).
2. C.W. Hartwig; D.I. Rousseau and S.F.S. Porto; Phys. Rev. 183, 1322 (1969).
3. G.L. Thayer, P.A. Dasannacharya, A. Sequiera and P.K. Iyengar; Solid State Comm. 9, 457 (1970).
4. G. Kartha; Proc. Ind. Acad. Sci. 36A, 501 (1952)
5. A.A. Silvidi, J.T. McGrath and D.F. Holcomb; J. Chem. Phys. 41, 105 (1964).

though give the frequencies in the same region as the ones measured experimentally, are certainly not accurate enough for assignment purposes.

V.S. Tomar

1) The assignment of T, R and W modes at 392, 457 and 570 cm^{-1} is in line with the simple picture that if the torque constants (c) are not too different for the three motions, the three librational frequencies should fall in the order (W) (T) (R). However, on the basis of single crystal polarization studies your assignment of 457 cm^{-1} mode as a rocking mode seems definite. Hence we thought it would be appropriate to assign the lowest mode as twisting mode which is allowed on crystal symmetry arguments, as discussed ⁱⁿ of the body of the paper.

2) The 570 cm^{-1} band is definitely due to some kind of water libration in $\text{KBr} + \text{Ba}(\text{ClO}_3)_2 \cdot \text{H}_2\text{O}$ system in the pellets. However we do not find it in the spectra taken by Nujol mull technique. The band does show shift on deuteration. However, its intensity depends on the manner of preparation of the KBr pellets. Due to such type of anomalous behaviour, we have kept a question mark (?) for this assignment.

3) About your calculations (ref.3) we do realise the approximations and do not intend to attach much significance for the calculated W mode (575 cm^{-1}).

C.L. Thaper

The criterion $\nu(W) > \nu(T) > \nu(R)$ is too crude to be used for assignments in crystal hydrates. This condition is definitely violated in $Ba(ClO_3)_2 \cdot H_2O$, for, rocking is not the lowest frequency.

HARD-CORE POTENTIAL FOR RARE-GAS SOLIDS

T.N. Agarwal, R.K. Gupta and G.L. Gupta
Physics Department, University of Jodhpur, Jodhpur.

I. INTRODUCTION

Lattice dynamics of rare-gas solids has been studied by number of workers in the field, using either Lennard-Jones (12,6) potentials or Buckingham (exp,6) potentials in various forms. It has been pointed out by Rossi and Danon⁽¹⁾ that if the pair potential of Kihara core model of molecules is used, there is an improvement over the results calculated with Lennard-Jones (12,6) potential. It has been shown^(2,3) that Kihara potential is considerably better than the Lennard-Jones for the gas-phase equilibrium properties and fits the transport properties as well⁽⁴⁾. It is therefore, worthwhile to investigate the applicability of such a hard-core potential to solid state of rare gases. In this paper we have calculated the inter-molecular potential parameters of solid Ne, Ar, Kr and Xe for hard-core potential using crystal data. These parameters have been used to study the vibrational properties of rare-gas solids.

II. THE HARD-CORE POTENTIAL AND ITS PARAMETERS

The hard-core potential of Kihara for a pair of atoms separated by a distance r can be written in the form

$$\phi(j,j') = 4\epsilon \left[\left(\frac{1-\gamma}{\frac{z_{jj'}}{\sigma} - \gamma} \right)^{12} - \left(\frac{1-\gamma}{\frac{z_{jj'}}{\sigma} - \gamma} \right)^6 \right] \dots (1)$$

where ϵ is the depth of the potential well for two molecules at equilibrium separation σ , and γ is the effective hard-core parameter. The potential parameters ϵ and σ for various values of γ have been determined using the following equations:

$$F_0 = -L_0 = \Phi_0 + E_z \dots (2)$$

$$-p = 0 = \left(\frac{d\Phi_0}{dv} \right)_{0^\circ K} + \left(\frac{dE_z}{dv} \right)_{0^\circ K} \dots (3)$$

The first equation relates the Helmholtz free energy F_0 of the lattice at $T = 0^\circ K$ (the sublimation energy L_0) to the static lattice energy Φ_0 and the zero-point energy E_z . The second equation relates the external pressure ($p = 0$) to the lattice pressure and the zero-point pressure. The parameters obtained from these calculations are presented in Table 1.

III. PHONON DISPERSION

Proceeding in the usual way, the phonon frequencies are determined by solving the secular determinant written as:

$$\left| \frac{D}{\omega} \left(\frac{q}{kk} \right) - 4\pi^2 m \omega^2 \left(\frac{q}{\omega} \right) \frac{I}{\omega} \right| = 0 \dots (4)$$

TABLE I

Hard-core Potential Parameters

Solid	$\sqrt{}$	σ (10^{-8} cm)	ϵ (10^{-15} erg)
Neon	0.20	2.778	52.06
	0.35	2.797	53.82
	0.10	2.811	55.60
	0.15	2.825	56.78
	0.185	2.835	58.58
	0.20	2.839	59.10
Argon	0.00	3.399	166.48
	0.05	3.405	173.93
	0.08	3.406	175.24
	0.10	3.414	179.91
	0.164	3.427	186.82
Krypton	0.00	3.639	227.03
	0.10	3.649	246.55
Xenon	0.00	3.962	318.81
	0.10	3.971	345.48

$$\phi(j,j') = 4\epsilon \left[\left(\frac{1-\gamma}{\frac{z_{jj'}}{\sigma} - \gamma} \right)^{12} - \left(\frac{1-\gamma}{\frac{z_{jj'}}{\sigma} - \gamma} \right)^6 \right] \dots (1)$$

where ϵ is the depth of the potential well for two molecules at equilibrium separation σ , and γ is the effective hard-core parameter. The potential parameters ϵ and σ for various values of γ have been determined using the following equations:

$$E_0 = -L_0 = \Phi_0 + E_z \dots (2)$$

$$-p = 0 = \left(\frac{d\Phi_0}{dV} \right)_{0^\circ K} + \left(\frac{dE_z}{dV} \right)_{0^\circ K} \dots (3)$$

The first equation relates the Helmholtz free energy E_0 of the lattice at $T = 0^\circ K$ (the sublimation energy L_0) to the static lattice energy Φ_0 and the zero-point energy E_z . The second equation relates the external pressure ($p = 0$) to the lattice pressure and the zero-point pressure. The parameters obtained from these calculations are presented in Table 1.

III. PHONON DISPERSION

Proceeding in the usual way, the phonon frequencies are determined by solving the secular determinant written as:

$$\left| \underline{D} \left(\underline{\tilde{q}}_{kk} \right) - 4\pi^2 m V^2(\underline{\tilde{q}}) \underline{I} \right| = 0 \dots (4)$$

TABLE I

Fard-core Potential Parameters

Solid	$\sqrt{}$	σ (10^{-8} cm)	E (10^{-15} erg)
Neon	0.00	2.778	52.06
	0.05	2.737	53.82
	0.10	2.811	55.60
	0.15	2.825	56.78
	0.185	2.835	58.58
	0.20	2.839	59.10
Argon	0.00	3.399	166.48
	0.05	3.405	173.93
	0.08	3.406	175.24
	0.10	3.414	179.91
	0.164	3.427	186.82
Krypton	0.00	3.639	227.03
	0.10	3.649	246.55
Xenon	0.00	3.962	318.81
	0.10	3.971	345.48

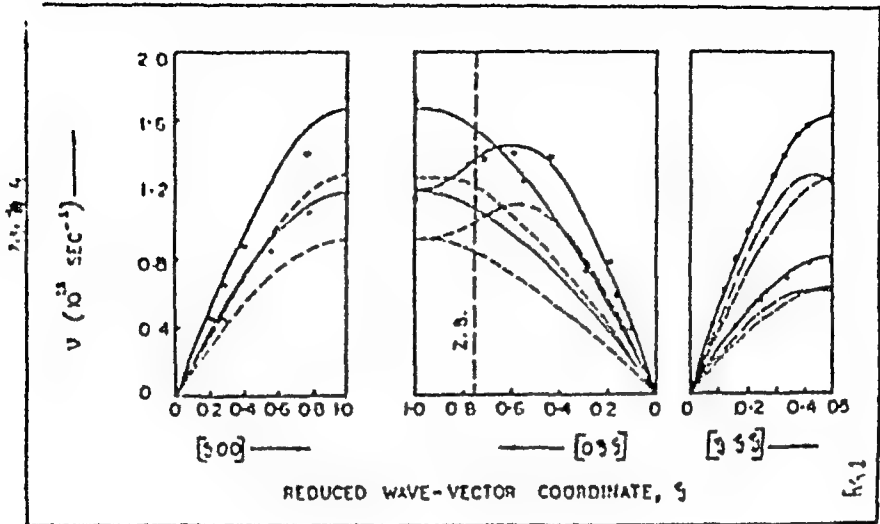


Fig. 1 Dispersion curve for Neon at 0°K

———— Present work,

- - - Theoretical curve of Gupta and Gupta
(Ref. 5)

- . - Theoretical curve of Horton and Leech
(Ref. 6)

Experimental Points at 4.7°K (Ref. 7)

(■) Longitudinal (●) Transverse

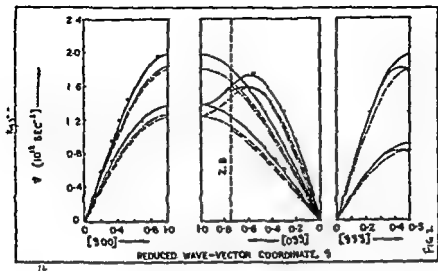


Fig. 2 Dispersion curve for argon at 0°K

———— Present work,

----- Theoretical curve of Gupta and Gupta
(Ref. 5)

- - - - Theoretical curve of Horton and Leech
(Ref. 6)

Experimental Points at 4.2°K (Ref. 8)

(•) Longitudinal (Δ) Transverse

Here \underline{D} is the dynamical matrix, \underline{I} the unit matrix of order three and m is the mass of atoms constituting the monatomic lattice. Due to lack of space, only dispersion curves of neon and argon for the $[100]$, $[110]$ and $[111]$ symmetry directions are shown in Fig. 1 and Fig. 2. These curves are drawn using parameters giving best fit with experimental results. They correspond to $\sqrt{V} = 0.185$ for neon and $\sqrt{V} = 0.06$ for argon.

However, to test the applicability of the hard-core potential, these results are not sufficient. We must also calculate the specific heat and the thermal expansion and compare them with experimental data. The preliminary calculations give encouraging results. It is not possible to discuss the detailed results here. They will be published elsewhere.

REFERENCES

1. J.C.Rossi and F.Danon; J.Chem.Phys., 43, 762(1965).
2. P.G.Francis and C.R.Luckhurst; Trans.Faraday Soc., 59, 667(1963).
3. A.E.Sherwood and J.M.Prausnitz; J.Chem.Phys., 41, 413 (1964).
4. J.A.Barker, W.Fock and F.Smith; Phys.Fluids, 7, 897 (1964).
5. N.P.Gupta and R.K.Gupta, Can.J.Phys; 47, 617(1969).
6. G.K.Horton and J.W.Leech; Proc.Phys.Soc., 32, 816(1963).
7. J.A.Leake, W.B.Daniels, J.Skalyo, Jr., B.C.Frazer and G.Shirane; Phys.Rev., 181, 1251 (1969).
8. H.Egger, M.Gsanger, E.Lüscher and B.Dorner; Phys.Letters, 28, 433 (1968).

DISCUSSION-

B.K. Agrawal

Solid Neon is a quantum crystal and it has a large zero point energy. One can't use harmonic approximation. Have you compared your result of dispersion curves etc. with the self consistent Harmonic approximation developed by Koheler and others? If so, what is the agreement.

R.K. Gupta

Neon is very close to Helium having large zero-point energy. The agreement obtained by us is due to varying values of γ which itself is not exact. Theory developed by Koheler is to be applied to this solid.

M.P. Verma

The hard core parameter γ you get for the best fit in case of the various solids do not show a systematic variation as you go from Neon to Xenon. I feel this must be. Or else, it appears that some thing is being missed, may be anharmonicity.

R.K. Gupta

The anharmonicity at zero-point definitely has effect on these parameters. The calculation of anharmonic parameters have been made by Gupta and Gupta (1) and by Brown in the case of (12,6) potential. For our case calculations are not yet complete. It is difficult to make precise comments.

1. Proc. Nucl. Solid State Phys. Symposium, 1968.

PSEUDOMOLECULAR MODEL FOR A SUBSTITUTIONAL
IMPURITY IN A LATTICE OF POLARISABLE ATOMS

M. Sachdev and J. Mahanty
Indian Institute of Technology, Kanpur-16

The object of this paper is to discuss an approach, based on the pseudomolecular model⁽¹⁾, to study of vibrational features of point defects in a lattice of polarisable atoms. Such lattices are usually studied in the framework of the shell-model.

In the notation of Cowley et al.⁽²⁾, the equations of motion of the lattice in the shell-model can be written as

$$\begin{pmatrix} \hat{\Phi}_{cc} - \omega^2 \hat{M}_c & \hat{\Phi}_{cs} \\ \hat{\Phi}_{cs} & \hat{\Phi}_{ss} \end{pmatrix} \begin{pmatrix} \underline{U} \\ \underline{V} \end{pmatrix} = 0 \quad (1)$$

where \underline{U} and \underline{V} denote the displacements of cores and shells, respectively, from their equilibrium positions. $\hat{\Phi}_{cc}$, $\hat{\Phi}_{cs}$ and $\hat{\Phi}_{ss}$ are matrices of the force constants between cores and cores, cores and shells and between shells and shells, respectively. Each of these $\hat{\Phi}$ matrices consists of a short-range part $\hat{\Phi}^R$ and a long-range part (arising from Coulomb forces) such that

$$\hat{\Phi}_{cc} = \hat{\Phi}_{cc}^R + \hat{X} \hat{C} \hat{X} \quad ; \quad \hat{\Phi}_{cs} = \hat{\Phi}_{cs}^R + \hat{X} \hat{C} \hat{Y} \quad \text{and} \quad \hat{\Phi}_{ss} = \hat{\Phi}_{ss}^R + \hat{Y} \hat{C} \hat{Y} \quad (2)$$

where \hat{X} and \hat{Y} are diagonal matrices of the core and shell charges, respectively. \hat{C} is a matrix of Coulomb coefficients. Eliminating \underline{V} from eqn. (1) we get

$$\left(\hat{\Phi}_{cc} - \hat{\Phi}_{cs} \hat{\Phi}_{ss}^{-1} \hat{\Phi}_{cs}^T \right) \underline{U} = 0 \quad (3)$$

As discussed by Iax⁽³⁾, $\hat{\Phi}_{cs}^R \hat{\Phi}_{ss}^{-1} \hat{\Phi}_{cs}^T$ is a long-range term due to the occurrence of $\hat{\Phi}_{ss}^{R-1}$ in it. Though in principle eqn. (3) can be partitioned in the same way as done earlier⁽¹⁾, this is of no special advantage here as the long-range nature of $\hat{\Phi}_{ss}^{-1}$ $\hat{\Phi}_{cs}^T$

makes it cumbersome to take into account changes in shell-parameters at the point defect. We shall show here that if the core and shell coordinates are taken together to form the pseudomolecule and if the long-range Coulomb terms in eqns. (2) and (3) are assumed to remain unchanged, a local effective interaction term can be obtained in terms of the defect parameters.

We define a unitary transformation matrix \hat{S} as follows:

$$\hat{S} = \begin{matrix} & \begin{matrix} n_1 & n_2 & n_1 & n_2 \end{matrix} \\ \begin{matrix} n_1 \\ n_1 \\ n_2 \\ n_2 \end{matrix} & \begin{pmatrix} \hat{I} & 0 & 0 & 0 \\ 0 & 0 & \hat{I} & 0 \\ 0 & \hat{I} & 0 & 0 \\ 0 & 0 & 0 & \hat{I} \end{pmatrix} \end{matrix} \quad (4)$$

where 1 and 2 refer to indices of regions I and II of the lattice and n_1, n_2 (with $n_1 + n_2 = N$) denote the number of degrees of freedom associated with regions I and II, respectively.

Applying the transformation \hat{S} to eqn. (1) we get

$$\hat{\Phi}_s \underline{\chi} = 0 \quad (5)$$

$$\text{where } \hat{\Phi}_s = \hat{S} \hat{\Phi} \hat{S}^{-1} \text{ and } \underline{\chi} = \begin{pmatrix} \chi_1 \\ \chi_2 \end{pmatrix} \text{ with } \underline{\chi}_1 = \begin{pmatrix} u_1 \\ v_1 \end{pmatrix}, \underline{\chi}_2 = \begin{pmatrix} u_2 \\ v_2 \end{pmatrix} \quad (6)$$

We partition $\hat{\Phi}_s$ and $\hat{\Phi}_s^{-1}$ as

$$\hat{\Phi}_s = \begin{pmatrix} \hat{\Phi}_{11}^s & \hat{\Phi}_{12}^s \\ \hat{\Phi}_{12}^s & \hat{\Phi}_{22}^s \end{pmatrix} \text{ and } \hat{\Phi}_s^{-1} = \begin{pmatrix} G_A & G_B \\ \tilde{G}_B & G_0 \end{pmatrix} \quad (7)$$

Using eqns (6) and (7) in eqn. (5), Equation for $\underline{\chi}_2$ can be shown to be

$$\left(\hat{\Phi}_{22}^s - \tilde{\hat{\Phi}}_{12}^s \hat{\Phi}_{11}^{s^{-1}} \hat{\Phi}_{12}^s \right) \underline{\chi}_2 = G_c^{-1} \underline{\chi}_2 = 0 \quad (8)$$

We shall consider here only those substitutional point defects which do not change the degrees of freedom associated with the lattice and the long-range Coulomb terms in eqn. (2). The formalism developed may be useful in many physical situation e.g., for defects like

Li^+ and K^+ in NaI crystals which have been treated essentially as mass defects⁽⁴⁾. For such defects, submatrices $\hat{\Phi}_{12}^s$, $\hat{\Phi}_{11}^{s^{-1}}$ & $\hat{\Phi}_{12}^s$ in eqn. (8) remain unaltered if the pseudomolecule (i.e. χ_2) is chosen such that the short-range force constants between the peripheral atoms of the pseudomolecule and those of the unperturbed region do not change. The change in matrix $\hat{\Phi}_{22}^s$ (eqn. 8) due to the defect can be determined in terms of the shell-model parameters of the perturbed region II only.

Equation for the imperfect pseudomolecule can therefore be written from eqn. (8) as

$$\left(\hat{\Phi}_{22}^{s'} - \hat{\Phi}_{22}^s + \hat{\Phi}_0^{-1} \right) \chi_2' = 0 \quad (9)$$

where primes denote perturbed matrices.

As an example we have studied the vibrational modes of a substitutional impurity in the isotropic simple cubic lattice. The pseudomolecule and the shell-model parameters are as shown in Figs 1a & 1b respectively. A group-theoretic analysis of the modes shows that there are $4A_g$, $2F_{1u}$ and $2E_g$ modes. The eigen value equation for the E_g modes $(0,1,1,\bar{2},1,1,\bar{2},0,0,0,0,0,0,0,0)$ and $(0,0,0,0,0,0,0,0,1,1,\bar{2},1,1,\bar{2})$,

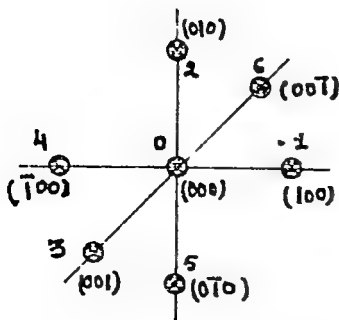
for example, is

$$\begin{pmatrix} \Delta\epsilon + \Delta F + \frac{c_{ss}(0) - 2c_{ss}(3) + c_{ss}(2)}{|\hat{v}^+ \hat{\Phi}_0 \hat{v}|_{E_g}} & \frac{c_{cs}(0) - 2c_{cs}(3) + c_{cs}(2)}{|\hat{v}^+ \hat{\Phi}_0 \hat{v}|_{E_g}} \\ \frac{c_{sc}(0) - 2c_{sc}(3) + c_{sc}(2)}{|\hat{v}^+ \hat{\Phi}_0 \hat{v}|_{E_g}} & \Delta\epsilon + \Delta F + \frac{c_{cc}(0) - 2c_{cc}(3) + c_{cc}(2)}{|\hat{v}^+ \hat{\Phi}_0 \hat{v}|_{E_g}} \end{pmatrix} \begin{pmatrix} u_1 + u_2 \\ -2u_3 \\ +u_4 \\ +u_5 \\ -u_6 \\ u_1 + u_2 \\ -2u_3 \\ +u_4 \\ +u_5 \\ -2u_6 \end{pmatrix} = 0$$

where \hat{v} is a matrix of the symmetry adapted vectors,

$$\Delta\epsilon = \epsilon' - \epsilon; \Delta F = F' - F \text{ and } \Delta s = s' - s \text{ and}$$

$$|\hat{v}^+ \hat{\Phi}_0 \hat{v}|_{E_g} = \begin{pmatrix} c_{ss}(0) - 2c_{ss}(3) + c_{ss}(2) \\ c_{sc}(0) - 2c_{sc}(3) + c_{sc}(2) \end{pmatrix} \begin{pmatrix} c_{ss}(0) - 2c_{ss}(3) + c_{ss}(2) \\ c_{cs}(0) - 2c_{cs}(3) + c_{cs}(2) \end{pmatrix}$$



☯ Core
X Shell

FIG. (1a)

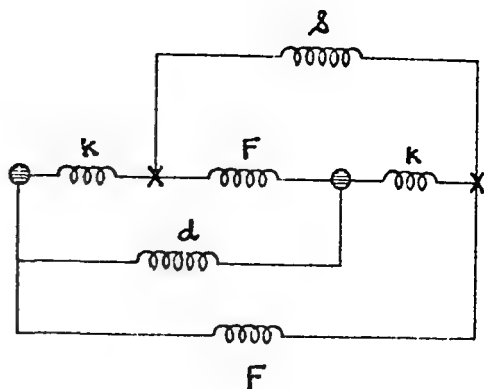


FIG. (1b)

Shell model parameters for the pseudomolecule

with $\hat{Q} = \hat{\Phi}^{-1} = \begin{pmatrix} \hat{Q}_{cc} & \hat{Q}_{cs} \\ \hat{Q}_{sc} & \hat{Q}_{ss} \end{pmatrix}$

and $G(\underline{R}, \underline{R}') = G(|\underline{R} - \underline{R}'|) = G(R_1 - R'_1, R_2 - R'_2, R_3 - R'_3)$

$$G(0) = G(000), \quad G(3) = G(1,1,0), \quad G(2) = G(2,0,0)$$

and $G(1) = G(1, 0, 0)$ denote the elements of Green function submatrices.

It may be remarked here that this method is quite similar to that given by Page and Strauch⁽⁵⁾. Their method enables one to take into account the changes in Coulomb terms due to the changes in core and shell charges as a local non-zero perturbation matrix in the full perturbation matrix. Calculations of Green functions in their treatment is
 . tly more involved. Both the methods can be generalized to the Breathing shell model.

- REFERENCES.** 1. M. Szechdev and J. Mahanty; *J. Phys.C*, 3, 1225 (1970)
2. R.A. Cowley, W. Cochran, B.W. Brockhouse and A.D.B.Woods;
Phys. Rev. 131, 1030 (1963).
3. M. Lax; *Lattice Dynamics*, Proc. Int. Conf., Copenhagen (Oxford:
Pergamon), Ed. R.F. Wallis, pp. 179 (1965).
4. I. Gunther; *Phys. Rev.* 138, A1697 (1965).
5. J.B. Page Jr. and D. Strauch; *Localized Excitations in Solids*
(Plenum Press), Ed. R.F. Wallis, pp 559 (1968).

THEORETICAL STUDY OF VACANCIES AND VACANCY PAIRS IN CsCl TYPE CRYSTALS

G.S.N. Murthy and Y.V.G.S. Murti
Department of Physics, I.I.T., Madras-36

I. INTRODUCTION

Cohesive energies under standard thermodynamic conditions (at 25°C and negligible pressures) for seven CsCl-type crystals (CsCl, CsBr, CsI, TlCl, TlBr, NH₄Cl and NH₄Br) have been calculated by the authors on the basis of Born model, considering explicitly the second neighbour repulsions and dispersion interactions. The repulsion parameters occurring in the Born-Mayer double exponential form are determined by employing the equation of state and its volume derivative appropriate to the crystal data used.⁽¹⁾ The close agreement with the experimental values indicates the predominance of ionic binding. The small discrepancies amounting to 4-6 Kcals/mole in the thallous and ammonium halides are attributed to contributions due to covalent and hydrogen bonding. Using the cohesion parameters of the above work, the formation of Schottky defects and neutral bound vacancy pairs is investigated.

II. ENERGY REQUIRED TO FORM ISOLATED VACANCIES

The work of extracting an ion (h_+) is evaluated as the negative of the average of the potential energies of the ion at the position of the vacancy before and after its creation. To determine the various energy terms in the distorted lattice the electronic moment and

the relaxation (ξ_R) of the eight first neighbours surrounding the vacancy are determined by balancing the forces on a $(\frac{1}{2}, \frac{1}{2}, \frac{1}{2})$ ion. The moments and the displacements of the farther ions assumed to behave harmonically, are calculated from the macroscopic polarisation caused by the effective charge of the defect. The Schottky defect formation energy (h_S) is then given by $h_+ + h_- - W_L$ where W_L is the lattice energy per ion pair excluding the vibrational part of the cohesive energy.

III. ENERGY REQUIRED TO CREATE A BOUND VACANCY PAIR

It is the negative of the average of the potential^t energies of the cation which is the nearest neighbour of an anion vacancy before and after its removal. The energy in the position of a cation near an anion vacancy is evaluated taking the polarisation of the lattice resulting from the presence of the anion vacancy. For calculating the potential energy of the cation after its removal, a model similar to Dienes⁽²⁾ is adopted for the core distortion (of the 14 ions) around the vacancy pair. The equilibrium outward displacement (γ_R) is computed by maximising the decrease in energy of the crystal upon distortion, considering separately all the interactions explicitly. The binding energy (B.E.) is then evaluated to be the difference between the energy required to extract a cation in the perfect lattice and the energy necessary to create the same neighbouring an anion vacancy.

TABLE I

Crystal	ξ	η	Schottky Defect Energy (e.v.)		B.B. (e.v.)
			Computed	Experi- mental	
CsCl	0.044	0.050	1.86	1.86	0.65
CsBr	0.045	0.0485	1.74	2.00	0.63
CsI	0.059	0.0495	1.40	1.90	0.52
TlCl	0.058	0.0595	1.27	1.30	0.43
TlBr	0.061	0.056	1.20		0.41
NH ₄ Cl	0.063	0.074	1.33	0.81	0.65
NH ₄ Br	0.067	0.0745	1.17		0.60

IV DISCUSSION

Comparison of the computed Schottky defect formation energies and the experimental values (Table I) indicated the reliability of the basic Mott - Littleton method⁽³⁾ when appropriate cohesion parameters are employed. The relatively low ground state vacancy pair binding energies for the thallous salts are qualitatively in accord with the rough estimates given by the electrostatic interaction ($e^2/\epsilon r$, where ϵ is the dielectric constant). The core distortion (η) is, in general, greater than the relaxation ξ (ξ) of the first neighbours of the isolated vacancy. This may be due to the $\langle 111 \rangle$ orientation of the vacancy pair.

ACKNOWLEDGEMENTS

We wish to thank Prof. C. Ramasastry for his kind interest in this work.

REFERENCES

1. C.S.N. Murthy and Y.V.G.S. Murti, J.Phys. C. 3, 122 (1970)
2. M.P. Tosi and F.G. Fumi, Nuovo Cimento, 7, 95 (1958)
3. C.S.N. Murthy and Y.V.G.S. Murti, J. Phys. C. (Accepted) 1970.

*

MODEL POTENTIAL FOR BCC METALS

S.S.Kushwaha and J.S.Rajput

Physics Department, Banaras Hindu University, Varanasi -5.

I. INTRODUCTION

Several theories have been developed for the phonon spectra of simple metals using model potentials and pseudopotentials. For such metals it is convenient to describe the mechanical system of electrons and forces by means of pseudopotential perturbation theory. Several simple local pseudopotential models have been used to calculate the thermodynamic properties and reasonably good agreement with experiment has been obtained. Wallace¹ has incorporated the Born Mayer repulsion between the ion cores and calculated phonon frequencies in the case of Na, K and Li using Harrison's modified point ion pseudopotential with two adjustable parameters. These calculations are in good qualitative agreement with the experimental results. Here we present a method to calculate the phonon dispersion relations in bcc metals using a two parameter model potential.

II. THEORETICAL MODEL

The total adiabatic potential for a simple metal consists of the electrostatic contribution of the direct Coulomb interaction of positive ions immersed in a uniform compensating background of negative charges, E^{es} ; the band structure energy, E^{bs} and the ion-core exchange energy, E^c . The electrostatic part of the dynamical matrix is determined in the usual way^{2,3} and the

which is of the Born-Mayer type is neglected here. We evaluate the band structure energy using a two parameter model potential. The Fourier transform of the total ion potential; which is separable into individual overlapping ion potentials centered upon individual ion at position \vec{r}_i , is given by

$$W_q = \Omega^{-1} \sum_i e^{-i\vec{q} \cdot \vec{r}_i} \int e^{-i(\vec{K} + \vec{q}) \cdot \vec{r}} \omega(\vec{r}) e^{i\vec{k} \cdot \vec{r}} d^3r \quad \dots(1)$$

The model potential for $\omega(\vec{r})$ is taken as

$$\omega(\vec{r}) = -\frac{Ze^2}{r} + \left(\frac{Ze^2}{r} + \beta\right) e^{-\alpha r} \quad \dots(2)$$

α and β are the two parameters.

The first order matrix element of the screening potential is written as

$$W_q \left[\left(1 + \frac{S_o(q)}{q^2}\right)^{-1} - 1 \right] \quad \dots(3)$$

where

$$S_o(q) = \frac{2 m e^2 Z k_F}{\pi \hbar^2} \left[1 + \frac{4 k_F^2 - q^2}{4 k_F q} \ln \left| \frac{2 k_F + q}{2 k_F - q} \right| \right] \quad \dots (4)$$

when exchange and correlation effects are introduced the dielectric function $\epsilon(q)$ is given by

$$\epsilon(q) = 1 + S_o(q)^{-2} \left[1 - \frac{1}{2(q^2 + \xi k_F^2) S_o(q)} \right]^{-1} \quad \dots (5)$$

where τ is defined by

$$\tau = 2 \left[1 + 0.153 / (\pi a_0 k_F) \right]^{-1} \quad \dots (6)$$

The expression for E^{bs} is written as

$$E^{bs} = -\frac{\Omega_0}{8\pi ze^2} \sum_q' S(q)^2 \omega_q^2 \left[\frac{\epsilon(q)-1}{\epsilon(q)} \right] \quad \dots (7)$$

is the Fourier transform of $\omega(\vec{r})$ and the structure factor $S(q)$ is defined as

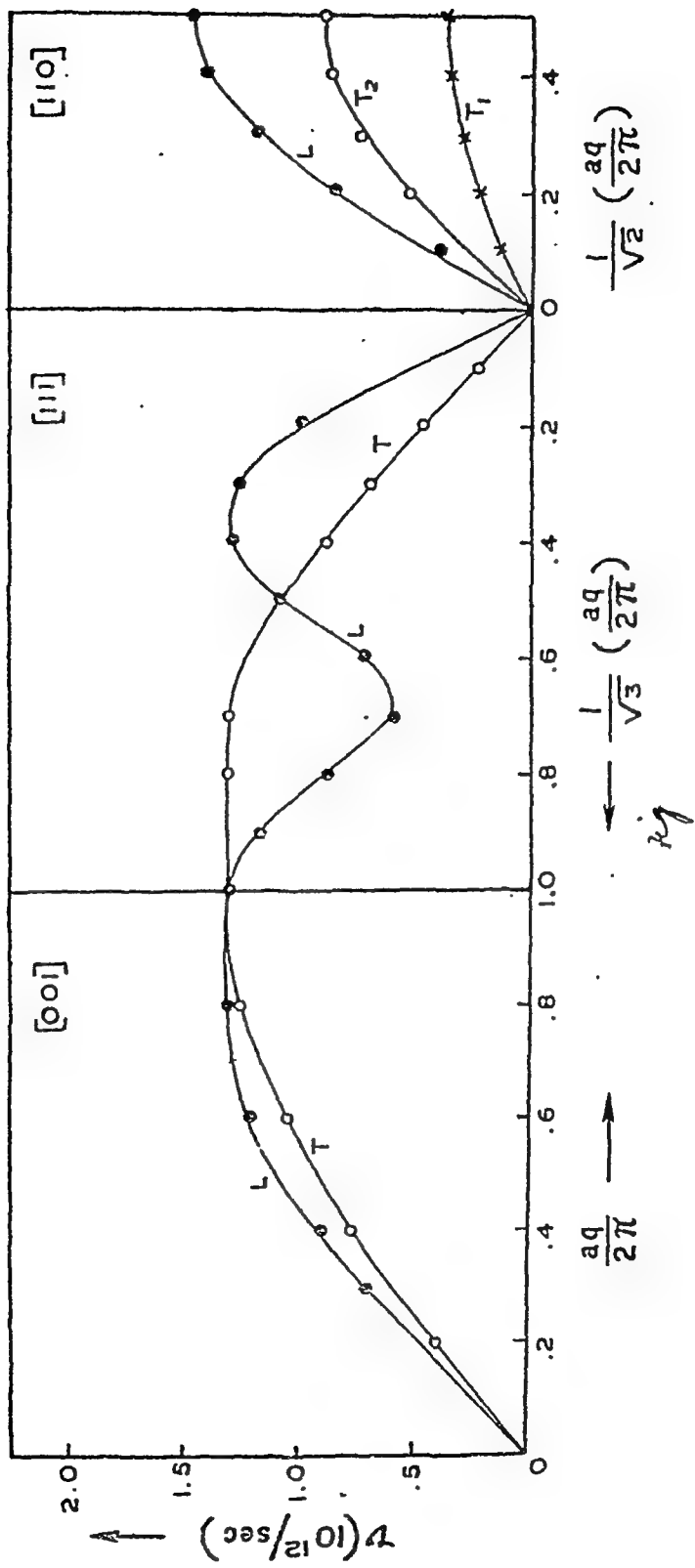
$$S(q) = (N)^{-1} \sum_v e^{-i\vec{q} \cdot \vec{r}_v} \quad \dots (8)$$

III. RESULTS

The parameters α and β are determined by fitting the observed crystal energy and its volume derivatives³. In the specific case of rubidium, we find $\alpha = 2$ and $\beta = 12$. The parameter τ comes out to be 2.02.

The convergence problem in the band structure energy part of the dynamical matrix due to oscillations of the Fourier transform of the actual potential at large values has been eliminated by multiplying the potential $(\frac{ze^2}{r} + \beta)$

by a factor $e^{-\alpha r}$. The dispersion curves along the symmetry directions $[100]$, $[111]$ and $[110]$ have been obtained and there compare well with the neutron scattering results of Copley and Brockhouse⁵.



REFERENCES:

1. D.C. Wallace , Phys. Rev. 176(1968) 832
2. E.W.Kellerman , Phil., Trans.Roy Soc.(London)
A238(1940) 873
3. P.P. Ewald , Ann.Physik, 64 (1921) 253
4. S.S.Kushwaha , Ph.D. Thesis submitted to Banaras Hindu
University . 1970
5. J.R.D. Coupley and B.K.Brockhouse , Neutron
inelastic scattering , Vol . 1,
IAEA , Vienna , 1968 .

DISCUSSION

S.K. Joshi:

A stage has reached in the study of simple alkali metals where one has fairly satisfactory understanding about the dielectric function (Singwi et al) and the model potential. A good agreement of calculated phonon frequencies with experimental data by badgering both the model potential and the dielectric function should not be attempted. It is suspected that the inadequacies of your model potential and the dielectric function balance each other and lead to the so called "good fit" with the experiment.

LATTICE DYNAMICS OF TRANSITION METALS

Satya Prakash and S.K. Joshi
Department of Physics, University of Roorkee, Roorkee

I. INTRODUCTION

We had proposed the non-interacting band model for the dielectric screening in transition metals.¹ We had concluded that the major contribution to the dielectric screening is from the unfilled d and d bands. In this paper we deduce the general formalism to calculate the phonon frequencies in transition metals assuming that the electrons, distributed in the unfilled s and d bands behave as the conduction electrons.

II. THEORETICAL DISCUSSION AND RESULTS

In the harmonic approximation the angular frequencies $\omega_{\underline{q}p}$ of lattice vibrations of a monatomic metal are obtained from the solution of the determinantal equation:

$$\det [D_{\alpha\beta}(\underline{q}) - M \omega_{\underline{q}p}^2 \delta_{\alpha\beta}] = 0. \quad (1)$$

Here \underline{q} is the phonon wave vector, p is the polarisation branch, M is the mass of the ion, $D_{\alpha\beta}(\underline{q})$ are the elements of the dynamical matrix and α, β are the Cartesian components (x, y, z). $D_{\alpha\beta}(\underline{q})$ is expressible as the sum of the three terms

$$D_{\alpha\beta}(\underline{q}) = D_{\alpha\beta}^{(C)}(\underline{q}) + D_{\alpha\beta}^{(R)}(\underline{q}) + D_{\alpha\beta}^{(E)}(\underline{q}). \quad (2)$$

$D_{\alpha\beta}^{(C)}(\underline{q})$ originates from the bare Coulomb interaction between the ions. $D_{\alpha\beta}^{(C)}(\underline{q})$ is evaluated by Ewald's method for a given ionicity and the crystal structure. $D_{\alpha\beta}^{(R)}(\underline{q})$ is the contribution from overlap potential between ions. We neglect $D_{\alpha\beta}^{(R)}(\underline{q})$, assuming that the overlapping between the cores is negligible. $D_{\alpha\beta}^{(E)}(\underline{q})$ stems for the ion-electron-ion

interaction. We deduce the general expression for $D_{\alpha\beta}^{(E)}(\underline{q})$ in the Hartree-Fock approximation with the help of second order perturbation theory. In actual calculations we limit ourselves to the Hartree approximation. The final expression for $D_{\alpha\beta}^{(E)}(\underline{q})$ is:

$$D_{\alpha\beta}^{(E)}(\underline{q}) = \frac{N}{\Omega} \sum_{\underline{G}} \frac{1}{v(\underline{q}+\underline{G})} \left\{ \frac{1}{\epsilon(\underline{q}+\underline{G})} - 1 \right\} (\underline{q}+\underline{G})_{\alpha} (\underline{q}+\underline{G})_{\beta} |U_b(\underline{q}+\underline{G})|^2 \quad (3)$$

Here N is the number of unit cells in the crystal, \underline{G} is the reciprocal lattice vector, $v(\underline{q}+\underline{G})$ and $U_b(\underline{q}+\underline{G})$ are the Fourier transform of the electronic Coulomb potential and of the bare-ion potential respectively, and $\epsilon(\underline{q}+\underline{G})$ is the dielectric function.

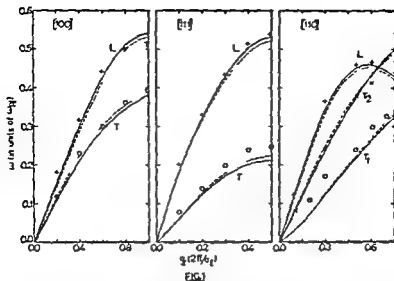
To reduce the heavy computational efforts we construct on isotropic two-band model for the static dielectric function based on the results of our earlier calculations¹. The final expression for the isotropic two band model dielectric function is:

$$\epsilon(p) = 1 + \frac{2e^2}{\pi \hbar^2 p^2} \left\{ m_s k_{Fs} \left[1 + \frac{4k_{Fs}^2 - p^2}{4k_{Fs}p} \ln \left| \frac{2k_{Fs} + p}{2k_{Fs} - p} \right| \right] + m_{d1} k_{Fd1} |\Delta_{21,21}(p)|^2 \left[1 + \frac{4k_{Fd1}^2 - p^2}{4k_{Fd1}p} \ln \left| \frac{2k_{Fd1} + p}{2k_{Fd1} - p} \right| \right] \right\}, \quad (4)$$

where $\underline{p} = \underline{q}+\underline{G}$. m_s and k_{Fs} are the effective mass and the Fermi momentum for the s band while m_{d1} and k_{Fd1} are the effective mass and the Fermi momentum for the unfilled d band. $\Delta_{21,21}(p)$ is a function of p and the 3d radial wave function.

The bare ion potential is replaced by the model pseudopotential and this corrects in an approximate manner the effects of the orthogonality of the wavefunctions. The Fourier transform of the modified bare ion potential is

$$U_b(p) = -\frac{4\pi ze^2}{p^2} + \frac{\beta}{[1 + (\beta r_c)^2]^2}. \quad (5)$$



Phonon frequencies for the paramagnetic nickel. The solid lines are for the configuration $(3d)^9(4s)^1$ while the dash lines are for the configuration $(3d)^{9.4}(4s)^{0.6}$. The experimental points are represented by O, + and x.

The parameters β and r_c are adjusted to achieve the rapid convergence of the sum in (3) and force a fit between the calculated and experimental phonon frequencies.

We limit the core of the paramagnetic nickel upto $(3d)^8$ configuration and neglect the core polarization effects. The physical constants and the other parameters are the same as in the reference [1]. The phonon frequencies are calculated for the configuration $(3d)^9(4s)^1$ along the three principal symmetry directions $[100]$, $[110]$ and $[111]$. The best possible agreement with the experimental measurements² is obtained for $\beta = 16.0$ and $r_c = 0.30$. We also repeated the calculations for the configuration

$(3d)^{9.4}(4s)^{0.6}$ for the same values of β and r_c . The calculated phonon frequencies are shown in the Fig.1. The calculated phonon frequencies of Ni for both the configurations differ at the most by 3%. While comparing we should remember that our calculations are for the paramagnetic phase and the experimental phonon frequencies are measured at 296°K for the ferromagnetic phase.

REFERENCES

1. S. Prakash and S.K. Joshi, Phys. Rev. B2, 915 (1970).
2. R.J. Birgeneau, J. Cordes, G. Dolling and A.D.W. Woods Phys. Rev. 136, A1359 (1964).

DISCUSSION

G. Venkataraman

I believe you used the Hartree approximation for the calculation of the dielectric screening function. Considering that you are dealing with magnetic materials would you not expect exchange effects to be important?

Satya Prakash

Yes, exchange and correlation effects are quite important in transition metals. If we include the exchange potential in any of the modified HFS scheme where correlation effects are also included in an approximate fashion, we get simply $\epsilon(p) = 1 + (1 - f(p)) \chi(p)$ where $f(p)$ is given by many workers. It will simply give a lot of data on frequency but nothing to understand the magnetic behaviour. I feel s-d interaction should be considered first to include in the dielectric function and then, one should think of exchange correlation part.

ELECTRICAL AND THERMAL RESISTIVITIES OF CAESIUM

SATYA PAL

Physics Department, Allahabad University, Allahabad.

I. INTRODUCTION

One of the basic tasks of solid state theory has been to account for the transport properties of metals. The problem is by no means straightforward and has been the subject of investigation by many workers⁽¹⁻⁹⁾. The transport phenomenon in metals depends in a complicated way upon the electronic band structure and the anisotropy of the lattice spectrum which complicate the evaluation of the scattering probability of the conduction electrons.

The calculations of the temperature variation of electrical and thermal resistivities of caesium using Bhatia's⁽¹⁰⁾ lattice dynamical model for the phonon spectrum are presented herein.

II. THEORY

For a lattice of cubic symmetry the first order solution of the Boltzmann equation giving the electrical resistivity ρ can be written as⁽¹¹⁾

$$\rho = \frac{3\pi^2}{2e^2 k_B k_F^2} \frac{1}{M N T S_P^2} \frac{1}{P} \frac{K^2 (\underline{K} \cdot \underline{e}_{q,p})^2 C^2(K)}{v v' (e^{\beta \omega_{q,p}} - 1) (1 - e^{-\beta \omega_{q,p}})} dS_P dS_P' \dots\dots\dots (1)$$

where $\omega_{q,p}$ is the angular frequency of phonon of wave vector \underline{q} and mode of vibration p , $\underline{e}_{q,p}$ the polarization vector of \underline{q} - p lattice mode, $\underline{K} = \underline{K}' - \underline{K}$ the scattering vector, and $\beta = 1/k_B T$. $C(K)$ is the Bardeen matrix element

for the transition of an electron from the initial state \underline{k} to the final state \underline{k}' and for a free electron model is given by⁽²⁾

$$C(K) = \frac{[E_0 - V_0(r_0)] K^2 + W(K) q_s^2}{q_s^2 + K^2} G(qr_0)$$

where $E_0 - V_0(r_0)$ is the kinetic energy of an electron in the lowest state at the surface of atomic polyhedra of radius r_0 and q_s is the screening parameter defined by

$$q_s^2 = \frac{4\pi n e^2}{W(K)}, \quad n \text{ being the electron density and}$$

$$W(K) = \frac{2}{3} E_F \left[\frac{1}{2} + \frac{4k_F^2 - K^2}{8k_F K} \ln \left| \frac{2k_F + K}{2k_F - K} \right| \right]^{-1},$$

$$G(x) = 3(\sin x - x \cos x) / x^3.$$

As the phonon frequencies $\omega_{\underline{q},p}$ and the factor $(\underline{K} \cdot \underline{e}_{\underline{q},p})$ depend upon the direction of the scattering vector \underline{K} , the evaluation of the double surface integral in eqn. (1) becomes difficult. Following Bailyn's⁽³⁾ method the right hand side of eqn. (1) can be reduced to

$$\frac{1}{S_F^2} \iint F(\underline{K}) dS_F dS_F' = \frac{1}{2\pi^2 k_F} \int dK \int d\Omega F(K) (1-u^2)^{1/2} \dots (2)$$

where $u = K/2k_F$.

Thus making use of relation (2) the expression (1) for the electrical resistivity due to phonon scattering becomes

$$\rho = \frac{3\hbar}{4\pi k_B e^2 v_F^2 k_F^3 M N T} \sum_P \int d\Omega \int \frac{K^2 (1-u^2)^{1/2} (\underline{K} \cdot \underline{e}_{\underline{q},p})^2 C^2(K)}{(e^{\beta\omega_{\underline{q},p}} - 1)(1 - e^{-\beta\omega_{\underline{q},p}})} dK, \dots (3)$$

Similarly by following the above procedure the final expression for the thermal resistivity can be deduced as

$$W_L = \frac{9K}{4\pi e^2 \kappa_B k_F^3 v_F^2 L_0 K H T^2} \int d\Omega \int B(K) dK \quad (4)$$

where

$$B(k) = \frac{1}{P} \frac{(1-u^2)^{1/2} K^2 (\underline{K} \underline{e}_{q,p})^2 C^2(K)}{(\omega_{q,p}^2 - 1)(1 - e^{-\beta\omega_{q,p}})} \times$$

$$\left[\frac{K^2}{3} - \left(\frac{\beta\omega_{q,p}}{\pi} \right)^2 \left(\frac{K^2}{6} - k_F^2 \right) \right],$$

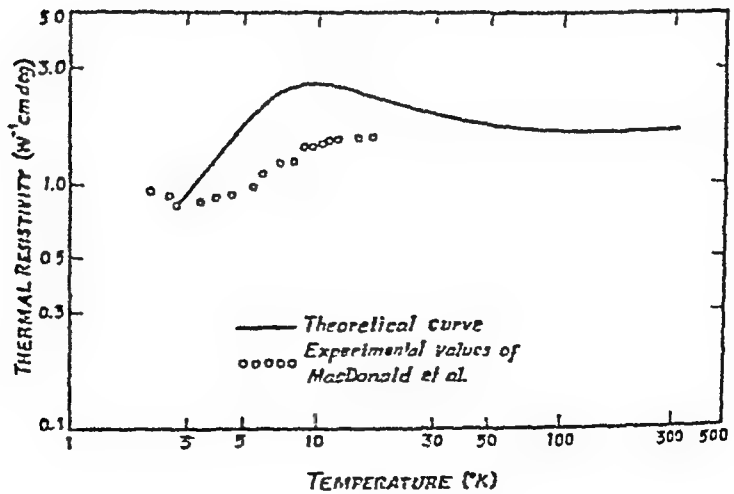
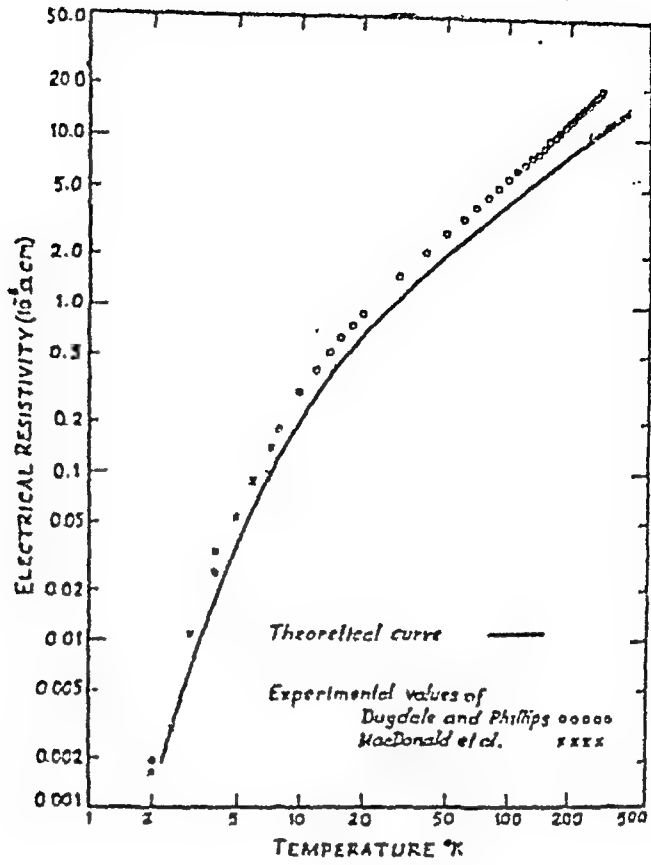
III NUMERICAL COMPUTATION

The phonon frequencies $\omega_{q,p}$ and the polarization vectors $\underline{e}_{q,p}$ have been obtained from the solutions of Bhatia's ⁽¹⁰⁾ secular determinant for a body-centred cubic crystal. The integration over \underline{K} has been performed numerically while the integration over the solid angle has been carried out with the help of the modified Houston's six-term procedure as developed by Betts et al ⁽¹²⁾. While integrating over \underline{K} a separation between the Normal and Umklapp processes has been affected. The U-processes occur subject to the condition

$$\underline{K} = \underline{K}' - \underline{k} = \underline{q} + \underline{g} \quad \dots (5)$$

where \underline{g} is the reciprocal lattice vector. The minimum value of \underline{K} at which U-processes set in can easily be determined.

The numerical values of elastic constants ⁽¹³⁾ and other parameters used in the calculation are . $C_{11} = 24.65 \times 10^9$ dyn cm⁻², $C_{12} = 20.55 \times 10^9$ dyn cm⁻², $C_{44} = 14.80 \times 10^9$ dyn cm⁻², lattice parameter $a = 6.057 \text{ \AA}$ density $\rho = 1.98 \text{ g cm}^{-3}$. Fermi energy $E_F = 1.61 \text{ eV}$ and $V(r_0) - E_0 = 0.0001 \text{ eV}$



IV: RESULTS AND DISCUSSION

The calculated values of electrical and thermal resistivities of caesium at different temperatures together with the experimental data have been plotted in fig. 1 and fig. 2 respectively. The contribution of the U-processes to the total electrical resistivity is of the order of 30% while for the thermal resistivity the contribution varies from 20% at 10°K to 35% at 300°K . It is seen that though theoretical electrical resistivity values of caesium are in fair agreement with experimental data of MacDonald et al.⁽¹⁴⁾ and Dugdale and Phillips⁽¹⁵⁾ the thermal resistivity values are uniformly higher than the experimental points of MacDonald et al.⁽¹⁴⁾

The discrepancy between theory and experiment may be attributed to the approximate calculation of the electron-phonon matrix element, to the anisotropy of the Fermi surface of caesium and to the neglect of the temperature dependence of elastic constants and other anharmonic effects.

REFERENCES

1. F. Bloch, Z. Physik 52, 555 (1928).
2. J. Bardeen, Phys. Rev. 52, 688 (1937).
3. M. Bailyn, Phys. Rev. 112, 1587 (1958); *ibid* 120, 381 (1960).
4. J.G. Collins, Proc. Roy. Soc. A263, 531 (1961).
5. J.G. Collins and J.M. Ziman, Proc. Roy. Soc. A264, 60 (1961).
6. H. Brons and A. Holz, Phys. Stat. Solidi 3, 1141 (1963).
7. A. Hasegawa, J. Phys. Soc. 19, 504 (1964).
8. J.K. Darby and N.H. March, Proc. Phys. Soc. 84, 591 (1964).
9. M.P. Greene and W. Kohn, Phys. Rev. 137, A513 (1965).
10. A.B. Ehtala, Phys. Rev. 97, 363 (1955).

11. J.M. Ziman, Electrons and Phonons, Clarendon Press, Oxford, England (1960).
12. D.D. Betts, A.B. Bhatia, and M. Wyman, Phys. Rev. 104, 37 (1956).
13. F.J. Kollarits and J. Trivisonno, J. Phys. Chem.Solids 29, 2133 (1968).
14. J.K.C. MacDonald, G.K. White, and S.B. Woods, Proc. Roy. Soc. A235, 358 (1956).
15. J.S. Dugdale and D. Phillips, Proc.Roy. Soc. A287, 381 (1965).

VARIATIONAL TREATMENT OF ZIMAN LIMIT OF THERMAL RESISTANCE DUE TO UMKLAPP PROCESSES

G.P. Srivastava and G.S. Verma
Department of Physics, B.H.U.,
Varanasi-5.

I. INTRODUCTION

Hamilton and Parrott⁽¹⁾ have used variational principle to calculate the thermal conductivity of Ge. Also an improved variational principle has recently been formulated by Banin⁽²⁾, which gives emphasis on the bounds on the transport coefficients. The method used by Hamilton and Parrott is no doubt an elegant one but is quite lengthy so far as the computation of resistivity due to any three phonon process is concerned. Moreover they have used an isotropic continuum model.

Here we develop a simple method to calculate Umklapp resistances for different three-phonon processes. A rigorous approach regarding many unknown geometrical factors depending on polarization, anisotropy and lattice structure etc., is attempted to make the formalism more realistic.

II. ZIMAN LIMIT OF THE UMKLAPP RESISTANCE

The Boltzmann equation in the presence of temperature gradient is

$$-\frac{\vec{E}(\vec{q}) \cdot \vec{v}}{T} \frac{\hbar \omega}{k_B T} N(N+1) = -\frac{\partial N}{\partial \epsilon} \Big|_{\text{scatt}} \quad \text{--- (1)}$$

or

$$\vec{X} = P \vec{Y}$$

Here $\vec{C}_s(\vec{q})$ is the group velocity of an phonon (\vec{q}, s) , T is the temperature gradient, $P(\vec{q}, \vec{q}')$ represents the total effect of the scattering processes, T is the absolute temperature, k_B Boltzman constant and γ_q is a measure of the deviation of the actual distribution $N_s^q(\equiv N)$ from the equilibrium (Planck) distribution $\bar{N} (\equiv \bar{N}_s^q)$ and is defined by

$$N = \bar{N} + \gamma_q \bar{N} (\bar{N} + 1) \quad \text{--- (3)}$$

Using $\vec{\Phi}_q = - \vec{q} \cdot \nabla T / T$ (where $\vec{\Phi}_q = \gamma_q + \delta \vec{\Phi}_q$), --- (4)

$$\bar{P}_{\vec{q}s, \vec{q}'s'} = \frac{\pi \hbar}{4 \rho^3 N_0 \Omega} \frac{\vec{q}^2 \vec{q}'^2 \vec{q}''^2}{\omega \omega' \omega''} \left| A_{\vec{q}\vec{q}'\vec{q}''} \right|^2 \bar{N} \bar{N}' (\bar{N}'' + 1) \delta(\omega + \omega' - \omega'') \delta_{\vec{q}+\vec{q}', \vec{q}''} \quad \text{--- (5)}$$

and $\vec{G} = 2 q_D \hat{q}''$ (q_D is Debye radius) --- (6)

we obtain

$$\langle \vec{\Phi}, P \vec{\Phi} \rangle_{ss's''} = \frac{N_0 \Omega q_D^{10}}{3 \pi^4 \rho^3 \alpha \alpha' C_L^4} \int dx \int dx' x^2 x'^2 (\alpha x + \alpha' x') (2 - \alpha x - \alpha' x') \times \left| A_{\vec{q}\vec{q}'\vec{q}''} \right|^2 \bar{N} \bar{N}' (\bar{N}'' + 1) \quad \text{--- (7)}$$

and

$$\langle \vec{\Phi}, \chi \rangle_s = N_0 \Omega \frac{q_D^5 \hbar C_s^2}{6 \pi^2 k_B T} \int dx x^4 \bar{N} (\bar{N} + 1) \quad \text{--- (8)}$$

where $\alpha = C_s / C_{s'}$, and $\alpha' = C_s / C_{s''}$, ρ = mass

density, $N_0 \Omega$ = Volume of crystal. Thus the upper bound⁽²⁾ of the Ziman limit of thermal resistance due to Umklapp processes is given by

$$W_{0,U}^{>} = \langle \vec{\Phi}, P \vec{\Phi} \rangle_{ss's''} / \langle \vec{\Phi}, \chi \rangle_s^2 \quad \text{--- (9)}$$

$$= \frac{12 (k_B T)^2}{\rho^3 \hbar^2 \alpha^5 \alpha' C_L^8} \frac{\int dx \int dx' x^2 x'^2 (\alpha x + \alpha' x') (2 - \alpha x - \alpha' x') \left| A_{\vec{q}\vec{q}'\vec{q}''} \right|^2 \bar{N} \bar{N}' (\bar{N}'' + 1)}{\left[\int dx x^4 \bar{N} (\bar{N} + 1) \right]^2} \quad \text{--- (10)}$$

III. HIGH AND LOW TEMPERATURE APPROXIMATIONS OF THE ZIMAN LIMIT

At low temperatures one can replace the distribution functions N etc., by exponentials so that

$$\overline{N}^n (\overline{N}^n + 1) = \exp(-\hbar\omega_0/k_bT) \exp\{-\hbar(\omega'' - \omega_0)/k_bT\},$$

where $\omega'' = \omega_0$ is the frequency where U-processes start.

Consider a geometry where $x \sim x_0$ and $x' \sim 0$ when $\omega'' = \omega_0$. In this case

$$\int dx' x'^2 (\alpha x + \alpha' x') (2 - \alpha x - \alpha' x') e^{-\frac{\hbar}{k_bT}(\omega'' - \omega_0)} \propto (x - x_0)^3 \exp\{-\hbar(\omega - \omega_0)/k_bT\}$$

In the same case no. of states of $x \propto (x - x_0) dx$, so that the whole integral in the numerator of (10) would behave like

$$\exp(-\hbar\omega_0/k_bT) \int dx (x - x_0)^4 \exp\{-\hbar(\omega - \omega_0)/k_bT\} \propto \exp(-\hbar\omega_0/k_bT) T^5$$

The integral in the denominator of (10) becomes

$$\int dx x^4 \exp(-\hbar\omega_0/k_bT) \propto T^5$$

Hence

$$\chi_{s's''}^c \propto T^{-3} \exp(-\hbar\omega_0/k_bT) \quad (T < \Theta) \quad \text{--- (11)}$$

($\Theta = \text{Debye Temp}$)

This agrees with the results obtained by Ziman.

At high temperatures one can replace N etc., by their classical values $\overline{N} \sim \frac{k_bT}{\hbar\omega_0}$. The integral in the numerator of (10), then, becomes

$$\left(\frac{k_bT}{\hbar\omega_0}\right)^3 \frac{1}{\alpha\alpha' C_L^2} \int dx \int dx' x x' (2 - \alpha x - \alpha' x') \left| A_{s's''}^{\hbar\omega_0/\hbar\omega} \right|^2$$

and the integral in the denominator of (10) becomes

$$\left(\frac{k_0 T}{\hbar q_D}\right)^2 \int x^2 dx$$

Hence at high temperatures we get

$$W_{0,U}^{>} \sim \frac{108 q_D (k_0 T)^2}{e^3 \hbar \alpha^6 \alpha' C_L^{12}} \int dx \int dx' (2 - \alpha x - \alpha' x') \left| A_{ss's''}^{\bar{q}\bar{q}'\bar{q}''} \right|^2 \quad \text{--- (14)}$$

This shows that

$$W_{0,U}^{>} \propto T \quad (T > \theta) \quad \text{--- (15)}$$

This is in agreement with the well known experimental result that at high temperatures thermal resistivity is directly proportional to temperature.

REFERENCES

1. R.A.H. Hamilton and J.E. Parrott, Phys. Rev. 178, 1284 (1969).
2. David Banin, Phys. Rev. B1, 2777 (1970).
3. J.M. Ziman, Electrons and Phonons (Oxford at the Clarendon Press, (1960). Chapters 7 and 8.

ELECTRON-PHONON SCATTERING IN Te-DOPED GaSb AT LOW TEMPERATURES

P. C. Sharma and G. S. Verma

Physics Department, Banaras Hindu University, Varanasi-5

Recently Poujade and Albany¹ have measured the thermal conductivity K at low temperatures in Te-doped GaSb samples with excess donor electron concentration n ranging between 10^{17} and $2 \times 10^{18} \text{ cm}^{-3}$. As the concentration of donor electron increases, K decreases drastically below the conductivity maximum. They could explain their experimental results at temperatures beyond the conductivity maximum only, the region where phonon-phonon scattering dominates over other phonon scattering processes. While discussing the various possibilities for this drastic reduction in the phonon conductivity at temperatures below the conductivity maximum, they realised that electron-phonon scattering, which leads to $\tau^{-1} \propto n^2$, may be responsible for the observed behaviour. They simply discussed this as well as other possibilities but made no attempt to explain their data and reach at any definite conclusions. In the present work it has been established that one can explain the drastic reduction in the phonon conductivity with doping on the basis of Ziman scattering, which is valid only for those cases for which impurity levels merge with the conduction band. The present calculations support that with the increase in donor electron concentration the density-of-states effective mass increases. (See last column of Table

Table 1

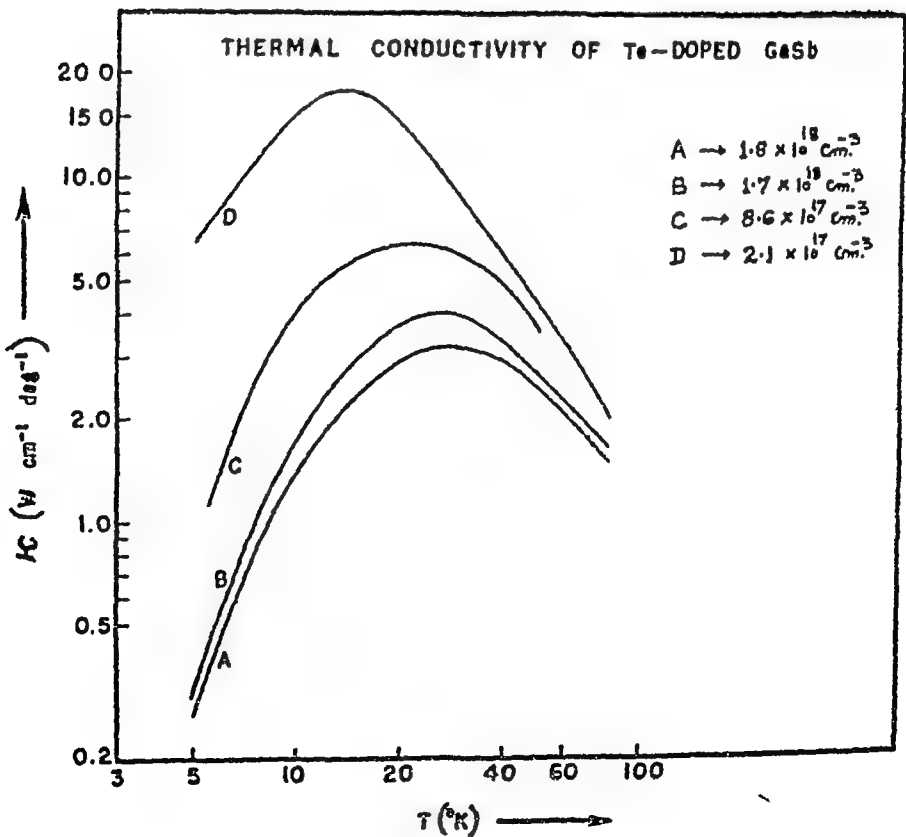
Following numerical values have been used in this work.

$$A = 0.813 \times 10^{-44} \text{ sec}^3 ; E_f = 0.0517 \text{ e.v.}$$

$$C_L = 3.09 \times 10^5 \text{ cm/sec} ; \epsilon = 16.3 \text{ e.v.}$$

$$B = 0.7 \times 10^{-22} \text{ sec. deg}^{-3}.$$

Sample	$n(\text{cm}^{-3})$	m_d^2
40 f	1.8×10^{18}	0.488
40 d	1.7×10^{18}	0.46
74 a	8.6×10^{17}	0.30
34 a	2.1×10^{17}	0.064



The phonon conductivity in the Debye's approximation is given by

$$\chi = \frac{k_0}{2\pi^2 c} \left(\frac{k_0}{h}\right)^3 T^3 \int_0^{\Theta_D/T} \frac{x^2 e^x / (e^x - 1)^2}{\tau_c^{-1}} dx$$

where τ_c is the combined relaxation time. Assuming the additivity of inverse relaxation times one can express

$$\tau_c^{-1} = \tau_0^{-1} + \tau_{pt}^{-1} + \tau_{3\mu}^{-1} + \tau_{ep}^{-1}$$

where $\tau_0 = L/c$ is the relaxation time for the boundary scattering of phonons.

$\tau_{pt}^{-1} = A\omega^4$ is the relaxation time for impurity scattering.

$\tau_{3\mu}^{-1} = B\omega^2 T^3$ is the relaxation time for three phonon² Normal and Umklapp processes.

$$\tau_{ep}^{-1} = DT \ln \frac{1 + \exp[\gamma^* - N/T - \rho T x^2 + x/2]}{1 + \exp[\gamma^* - N/T - \rho T x^2 - x/2]}$$

is the relaxation time for the scattering of phonons by electrons. (Ziman scattering)³

$$\text{where } D = \frac{\varepsilon^2 m_d^{*2} k_0 \delta^3}{2\pi \hbar^4 M c_L}, \quad N = \frac{m_d^* c_L}{2 k_0}$$

$$\text{and } \rho = \frac{k_0}{8 m_d^* c_L^2}$$

Here ϵ is the deformation potential constant, δ^3 is the atomic volume, M is the mean atomic weight, c_L is the velocity for longitudinal phonons and m_d^* is termed as density-of-states effective mass.

This work suggests that with the change in the carrier concentration of donor electrons the density-of-states effective mass changes. Ziman³ scattering is valid for the samples where the concentration of donor electron is more than 10^{17} cm^{-3} . Contribution of electron phonon scattering seems to be maximum at lowest temperatures and a sharp reduction is obtained as one goes to temperatures above the conductivity-maximum temperature. The electron phonon scattering effect is prominent rather dominant upto 20°K in the present calculations.

REFERENCES:

1. A.M. Poujade and H.J. Albany, Phys. Rev. 182, 802 (1969).
2. J. Callaway, Phys. Rev. 113, 1039 (1959).
3. J.M. Ziman, Phil. Mag 1, 191 (1956).

PHONON CONDUCTIVITY OF GaAs IN THE TEMPERATURE RANGES 2 TO 300°K AND GUTHRIE'S TEMPERATURE DEPENDENCES.

K.S. Dubey and G. S. Verma
Department of Physics, B.H.U.,
Varanasi-5.

The frequency and temperature dependences of three phonon relaxation rate can be expressed in the form

$\tau_{3ph}^{-1} \propto g(\omega)f(T)$. So far the phonon conductivity results in different semiconductors have been explained on the basis of some explicit relations for $g(\omega)$ and $f(T)$ obtained by Peials¹, Kloxens², Herring³ and Holland⁴. Recently Guthrie⁵ has obtained the extremum values of the temperature dependence of three phonon scattering processes by expressing $f(T) = T^m$, where the exponent m also depends upon temperature $m = m(T)$. He has obtained the maximum and minimum values of m as a function of temperature for class I and class II events. Class I events are those processes in which the carrier-phonon is annihilated by combination. Class II refer to those processes in which the carrier phonons are annihilated by splitting. In principle, this approach led to correct results both at high and low temperatures, but it was of no use as m depends continuously upon temperature. However, in the present work we have shown that if one expresses $T^{m(T)} = (1 + \Theta/kT) T^{m_{av}}$ and $\tau_{3ph}^{-1} \propto g(\omega) T^{m(T)} e^{-\Theta/kT}$, it is possible to explain not only the phonon conductivity results but also one can

obtain information regarding the temperature dependence of $m(T)$. Guthrie has been able to obtain information regarding the maximum and minimum values of $m(T)$ but with the present approach it has been possible to obtain the actual temperature dependence of m . In the present paper, we present the results for GaAs.

Using Holland's⁴ formulation one can write

$$\kappa = \kappa_T + \kappa_L$$

$$\kappa_T = \frac{2}{3} \frac{k_B}{2\pi^2} \left(\frac{k_B T}{\hbar} \right)^3 \left[\left(\nu_{T1}^{-1} \right) \int_{0 < \omega < \omega_1} \frac{\Theta_1/T}{\tau_B^{-1} + \tau_{pt}^{-1} + \beta_T \omega T^{m_T(T)}} \frac{x^4 e^x (e^x - 1)^{-2} (1 + \gamma_1 \omega^2)^2 (1 + 3\gamma_1 \omega^2)^{-1} dx}{e^{-\Theta/\kappa T}} \right. \\ \left. + \left(\nu_{T2}^{-1} \right) \int_{\omega_1 < \omega < \omega_2} \frac{\Theta_2/T}{\tau_B^{-1} + \tau_{pt}^{-1} + \beta_T \omega T^{m_T(T)}} \frac{x^4 e^x (e^x - 1)^{-2} (1 + \gamma_2 \omega^2)^2 (1 + 3\gamma_2 \omega^2)^{-1} dx}{e^{-\Theta/\kappa T}} \right]$$

$$\kappa_L = \frac{1}{3} \frac{k_B}{2\pi^2} \left(\frac{k_B T}{\hbar} \right)^3 \left[\left(\nu_{L1}^{-1} \right) \int_{0 < \omega < \omega_4} \frac{\Theta_4/T}{\tau_B^{-1} + \tau_{pt}^{-1} + (\beta_{LI} T^{m_L(T)} + \beta_{LII} T^{m_{LI}(T)}) \omega^2} \frac{x^4 e^x (e^x - 1)^{-2} dx}{e^{-\Theta/\kappa T}} \right. \\ \left. + \left(\nu_{L2}^{-1} \right) \int_{\omega_4 < \omega < \omega_3} \frac{\Theta_3/T}{\tau_B^{-1} + \tau_{pt}^{-1} + (\beta_{LI} T^{m_L(T)} + \beta_{LII} T^{m_{LI}(T)}) \omega^2} \frac{x^4 e^x (e^x - 1)^{-2} (1 + \gamma_3 \omega^2)^2 (1 + 3\gamma_3 \omega^2)^{-1} dx}{e^{-\Theta/\kappa T}} \right]$$

Where for class I events

$$m_I(T) = \frac{1}{2} x_{\max} + \frac{x_{\max}}{(e^{x_{\max}} - 1)} + \frac{\log(1 + \Theta/\kappa T)}{\log T}$$

and for Class II events

$$m_{II}(T) = 0.5 \frac{x_{\max}}{(e^{x_{\max}} - 1)} e^{0.5 x_{\max}} + 0.5 + \frac{\log(1 + \Theta/\kappa T)}{\log T}$$

Here $x = \hbar\omega/k_B T$ and α is a constant which depends upon the structure of the crystal. The factor $(1 + \gamma_i \omega^2)^2 (1 + 3\gamma_i \omega^2)^{-1}$ is the correction term which v_g/v_p^2 and taken into account the dispersion of ω vs. q curves.

The values of the various parameters used in the

Table No. 1.

The parameters which are used in analysis are given below.

$$\Theta_1 = 90^\circ \text{K}$$

$$\Theta_2 = 101.5^\circ \text{K}$$

$$\Theta_3 = 313^\circ \text{K}$$

$$\Theta_4 = 187^\circ \text{K}$$

$$v_{T1} \omega_1 \omega_2 \omega_3 = 2.48 \times 10^5 \text{ cm/sec}$$

$$v_{T2} \omega_1 \omega_2 \omega_3 = 0.90 \times 10^5 \text{ cm/sec}$$

$$v_L = 4.73 \times 10^5 \text{ cm/sec}$$

$$\gamma_{ax} = 2.084 \times 10^{-27} \text{ sec}^2$$

$$[\gamma_1]_{100} = 2.060 \times 10^{-27} \text{ sec}^2$$

$$[\gamma_1]_{111} = 2.107 \times 10^{-27} \text{ sec}^2$$

$$[\gamma_2]_{100} = 6.056 \times 10^{-27} \text{ sec}^2$$

$$[\gamma_2]_{111} = 8.393 \times 10^{-27} \text{ sec}^2$$

$$[\gamma_3]_{100} = 1.283 \times 10^{-28} \text{ sec}^2$$

$$[\gamma_3]_{111} = 1.042 \times 10^{-28} \text{ sec}^2$$

$$\alpha = 2$$

$$\beta_T = 1.57 \times 10^{-6} \text{ deg}^m$$

$$\beta_{LII} = 2.07 \times 10^{-18} \text{ sec deg}^m$$

$$\beta_{LII} = 1.0 \times 10^{-24} \text{ sec deg}^m$$

(can be neglected)

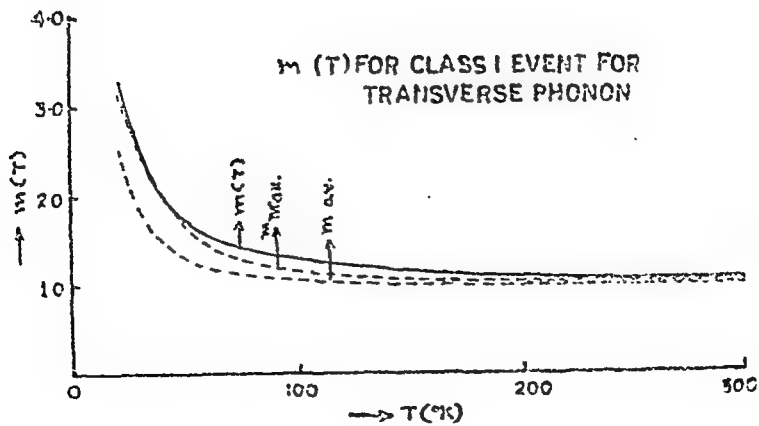
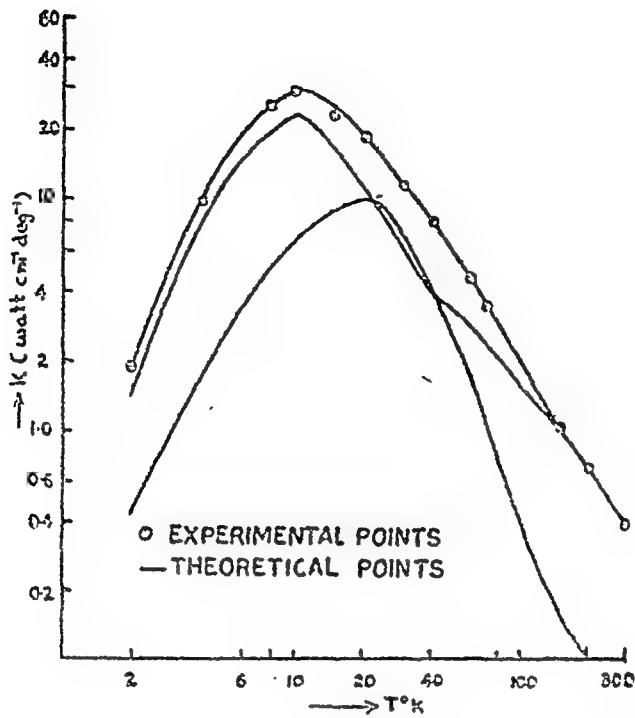
$$\gamma_{av} = 7.224 \times 10^{-27} \text{ sec}^2$$

$$\gamma_{av} = 1.163 \times 10^{-28} \text{ sec}^2$$

$$\Theta_0 = 345^\circ \text{K}$$

$$\tau_B^{-1} = 5.94 \times 10^5 \text{ sec}^{-1}$$

$$A = 1.30 \times 10^{-44} \text{ sec}^3$$



analysis of the phonon conductivity data are given in table I. Fig. 1 shows the comparison between the theoretical and experimental values of phonon conductivity of GaAs in the temperature range 2 to 300°K⁶. The temperature dependence of $\kappa(T)$ for Class I events for T phonons is shown in Fig. 2. It may be seen from this figure.

References

1. H.E. Peierls, quantum Theory of Solids
(Clarendon Press, Oxford, England, 1955)
2. P.O. Klenows, Proc. Phys. Soc. (Lond.) A68, 1113 (1955)
3. G. Herring, Phys. Rev. 95, 954 (1954)
4. M.C. Holland, Phys. Rev. 132, 2461 (1963)
5. G.L. Guthrie, Phys. Rev. 152, 801 (1968)
6. M.C. Holland, Phys. Rev. 134, A471 (1964)

DISCUSSION

K.N. Pathak

What is the importance of four phonon processes on thermal conductivity of insulators?

G.S. Verma

Four phonon processes become important in the high temperature region and it has been already established by us that one cannot explain the phonon conduc-

tivity of Si and Ge beyond 500°K without taking four phonon processes into account. The four phonon relaxation rate is given by $\tau_{4 \text{ phonon}}^{-1} = B_H \omega^2 T^2$. This is to be included in the

$$\tau_{\text{cond. band}}^{-1} = \tau_{\substack{\text{other} \\ \text{processes}}}^{-1} + \tau_{4\text{-phonon}}^{-1}$$

THE THERMAL CONDUCTIVITY OF NICKEL

M.S.R. Chari
National Physical Laboratory
New Delhi-12

I. INTRODUCTION

The electrical resistivity of ferro-magnetic metals has been analysed by Weiss and Marotta⁽¹⁾ assuming the intrinsic electrical resistivity ρ_i to be given by the Bloch-Gruneisen expression. For temperatures T above T_c (the Curie temperature) and θ (the Debye temperature), the Bloch-Gruneisen term reduces to AT/θ (A being a constant for the metal) and the magnetic term is independent of T . Since the experimental ρ - T curves at such temperatures are linear, the slope gives A/θ , whereby ρ_i at the temperature T can be obtained.

The magnetic (w_{em}) and the residual (w_{eo}) components of the electronic thermal resistivity (w_e) are obtained from the corresponding electrical resistivity components using the normal Sommerfeld value (L_n) of the electronic Lorenz number (L_e). For obtaining the intrinsic component (w_{ei}) of w_e from ρ_i , one should use the Makinson value⁽²⁾ of L_e .

An analysis⁽³⁾ of the thermal conductivity (k) of iron in this manner gave the electronic (k_e) and lattice (k_g) components agreeing with those obtained by employing a modified Wiedemann-Franz-Lorenz relation due to Lindo and Backlund⁽⁴⁾.

In the case of nickel, the analysis⁽⁵⁾ based on

Backlund's method led to the illogical result of the k_g rising with T even at temperatures as high as 400 K. (We will confine ourselves to the temperature region above 400 K). It is shown in this paper that this can be traced to the high sensitivity of the thermal properties of nickel to impurities.

II. ANALYSIS OF DATA

According to the Backlund method, w_{ei} is given by the modified Wiedemann-Franz relation.

$$w_{ei} = (\rho_1 + \bar{\rho}_0) / L_n T \dots\dots\dots(1)$$

where $\bar{\rho}_0$ is ρ_0 times the intercept on the negative side of the resistivity axis of the rectilinear ρ_1 - T plot and is presumably due to zero-point energy. It is evident that $\bar{\rho}_0$ will be the larger, the steeper the ρ_1 - T curve. Owing to the essentially inelastic nature of the electron-phonon interaction at these temperatures, it would be appropriate to use the electronic Lorenz number deduced by Makinson (for the case of a monovalent metal rather than L_n . However, if $\bar{\rho}_0$ is large enough, it compensates somewhat for the inappropriate use of L_n in equation (1). This is why the analysis of the conductivity of iron by earlier method leads to similar results.

Powell et al⁽⁵⁾ give 27 and 31 respectively (in units of 10^{-11} ohm-m/K) for $d\rho/dT$ of their nickel samples No. 5 and No. 1 in the paramagnetic state. Their data on the former show that i) using L_n leads to a $k_g(T)$ larger than the measured (total) thermal conductivity and ii) using the Backlund method leads to k_g

increasing with the rise of temperature. Neither of these conform to our present-day concepts of the transport properties of metals. On the other hand, using the Makinson value of the electronic Lorenz number, we find the components k_e and k_g conforming to expectations. w_e presents a rather shallow peak (of 2 mK/°) at T_c . k_g presents a minimum at 570 K and a maximum at 770 K. The magnon conductivity is considered as included in k_g .

The recent data of Kirichenko and Mikryukov⁽⁶⁾ on nickel of better than 99.999 percent purity give dP/dT equal to 35 above T_c . For this, the analysis based on the Backlund method and our method using the Makinson value of L_0 give comparable results. The Backlund method fails for the less pure nickel specimens on which data is available. This is to be traced to a smaller value of dP/dT (in the paramagnetic state) and a correspondingly smaller value of $\bar{\rho}_0$. This is not able to compensate for the inappropriate use of L_H (in place of the Makinson value).

The data of Kirichenko and Mikryukov⁽⁶⁾ for the very dilute Nickel-Rhenium alloys show a larger drop in the thermal conductivity at 400 K as compared with that for their pure nickel. The sensitivity of the thermal conductivity and diffusivity of pure nickel to impurities as also pointed out by Sidles and Danielson.⁽⁷⁾

REFERENCES

- R.J. Weiss and A.S. Kirovta; J. Phys. Chem. Solids
2, 302 (1950).
R.E.B. Makinson; Proc. Camb. Phil. Soc.
34, 474 (1929).

3. M.S.R. Chari; Phys. Stat. Sol.
19, 169 (1967).
4. N.G. Backlund; J. Phys. Chem. Solids,
20, 1 (1961).
5. R.W. Powell, R.P. Tye and M.J. Hickman; Int.J.Mass
Heat Transfer 8, 679 (1965).
6. P.I. Kirichenko and V.E. Mikryukov; High Temp.,
2, 176 (1964).
7. P.H. Sidles and G.C. Danielson; 'Thermo-electricity'
Ed. P.G. Egli (1960), p 270.

MAGNETIC PROPERTIES OF SOLIDS

MAGNETIC PROPERTIES OF SOLIDS

CONFIGURATION INTERACTION AND COVALENT METAL LIGAND INTERACTION OF Cu^{2+} IN DODECAHEDRAL DISPOSITION.

A. K. Roy and S. Roy, Saha Institute of Nuclear Physics, Calcutta-9, and A. K. Pal, Indian Association for the Cultivation of Science, Magnetism Department, Calcutta-12.

I. INTRODUCTION

Magnetic studies of dodecahedrally co-ordinated copper complex, copper calcium acetate hexahydrate and Cu^{2+} doped in isomorph cadmium calcium acetate hexahydrate host lattice were reported in the last symposium held at Borker, India, 1969. In the present communication, the spin-Hamiltonian parameters and the optical polarized data are utilized for the assignment of the ligand field levels conforming to the D_{2d} symmetry and for estimation of covalent character of the ligand field.

II. RESULTS AND DISCUSSIONS OF THE SPIN HAMILTONIAN PARAMETERS

The expression for the spin-Hamiltonian parameters can be written, following Pal and Pal², as

$$g_1 = 2 \left[1 - \frac{4b^2 R_{14} k_{14} \zeta_A}{\Delta_{41}} - \frac{b^4 R_{12}^2}{\Delta_{21}^2} \left(\zeta_A^2 - 2\gamma^2 \zeta_A \zeta_B + \gamma^4 \zeta_B^2 \right) - \frac{b^6 R_{12}^2 k_{12}^2}{2\Delta_{21}^3} \left(\zeta_A - \gamma^2 \zeta_B \right) \left(\zeta_A - \gamma^2 \zeta_A - \gamma^2 \zeta_B + \gamma^4 \zeta_B \right) - \frac{2b^4 R_{12} R_{14} k_{14}}{\Delta_{21} \Delta_{41}} \left(\zeta_A^2 - \gamma^2 \zeta_A \zeta_B \right) \right]$$

$$g_2 = 2 \left[1 - \frac{b^4 R_{12} k_{12}}{\Delta_{21}} (1 - \gamma^2) (\zeta_A - \gamma^2 \zeta_B) - \frac{b^4 R_{12}}{2\Delta_{21}^2} \times (\zeta_A^2 - 2\gamma^2 \zeta_A \zeta_B + \gamma^2 \zeta_B^2) \{ R_{12} - b^2 R_{12} k_{12} (1 - \gamma^2) \} + \frac{b^4 R_{14}}{\Delta_{21} \Delta_{41}} \{ R_{12} k_{14} (\zeta_A^2 - \gamma^2 \zeta_A \zeta_B) - R_{14} k_{12} (1 - \gamma^2) \zeta_A^2 \} - \frac{2b^2 R_{14}^2 \zeta_A^2}{\Delta_{41}^2} \right]$$

$$A_{11} = -k_0 R_{11} p^2 [P_d + \gamma^2 P_p] - R_{11} p^2 [4/7 P_d - 4/5 P_p] \\ + (2I_1 - 2) \frac{R_{14}}{k_{14}} P_d + (2I_1 - 2) \frac{R_{12}}{k_{12}(1-\gamma^2)} [3/7 P_d + 3/5 \gamma^2 P_p]$$

$$A_{-1} = -k_0 R_{11} p^2 [P_d + \gamma^2 P_p] + R_{11} p^2 [2/7 P_d - 2/5 \gamma^2 P_p] \\ + \frac{(2I_1 - 2) R_{12}}{k_{12}(1-\gamma^2)} [11/14 P_d - 13/10 \gamma^2 P_p]$$

where k_{ij} and R_{ij} are orbital and spin-orbit reduction parameters³; $\Delta_{ij} (= E_i - E_j)$ are ligand field splitting corresponding to i th and j th ligand field level. $p^2 = \frac{1}{1+\gamma^2}$; γ^2 represents the average $4p$ contribution towards $2p$ ($3d$) orbitals; ζ_p and ζ_d are spin orbit coupling coefficients of $Cu(4p)$ and $Cu(3d)$ orbitals related as

$$\frac{\zeta_p}{\zeta_d} = \frac{P_p}{P_d} = (925 \pm 40) \pm 829 \quad \text{for free copper ion} \\ \text{(Bates, 1962)}$$

The parameter k_0 takes into account isotropic Fermi type interaction and has a value of about 0.43 ± 0.02 for free Cu^{2+} ion (Abragam et al., 1955).

Although the analysis of the polarised optical spectra in the doped crystal shows $\Delta_{21} = 14000 \text{ cm}^{-1}$ ($2B_2 \rightarrow 2B_1$), $\Delta_{51} = 12800 \text{ cm}^{-1}$ ($2B_2 \rightarrow 2A_1$), there is uncertainty in the value of the energy separation Δ_{41} (i.e. $2B_2 \rightarrow 2B_1$). On the other hand, the number of theoretical parameters to be evaluated outnumber the no of observables. Some simplifying assumptions⁴ are made viz $R_{1j} \approx N_1 N_j$ (N_1 and N_j are normalisation constants connected with i th and j th levels respectively) since the spin-orbit coupling of oxygen ligands is small compared to that of Cu^{2+}

and $k_{ij} \approx R_{ij}$. It may be noted that for a fixed value of 4p admixture, no improvement in the fitting of hyperfine coupling constants by taking $k_{ij} \neq N_i N_j$ is obtained. The results are shown in the Table I.

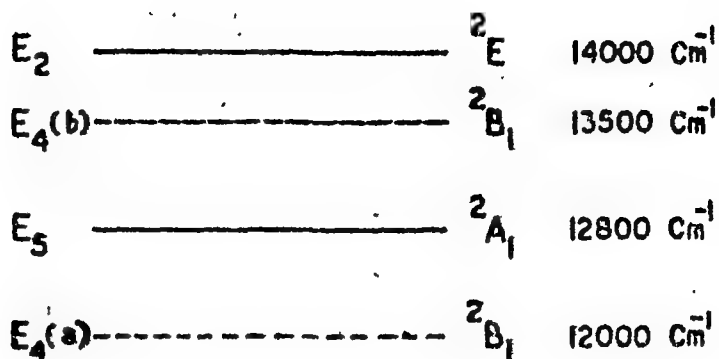
Table I - Results of theoretical fitting of spin-Hamiltonian parameters

Parameters	Theoretical value	Experimental value	$k_0 = 0.41$	$\gamma^2 = 0.02$
$g_{ }$	2.36	2.36	$C_p = -885 \text{ cm}^{-1}$	$C_d = -829 \text{ cm}^{-1}$
g_{\perp}	2.07	2.07		
$A_{ }$	-0.01185 cm^{-1}	-0.0119 cm^{-1}	$N_1^2 = 0.76$	$N_2^2 = 0.90$
A_{\perp}	-0.0017 cm^{-1}	-0.0015 cm^{-1}	$N_4^2 = 0.88 \text{ to } 1.0$	

It is found that 4p admixture in 2_{B_2} and 2_{B_1} states is small (at most 2%) whereas the covalencies of the states are 25% and 10% respectively. It is further realised that $2_{B_1} \leftrightarrow 4_{B_1}$ repulsion can not exceed 13500 cm^{-1} because of the restriction that covalency parameter N_4^2 connected with 2_{B_1} level can be at most equal to unity for purely ionic cases. 2_{B_1} state lies somewhere between 13500 cm^{-1} and 12000 cm^{-1} above the ground state. Maximum covalency that can be assigned to this state is about 12%. The proposed ligand field scheme is shown in Fig.1.

III. REFERENCES

1. A. K. Roy, E. Roy and A. K. Pal, Proc. Nuclear & Solid State Physics Symposium, Bhubaneswar, India (1969).
2. A. K. Pal and D. Pal (nee Mukhopadhyay), Proc. Nuclear & Solid State Physics Symposium, Bhubaneswar, India (1969).
3. K. R. W. Stevens, Proc. Roy. Soc. (London), A219, 542 (1953).
4. A. A. Missetich and T. Buch, J. Chem. Phys., 41, 2524 (1964).



²D, ³F₄



FREE ION

D_{2d} FIELD

PROPOSED LIGAND FIELD SCHEME

Fig-1

DISCUSSION

J.R. Perumareddi

Should not there be another orbital singlet in the energy diagram? Why is it missing?

A.K. Pal

Transition to that level is forbidden, so it is not included.

H.D. Bist

You have not considered at all the effect of vibronic interaction. The 1200 cm^{-1} difference between 12800 and 14000 cm^{-1} could very well be explained as a CO vibrational frequency in the excited state?

A.K. Pal

The observed bands have intensity characteristics of d-d bands so the occurrence of CO vibrational band does not arise in the present case.

R. Srinivasan

ESE work on this system has also been reported by Dr. Herring and collaborators from the University of British Columbia, Vancouver.

MAGNETIC STUDIES OF TRIGONAL BIPYRAMIDAL [Cu(II)N₃] COMPLEX IN COPPER TREN ISOTHIOCYANATE

A.K.Pal, D.Pal and C.Bose

Magnetism Department, Indian Association for the Cultivation of Science, Calcutta-32

I. INTRODUCTION

In a communication to the previous year's Symposium at Roorkee¹ the possible consequences of the ligand field due to trigonal bipyramidal mode of arrangement of primary ligand cluster of Cu(II) on the spin-Hamiltonian parameters (g and A) and on magnetic susceptibilities have been discussed. In the present work, measurements of g -factors, mean magnetic susceptibility and crystalline anisotropies of copper tren isothiocyanate in the temperature range 300°K - 90°K and hyperfine structure in inert solvent (methanol) at 300°K have been reported. Covalent reduction parameters have also been estimated from a semiempirical analysis of the experimental findings.

II. EXPERIMENTAL

Magnetic susceptibility of the powdered sample and crystalline anisotropies ($\chi_0 \sim \chi_a$) and ($\chi_c \sim \chi_b$) have been measured by very sensitive photo-electrically controlled Curie² and magnetic anisotropy³ balances constructed in this laboratory. Angular variations of g -factors have been measured in three principal crystalline planes [100], (010) and (001)] of the orthorhombic crystal (space group P_{212121} , $Z \approx 4$)⁴ by a reflection type X-band E.P.R. spectrometer. Hyperfine splitting in methanol solution has been observed at room temperature. Although there are two magnetically inequivalent Cu(II) complexes per unit cell, only one signal has been detected in all directions probably due to minor effects of exchange interaction (nearest Cu neighbors are at $\sim 7\text{\AA}$ apart). Moreover, magnetic units are situated at general positions. So, even on axial approxi X

determined direction cosines (α, β, γ) of the symmetry axis of $[\text{CuN}_5]$ cluster are required for derivation of ionic g -factors (g_{11}, g_{\perp}) and susceptibilities (K_{11}, K_{\perp}) from respective crystalline values (g_a, g_b , and g_c ; X_a, X_b and X_c) :

$$g_{11}^2 \sim g_{\perp}^2 = \frac{g_a^2}{\alpha^2 \sim \beta^2} = \frac{g_b^2}{\beta^2 \sim \gamma^2} = \frac{g_c^2}{\gamma^2 \sim \alpha^2} \dots\dots\dots(1)$$

$$K_{11} \sim K_{\perp} = \frac{X_a}{\alpha^2 \sim \beta^2} = \frac{X_b}{\beta^2 \sim \gamma^2} = \frac{X_c}{\gamma^2 \sim \alpha^2} \dots\dots\dots(2)$$

From measurements it has been established that $g_b > g_c > g_a$ and $X_b > X_c > X_a$ in the temperature interval $300^\circ\text{K} - 90^\circ\text{K}$. With the values of X-ray determined α, β and γ although it has been found from room temperature measurements that $g_{\perp} > g_{11}$ and $K_{\perp} > K_{11}$ in accordance with theoretical expectation¹, g_{11} comes out to be much less than 2. Evidently

TABLE I

$g'_{12}, \bar{A} \text{ \& } \Delta_{12} :$

$g_{11} = 1.993 \text{ (1.993)}$
 $g_{\perp} = 2.194 \text{ (2.193)}$

$\bar{A} = |1.0048| \text{ cm}^{-1} (-0.0048 \text{ cm}^{-1})$
 $\Delta_{12} ({}^2A' \rightarrow {}^2E'') = 12 \text{ kK (12 kK)}$

Magnetic susceptibility :

Temp ($^{\circ}\text{K}$)	300	240	200	140	90
$\Delta K (= K_{\perp} - K_{11}) \times 10^6$	341.5 (340.4)	412.2 (405.9)	481.5 (471.3)	555.4 (539.6)	976.7 (951.1)
$\bar{K} (= \bar{X}) \times 10^6$	1469 (1468)	1828 (1823)	2187 (2177)	3109 (3087)	4818 (4772)

Covalency reduction parameters :

$R_{12} = .777 ; R_{13} = .630 ; R_{11} = .568$

this can not be accounted for by postulation of any ligand field of symmetry lower than D_{3h} (i.e D_2, C_2 or C_{2v}). On the other hand, it appears that magnetic and geometric axes are not in one to one correspondance. Under the circumstances, we have evaluated α, β and γ by a trial and error procedure so that the derived values of $(g_{\perp}^2 - g_{11}^2)$

and $(K_{\perp} - K_{\parallel})$ from measurements in three principal planes at room temperature are quite consistent with each other, giving due attention to the fact that $g_{\perp\parallel}$ is just less than 2 (as theoretically follows for D_{3h} symmetry). The magnetic symmetry axis so derived has been found to be tilted from the X-ray determined approximate symmetry axis by about 4.8° . This is presumably due to substantial role played by the secondary ligands in modifying the magnetic ellipsoid. The thermal variation of mean susceptibility (\bar{K}) , derived $(K_{\perp\parallel} - K_{\parallel})$, $g_{\perp\parallel}$ and g_{\perp} are given in table I.

III RESULTS OF FITTING OF g-FACTORS, \bar{A} AND MAGNETIC SUSCEPTIBILITIES :

Theoretical expressions for g's, A's and K's are¹

$$g_{\perp\parallel} = 2 \left[1 - \frac{3Q^2 R_{12}^2 S_d^2}{\Delta_{21}^2} \left(1 - \frac{k_{22}}{2} \right) \right]$$

$$g_{\perp} = 2 \left[1 - \frac{3Q^2 R_{12}^2 k_{12} S_d}{\Delta_{21}} - \frac{3Q^2 R_{12}^2 S_d^2}{2 \Delta_{21}^2} - \frac{3Q^2 R_{12} R_{22} k_{12} S_d^2}{2 \Delta_{21}^2} \right]$$

$$A_{\perp\parallel} = -K_0 Q^2 (P_d R_{11} + P_s d^2) - \frac{4}{7} Q^2 P_d R_{11} \frac{1}{7} (g_{\perp} - 2) \frac{R_{12}}{k_{12}} P_d$$

$$A_{\perp} = -K_0 Q^2 (P_d R_{11} + P_s d^2) + \frac{2}{7} Q^2 P_d R_{11} \frac{15}{14} (g_{\perp} - 2) \frac{R_{12}}{k_{12}} P_d$$

$$K_{\perp\parallel} = \frac{N\beta^2}{4kT} \cdot g_{\perp\parallel}^2$$

$$K_{\perp} = \frac{N\beta^2}{4kT} g_{\perp}^2 + 2N\beta^2 \cdot \frac{3Q^2 k_{12}}{\Delta_{21}}$$

Where R_{ij} and k_{ij} are called covalent reduction parameters,

Δ_{21} is the energy separation between the ground level $^2A'$ and excited level $^2E''$. Polarised spectral study of Hathaway et al⁵ in similarly constituted $[\text{Cu}(\text{NH}_3)_2] \text{Ag}(\text{SO}_3)$ definitely establishes that $^2E''$ lies lower than $^2E'$ and hence of the two bands observed by Barbucci et al⁶ in copper tren isothiocyanate in powdered state and in methanol the lower band at 12 kK can be assigned as $^2A' \rightarrow ^2E''$ transition i.e. $\Delta_{21} = 12 \text{ kK}$. Since there are effectively three observables i.e. g_{\perp} , K_{\perp} and \bar{A} , we have made two important assumptions in order to arrive at a

unique solution of the problem : (i) $4s$ orbital admixture with d_{z^2} orbital is taken to be negligible i.e. $Q=1$ and $\alpha=0$. (ii) average values of reduction parameters have been assumed in estimating third order contributions. The results of fitting $\Delta K, \bar{K}$, g 's and \bar{A} are shown in Table I (within parenthesis). There are small and systematic deviations of the experimental values from those theoretically obtained (2.5% and 1% ΔK and \bar{K} respectively at $90^\circ K$). It will be seen from theoretical fitting of \bar{A} that theoretically obtain values of A_{11} and A_1 are -0.0213 cm^{-1} and $+0.0034 \text{ cm}^{-1}$ respectively in conformity with the theoretical prediction¹ that $|g_{11}| < |g_1|$ whereas $|A_{11}| > |A_1|$. Values^{of} reduction parameters (vide Table I) are also indicative of profound covalent character of the ligand field levels 2A_1 and 2E_g .

Acknowledgments : The authors are indebted to Prof. A. Bose, D.Sc.F.N.A. for his valuable suggestions and advice. The authors are thankful to Prof. K.N.Raymond of University of California, Berkeley for the generous supply of the copper tren compound.

REFERENCES

1. A.K.Pal & D.Pal (née Mukhopadhyay) ; Proc.Nucl.Phys. Solid State Phys.Symposium,Roorkee,Vol.III(1969).
2. A.Bose, S.K.Dutta Roy,P.K.Ghosh & S.Mitra;Indian J. Phys.37,505(1963).
3. D.Guha Thakurta & D.Mukhopadhyay; Indian J.Phys. 40,69(1966).
4. P.C.Jain & E.C.Lingafelter;J.Am.Chem.Soc.89,4131(1967).
5. B.J.Hathaway,D.E.Billing,R.J.Faraday & A.A.G.Tomlinson; J.Chem.Soc. (A),806 (1970).
6. R.Barbucci, G.Cialdi, G.Ponticelli & P.Paoletti ; J. Chem.Soc.(A), 1775(1969).

J.R. Perumareddi

The actual symmetry is probably less than D_{3h} . In that case deducing covalency merely from the reduction of spin-orbit parameter (neglecting lower symmetry) may not make much sense!

A.K. Pal

The corresponding Ni complex is D_{3h} so we assumed D_{3h} . EPR results should show the proper symmetry.

CRYSTAL FIELD-SPIN ORBIT TREATMENT OF LIGAND FIELD LEVELS OF DISTORTED OCTAHEDRAL COPPER(II) SYSTEM

A.K.Pal, D.Pal and A.K.Ghoshal
Magnetism Department, Indian Association
for the Cultivation of Science, Calcutta-32

I. INTRODUCTION

In copper salts spin-orbit effect on the relative positions of ligand field levels may be comparable to those of axial and orthorhombic components of the crystal field. Well-authenticated examples demonstrating such effects are trigonal bipyramidal copper ammonium silver thiocyanate¹ and pseudo tetrahedral copper cesium chloride². In the present communication, in an attempt to interpret the recent magnetic³ and optical observations⁴ in (Cu,Zn) potassium Tutton salts, the generalised 'crystal field-spin orbit' treatment of the tetragonally distorted Cu(II) system has been dealt with.

II CRYSTAL FIELD-SPIN ORBIT CALCULATION OF LIGAND FIELD LEVELS

We will have to envisage the combined crystal field-spin orbit interaction $H' = V_{LF}(\tau, \theta, \phi) + 5\bar{L} \cdot \bar{S}$ on Cu^{2+} ($3d^9$) ion. This has been done by first constructing symmetry eigenfunctions comprising of both orbital and spin functions approximate to double groups D_{4h}' and C_{4v} and then setting up the relevant crystal-spin orbit matrix which subsequently breaks up into two submatrices (2×2 and 3×3 of Γ_8 and Γ_7 representations respectively). Neglecting second order spin-orbit contribution and assuming isotropic reduction of free ion spin-orbit coefficient $\zeta = 828 \text{ cm}^{-1}$, we finally obtain the following eigen states and eigen values for D_{4h}' ligand field :

$$\begin{aligned} \Gamma_7^a (B_{1g}) : & -\frac{4}{7} F_2(\tau) + \frac{2}{21} \langle f_4^0(\tau) \rangle + \frac{19}{21} \langle f_4^2(\tau) \rangle \\ \Gamma_6^a (A_{1g}) : & +\frac{4}{7} F_2(\tau) + \frac{4}{7} \langle f_4^0(\tau) \rangle + \frac{3}{7} \langle f_4^2(\tau) \rangle \dots \dots (1) \\ \Gamma_8^b (E_g) : & +\frac{2}{7} F_2(\tau) - \frac{8}{21} \langle f_4^0(\tau) \rangle - \frac{2}{7} \langle f_4^2(\tau) \rangle \end{aligned}$$

$$\Gamma_7^{b,c}(B_{2E}, E, \xi) = -\frac{1}{7} F_2(r) - \frac{1}{7} \langle \rho_4(r) \rangle - \frac{11}{21} \langle \rho'_4(r) \rangle + \frac{\xi'}{4} + \frac{1}{2} \left[\frac{3}{2} \xi'^2 + x^2 + 8x \right]^{1/2}$$

$$\text{where } x = \frac{2}{7} F_2(r) - \frac{10}{63} \left[\langle \rho_4(r) \rangle + \langle \rho'_4(r) \rangle \right]$$

$$F_2(r) = \langle \rho_2(r) \rangle - \langle \rho'_2(r) \rangle$$

$$\langle \rho_n(r) \rangle = \frac{eq}{R^{n+1}} \cdot \langle r^n \rangle, \quad \langle \rho'_n(r) \rangle = \frac{eq}{R^{n+1}} \langle r^n \rangle$$

ξ' is the reduced spin-orbit coupling coefficient.

The unprimed and primed quantities are for ligands situated on Z and (X,Y) axes respectively. For C'_{4v} field, we need only to replace $\langle \rho_n(r) \rangle$ in the above by $\frac{1}{2} [\langle \rho_n^{(1)}(r) \rangle + \langle \rho_n^{(2)}(r) \rangle]$ where superscripts (1) and (2) are for ligands situated on the z-axis at unequal distances from the central metal ion.

III ANALYSIS OF SPECTROSCOPIC RESULTS OF MATHUR et al⁴

Mathur et al⁴ observed three d-d bands in the region 11.50 kK-13.50 kK in mixed (Cu,Zn) Tutton single crystals and ascribed them as due to transitions from the ground level to the three split levels of the upper triplet $T_{2g} (O_h)$ under orthorhombic symmetry. However, polarisation characteristics of the bands do not advocate such an explanation. Since the overall splitting of the triplet is rather small (about 1.5 kK) and the axial field together with s.o. perturbation also is capable in complete removal of the degeneracy of the triplet as evident from our preceding calculations, probable optical selection rules in conjunction with requisite magnetic anisotropy informations (for both the possibilities $K_{||} > K_{\perp}$ and $K_{\perp} > K_{||}$) [Table I] have been examined in order to fit the observed polarised spectra. It has been found that the absorption bands in Cu+5.15 Zn (I) and Cu+ 13.93 Zn (II) mixed crystals can be reasonably accounted for with the assumption of C'_{4v} and D_{4h} site symmetries (selection rules given in Table II). The assignments of the bands have been presented in Table III. The respective ground levels for I and II mixed crystals are B_1 and B_{1g} . Thus Mookherjee & Lal³

and Mathur et al⁴'s speculation that $[Z^2]$ is the ground state for the more dilute salt is not justified. It appears that they have unduly relied on the room temperature E.P.R. findings of Bagguley and Griffith³ i.e. $J_A > J_B$, ignoring the fact that Bagguley and Griffith actually worked with far greater dilution (less than 1% of the copper salt in the mixed crystal).

TABLE I. Angle $K_{II} \hat{C}$ from Kookerjee & Lal³:

(Cu + Zn) $(K_2SO_4)_2 \cdot 6H_2O$	$K_{II} \hat{C} (^\circ)$	
	$K_{II} > K_A$	$K_A > K_{II}$
Cu + 4.38 Zn	93.3	24.3
Cu + 13.04	68.2	38.1

TABLE II. Polarisation selection rule for C_{4v} and D_{4h} site symmetry:

C_{4v} With electronic coupling Z (") x, y (+)			D_{4h} Vibronic coupling z (") x, y (+)		
$\Gamma_7(B_1) \rightarrow \Gamma_7(B_2)$	Allowed	Allowed	$B_{1g} \rightarrow B_{2g}$	Forbidden	Allowed
$\Gamma_7(B_1) \rightarrow \Gamma_7(E)$	Allowed	Allowed	$B_{1g} \rightarrow E_g$	Allowed	Allowed
$\Gamma_7(B_1) \rightarrow \Gamma_6(E)$	Forbidden	Allowed	$B_{1g} \rightarrow A_g$	Forbidden	Allowed
$\Gamma_7(B_1) \rightarrow \Gamma_6(A)$	Forbidden	Allowed			

TABLE III. Assignments of the bands of Mathur et al⁴

Cu + 5.15 Zn (site symmetry C_{4v})	Cu + 13.93 Zn (site symmetry D_{4h})
11.76 kK : $\Gamma_7(B_1) \rightarrow \Gamma_7(B_2)$	13.00 kK : $\Gamma_7(B_{1g}) \rightarrow \Gamma_6(E_g)$
12.50 kK : $\Gamma_7(B_1) \rightarrow \Gamma_7(E)$	12.80 kK : $\Gamma_7(B_{1g}) \rightarrow \Gamma_7(E_g)$
13.03 kK : $\Gamma_7(B_1) \rightarrow \Gamma_6(E)$	11.70 kK : $\Gamma_7(B_{1g}) \rightarrow \Gamma_7(B_{2g})$
(Absent $\perp C$)	(Absent $\perp C$)

IV. ASSESSMENT OF LIGAND FIELD PARAMETERS

In view of a large number of ligand field parameters (more so for C_{4v} ligand field) occurring in the expression (1) for energies of the ligand field levels, it is essential

Take cognizance of the following for atleast a qualitative delineation of the nature of the ligand field :

(i) In many cases s.o. coupling effects for ions in crystals are about 20% less than for free ions⁶, a value of -664 cm^{-1} for S' may be reasonably assumed. (ii) Smith's semiempirical calculation for octahedral $[\text{CuO}_6]$ system leads to $\langle r^2 \rangle = 1.4a_0^2$ and $\langle r^4 \rangle = 5.0 a_0^4$. So, taking the least Cu-O separation observed among isomorphous Tutton salts^{7,8} i.e. $3.7 a_0$ for R^2 , $\rho' (= \langle \rho'_2(r) \rangle / \langle \rho'_4(r) \rangle)$ should not be less than 3.83. Obviously, fitting of spectral results for (II) crystal have been attempted which yields two values of x i.e. $+302 \text{ cm}^{-1}$ and -80 cm^{-1} . By giving different values to the ratio R'/R both ρ' and $\Delta E [= E(\Gamma_6 A_{1g}) - E(\Gamma_7 B_{1g})]$ may be estimated for both values of x . From inspection of Table IV it readily follows that positive value of x together with $R' < R$ is only consistent with the choice of B_{1g} as the ground level and the value of $\rho' > 3.83$. This means that the magnetic ellipsoid at the paramagnetic site is elongated in sharp contrast with the observed compressed geometry of primary ligand clusters in isomorphous Tutton salts^{7,8}. It appears that the manner of disposition of secondary ligands and also of water protons may be responsible for such discrepancy and a more satisfactory correlation may be possibly achieved by incorporating such effects. Theoretical investigations in this line are presently being pursued in this laboratory. Detailed polarised spectral measurements on the series of copper Tutton salts at different temperatures with the main interest in tracking $B_{1g} \rightarrow A_{1g}$ transition have also been planned.

TABLE IV (Cu + 13.93 Zn) $(\text{K}_2\text{SO}_4) \cdot 6\text{H}_2\text{O}$

$$S' = -664 \text{ cm}^{-1}. \Delta E = E(\Gamma_6 A_{1g}) - E(\Gamma_7 B_{1g})$$

$$x = \frac{2}{7} [\langle \rho'_2(r) \rangle - \langle \rho'_4(r) \rangle] - \frac{10}{63} [\langle \rho'_6(r) \rangle + \langle \rho'_4(r) \rangle]$$

R'/R	$x = +302 \text{ cm}^{-1}$ ρ'	$\Delta E (\text{kK})$	ρ'	$x = -80 \text{ cm}^{-1}$ $\Delta E (\text{kK})$
0.980	3.380	1.982	0.307	0.528
0.985	4.182	1.795	0.119	0.324
1.004	negative	-	3.880	- 0.497
1.010	negative	-	2.107	- 0.761

Acknowledgements : The authors are indebted to Prof. A. Bose, D.Sc., F.N.A., for his valuable suggestions and advice.

REFERENCES

1. B.J.Hathaway, D.E.Billing, R.J.Dudley, R.J. & A.A.G. Tomlinson; J.Chem.Soc.(A), 808(1970).
2. J.Ferguson; J.Chem.Phys., 40, 3405(1964)
3. A.Nookherji & R.B.Lal; Indian J.Pure & Appl.Phys., 3, 288(1965).
4. S.C.Mathur, P.R.Suri & V.P.Goel; Indian J.Pure & Appl. Phys., 8, 345(1970).
5. D.M.S.Bagguley & J.H.E.Griffith; Proc. Phys. Soc.A, 65, 394(1952).
6. J.Owen; Proc. Roy.Soc.A, 227, 183(1955)
7. H.Montgomery & E.C.Lingafelter; Acta. Cryst. 17, 1295, 1478(1964); *ibid*, 20, 659, 728 (1966).
8. H.Montgomery, R.V.Chastian, J.J.Natt, A.M.Witkowska & E.C.Lingafelter; Acta.Cryst. 23, 775(1967)

DISCUSSION

J.R. Perumareddi

Spin-orbit calculations on d^1 in trigonal and tetragonal symmetry which are applicable to d^9 by the principle of hole formalism have been carried out ten years ago by Dr.A.D. Liehr (J. Phys.'Chem. 1960).

A.K. Pal

We wanted to use the axial fields also as major perturbations along with cubic fields, so we have repeated the calculations.

EFFECT OF THE CRYSTALLINE FIELD ON THE SPIN AVERAGE OF Sm^{3+} IN SAMARIUM INTERMETALLICS

S.K. Malik and R. Vijayaraghavan
Tata Institute of Fundamental Research, Colaba, Bombay-5.

I INTRODUCTION

In the case of Sm^{3+} ion the energy separation between the ground and the excited J state is only 1500°K . White and Van Vleck⁽¹⁾ have shown that there is large temperature independent contribution, associated with the second order Zeeman effect, to the spin average and the susceptibility of Sm^{3+} ion. As a consequence of this the spin average $\langle S_z \rangle_{\text{av}}$ reverses sign at about 300°K (henceforth called the crossover temperature and denoted by T_{CO}). Moreover $\langle S_z \rangle_{\text{av}}$ does not remain proportional to the susceptibility.

The spin average of the rare-earth ion can be measured by measuring the Knight shift of the non-magnetic constituent of the rare-earth alloy e.g. Sn in SmSn_3 etc. In rare-earth intermetallics it has been shown⁽²⁾ that the Knight shift can be written as

$$K - K_0 = -K_0 J_{sf} \langle S_z \rangle_{\text{av}} / g_s \beta H \quad (1)$$

where J_{sf} is the exchange constant between the 4f electron spins and conduction electron spins and K_0 is the Knight shift in the absence of any exchange interaction. The crossover of $(K - K_0)$ has been observed in a variety of Samarium compounds⁽³⁻⁵⁾ except in SmSn_3 ⁽⁵⁾ and SmAl_2 ⁽⁵⁾. Crystal fields are known to affect considerably the susceptibility of the rare-earth ions. We have investigated the effect of crystalline fields on the spin average of Sm^{3+} and find that the crossover temperature in SmSn_3 and SmAl_2 may be suppressed altogether due to strong crystalline fields which cause admixture of excited J states into the ground state of Sm^{3+} .

II CALCULATIONS AND RESULTS

The site symmetry of Sm^{3+} in SmSn_3 and SmAl_2 is cubic. The Hamiltonian for the cubic crystalline field can be written as⁽⁷⁾

$$\mathcal{H}_c = A_4^0 \sum_i \left\{ (35 z_i^4 - 30 z_i^2 r_i^2 + 3 r_i^4) + 5(x_i^4 - 6 x_i^2 y_i^2 + y_i^4) \right\} + \text{sixth degree terms} \quad (2)$$

This Hamiltonian has two effects, in first order it splits the ground state into various energy levels and in second order it causes admixture of excited J states into the ground J state. We shall first neglect this admixture and show that crystal fields do not alter the crossover temperature substantially. Subsequently we shall include the admixture and show that now the crossover temperature depends strongly on the crystal field strength.

Within a manifold of constant J the above Hamiltonian can be written as⁽⁷⁾

$$\mathcal{H}_c = B_4^0 \left[O_4^0 + 5 O_4^4 \right] + B_6^0 \left[O_6^0 - 21 O_6^4 \right] \quad (3)$$

where $B_4^0 = A_4^0 \beta \langle r^4 \rangle$ and β is the Stevens multiplication

constant. Sixth degree terms have no effect on the ground state

$J = 5/2$ of Sm^{3+} , while the fourth degree term splits $J = 5/2$ into quartet and doublet energy levels with a separation $h \nu_c = 360 B_4^0$.

The doublet lies lowest if $B_4^0 > 0$ and quartet lowest if $B_4^0 < 0$.

In the absence of crystal fields and exchange effect, the expression for spin average is given to be⁽³⁾

$$\langle S_z \rangle_{av} / H = - \sum_J p(J) \left[\frac{(g_J - 1)a}{g_J T} + b \right] \quad (4)$$

The effect of the crystalline field splitting is to reduce the $\frac{a}{T}$ term from $J = 5/2$ by the factor⁽⁸⁾

$$f(T) = \left[5 + 26 e^{-x} + (32/x) (1 - e^{-x}) \right] / 21(1 + 2 e^{-x}) \quad (5)$$

where $x = h \nu_c / kT$. Dotted curve in Fig. 2 shows the variation of

crossover point (where $\langle S_z \rangle_{av} = 0$) with B_4^0 and it is to be

noticed that T_{CG} is not altered much.

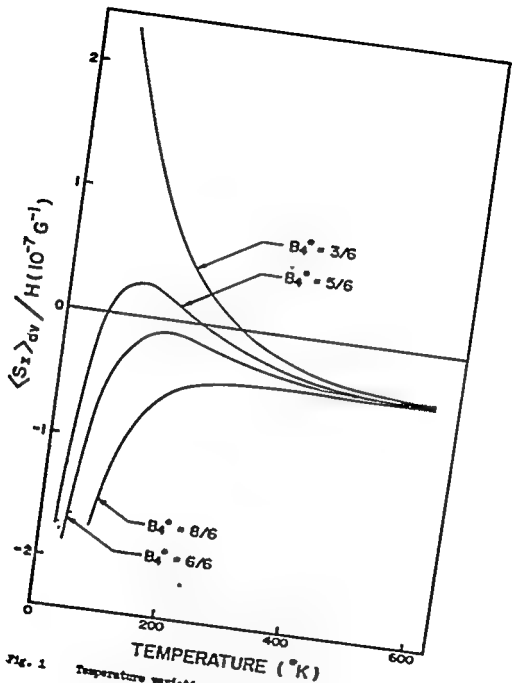


Fig. 1 Temperature variation of $\langle S_z \rangle_{av} / H$ for various values of crystal field parameter B_4^0 .

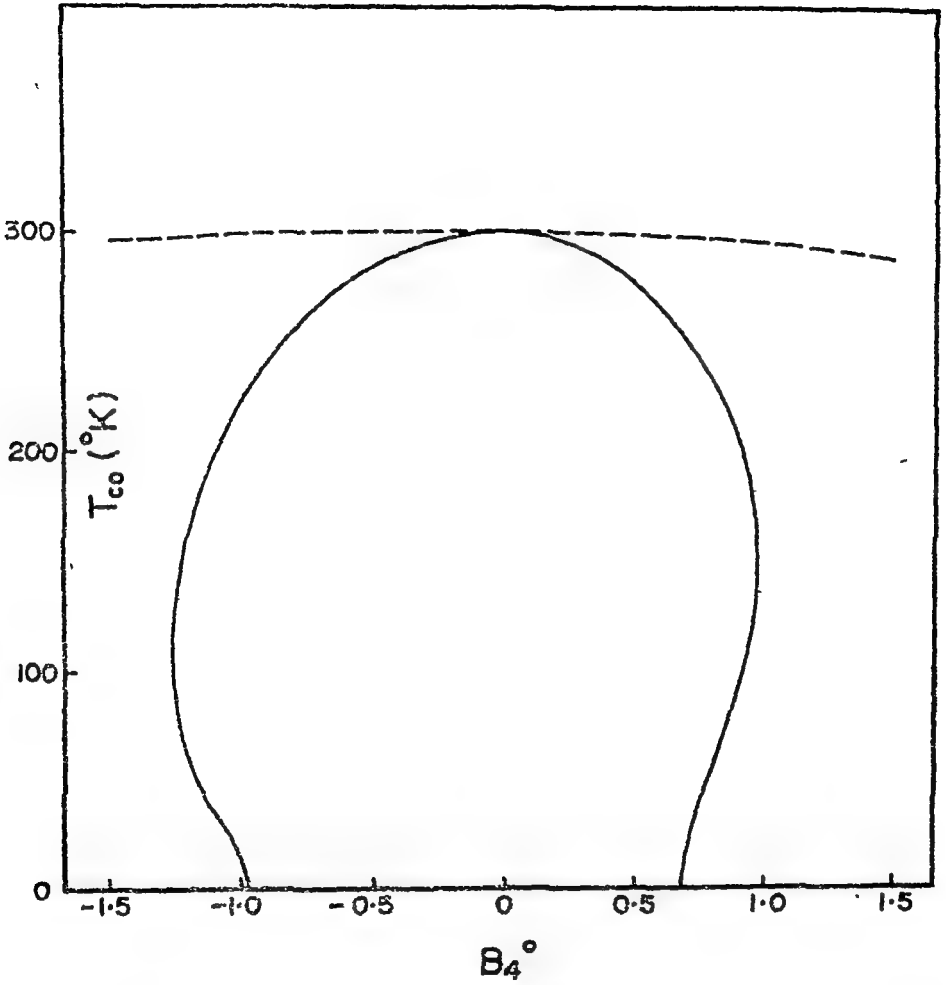


Fig. 2 Variation of crossover temperature with B_4° ; dotted curve without admixture and solid curve with admixture of $J = 7/2$ state into $J = 5/2$ state.

We now take into account admixture of excited J states into the ground state of Sm^{3+} . For simplicity we shall not include 6th degree terms in \mathcal{H}_C . The operator equivalent does not hold now. The relevant matrix elements of \mathcal{H}_C of Eq. 1 between different J states have been evaluated by Elliot⁽⁹⁾ et al and Judd⁽¹⁰⁾. Although \mathcal{H}_C can mix J states differing by ± 4 , the only non-vanishing matrix elements of S_z nondiagonal in J are those between adjacent J values. Therefore we have considered the admixture of only $J = 7/2$ into $J = 5/2$. The 14×14 secular determinant of \mathcal{H}_C and the Zeeman terms is diagonalised for various values of B_4^0 (though we use \mathcal{H}_C of Eq. 1, we still use B_4^0 as the crystal field strength parameter) to get energy eigenvalues and wavefunctions which are subsequently used to calculate the spin average. The variation of $\langle S_z \rangle_{av}/H$ with temperature for various values of B_4^0 is shown in figure 1. It is seen that for small values of B_4^0 the admixture of $J = 7/2$ state has no effect and crossover still occurs around 300°K . However, for very large values of B_4^0 the crossover has disappeared completely. There is a marked contrast between the temperature dependence of $\langle S_z \rangle_{av}/H$ for strong and weak fields, in the former it is negative and becomes more negative while in the latter it becomes more positive at lower temperatures. For intermediate values of B_4^0 two crossovers may occur.

To summarise the absence of crossover of $\langle S_z \rangle_{av}$ in SmSn_2 and SmAl_2 may arise due to strong crystalline fields. Large crystal fields have in fact been observed in other rare-earth - Al_2 compounds⁽¹¹⁾.

REFERENCES

1. J.A. White and J.H. Van Vleck; *Phys. Rev. Letters* 6, 412 (1961).
2. V. Jaccarino, B. Matthias, M. Peter, H. Suhl and J.H. Wernick;
Phys. Rev. Letters 5, 251 (1960).
3. H.W. de Wijn, A.M. Van Diepen and K.H.J. Buschow; *Phys. Rev.*
161, 253 (1967).
4. E.D. Jones; *Phys. Rev.* 180, 455 (1969).
5. S.K. Malik; *Phys. Letters* 31A, 33 (1970).
6. K.H.J. Buschow, A.M. Van Diepen and H.W. de Wijn; *Phys. Letters*
24A, 536 (1967).
7. For details see M.T. Hutchings, in Solid State Physics, edited
by F. Seitz and D. Turnbull (Academic Press, New York and
London 1964) Vol. 16, p 227 ff.
8. A. Frank; *Phys. Rev.* 48, 765 (1935).
9. R.J. Elliot and K.W.H. Stevens; *Proc. Roy. Soc. London* 218A,
553 (1953).
10. B.R. Judd; *Proc. Roy. Soc. London* 227A, 552 (1954).
11. J.A. White, H.J. Williams, J.H. Wernick and R.C. Sherwood;
Phys. Rev. 131, 1039 (1963).

SINGLE CRYSTAL EPR STUDIES OF PLANAR COPPER(II) BIS (N-PHENYLSALICYLALDIMINE)

SUBRATA LAHIRI

Dept. of Chemistry, University of Delhi, Delhi-7.

Introduction: The single crystal EPR studies on planar copper (II) complexes are quite limited, these include copper (II) acetylacetonate doped into Palladium (II) acetylacetonate¹, copper (II) bis (n-propylsalicylal-dimine)³, and copper (II) bis (salicylal-dimine)² in diluted salt. These studies show a slight orthorhombicity in the ionic g-tensor in some of these compounds. No study has been made regarding their linewidth variation.

We undertook this work to find out the orthorhombicity in the g-tensor, their direction cosines, location of the ground orbital state for the hole , in (A) $3d^9$ configuration and a study of the linewidth variation with temperature.

Copper (II) bis (N-phenylsalicylal-dimine)⁴ belongs to the monoclinic space group, $P2_1/a$, $\beta = 111^\circ 24'$ with two formula units in the unit cell. Copper (II) ion is coordinated to oxygens and nitrogens of the two salicylal-dimine groups forming a centrosymmetric square plane. The symmetry of the complex is essentially tetragonal.

Experimental: The compound was prepared by the interaction of copper (II) bis salicylaldehyde prepared from copper acetate and salicylaldehyde, with . . . crystals were prepared by slow ev

solution of the compound in chloroform. Crystals were analysed for metal and nitrogen.

Identification of the axes were made by X-ray goniometry.

EPR measurements were made at X-band using a Hilger Microspin Spectrometer using 100 KHz field modulation phase sensitive detection system. The derivative curve was recorded and DPPH was used as the marker.

RESULTS: Measurements were made in the crystallographic ac (010) plane containing g_1 and g_2 (where $g_1 > g_2$), along the b -axis (g_3), in g_1g_3 and g_2g_3 planes, where g_1, g_2, g_3 are the principal crystalline g -tensors. In all these measurements the magnet was rotated. It is calculated from X-ray results that there are two magnetically inequivalent ions in the unit cell. But, measurements in any direction in different planes gave only one resonance signal at room temperature; even the measurements in g_1g_3 plane containing the two tetragonal axes (assuming $g_{11} > g_1$) showed only one signal. The line was quite broad (as evident from the video detection system) keeping in mind the magnetic dilution produced by the bulky diamagnetic ligand.

On the assumption of tetragonal symmetry and assuming $g_{11} > g_1$, we can calculate from crystalline g -value measurements in ac plane and along the b -axis the principal axial g -values as $g_{11} = 2.141$ and $g_1 = 2.05$, and the angle between the two tetragonal axes as $\sim 69^\circ$. This is consistent with the angle $\sim 70^\circ$, calculated from room temperature anisotropy data⁵.

If the assumption $g_{\parallel} > g_{\perp}$ is correct, the tetragonal (symmetry) axis should be perpendicular to the molecular plane and a calculation of the principal ionic g -values using direction cosines of the tetragonal axis from X-ray structural parameters, and the appropriate crystalline g -values shows g_{\perp} to be greater than g_{\parallel} . However, if the tetragonal axis lies in the molecular plane then g_{\parallel} becomes greater than g_{\perp} .

The preliminary study of linewidth (peak to peak linewidth of the derivative curve) variation in ac plane where the two ions are equivalent shows a main maximum along (or very close to) the c-axis, a subsidiary maximum practically at right angles and two minima. This trend in variation of linewidth appears to be consistent with the magnetic dipolar linewidth (governed by the factor, $1-3\cos^2\theta$, apart from other terms) due to the two nearest ions at $(0,0,\pm 1)$, although the effect due to distant ions is quite evident. This point will be clear when we extend the measurement to low temperature. And, the relative importance of the exchange interaction, if any, will also be clarified with measurements of the diluted salts.

We have undertaken a broad programme of studying a number of planar complexes as concentrated and diluted salts including magnetic and optical studies and a complete ligand field theory which is being worked out will be reported in due course.

References:

1. A. H. Maki and B.R. McGarvey, J.Chem.Phys. 29, 31 (1958)
2. Idem, ibid, 29, 35 (1958)
3. C.W. Reimann & H. C. Allen Phys. & Chem. Jour. of Res. NBS 70A, 1 (1966).
4. E.C. Lingafelter, Acta Cryst. 17, 1058 (1964)
5. S. Lahiry, unpublished result. (In preparation)

EXCHANGE COUPLED PAIRS IN COPPER DIETHYLDITHIOCARBAMATE

R.Kumari Cowaik, G.Rangarajan and R.Srinivasan
 Department of Physics, Indian Institute of Science,
 Bangalore-12

I. INTRODUCTION

In this paper we report the single crystal ESR study of exchange coupled pairs of copper diethyldithiocarbamate (dto) molecules. The study was carried out using mixed crystals of Cu(dto)_2 and Zn(dto)_2 prepared as described by Reddy and Srinivasan¹.

The X-ray structural analysis of Cu(dto)_2 and Zn(dto)_2 were performed by Bonamico et al^{2,3}. Both Cu(dto)_2 and Zn(dto)_2 belong to the monoclinic space group $\text{P2}_1/\text{c}$, $Z = 4$. Each pair of centrosymmetrically related copper atoms separated by 3.59Å share sulphur atoms, forming a bimolecular unit (Fig.1). The geometry of coordination of each copper is a distorted tetragonal pyramid, copper being bounded to four sulphurs in a plane with a sulphur atom from the centrosymmetrically related molecule at the fifth position. In Zn(dto)_2 , only small changes in the atomic positions of the metal atoms from those in Cu(dto)_2 produce the differences in the coordination geometry leaving the general size and shape of the molecule unaltered. Therefore, the zinc complex can be considered to be isostructural with the copper complex with the zinc atom also in a tetragonal pyramidal environment. This is supported by the fact that we could grow mixed crystals in all proportions.

II. EXPERIMENTAL

The ESR measurements were made at x-band using 100 kc/s modulation. A proton probe was used for magnetic field measurements. Experiments were made in the temperature range 300°K to 4.2°K.

The spin Hamiltonian parameters of the single crystal ESR study of Cu(dto)_2 ¹ are:

$$g_{11} = 2.108, g_{\perp} = 2.023, A^{63} = 142.4 \times 10^{-4} \text{ cm}^{-1}, \\ A^{65} = 152.1 \times 10^{-4} \text{ cm}^{-1} \text{ and } B = 22.4 \times 10^{-4} \text{ cm}^{-1}.$$

Using magnetically more concentrated crystals, we have now observed the spectrum due to a pair of copper atoms coupled by an exchange interaction. This exchange interaction produces a diamagnetic singlet state and a paramagnetic triplet state. ESR transitions are observed between the states of the triplet. Due to equal coupling to the copper nuclei of the pair, each of the two fine structure transitions, arising from a zero field splitting of the triplet, are split into seven hyperfine components with an intensity distribution 1:2:3:4:3:2:1 (Fig.2).

The principal values and axes of the g-tensor and the principal axes of the hyperfine tensor of the coupled pair are the same as those of the uncoupled ion. The hyperfine separation for the triplet is half that for the doublet in all orientations in accordance with what one would expect when $J \gg A$. The angular variation of the spectrum can be fitted to a spin Hamiltonian,

$$\mathcal{H} = \beta [g_{11} H_z S_z + g_{\perp} (H_x S_x + H_y S_y)] + D [S_z'^2 - \frac{1}{3} S(S+1)] \\ + E(S_x'^2 - S_y'^2) + A S_z I_z + B(S_x I_x + S_y I_y) \dots\dots (1)$$

with $S = 1$, $I = 3$. A value of $276 \times 10^{-4} \text{ cm}^{-1}$ was obtained for D with $E \approx 0$.

Temperature variation of the relative intensities of the triplet and doublet spectra indicated that the exchange is ferromagnetic with $J \approx 40^\circ \text{K}$. Gregson and Mitra⁴ have estimated J to be of the order of -8 cm^{-1} from susceptibility measurements.

III. DISCUSSION

The contribution to D from direct dipolar interaction is estimated to be about 0.05 cm^{-1} . Corresponding to $J = 40^\circ \text{K}$ the pseudodipolar contribution⁵ is

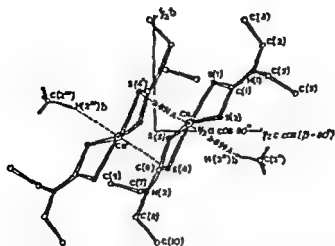


Fig.1. Orthographic Projection of the crystal structure of copper diethyldithiocarbamate down the line which makes an angle of 90° with the b axis and $60^\circ - (\beta - 90^\circ)$ with the c axis.

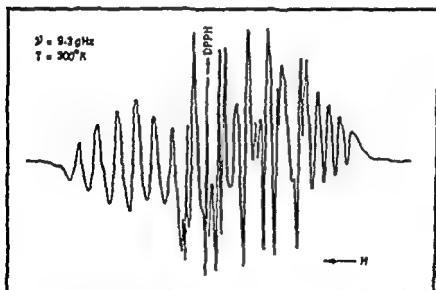


Fig.2. A typical ESR recording showing the lines due to isolated Cu ions and Cu-Cu pairs.

about 0.007 cm^{-1} . Thus the main contribution to the zero-field splitting comes from dipolar interaction.

Two possibilities appear to exist for the exchange interaction between the two molecules—one depending on transfer of electron correlation information through ligand sulphurs and the other making use of the direct overlap of the copper (d_{yz} , d_{xz}) wave functions at the two sites. The isolated molecule ESR study has shown the Cu-S binding to be considerably covalent, with the unpaired electron in the B_1 orbital. The unpaired electron density on the sulphur could polarise its doubly occupied orbital pointing towards the neighbouring copper and overlapping with the A_1 orbital of the latter. The B_1 orbital on the second copper being orthogonal to its A_1 orbital, this could lead to ferromagnetic coupling. The direct exchange interaction could arise because of the overlap of the d_{xz} orbitals of the two coppers (assuming that the Cu-Cu direction is in the XZ-plane). The unpaired electron character is introduced into the copper d_{xz} orbital by spin-orbit admixture with the Cu $d_{x^2 - y^2}$ orbital. It has not been possible to decide as to the relative importance of these two models in the present situation.

REFERENCES

1. T.Ramasubba Reddy and R.Srinivasan; J. Chem. Phys. 43, 1404 (1965).
2. M.Bonamico, G.Dessy, A.Mugnoli, A.Vacaigo and L.Zambonelli; Acta Cryst. 19, 886, (1965).
3. M.Bonamico, G.Mazzzone, A.Vacaigo and L.Zambonelli; Acta Cryst. 19, 898 (1965).
4. A.K.Gregson and S.Mitra; J. Chem. Phys. 49, 3696, (1968).
5. B.Bleaney and K.D.Bowers; Proc. Roy. Soc. (Lond.) A214, 451, (1952).

DISCUSSIONS. Mitra

Have you studied the concentration Cu(II) diethyl dithiocarbamate?

R. Srinivasan

Yes. We found only a single exchange narrowed line in all direction (Reddy and Srinivasan, J. Chem. Phys. 1965).

A.B. Biswas

In view of the Cu-Cu distance to be $\sim 3.6 \text{ \AA}$ in this compound compared to 2.6 \AA in Cu-acetate, is it not possible to prefer the indirect exchange rather than direct exchange?

R. Srinivasan

It is likely that what you suggest is true. We are attempting some calculations to see the relative importance of the two models. It has not been possible to decide from the experiments done so far.

V.D. Singh

Is it worthwhile to consider the interaction of Cu-Cu ions in these crystals?

R. Srinivasan

EPR results, in particular the equivalent coupling to two Cu nuclei, confirms that the pair coupling exists. Further, the temperature dependence of the magnetic nature of the coupling. erro-

g - ANISOTROPY OF O_3^- TRAPPED IN SODIUM CHLORATE CRYSTALS

C. Ramasastry and V.S. Murty
 Indian Institute of Technology, Madras-36.

I. INTRODUCTION

Free radicals produced by radiation damage in ionic crystals are identified by analysing the esr spectra (provided the radical is paramagnetic) and the corresponding optical absorption curves. If the radical under investigation possesses low g-anisotropy then working at higher frequencies will be helpful in determining the principal values of the g-tensor without any ambiguity.

The present work reports the g-parameters of the ozonide ion (O_3^-) trapped in x-ray irradiated sodium chlorate crystals using a k-band esr spectrometer.

II. EXPERIMENTAL

The crystals were grown from saturated solution by slow evaporation. They are irradiated by x-ray from a copper target operating at 30 KV 10 ma. Both the faces of the crystal were exposed to the x-radiation for equal times to achieve a greater uniformity in colouration. Using the past experience of this laboratory, these coloured crystals were thermally bleached at 200°C for one hour and then slowly cooled to bring out the lonely spin resonance peak attributable to the O_3^- formed and trapped in the lattice.

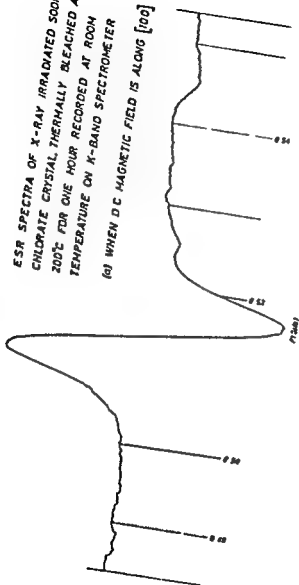
The k-band spectrometer employed 400 Hz modulation and the d.c magnetic field at the location of the crystal was measured using a proton resonance probe in conjunction with a HP frequency counter. The klystron frequency was found to be $23,972 \pm 20$ MHzs. The crystal is rotated about one of its $[100]$ axes kept perpendicular to the d.c magnetic field.

III. RESULTS AND DISCUSSION

The spectra obtained have interesting features. The single resonance peak observed when d.c magnetic field is along $[100]$, (fig 1a) is clearly split into two when the angle is about 20° and the separation between the two peaks is maximum when the angle is 45° with $[100]$ (fig 1b). For a general orientation four lines are expected for the site symmetry $3m$.^{1,2} If the crystal is rotated along $[100]$ kept perpendicular to the d.c magnetic field we expect two lines for positions other than when H is along $[100]$ or perpendicular to $[100]$. As the g-tensor of O_3^- ion exhibits cylindrical symmetry in γ -irradiated sodium bromate which has same structure as sodium chlorate, we assumed cylindrical symmetry for the g-tensor of O_3^- in sodium chlorate lattice and deduced g_{\perp} and g_{\parallel} from fig 1b which are $g_{\perp} = 2.0119$, $g_{\parallel} = 2.0070 \pm .0001$. These values are in agreement with the earlier reported values for O_3^- ^{3,4,5}. Then g values for the remaining orientations are calculated using the expression $g^2 = g_{\parallel}^2 \cos^2 \theta + g_{\perp}^2 \sin^2 \theta$ where

ESR SPECTRA OF X-RAY IRRADIATED SrSO_4
 CHLORATE CRYSTAL, THERMALLY BLEACHED AT
 200°C FOR ONE HOUR RECORDED AT ROOM
 TEMPERATURE ON K-BAND SPECTROMETER

(a) WHEN DC MAGNETIC FIELD IS ALONG $[100]$



(b) WHEN D.C. MAGNETIC FIELD IS 45° TO $[100]$
MAGNETIC FIELD IS MARKED IN UNITS OF KILO
GAUSS.

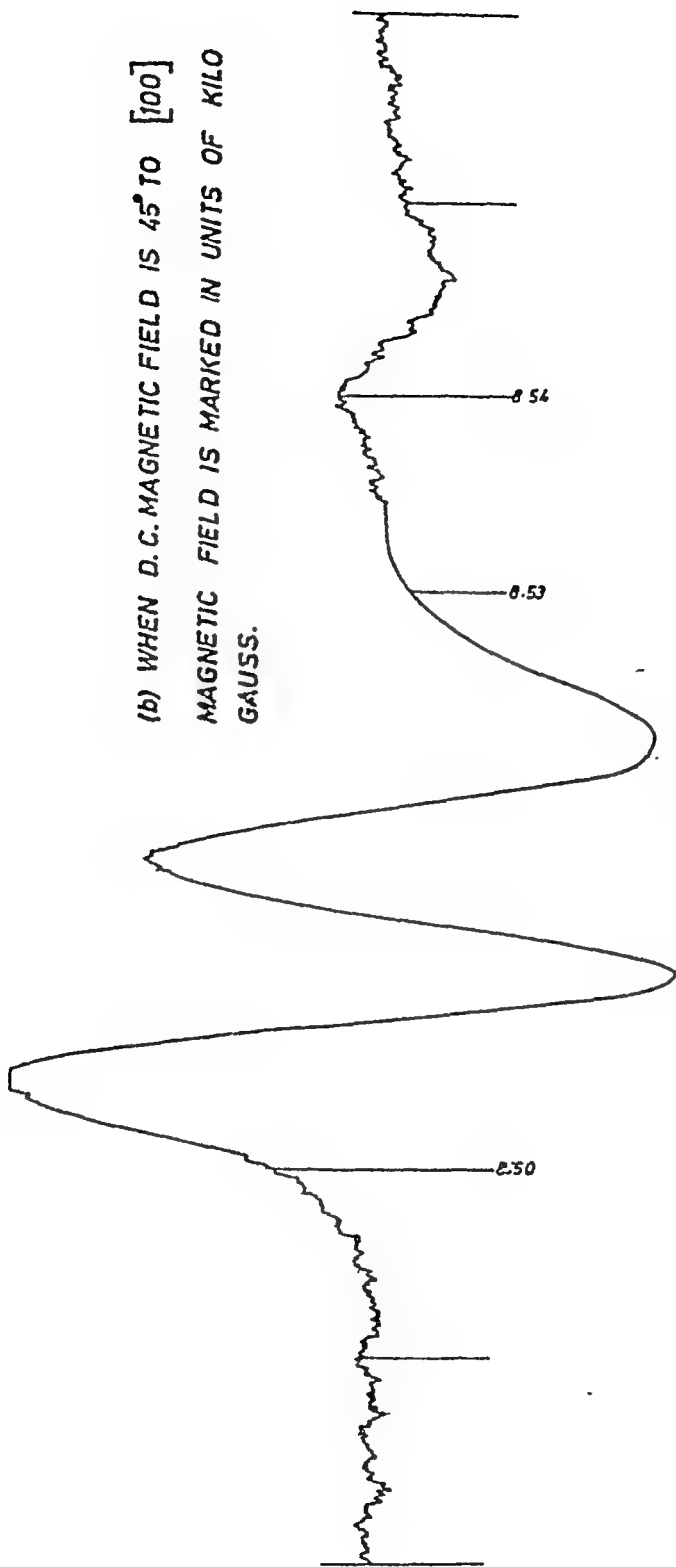


FIG. 1 (b)

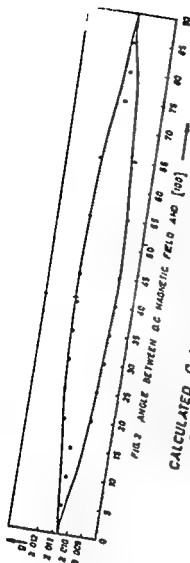


FIG. 2. CALCULATED g -VALUES USING $g^2 = g_{\parallel}^2 \cos^2 \theta + g_{\perp}^2 \sin^2 \theta$ (PLOTTED ON Y-AXIS) SHOWN AS CONTINUOUS CURVE THE ANGLE BETWEEN DC MAGNETIC FIELD WITH $[100]$ ON X-AXIS EXPERIMENTAL g -VALUES ARE SHOWN AS BLACK CIRCLES

is the angle between the symmetry axis and the magnetic field. The observed and calculated values of g are shown in fig.2. As the agreement is satisfactory, we are now convinced that the g tensor of O_3^- ion trapped in sodium chlorate has cylindrical symmetry.

Regarding the structure of ozonide ion, one will be tempted to assume that O_3^- ion is formed as an equilateral triangle in the host lattice. But the structure of the free ozonide ion is known as a bent structure with a bond angle of $110 \pm 5^\circ$ ^{6a, 6b}. In order to explain the observed cylindrical symmetry of O_3^- in sodium bromate Cosgrove et al assumed that the ozonide ion is undergoing rapid reorientations among its three possible structures amounting to a rotation about $[111]$. In potassium ³ chlorate the oxygens are arranged in equilateral triangle whereas the O_3^- formed on γ -irradiation showed C_{2v} symmetry. In this case of sodium chlorate with the available data we cannot comment about the structure of ozonide ion.

IV. REFERENCES

1. A.D. Rae; J. Chem. Phys. 50, 2672 (1969)
2. G. Wyckoff; Crystal structures, Vol.II, VII-A; 1 (4)
3. P.W. Atkins, J.A. Brivati, N. Keen, M.C.R. Symons and P.A. Trevalion; J. Chem. Soc. 1962, 4785
4. R.S. Eachus, P.R. Edwards, S. Subramaniam and M.C.R. Symons; ibid, A1968, 1704.
5. K. Tagaya and T. Nogaito; J. Phys. Soc. Japan 23, No.1, July 1967 p.70.
6. a. P. Smith; J. Phys. Chem. 60, 1471, (1956)

- b. Linuspauling; The nature of the Chemical bond
1963, p.354.
7. M.M. Cosgrove and M.A. Collins; J. Chem. Phys. 52,
p.989 (1970).

DISCUSSION

S. Radhakrishna

What is the mechanism of formation of O_3^- ?

V.S. Murty

It appears that the incident radiation on sodium chlorate has resulted in release of not only chlorine but also some oxygen atoms. It is possible that these oxygens regroup themselves into a O_3^- radical.

A COMPARATIVE STUDY OF THE EPR OF Mn^{2+} IN ISO-STRUCTURAL SINGLE CRYSTALS OF SOME DIAMAGNETIC AND PARAMAGNETIC SALTS

R. Janakiraman and G.C. Upreti
Department of Physics,
Indian Institute of Technology, Kanpur-16

1. INTRODUCTION

In the study of electron paramagnetic resonance (EPR) of paramagnetic ions in single crystals, diamagnetic ions are commonly used as the dilutants in the magnetically dilute mixed crystals⁽¹⁾. There are certain paramagnetic ions whose ground state is non-magnetic, in the absence of the applied static magnetic (Zeeman) field, because of the complete removal of its orbital and spin degeneracies in the presence of crystalline fields of lower-than-axial symmetry. When the Zeeman field is set on, magnetic moments are induced on these ions due to polarization effect, and this introduces additional interactions in the EPR of paramagnetic ions introduced in a crystal where these ions are used as dilutants⁽²⁾. In the iron group series of transition metal ions, octahedrally coordinated Ni^{2+} is a good example of this class of paramagnetic ions. A study of the EPR of Mn^{2+} in isostructural single crystals of nickel and magnesium salts will give information about the effect of Ni^{2+} on the EPR of Mn^{2+} . The present paper deals with the EPR of Mn^{2+} in single crystals of nickel acetate tetrahydrate $[Ni(CH_3COO)_2 \cdot 4H_2O]$, nickel sulfate heptahydrate $(NiSO_4 \cdot 7H_2O)$, and magnesium sulfate heptahydrate $(MgSO_4 \cdot 7H_2O)$, at room temperature ($\sim 300^\circ K$)⁽³⁾. For comparison, results of the EPR of Mn^{2+} -doped magnesium

$[\text{Mg}(\text{CH}_3\text{COO})_2 \cdot 4\text{H}_2\text{O}]^{(4)}$ are also included.

II. RESULTS AND DISCUSSION

$\text{Ni}(\text{CH}_3\text{COO})_2 \cdot 4\text{H}_2\text{O}$ and $\text{Mg}(\text{CH}_3\text{COO})_2 \cdot 4\text{H}_2\text{O}$ are isostructural⁽⁵⁾ with monoclinic unit cell symmetry, and $\text{NiSO}_4 \cdot 7\text{H}_2\text{O}$ and $\text{MgSO}_4 \cdot 7\text{H}_2\text{O}$ are isostructural⁽⁶⁾ with orthorhombic unit cell symmetry. In all these compounds the cation (Ni^{2+} or Mg^{2+}) is coordinated, with four H_2O 's and two oxygen atoms in the case of acetates and with six H_2O 's in the case of sulfates, forming a slightly distorted octahedron. The experiments were conducted at room temperature, with Varian V-4502 X-band EPR spectrometer.

The different magnetic complexes of Mn^{2+} in these systems were found by studying the angular variation of the resonance spectrum. The spectra along the principal z axis were analyzed using the spin Hamiltonian

$$\mathcal{H} = \beta g_z H_z S_z + D \left[(S_z^2 - S(S+1)/3) \right] + E(S_x^2 - S_y^2) + A S_z I_z + B(S_x I_x + S_y I_y) \quad (1)$$

The spin-Hamiltonian parameters, assuming the sign of A to be negative, are given in Table I.

TABLE I

Spin-Hamiltonian Parameters of Mn^{2+} in Isostructural Single Crystals of Nickel and Magnesium

Host Crystal	g_z	D	A	E	B
			(in units of gauss)		
$\text{Ni}(\text{CH}_3\text{COO})_2 \cdot 4\text{H}_2\text{O}$	1.996 ± 0.005	$+462 \pm 5$	-90 ± 5	93 ± 10	90 ± 10
$\text{Mg}(\text{CH}_3\text{COO})_2 \cdot 4\text{H}_2\text{O}$	2.007 ± 0.003	-430 ± 3	-90 ± 1	68 ± 10	96 ± 3
$\text{NiSO}_4 \cdot 7\text{H}_2\text{O}$	1.995 ± 0.005	$+448 \pm 5$	-91 ± 5	74 ± 10	87 ± 10
$\text{MgSO}_4 \cdot 7\text{H}_2\text{O}$	2.003 ± 0.005	$+412 \pm 5$	-92 ± 5	95 ± 10	87 ± 10

As far as the general resonance properties of the resonance spectra - like the symmetry and strength of the crystalline field, the angle between the axes - are concerned, the EPR of Mn^{2+} in

nickel and magnesium salts is similar. The deviations in the EPR of Mn^{2+} in single crystals of Ni^{2+} have been, (a) a negative g-shift from the corresponding factor in isostructural magnesium salt, and (b) a regular increase in the linewidth of Mn^{2+} resonance lines with the Zeeman-field intensity.

The ground state of Ni^{2+} ($3d^8$ outershell configuration) is 3F_4 . In an octahedral crystalline field of lower-than-axial symmetry, the orbital and spin degeneracies of this ground state are completely removed⁽⁷⁾. The separations between the ground state spin triplet (ZFS) are much greater than the energy of X-band microwave frequency. Moriya and Obata⁽²⁾ have given a detailed account of the effect of Ni^{2+} diluting ions on the EPR of Mn^{2+} . When the Zeeman field is set on, magnetic moments are induced on these ions due to polarization effect. This introduces additional magnetic field at the site of Mn^{2+} ion, proportional to the magnitude of the thermal of equilibrium value of Ni^{2+} spin, at room temperature, and the coupling constant between the Mn^{2+} and Ni^{2+} spins. This causes the g-shift as observed in the Ni^{2+} systems. The frequency dependence of the fluctuations of Ni^{2+} spin about its thermal equilibrium value gives rise to Zeeman-field dependence of the spin-spin and spin-lattice relaxation times, and hence the linewidth dependence on the Zeeman-field intensity.

From the magnitudes of the g-shift of the EPR of Mn^{2+} in Ni^{2+} salts, from the corresponding factors in Mg^{2+} salts, assuming the shift to be entirely due to the additional magnetic field at Mn^{2+} , the magnitudes are $\sim 20\text{G}$ in the case of Mn^{2+} : $\text{Ni}(\text{CH}_3\text{COO})_2 \cdot 4\text{H}_2\text{O}$, and

~ 15 G in the case of $\text{Mn}^{2+}:\text{NiSO}_4 \cdot 7\text{H}_2\text{O}$.

The linewidths in the case of $\text{Mn}^{2+}:\text{Mg}(\text{CH}_3\text{COO})_2 \cdot 4\text{H}_2\text{O}$ and $\text{Mn}^{2+}:\text{MgSO}_4 \cdot 7\text{H}_2\text{O}$ are ~ 10 G, for all the resonance lines. Some representative values of the linewidths of $\text{Mn}^{2+}:\text{Ni}(\text{CH}_3\text{COO})_2 \cdot 4\text{H}_2\text{O}$ and $\text{Mn}^{2+}:\text{NiSO}_4 \cdot 7\text{H}_2\text{O}$ are given in Table II.

TABLE II

Some Representative Values of the Zeeman-Field Intensity (H) And the Corresponding linewidth (ΔH) of Mn^{2+} Resonance Lines in $\text{Ni}(\text{CH}_3\text{COO})_2 \cdot 4\text{H}_2\text{O}$ and $\text{NiSO}_4 \cdot 7\text{H}_2\text{O}$.

$\text{Mn}^{2+}:\text{Ni}(\text{CH}_3\text{COO})_2 \cdot 4\text{H}_2\text{O}$		$\text{Mn}^{2+}:\text{NiSO}_4 \cdot 7\text{H}_2\text{O}$	
H	ΔH	H	ΔH
(in gauss)		(in gauss)	
1285	20.3	2510	13.1
2570	33.9	3569	18.1
4013	47.5	4448	20.3
4478	48.8	5266	22.0

The authors are thankful to the Council of Scientific and Industrial Research for financial assistance.

REFERENCES

1. B. Bleaney and D.J.E. Ingram, Proc. Phys. Soc. (London) A63, 408 (1950).
2. T. Moriya and Y. Obata, J. Phys. Soc. Japan 13, 1333 (1958).
3. R. Janakiraman, Ph.D. Thesis, Indian Institute of Technology, Kanpur (1970).
4. T.J. Manakkil, Ph.D. Thesis, New Mexico State Univ.; USA, (1967).
5. R.W.G. Wyckoff, "Crystal Structures", Interscience Pub. New York, Vol. 5 (1966).
6. R.W.G. Wyckoff, "Crystal Structures", Interscience Pub. New York, Vol. 3 (1965).
7. R. Schlapp and W.G. Penney, Phys. Rev. 42, 666 (1932).

III. RESULTS

At 300°K where the crystal has a b.c.c. structure, the EPR spectrum of Mn^{2+} at 9.5 and 35GHz consists of a single isotropic sextet. This suggests that Mn^{2+} very likely enters the lattice substitutionally at $(\text{Mg})^+$ site with remote charge compensation. The zero field splitting of ^6S of Mn^{2+} is reported to be small in moderate cubic fields giving us an unresolved fine structure and hence the single isotropic sextet. The spectrum was analysed using the spin Hamiltonian

$$\mathcal{H} = g \beta H.S + A.I$$

with $S = 1/2$ and $I = 5/2$. This gives $g = 2.003$ and $A = 87.5 \times 10^{-4} \text{ cm}^{-1}$.

The EPR spectrum at 9.5GHz at low temperature with the magnetic field parallel to one of the original cubic axes showed five groups of sextets together with a few very weak lines. Further it was observed that different hyperfine sextets have unusual intensities with no apparent regularity of the hyperfine separations of different sextets. This type of a behaviour could be understood⁶ by considering the energy expressions⁷ correct to third order. The spreads of the hyperfine sextets for various fine structure transitions are given by

$+5/2 \rightleftharpoons +3/2$	$5A + 10A^2/H_{5/2} - 20A^2 D/H_{5/2}^2$
$+3/2 \rightleftharpoons +1/2$	$5A + 5A^2/H_{3/2} - 25A^2 D/H_{3/2}^2$
$+1/2 \rightleftharpoons -1/2$	$5A + 40A^2/H_{1/2}^2$
$-1/2 \rightleftharpoons -3/2$	$5A - 5A^2/H_{-1/2} + 25A^2 D/H_{-1/2}^2$
$-3/2 \rightleftharpoons -5/2$	$5A - 10A^2/H_{-3/2} - 20A^2 D/H_{-3/2}^2$

where H_{\pm} is the resonant field value corresponding to the transition $M_S \rightleftharpoons M_S - 1$. Here the parameters A and D are expressed in gauss.

ELECTRON PARAMAGNETIC RESONANCE STUDIES OF DIVALENT MANGANESE IN
AMMONIUM BROMIDE SINGLE CRYSTALS

P.A. Narayana, G.Nageswara Rao, M.D. Sastry, T.M. Srinivasan
and Putcha Venkateswarlu
Department of Physics, Indian Institute of Technology, Kanpur

I. INTRODUCTION

Electron paramagnetic resonance has been found to be a most effective tool to study the nature of the environments of the impurity magnetic ions in single crystals. The EPR studies of Mn^{2+} in f.c.c. alkali halides^(1,2) show that Mn^{2+} enters substitutionally at cation site, the charge compensation being achieved by the production of cation vacancies or by the presence of impurity negative ions. However the work so far reported^(3,4) in the case of b.c.c. lattices like CsCl or NH_4Cl shows that Mn^{2+} does not enter substitutionally at the cation site but enters interstitially. Here we present evidence of substitutional Mn^{2+} in a b.c.c. NH_4Br lattice. Further ammonium bromide has a phase transformation at $235^\circ K$ below which the crystal has an ordered tetragonal phase⁽⁵⁾ and the EPR studies are expected to throw some light on the nature of the phase transition.

II. EXPERIMENTAL

Ammonium bromide single crystals were grown by slow evaporation of solution containing 0.2 mole percent of $MnBr_2$ by weight. 10 percent of urea by weight was added to the growth solution to stimulate the cubic habit of the crystals. EPR spectra were recorded at $300^\circ K$ and $80^\circ K$ at 9.5 GHz and 35 GHz.

The third order terms become very small at 35GHz and therefore can be neglected. So all the sextets are expected to have the same hyperfine separations at this frequency. In fact this is what we observed. Further it was found that at this frequency when the static magnetic field was made parallel to one of the original cubic axes, a sixty line spectrum was observed. When the direction of the static magnetic field was changed by 20° , more than sixty lines were observed. These features could be explained if it is assumed that in the ordered tetragonal phase, NH_4Br consists of domains of tetragonal crystallites with their unique axes lying arbitrarily along one of the original cubic axes. One will then expect three sets of thirty lines along an arbitrary direction. On the other hand if H is parallel to $\langle 100 \rangle$ axis, the two complexes with their unique axes along $\langle 010 \rangle$ and $\langle 001 \rangle$ become equivalent and therefore only sixty lines, thirty corresponding to zero degree parts and thirty corresponding to perpendicular parts are expected. This is consistent with our observation. When the magnetic field is parallel to $\langle 111 \rangle$ axis all the three complexes become equivalent and only thirty lines are expected. To verify this the crystal was cut in the $[110]$ plane and the angular variation was studied in this plane. When the magnetic field was parallel to $\langle 111 \rangle$ axis the spectrum obtained was not well resolved. This is not surprising in view of the fact that an axial spectrum is expected to exhibit a $(3 \cos^2 \theta - 1)$ type of angular variation.⁸

The low temperature spectrum obtained at 35GHz was analysed using the usual spin Hamiltonian appropriate for the axial symmetry and the parameters obtained are $g = 0.02$, $D = 510 \times 10^{-4} \text{ cm}^{-1}$ and $A = 85 \times 10^{-4} \text{ cm}^{-1}$.

Further work at helium temperatures is in .

REFERENCES

1. G.D. Watkins; Phys. Rev. 112, 99(1959)
2. K.N. Shrivastava and Putcha Venkateswarlu; Proc. Ind. Acad. Sci. 63A, 234(1966)
3. A. Forman and J.A. Van Wyke; J. Chem. Phys. 44, 73 (1966)
4. A. Forman and J.A. Van Wyke; Can. J. Phys. 45, 2381 (1967)
5. H.A. Levy and S.W. Peterson; J. Am. Chem. Soc. 75, 1536(1952)
6. H.D. Sastry; Ph.D. Thesis, Indian Institute of Technology, Kanpur (1967)
7. T.J. Folen; Phys. Rev. 139, a1961(1965)
8. V. Lox; Paramagnetic Resonance in Solids (Academic Press, New York and London, 1960.)

90° SUPER-EXCHANGE INTERACTION IN TRANSITION METAL
PHTHALOCYANINES

S. Mitra

Tata Institute of Fundamental Research, Bombay - 5.

and

C.C. Barraclough, R.L. Martin and R.C. Sherwood
University of Melbourne, Australia

INTRODUCTION

X-ray structural data¹ on the transition metal phthalocyanines show that the magnetic interaction occurs through its developed π -system via a 90° metal-ligand-metal pathway, and the molecules are stacked in the lattice in such a way that it forms approximately discrete linear chains. Since the electronic structures of these compounds are now known, the low temperature magnetic studies on the metal phthalocyanines (abbreviated henceforth as M Pc like CoPc etc.) promises to offer good scope to test the theoretical results on the linear chains and the 90° super-exchange mechanism.

EXPERIMENTAL

Magnetic susceptibility measurements were made between 293° - 1.5°K on CoPc, CuPc and NiPc using a null-coil pendulum magnetometer by R.C. Sherwood. Magnetisation measurements were done between the magnetic field-strengths of 1000 - 15,000 oe.

RESULTS AND DISCUSSION

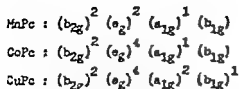
CuPc ($3d^9$, $S = \frac{1}{2}$) has a magnetic moment of 1.82 B.M. at room temperature, which remains constant down to 1.5°K. The magnetisation data obtained at 1.5°K closely conform to the Brillouin function for $S = \frac{1}{2}$.

CoPc ($3d^7$, $S = \frac{1}{2}$) shows evidence of antiferromagnetic interaction below about 60°K . The magnetic moment of this compound at higher temperatures correspond to unpaired spin ($\mu = 2.2$ B.M. at 100°K). Below 60°K , it however decreases fast and at 1.5°K , $\mu = 1.1$ B.M. The magnetisation results at 1.5°K show large deviations from the Brillouin function for $S = \frac{1}{2}$.

The measurements on MnPc ($3d^5$, $S = 3/2$) establish ferromagnetic metal-metal interaction in this compound. The magnetic moment rises steadily from its room temperature value of 4.3 B.M. to about 7.5 B.M. as the temperature is lowered to the liquid hydrogen temperature range. The magnetisation data at 4.2 and 1.5°K confirm the occurrence of ferromagnetic interaction.

We shall first discuss the 90° superexchange mechanism. The sign of the exchange coupling constant for each superexchange pathway will be determined, in part, by orthogonality relationships between the relevant metal and phthalocyanine orbitals, and in part, by the electron distribution in these some orbitals. In the point group D_{4h} , the $3d$ metal orbitals are classified as a_{1g} , b_{1g} , b_{2g} and e_g while the π -molecular orbitals of the phthalocyanine are A_{1u} , A_{2u} , B_{1u} , B_{2u} and E_g . The sign of the magnetic exchange associated with a particular pathway may be inferred from essential qualitative considerations. These have been discussed in detail elsewhere² and we summarise here only the results of nearest neighbor interaction in Table 1.

The electronic configuration of all these compounds have been deduced by us^{3,2}, and the results are again summarised below for reference:



The absence of any magnetic interaction in CuPe, as experimentally observed, is supported from Table 1. The ferromagnetic interaction observed in MnPe appears to be also consistent with the theoretical prediction. However, Table 1 would predict ferromagnetic interaction in CoPe with unpaired electron in a_{1g} orbital while we observe experimentally that the interaction is antiferromagnetic. We believe that, in CoPe, the next-nearest neighbour interaction which will be antiferromagnetic in this case, probably dominates the weak nearest-neighbour ferromagnetic one with the result that the net sign of interaction is antiferromagnetic.

We have fitted our data on MnPe and CoPe to the existing models for linear chains. CoPe conforms very well to the Fischer-Jensen model for $\nu = 3$ with $J = 2 \text{ cm}^{-1}$. For MnPe we have used the model of Griffith deduced in the classical spin limit. Suitable adaption of this theory for the present case with $\nu = 3/2$ gives reasonable agreement at low temperatures with $J = +5 \text{ cm}^{-1}$.

REFERENCES

1. J.M. Robertson : J. Chem. Soc., 615 (1935), 219 (1937).
2. C.G. Barraclough, P.L. Martin, S. Mitra and R.C. Sherwood, J. Chem. Phys. 53 (1970) 1122.
3. R.L. Martin and S. Mitra, Chem. Phys. Letters, 3 (1969) 183; Inorg. Chem. 9 (1970) 183.

TABLE 1

Predicted sign of nearest-neighbour interaction
in the 90° superexchange process

Phthalocyanine M.O.	Half-filled metal orbitals			
	a_{1g}	e_g	b_{2g}	b_{1g}
A_{2u}	Ferro.	Ferro.	Nil	Nil
E_g	Ferro.	Antiferro.	Nil	Nil
B_{2u}	Nil	Ferro.	Nil	Nil
A_{1u}	Nil	V. Weak Ferro.	Nil	Nil
B_{1u}	Ferro.	Ferro.	Nil	Nil

MOSSBAUER AND MAGNETIC SUSCEPTIBILITY MEASUREMENTS ON CADMIUM FERRICYANIDE

G.R. Kanekar, V.R. Marathe, A.C. Kunwar and S.K. Date
Tata Institute of Fundamental Research, Bombay 5

I. INTRODUCTION

Cadmium ferricyanide is one of the typical compound of the type $M_3^{2+} [Fe^{III} (CN)_6]_2$, where M is the divalent metal atom. These compounds are quite interesting from the point of view of studying hyperfine interactions of the iron nuclei with an effective spin $S = 1/2$. It is very well-known from earlier studies⁽¹⁻³⁾ that the hf interactions in such low-spin compounds are quite different from the usual high-spin compounds with effective spin $S = 5/2$. For example, whereas the electric field gradient is of lattice origin in high-spin compounds (essentially temperature independent) that in low-spin ferricyanide complexes is predominantly of valence origin (and therefore, it is temperature dependent). We, therefore, thought of studying this typical member of the series with a view to understand in detail the temperature dependence of the quadrupole interaction observed in Mossbauer spectra, and to correlate this data with the magnetic measurements. In the present paper, we report the Mossbauer and magnetic susceptibility measurements on $Cd_3 [Fe (CN)_6]_2 \cdot 12H_2O$ between 77°K and 300°K. Our data has been analyzed on the basis of ligand field theory taking into account the interaction of the central metal atom with the surrounding CN^- ligands by a static potential which reflects the symmetry of the local environments. The computed crystal field

TABLE 1

Predicted sign of nearest-neighbour interaction
in the 90° superexchange process

Phthalocyanine M.O.	Half-filled metal orbitals			
	a_{1g}	e_g	b_{2g}	b_{1g}
A_{2u}	Ferro.	Ferro.	Nil	Nil
E_g	Ferro.	Antiferro.	Nil	Nil
B_{2u}	Nil	Ferro.	Nil	Nil
A_{1u}	Nil	V. weak Ferro.	Nil	Nil
B_{1u}	Ferro.	Ferro.	Nil	Nil

MOSSBAUER AND MAGNETIC SUSCEPTIBILITY MEASUREMENTS ON CADMIUM FERRICYANIDE

C.R. Kanekar, V.R. Marathe, A.C. Kumar and S.K. Date
Tata Institute of Fundamental Research, Bombay 5

1. INTRODUCTION

Cadmium ferricyanide is one of the typical compound of the type $M_3^{2+} [Fe^{III} (CN)_6]_2$, where M is the divalent metal atom. These compounds are quite interesting from the point of view of studying hyperfine interactions of the iron nuclei with an effective spin $S = 1/2$. It is very well-known from earlier studies⁽¹⁻³⁾ that the hf interactions in such low-spin compounds are quite different from the usual high-spin compounds with effective spin $S = 5/2$. For example, whereas the electric field gradient is of lattice origin in high-spin compounds (essentially temperature independent) that in low-spin ferricyanide complexes is predominantly of valence origin (and therefore, it is temperature dependent). We, therefore, thought of studying this typical member of the series with a view to understand in detail the temperature dependence of the quadrupole interaction observed in Mossbauer spectra, and to correlate this data with the magnetic measurements. In the present paper, we report the Mossbauer and magnetic susceptibility measurements on $Ca_3[Fe(CN)_6]_2 \cdot 12H_2O$ between 77°K and 300°K. Our data has been analysed on the basis of ligand field theory taking into account the interaction of the central metal atom with the surrounding CN^- ligands by a static potential which reflects the symmetry of the local environments. The computed crystal field

parameters from these two measurements agree amongst themselves.

II. EXPERIMENTAL

Cadmium ferricyanide was prepared by the usual method; by double decomposition of potassium ferricyanide and cadmium bromide. Analysis of cadmium, iron and thermogravimetric analysis have confirmed the molecular formula $\text{Cd}_3[\text{Fe}(\text{CN})_6]_2 \cdot 10\text{H}_2\text{O}$.

The Mossbauer spectra were recorded between 77 and 300°K in a 400-channel analyser operated in pulse height mode. Assuming a Lorentzian lineshape, the spectra were analysed by the least-square method. The magnetic susceptibility was measured from liquid nitrogen to room temperature using the Guoy balance.

III. RESULTS AND DISCUSSION

In all ferricyanides, six CN^- ligands surround the iron atom and form an octahedral complex with d^2sp^3 hybridization. Because of strong covalent bonding between the central iron ion and surrounding ligands, Hund's principle is violated; the five-fold degeneracy of the 3d-orbitals is removed by the interaction and are split into a low-lying threefold degenerate t_{2g} level and a doubly degenerate e_g level lying higher in energy by about 35000 cm^{-1} . Due to the presence of such strong ligand fields, all the five 3d-electrons occupy the lower t_{2g} level i.e. all ferricyanides are spin-paired with only one unpaired electron. If these are degenerate, the unpaired electron is distributed equally among the three t_{2g} orbitals and no quadrupole splitting will be observed in the Mossbauer spectra. However, the outer divalent cation may distort the octahedral symmetry of CN^- ligands and in turn produce the net

EFG at the iron nucleus [Fig. 1(a)].

In Fe^{57} Mossbauer spectrum, the quadrupole splitting is given by

$$\Delta E_Q = \frac{1}{2} e^2 q Q \left[1 + \frac{\eta^2}{3} \right]^{\frac{1}{2}}$$

$$\text{with } q = \frac{V_{zz}}{r^3} = (1-R) q_{\text{val}} + (1-V_{\infty}) q_{\text{lattice}}$$

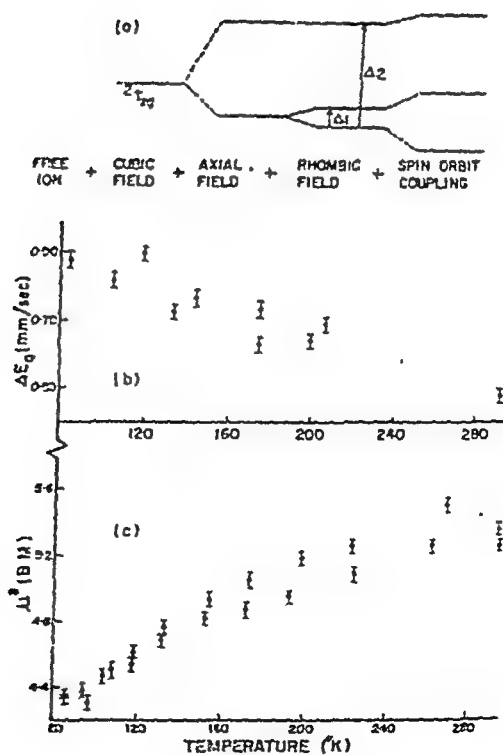
Figure 1(b) shows the temperature dependence of quadrupole splitting observed for cadmium ferricyanide between 77 and 300°K. In order to calculate the ligand-field parameters, Δ_1 and Δ_2 , we have followed the formalism of Golding⁽⁴⁾, put forward for low-spin complexes. We have assumed the spin-orbit coupling constant $\lambda = -278 \text{ cm}^{-1}$ and orbital reduction factor $K = 0.87$, which are taken from earlier ESR work⁽⁵⁾ on single crystal of potassium ferricyanide. The contribution to the EFG due to the non-cubic charge distribution in the lattice is estimated from Co^{59} NMR measurements on $\text{Cd}_3[\text{Co}(\text{CN})_6]_2$. By least-square analysis, we have computed the two parameters and are given as $\Delta_1 = 112 \text{ cm}^{-1}$ and $\Delta_2 = 615 \text{ cm}^{-1}$.

Taking into account the effect of these distortions, spin-orbit coupling and Zeeman field splitting on $2T_{2g}$ state and using Van Vleck's formula, the magnetic moments of cadmium ferricyanide at various temperatures were calculated. Figure 1(c) shows the variation of M^2 against temperature. By fitting the experimental variation to the calculated values of magnetic moments at various temperatures by least-square method, the two crystal field parameters were evaluated and are given as $\Delta_1 = 92 \text{ cm}^{-1}$ and $\Delta_2 = 593 \text{ cm}^{-1}$. Even though there are quite a few assumptions in evaluation of these parameters from the data obtained by these two techniques, the close

agreement observed gives us confidence in the reliability of values of the estimated parameters.

REFERENCES

1. W. Karler et al.; Z. Phys. 173, 321 (1963).
2. A.Z. Hrynkiowicz, B.D. Sawicka and J.A. Sawicki; Phys. Stat. Solidi 38, K111 (1970), 38, K115 (1970).
3. W.T. Oosterhuis and G. Laug; Phys. Rev. 178, 439 (1969).
4. R.M. Golding; Mol. Phys. 12, 13 (1967).
5. J.M. Baker, B. Bleaney and K.D. Bowers; Proc. Phys. Soc. 69, 1205 (1956); 69, 1216 (1956).



MAGNETIC HEAT CAPACITY OF THULIUM ETHYLSULPHATE

H.V. Keer, Department of Chemistry, Indian
Institute of Technology, Powai, Bombay-76 (India)

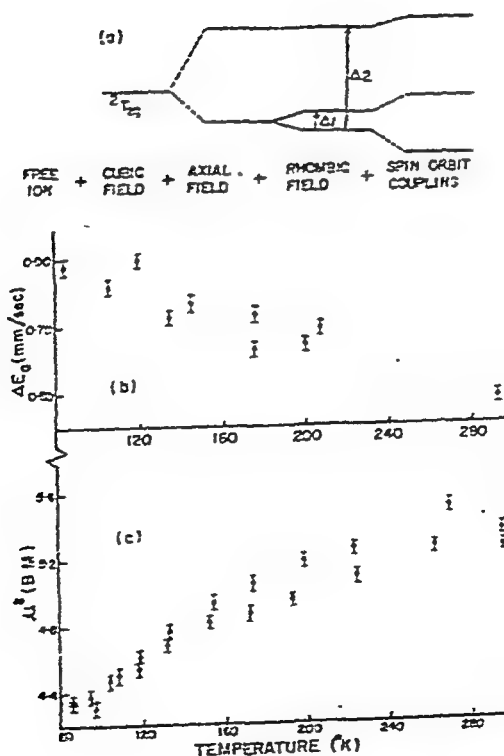
Rare-earth ethylsulphates have been the object of numerous experiments since cerium ethylsulphate was first used in adiabatic demagnetization. They form an isomorphous series of salts with the general formula $M(C_2H_5SO_4)_3 \cdot 9H_2O$ where M is the trivalent rare-earth ion. Gerstein *et al.*⁽¹⁾ measured the heat capacity of thulium and lutecium salts, hereinafter referred to as TmE.S and LuE.S respectively, over the temperature range $15^\circ - 300^\circ K$. The contribution of the 4f electrons in Tm to the heat capacity was also calculated by the above authors⁽¹⁾, using the angular part of the crystal field matrix elements calculated by Stevens and Elliott and two sets of parameters given by Wong and Richman⁽²⁾ and Gruber and Conway⁽³⁾. The calculations predicted that maxima may exist at about $16^\circ K$, $45^\circ K$ and $80^\circ K$ respectively. Gerstein *et al.*⁽¹⁾ did attempt to evaluate the anomalous (magnetic) heat capacity (C_m) ; but many assumptions were made in their calculations. For example, they assumed that the maximum in C_m at $16^\circ K$ was to be 7 J/g at.wt.deg. The present purpose is to suggest a method which enables estimation of C_m from the thermal data alone.

Since the formula weights of the isomorphous TmE.S and LuE.S are not widely different, it may be assumed that the vibrational contribution to the entropy

agreement observed gives us confidence in the reliability of the values of the estimated parameters.

REFERENCES

1. W. Karlar et al.; Z. Phys. 173, 321 (1963).
2. A.Z. Hryniewicz, B.D. Sawicki and J.A. Sawicki; Phys. Stat. Solidi 38, K111 (1970), 38, K115 (1970).
3. W.T. Costerhuis and G. Laug; Phys. Rev. 178, 439 (1969).
4. R.M. Golding; Mol. Phys. 12, 13 (1967).
5. J.M. Baker, B. Bleaney and K.D. Bowers; Proc. Phys. Soc. (B) 69, 1205 (1956); 69, 1216 (1956).



MAGNETIC HEAT CAPACITY OF THULIUM ETHYLSULPHATE

H.V. Keer, Department of Chemistry, Indian
Institute of Technology, Powai, Bombay-76 (India)

Rare-earth ethylsulphates have been the object of numerous experiments since cerium ethylsulphate was first used in adiabatic demagnetization. They form an isomorphous series of salts with the general formula $M(C_2H_5SO_4)_3 \cdot 9H_2O$ where M is the trivalent rare-earth ion. Gerstein *et al.*⁽¹⁾ measured the heat capacity of thulium and lutecium salts, hereinafter referred to as TmE.S and LuE.S respectively, over the temperature range $15^\circ - 300^\circ K$. The contribution of the 4f electrons in Tm to the heat capacity was also calculated by the above authors⁽¹⁾, using the angular part of the crystal field matrix elements calculated by Stevens and Elliott and two sets of parameters given by Wong and Richman⁽²⁾ and Gruber and Conway⁽³⁾. The calculations predicted that maxima may exist at about $16^\circ K$, $45^\circ K$ and $80^\circ K$ respectively. Gerstein *et al.*⁽¹⁾ did attempt to evaluate the anomalous (magnetic) heat capacity (C_m) ; but many assumptions were made in their calculations. For example, they assumed that the maximum in C_m at $16^\circ K$ was to be 7 J/g at.wt.deg. The present purpose is to suggest a method which enables estimation of C_m from the thermal data alone.

Since the formula weights of the isomorphous TmE.S and LuE.S are not widely different, it may be assumed that the vibrational contribution to the entropy

and heat capacity of these compounds obey a law of corresponding states. Then the lattice entropy $S(\text{lat.}) = \Phi(T/\theta)$, and the lattice heat capacity $C_p(\text{lat.}) = (T/\theta) \Phi'(T/\theta)$, where Φ is the same function for both TmE.S and LuE.S but θ is a characteristic temperature different for each compound. Now, one can find a temperature T' , where LuE.S has the same heat capacity as does TmE.S at temperature T and denote the ratio T'/T by $r(\text{TmE.S}, C_p)$. It follows from thermodynamics that

$$C_p(\text{lat.}) = C_p(\text{LuE.S}, rT) \left[1 + \frac{d \ln r}{d \ln T} \right]$$

Once the lattice contribution has been estimated, the magnetic one (C_m) can be obtained by subtracting the former from the measured total. The value of $r(\text{TmE.S}, C_p)$ evaluated at about 298°K, using the data of Gerstein et al.⁽¹⁾, was found to be 1.002. The values of C_m at regular intervals of temperature are plotted in Fig.1.

It will be seen from Fig.1 that two humps in C_m have been observed around 16°K and 80°K respectively. These results are in agreement with those obtained by using the crystal field parameters of Wong and Richman⁽²⁾ (see Fig.1). Results based on constants of Gruber and Conway⁽³⁾ predict a hump around 45°K and are in disagreement with our calculations. Hence it may be concluded that the parameters of Wong and Richman⁽²⁾ are more nearly correct. Gerstein et al.⁽¹⁾ also

obtained agreement with Wong and Richman⁽²⁾, but it is fortituous, since it was assumed a priori in their calculations that a hump does exist at about 16°K. However, it is gratifying to note that an estimation of the magnetic heat capacity has been made using the thermal data alone and without resorting to any simplifying assumptions.

REFERENCES

1. B.C. Gerstein, L.D. Jennings and P.H. Spedding;
J.Chem.Phys. 37 1496 (1962).
2. E.Y. Wong and I. Richman;
J.Chem.Phys. 34 1182 (1961).
3. J.B. Gruber and J.G. Conway;
J.Chem.Phys. 32 1531 (1960).

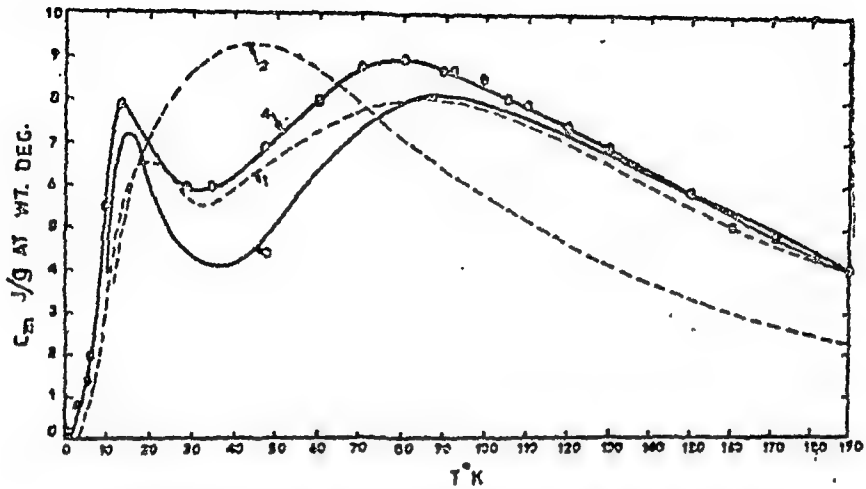


FIG. 1. MAGNETIC HEAT CAPACITY OF THULIUM ETHYLSULPHATE.

1. Wong's XTL field constants
2. Gruber's XTL field constants
3. Gerstein et.al.
4. Present work.

THERMAL AND MAGNETIC PROPERTIES OF Pr^{3+} AND Er^{3+} IONS IN A CRYSTAL FIELD WITH C_{3h} SITE SYMMETRY

Vishveshmittar, S.P.Taneja and S.P.Puri
Department of Physics, University of Roorkee, Roorkee

The Pr^{3+} ($4f^2, {}^3H_4$) and Er^{3+} ($4f^{11}, {}^4I_{15/2}$) ions when substituted into the LaBr_3 and GdCl_3 crystals see an electrostatic field of C_{3h} point symmetry, which can be replaced by D_{3h} pseudosymmetry. The complete Hamiltonian for such a system in a magnetic field can be written as

$$H = H_0 + A_2^0 V_2^0 + A_4^0 V_4^0 + A_6^0 V_6^0 + A_6^6 V_6^6 + g_L \mu_B H \cdot J \quad (1)$$

Using the operator equivalent method and omitting the magnetic field operator, the matrices obtained by using the C.F. parameters reported (1-3) for Pr^{3+} ; LaBr_3 , Er^{3+} ; GdCl_3 and Er^{3+} ; LaBr_3 are diagonalized to yield the eigenvectors and their corresponding eigenvalues E_1^0 ; the latter are used to calculate the Schottky specific heat, C_s (4). The Zeeman splittings of the Stark levels are found by employing the perturbation technique and the first and second order energies corresponding both to H parallel and perpendicular to the c-axis are calculated to use the VanVleck formula (5) for g.at. susceptibility of a multiplet system. The principal susceptibilities χ_0 and χ_a so generated are used to find the anisotropy, $\Delta\chi = \chi_a - \chi_0$, and the μ_{eff} values in the temperature range 10-400°K.

Thermal Properties The Schottky specific heat is found to be prominent at liquid oxygen or lower temperatures and it is maximum at about 62°K for Pr^{3+} ; LaBr_3 (6.7 J/g.at.wt.deg.); 40°K for Er^{3+} ; GdCl_3 (8.5 J/g.at.wt.deg.); and 36°K for Er^{3+} ; LaBr_3 (2.6 J/g.at.wt.deg.). The peak positions and peak values for the Er^{3+} compounds are in good accord with the corresponding values of 40-50°K and 8.0 J/g.at.wt.deg. determined experimentally (6) for $\text{Er}(\text{C}_2\text{H}_3\text{CO}_2)_3 \cdot 9\text{H}_2\text{O}$. The entropy associated with the Schottky anomaly comes to be 12.31, 17.04 and

17.07 J(g.at.wt.deg.)⁻¹ for Pr³⁺: LaBr₃, Er³⁺: GdCl₃, and Er³⁺: LaBr₃, respectively. These values compare well with the values 12.51 and 17.29 for Pr³⁺ and Er³⁺ ions, obtained from the theoretical entropy expression for a system with doublet ground state, $S = Nk \times \log_0(2J+1/2)$.

Magnetic Properties The magnetic susceptibilities are found to vary with temperature in accordance with the Curie-Weiss law, $\chi = C/(T + \theta_p)$

The results for the mean susceptibility are:

$$\begin{array}{lll} \text{Pr}^{3+}: \text{LaBr}_3 & \bar{K} = 1.630/(T + 10.57) & T \geq 190^\circ\text{K}, \\ \text{Er}^{3+}: \text{GdCl}_3 & \bar{K} = 11.665/(T + 6.31) & T \geq 100^\circ\text{K}, \\ \text{Er}^{3+}: \text{LaBr}_3 & \bar{K} = 11.508/(T + 2.84) & T \geq 80^\circ\text{K}. \end{array}$$

The positive sign of θ_p in \bar{K} dependence suggests the possibility of existence of antiferromagnetic interaction in the three systems. It may be pointed out that the \bar{K} -values can be taken as following Curie-Weiss law with slightly different parameters down to about 60°K. However, at still lower temperatures appreciable departure is indicated. The values of Curie constants compare favourably with the values 1.585 and 11.2 for Praseodymium and Erbium metals⁽⁷⁾. In

Pr³⁺:LaBr₃ the relative anisotropy $\Delta K/\bar{K}$ increases from 0.079 to 0.145 as temperature decreases from 400°K to 125°K. As temperature is lowered further the $\Delta K/\bar{K}$ value decreases and changes sign at about 52°K. This reversal of anisotropy is not surprising in light of the observation made by Rosenberg⁽⁴⁾. However, the value of $\Delta K/\bar{K}$ falls from -0.070 and -0.072 to -1.299 and -1.307 for Er³⁺: GdCl₃ and Er³⁺: LaBr₃, respectively, as temperature is lowered from 400°K to 10°K. The results for Er³⁺ systems are in good agreement with the experimental findings for isosymmetric Er(C₂H₅SO₄)₃·9H₂O⁽⁸⁾. The μ_{eff} of paramagnetic ion does not depart more than 3% from the room temperature value down to 140°K in Pr³⁺:LaBr₃, 80°K in Er³⁺:GdCl₃,

and 70°K in $\text{Er}^{3+}:\text{LaBr}_3$. The room temperature values 3.55 B.M. ($\text{Pr}^{3+}:\text{LaBr}_3$), 9.56 B.M. ($\text{Er}^{3+}:\text{GdCl}_3$), and 9.55 B.M. ($\text{Er}^{3+}:\text{LaBr}_3$) match fairly well with the values 3.53 B.M. and 9.58 B.M. for Pr^{3+} and Er^{3+} ions obtained from Hund's formula and those 3.56 B.M. and 9.52 B.M. for the two metals^(9,10). Furthermore, the calculated g-values for the lowest Stark level are quite consistent with the corresponding experimental values in the isosymmetric systems:

Compound	$g_{\parallel}(\approx g_{\parallel})$	$g_{\perp}(\approx g_{\perp})$
$\text{Pr}^{3+}:\text{LaBr}_3$	0.965	0.000
$\text{LaCl}_3^{(11)}$	1.035 ± 0.005	0.1 ± 0.15
$\text{Er}^{3+}:\text{GdCl}_3$	1.826	8.866
LaBr_3	1.544	8.889
$\text{LaCl}_3^{(11)}$	1.989 ± 0.001	8.757 ± 0.002
$\text{Er}(\text{C}_2\text{H}_3\text{SO}_4)_3 \cdot 9\text{H}_2\text{O}^{(12)}$	1.47 ± 0.03	8.85 ± 0.05

These results suggest that the ratio of the parameters A and B occurring in the expression for interaction of nuclear magnetic moment with the magnetic field of the electrons⁽¹³⁾ will be 0.206 and 0.174 for $\text{Er}^{3+}:\text{GdCl}_3$ and $\text{Er}^{3+}:\text{LaBr}_3$; whereas B should be zero for $\text{Pr}^{3+}:\text{LaBr}_3$.

The nice agreement observed for the thermal and magnetic properties indicates that the crystal - field parameters reported for these compounds are reliably good.

We wish to thank the C.S.I.R. for their financial assistance and the S.E.R.C., Roorkee, for access to their IBM 1620 Computer.

REFERENCES

1. E.Y. Wong and I. Richman; J. Chem. Phys. **36**, 1827 (1962).
2. H.M. Crosswhite and H.W. Moos; Optical Properties of Ions in Crystals Eds. H.M. Crosswhite and H.W. Moos [Interscience Pub., New York], p.3 (1967).

3. N.H.Kiess and G.H.Dieke; J.Chem.Phys. 45, 2729 (1966).
4. H.M.Rosenberg; Low Temperature Solid State Physics (Clarendon Press, Oxford), p.23, p.306 (1963).
5. J.H.Van Vleck; The Theory of Electric and Magnetic Susceptibilities (Univ.Press, Oxford), p.182 (1932).
6. B.C.Gerstein, G.J.Penney and F.H.Spedding; J.Chem.Phys. 37, 2610 (1962).
7. E.V.Kleber and B.Love; The Technology of Scandium, Yttrium and the rare-earth metals (Pergamon Press, Oxford), p.76, (1963).
8. A.H.Cooke, R.Lazenby and M.J.M.Leask, Proc.Phys.Soc. 85, 767 (1965).
9. H.Nagasawa and T.Sugawara; J Phys.Soc.Japan 23, 701 (1967).
10. I.Pop; Studii Cercetari Fiz. 17, 755 (1965).
11. C.A.Hutchison and E.Wong; J.Chem. Phys. 29, 754 (1958).
12. R.J.Elliot and K.W.H. Stevens; Proc. R. Soc A 219, 387 (1953).
13. _____; Proc. R.Soc. A 218, 553 (1953).

O' AVALUS 'AG'ETIC AND THERMODYNAMIC PROPERTIES
OF $\text{CoF}_2 \cdot 5\text{H}_2\text{O}$, $\text{CoSiF}_6 \cdot 6\text{H}_2\text{O}$ AND $\text{CoZrF}_6 \cdot 6\text{H}_2\text{O}$

B. Ghosh and S. K. Dutta Roy

Department of Physics

Indian Institute of Technology, Kharagpur

INTRODUCTION

In recent years there has been much interest in the phase transition study of paramagnetic crystals. The six coordinated Co^{2+} complexes (e.g. $\text{CoF}_2 \cdot 5\text{H}_2\text{O}$, $\text{CoSiF}_6 \cdot 6\text{H}_2\text{O}$ and $\text{CoZrF}_6 \cdot 6\text{H}_2\text{O}$) are of special interest because of their simple crystal structure at room temperature (trigonal symmetry with one ion in the unit cell). All these crystals undergo phase transition at 246°K [1-4]. The specific heat data of these crystals have also shown a λ type anomaly at a temperature where the phase transition disappears. This paper describes the interpretation of the magnetic and the sp. heat results in the light of the model proposed by the authors in an earlier communication [3, 4].

RESULTS AND DISCUSSION

The results are shown in fig.1. It is evident from the fig. that the phase transition is associated with the appearance of magnetic anisotropy in the symmetry plane and λ -anomaly in the specific heat. The X-ray evidence of $\text{CoSiF}_6 \cdot 6\text{H}_2\text{O}$ [1, 5] show that below 246°K two types of Co^{2+} ions in the unit cell are oriented at an angle ϕ w.r.t room temperature trigonal axis.

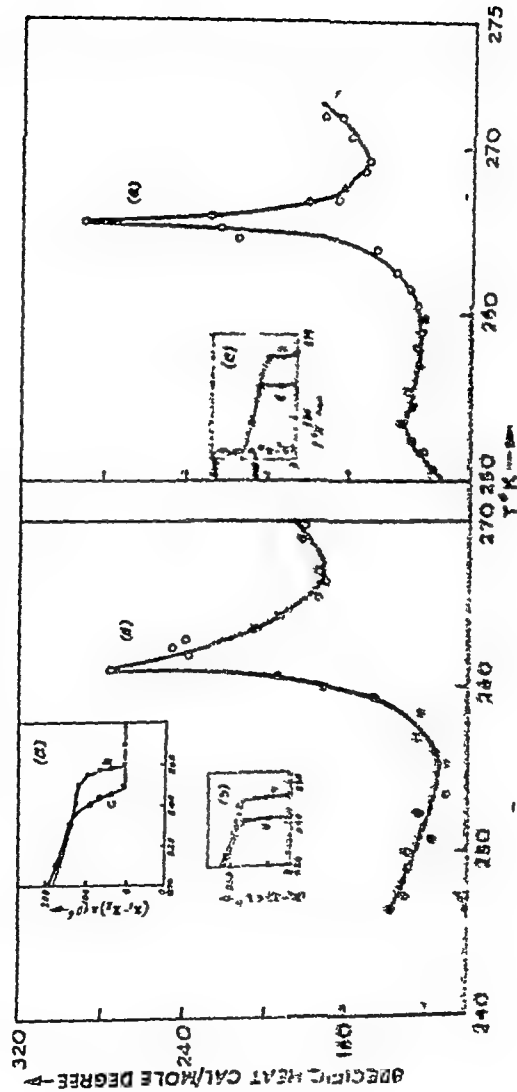


FIG. 1

Magnetic anisotropy in the symmetry plane. (a) $GdFe_3W_6$, $11H_2O$, (b) $Gd_2Fe_{12}W_6$, $11H_2O$. Specific heat of (a) $GdFe_3W_6$, $11H_2O$ (c) $Gd_2Fe_{12}W_6$, $11H_2O$

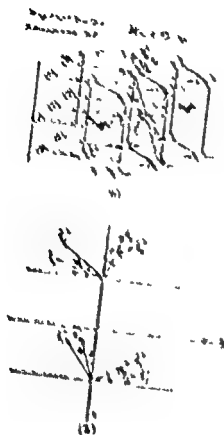


FIG. 2

FIG. 2. (a) Proposed spin structure for parallel dipole-dipole interaction (after Chakrabarti, 1974). (b) The various coordinate systems in the two sublattice models. The top system is the crystallographic system, the bottom is the spin system, and the middle is the coordinate system in which the dipole-dipole interaction is diagonal and the system is in equilibrium.

REFERENCES

1. S.Roy Ind. J. Phys 38, 176 (1966)
2. V.Vazumder and S.K.Datta J.Chem.Phys 42, 418 (1965)
3. S.K.Dutta Roy and B.Ghosh J Phys Chem.Solids 29,1511 (1968)
4. " " and Supratik Kar J.Phys Chem Solids (1970) inpress
5. T.Hatanabe J.Phys Soc Japan 20 82 (1965)
6. A Abragam and V.H.L Pryce Proc Roy Soc A208 173 (1953)
7. A.Bose. A.S.Chakraborty and R.Chatterji Proc Roy Soc A261, 43 (1961)
8. I.F.Silvera, J.H.V.Thornley and M.Tinkham., Phy.Rev 136, A695 (1964)
9. B.Eleaney and D.J.E Ingram, Proc Roy Soc A208,143(1961)
- 10.A.Ohtsubo J. Phy Soc Japan 20, 82 (1965)

Acknowledgement.

One of us (B.G.) is grateful to CSIR for the award of Senior Research Fellowship.

DISCUSSION

E.S.R. Gopal

The observation of a thermal hysteresis is reported. What were the and the heating rates?

B. Ghosh

At the rate of

B.

a point

y ob

hyste

he

observe any latent heat? If the above observation are confirmed then the transition is of first order. Then transition cannot be λ -type.

R. Ghosh

No.

MAGNETIC AND THERMODYNAMIC STUDIES OF CoO(I) AND CoO(II)

V.K.Goswami, B. Ghosh, and K.S.De.
 Indian Institute of Technology, Kharagpur-2.

I. INTRODUCTION

Cobaltous Oxide is known to be a good catalyst for oxidation reactions. In recent times, existence of two forms of Cobaltous Oxide possessing different physico-chemical properties have been reported¹. The form I, CoO(I) (prepared by heating cobalt metal in carbondioxide at 1000°C) has a NaCl structure and the form II, CoO(II) (prepared by decomposing cobalt carbonate at 300°C in vacuum) has a NaCl structure with half of its (+)ve ion sites and half of its (-)ve ion sites vacant. The density measurements¹ have shown that CoO(I) has a density of 6.4 gms/cm^3 whereas CoO(II) has a density of $4.8 \pm 0.5 \text{ gms per cm}^3$. The same authors¹ have also found that CoO(II) transforms noticeably to CoO(I) at about 300°C , giving CoO(I,II) - a mixture of form I and II.

It remains to be investigated which of the two forms of cobaltous oxide is mainly responsible for the catalytic activity, through a study of the physical properties of the two forms and their catalytic activities.

In the present paper the results of magnetic measurements and Differential Thermal Analysis (DTA) are presented.

II. EXPERIMENTAL

CoO(II) , CoO(I) , CoO(I,II) have been prepared following the methods described by Ok and Mullen¹. In

addition to this, $\text{CoO}(\text{I})$, and $\text{CoO}(\text{I,II})$ have also been prepared by a second method.

The magnetic susceptibilities of $\text{CoO}(\text{II})$, $\text{CoO}(\text{I})$, $\text{CoO}(\text{I,II})$ have been measured² over the temperature region 300 - 700°K.

The DTA measurements on $\text{CoO}(\text{II})$ in the temperature region 300 - 850°K in vacuum and Ar. atmosphere were done in sealed pyrex glass ampules by using the conventional DTA apparatus.

III. RESULTS

The results of magnetic susceptibility measurements* and DTA are shown in figure 1 and 2 respectively.

The magnetic susceptibility data of the two forms of CoO and the mixture show that $\text{CoO}(\text{II})$ has got the highest magnetic susceptibility value at room temperature (5231×10^6 gms/mole), in comparison to the room temperature susceptibility values of $\text{CoO}(\text{I})$ (4684×10^6 gms per mole) and $\text{CoO}(\text{I,II})$ (4762×10^6 gms/mole). This arises from the low density of $\text{CoO}(\text{II})$, compared^b $\text{CoO}(\text{I})$ and $\text{CoO}(\text{I,II})$ °

Along with the temperature dependence of magnetic susceptibility of $\text{CoO}(\text{I,II})$, $\text{CoO}(\text{I})$ and $\text{CoO}(\text{II})$, the magnetic susceptibility data of LaBlanchetais³ has also been shown in figure 1. The sample to sample variation in the region 300 - 600°K indicates that the magnetic

* The authors gratefully acknowledge the sustained help of Dr. S.K.Dutta Roy and Mr. S.N.Kaul, during magnetic measurements.

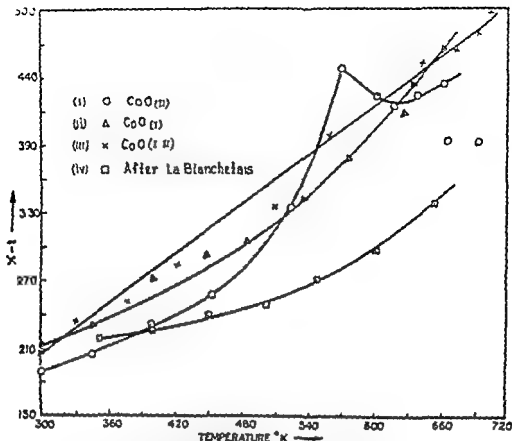


FIG-1 TEMP DEPENDENCE OF SUSCEPTIBILITY OF COBALT OXIDE

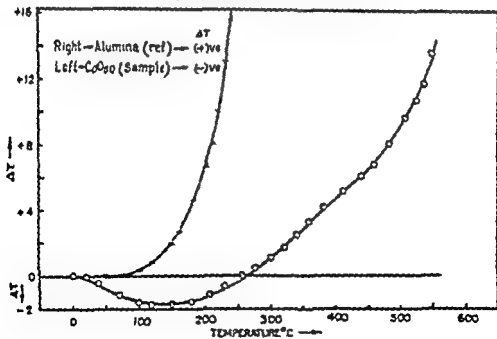


FIG-2 DTA THERMOGRAPH OF CoO_{90}

These data are shown graphically on the sample preparation diagram. The curve of χ vs T in $\text{CoO}_{(I,II)}$ follows a similar relationship. In $\text{CoO}_{(I)}$ shows a slight curvature towards the temperature axis. This curvature increases in the case of $\text{CoO}_{(II)}$. Further, in $\text{CoO}_{(II)}$ the susceptibility shows an anomalous behaviour in the temperature region $550 - 600^\circ\text{K}$ indicating that in this temperature range $\text{CoO}_{(II)}$ slowly passes into $\text{CoO}_{(I)}$. Beyond the transition region all the samples show a similar behaviour. This result is in conformity with the Mossbauer data¹. The transition observed in $\text{CoO}_{(II)}$ is not of magnetic origin since the sample is paramagnetic both below and above the transition temperature. But, the large density difference between the two forms suggests that the transition is probably of first order. The evaluation of exchange parameter appears difficult due to the magnetic anomaly in the region $300 - 200^\circ\text{K}$.

The DTA measurements on $\text{CoO}_{(II)}$ shows that the endothermic pattern of thermograph changes at about $550 \pm 5^\circ\text{C}$ indicating a change in the form of CoO . Such a change might be due to contraction of the lattice.

On the basis of the observed differences in the physical properties of the two specimen of CoO , the catalytic activity is being investigated by us.

REFERENCES

1. Ok and Mullen, The Phy. Rev., 168, 2, 550-552, (1968).
2. A. Subrahmanyam, Indian J. of Phy., XL, 9, 527, (1966).
3. LaBlanchette, J. Phy. Radium, 12, 765, (1951).

DISCUSSION

H.V. Kcer

How have you evaluated the exchange parameters. The transition is crystallographic and not magnetic in the real sense. So no evaluation of exchange parameters is possible.

V.K. Goswami

It has not been possible to evaluate the exchange parameter from the above data.

NATURE OF LIGAND FIELDS IN FERROUS AMMONIUM SULPHATE HEXAHYDRATE AND FERROUS POTASSIUM SULPHATE HEXAHYDRATE

D.Pal, D.Ghosh and A.K.Pal
Magnetism Department, Indian Association for the
Cultivation of Science, Calcutta-32

I. INTRODUCTION

There have been some studies of magnetic properties¹⁻⁶ of ferrous Tutton salts, of which the most extensive is that of ferrous ammonium sulphate hexahydrate. Recent measurement⁷ of principal crystalline susceptibilities by very sensitive magnetic balances prompts us to reinvestigate the nature of ligand fields in these salts on the basis of rigorous theory of Bose *et al.*⁸ In absence of resonance data which only can give the true magnetic symmetry and orientation of the ligand clusters the best thing to do is to assume an approximate tetragonal symmetry and calculate ionic susceptibilities K_{11} and K_{\perp} from crystalline susceptibilities considering both the possibilities viz $K_{11} > K_{\perp}$ and $K_{11} < K_{\perp}$ and finally omitting the one which does not tally with all the available data.

II. THEORETICAL CONSIDERATIONS

In ligand field of D_{4h} symmetry, either of the two levels 5B_2 or 5E leading to quite different magnetic properties can be the lowest in the ligand field energy pattern depending on the sign of the axial field parameter. 3A_1 and 5B_2 levels lying at $\sim 10^4 \text{ cm}^{-1}$ above the ground state are not important for paramagnetism. Following Bose *et al.*⁸ it can be shown that ionic susceptibilities are functions of orbital reduction parameters ($k_{||}, k_{\perp}$), reduced spin-orbit coupling coefficients ($S_{||}, S_{\perp}$) and Δ

III. LIGAND FIELD INFORMATION FROM THEORETICAL FITTING OF MAGNETIC AND OTHER ALLIED PHYSICAL DATA

(1) Ferrous Ammonium Sulphate Hexahydrate :

The fitting procedure adopted is to select a set of $\Delta, k_{11}, k_{\perp}, S_{11}$ and ζ which will enable best fitting of both anisotropy in moment square ($P_{11}^2 \sim P_{\perp}^2$) and mean moment square ($\overline{P^2}$) data at room temperature with minimum deviation at all other temperatures in the temperature range $300^\circ\text{K} - 68^\circ\text{K}$. It will be seen (vide Table I) that the deviation of $\overline{P^2}$ are well within 1% of the calculated values at different temperatures but those in anisotropy $P_{11}^2 \sim P_{\perp}^2$ are quite pronounced being ~10% in the case of $K_{11} > K_{\perp}$ ($\Delta +ve$) and ~4% in the case of $K_{11} < K_{\perp}$ ($\Delta -ve$). This deviation may be due to our neglect of the departure from axial symmetry or due to taking the field parameters as independent of temperature or due to both and so the proper choice of relative magnitude of K_{11} and K_{\perp} remains undecided. It is however interesting to note that the theoretical curve for $\sqrt{\overline{P^2}}$ obtained from derived parameters at room temperature for positive Δ has not the least resemblance with the experimental curve below 10°K (Figure 1) and the position does not improve by varying Δ . On the other hand, in the negative Δ case theoretical curve closely follows the trend of the experimental curve. Moreover it has been observed that by increasing Δ from -400 cm^{-1} to -800 cm^{-1} the theoretical curve can be made to pass through the mean of the experimental data of various authors. In this connection it seems useful to analyse observed Schottky anomalies⁹ in specific heat at 3.8°K & 20°K in the light of Stark pattern. It is found that orthorhombic ligand field with zero field parameter

$D_z = 12 \text{ cm}^{-1}$ (corresponding $\Delta = -500 \text{ cm}^{-1}$) and asymmetry parameter η ($= \frac{D_x - D_y}{3D_z}$) = 0.37 for the ground spin quintuplet can only satisfactorily explain the said peaks. With these parameters and adopting $S=1$ formalism (valid below $\sim 7^\circ \text{K}$) calculated $\sqrt{P^2}$ are also quite consistent with the experimental values for temperatures below 7°K (vide Fig 1)

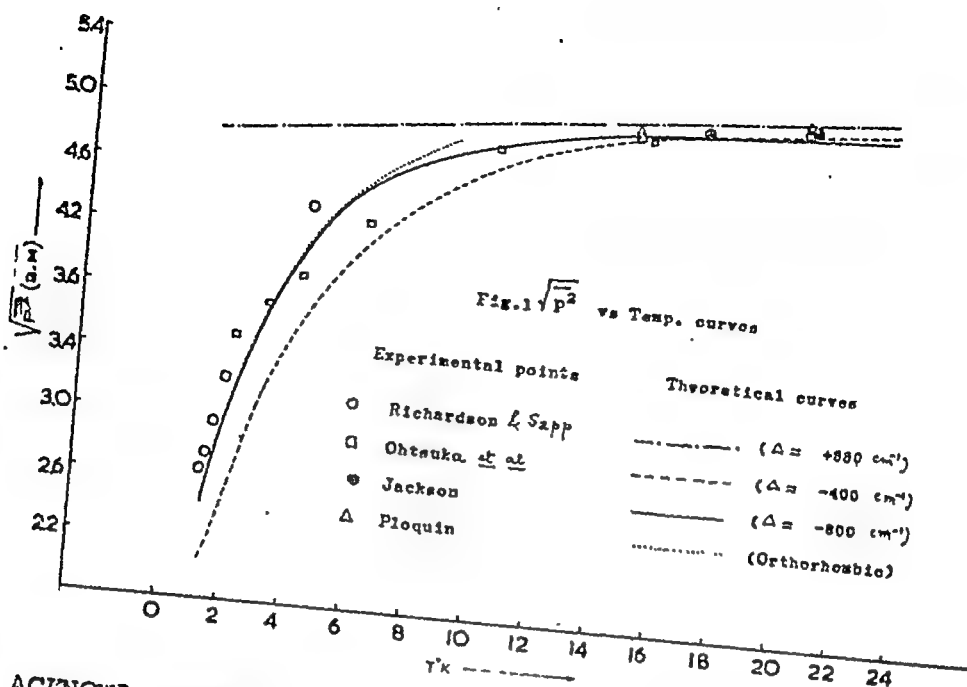
TABLE I

Results of fitting for ferrous ammonium sulphate hexahydrate. Values within parentheses are theoretically obtained.

Temp $^\circ \text{K}$		300	200	100	68
$\Delta = -400 \text{ cm}^{-1}$ $k_{11} = k_{\perp} = 0$ $S_{11}S_{\perp} = -80 \text{ cm}^{-1}$	$P_{\perp}^2 - P_{11}^2$	6.286 (6.269)	10.46 (10.25)	17.63 (17.01)	22.00 (21.14)
	$\overline{P^2}$	28.98 (29.07)	29.38 (29.30)	29.09 (28.90)	28.73 (28.53)
$\Delta = 880 \text{ cm}^{-1}$ $k_{\parallel} = 0, k_{\perp} = 8$ $S_{\parallel} = 88 \text{ cm}^{-1}$ $S_{\perp} = -80 \text{ cm}^{-1}$	$P_{11}^2 - P_{\perp}^2$	11.23 (11.26)	18.52 (18.24)	31.61 (34.83)	40.11 (44.66)
	$\overline{P^2}$	28.98 (28.94)	29.38 (29.70)	29.09 (30.36)	28.73 (30.01)

(ii) Ferrous Potassium Sulphate Hexahydrate :

Experimental results⁷ directly invalidates " $k_{\perp} > k_{11}$ approximation". With the other approximation i.e positive Δ and following similar procedure in fitting as for ammonium salt wide divergences are encountered in case of anisotropy $P_{11}^2 - P_{\perp}^2$ (about 75%). Since low temperature specific heat and susceptibility data are lacking, it can only be guessed that presence of pronounced orthorhombicity (more than that in ammonium salt) is mainly responsible for such large discrepancy.



ACKNOWLEDGMENTS

The authors are deeply indebted to Prof. A. Bose, D.Sc, F.N.I. for his valuable suggestions and advice.

REFERENCES

1. L.C. Jackson ; Phil. Trans. Roy. Soc. (London) A 224, 1 (1924)
2. A. Bose; Indian. J. Phys. 22, 276 (1948)
3. D.M.S. Bagguley, B. Bleaney, J.H.E. Griffiths, R.P. Penrose and B.I. Plumpton; Proc. Phys. Soc. 61, 542, 551 (1948)
4. J. Ploquin ; Compt. Rend. 233, 162 (1951)
5. T. Ohtsuka, H. Abe and E. Kanda; Sci. Rept. Toho Ku University 9A, 476 (1957)
6. J.T. Richardson and R.C. Sapp; J. Chem. Phys. 29, 337 (1958)
7. D. Guha Thakurta and D. Mukhopadhyay, Indian J. Phys. 40, 69 (1966)
8. A. Bose, A.S. Chakraborty and R. Chatterjee; Proc. Roy. Soc. (London) A261, 207 (1961)
9. R.W. Hill and P.L. Smith; Proc. Phys. Soc (London) A66, 228 (1953)

PARAMAGNETIC ANISOTROPY AND ELECTRONIC STRUCTURE
OF SQUARE PLANAR TRANSITION METAL COMPOUNDS

S. Mitra
Tata Institute of Fundamental Research
Bombay-5

and,

C.G. Barraclough and R. L. Martin
University of Melbourne, Australia

I. INTRODUCTION

The electronic structures of square-planar paramagnetic transition metal compounds have been the subject of extensive studies. Optical absorption and electron spin resonance spectroscopy are the only methods which have been widely used for this purpose. While absorption spectroscopy in the visible and ultraviolet region is quite versatile in its applications, the occurrence of intense charge-transfer bands often obscures the much weaker d-d transitions and so makes the identification and assignment of ground and excited states difficult. Electron spin resonance has been successfully applied to several square-planar systems, but its application is often limited by relaxation and other phenomena.

We have been recently interested to apply the method of paramagnetic anisotropy to deduce the electronic structures of square-planar transition metal compounds, and have applied it successfully to a number of square planar copper (II), cobalt (II), manganese (II) and iron (II) compounds.¹⁻⁴ The present paper presents a summary of the results obtained by us.

Square-planar stereochemistry is not very common for the transition metal compounds. The phthalocyanines provide the classic

example where the metal atoms almost achieve square planar geometry. During the past few years many square planar compounds of Cu(II) and Co(II) have, however, been discovered. Our measurements are only confined to the representative compounds.

II. RESULT AND DISCUSSION

Our susceptibility and magnetisation measurements between 300° and 1.5° K on manganese (II) phthalocyanine ($3d^5$) establish that the compound belongs to the rare intermediate spin situation $S = 3/2$. The study of paramagnetic anisotropy shows that the principal moment along the symmetry axis of the molecule, $\mu_{\parallel} = 4.0$ B.M. remains constant, while the principal moment perpendicular to the symmetry axis increases from 4.4 B.M. (300° K) to 5.0 B.M. (90° K). Calculation shows that this magnetic anisotropy is consistent with a $^4A_{2g}$ ground term deriving from the configuration $(b_{2g})^2 (e_g)^2 (a_{1g})^1$. Alternative possibilities for the ground term can be eliminated on the basis of the anisotropy data.

The electronic structure of iron (II) phthalocyanine ($3d^6$) has been the subject of controversy. Our magnetic susceptibility, magnetic anisotropy and magnetisation data between $300 - 1.5^{\circ}$ K that the compound belongs to the $S = 1$ spin case, deriving from the configuration $(e_g)^4 (b_{2g})^1 (a_{1g})^1$. The ground term is then $^3B_{2g}$. The magnetic moment () of the compound at room temperature is 3.9 B.M. and remains nearly constant down to about 80° K, below which it decreases rapidly so that at 1.5° K, $\mu_{\text{eff}} = 0.5$ B.M. The magnetisation data at 1.5° K show vanishing magnetisation. The crystals of the compound are fairly anisotropic at high temperatures. At low temperatures, the anisotropy, however, increases very fast,

with g decreasing fast with lowering of temperature, and increasing. These observations are consistent with a large zero-field splitting of the ground term ${}^3B_{2g}$ such that $M_s = 0$ lies about 65 cm^{-1} below $M_s = \pm 1$. The magnetic anisotropy, in this case, appears to arise from the zero-field splitting since we deduce

Cobalt (II) phthalocyanine ($3d^7$) is low spin ($S = \frac{1}{2}$) and has one unpaired electron which may lie in any of the (d_{xz}, d_{yz}), d_{xy} or d_{z^2} orbitals. If it lies in the (d_{xz}, d_{yz}), then which is opposite to our experimental observation. If the unpaired electron lies in d_{xy} , then both g_x and g_y are expected to vary appreciably with temperature, which is not supported by experiment. If the unpaired electron lies in d_{z^2} orbital, then g_z and while g_x will be independent of temperature, g_y will vary considerably with it. This is exactly what is observed experimentally.

Cobalt (II) dithioacetylacetonate is another example of low-spin planar Co(II) compound. The x and g -tensors are given below:

$$\begin{aligned} g_x &= 3.280, & g_y &= 1.904, & g_z &= 1.899 \\ &= 2.93, & &= 1.89, & &= 1.77 \quad (\text{in d.u.}) \end{aligned}$$

Here x and y axes lie in the molecular plane and the z axis perpendicular to it. Note the large in-plane anisotropy in this compound compared to the near in-plane isotropy in the cobalt phthalocyanine. The unpaired electron is deduced to lie in the d_{z^2} orbital and the large in-plane anisotropy is shown to arise from the proximity of the d_{z^2} and d_{xy} levels relative to d_{xz} .

Copper (II) phthalocyanine (d^9) has one unpaired electron. While the ground term of this compound is known ($^2B_{1g}$), there are controversies regarding the ordering of the excited terms. Our measurements of its paramagnetic anisotropy has been helpful in deciding the correct ordering of the excited terms.²

We finally note that the measurement of paramagnetic anisotropy promises to be very helpful in elucidating the electronic structure of transition metal compounds, and its application to the compounds of other stereochemistries will be interesting. One such recent application of this technique to the octahedrally coordinated binuclear copper (II) acetate monohydrate has proved to be rewarding⁵.

REFERENCES

1. R.L. Martin and S. Mitra, Chem. Phys. Letters 3 (1969) 183.
2. R.L. Martin and S. Mitra, Inorg. Chem. 9 (1970) 182.
3. G.G. Barraclough, R.L. Martin, S. Mitra and R.C. Sherwood, J. Chem. Phys. 53 (1970) 1638, 1643.
4. A.K. Gregson, R.L. Martin and S. Mitra, Chem. Phys. Letters 5 (1970) 310.
5. A.K. Gregson, R.L. Martin and S. Mitra, Proc. Roy. Soc. (Lond.), in press.

DETERMINATION OF THE PRINCIPAL AXES OF THE FIELD GRADIENT TENSOR FROM THE ZEEMAN SPLIT NQR SPECTRA.

A. K. Saha, R. Roy and S. Sengupta, Saha Institute of Nuclear Physics, Calcutta-9.

I. Introduction

The asymmetry parameters and the orientation of the principal axes of the field gradient tensor from the Zeeman split NQR spectra have been determined on the basis of the theory suggested by Saha¹. The Zeeman spectra corresponding to the rotation of a single crystal of $\text{Ba}(\text{ClO}_3)_2 \cdot \text{H}_2\text{O}$, - around the E.F. (X) axis and an axis (Y) perpendicular to both the E.F. and Zeeman field axis (Z), have been analysed. The orientation parameters of the field gradient tensor within the crystal with respect to the crystallographic axes have been determined.

With the application of Zeeman field, the pure NQR line splits up into a quadruplet and we define a splitting function k as

$$k = \frac{1}{\omega_z} (f_{M'}^2 + g_{M'}^2)$$

where, $f_{M'}$ and $g_{M'}$ are the separations of the outer pair and the inner pair of the split lines.

For rotation of the crystal around X-axis, the splitting function

$$\begin{aligned} h(\alpha_s) &= p_x + q_x \cos 2\alpha_s + r_x \sin 2\alpha_s \\ &= p_x + \lambda_x \cos 2(\alpha_s - \Theta_s) \end{aligned}$$

$$\text{where, } \cos 2\Theta_x = \frac{q_x}{\Lambda_x} \quad \text{and } \sin 2\Theta_x = \frac{r_x}{\Lambda_x}$$

The values of p_x and Λ_x can be obtained from the curve of $k(\alpha_x)$ as,

$$p_x = \frac{k(\alpha_x)_{\max} + k(\alpha_x)_{\min}}{2}$$

$$\Lambda_x = \frac{k(\alpha_x)_{\max} - k(\alpha_x)_{\min}}{2}$$

θ_{x0}, ϕ_{x0} the polar angles of the R.F. axis with respect to the principal axes frame for initial position of the crystal, are obtained from

$$p_x = b + \frac{\sin^2 \theta_{x0}}{2} (a - b - c \cdot \cos 2\phi_{x0})$$

$$q_x = p_x - b + c \cdot \cos 2\phi_{x0}$$

$$r_x = -c \cdot \cos \theta_{x0} \sin 2\phi_{x0}$$

If ϕ_x is the angle where $k(\alpha_x)$ is maximum, the possible values of α_{x0} , the angle between Z-principal axis and X-meridian are $\alpha_{x0} = -(\phi_x \pm \Theta_x)$, $[\pi - (\phi_x \pm \Theta_x)]$. The correct value of α_{x0} is settled by observing a doublet spectrum at a separation of $2\omega_z$ which can be obtained by an (A.C.) rotation of around X axis and a (C) or (A.C.) rotation through $\left(\frac{\pi}{2} - \theta_{x0}\right)$ around Y, when Z_p becomes aligned along Z.

For spin $I = \frac{3}{2}$, a, b, c are not known in which case the crystal is brought back to the initial position and the split

spectrum corresponding to Y-rotation is recorded. From spherical trigonometry, we know $\cos\theta_{Y0} = \sin\theta_{X0} \sin\eta \sin\alpha_{X0}$, which again can be expressed as a function of η . $\cos\theta_{Y0}$ as obtained from Y-rotation pattern can also be plotted as a function of η . The intersection of these two curves gives the value of η .

II. Experimental

Before setting the single crystal of $\text{Ba}(\text{ClO}_3)_2 \cdot \text{H}_2\text{O}$ in the goniometer, the orientation of the crystal axes $X_0 Y_0 Z_0$ relative to the laboratory frame of axes XYZ was determined. The laboratory frame of axes is such that the R.F. field is parallel to the Z-direction and the Y-axis is perpendicular to R.F. field and Zeeman field. The single crystal used here being large, the orientation of these axes were determined following back-reflection X-ray method of Laue. For rotation around X-axis, two sets of quadruplet lines for the two system of molecules were found. The initial orientation was such that the absolute values of the direction cosines in the two systems of the principal axes were identical and for Y-rotations only one set of superposed quadruplet lines were observed. The parameters β_{X1} , Λ_{X1} , β_{Y1} , Λ_{Y1} corresponding to X-rotation and β_Y , Λ_Y corresponding to Y-rotation are obtained from the experimental curves. The plot of $\cos\theta_{Y0}$ as a function of η gives the value $\eta = .027$. η being known, all the angles α_{X0} , θ_{X0} , ϕ_{X0} can be computed. The direction cosines of the principal axes $X_P Y_P Z_P$ of the field gradient tensor with respect to the crystallographic axes are then computed as detailed in the table below :

Table 1

Direction Cosines of $X_p Y_p Z_p$ with respect to $X_o Y_o Z_o$

	Mol 1			Mol 2		
	X_c	Y_c	Z_c	X_o	Y_o	Z_o
X_p	.66413	-.40445	-.62373	.66413	.74151	.69519
Y_p	.28923	.63651	-.71496	-.28923	-.13745	-.94732
Z_p	.68940	.65669	.30575	-.68940	.65669	-.30575

III. Discussion

Zeldes and Livingston² from a study of Zeeman split NQR spectra of $Ba(ClO_3)_2 \cdot H_2O$ estimated that η cannot exceed 0.05. Their analysis was based on the fact that there was no residual splitting when the Zeeman field was oriented 90° to the Z-principal axis. The precise value of η obtained by this method is free from the uncertainty reported by the earlier workers.

Work is in progress for estimating theoretically values of η and the direction cosines of the principal axes of the field gradient on the basis of the X-ray data of the crystal for ultimate comparison with the experimental values.

IV. References

1. A. K. Saha, Proceedings of the Symposium on Solid State Physics, Calcutta, 1965.
2. R. Zeldes and R. Livingston, J.C.P., 26, 1102, 1957.

DISCUSSION

B.D. Nageswara Rao

What is the accuracy with which you can determine the orientation of the principal axes of the ZPG?

S. Sengupta

It depends on the accuracy of measurement of the split lines and we can claim an accuracy of 1% in our experimental results.

B.D. Nageswara Rao

How do your η values on Mercuric Chloride compare with those of Dinesh and Narasimhan?

S. Sengupta

They do not compare well with those of Dinesh and P.T. Narasimhan. Their values are rather large and are not consistent with theoretical considerations.

NUCLEAR MAGNETIC RESONANCE STUDIES OF ^{35}Cl IN $\text{K}_2\text{CuCl}_4 \cdot 2\text{H}_2\text{O}$

L.C. Gupta and D.L. Padmakrishna Setty
Tata Institute of Fundamental Research
Homi Bhabha Road, Bombay-5

I. INTRODUCTION

The purpose of this note is to report the experimental and calculated values of the nuclear quadrupolar interaction parameters of ^{35}Cl in $\text{K}_2\text{CuCl}_4 \cdot 2\text{H}_2\text{O}$.

II. EXPERIMENTAL

The nuclear magnetic resonance experiments at about 10,000 Gauss were performed on a single crystal (approximate dimensions 1 cm x 1 cm x 0.5 cm) whose axes were identified by neutron diffraction. Only the central transition ($\frac{1}{2} \leftrightarrow -\frac{1}{2}$) of ^{35}Cl isotope could be observed.

The preliminary studies showed that the spectrum, in general, consists of four lines which can be grouped into two sets, each set containing two lines. One of the sets (to be referred as Set I) was very sensitive to the crystal orientation in the magnetic field. With the limited accuracy ($\pm 2^\circ$) of our fixing the orientation of the crystal, it was difficult to follow this set as a function of the orientation. The other two lines (Set II) could be followed comfortably.

The bimolecular tetragonal unit cell of $\text{K}_2\text{CuCl}_4 \cdot 2\text{H}_2\text{O}$ with edge dimensions $a = b = 7.44 \text{ \AA}$ and $c = 7.88 \text{ \AA}$ has two crystallographically non-equivalent Cl-sites, Cl(1) and Cl(2), four chlorines belonging to each of the two sites¹. The distance Cu-Cl(1) ($= 2.51 \text{ \AA}$) is smaller than the distance Cu-Cl(2) ($= 2.94 \text{ \AA}$). Further the four crystallographically equivalent chlorines are arranged in such a way that the Cl-Cu-Cl line is parallel to two

chlorines while it is parallel to $[1\bar{1}0]$ for the other two chlorines, thus giving rise to two physically non-equivalent sites in the presence of a magnetic field. This accounts for the observed two NMR lines in each set.

The crystal was rotated about $[110]$, $[1\bar{1}0]$ and $[001]$ keeping these axes perpendicular to the magnetic field, H_0 . From the nature of the spectrum one concludes² that these directions are the principal axes of the electric field gradient (EFG) tensor. A complete rotation pattern about $[110]$ is shown in Fig. 1. The rotation pattern about $[1\bar{1}0]$ was identical to that shown in Fig. 1 as required by the symmetry of the crystal.

III. RESULTS

The rotation patterns were analysed by diagonalising the Hamiltonian

$$\mathcal{H} = \frac{eQ}{4I(2I-1)} \left[eq_{zz} (3I_z^2 - I^2) + \frac{e}{2} (q_{xx} - q_{yy}) (I_+^2 + I_-^2) \right] + \gamma \hbar \vec{I} \cdot \vec{H}(\theta)$$

where the symbols have their usual meaning³. The quadrupole coupling tensor parameters so obtained from the observed spectra, for one of the physically non-equivalent site, are given in Table I.

A point charge calculation of the EFG within a sphere of 100 \AA was performed on the CDC 3600 computer. The formal charges used in this calculation are

$$Z_K = +1, Z_{Cu} = +2, Z_{Cl} = -1, Z_H = 0.3 \text{ and } Z_O = -0.6$$

The calculated values of the quadrupole coupling tensor are given in Table 1. The value of the antishielding factor for ^{35}Cl in these calculations, has been taken to be -27.1^4 . These results

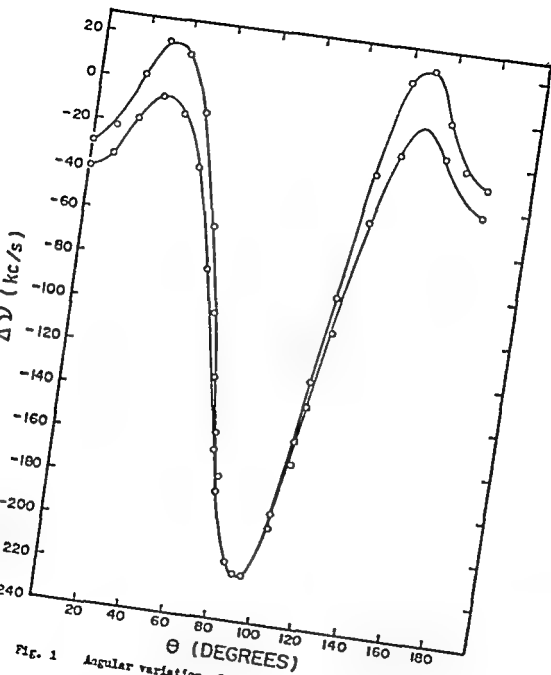


Fig. 1 Angular variation of the second order shift of ^{35}Cl NQR ($\frac{1}{2} \leftrightarrow -\frac{1}{2}$) transition in a single crystal of $\text{K}_2\text{CuCl}_4 \cdot 2\text{H}_2\text{O}$.

TABLE I

The Quadrupole coupling constant tensor parameters
of ^{55}Cl in $\text{K}_2\text{CuCl}_4 \cdot 2\text{H}_2\text{O}$

	<u>Directions of principal axes</u>			$e^2 Q_0$ $_{zz}$ (Mc/s)	η , the asymmetry parameter
	X	Y	Z		
Cl(1) (Calc.)	$[\bar{1}10]$	$[001]$	$[110]$	- 15.2	0.24
Cl(2) (Calc.)	$[001]$	$[\bar{1}10]$	$[110]$	- 4.01	0.30
Cl(2) (Expt.)	$[001]$	$[\bar{1}10]$	$[110]$	$\pm 3.32 \pm 0.02$	0.90 ± 0.01

suggest that Cl(1) - site is responsible for the set I and Cl(2)-site for Set II. Though the directions of the principal axes of the calculated EFG agree with those determined experimentally, the magnitudes are not in good agreement. This is expected due to the crude nature of these calculations. The introduction of Cu-Cl covalent bond, giving rise to an axially symmetric EFG about the bond axis, does not improve the situation.

The authors wish to thank Drs. S.K. Sikka and A. Sequeira for identifying the axes of the crystal by Neutron Diffraction and Dr. R. Vijayaraghavan for valuable discussion.

REFERENCES

1. R.W.G. Wyckoff; Crystal Structures, 2nd Ed., Vol. 3 (Interscience New York, 1965), p. 618.
2. H.E. Petch, N.G. Granna and G.M. Volkoff; Can. J. Phys., 31, 857 (1955).

3. C.P. Slichter, *Physics of the Earth*, Science,
 New York, 1963], p. 111.
4. G. Burns and E.C. ~~Went~~, *Phys. Rev.* ~~131~~, 1964, 1711. Dipole
 earlier by
 of the
 tied over a
 ent work on
 ify the results
 The Zeeman
 14-dinitrobenzene

oxide and
 from melt. The
 two Helmholtz coils
 and the hori-

th four
 out

ZEEMAN EFFECT OF CHLORINE NUCLEAR QUADRUPOLE RESONANCE IN MERCURIC CHLORIDE AND 1-CHLORO-2:4-DINITROBENZENE

H.S.Vijaya and J.Ramakrishna

Department of Physics, Indian Institute of Science,
Bangalore-12.

The Zeeman effect of chlorine pure quadrupole resonance in mercuric chloride was studied earlier by a number of investigators.¹⁻³ The value of the asymmetry parameter η obtained by them varied over a wide range, viz., 0.08 to 0.8. The present work on mercuric chloride was undertaken to verify the results obtained by the earlier investigators. The Zeeman effect of Cl^{35} resonance in 1-chloro-2:4-dinitrobenzene was studied for the first time.

Single crystals of mercuric chloride and 1-chloro-2:4-dinitrobenzene were grown from melt. The Zeeman effect assembly consisted of two Helmholtz coils capable of rotation about the vertical and the horizontal axis.

Mercuric chloride is orthorhombic with four molecules per unit cell the molecules being essentially linear.⁴ It gives two resonance lines corresponding to the two chemically inequivalent chlorine atoms in the molecule. Zeeman effect studies show that there are two physically inequivalent chlorine atoms in the crystal and these two correspond to the chlorine atoms in the two adjacent molecules oriented in different directions. The locus of zero-splitting was obtained for both the resonance lines.

1-chloro-2:4-dinitrobenzene belongs to the orthorhombic system with eight molecules per unit cell. Three zero-splitting loci were observed in this compound indicating the presence of three physically inequivalent field gradient z directions. Since there are eight molecules in the unit cell, it is suspected that one locus might have been missed in the experiment.

Further investigations are in progress.

RESULTS AND DISCUSSION

The equation for the zero-splitting locus for Cl^{35} ($I = 3/2$) resonance is given by

$$\sin^2 \theta_0 = \frac{2}{3 - \gamma \cos 2 \phi_0} \quad \dots \quad (1)$$

where θ_0 and ϕ_0 are the polar coordinates of the zero-splitting direction of the magnetic field with respect to the principal axes system. The zero-splitting locus is in general an ellipse and the eccentricity of the ellipse is proportional to the asymmetry parameter γ . The normal to the plane of the ellipse gives the direction of the principal z axis.

An average value of 0.10 is obtained for γ in 1-chloro-2:4-dinitrobenzene while those obtained in mercuric chloride are 0.12 and 0.17 for the two chemically inequivalent chlorines.

In mercuric chloride the angle between the two physically inequivalent z directions is about 70° which agrees to better than 5° with the value obtained from structural data. Our results indicate that mercuric chloride has a low value for γ and is thus in fair agreement with the results of Negita et al.³ The orientation of the three inequivalent field gradient tensors in the laboratory system is calculated for 1-chloro-2:4-dinitrobenzene and is shown in Table 1.

TABLE 1

1-chloro 2:4 dinitrobenzene.

Orientation of the C-Cl bonds with respect to the laboratory fixed system. A,B and C refer to the three physically inequivalent sites observed.

	ϕ_z	ϕ_x
C - Cl _A	62°3'	1°41'
C - Cl _B	77°49'	44°2'
C - Cl _C	46°57'	87°18'

REFERENCES

1. J.Ramakrishna; Phil. Mag. 14, 589, (1966).
2. Dinesh and P.T.Narasimhan; J. Chem. Phys. 45, 2170, (1966).
3. H.Kegita, T.Tanaka, T.Okuda and H.Shimada; Inorg. Chem. 5, 2126, (1966).
4. H.Braekken and W.Scholten; Z. Krist. 89, 448, (1934).
5. E.M.Gopalakrishna; Z. Krist. 111, 159, (1959).

ON THE QUADRUPOLE COUPLING CONSTANTS OF ^{197}Au , ^{182}W AND ^{183}W COMPOUNDS

Vishwanittar* and S.P.Puri

Department of Physics, University of Roorkee, Roorkee.

I. INTRODUCTION

Recently a number of groups⁽¹⁻⁴⁾ has reported data for the nuclear quadrupole coupling constants (QCC) in various compounds of ^{197}Au , ^{182}W and ^{183}W , using the techniques of Mössbauer effect and N.Q.R.. In the present work, an attempt is made to elucidate the available data in terms of ligand field theory. Following Ingalls⁽⁵⁾ and neglecting the lattice contributions to QCC we may write, for the case of axial symmetry ($\eta=0$),

$$\Delta E = C \gamma \langle \varphi | Y_2^0 | \varphi \rangle. \quad (1)$$

Here C is a constant for a particular nucleus and is determined by its spin, Sternheimer factor and quadrupole moment, the temperature of study and the spin-orbit coupling constant for the free ion; γ is the covalency factor and φ is the ground level wavefunction for the atom in the crystalline lattice.

II. QCC OF Au COMPOUNDS

The X-ray diffraction work of Jagodzinski⁽⁶⁾ reveals that the Au and I atoms in AuI are linearly arranged in the form of a zig-zag chain in the tetramolecular unit cell. The aureous chloride and bromide, being unstable are not yet investigated crystallographically and are assumed to have a structure similar to that of AuI. Accordingly, the Au atom in these compounds must be using the $(s-6p_x)$ hybrid orbitals for chemical bonding with the halogen atoms. Thus, the $6p_x$ electron will be contributing to the EFG at the nucleus, and in the spirit of Townes and Dailey theory⁽⁷⁾, we can take for an elec-

* C.S.I.R. Fellow.

-tropositive atom,

$$\gamma \mathcal{L} U_p = -(1+s)(1-s); \quad (2)$$

here the amount of s hybridization will be 0.5 and the ionicity i will be different for different halides. Using the ionic character vs. electronegativity difference curve of Dailey and Townes⁽⁸⁾, we find that the values of U_p for AuCl, AuBr and AuI will be -0.58, -0.54 and -0.51, respectively, and their order is in a good agreement with the observed relative magnitudes of e^2qQ — 1.168:1.063:1.⁽⁴⁾

This, therefore, supports the belief that the values of s and hence the bond angles are nearly same in the Aurous halides. Furthermore, from the experimental value of e^2qQ and taking $Q=0.594$ barn⁽⁹⁾ for ^{197}Au the value of atomic EFG eq_{611} for Au is estimated to be

-6.82×10^{18} volt/cm². This when substituted in the following relation⁽⁷⁾

$$eq_{611} = -(21e/21+3) \langle r^{-3} \rangle_{6p} \quad (3)$$

gives $\langle r^{-3} \rangle_{6p} = 118.4 \times 10^{24} \text{ cm}^{-3}$. This value is in nice agreement with the one calculated from the hyperfine structure constant $a_{6p_{3/2}}$ obtained spectroscopically by Kelly⁽¹⁰⁾ ($\langle r^{-3} \rangle_{6p} = 114.8 \times 10^{24} \text{ cm}^{-3}$), but differs appreciably from those obtained from $a_{6p_{1/2}}$ ($\langle r^{-3} \rangle_{6p} = 44.8 \times 10^{24} \text{ cm}^{-3}$) and the fine structure constant ($\langle r^{-3} \rangle_{6p} = 33.2 \times 10^{24} \text{ cm}^{-3}$).

The AuCl₃ crystals are built up of planar Au₂Cl₆ molecules, and the arrangement around Au^{III} is nearly square-planar (D_{4d});⁽¹¹⁾

the arrangement of ligands in AuBr₃, NaAuCl₄, KAuCl₄ and KAuBr₄ is also almost planar⁽¹²⁾. In the crystal field approximation the

$^1G(3d^8)$ ground term of low spin Au^{III} in D_{4d} field will give

$\varphi = c_1 \langle 4,4 \rangle + c_2 \langle 4,0 \rangle + c_1 \langle 4,-4 \rangle$ as the ground level, which for $Ze^2 \langle r_2^2 \rangle / a^3 = Ze^2 \langle r_2^4 \rangle / a^5$ becomes $\varphi = 0.7052 (\langle 4,4 \rangle + \langle 4,-4 \rangle) + 0.0728 (\langle 4,0 \rangle)$. For this state $G \langle \varphi | Y_2^0 | \varphi \rangle = 36.52$ mm/sec; here Sternheimer factor is not included and the spin-orbit coupling -

temperature parameter is taken unity. Using ΔE values from Ref. (4) we obtain the covalency factors γ for AuCl_3 , AuBr_3 , NaAuCl_4 , KAuCl_4 and KAuBr_4 as 0.041, 0.070, 0.070, 0.070 and 0.062, respectively. It may be pointed out that (i) the same level remains the lowest whether the above choice guided by observations of Spees et al.⁽¹³⁾ is true or not; and (ii) the $\langle \varphi | Y_2^0 | \varphi \rangle$ value obtained by one electron picture is 36.85 m/sec., which suggests that interelectronic interaction in these calculations is not very important.

III. QOC OF W COMPOUNDS

The trigonal field at W^{IV} in hexagonal WC will split the $3\gamma(d^2)$ ground term to give $^3A_2 (= \langle 3,0 \rangle)$ as the ground state, for which $\langle \varphi | Y_2^0 | \varphi \rangle = -8/35$. The W site symmetry in the tungsten sulphide is also trigonal, so that the said matrix element will be $-(8/35)$ for WS_2 too. But it is well established that the carbides are more covalent than the sulphides even though the Pauling's electronegativity values for C and S are same. Therefore, the factor

γ and hence QOC for WC will be smaller than that for WS_2 . This is in accord with the results of Refs (1,2). Nonetheless, our calculations show that the EFC for these two compounds of ^{182}W as well as ^{183}W is negative, which is borne out by experiments for WS_2 ⁽²⁾. Also the valence contribution $e_v = -1.51 \times 10^{18}$ volt/cm² calculated with the assigned pure ground state and taking $\langle r^{-3} \rangle_{\text{rel}} = 6.81 a_0^{-3}$ ⁽¹⁴⁾ compares fairly well with the experimental value $e_v = -(1.86 \pm 0.05) \times 10^{18}$ volt/cm² in WS_2 ⁽²⁾.

The MO calculations for these compounds are in progress.

REFERENCES

1. E.A. Phillips and L. Grodzins; Perturbed Angular Correlations, Eds Karlsson, Matthias and Siegbahn (North-Holland Pub.Co.), p. 201 (1964).

2. D. Agresti, E. Kankaleit and B. Persson, Phys. Rev. 155, 1342 (1967).
3. P. Machmer; J. Inorg. Nucl. Chem. 30, 2627 (1968).
4. H.O. Faltens and D.A. Shirley; J. Chem. Phys. (to be published), (1970).
5. R. Ingalls; Phys. Rev. 133, A787 (1964).
6. H. Jagodzinski; Z. Krist. 112, 80 (1959).
7. C.H. Townes and B.P. Dailey; J. Chem. Phys. 17, 782 (1949).
8. B.P. Dailey and C.H. Townes; J. Chem. Phys. 23, 118 (1955).
9. A.G. Blachman, D.A. Landman and A. Lurio; Phys. Rev. 161, 60 (1967).
10. F.H. Kelly; Proc. Soc. A65, 250 (1952).
Phys.
11. E.S. Clark, D.H. Templeton and C.H. MacGillavry; Acta Cryst. II, 284 (1958).
12. P.J. Durrant and B. Durrant; Introduction to Advanced Inorganic Chemistry (Green & Co., London), 1966.
13. S.T. Speers, J.R. Perumareddi and A.W. Adamson; J. Phys. Chem. 72, 1822 (1968).
14. J.B. Mann; Los Alamos Report 3691, part II (1968).

MÖSSBAUER ELECTRIC FIELD GRADIENT PARAMETERS IN $\text{Fe}(\text{KSO}_4)_2 \cdot 6\text{H}_2\text{O}$ SINGLE CRYSTALS

V.K.Garg and S.P.Puri

Department of Physics, University of Roorkee, Roorkee.

I. INTRODUCTION

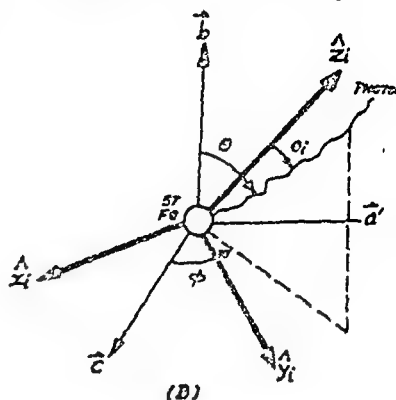
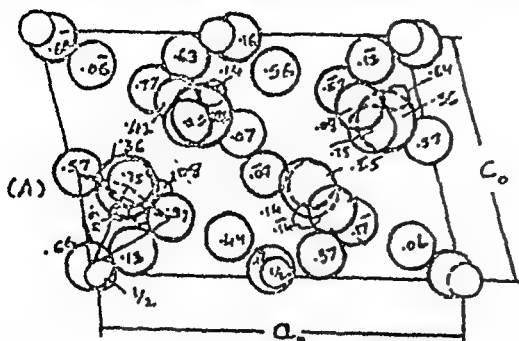
Numerous methods have been employed to determine the EFG tensor parameters of asymmetry η and electric field gradient q . When a single crystal, having a fixed direction for the EFG, is used as absorber, there is observed a variation of the intensity of hyperfine components with the angle of incidence of γ -rays. This method has been successfully employed for the complete determination of all the five independent parameters of the EFG tensor in the case of $\text{FeCl}_2 \cdot 4\text{H}_2\text{O}^{(1)}$, $\text{FeSO}_4 \cdot 7\text{H}_2\text{O}^{(2)}$, $\text{Fe}(\text{NH}_4\text{SO}_4)_2 \cdot 6\text{H}_2\text{O}^{(2,3)}$, $[\text{Fe}_2\text{Fe}(\text{CN})_5\text{NO}] \cdot 2\text{H}_2\text{O}^{(4,5)}$ and $\text{FeSO}_4 \cdot 4\text{H}_2\text{O}^{(6)}$ single crystals. The present investigation is a report on $\text{Fe}(\text{KSO}_4)_2 \cdot 6\text{H}_2\text{O}$ which gives angular variation of the Mössbauer hyperfine interaction and its relation with the molecular structure of the compound.

II. CRYSTAL STRUCTURE AND EXPERIMENTAL

$\text{Fe}(\text{KSO}_4)_2 \cdot 6\text{H}_2\text{O}$ is a monoclinic crystal⁽⁷⁾, space group $P2_1/a$ with unit cell dimensions $a = 9.28$, $b = 12.58$ and $c = 6.22\text{\AA}$ and $\beta = 106^\circ 50'$. A unit cell contains two equivalent Fe^{2+} ions; these ions are in a spin free state surrounded by a distorted octahedron formed from six water molecules. These octahedron get transformed into each other by a rotation of 180° about b axis, disregarding the translation, for it is the orientation of the site relative to the crystal axes which is important.

Single crystals were grown from aqueous solution of equimolar K_2SO_4 and $\text{FeSO}_4 \cdot 7\text{H}_2\text{O}$ by repeated crystallisation at room temperature. In order to render them suitable for transmission

the crystals were ground down to $0.5 \times 0.5 \times 0.02$ cm³ platelets. The thickness of the absorber used was ≤ 0.02 cm which is suitable in the thin absorber approximation (nfc. < 1)



(A) Projection diagram along [010] of isomorphous $\text{Mg}(\text{NH}_4\text{SO}_4)_2 \cdot 6\text{H}_2\text{O}$
 (B) Schematics of absorption of γ -rays.

III. ANALYSTS

For a monochromatic unpolarised source and a single crystal absorber with 1 equivalent sites per unit cell. The final expression for the area ratios of higher velocity (a_3) to lower velocity (a_1) after Zory⁽¹⁾ is

$$\frac{a_3}{a_1} = \frac{\sum_{\text{sites}} \{ [4(\frac{3+\eta}{3})^2]^{k_2} + (3k-1+\eta k') \}}{\sum_{\text{sites}} \{ [4(\frac{3+\eta}{3})^2]^{k_2} - (3k-1+\eta k') \}}$$

$$\begin{aligned} \text{where } K &= \sin^2 \Theta \left[(\cos^2 \phi) Z_a^2 + (\sin^2 \phi) Z_c^2 \right] + (\cos^2 \Theta) Z_b^2 \\ &+ (\sin^2 \Theta \sin 2\phi) Z_a \cdot Z_c + \sin 2\Theta + [(\sin \phi) Z_c Z_b + (\cos \phi) Z_a Z_b] \sin 2\Theta \\ K' &= \sin^2 \Theta (\cos^2 \phi) (X_a^2 - Y_a^2) + (\sin^2 \phi) (X_c^2 - Y_c^2) \\ &+ (\cos^2 \Theta) (X_b^2 - Y_b^2) + (\sin^2 \Theta \sin 2\phi) (X_a X_c - Y_a Y_c) \\ &+ \sin 2\Theta \left[(\cos \phi) (X_a X_b - Y_a Y_b) + (\sin \phi) (X_c X_b - Y_c Y_b) \right] \end{aligned}$$

The symbols X_a , Y_b and Z_c denote the direction cosines \overline{X}_a , \overline{Y}_b and \overline{Z}_c . Calculated and least square fit experimental area ratios in the table I, are on the following specifications of the EFG tensor.

1. OW_9-OW_9 is the direction of \hat{Z} axis of the EFG whereas OW_7-OW_7 and OW_8-OW_8 correspond to \hat{Y} and \hat{X} respectively
2. The higher velocity $(\pm 3/2 \rightarrow \pm 1/2 \text{ transition})$ to lower velocity $(\pm 1/2 \rightarrow \pm 1/2 \text{ transition})$ peak area ratio is

a_3/a_1 and not a_1/a_3 implying thereby that e_q is positive.

3. $\eta = 0.7$



Distances between the water molecules around Fe^{++} and angles between octahedron axes.

TABLE I

Θ	Φ	Experimental 300°K	Calculated $\eta=0.7$
1. 0	0		
2. $\pi/2$	0	1.00	
3. $\pi/2$	$-\pi/4$	1.18	1.00
4. $\pi/2$	$\pi/2$	0.57	1.15
5. $\pi/4$	$\pi/2$	0.90	0.47
6. $\pi/4$	0	0.91	0.83
7. Polycrystalline		0.99	0.94
		0.97	1.07
			1.00

Grant (8) et al. studied the spectrum of $Fe(NH_4SO_4)_2 \cdot 6H_2O$ in an external field of 35 KOs and set the lower limit of $\eta \geq 0.7$. They inferred that the sign of e^2qQ cannot be determined by the magnetic perturbation technique; since η is very large but however pointed out that the data seem to favour a positive sign for e^2qQ . Our single crystal absorption measurements decide that the assignment of positive sign to the quadrupole coupling constant is correct and further confirm that $\eta = 0.7$.

REFERENCES

1. P.Zory, Phys.Rev. 140, A1401 (1965).
2. K.Chandra and S.P.Puri, Phys.Rev. 169 (2), 272 (1968).
3. R.Ingalls, K.Ôno and L.Chandler, Phys. Rev. 172 No.2,295 (1968).
4. J.Danon and L.Iannabrella, J.Chem.Phys. 47, 382 (1967).
5. R.W.Grant, R.M. Houseley and U.Gonser, Phys.Rev. 178 No.2 523 (1969).
6. V.K.Garg and S.P.Puri, J.Chem. Phys. Nov.1970.
7. H.Montgomery, R.V.Chastain, J.J.Natt, A.M.Witkowska and E.C.Lingafelter, Acta.Cryst. 1967, 22 , (775/780).
8. R.W.Grant et al., J.Chem.Phys. 45, 1015-1019 (1966).

THE SECRETARY OF THE ARMY
WASHINGTON, D. C.
JANUARY 1, 1918

TO THE SECRETARY OF THE ARMY
FROM THE SECRETARY OF THE ARMY
SUBJECT: [illegible]

THE SECRETARY OF THE ARMY
WASHINGTON, D. C.
JANUARY 1, 1918

THE SECRETARY OF THE ARMY
WASHINGTON, D. C.
JANUARY 1, 1918

280 320

SEQUENCE IN

There has not been much data on the divalent chlorates of barium, calcium and strontium and hence a systematic study of these has been undertaken by the authors. A preliminary report on the temperature dependence is given and compared with the data on monovalent chlorates.

II. EXPERIMENTAL

A super-regenerative oscillator based on Dean's circuit and described earlier⁽⁵⁾ has been used for detecting the NQR frequencies at different temperatures. Petroleum ether was used as the temperature bath and liquid nitrogen as the coolant. The resonance frequencies were determined using a Marconi Signal Generator Model No. MO02/27 and are accurate upto 8 KHz.

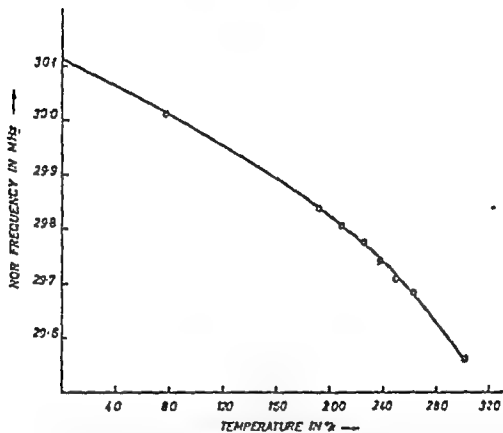
III. RESULTS

The NQR frequencies in barium and calcium chlorates were determined at various temperatures starting from 77°K. The results on calcium chlorate are presented here. Fig. (1) gives the temperature dependence of ³⁵Cl NQR frequency in Ca(ClO₃)₂ · 2H₂O. The rate of change of NQR frequency with temperature has been determined in the case of all the chlorates investigated and are presented in table (1).

Table(1)

Substance	NQR frequency at 77°K in MHz	NQR frequency at 0°K in MHz	$\left(\frac{1}{\nu} \frac{d\nu}{dT}\right) \times 10^{-4}$
NaClO ₃	30.635	30.79	1.13
KClO ₃	28.950	29.25	1.40
Ba(ClO ₃) ₂ · H ₂ O	29.918	30.085	0.74
Ca(ClO ₃) ₂ · 2H ₂ O	30.013	30.115	0.67

FIG. I



TEMPERATURE DEPENDENCE OF CHLORIDE NQR FREQUENCY IN
CALCIUM CHLORATE DIHYDRATE.

From table (i), it can be seen that the temperature coefficient in the case of divalent chlorate is much smaller when compared to that in the monovalent chlorates.

Since the crystal structure data is not available on $\text{Ca}(\text{ClO}_3)_2 \cdot 2\text{H}_2\text{O}$ other methods are being tried to interpret these results on the basis of Bayer-Kushida theory.

The authors are grateful to the Council of Scientific and Industrial Research for the grant of a research scheme. Thanks are also due to Dr. N. Hariham for supplying calcium chlorate from Sweden.

REFERENCES

1. H. Bayer, Z.Physik 130, 227 (1951)
2. T. Kushida, J.Sci.Hiroshima Univ. Ser.A-II 19, 327 (1955)
3. C.V. Ramanathan and J. Sobhanadri, Ind.J.Pure and Appl. Phys. (communicated)

TEMPERATURE DEPENDENCE OF PURE QUADRUPOLE RESONANCE IN SODIUM CHLORATE AND COPPER CHLORATE

M.S. Vijaya and J. Ramakrishna

Department of Physics, Indian Institute of Science,
Bangalore-12, India.

The temperature dependence of chlorine pure quadrupole resonance (PQR) was studied in sodium chlorate and copper chlorate. The PQR in sodium chlorate was reported by Wang¹ at three temperatures viz., 78°K, 273.4°K and 296.8°K. Partlow and Moulton² studied the temperature dependence of PQR in sodium chlorate in the temperature range 4.2-77°K. The resonance frequency in copper chlorate was reported by Bray³ at liquid nitrogen temperature and later by Moshier⁴ at room temperature.

In the present work the temperature dependence of PQR in the two chlorates was studied in the temperature range 90-300°K.

A frequency modulated super-regenerative oscillator working in the range 20-40 MHz was used to observe the resonances and the frequencies were measured with a BC-221 frequency meter using Oscilloscope display. Low boiling petroleum ether was used as the bath liquid and liquid air was the coolant. Temperatures were measured with an iron-constantan thermocouple and frequencies were measured at intervals of 5°C.⁵

According to Bayer's⁶ theory the temperature dependence of PQR frequencies for axially symmetric field gradients is given by

$$\frac{\nu_r}{\nu_0} = 1 - \frac{3h}{8\pi^2 A_A f_A} \frac{1}{e^{h\nu_A/kT_A}} - \frac{3h}{8\pi^2 A_T f_T} \frac{1}{e^{h\nu_T/kT_T}} \dots (1)$$

In the above equation it is assumed
resonance frequency of the stationary

is equal to, ν_0 the resonance frequency at 0°K. f_x and f_y are the torsional frequencies of the molecule about the x and y axes of the field gradient tensor and A_x and A_y are the corresponding moments of inertia.

Kushida⁷ extended Bayer's equation by including all the normal modes of vibration of the molecule in equation (1). But Kushida's theory reduces to the simple Bayer's theory if it is assumed that the main contributions to the temperature dependence of PQR comes only from the torsional frequencies about the principal x and y axes of the field gradient tensor and that these are normal modes of vibration of the molecule.

For metal chlorates the principal z axis of the field gradient tensor is along the 3-fold symmetry axis of the chlorate pyramid and hence the asymmetry parameter $\eta \approx 0$. The principal x and y axes are taken perpendicular to the z axis and passing through the centre of gravity of the chlorate group.

Bayer's equation (1) is expected to hold good exactly for the case of metal-chlorates, because the principal x and y axes of the field gradient tensor defined above, are also the principal axes of moment of inertia of the chlorate group, and hence the torsional motion about these axes would be normal modes of vibration of the molecule. Also it has been shown^{7,8} in the case of sodium chlorate that the contribution to the temperature dependence of PQR from the high frequency vibrations and from the effect of volume expansion are negligible. Therefore the torsional frequencies of chlorates, calculated using Bayer's equation may be expected to be very close to the true values.

The moments of inertia A_x and A_y calculated using the known structural data of the chlorates, are

found to be very nearly equal. This is expected, because of the axial symmetry of the chlorate group. Since λ_x and λ_y are nearly equal it is reasonable to assume that the corresponding torsional frequencies f_x and f_y would also be equal. Assuming that $\lambda_x = \lambda_y = \lambda_t$ (where λ_t is the average of λ_x and λ_y) and $f_x = f_y = f_t$ Bayer's equation takes the form

$$\frac{\gamma_T}{\gamma_0} = 1 - \frac{3h}{4\pi^2 A_t f_t} \frac{1}{e^{Ah/hT} - 1} \quad \dots (2)$$

Using the experimental values of γ_T and γ_0 (obtained by extrapolation of γ_T versus T curve) and the calculated value of λ_t the value of f_t was evaluated at each temperature using equation (2). The calculations were made using an Elliot 807 computer.

RESULTS AND DISCUSSION

The experimental values of γ_T at 297°K (room temperature) and 90°K, and the calculated values of f_t at the two temperature are given in Table 1. It is found that the variation of f_t with temperature is not quite linear for both the chlorates and this observation is not in agreement with Brown's⁹ assumption that f_t varies linearly with T . The calculated value of f_t at room temperature for sodium chlorate compares favourably with that obtained from Raman spectroscopy.¹⁰ Though the low frequency Raman spectroscopy data are not available for copper chlorate it is reasonable to assume that the vibrational frequencies of the chlorate group, would be more or less the same for all chlorates.

TABLE I

Compound	A_t cm ² gm.	τ MHz at $T = 297^\circ\text{K}$	τ MHz at $T = 90^\circ\text{K}$	f_t cm ⁻¹ at $T = 297^\circ\text{K}$	f_t cm ⁻¹ at $T = 90^\circ\text{K}$	Tors. freq. from Raman Spectroscopy at R.T. -1 cm
Sodium chlorate	83.38×10^{-40}	29.920	30.576	115.60	138.80	122.7, 103.0
Copper chlorate	83.38×10^{-40}	29.104	29.980	101.14	128.06	-

REFERENCES

1. T.C.Wang; *Phy. Rev.* 99, 568 (1955).
2. W.D.Partlow and W.G.Moulton; *J. Chem. Phy.* 24, 1114 (1956).
3. P.J.Bray; *J. Chem. Phys.* 23, 702 (1955).
4. R.W.Moshier; *Inorg. Chemistry* 3, 199 (1964).
5. J.Ramakrishna; *Indian J. Pure and Appl. Phys.* 1, 314 (1963).
6. H.Bayer; *Z. Physik* 130, 227 (1951)
7. T.Kushida; *J. Sci. Hiroshima Univ. Ser. A* 19, 327 (1955).
8. T.Kushida, G.B.Benedek and H.Bloembergen; *Phy. Rev.* 104, 1364 (1956).
9. R.J.C.Brown; *J. Chem. Phys.* 32, 116 (1960).
10. C.Shantakumari; *Proc. Ind. Acad. Sci. Sect. A.* 28, 500 (1943).

DISCUSSION

B. Venkataraman

There are too few points on the temperature dependence curves in the low temperature region where the curves are expected to be non-linear. One should be careful in drawing any conclusions from so few experimental points.

J. Ramakrishna

I agree with you. We are collecting data in that region also.

V.S. Tomar

What is the Torsional frequency
of LaClO_3 etc? How does it vary with .

J. Ramakrishna

The torsional frequencies at 90°K and room temperature are indicated in Table I. The variation with temperature is almost linear but not quite linear.

B.D. Nageswara Rao

Brown's assumption is meant for the compound of his interest and was not meant to be any more profound. If you found deviations from linearity in that the quadratic term is present it is a natural extension of the linear variation rather than a flaw in Brown's work.

J. Ramakrishna

I agree with your comment. I only wanted to point out that linear variation of f_t may not hold good at lower temperatures in chlorates. In Benzene compounds we find that linear variation is good enough.

Fe^{57} INTERNAL FIELDS IN NICKEL-MANGANESE ALLOYS

Girish Chandra and T. S. Radhakrishnan
Tata Institute of Fundamental Research, Bombay-5

I. INTRODUCTION

The internal fields at impurity nuclei in several host systems have been measured. In alloys of iron with cobalt, nickel, manganese, vanadium and chromium, the variation of hyperfine field at Fe^{57} nuclei with electron concentration has been reported⁽¹⁾ to be qualitatively similar to that of the saturation magnetic moment of the alloys. Extension of this to several other ferromagnetic host systems leads to a phenomenological expression⁽²⁾,

$$B_{\text{eff}} = \alpha \mu_{\text{local}} + \beta \bar{\mu}$$

where B_{eff} is the field at the impurity nucleus, μ_{local} is the magnetic moment associated with the impurity atom and $\bar{\mu}$ is the average magnetic moment of the host system. The first term is usually identified with the core-polarisation, while the second term covers the conduction electron effects. However, the inadequacy of this expression to explain the observed magnetic fields is borne out by many systems, especially, when the average magnetic moment of the host is small⁽³⁾. Hence the hyperfine field at an impurity nucleus depends on the impurity and host moments in a complex way.

Nickel-manganese alloy system shows very complex magnetic behaviour, depending strongly on states of atomic order and disorder, which can be controlled by heat treatment. The variation of average magnetic moment per atom, $\bar{\mu}$, plotted against Mn concentration is shown in Fig.1 for both the ordered and disordered alloys. Piercy and Morgan⁽⁴⁾ have described the heat treatments which produce various degrees of ordering.

We report here the studies of Fe^{57} internal

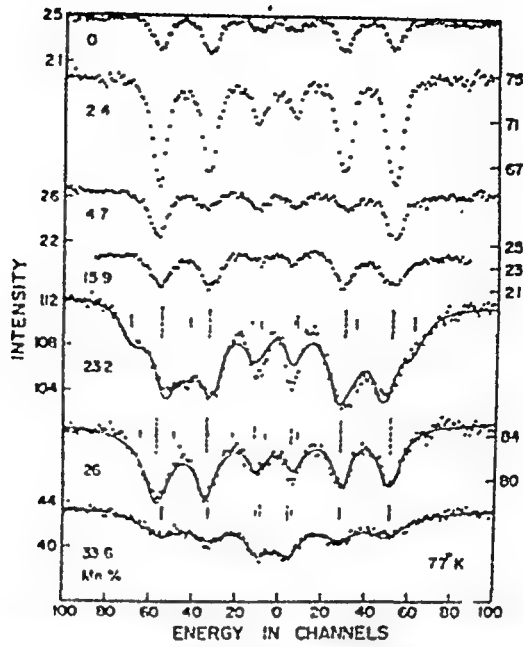


Fig.1. Fe^{57} spectra showing experimentally scanned points. The solid lines are best fits. The vertical lines are the individual absorption components, the heights being proportional to their intensities.

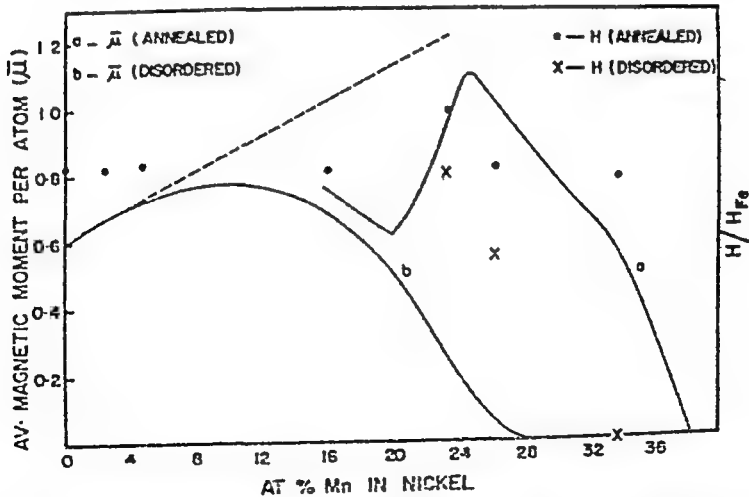


Fig.2. Saturation magnetic moments and Fe^{57} internal fields against Mn concentration. The broken line shows the trend of $\bar{\mu}$, in the absence of Mn-Mn interactions.

annealed and quenched alloys of nickel and manganese, at various compositions.

II. EXPERIMENTAL

Ni-Mn alloys of Mn concentrations 0, 2.4, 4.7, 15.9, 22.5, 24.3, 32.5 at % (as later checked by chemical analysis) were made by induction melting and thin foils were prepared by cold rolling. Co^{57} activity was electroplated on the foils and diffused in vacuum at 900°C . The foils were annealed as described⁽⁴⁾ for maximum ordering. Mössbauer spectra of all samples were obtained at room temperature and at 77°K against a stainless steel absorber enriched with Fe^{57} . A liquid nitrogen cryostat was built for this purpose with Mylar window in which liquid nitrogen could last for about 20 hrs. without the need for continuous pumping.

III. DISCUSSION

Fig.1 shows the spectra obtained at 77°K for all the alloys studied. The ones upto 16 at % Mn, consist of simple magnetic h.f.s., while the other alloys show complex pattern.

In the higher Mn concentration range, comparison of the patterns obtained at room temperature and at 77°K suggests the co-existence of long-range ordered and disordered regions, both the phases being ferromagnetic with different curie temperatures. Kroger⁽⁵⁾ et al have observed such coexistence in Ni_2Mn . On this basis the higher concentration alloys were resolved into spectra characteristic of two sets of hyperfine fields. The good agreement obtained between the computer fitted curve and the experimental points justify such a reasoning. Accordingly the 23.2% alloy consists of two Fe^{57} sites, the field at one site being about 20% higher than the field at the other. That the higher field originates from the Fe^{57} nuclei in the long-range ordered domains was checked later, by quenching the sample

from 850°C. This treatment results in the disordered phase. This produced only a single magnetic h.f.s. corresponding to the lower value.

Fig.2 shows the Fe^{57} internal fields in both the ordered and disordered phases, as a function of alloy composition. The fields are normalised to the field at Fe in metallic iron. The disordered phase of the 26% alloy has a much lower field. The curie point being low for this phase, the saturation value would be very much different than the value at 77°K. The disordered phase of the 33.6% alloy gives just a quadrupole doublet. Further, the line widths are larger in the case of disordered phases by almost 100%. This we believe is because of the Fe^{57} atoms having different near neighbours, each neighbour configuration⁽⁵⁾ having a different curie temperature, so that at any temperature there would be a distribution of internal fields. Further discussion on this is possible only after a detailed study of the line shapes at different temperatures is undertaken.

IV. CONCLUSION

For Fe^{57} , the hyperfine field is in large part independent of the host's magnetic moment in Ni-Mn alloys except for the ordered phase near Ni_3Mn . Considering that the major contribution to the internal fields in such systems is due to core polarisation, the constancy of the field could mean that there is very little change in the atomic configuration of the iron in these alloys. Wertheim⁽³⁾ et al have explained similar results in Ni-Cu alloys the same way.

We thank Prof. B.V. Thosar for his interest in the work.

REFERENCES

1. C.E. Johnson, M.S. Ridout and T.S. Granshaw; Proc.Phys. Soc., 81, 1079 (1963).
2. I.A. Campbell; Proc. Roy. Soc. A 311, 131 (1969).

3. G.L. Wertheim and J.R. Wernick; Phys. Rev. 123, 755 (1961).
4. G.R. Piercy and E.R. Morgan; Canadian J. Physics, 31, 527 (1953).
5. M.J. Marcinkowski and R.M. Poliak; Phil. Mag. 8, 1023 (1963).

DISCUSSION

B. Viswanathan

1) In Ni - Mn alloys you spoke of coexisting ordered and disordered regions, with higher Mn concentrations. Can you elaborate on this?

2) Is there a critical point where such coexistence terminates?

T.S. Radhakrishnan

1) These refer to atomic ordering, the degree of ordering defined by short-range ordering and long-range ordering parameters. The degree of ordering can be controlled by heat treatment. For example if one takes the sample to a high temperature (above a temperature called the ordering temperature) and cools it suddenly, a disordered structure exists. This means that the positions of Ni and Mn atoms in the f.c.c. lattice can be described by a probability distribution. Whereas in the ordered case (Ni_3Mn) obtained by slow annealing, Ni atoms occupy face-centres while the Mn atoms occupy the cube-corners.

2) The co-existence is a function of temperature (heat treatment). There is a temperature, the ordering temperature, above which the long-range ordered phase disappears. These have been extensively described by Marcinkowski and Brown, J. Appl. Phys. P.375 (1961)

from 850°C. This treatment results in the disordered phase. This produced only a single magnetic h.f.s. corresponding to the lower value.

Fig.2 shows the Fe^{57} internal fields in both the ordered and disordered phases, as a function of alloy composition. The fields are normalised to the field at Fe in metallic iron. The disordered phase of the 26% alloy has a much lower field. The curie point being low for this phase, the saturation value would be very much different than the value at 77°K. The disordered phase of the 33.6% alloy gives just a quadrupole doublet. Further, the line widths are larger in the case of disordered phases by almost 100%. This we believe is because of the Fe^{57} atoms having different near neighbours, each neighbour configuration⁽⁵⁾ having a different curie temperature, so that at any temperature there would be a distribution of internal fields. Further discussion on this is possible only after a detailed study of the line shapes at different temperatures is undertaken.

IV. CONCLUSION

For Fe^{57} , the hyperfine field is in large part independent of the host's magnetic moment in Ni-Mn alloys except for the ordered phase near Ni_3Mn . Considering that the major contribution to the internal fields in such systems is due to core polarisation, the constancy of the field could mean that there is very little change in the atomic configuration of the iron in these alloys. Wertheim⁽³⁾ et al have explained similar results in Ni-Cu alloys the same way.

We thank Prof. B.V. Thosar for his interest in the work.

REFERENCES

1. C.E. Johnson, M.S. Ridout and T.E. Cranshaw; Proc.Phys. Soc., 81, 1079 (1963).
2. I.A. Campbell; Proc. Roy. Soc. A 311, 131 (1969).

3. G.K. Wertheim and J.H. Wernick; *Phys. Rev.* **123**, 755 (1961).
4. G.R. Piercy and E.R. Morgan; *Canadian J. Physics*, **31**, 523 (1953).
5. M.J. Marcinkowski and E.N. Polisk; *Phil. Mag.* **8**, 1023 (1963).

DISCUSSION

B. Viswanathan

1) In Ni - Mn alloys you spoke of coexisting ordered and disordered regions, with higher Mn concentrations. Can you elaborate on this?

2) Is there a critical point where such coexistence terminates?

T.S. Radhakrishnan

1) These refer to atomic ordering, the degree of ordering defined by short-range ordering and long-range ordering parameters. The degree of ordering can be controlled by heat treatment. For example if one takes the sample to a high temperature (above a temperature called the ordering temperature) and cools it suddenly, a disordered structure exists. This means that the positions of Ni and Mn atoms in the f.c.c. lattice can be described by a probability distribution. Whereas in the ordered case (Ni_3Mn) obtained by slow annealing, Ni atoms occupy face-centres while the Mn atoms occupy the cube-corners.

2) The co-existence is a function of temperature (heat treatment). There is a temperature, the ordering temperature, above which the long-range ordered phase disappears. These have been extensively described by Marcinkowski and Brown, *J. Appl. Phys.* **P** 5 (19

EMI IN Co^{57} DOPED Mn_5Ge_3

R. Nagarajan, T.S. Radhakrishnan and S.V. Lato
Tata Institute of Fundamental Research, Bombay-5

I. INTRODUCTION

Mn_5Ge_3 is a ferromagnetic intermetallic compound with a Curie temperature of 304°C and has been studied by various techniques. It has a D_{3d} structure having two non-equivalent Mn sites denoted by 6(g) and 4(d) and a 6(g) Germanium site. The N.M.R. and nuclear specific heat experiments⁽¹⁾ revealed a hyperfine fields of 393 kOe at the 6(g) Mn site and 195 kOe at the 4(d) site. They also reported quadrupole interaction at both the sites. They found consistency for these field values in the then unpublished⁽²⁾ neutron diffraction work of Forsyth and Brown which gave magnetic moments as 2.9 B.M. and 1.85 B.M. for the two sites respectively. The earlier neutron diffraction work of Ciszewski⁽³⁾ has given contradicting values of 2 M.B. for the 6(g) Mn site which is reported to be having a higher field of 393 kOe and 3.0 M.B. for the 4(d) site to which Jackson et al. ascribed the lower field of 195 kOe. We report in this paper the Recoil-less Gamma Resonance studies on Co^{57} doped single crystal of Mn_5Ge_3 .

II. EXPERIMENTAL

Co^{57} in the form of neutral CoCl_2 was deposited and dried on a single crystal* of Mn_5Ge_3 . It was a disc of 6 mm. diameter and 1 mm. thickness. The diffusion was done under hydrogen atmosphere at 500°C for about 8 hrs. The Mossbauer spectra were taken at room temperature and at 77°K . Since these did not show a resolved pattern, a further diffusion was done for 3 hrs. at 500°C . Spectra were also taken at 4.2°K , 77°K and at 400°K .

* The single crystals were kindly donated by Dr.

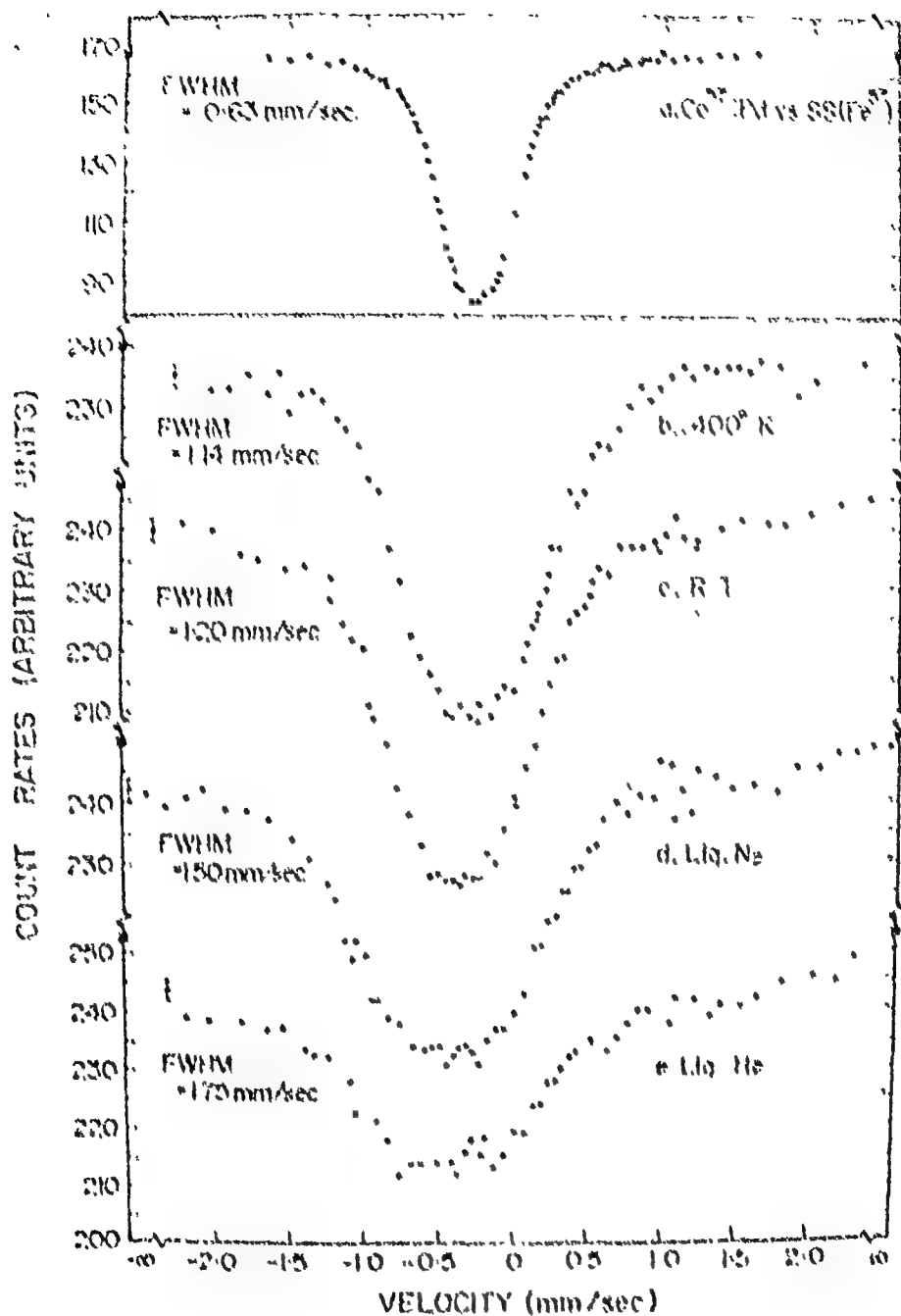


Fig.1. Mössbauer spectra taken from the front side of the crystal at various temperatures.

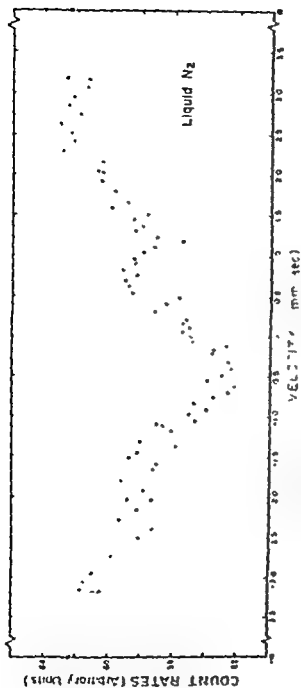


Fig. 2. 165keV gamma-ray spectrum at 77°K from the reverse side of the crystal.

III. RESULTS AND DISCUSSION

Fig.1 shows the spectra obtained at various temperatures from the front side. A standard spectrum is also shown for comparison purposes. The features are:

- 1) Down to liquid helium temperature there is no suggestion of a resolved splitting which is magnetic in nature.
- 2) The line gets broader and broader as the temperature is lowered which can perhaps account for a small hyperfine field at Fe nuclei.
- 3) The spectrum in the paramagnetic region, (at 400°K) has nearly twice the width compared to that of a standard spectrum taken with Co^{57} in palladium matched against a stainless steel absorber.

These are completely surprising in view of the magnetic properties of the solid detailed earlier. It can now be mentioned that the Co^{57} atoms that were doped are expected to occupy the Mn sites on size considerations and also on considerations of electronic configuration. Additional support for this can be derived from the fact that Mossbauer studies⁽⁴⁾ on Fe_5Ge_3 , a similar intermetallic compound, used both as absorber and as source, gave identical results. In view of this situation and also to ensure that the spectra obtained are not characteristic of the undiffused surface activity, spectra were obtained at room temperature and at 77°K (fig.2) from the reverse side of the crystal. In this case, whereas the room temperature spectrum is a single line having a full width of 1.2 mm/sec. the spectrum at 77°K has a broad region with a resolved outer line. On the basis of this line, one can put a rough upper limit of 100 kOe acting at an Fe^{57} site. Apart from this, it is difficult to say anything about the individual contributions from the two sites. As to the difference in the nature of the spectra obtained from the two sides of the crystal, we can only say that the characteristic hyperfine structure at the

first instance has been masked by the contribution from the surface activity still adsorbed to the surface, even though we had given it a mechanical rubbing. For further interpretation, more work is in progress.

We thank Professors B.V. Thosar and C.R. Kanekar and Dr. Girish Chandra for their interest in the work.

REFERENCES

1. K. Kanenatsu; J. Phys. Soc. Japan, 17, 85 (1962).
2. R.F. Jackson, R.G. Scurlock, D.B. Otton and E.L. Bray; Proc. Phys. Soc. 85, 127 (1965).
3. R. Ciszewski; Phys. Stat. Sol. 3, 177 (1963).
4. V.G. Shide and S.K. Date; Solid State Comm. 5, 435 (1967).

DISCUSSION

P.K. Iyengar

Why don't you see resolved hyperfine spectra in the ordered compound Mn_3Ge_3 ?

T.S. Radhakrishnan

Hence the interest. We do see a structure on the basis of which a small field (100 Oe) could be estimated. I can only say that the magnetism of manganese is quite uncertain and point out a parallel instance of FeMnGe where Fe does not see appreciable field in its first ferrimagnetic phase.

THE MAGNETIC SUSCEPTIBILITY AND ELECTRICAL RESISTIVITY OF FeCo_2 NEAR ITS NEEL TEMPERATURE

U.R.K. Rao and J.V. Yakhai

Bhabha Atomic Research Centre, Chemistry Division, Trombay, Bombay 85

1. INTRODUCTION

The intermetallic compound FeCo_2 has a tetragonal⁽¹⁾ structure of the C^{16} type, with the space group $D_{4h}^{22}(\text{I4/mcm})$, with $a = 5.91 \text{ \AA}$ and $c = 4.96 \text{ \AA}$.

Tasukochi et al⁽²⁾ investigated the magnetic properties of FeCo_2 and found it to have a weak paramagnetic ferrimagnetism having its $T_N = 190^\circ\text{K}$. Several workers⁽³⁻⁷⁾ studied this alloy using neutron diffraction technique. The interpretation of the data given by these groups differ in finer detail regarding the magnetic structure of the compound and the temperature of ordering, T_N . Nevertheless, they all agree that FeCo_2 is antiferromagnetic at low temperatures.

Magnetic susceptibility (χ) measurements on FeCo_2 by Airoldi and Fauthenet⁽⁸⁾ revealed the absence of any weak ferromagnetism in the range $2^\circ - 950^\circ\text{K}$ (measurements at intervals of $\sim 20^\circ$), for fields upto 20KO_e . They also did not find any evidence of a peak in χ vs. T curve either, which is indicative of antiferromagnetic ordering. Geist et al⁽⁹⁾ made a more detailed study of FeCo_2 by measuring the χ for stoichiometric, sub- and super-stoichiometric samples. They did not observe any evidence of antiferromagnetism in stoichiometric or Fe-deficient samples (a field of 5KO_e was used). But the Fe-rich alloy showed ferromagnetism, and it is possible that either⁽²⁾ samples may have been contaminated by ferromagnetic impurity, as was argued by Forsyth et al⁽³⁾. Mossbauer studies on FeCo_2 by Forsyth et al⁽⁵⁾ gave $T_N = 267 \pm 2^\circ\text{K}$. Thus although the neutron diffraction studies definitely show antiferromagnetic order, the magnetization studies

do not.

Since magnetic ordering is a second order phase transition⁽¹⁰⁾, one would expect to observe anomalies in non-magnetic properties e.g. electrical resistivity (ρ), sp.heat etc., close to T_N . So we undertook a detailed study of ρ and χ at close intervals of 2°C in the neighborhood of T_N .

II EXPERIMENTAL

FeGe_2 was prepared by melting the constituents in appropriate quantities in an evacuated and sealed quartz tube for several hours and annealing at 950°K for 24 hours. After finely powdering it, the alloy was reannealed in vacuum at 950°K to relieve any mechanical strain that might be introduced in the process of powdering. These thoroughly annealed samples were used for χ measurements. The X-ray pattern of this powder was indexed in terms of the tetragonal cell of the dimensions already mentioned. For measurements of ρ , samples in the form of rods of 6 mm dia. and 10 mm length were prepared and reannealed as above.

Conventional Gouy technique was employed for χ measurements. The rate of heating was $2^\circ\text{C}/\text{hour}$ and measurements taken at intervals of 2°C .

The value of the electrical resistivity for FeGe_2 being as low as about 180×10^{-6} ohm cm., to observe changes in resistivity as a function of temperature at small temperature intervals the conventional potentiometric technique was modified⁽¹¹⁾. In this modification the drop across the sample is matched against the potential drop across a standard 1Ω resistance using a null-detector (I & N, model No.9834). This drop in turn is magnified 1000 times and measured with the help of a microvolt potentiometer (Biddle Guarded Universal

Potentiometer). Similarly, the drop across a reference resistance ($.001\Omega$) is also measured to calculate the current in the sample circuit. The accuracy of measurement of voltage in this way was better than $0.01\mu V$. Effects of thermal e.m.f's were minimised by the usual technique of current reversal. The standard 4-probe D.C. technique was used.

The alloy $FeGe_2$ exhibits metallic behaviour as can be deduced from its value of ρ (about $180\mu\Omega cm$). Fig.1 shows the behaviour of ρ vs. T as the sample is cycled through T_N . There are two faint peaks in ρ vs. T curve. It can be seen that on recycling the peaks shift to lower temperatures.

Fig.2 shows χ vs. T plot wherein one can see a small but perceptible peak. Here also on cycling the peak shifts to lower temperatures. Nonetheless the χ -values increase at lower temperatures. It must be mentioned in these measurements, the errors are larger, since the temperature intervals are smaller. Still the existence of the peak is unambiguous.

III DISCUSSION

The χ vs. T plot shows a faint but perceptible peak characteristic of antiferromagnetic ordering. Possibly the earlier workers missed it since they measured χ at large temperature intervals. The χ vs. T curve rises again below T_N . Since the magnetisation studies involve application of external magnetic fields whereas the neutron diffraction does not, one would be tempted to attribute this paramagnetic behaviour shown by $FeGe_2$ below T_N to the opening up of the spins by the applied fields^(12,13). But one is hesitant to say whether the strength of the fields applied by us (~ 170 Oe) is really sufficient enough to do so.

1111.

The thermoelectric effect is a second order phase transition⁽¹⁰⁾,
in which aspect the observed anomalies in thermoelectric properties e.g.,
longitudinal resistivity (ρ_{xx}), optical etc., close to T_H . It is interesting
to study the effect of ρ_{xx} and ρ_{xy} at some intervals of T in the
neighborhood of T_H .

2.2.2. Sample

Sample was prepared by melting the constituents in appropriate
proportions in an evacuated and sealed quartz tube of a several hours
duration at 1000°C for 24 hours. After slowly cooling it, the
tube was resealed in vacuum at 10^{-6} Torr to remove any incidental
contaminants that might be introduced in the process of pulverizing. These
only analytical samples were used for measurements. The density
of the sample was inferred in terms of the tetrahedral cell of
silicon already mentioned. For measurements of ρ_{xx} , samples in
form of rods of 1 mm dia. and 10 mm length were prepared and
used for studies.

For the study of thermoelectric effect was employed for measurements.
The sample was heated in a furnace and measurements taken at intervals
of 10°C .

The value of the electrical resistivity for FeGe_2 being as
low as about 10^{-3} ohm cm. , to observe changes in resistivity as
a function of temperature at small temperature intervals the conven-
tional potentiometric technique was modified⁽¹¹⁾. In this modification
the drop across the sample is matched against the potential drop
across a standard 10 resistance using a null-detector (L & N, model
No. 9314). This drop in turn is magnified 1000 times and measured
with the help of a microvolt potentiometer (Biddle Guarded Universal

Potentiometer). Similarly, the drop across a reference resistance ($.001\Omega$) is also measured to calculate the current in the sample circuit. The accuracy of measurement of voltage in this way was better than $0.01\mu V$. Effects of thermal emf's were minimised by the usual technique of current reversals. The standard 4-probe D.C. technique was used.

The alloy $FeGa_2$ exhibits metallic behaviour as can be deduced from its value of ρ (about $180\mu\Omega cm$). Fig.1 shows the behaviour of ρ vs. T as the sample is cycled through T_N . There are two faint peaks in ρ vs. T curve. It can be seen that on recycling the peak shift to lower temperatures.

Fig.2 shows χ vs. T plot wherein one can see a small but perceptible peak. Here also on cycling the peak shifts to lower temperatures. Nonetheless the χ -values increase at lower temperatures. It must be mentioned in these measurements, the errors are larger, since the temperature intervals are smaller. Still the existence of the peak is unambiguous.

III DISCUSSION

The χ vs. T plot shows a faint but perceptible peak characteristic of antiferromagnetic ordering. Possibly the earlier workers missed it since they measured χ at large temperature intervals. The χ vs. T curve rises again below T_N . Since the magnetisation studies involve application of external magnetic fields whereas the neutron diffraction does not, one would be tempted to attribute this paramagnetic behaviour shown by $FeGa_2$ below T_N to the opening up of the spins by the applied fields^(12,13). But one is hesitant to say whether the strength of the fields applied by us (~ 110 G) is really sufficient enough to do so.

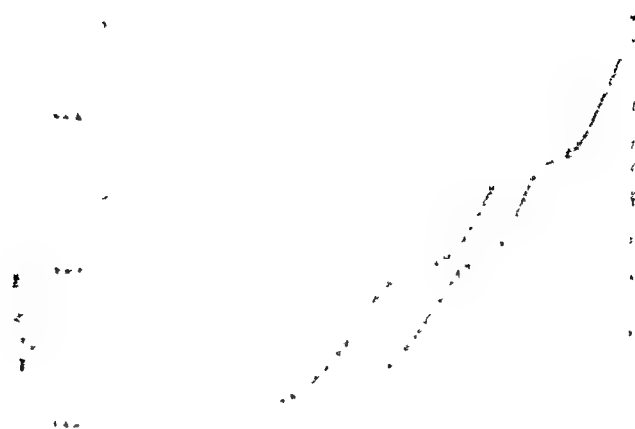


Fig. 1. Dependence of the activation energy E on the temperature T for the reaction of the oxidation of FeO and Fe₂O₃.

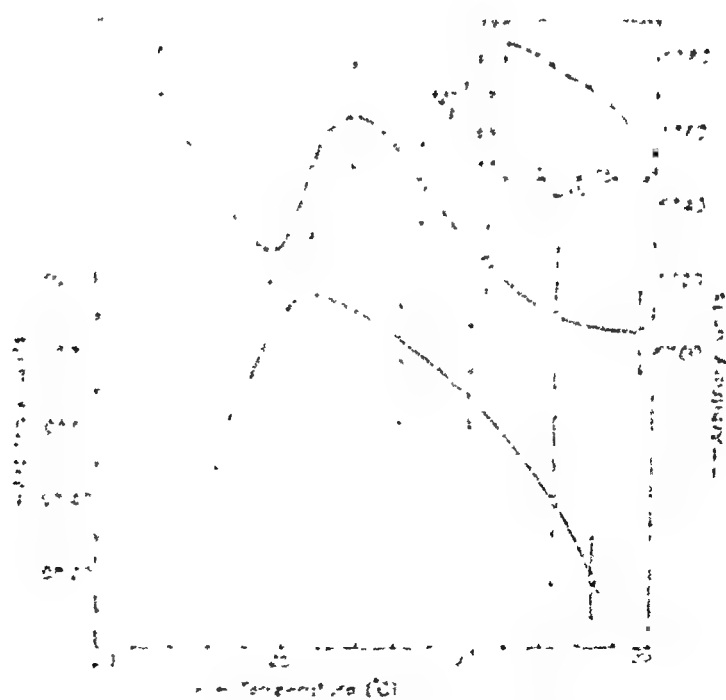


Fig. 2. Conversion degree vs. Temperature of FeO and Fe₂O₃.

In alternate explanation for the presence of a weak peak in the χ vs. T curve is that there is a paramagnetic phase all through over which a weak anti-ferromagnetic phase is superposed. And this paramagnetic phase could come into existence due to the onset of "giant" moments out of FeCo_2/Fe dilute alloy where Fe concentration is too small to be detected by the usual X-ray technique. Also the peaks in P vs. T curve could then be attributed to a Kondo type anomaly and a magnetic anomaly together.

We are grateful to Dr M.D.Karthanavala and Dr C.Monchar of RARC and Dr A.P.B.Sinha of ICL, Poona for helpful discussions and advice. We also record our thanks to the Metallurgy Division, RARC for help in preparing the alloy.

REFERENCES

1. Wallbom H.J; *Z.Metallkunde* 35 (1945) 218.
2. Yasukochi K, Kanematsu K and Ohoyama T; *J.Phys.Soc.Jap.* 16 (1961) 429.
3. Forsyth J.B, Johnson C.E. and Brown P.J; *Phil.Mag.* 10 (1964) 713.
4. Krón Z. and Szabó P; *Physics Letters* 11 (1964) 215
5. Adelson E. and Austin A.E. *J.Phys.Chem.Solids* 26 (1965) 1795
6. Austin A.E. *Technical Review*, Vol.14, No.12, p.13 (1965)
7. Satyamurthy N.S., Begun R.J., Somanathan C.S. and Murthy M.R.L.N. *Solid State Communications* 3 (1965) 113
8. Airoidi G. and Pauthenet R. *C.R.Acad.Sc.Paris* 258 (1964) 3994
9. Geist D., Kunz R., and Ederelt G., *Z.Physik* 191 (1966) 174
10. Belov K.P. *Magnetic Transitions*. Chapter 1. Consultants Bureau, New York, 1961.
11. Rao U.R.K., Yakhai J.V. and Karthanavala M.D; *RARC Report* (In Press).
12. Shapira Y., Foner S. and Oliveira V.P.Jr. *Phys.Letters* 37A (1970) 323.
13. Pickart S.J. and Algerin E.A. *Phil.Mag.* 10 (1965) 32.

NEUTRON DIFFRACTION STUDIES IN SOME TERNARY ALLOYS

K.R.L.N. Murthy, R.J. Begun and N.S. Satya Murthy

Nuclear Physics Division, Bhabha Atomic Research Centre, Trombay,
Bombay-85.

INTRODUCTION

In this paper we report neutron diffraction studies on CoRhSb and CoFeGeHf type structures. It was thought that the question of magnetic ordering mechanism in Heusler alloys would become somewhat clearer if the Cu or Pd sites were substituted by a magnetic atom such as cobalt. However an alloy of composition Co_2RhSb does not seem to form; instead an alloy of the stoichiometric formula CoRhSb can be made.

RESULTS

CoRhSb : A least-square analysis of the neutron diffraction data on CoRhSb at 300°K showed that the observed intensities are in good agreement with a Cl_2 structure with $a_0 = 5.632 \text{ \AA}$; the atoms having the following distributions:

Rh	=	A Site	(000)
Sb	=	C Site	$(\frac{1}{2} \frac{1}{2} \frac{1}{2})$
Co	=	D Site	$(\frac{1}{2} \frac{1}{2} \frac{1}{2})$

However, the intensities are also in good agreement with a L2_1 type of structure in which Rh and Sb occupy the A and C sites respectively while the Co atoms are statistically disordered between B and D sites. Both Kowotny⁽¹⁾ and Castellan⁽²⁾ reported CoRhSb to have the Cl (CaF_2) structure. But none of the possible distributions in this model could account for the observed intensities. The calcula-

ted relative intensities based on various models as well as the observed intensities are shown in Table I.

Table I.

Nuclear Intensities in CoMnSb at 300°K

hkl	Observed intensities	Calculated Intensities			
		L2 ₁	Cl _b	Cl Mn at A	Cl Co at A
111	128.49	130.64	130.64	130.64	130.64
200	0	0.56	0.52	716.06	7.46
220	15.48	15.00	13.95	90.74	198.74
311	100.00	100.00	100.00	100.00	100.00
222	0	0.24	0.22	298.09	3.11
400	< 2	3.53	3.28	21.36	46.79

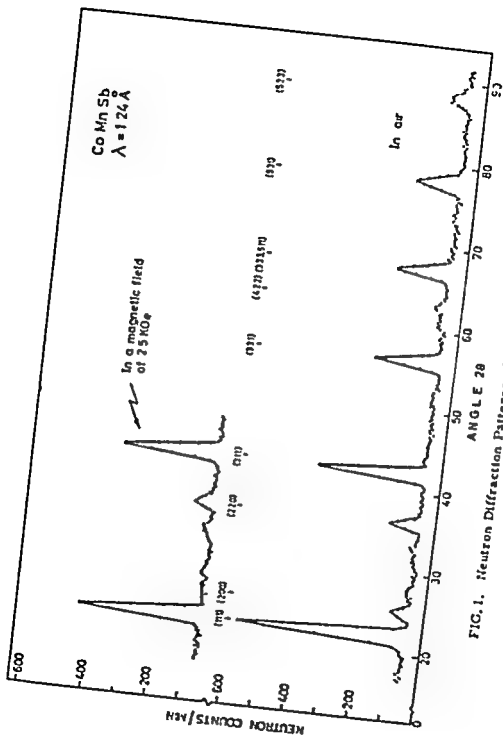
$$\text{Debye-Waller Factor } B = 1.4 \times 10^{-16} \text{ cm}^2$$

Although the CaF₂ structure is ruled out, no choice could be made between Cl_b and L2 structures. Fig.1 illustrates the unpolarised neutron diffraction patterns of CoMnSb taken at 300°K. The upper pattern shows the effect of an external magnetic field of 2.5 KOe, applied parallel to the scattering vector and sufficient to saturate the sample. The magnetic structure of the alloy was determined by a least squares refinement of the observed intensities. The results show that a ferromagnetic coupling exists between Mn and Co atoms with the following moments:

Atom	300°K	85°K
Mn	3.6 ± 0.1 μ _B	4.2 ± 0.1 μ _B
Co	0.5 ± 0.1 μ _B	0.8 ± 0.1 μ _B

The temperature dependence of (III) reflection yielded a value of 430° ± 5°K for T_c.

CoFeGe: A preliminary analysis of the nuclear intensities shows that the alloy has the disordered L2₁ structure. The A and D sites are occupied by Co and Ge atoms respectively while the iron atoms are



statistically disordered between B and C sites. The magnetic intensity analysis reveals a ferrimagnetic alignment between Co and iron atoms.

DISCUSSION

In a Heusler alloy or $L2_1$ structure, there are four lattice sites, namely A(000), $B(\frac{1}{2} \frac{1}{2} \frac{1}{2})$, $C(\frac{1}{2} \frac{1}{2} \frac{1}{2})$ and $D(\frac{3}{2} \frac{3}{2} \frac{3}{2})$. The C1 and $C1_b$ structures result when there is incomplete filling of the above sites. In the C1 or CaF_2 type of structure the Ca atoms occupy the A sites while the F atoms fill the B and D sites. When further ordering between the B and D sites takes place the structure becomes the $C1_b$ type.

It is possible that an alloy like $Co_{1.5}MnSb$ which has the $C1_b$ type of ordering may at higher temperatures go over to $L2_1$ type of ordering because of the jumping of atoms from the A to the C sites. This is plausible energetically, because of the small, if any, difference in energy for occupation of these two sites by the same atom. This will mean a transition to a state of higher symmetry and is thermodynamically reasonable. It is probable that both the structures coexist at 300°K.

The magnetic moment values obtained agree closely with those reported for $Co_2MnSn^{(3)}$ which is a Heusler alloy. This indicates that the nature of interactions are similar in both these alloys.

References:

1. H. Nowotny and B. Glatz, Montash. Chem. 83, 237 (1952).
2. L. Castelliz, Z. Metallkde 46, 198 (1955)
3. T. Shinohara and H. Watanabe, J. Phys. Soc. Japan, 21, 1658 (1966).

THE ATOMIC AND MAGNETIC STRUCTURE OF Co_2TiO_4

R.J. Begum, L. Mahesh Rao and N.J. Satya Murthy.
Nuclear Physics Division, Bhabha Atomic Research Centre,
Trombay, Bombay 85.

I. INTRODUCTION

Co_2TiO_4 was first reported by Romeijn⁽¹⁾ to have the cubic spinel structure. Magnetisation measurements by Sakamoto and Yamaguchi⁽²⁾ revealed some interesting properties. They reported it to be ferrimagnetic below 55°K. On lowering the temperature, they found that the spontaneous magnetic moment increases at first, rises to a maximum of 0.04 μ_B /mole at 45°K and then decreases to zero at 30°K. However, the specific heat measurements of Ogawa and Waki⁽³⁾ showed an anomaly at 49°K which they attributed to a magnetic transition. The present neutron diffraction study was taken up in an attempt to solve the atomic and magnetic structure of Co_2TiO_4 .

II. EXPERIMENT AND RESULTS

Neutron diffraction patterns of the sample were obtained at 300°K, 90°K and 4.2°K. From a least square analysis of the Bragg intensities of the room temperature pattern, the cation distribution and the oxygen parameter were determined. The sample was found to be normal within an accuracy of better than 1%. From the combined data using both γ -rays and neutrons, the lattice constant a_0 was determined to be 8.430 ± 0.003 Å.

Except for thermal effects, no change in the neutron diffraction pattern was observed, as the temperature was lowered from 300°K to 90°K. The pattern at 4.2°K, however, developed new features as shown in Fig. 1. A broad peak at the (111) position and several magnetic satellite peaks appeared. From the temperature dependence of the (111) peak intensity, the Neel temperature was measured to be $48 \pm 2^\circ\text{K}$, which is in good agreement with the value obtained from the specific heat measurement⁽³⁾ but appreciably lower than the earlier estimate of 55°K by Sakamoto and Yamaguchi⁽²⁾.

III. DISCUSSION

Co_2TiO_4 belongs to the group of the so-called "2-4" spinels and its cation distribution can be written as



Sakamoto and Yamaguchi⁽²⁾ tried to explain the low saturation moment on the basis of incomplete quenching of the orbital moments on the A and B sites. They also put forward the possibility of the existence of Yafet-Kittel angles between the moments. However, the magnetic satellite peaks obtained in the present study can be explained only as due to a complicated spiral structure. The resolution of the magnetic satellite lines is not sufficient to solve the magnetic structure of this spinel completely. Nevertheless, from the major qualitative features of the present neutron diffraction pattern, the

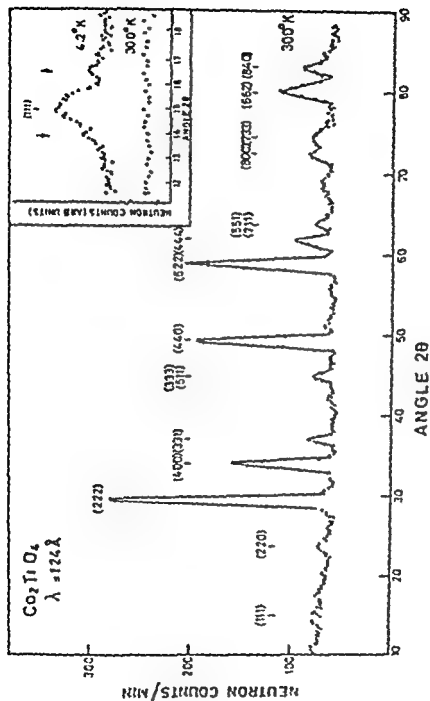


FIG. 1 Neutron diffraction patterns of Co₂TiO₄. The arrows in the inset indicate the positions of the satellite reflections.

following important conclusions can be drawn (1) Both the Neel and Yafet-Kittel type of magnetic ordering can be ruled out (2) The observation of a single pair of magnetic satellite lines together with substantial magnetic contribution to the normal spinel reflections can be explained on the basis of a conical spiral structure. The magnetic moment values indicate orbital contributions to both the A and B sites. The Neel temperature is quite low and it is probable that the spin-orbit energy is comparable with the exchange energy. A competition between these two types of interaction renders the magnetic ordering more complicated than a simple antiferromagnetic alignment of the $\text{Co}^{2+}(\text{A})$ and $\text{Co}^{2+}(\text{B})$ moments.

REFERENCES

1. F.C. Romeijn, Philips Res. Repts. 8, 304 (1953).
2. N. Sakamoto and Y. Yamaguchi J. Phys. Soc. Japan, 17, B-I, 276 (1962).
3. S. Ogawa and S. Waki J. Phys. Soc. Japan 20, 540 (1965).

DISCUSSION

N. P. Sastry

In Co_2TiO_4 , the large value of $3.5 \mu_B$ on Co^{2+} is attributed partly to orbital contribution. Is the sign of λ in $\lambda \underline{L} \cdot \underline{S}$ which tends to align \underline{L} to \underline{S} in agreement with the fact that $3.5 \mu_B$ is greater than $3 \mu_B$?

L. Madhav Rao

λ is negative for Co^{2+} ion (ion with more than half filled d shell) and the effective 'g' factor is greater than 2.

EXCHANGE INTEGRALS IN SOME SPINEL FERRITES

R.J. Begum, L. Mahav Rao, S.K. Paranjpe and
N.S. Satya Murthy

Nuclear Physics Division, Bhabha Atomic Research Centre,
Trombay, Bombay - 85.

I. INTRODUCTION

A knowledge of the exchange integrals operative between the magnetic ions is important to understand its basic magnetic properties. In this paper we report measurements of the relevant exchange integrals in the mixed ferrite system $\text{Mg}_x\text{Mn}_{1-x}\text{Fe}_2\text{O}_4$. We have employed a combination of the paramagnetic neutron scattering data^(1,2) interpreted in the de Gennes formalism and the molecular field analysis of the neutron diffraction data.

II. PRINCIPLE AND EXPERIMENT

Assuming only three exchange interactions J_{AB} , J_{AA} and J_{BB} , and using the fact that the A sub-lattice magnetisation is directed opposite to the net magnetisation, we arrive at the following molecular field expressions:

$$-M_A = M_A(0) B_{SA} \left[\frac{2M_{SA}(0)}{g^2 T} \left\{ -J_{AA} Z_{AA} M_A + J_{AB} Z_{AB} M_B \right\} \right]$$

$$M_B = M_B(0) B_{SB} \left[\frac{2M_{SB}(0)}{g^2 T} \left\{ -J_{AB} Z_{BA} M_A + J_{BB} Z_{BB} M_B \right\} \right]$$

In these expressions, $M_{SA}(0)$ and $M_{SB}(0)$ represent the

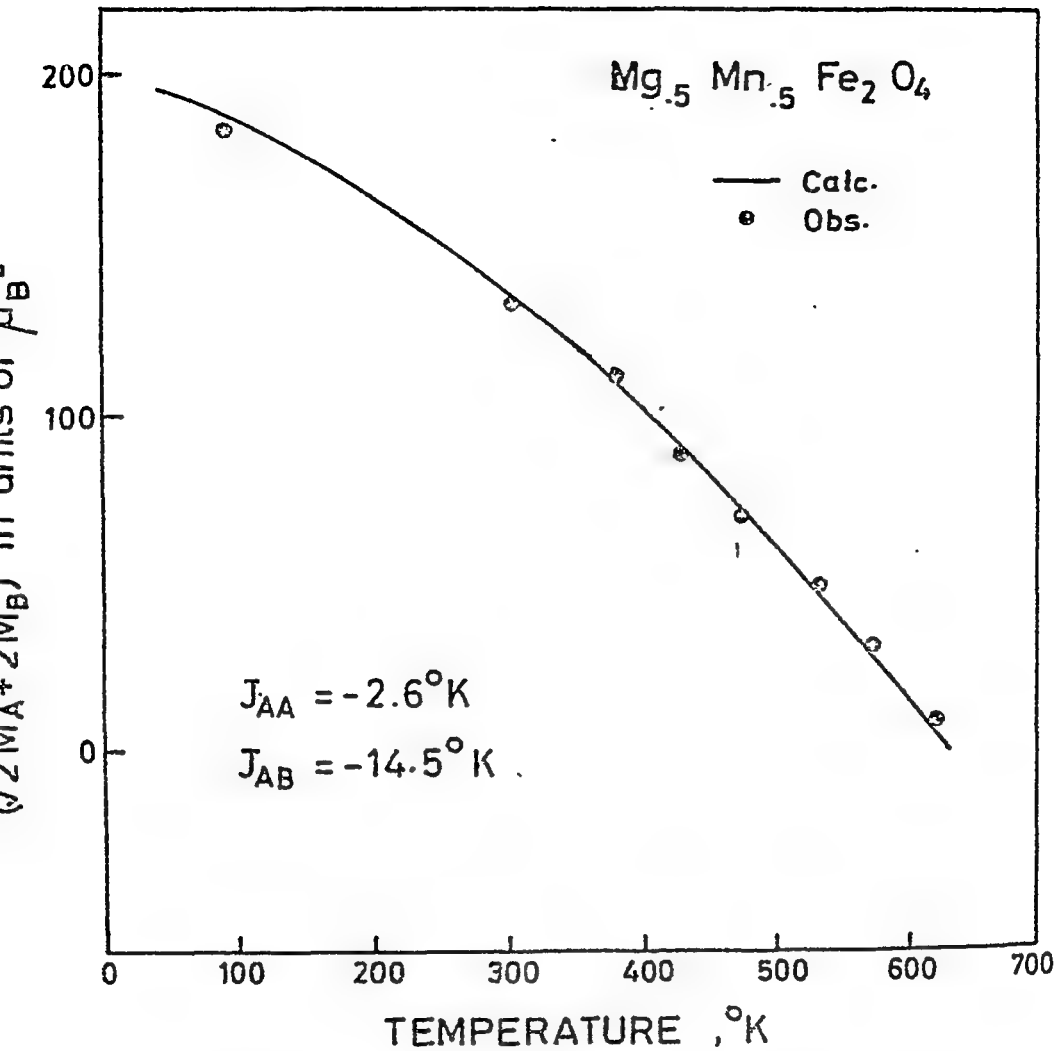


FIG. 1.

The calculated and the observed temperature dependence of the (111) magnetic reflection in $\text{Mg}_{.5}\text{Mn}_{.5}\text{Fe}_2\text{O}_4$. The dots correspond to the observed values while the smooth curve is the theoretically calculated one using $J_{AA} = -2.6^\circ\text{K}$, $J_{AB} = -14.5^\circ\text{K}$ and $J_{BB} = 1^\circ\text{K}$.

are -18.4°K and -12.1°K respectively). The calculated J_{AB} values in the above Table, are based on the present J_{AB} 's obtained from the MgFe_2O_4 and MnFe_2O_4 data. The agreement between the calculated and observed effective J_{AB} 's is seen to be quite good, except in the case of $\text{Mg}_{0.25}\text{Mn}_{0.75}\text{Fe}_2\text{O}_4$. This discrepancy is perhaps due to the neglect of $J_{AB}(\text{Mn}^{2+}-\text{Mn}^{2+})$ in our calculations and which cannot be isolated from our data.

As an example we have shown in Fig.1 the observed and calculated temperature dependence of the (111) magnetic reflection in $\text{Mg}_{0.5}\text{Mn}_{0.5}\text{Fe}_2\text{O}_4$.

(b) ZnCr_2O_4 : Our neutron diffraction study shows this spinel to be completely normal with all the Cr^{3+} ions on the B sites. Thus only $J_{BB}(\text{Cr}^{3+}-\text{Cr}^{3+})$ is operative. The cold neutron time-of-flight technique was employed to measure the neutron spectrum from paramagnetic ZnCr_2O_4 . The data was analysed in the manner outlined previously⁽¹⁾ and the value of $J_{BB}(\text{Cr}^{3+}-\text{Cr}^{3+})$ was determined to be 2.08°K .

REFERENCES

1. N.S. Satya Murthy and L. Madhav Rao, Nuclear Physics and Solid State Physics Symposium, Bombay 1968. Invited Paper, Vol. 1, p. 167.
2. N.S. Satya Murthy, L. Madhav Rao, M.G. Satera and J.I. Youssef, International Conf. on Ferrites, Kyoto, Japan 1970.
3. R.J. Begun Ph.D. Thesis, University of Bombay 1970.
4. G.A. Sawatzky, F. Van Der Louie and A.M. Morrish, Phys. Rev. 187, 747 (1969).

DISCUSSION

H. V. Keer

What is the heat treatment, quenching, annealing etc. given to the $Mg_x Mn_{1-x} Fe_2 O_4$ samples, since the cation distribution is sensitive to such treatment and hence the magnetic behaviour will be accordingly affected? Has any specific heat measurements reported for these compounds?

L. Madhav Rao

The cation distribution in $Mg_x Mn_{1-x} Fe_2 O_4$ samples, used in the present experiment, has been determined by our group using neutron diffraction technique (see paper no. S144, DAE Symposium, Solid State Physics, Roorkee, 1969). The samples were all fired at 1250°C and then furnace cooled.

As far as I know, no specific heat measurements have been reported for the mixed ferrites.

EFFECT OF MICRO STRUCTURE ON KOOSBANER LINE SHAPES IN NICKEL ZINC FERRITE

P. Raj and S.K. Kulshreshtha
Bhabha Atomic Research Centre, Chemistry Division, Trombay, Bombay 85

I. INTRODUCTION

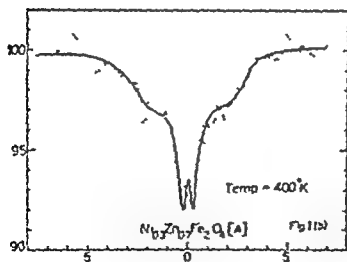
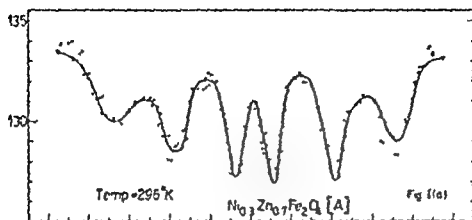
In our recent investigations⁽¹⁾ of relaxation times in nickel zinc ferrite by Mossbauer effect, the observed line shapes were found to be characteristic of relaxation behaviour in a large range of temperature. Well resolved sextets were not observed even at temperatures well below the reported Neel temperatures and spectra characteristic of paramagnetic were obtained. The results were explained on the assumption of collective spin-flipping due to relatively smaller spin flip barrier (IV) of these soft ferrites. The magnetic properties like magnetic anisotropy, susceptibility or permeability, resonance frequency, hysteresis and magnetostriction are intimately related to each other and also depend on the micro-structure. The sample characteristics are quite sensitive to the fabrication parameters such as calcination temperature, grinding (dry or wet) time and sintering time and temperature. Rao Prasad⁽²⁾ has prepared many samples of the same chemical composition i.e. $\text{Ni}_{0.3}\text{Zn}_{0.7}\text{Fe}_2\text{O}_4$ but under varying fabrication conditions. The samples were found to show a great variation in their permeability values from 200 to approximately 2200 due to difference in their micro-structure. As the larger value of permeability implies lower values of anisotropy, the different samples should have different spin flip barrier. The difference in Mossbauer line shapes, if present, in accordance with our earlier work⁽¹⁾ should ascertain our views and with this in mind, we are reporting our Mossbauer studies on two of the representative samples.

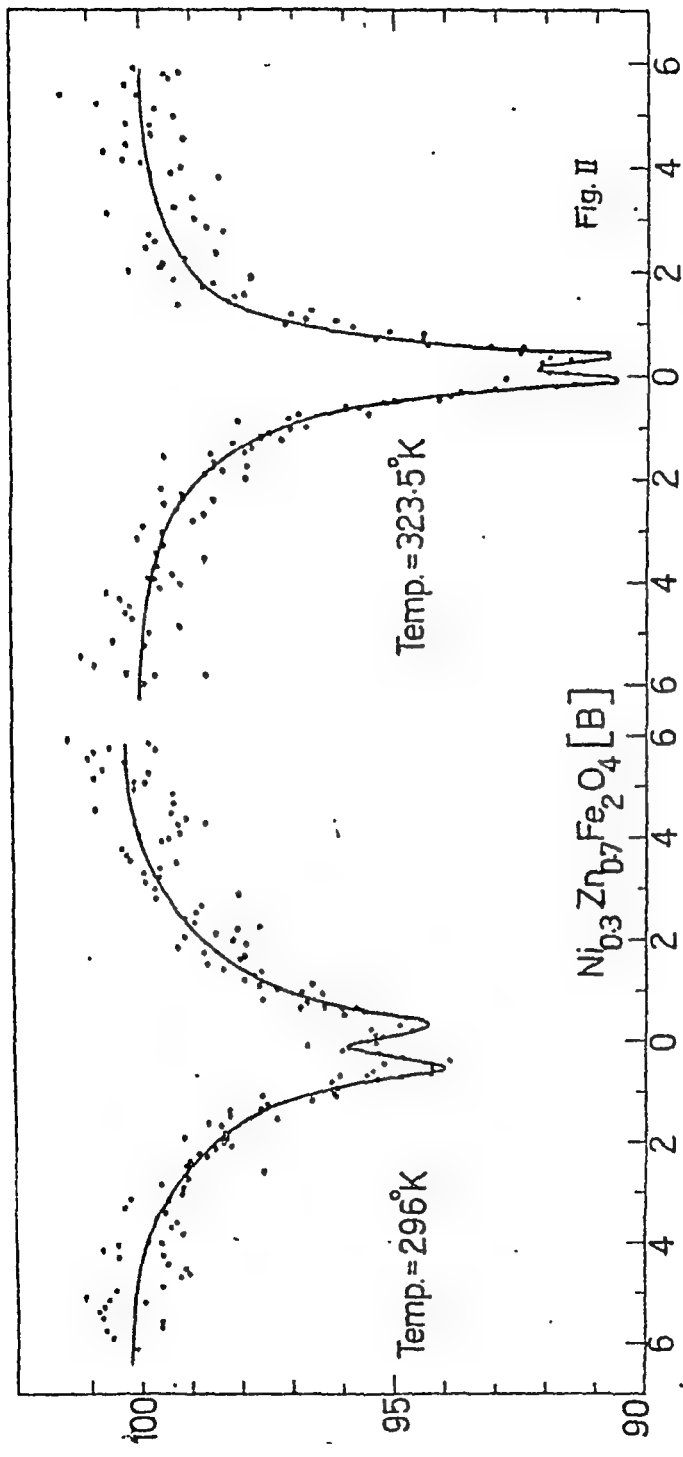
II. EXPERIMENTAL

The method of preparation of the samples has already been reported⁽²⁾ and employs the usual ceramic techniques. Starting with oxides both the samples were double calcined at 1200°C for 2 hours with interpaced wet grinding for 24 hours in a steel ball mill. After second calcination the sample [A] was sintered at 1200°C for 2 hours and was resintered for another 8 hours at the same temperature. For sample [B] the double calcined powder was ground for 200 hours and sintered at 1500°C for 2 hours. Mossbauer spectra of these samples have been taken at various temperatures using a mechanical Cam drive and a proportional counter. Source used was Co^{57} in Pd matrix and the absorbers contained approximately $0.5 \text{ mg Fe}^{57}/\text{cm}^2$. The control of sample temperature was better than $\pm 1^{\circ}\text{C}$.

III. RESULTS AND DISCUSSION

Fig.I(a) and (b) are the Mossbauer spectra of sample [A] and Fig.II shows the M.S. for the sample [B] at temperatures given on the graphs. The value of the initial permeability for the two samples [A] and [B] are 360 and 2000 respectively at frequency of 1 KC/sec. The micrographs⁽²⁾ of the two samples show a definite difference in their grain size, shapes and distribution. The sample [B] which is sintered at a higher temperature has larger grains and shows larger permeability value due to easier wall displacements. For a high value of permeability it is essential to have a combination of high K_s value with low K_f and λ values. The two factors which determine the anisotropy are (i) Crystal structure and (ii) Kind of magnetic ions. The anisotropy is built up from the single ion contribution and because the contribution of both signs have been





in nickel zinc ferrite system is due to this type of compensation and that is why the system forms a back-bone of soft ferrites which are characterized by a narrow S-shaped hysteresis curve.

The salient features of the observed M.S. are the following:

(i) At a given temperature, the Mossbauer line shapes for two samples are different and they show paramagnetic doublets at different temperatures. Vanishing of h.f.s. below the reported T_N shows that T/T_N is not a determining parameter.

(ii) As the temperature is increased, the ratio S_{16}/S_{54} also increases beyond 6.35. In a range of temperature, whereas the line widths of the outermost pair increase with increase in temperature, the innermost lines become narrow and increase in intensity. These features cannot be explained by assuming a static hyperfine field at the nucleus.

(iii) While passing from the magnetically ordered state to the paramagnetic state no asymmetric L.S. is observed which is expected on the basis of relaxation formalism⁽⁵⁾.

In order to explain similar observations⁽¹⁾ it was necessary to assume the super paramagnetic behaviour, where flipping time τ_c is given by

$$\tau_c = \tau_0 \exp \left(\frac{KV}{RT} \right)$$

Where K is the anisotropy per unit volume and V is the effective volume and KV determines the spin flip barrier. Since the value of KV at any temperature is different for the two samples, different line shapes are observed. $\Omega \cdot \frac{1}{\tau_c}$ determines the rate of magnetization reversal and therefore gives the rate at which the hyperfine field at the nucleus is fluctuating regardless of the value of magnetisation. (η). Under these conditions the Mossbauer line separation does not follow magnetisation and only KV determines the line shapes. In order

to fit relaxation times to the experimentally observed $M_S^{(1)}$ it was found necessary to change δ also in addition to Ω . Decreasing value of δ required to fit the line positions alone, at higher temperatures, explains why asymmetric O.S. is not observed when passing from the magnetically ordered state to the paramagnetic state which is a general observation.

We are thankful to Dr P.G.Khubchandani for valuable discussions, to Mr Ram Prasad for supplying the samples and to Mr B.R. Vyas for micrographs.

REFERENCES

- (1) P. Raj and S.K. Kulshreshtha., Phys. Stat.Sol.(To be published)
- (2) Ram Prasad and V.K. Moorthy., BARC report 477 (1970)
- (3) M. Blume "Hyperfine Interaction and Nuclear Radiation"
(North Holland Publishing Company Amsterdam 1968)

SPIN RELAXATION OF Fe^{3+} ION IN FERRITES USING MÖSSBAUER EFFECT

P.K. Tyengar and H.C. Rangan
Nuclear Physics Division
Bhabha Atomic Research Centre,
Trombay, Bombay - 85.

INTRODUCTION

Mössbauer Effect has been used to study the hyperfine interactions in Solids. A necessary condition to observe the hyperfine structure being that the ionic spin fluctuations should be either very fast or very slow compared to nuclear precession frequency. In case these two are comparable in magnitude, the shape of Mössbauer spectrum is very sensitive to these fluctuation rates, and is characterised by intense central lines compared to broadened outer lines.

In this paper results of Mössbauer measurements on Fe^{3+} in $\text{Co}_{1-x}\text{Zn}_x\text{Fe}_2\text{O}_4$, for $x = 0.5$ and 0.7 , are described which show these features clearly at temperature below their respective Neel temperatures.

The shape of the spectra are related to the dynamical properties of the ionic spin system using stochastic model for spin fluctuations in which the nature of spin flip is assumed to be stationary Markoff process⁽¹⁻³⁾.

CALCULATION OF RELAXATION SPECTRA for $\text{Co}_{0.5}\text{Zn}_{0.5}\text{Fe}_2\text{O}_4$.

The spectra at 90°K and 455°K show that the magnitude of quadrupole interaction is small and is ignored in the following calculations. The molecular field at the ion removes the six fold degeneracy of the 3-state. The relaxation causes the ionic spin to change its orientation with respect to the molecular field

and thereby changing the magnitude of the internal field at the nucleus. The shape in presence of these fluctuations is given by

$$P(\omega) = \sum_{m^*m} \frac{2}{T} p_{m^*m} \operatorname{Re} \left\{ \tilde{W} \cdot \tilde{A}^{-1} \cdot 1 \right\}$$

where $\tilde{1}$ is unit matrix, p_{m^*m} describes probability of transition from nuclear excited state m^* to ground state m , \tilde{W} is the row vector $\{\delta^5, \delta^4, \delta^3, \delta^2, \delta, 1\}$

where $\delta = \exp\left(-\frac{2\beta H a}{kT}\right)$

and \tilde{A} is (6 x 6) matrix depending on Ω_e, δ, T and δ

where

$$\Omega_e = \frac{1}{7(1+\delta)\tau_s}$$

and

$$\delta = \frac{A^* m^* - A m}{2h}$$

All parameters, except δ , δ and Ω_e were determined from spectrum at 90°K. Comparison of theoretical spectra with experimental data gave values of parameters described in Table 1.

DISCUSSION

For ions in S-state, the spin-spin relaxation is expected to be the dominant mode of relaxation. The Hamiltonian involved in spin-spin relaxation is temperature independent but the actual transition rates depends on temperature due to its dependence on δ also⁴.

From the table it is seen that relaxation time is not strongly dependant on temperature. However, a weak dependence on temperature cannot be ruled out due to the small amount of uncertainty in the values of the derived parameters.

TABLE - I

TEMPERATURE (°K)	β	Relaxation time ($\times 10^{-7}$ Sec.)	($\times 10^7$)
455	1	—	—
433	1	—	0.4581
413	1	—	0.9
387	0.93	3.7 to 7.4	1.113
367	0.77	4.0	1.24
359	0.65	1.2	1.2743
340	0.585	9	1.275
313	0.484	2	1.396
292	0.44	1	1.482
222	0.293	1	1.61
190	0.222	2.33	1.66
90	0.033	—	1.89

Spin-spin relaxation, unlike spin-lattice relaxation, is however concentration dependent. So the concentration of Zn^{2+} ions was changed. The spectra for $\text{Co}_{0.3}\text{Zn}_{0.7}\text{Fe}_2\text{O}_4$ indicate qualitatively a change in relaxation time with concentration. These spectra are being analysed to establish the mode of relaxation with certainty.

REFERENCES

1. Blume, M., Phys. Rev. Letters 18, 305 (1967)
2. Wickham H.H., and Nowik, I., Phys. Rev. 142, 113 (1966)
3. Van der Woude, F., and Dekker, A.J. Phys. Status Solidi 9, 775 (1965)
4. Boyle, A.J.P., and Gabriel, J.R., Phys. Letters 19, 471 (1966).

MAGNETIC ANISOTROPY IN $(1-x)\text{Fe}_2\text{O}_3 - x\text{Al}_2\text{O}_3$ SYSTEM

J.K. Srivastava and R.P. Sharma
Tata Institute of Fundamental Research, Bombay-5

It is known that some of the anti-ferromagnetic systems such as $\alpha\text{-Fe}_2\text{O}_3$, MnCO_3 etc exhibit extremely small spontaneous magnetization above a certain temperature known as phase transition temperature. In $\alpha\text{-Fe}_2\text{O}_3$ below this transition temperature, $T_M = 260^\circ\text{K}$, the Fe^{3+} ion spins point along the trigonal $\langle 111 \rangle$ direction, while above this temperature within the range $260^\circ < T < 956^\circ\text{K}$ these spins flip over to the basal plane.⁽¹⁾ Oyaloshinaki⁽²⁾ has shown that the observed weak ferromagnetism in the later temperature range is due to a slight canting of the sublattice magnetizations, while the Morin phase transition as such is due to a sign change in the phenomenological C-axis anisotropy.⁽⁵⁾ In the present work Mössbauer measurements have been carried out to study the effect of magnetic dilution on this spin transition temperature. The $\alpha\text{-Fe}_2\text{O}_3$ lattice has been magnetically diluted by introducing different concentrations of diamagnetic $\alpha\text{-Al}_2\text{O}_3$.

The samples of $(1-x)\text{Fe}_2\text{O}_3 - x\text{Al}_2\text{O}_3$ were first made in the form of a tablet under high pressure of ~ 1 ton and then fired at 1100°C for a period of 12 hours. The tablet was then crushed and the powder was used as an absorber in the study of Mössbauer spectra at different temperatures. The x-ray analysis using Nb K_α line confirmed that both the constituents of the solid solution were in the α -form.

Typical Mössbauer spectra for the $x = 1.96\%$ at three different temperatures are shown in Fig.1. At 25°K the spacing between the first two lines $\Delta_{1,2}$ is less than the spacing between the last two lines $\Delta_{5,6}$. As the temperature is increased the

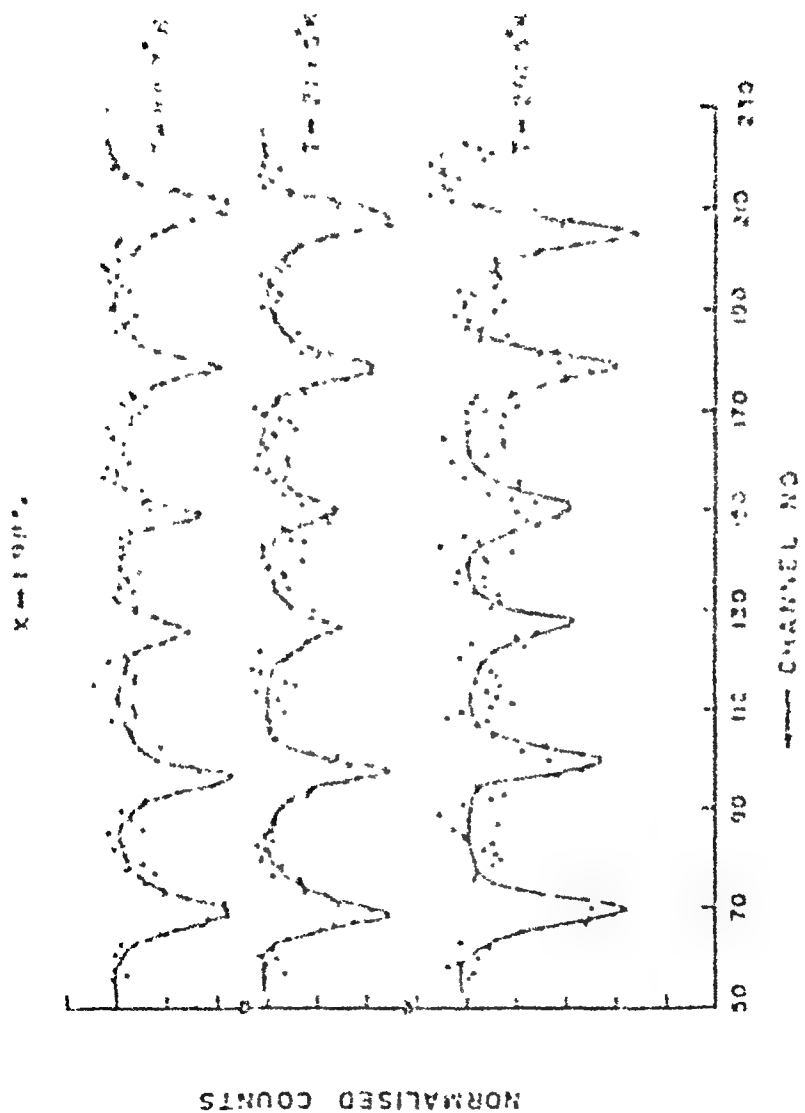


Fig.1

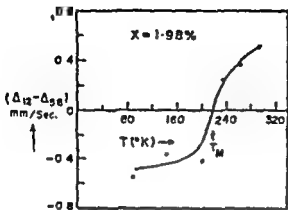


Fig. 2

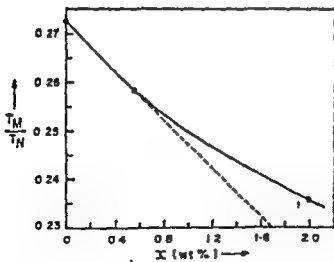


Fig. 3

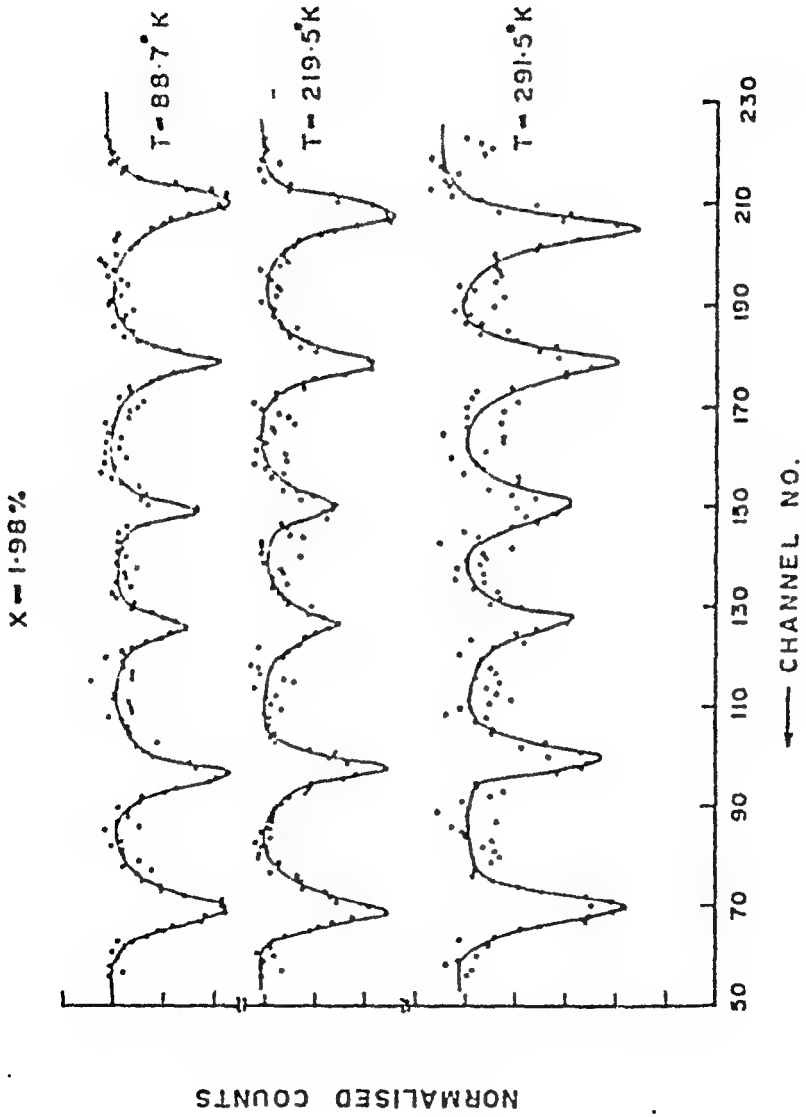


Fig. 1

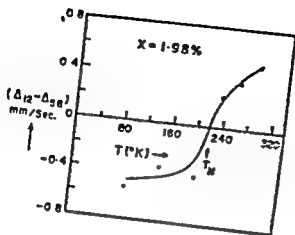


Fig. 2

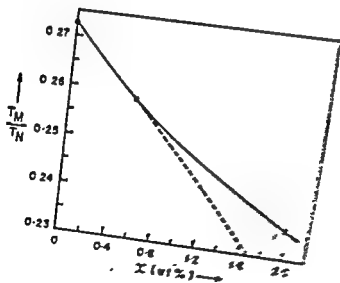


Fig. 3

difference $|\Delta_{1,2} - \Delta_{5,6}|$ decreases and finally changes sign. The variation of $(\Delta_{1,2} - \Delta_{5,6})$ at different temperatures is shown in Fig.2. It is evident from this figure that as the temperature is increased the value of θ , i.e. the angle between the c -axis and the spin direction, changes continuously from 0 to 90° , indicating that there is a spread in the Morin phase transition. A similar measurement was carried out for $x = 0.56\%$, 10% and 20% .

The Néel temperature for all the concentrations was determined in the usual way by the stationary absorber technique. The variation of Néel temperature T_N with concentration has been found to follow a linear trend.

RESULTS

The results are shown in table 1. Their analysis has shown that the variation of T_M with concentration is not linear which is contradictory to the earlier results⁽³⁾ obtained from the remanent magnetization measurements. Actually the value T_M for 10 and 20% concentration is much lower (below 90°K) than that given in earlier measurement⁽³⁾. It may be mentioned here that a temperature hysteresis in the Morin phase transition was found for all the concentrations, similar to what has been reported in the case of $\alpha\text{-Fe}_2\text{O}_3$ ⁽¹⁾.

Table 1

Sr. No.	x (wt. %)	$T_M(^{\circ}\text{K})$	$T_N(^{\circ}\text{K})$	T_M/T_N
1	0.0	260	954	0.2725
2	0.56	244.5	947	0.2582
3	1.98	220	933	0.2358
4	10.17	$< 90^\circ\text{K}$	866	-
5	20	$< 90^\circ\text{K}$	-	-

The T_M/T_N vs x plot is shown in Fig.3. Here again the trend is not linear and it is opposite to what has been predicted by the anisotropy theory^(4,5). Also it is difficult to understand the spread in the spin transition temperature.

REFERENCES

1. F. Vander Woude; Phys. Stat. Solidi 17, 417 (1966).
2. I. Dzyaloshinski; J. Phys. Chem. Solides 4, 241 (1958).
3. G. Haigh; Phil. Mag. 2, 505 (1957).
4. J.O. Artman, J.C. Murphy and S. Foner; J. Appl. Phys. 36, 986 (1965).
5. J.O. Artman, J.C. Murphy and S. Foner; Phys. Rev. 138, A912 (1965).

DISCUSSION

H.V. Keer

Can you comment on the fact that T_N varies linearly with composition. Most of the theories predict a non-linear dependence.

J.E. Srivastava

In the Ising model calculations^(1,2) the variation of T_N with concentration, x , is linear upto about $x \sim 70\%$, where x is the concentration of the diamagnetic atoms in the magnetic lattice. In the range $70\% \leq x \leq 100\%$, the variation is non-linear although this range can be exactly calculated only if the number of interacting nearest neighbours, Z is known. In the framework of Heisenberg model calculations⁽²⁾, T_N vs. x is linear upto $x \sim 70\%$ if $Z = 12$ or upto $x \sim 55\%$ if $Z = 8$.

However, in any case, T_K vs. x is always linear in the composition range in which we have presented the experimental results viz. $0 \leq x \leq 2\%$. Thus there is an agreement between the theory and experiment.

1. H. Sato, A. Inoue and T. Shimizu; J. Phys. Chem. Solids 10, 19 (1959).
2. T. Ogiuchi and T. Ohtake; J. Phys. Soc. Japan 27, 1111 (1959).

CRYSTAL FIELD EFFECTS ON TIME DEPENDENT HYPERFINE INTERACTIONS

J.L. Srivastava

Tata Institute of Fundamental Research, Bombay-5

I. INTRODUCTION

Time dependent hyperfine interactions have recently been observed in Mössbauer spectra of some Fe^{2+} compounds⁽¹⁻⁴⁾ and also in the time-integral perturbed angular correlation studies of the rare-earth ions implanted into copper lattices⁽⁵⁾. In the former case, the experimentally observed line-shapes are compared with the theories of Blume et al⁽⁶⁾ and Vander Woude et al⁽⁷⁾. This comparison has shown unusually large values of relaxation time for Fe^{2+} ions in some paramagnetic systems⁽³⁾. In the case of PAC studies⁽⁵⁾, relaxation time is deduced by comparing the experimentally observed values of G_2/G_4 with the calculated ones using Blume's theory⁽⁸⁾. A poor agreement between the theory and the experiment is found, particularly in the case of ^{152}Gd , ^{174}Yb and ^{166}Er ⁽⁵⁾. In the present work, crystal field and ionic spin-orbit interactions have been taken into account while calculating Mössbauer line shapes and the values of G_2/G_4 . It shows a large effect of these interactions on G_2/G_4 . Also it is found that the relaxation times obtained for paramagnetic Fe^{2+} compounds⁽³⁾ are not very large if these interactions are taken into account.

II. THEORY AND CALCULATIONS

In presence of relaxing electronic spins, the Hamiltonian describing the electron-nuclear hyperfine interaction can be written as^(6,8),

$$H(t) = H_0 + 2\beta_n I_z f(t) \quad \text{----- (1)}$$

Since the above mentioned theories⁽⁶⁻⁸⁾ assume an ionic spin $S = \frac{1}{2}$, they discuss a 2-level relaxation process in which the ionic spin fluctuates between two levels $m_s = +\frac{1}{2}$ and $m_s = -\frac{1}{2}$.

the crystal field and spin-orbit interactions into account, the ion Hamiltonian is

$$H = H_0 + H_{CF} + H_{LS} + H_{ex}. \quad \text{----- (2)}$$

Now the energy level diagram of a Fe^{2+} ion or a rare earth ion is complex. The exact number of levels involved in the relaxation process depends both on the crystal symmetry and on the relative magnitudes of the different terms in eq. (2). Assuming $H_{CF} > H_{LS} > H_{ex}$ and taking the cubic crystal field to be larger than the axial or rhombic field, the number of levels involved in the relaxation process in Fe^{2+} systems⁽¹⁻⁴⁾ is given in Table 1. Both the above assumptions are satisfied in all the experimental cases⁽¹⁻⁴⁾. In the case of rare-earth ions in copper⁽⁵⁾, the ionic ground state is either a triplet or a singlet i.e. $n = 3$ or 1. In the singlet case, relaxation is possible only if the ground state mixes with the higher J-multiplets.

Table 1

Crystal symmetry	Experimental case	Number of levels involved (n)
1. Cubic Octa.	$KFeF_3$ at $110^\circ K$ ⁽¹⁾	3
2. Cubic Octa.+axial		
(i) Singlet is ground state	-	5
(ii) Doublet is ground state	(a) $Fe^{2+} : CoCO_3$ at $27^\circ K$ ⁽²⁾ (b) $FeCO_3$ ⁽⁴⁾	2
3. Cubic Octa.+Rhombic	$(Fe_xMg_{1-x})SiO_3$ at $4^\circ K$ ⁽³⁾	5

Thus we see that a 2-level relaxation process is a correct description of the relaxation process only in some cases, but not always.

We now consider a general n-level relaxation process by extending the previously existing theories⁽⁶⁻⁸⁾ on the basis of Kubo-Anderson model. In the Mössbauer case the expression for the line-shape,

within a multiplicative constant, is given by

$$I(\omega) = -\text{Re} \sum_{m, m'} \langle \chi_m | \chi_{m'}^{(0)} | \chi^* m'' \rangle \{ \vec{W} \cdot \vec{A}^1 \cdot \vec{I} \} \quad \text{----- (3)}$$

Assuming a Boltzmann distribution for the ionic spins over different

m states, \vec{W} is given by: $\vec{W} = [\beta^{n-1}, \beta^{n-2}, \dots, \beta^2, \beta, 1]$,

where $s = \exp(-\Delta/kT)$, Δ being the energy separation between any two successive spin states. $\vec{1}$ denotes a n -dimensional column vector and the matrix \vec{A} is given by:

$$\vec{A} = \omega (\vec{\omega} - \omega \vec{E}) + \vec{\Gamma} \quad \text{--- (4)}$$

\vec{E} is a n -dimensional unit matrix and ω is the emission or absorption frequency of a particular nuclear transition, $|i^*, m^* \rangle \leftrightarrow |i, m \rangle$

$\vec{\omega}$ is a diagonal matrix, whose elements are the values assumed by $\omega(t)$ when $f(t)$ takes on different values. $\vec{\Gamma}$ is the matrix of transition probabilities. In presence of an axially symmetric ZFG parallel to the fluctuating field, $\omega \vec{E}$ in (4) should be replaced by $[\omega - P(3m^2 - 1/2)] \vec{E}$. We consider such a case here.

In the PaG studies, the effect of time dependent perturbation is given by the attenuation factor⁽⁶⁾:

$$G_{kk}(t) = \frac{1}{2k+1} \sum_{n=-k}^{+k} \bar{a}_n e^{-\gamma_{1/2} \beta_n \tau_n \int_0^t f(t') dt'}$$

where the bar indicates the stochastic average. Assuming $f(t)$ to be a stationary Markoff function,

$$G_{kk}(t) = \frac{1}{2k+1} \cdot \sum_{n=-k}^{+k} \vec{W}_n \cdot \exp(\vec{B} t) \cdot \vec{1},$$

where $\vec{B} = \omega \vec{F} + \vec{\Gamma}$; $\omega = \gamma_{1/2} \beta_n \tau_n$ and \vec{F} is a diagonal matrix whose elements are the possible values of $f(t)$. The total time-integrated attenuation factor is:

$$\begin{aligned} \overline{G_{kk}(\infty)} &= \frac{1}{\tau_n} \int_0^\infty dt e^{-t/\tau_n} G_{kk}(t) \\ &= -\frac{1}{(2k+1)\tau_n} \text{Re} \sum_{n=-k}^{+k} \{ \vec{W}_n \cdot \vec{A}^{-1} \cdot \vec{1} \}, \end{aligned}$$

where τ_n = Nuclear lifetime and $\vec{A} = \vec{B} - 1/\tau_n$.

III. RESULTS AND DISCUSSION

Mossbauer line shape calculations done for $n = 2, 3, 5, 6$ and 9 show an exponential decrease in relaxation-time with an increase in n . This is shown in Fig.1 where I_1/I_2 is the amplitude-ratio of the two peaks in the asymmetric quadrupole doublet. τ_n is the relaxation time

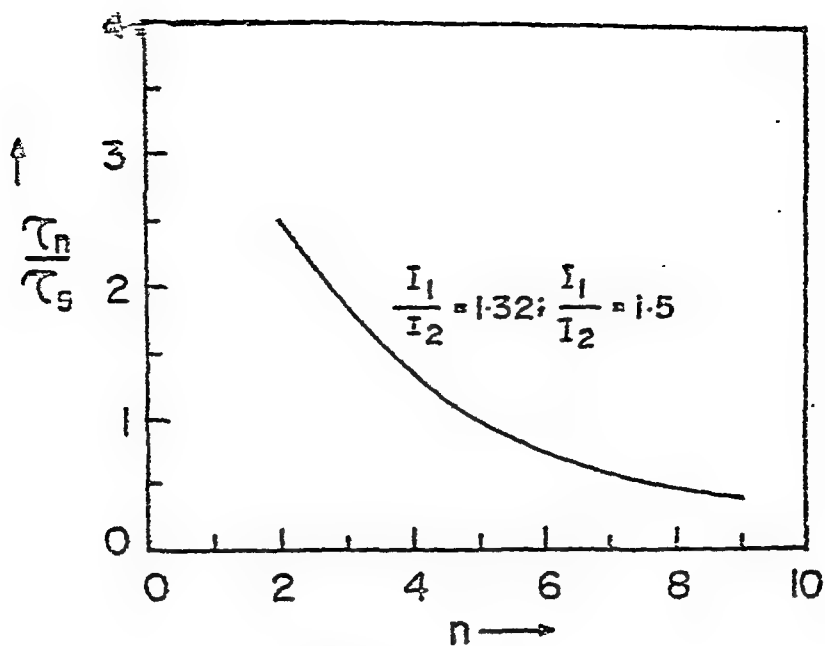


Fig. 1

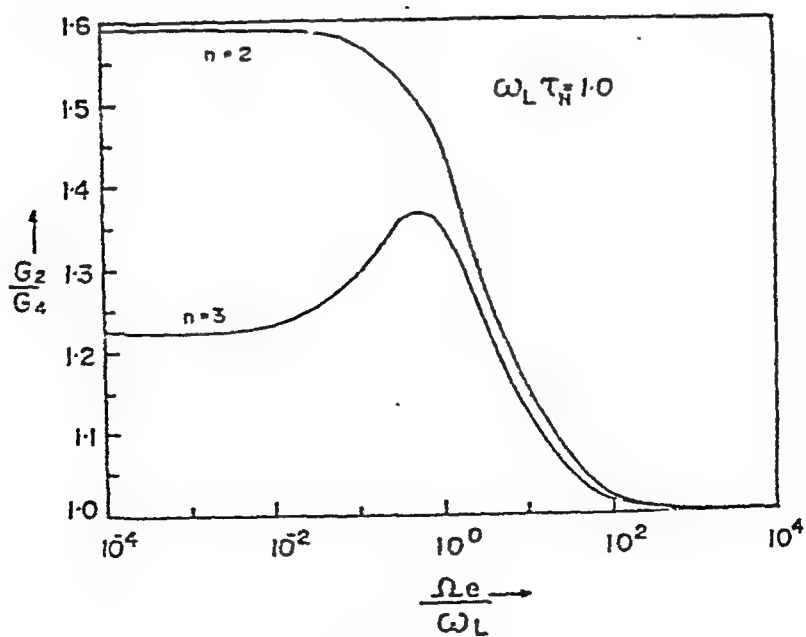


Fig. 2

obtained for a particular shape when n levels are assumed to take part in the relaxation process. The τ_1/τ_2 vs. n curve has been found to be independent of the value of I_1/I_2 . Calculations done for $P = 3.7\%$, 4.5% and 5.0% (where Γ = level width of the excited nuclear state) and for $H_{eff} = 130, 150$ and 200 KG show that this curve is independent of the value of P and H_{eff} . Hence it can be used as a standard curve in all the cases. To now explain the experimental results, in $(Fe_x Nb_{1-x})SiO_3$ system⁽³⁾, 2-level relaxation theory⁽⁶⁾ has shown a large value of τ . If we include crystal field effects, Table 1 shows in this case $n = 5$ and thus the actual relaxation time will be less as shown in Fig. 1.

Fig. 2 shows the values of τ_1/τ_2 for $n = 2$ and 3 to a function of the ratio of the spin flip frequency ω_{sf} and the nuclear Larmor precession frequency ω_n . The difference between the two curves is evident.

References

1. E. Prins, *in: Solid State Physics*, Vol. 10, Academic Press, New York, 1962, p. 1.
2. E. L. Hahn, *Phys. Rev.*, **80**, 1305 (1950).
3. E. L. Hahn, *in: Relaxation and Phase Transitions*, Gordon and Breach, London, 1963, p. 1.
4. E. L. Hahn, *in: Solid State Physics*, Vol. 10, Academic Press, New York, 1962, p. 1.
5. E. L. Hahn, *in: Solid State Physics*, Vol. 10, Academic Press, New York, 1962, p. 1.
6. E. L. Hahn, *in: Solid State Physics*, Vol. 10, Academic Press, New York, 1962, p. 1.
7. E. L. Hahn, *in: Solid State Physics*, Vol. 10, Academic Press, New York, 1962, p. 1.
8. E. L. Hahn, *in: Solid State Physics*, Vol. 10, Academic Press, New York, 1962, p. 1.

CRITICAL ATTENUATION IN NICKEL

B.K.Basu

Tata Institute of Fundamental Research, Bombay.

I. INTRODUCTION

It is well known⁽¹⁾ that ultrasonic waves show a sharp increase in attenuation in the vicinity of magnetic phase transition temperature. The peak of the attenuation occurs at a temperature given by the condition

$$\omega \tau = 1, \quad T < T_c \quad \dots (1)$$

where ω is the angular frequency of the ultrasonic wave, T the absolute temperature, and T_c is the transition temperature. τ above is the relaxation time for spin fluctuations that occur near the transition temperature. For ferromagnets the theory of Landau and Khalatnikov⁽²⁾ gives $\tau \propto \epsilon^{-1}$ whereas recent dynamical scaling theory^(3,4) predicts $\tau \propto \epsilon^{-5/3}$, where $\epsilon = \left| \frac{T - T_c}{T_c} \right|$.

We have reported earlier some work on critical attenuation in nickel⁽⁵⁾. This paper is a continuation of this work with a specific objective of examining relation (1). So far, such measurements in magnetic systems are not available.

II. EXPERIMENTAL

The relative positions of the peaks have been obtained by measuring echo-amplitudes for two frequencies simultaneously. Figure 1 shows the block diagram of the experimental arrangement. Two units, each consisting of an attenuation comparator, amplifier, and integrator,

and a recorder were used. The attenuation comparators were operated in alternate phase by the synchronizing circuit. In addition we found it necessary to use an interference suppressor to avoid interference of the two units.

The crystal was heated in a vacuum furnace of large thermal mass. Near Curie point the temperature of the furnace was varied at the rate of a few degrees per hour. Using charts with appropriate speeds an accuracy better than 10 millidegrees in relative temperature measurements were obtained.

III. RESULTS.

Here we give only preliminary results. Figure 2 shows echo-amplitude measurements for two frequencies 14 Mc/s and 100 Mc/s. Relation (1) predicts the peak for higher frequency to occur at a lower temperature. This is quite evident from the figure. The experimental shift is 180 ± 40 mdeg. This result is similar to first sound attenuation measurement near λ transition in liquid He. At the present time complete data are not available to make a deterministic comparison with the theoretical predictions. However, a preliminary check using our data together with the results of Golding et. al⁽⁶⁾ from Bell Telephone Laboratory (who finds the separation between 20 and 60 Mc/s as 80 ± 20 mdeg.) and assuming a power

ture

$T_c?$

hour
mpera-
tal
lock of

• order
r is
tuation

law relation for χ , shows that the variation of χ is closer to the relation $\chi \propto e^{-1}$, and has certainly a weaker temperature dependence than that given by neutron diffraction result⁽⁷⁾.

IV. REFERENCES

1. B.Luthi and T.J.Moran, J.Phys.Chem.Solids, 31, 174 (1970).
2. L.D.Landau and I.M.Khalatnikov, Dokl.Akad.Nauk SSSR, 96, 459(1954).
3. K.Kawasaki, Prog.Theo.Phys. 39, 285(1968).
4. B.I.Halperin and P.C.Hohenberg, Phys.Rev. 177, 952 (1969).
5. B.I.Basu, Phys,Stat.Sol. 38, 857(1970).
6. B.Golding and M.Barmatz, Phys.Rev.Letters, 23, 223 (1969).
7. V.J.Minkiewicz, M.F.Collins, R.Nathans and G.Shirar, Phys.Rev. 132, 624(1969).

DISCUSSION

D. K. Ghosh

This question is in the nature of a general enquiry:

Supposing you have a substance (e. g. NiO) which exhibits both magnetic transition and a transition corresponding to insulator to metallic state. If you measured the ultrasonic attenuation in such a substance will you expect the enhancement at the Neél transition temperature (T_N) or at the temperature T_c at which carrier density is suddenly increased?

B. K. Basu

The antiferromagnetic transition in NiO is rather complicated. If it turns out to be a second order phase transition it

will show an enhancement of attenuation near the Neel temperature T_N . I am not familiar with the other transition in NiO.

B. Viswanathan

- 1) What is the heating rate employed close to T_c in studying the attenuation as a function of temperature?
- 2) What about the thermal equilibrium problem near T_c ?

B. K. Basu

- 1) The rates employed are between 3°C and 6°C per hour
- 2) We have taken considerable pains to make the temperature gradient in the crystal as small as possible. The crystal size is about 5 cm^3 , and it is kept in contact with a large block of aluminium.

T. V. Ramakrishnan

The critical attenuation indices quoted are for the order parameter fluctuations. In this case, the order parameter is magnetization. How are the measurement of density fluctuation attenuations related to these indices?

B. K. Basu

The relation $\chi \propto E^{-1}$ holds, for the model of Landau and Khalatnikov, for density fluctuations as well as for magnetization fluctuation. Here $E = \left| (T - T_c)/T_c \right|$.

law relation for χ , shows that the variation of is closer to the relation $\chi \propto \epsilon^{-1}$, and has certainly a weaker temperature dependence than that given by neutron diffraction result⁽⁷⁾.

IV. REFERENCES

1. B.Luthi and T.J.Moran, J.Phys.Chem.Solids, 31, 1741 (1970).
2. L.D.Landau and I.M.Khalatnikov, Dokl.Akad.Nauk SSSR 96, 469(1954).
3. K.Kawasaki, Prog.Theo.Phys. 39, 285(1968).
4. B.I.Halperin and P.C.Hohenberg, Phys.Rev. 177, 952 (1969).
5. B.K.Basu, Phys,Stat.Sol. 38, 857(1970).
6. B.Golding and M.Barnatz, Phys.Rev.Letters, 23, 223 (1959).
7. V.J.Minkiewicz, M.F.Collins, R.Nathans and G.Shirane Phys.Rev. 132, 624(1969).

DISCUSSION

D. K. Ghosh

This question is in the nature of a general enquiry:

Supposing you have a substance (e. g. NiO) which exhibits both magnetic transition and a transition corresponding to insulator to metallic state. If you measured the ultrasonic attenuation in such a substance will you expect the enhancement at the Neel transition temperature (T_N) or at the temperature T_c at which carrier density is suddenly increased?

B. K. Basu

The antiferromagnetic transition in NiO is rather complicated. If it turns out to be a second order phase transition it

will show an enhancement of attenuation near the Neel temperature T_N . I am not familiar with the other transition in NiO .

B. Viswanathan

1) What is the heating rate employed close to T_c in studying the attenuation as a function of temperature?

2) What about the thermal equilibrium problem near T_c ?

B. K. Basu

1) The rates employed are between 3°C and 6°C per hour.

2) We have taken considerable pains to make the temperature gradient in the crystal as small as possible. The crystal size is about 5 cm^3 , and it is kept in contact with a large block of aluminium.

T. V. Ramakrishnan:

The critical attenuation indices quoted are for the order parameter fluctuations. In this case, the order parameter is magnetization. How are the measurement of density fluctuation attenuations related to these indices?

B. K. Basu

The relation $\chi \propto \epsilon^{-1}$ holds, for the model of Landau and Khalatnikov, for density fluctuations as well as for magnetization fluctuation. Here $\epsilon = \{(T - T_c)/T_c\}$.

MAGNON DISPERSION IN MAGNETO-ELECTRIC ANTIFERROMAGNETS

R.S.Tripathi, R.P.S.Kushwaha and K.G.Srivastava

U.P.Agricultural University, Pantnagar, Nainital.

I. Introduction

Magnetoelectric effect was predicted by Landau and Lifshitz¹. Dzyaloshinski,² on symmetry grounds demonstrated its existence in Cr_2O_3 . It was confirmed experimentally by Astrov³ and Rado⁴, measuring susceptibility of Cr_2O_3 in simultaneous presence of electric and magnetic fields.

The microscopic explanation rests on the higher order term in perturbation theory. Rado⁴ considered spin orbit interaction on a single ion and calculated susceptibilities in molecular field approximation. A good fit with experiment was reported. Later Hornreich and Shtrikman⁵ included the change in g-factor due to applied electric field also, and did the calculations in molecular field approximation. On the other hand Date et al⁶ considered exchange coupling via electric field between two ions in the same sublattice. Recently Yatom and Englman⁷ included all these interaction terms in the Hamiltonian and calculated the susceptibilities by thermodynamic Green's function in Callen decoupling approximation. Their calculations establish that the most dominant interaction term is single ion term due to Rado.

In the present paper we calculate the magnon eigenfrequencies of a two sublattice antiferromagnet subjected to electric and magnetic fields along the spin orientation, considering nearest neighbour interactions only.

II. HAMILTONIAN

We write down the Hamiltonian of our system

$$H = \frac{J}{2} \sum_{i,j} \mathbf{S}_i \cdot \mathbf{S}_j - \frac{I_a}{2} \sum_j (S_j^z)^2 + \mu a_{||}^{LS} E_z \sum_j \epsilon(j) (S_j^z)^2 - \mu H_z \sum_j S_j^z \quad [1]$$

where J denotes the exchange coupling between nearest neighbouring spins S_i and S_j which belong to different sublattices designated by 'a' and 'b', I_a is proportional to the anisotropy energy; H_z and E_z are the magnetic and electric fields along the z direction, coinciding with the spin orientation, $a_{||}^{LS}$ is the spin orbit coupling and $\epsilon(j) = \pm 1$ depending on 'a' or 'b' sublattices.

In order to calculate the magnon energy, we use the Holstein-Primakoff transformation and write down the

Hamiltonian(1) in magnon operator formalism :-

$$H = \text{Const.} + \sum_k \left[\lambda_k^\dagger c_k^\dagger c_k + \bar{\lambda}_k d_k^\dagger d_k + J_a S \gamma_a(k) (c_k d_k + c_k^\dagger d_k^\dagger) \right] \quad [2]$$

where c_k^\dagger , d_k^\dagger are the creation operators for 'a' and 'b' sublattices, and c_k , d_k are the corresponding annihilation operators. In the Hamiltonian(2) magnon-magnon interaction terms have not been included. Other symbols are given below

$$\begin{aligned} \lambda_k^\pm &= J_a S + I_a S (1 - \frac{1}{2S}) \pm \mu H_z \mp 2\mu S a_{||}^{LS} E_z (1 - \frac{1}{2S}) \\ \gamma_a(k) &= \frac{1}{z} \sum_j e^{i \cdot k \cdot \delta} \quad , \quad J_a = zJ \end{aligned} \quad [3]$$

where z is the number of the nearest neighbours and the sum over δ is limited to nearest neighbouring atoms only.

III. ENERGY EVALUATION

The magnon energies can now be calculated from the Green's function method. We define the single particle Green function

$$\hat{G}_{kk} = \begin{bmatrix} \langle c_k | c_k^\dagger \rangle & \langle d_k^\dagger | c_k^\dagger \rangle \\ \langle c_k | d_k \rangle & \langle d_k^\dagger | d_k \rangle \end{bmatrix} \quad [4]$$

The equation of motion of \hat{G}_{kk} can be written down in the usual manner. The magnon eigenfrequencies will be obtained from the pole of the Green's function. The final result is given below

$$\omega - \lambda_k + \frac{(J_d S \chi(k))^2}{\omega + \lambda_k} = 0 \quad [5]$$

Solving the quadratic equation (5) and setting $k=0$, we get the following expression for antiferromagnetic resonance frequencies,

$$\omega = \mu H - 2\mu S a_{||}^{LS} E_z \left(1 - \frac{1}{2S}\right) \pm \left[(J_d S + J_d S \left(1 - \frac{1}{2S}\right))^2 - (J_d S)^2 \right]^{\frac{1}{2}} \quad [6]$$

We find that the spin wave resonance frequency consists of two branches, as is the case in the presence of only magnetic field. The splitting factor depends on the electric field through the spin orbit coupling parameter $a_{||}^{LS}$. Antiferromagnetic resonance is normally used for evaluation of effective exchange and anisotropy fields in antiferromagnets. Our result vide equation (6) shows that measurement of Antiferromagnetic Resonance Frequencies should give the value of the spin orbit coupling coefficient².

REFERENCES

1. L.D.Landau and E.M.Lifshitz; Electrodynamics of Continuous Media (Addison-Wesley Publishing Co., Reading, Mass., USA, 1960) ,p.119.
2. I.E.Dzyaloshinski; Soviet Physics JETP, 10, 628, (1960)
3. D.N.Astrov; *ibid* 11, 708 (1960)
4. G.T.Rado; Phys.Rev. 128, 2546 (1962)
5. R.Hornreich and S.Shtrikman; Phys.Rev. 161, 506 (1967)
6. M.Date, J.Kanamori and M.Tachiki; J.Phys.Soc.Japan 16, 2589 (1961)
7. H.Yatom and R.Englman; Phys.Rev. 188, 793, (1969)

DISCUSSION

N. Kumar

How is it that the correction is zero for $S = 1/2$?

R.S. Tripathi

Magneto-electric effect in antiferromagnets is observed only where certain magnetic symmetries are present. It is not true for all the antiferromagnets. But if it is there for $S = 1/2$, then one might have to use higher order decoupling approximation.

THERMODYNAMIC BEHAVIOUR OF A HEISENBERG SYSTEM OF THREE LEVEL IONS

C.M.Bhandari and Ashok Kumar Gupta
Physics Department, Allahabad University, Allahabad-2.

We consider an exchange coupled system of triplet
($S = 1$) ions in presence of uniaxial anisotropy due to
crystalline field. The Hamiltonian for the system is

$$H = -\mu_B \sum_f S_f^z - D \sum_f (S_f^z)^2 \\ - \sum_{f_1 f_2} I(f_1, f_2) \left[S_{f_1}^z S_{f_2}^z + \phi S_{f_1}^+ S_{f_2}^- \right]. \quad (1)$$

The first, second, and the third terms refer to the
Zeeman energy, crystal field anisotropy energy, and the
exchange energy, respectively. The symbols have the same
meaning as in a previous paper by one of the authors⁽¹⁾.
We have to consider only two Green's functions^(2,3),
namely

$$G_{f_1 f_2}^{(0)}(t - t') = \langle S_{f_1}^+(t), S_{f_2}^-(t') \rangle, \quad (2a)$$

$$G_{f_1 f_2}^{(1)}(t - t') = \langle S_{f_1}^z(t) S_{f_1}^+(t), S_{f_2}^-(t') \rangle, \quad (2b)$$

We write down the time Fourier transformed
equations of motion and introduce the RPA decoupling
scheme for the higher order Green's functions

$$\langle S_{f_1}^z S_{f_2}^+ S_{f_3}^- \rangle_E \rightarrow \sigma \langle S_{f_2}^+ S_{f_3}^- \rangle_E, \quad (3a)$$

$$\langle S_{f_1}^z S_{f_1}^z S_{f_2}^+ S_{f_3}^- \rangle_E \rightarrow \sigma \langle S_{f_2}^+ S_{f_3}^- \rangle_E, \quad (3b)$$

where

$$\sigma = \langle S^z \rangle, \quad \text{and} \quad m = \langle (S^z)^2 \rangle.$$

On introducing the spatial fourier transforms, two coupled equations are obtained which are solved to give

$$G^{(0)}(\vec{k}, E) = \frac{1}{2\pi} \times \left[\frac{a_+(\vec{k})}{E - E_+(\vec{k})} + \frac{a_-(\vec{k})}{E - E_-(\vec{k})} \right], \quad (4a)$$

$$G^{(1)}(\vec{k}, E) = \frac{1}{2\pi} \times \left[\frac{b_+(\vec{k})}{E - E_+(\vec{k})} + \frac{b_-(\vec{k})}{E - E_-(\vec{k})} \right], \quad (4b)$$

where

$$a_{\pm} = \sigma \pm \frac{2}{(E_+ - E_-)} \left[\sigma E_1 + D(3m + \sigma - 2) \right], \quad (5a)$$

$$b_{\pm} = \frac{3m + \sigma - 2}{2} \pm \frac{1}{(E_+ - E_-)} \left[(3m + \sigma - 2) E_2 - 4\phi m I(\vec{k}) \right], \quad (5b)$$

$$\text{here } E_{\pm}(\vec{k}) = \frac{1}{2} \left[(E_1 + E_2) \pm \sqrt{(E_1 - E_2)^2 - 4E_3} \right], \quad (6)$$

$$E_1(\vec{k}) = \mu H - D + 2\sigma \left[I(0) - \phi I(\vec{k}) \right], \quad (7a)$$

$$E_2(\vec{k}) = \mu H + D + 2\sigma I(0), \quad (7b)$$

$$E_3(\vec{k}) = 4D\phi m I(\vec{k}), \quad (7c)$$

$I(\vec{k})$ is the Fourier transform of $I(\vec{r})$. We find that there are two spin wave modes $E_+(\vec{k})$ and $E_-(\vec{k})$. In the low temperature limit and in zero field when $\sigma = 1$, $m = 1$, we have

$$E_+(\vec{k}) = 2zJ (1 - \phi \gamma(\vec{k})) + D$$

$$E_-(\vec{k}) = 2zJ - D$$

From eqns.(4a) and (4b), we obtain the equal-time correlation functions using the standard formula⁽³⁾.

$$\begin{aligned}\langle S_g^- S_g^+ \rangle &= 2 - \sigma - n \\ &= \frac{1}{N} \sum_{\vec{k}} \left[a_+ f(E_+) + a_- f(E_-) \right], \quad (8a)\end{aligned}$$

$$\begin{aligned}\langle S_g^- S_g^z S_g^+ \rangle &= 2(1 - n) \\ &= \frac{1}{N} \sum_{\vec{k}} \left[b_+ f(E_+) + b_- f(E_-) \right], \quad (8b)\end{aligned}$$

here $f(E) = (e^{\beta E} - 1)^{-1}$.

From eqns.(8a) and (8b), we get magnetization σ and function n ⁽²⁾. The Curie temperature is obtained by putting $\sigma = 0$ and $n = 2/3$, we find $\beta_C = 1/k_B T_C$ is given by implicit equation,

$$1 = \frac{1}{N} \sum_{\vec{k}} \left[\frac{2\beta_C \{2I(0) - \phi I(\vec{k})\} - 3/2}{\beta_C^2 \{D^2 - (8/3) D \phi I(\vec{k})\}} \right] \quad .(9)$$

Other interesting thermodynamic behaviour of the system can be obtained from the expressions of magnetization and spin wave energy spectrum.

REFERENCES

1. C .M .Bhandari, Indn. J. Pure and Appl. Phys.,
8, in press (1970)
2. G. B. Taggart and R. A. Tahir-Kheli, Physica,
44, 321 (1969)
3. D. N. Zubarev, Usp. Fiz. Nauk., 71, 71 (1960),
English translation in Sov.
Phys. - USPEKHI, 3, 320(1960)

DISCUSSION

Ram Kishore

The order parameter Δ represents the x -component of the magnetization and therefore as long as

Δ is finite, system has magnetic moment in the x direction instead of z . In this case the system is ferromagnetic instead of being non-magnetic. And therefore transition described here is in the ferromagnetic system instead of being in the non-magnetic system.

A.K. Gupta

Δ which I have taken is $\langle a_i^\dagger a_i \rangle = \langle a_i^\dagger a_i \rangle$

A nonvanishing Δ will not mean a nonvanishing mag-

netization. If $\langle n_x \rangle = \langle n_y \rangle$, then the magnetisation will be zero. In no case nonvanishing Δ will imply a magnetization in x direction.

D.K. Ghosh

What happens if $(E_1 - E_2)^2 < 4E_3$, i.e. when the spin wave energies develop an imaginary part?

A.K. Gupta

Such a situation will arise when $4D^2 + 4\sigma^2 I^2(k) - 4D I(k) [m - \sigma] < 0$. Now $m > \sigma$ always, so this can happen near curie point. In that case it will imply that spin wave modes are damped. But simple RPA decoupling of the second order Green's function, as I have done, does not lead to spin wave life-time. It is apparant that the approximation will break down under the condition suggested by you.

PHASE TRANSITION IN NARROW ENERGY BAND HUBBARD MODEL

Ashok Kumar Gupta

Physics Department, Allahabad University, Allahabad-2

(1)

We employ the Hubbard model to discuss the metal-insulator phase transition, For a narrow s-band the Hamiltonian for the system is

$$H = \sum_{ij} T_{ij} a_i^\dagger a_j + \frac{1}{2} I \sum_i n_{i\uparrow} n_{i\downarrow}, \quad (1)$$

where

$$T_{ij} = N^{-1} \sum_{\vec{k}} \exp i \vec{k} \cdot (\vec{R}_i - \vec{R}_j) \quad . \quad (2)$$

The first term is the 'hopping' term while the second is the intra-atomic coulomb repulsion term between the electrons of opposite spin. The notations used are standard and self-explanatory.

It is clear that the system will be a metal at high temperatures due to the electron hopping from one atomic site to another with ease. At low temperatures, the motion is restricted due to the interaction term which favours only one electron at a particular lattice site. There is an energy gap corresponding to the fact that two electrons of opposite spin on the same site have higher energy as compared to one electron and one hole (of opposite spin) on the same site. The 'onset' of the 'insulating state' is characterized by the non-vanishing opposite spin electron-hole correlations. These are described by the 'anomalous' off-diagonal elements of the matrix Green's function

$$\hat{G}_{ij}^{\sigma\sigma'}(E) = \begin{vmatrix} G_{ij}^{\uparrow\uparrow}(E) & G_{ij}^{\uparrow\downarrow}(E) \\ G_{ij}^{\downarrow\uparrow}(E) & G_{ij}^{\downarrow\downarrow}(E) \end{vmatrix}, \quad (3)$$

where $G_{ij}^{\sigma\sigma'}(E)$ is the Fourier transform of

$$G_{ij}^{\sigma\sigma'}(t, t') = -i \theta(t-t') \left\langle \left[a_{i\sigma}(t), a_{j\sigma'}^+(t') \right]_{(+)} \right\rangle. \quad (4)$$

We write down the equation of motion of the Green's functions and introduce the decoupling scheme:

$$\begin{aligned} \left\langle \left\langle a_{i-\sigma} a_{i\sigma}; a_{j\sigma'}^+ \right\rangle \right\rangle_E &\rightarrow \left\langle \left\langle a_{i-\sigma} a_{i\sigma} \right\rangle \right\rangle \left\langle \left\langle a_{i\sigma} a_{j\sigma'}^+ \right\rangle \right\rangle_E \\ &- \left\langle \left\langle a_{i-\sigma} a_{i\sigma} \right\rangle \right\rangle \left\langle \left\langle a_{i-\sigma}; a_{j\sigma'}^+ \right\rangle \right\rangle_E. \end{aligned} \quad (5)$$

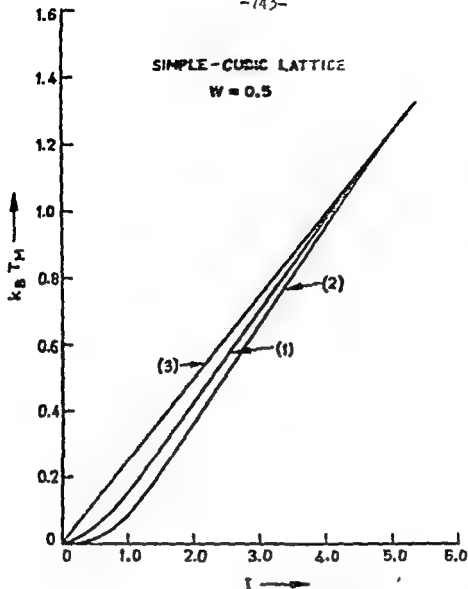
We treat only the non-magnetic solutions, where $\langle n_{\uparrow} \rangle = \langle n_{\downarrow} \rangle = \frac{1}{2}n$, and we put $\langle a_{\uparrow} a_{\downarrow} \rangle = \langle a_{\downarrow} a_{\uparrow} \rangle = \Delta / I$, Δ is the 'order parameter' for the insulating phase and it is to be determined self consistently. This procedure is analogous to the Gorkov method in the theory of superconductivity. In the case when $n=1$, and in the zero bandwidth limit, we get the following result

$$\Delta / I = \frac{1}{2} \tanh \left(\frac{\Delta}{2k_B T} \right). \quad (6)$$

It is easily seen that 2Δ is the energy gap parameter. The transition temperature T_M is determined by putting $\Delta = 0$, the transition is of the second order, we get

$$\frac{k_B T_M}{I} = \frac{1}{2}, \text{ and } \Delta(0) / \frac{k_B T_M}{I} = 2. \quad (7)$$

The gap $\Delta(0)$ gradually changes from $\frac{1}{2}I$ at $0^\circ K$ to zero at $T = T_M$.



The plot of $K_B T_M$ (T_M is the metal-insulator transition temperature) vs. I (the intra-atomic electron repulsion term) for a simple cubic lattice with the bandwidth $W = \frac{1}{2}$. (1) Our results and (2) the result of Langer, Plischke, and Mattis for exactly the same case. Quite close agreement of the two results is clearly evident. For comparison (3) shows the result in the zero bandwidth case.

In the finite bandwidth case, the coupled equations are self consistently solved by iteration. The results are shown in Fig. 1, for the simple cubic lattice and the s-bandwidth $W = \frac{1}{2}$. For comparison the result of the zero bandwidth approximation are also plotted. It is observed that these results compare very well with the calculations of Langer, Plische, and Mattis⁽²⁾. The details of the work are being reported elsewhere.

References;-

- (1) J. Hubbard, Proc. Roy. Soc. (London), Ser. A 276, 238 (1963);
 ibid, 277, 237(1963); ibid, 281, 401(1964);
 ibid, 285, 542(1965).

For a comprehensive review of the work on the metal-nonmetal transition, see D. Adler, in Solid State Physics, Vol. 21, eds. F. Seitz and D. Turnbull (Academic press Inc., New York, 1968).

- (2) W. Langer, M. Plischke, and D. Mattis, Phys. Rev. Letters, 23, 1448(1969).

DISCUSSION

D.K. Ghosh

1) For the Hamiltonian which you have written the total number of particles having a particular spin is conserved. Hence spin flip correlations $\langle a_{i\uparrow}^{\dagger} a_{j\downarrow} \rangle$ ($i \neq j$ or $i = j$, irrespective) are Zero from first principles.

I. Ramarao

- 1) You can get around the problem by introducing

symmetry breaking (total spin non-conserving) terms and define quasi-averages as done in superconductivity.

2) If one pushes the analogy with super conductors to the extreme, then would you not expect Josephson type effects in coupled Ferromagnets?

D.K. Ghosh

I agree with you when you say that the presence of a symmetry breaking term in the Hamiltonian will make the quasi-averages non-zero. For instance, in the spin density wave state these correlations are non-zero. But in the way the author has presented my comment stands.

A.K. Gupta

1) What Dr. Ghosh has suggested appears to be very interesting. I intend to carry out the programme and see the results.

2) I don't think that at this stage it will be possible to push the analogy too far. The analogy, which I have tried to focus into attention, is with the general theory of second-order phase transitions in many-fermion system and not exactly in superconductivity theory.

ON DYNAMICAL DISSIMILARITY OF MAGNON MODES FOR ANTIFERROMAGNETS

SP SAXENA

Department of Physics, National Defence Academy,
Dharwad, Poona - 23

INTRODUCTION

In the absence of external magnetic field, two magnon modes for two sub-lattice Heisenberg antiferromagnet are degenerate. However, if we were to consider the interaction of these modes with phonons, we find that the two modes are displaced unequally on renormalisation by phonon interaction. This significantly reflects the dynamical dissimilarity of two magnon (acoustical and optical) modes.

REORMALISED MAGNON ENERGY DUE TO PHONON-MAGNON INTERACTION

The total Hamiltonian¹ of two sub-lattice Heisenberg Antiferromagnet can be expressed as:-

$$H = H_m + H_p + H_{mp} \quad (1)$$

$$\text{where } H_m = \sum_q \hbar \omega_q^+ (\alpha_q^+ \alpha_q + \frac{1}{2}) + \hbar \omega_q^- (\beta_q^+ \beta_q + \frac{1}{2}) \quad (2)$$

$$H_p = \sum_q \hbar \omega_q (\gamma_q^+ \gamma_q + \frac{1}{2}) \quad (3)$$

$$\text{and } H_{mp} = \sum_q [A_{2q} (\alpha_q^+ \alpha_{q-y}^+ \gamma_q^+ - \alpha_q^+ \alpha_{q-y} \gamma_q) + B_{2q} (\alpha_q^+ \beta_{q-y} \gamma_q^+ - \alpha_q^+ \beta_{q-y}^+ \gamma_q) + A_{2q} (\beta_q^+ \beta_{q-y} \gamma_q - \beta_q^+ \beta_{q-y}^+ \gamma_q^+)] \quad (4)$$

where symbols have their usual meanings² and A and B_{2q} are coupling coefficients.

Considering Green's functions $\langle\langle \alpha_q(t); \alpha_q^+(t') \rangle\rangle$, $\langle\langle \beta_q(t); \beta_q^+(t') \rangle\rangle$ and $\langle\langle \gamma_q(t); \gamma_q^+(t') \rangle\rangle$ for two magnon modes and phonon modes respectively, we find that

$$\begin{aligned} \langle\langle \alpha_q; \alpha_q^+ \rangle\rangle &= \frac{1}{2\pi} \left[E - \hbar \omega_q^+ + \sum_q \frac{A_{2q}^2}{E - \hbar \omega_q^+ + \hbar \omega_q} (1 + N_q) \right. \\ &\quad + \sum_q \frac{B_{2q}^2}{E - \hbar \omega_q^+ - \hbar \omega_q} (1 + n_{q-y} - N_q) \\ &\quad \left. + \sum_q \frac{B_{2q}^2}{E + \hbar \omega_q^+ - \hbar \omega_q} (n_{q-y} - N_q) \right]^{-1} \quad (5) \end{aligned}$$

$$\begin{aligned} \langle\langle \beta_q; \beta_q^+ \rangle\rangle &= \frac{1}{2\pi} \left[E - \hbar \omega_q^- + \sum_q \frac{B_{2q}^2}{E + \hbar \omega_q^+ - \hbar \omega_q} N_q \right. \\ &\quad \left. + \sum_q \frac{A_{2q}^2}{E - \hbar \omega_q^+ - \hbar \omega_q} N_q \right]^{-1} \quad (6) \end{aligned}$$

Hence

$$\frac{1}{2\pi} \langle \langle \hat{a}_\lambda \cdot \hat{a}_\lambda^\dagger \rangle \rangle^{-1} = E - E_0 \cdot \lambda - \sum_m \frac{\lambda}{m} E(\lambda) \quad (7)$$

and $\frac{1}{2\pi} \langle \langle \hat{a}_\lambda \cdot \hat{a}_\lambda^\dagger \rangle \rangle^{-1} = E - E_0 \omega_\lambda - \sum_m \frac{\beta}{m} E(\lambda) \quad (8)$

The Principal parts of expressions $\sum_m \frac{\lambda}{m} E(\lambda)$ and $\sum_m \frac{\beta}{m} E(\lambda)$

give the renormalisation energies. If we replace in the integrands by unperturbed values and ignore anisotropy energy we find that

$$\sum_m \frac{\lambda}{m} E(\lambda) = (A_\lambda - E_0 T^4) \lambda \quad (9)$$

$$\sum_m \frac{\beta}{m} E(\lambda) = (A_\beta - E_0 T^4) \lambda \quad (10)$$

where A_λ , A_β and E_0 are functions of Debye temperature and $A_\beta = 0$

Thus the renormalised energies of magnon modes are:

$$E_\lambda = 2SJ \sqrt{z} \cdot \lambda \omega_\lambda + \beta u_0 H + (A_\lambda - E_0 T^4) \lambda \quad (11)$$

$$E_\beta = 2SJ \sqrt{z} \cdot \lambda \omega_\lambda - \beta u_0 H - E_0 T^4 \quad (12)$$

It will thus be seen that even in the absence of the magnetic field, two branches are no longer degenerate.

ESTIMATES AND DISCUSSIONS

For a typical antiferromagnet like NiF_2 the estimated values of A_λ , E_0 and A_β are as under:-

$$\begin{aligned} A_\lambda &= 0.14 \times 10^{-24} \text{ erg} \\ E_0 &= 6 \times 10^{-32} \text{ erg } (T^4) \text{ cm} \\ A_\beta &= 10 \times 10^{-32} \text{ erg } (T^4) \text{ cm} \end{aligned}$$

The zero-point contribution to percentage splitting in the absence of external magnetic field is of the order of 1%. The temperature dependent correction at 50°K is of the order of $0.8 \times 10^{-3}\%$ and is additive to zero-point contribution.

It is therefore reasonable to conclude that two magnon modes are no longer degenerate. This is not surprising in that the two modes are dynamically dissimilar. The splitting caused by magnon-phonon interaction may be explained by the following argument. In the second order the spin phonon effects after elimination of phonon coordinates lead to effective spin-spin interaction. Each sub-lattice sees an effective magnetic field. In as much as each sub-lattice interacts differently, the two modes are split up. One has to look for this splitting carefully

in experimental work.

REFERENCES:-

- 1 Upadhyaya and Sinha : Phy Review 130, 223 (1963)
- 2 Sarena SP: Ph D Thesis Agra University (1962)
- 3 Zubarev EM: Soviet Physics Uspekhi 3, 220 (1955)

ON VALIDITY OF HEISENBERG-BLOCH MODEL FOR FERROMAGNETS

SP SAIKHA

Department of Physics, National Defence Academy,
Kharakvasla, Poona-23INTRODUCTION

Recently, there has been a shift of emphasis in the theory of Ferromagnetism from Heisenberg localised model to itinerant electron model. The primary reason for this has been the presumption that the localised Heisenberg-Bloch model is unable to explain the temperature dependence of Dispersion constant, in the well-known magnon dispersion relation for the ferromagnet,

$$E_{\lambda} = D(\gamma) \lambda^2$$

It can, however, be shown that the renormalisation of Magnon Energy due to interaction of Magnon modes with phonons can explain this temperature dependence in a manner, consistent with experimental observations and theoretical requirements.

RENORMALISATION OF MAGNON ENERGY DUE TO MAGNON-PHONON INTERACTION

Total Hamiltonian of a typical Ferromagnet^{1,2} can be expressed in the form $H = H_m + H_p + H_{mp}$ (1)

where $H_m = \sum_{\lambda} \sum_{\gamma} \frac{\hbar}{2} \omega_{\lambda} (a_{\lambda\gamma}^{\dagger} a_{\lambda\gamma} + \frac{1}{2})$ (2)

$$H_p = \sum_{\gamma} \frac{\hbar}{2} \omega_{\gamma} (c_{\gamma}^{\dagger} c_{\gamma} + \frac{1}{2})$$
 (3)

and $H_{mp} = \sum_{\lambda, \gamma} \Phi_{\lambda\gamma} a_{\lambda\gamma}^{\dagger} a_{\gamma} + \text{hermitian conjugate}$ (4)

Here $\Phi_{\lambda\gamma}$ is the phonon-magnon coupling coefficient and other symbols have their usual meanings³ in the second quantisation representation.

We can define Magnon Green's function⁴ as:

$$G_{\lambda\lambda}(t-t') = \langle\langle a_{\lambda}(t), a_{\lambda}^{\dagger}(t') \rangle\rangle$$
 (5)

Considering the equations of motion for the Green's function and solving them for higher orders after making valid approximations, we find

$$\langle\langle a_{\lambda}; a_{\lambda}^{\dagger} \rangle\rangle = \frac{1}{2\pi} \left[E - A_{\lambda} + \frac{\sum_{\gamma} \Phi_{\lambda\gamma}^2 (N_{\lambda} - N_{\lambda-\gamma})}{E - A_{\lambda-\gamma} + \hbar \omega_{\gamma}} + \frac{\sum_{\gamma} \Phi_{\lambda\gamma}^2 (1 + N_{\lambda} + N_{\lambda-\gamma})}{E + A_{\lambda-\gamma} - \hbar \omega_{\gamma}} \right]^{-1}$$
 (6)

We can express the above result as:-

$$\frac{1}{2\pi} \langle\langle a_{\lambda}; a_{\lambda}^{\dagger} \rangle\rangle^{-1} = E - A_{\lambda} - E_{\lambda}(\lambda)$$
 (7)

where $\Sigma^{(1)}$ is the self-energy part complex in general. The principal part gives the renormalisation of the single particle of magnon energy. In the long wave length approximation in low temperature limit of validity of magnon concept integration over q leads to the result

$$\Sigma^{(1)} = -\frac{32}{3\pi^2} \left(\frac{J}{\hbar} \right)^2 \left(\frac{k_B T}{2Js} \right)^{\frac{3}{2}} \Gamma\left(\frac{3}{2}\right) \lambda^2 = -c T^{\frac{3}{2}} \lambda^2 \quad (8)$$

Thus the renormalised magnon energy for a typical ferronagnet is given by

$$E_\lambda = \tilde{A}_\lambda = (2Js\lambda^2 - cT^{\frac{3}{2}}) \lambda^2 = D_0 (1 - bT^{\frac{3}{2}}) \lambda^2 \quad (9)$$

$$D_0 = 2Js a^2 \quad a \sim 1 \quad b = \frac{c}{2Js a^2} \quad (10)$$

ESTIMATES AND DISCUSSION

Equation 9 above given us the temperature variation of spin-wave coupling parameter $D(T)$ in close accord with the experimental results of Phillips and Rosenberg⁴ on thin films of Cobalt and Nickel.

The value of the parameter 'b' is found to be of the order of 10^{-5} a value quite close to that obtained from spin-wave resonance measurements as well as the experimental value obtained from second-order magnetisation effects.

The percentage change in spin-wave coupling parameter D_0 for a temperature rise from 0 to 300°K is of the order of 10%, a right order of magnitude in accord with experimental observations.

The above calculations show that Heisenberg-Block Model for a ferromagnet can explain the temperature dependence of parameter D in the correct manner, if we invoke phonon-magnon renormalisation. To this extent, validity of the model is vindicated.

REFERENCES

1. KP Sinha and U.N. Upadhyaya : Phy. Rev. 127, 432 (1962)
2. Saxena, S.P-Magnon-Phonon Interaction and Renormalisation of collective Modes in Magnetic Systems (Ph D Thesis-Agra University-1968) to be published.
3. Zubarev D.N.-Soviet Physics Uspekhi, 8, 320 (1960)
4. T.G. Philips and H.M. Rosenberg: Proceedings of International Conference on Magnetism, Nottingham, 1965, 306.

ANTIFERROMAGNET WITH NEAREST NEIGHBOUR INTERACTIONS

J. Pasupathy

Tata Institute of Fundamental Research, Bombay 5

I. INTRODUCTION

The Heisenberg model of exchange between neighbouring atoms, has been a favourite candidate for the study of properties of anti-ferromagnets. Bethe⁽¹⁾ in (1931) showed that the eigenvalue problem for a chain of N spin- $\frac{1}{2}$ atoms with Hamiltonian

$$H = J \sum_{i=1}^N \vec{\sigma}_i \cdot \vec{\sigma}_{i+1} \quad (1)$$

$$\vec{\sigma}_{N+1} = \vec{\sigma}_1$$

where $\vec{\sigma}_i$ (the Pauli matrices) are the spin operator for the i^{th} atom and $J(>0)$ the exchange integral, could be reduced to that of solving a set of coupled transcendental algebraic equations. Seven years later Hulthen⁽²⁾ calculated the exact ground state energy and a few years ago Griffiths⁽³⁾ computed the magnetization curve at zero temperature. Even though the Heisenberg model has been solved exactly in principle, practical calculations have proved to be quite difficult. In view of this, there is no compelling virtue in restricting oneself to nearest neighbour interaction. Majumdar⁽⁴⁾ and his collaborators, have studied the effect of introducing an additional term to eq.(1)

$$H = J \sum_{i=1}^N \vec{\sigma}_i \cdot \vec{\sigma}_{i+1} + J_1 \sum_{i=1}^N \vec{\sigma}_i \cdot \vec{\sigma}_{i+2}$$

$$\vec{\sigma}_{N+1} = \vec{\sigma}_1$$

$$\vec{\sigma}_{N+2} = \vec{\sigma}_2 \quad (2)$$

and has pointed out that in the special case $2J_1 = J$, it may be possible to find simple and exact solution. In particular he has conjectured that the ground state wave function is the characteristic Keesom state with adjacent spins coupled in pairs.

SPIN PHONON INTERACTION IN FERROMAGNETIC INSULATOR AT LOW TEMPERATURES

S. K. Ghatak

Saha Institute of Nuclear Physics, Calcutta-9

INTRODUCTION

Recent experimental data on the acoustic attenuation in ferromagnetic insulators suggest that either the volume magnetostriction or the single ion magnetostriction plays the major role in the coupling between the spins and the phonons. The volume magnetostriction which at low temperatures, describes the scattering of magnon with simultaneous emission or absorption of one phonon has been considered by Pytte⁽¹⁾ and Yakovlev⁽²⁾. It has been shown that all the modes except $K = 0$ mode are effected by this interaction and this also contributes to the Dyson T^4 -term in the magnetization. In this paper, we study the effect of the single-ion magnetostriction on the spin-wave spectrum. We will see that because of the single-ion nature of the single-ion magnetostriction, it contributes mostly to the self-energy of the magnon with $K = 0$.

HAMILTONIAN

The single-ion magnetostriction interaction can be written in the form,

$$H_S = \sum_i G_i \epsilon_i \quad (1)$$

where G is the spin magnon coupling tensor and ϵ is the strain tensor crystal

which will be considered here we obtain the magnon-phonon Hamiltonian from eq. (1) after expressing ϵ in terms of phonon operator and spin in terms of magnon operator in H-P approximation⁽³⁾

$$H_{m-p} = \sum_{q,k} \Phi(q) b_{k-q}^\dagger b_k \varphi(q) + \sum_{k,q} \left[\Psi(q) b_{k-q} b_k \varphi(q) + c.c. \right] \quad (2)$$

where

$$\Phi(q) = \frac{1}{(2\pi\epsilon_0 NN)^{1/2}} \left(\frac{2G_{11}S}{2} \right) \left[\underline{e}(q) \cdot \underline{q} - 3\epsilon_z(q) q_z \right]$$

and

$$\Psi(q) = \frac{1}{(2\pi\epsilon_0 NN)^{1/2}} \left[\frac{3G_{11}S}{8} \left\{ \epsilon_+(q) q_+ + \epsilon_-(q) q_- \right\} + \frac{3q_z S}{4} \left\{ \epsilon_-(q) q_- - \epsilon_+(q) q_+ \right\} \right]$$

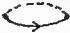
The first term describes the scattering of magnon with the emission or the absorption of one phonon and second term represents the fusion of the magnons into one phonon and the reverse.

Now the total Hamiltonian of the magnon-phonon system becomes $H = H_m + H_p + H_{m-p}$ where H_m is the magnon Hamiltonian in H-P approximation and H_p , the phonon Hamiltonian in harmonic approximation.

SELF ENERGY OF MAGNON

A. Scattering process

We use the diagrammatic Green's function theory⁽⁴⁾ to calculate the self-energy $\Sigma(k)$ of the magnon and the real part of $\Sigma(k)$ gives the change in magnon energy. Assuming the spin-phonon interaction to

be small we calculate $\Sigma(k)$ to the lowest order in spin-phonon interaction. The lowest order irreducible self-energy diagram is  where dotted line represents the phonon Green's function and solid line the magnon Green's function. The real part of the contribution of the above diagram is given by

$$\text{Re} \Sigma(k) = -\rho \int_q \frac{\Phi(q)\Phi(-q)}{2} \left\{ \frac{\coth \frac{\beta \omega_q}{2} - \coth \frac{\beta \Sigma_{k+q}}{2}}{\Sigma_k - \Sigma_{k+q} + \omega_q} + \frac{\coth \frac{\beta \omega_q}{2} + \coth \frac{\beta \Sigma_{k+q}}{2}}{\Sigma_k - \Sigma_{k+q} - \omega_q} \right\}$$

In Debye approximation, the $\text{Re} \Sigma(k)$ comes out to be


$$\text{Re} \Sigma(k) = -\frac{9G_{11}^2}{40\pi^2 m} \left[\frac{2}{c^2} + \frac{1}{c^2} \right] \left[I(T_D, T) + S^{\frac{1}{2}} \zeta(3/2) \Gamma(3/2) \left(\frac{kT}{J} \right)^{3/2} \right] + O(\vec{k}^2, T^3)$$

where

$$I(T_D, T) = S \left(\frac{kT_D}{J} \right) \left(q_{\text{od}} \right) \left[1 - \frac{2}{S} \left(\frac{kT_D}{J} \right) \frac{1}{(dq_0)^2} + \frac{2}{S^2} \left(\frac{kT_D}{J} \right)^2 \frac{1}{(dq_0)^4} \log \left(1 + S \left(\frac{T}{T_D} \right)^{q_{\text{od}}} \right) \right]$$

The part of $\text{Re} \Sigma(k)$ which depends on \vec{k}^2 is small compared to leading term which is independent of k .

B. Fusion process

The lowest order irreducible diagram for this process is  and the real part of the contribution of this diagram, within the above approximation is given by

$$\text{Re} \Sigma(k) = -\frac{2}{15\pi^2 m} \left[\frac{9G_{11}^2}{16} + \frac{G_{44}^2}{4} \right] \left[\frac{2}{c^2} + \frac{3}{c^2} \right] \left[I(T_D, T) + S^{\frac{1}{2}} \zeta(3/2) \Gamma(3/2) \left(\frac{kT}{J} \right)^{3/2} \right] + O(\vec{k}^2, T^3)$$

Again the term proportional to k^2 is small.

DISCUSSION

The analysis shows that the dominant contribution (neglecting terms proportional to K^2) to the magnon energy due to the single-ion magnetostriiction affects all the modes equally, and so the single-ion magnetostriiction interaction can be considered to give rise to an effective uniaxial anisotropy which reduces the magnon frequency for all K values. It shifts the ferromagnetic resonance frequency towards the lower frequency region and the energy gap (i.e. energy for $K = 0$) if already existing, will also be reduced. Therefore the spin-phonon interaction has to be considered in interpreting the data on energy gap measured by neutron diffraction method. This effect will obviously affect the dependence of magnetisation on the external field at low temperatures.

ACKNOWLEDGEMENTS

The author acknowledges many helpful discussions with Dr. S. S. Sinha and A. Ramakrishna.

REFERENCES

1. E. Pytte, Ann. Phys. (N.Y.), 32, 377 (1965).
2. E. K. Inakiev, Sov. Phys. Solid State, 4, 453 (1962).
3. E. Holstein and H. Primakoff, Phys. Rev. 55, 1038 (1940).
4. Abrikosov et al., Methods of Quantum Field Theory in Statistical Physics, (Prentice Hall, Inc., New Jersey, 1964.)

NUCLEAR SPIN PHONON INTERACTION IN METALS

A. Ramakanth

Saha Institute of Nuclear Physics, Calcutta-9.

INTRODUCTION

The study of many properties of metals fortifies the fact that conduction electrons play a vital role in the physical processes. So it is interesting to investigate any mechanism for spin phonon coupling involving conduction electrons. There are various indirect mechanisms via conduction electrons through which nuclei interact with each other. When averaged over conduction electrons these interactions depend on the internuclear distance. In the presence of an externally impressed ultrasonic beam, the internuclear distance becomes time dependent. Consequently these interactions are modulated giving rise to Waller like mechanism for spin phonon coupling. The present work reports an investigation when one of the above mentioned indirect interactions namely, the Ruderman Kittel interaction is thought to be modulated, thus coupling phonons with nuclear spins. Using this spin phonon coupling mechanism, the absorption coefficient α for resonant absorption of phonons by spins is calculated.

INTERACTION HAMILTONIAN :

The calculations are done with independent nuclei model. The Ruderman Kittel Hamiltonian for interaction between the representative nucleus and the s is given by¹

NUCLEAR SPIN PHONON INTERACTION IN METALS

A. Ramakanth

Saha Institute of Nuclear Physics, Calcutta-9.

INTRODUCTION

The study of many properties of metals fortifies the fact that conduction electrons play a vital role in the physical processes. So it is interesting to investigate any mechanism for spin phonon coupling involving conduction electrons. There are various indirect mechanisms via conduction electrons through which nuclei interact with each other. When averaged over conduction electrons these interactions depend on the internuclear distance. In the presence of an externally impressed ultrasonic beam, the internuclear distance becomes time dependent. Consequently these interactions are modulated giving rise to Waller like mechanism for spin phonon coupling. The present work reports an investigation when one of the above mentioned indirect interactions namely, the Ruderman kittel interaction is thought to be modulated, thus coupling phonons with nuclear spins. Using this spin phonon coupling mechanism, the absorption coefficient α for resonant absorption of phonons by spins is calculated.

INTERACTION HAMILTONIAN :

The calculations are done with independent nuclei model. The Ruderman kittel Hamiltonian for interaction between the representative nucleus and the j^{th} nucleus is given by¹

$$H_j' = \frac{|\Delta_{K_F K_F}|^2}{4(2\pi)^3 \hbar^2} \mathbf{I} \cdot \mathbf{I}_j \left[\frac{2k_F R_j \cos 2k_F R_j - \sin 2k_F R_j}{R_j^4} \right] \quad (1)$$

where \mathbf{I} and \mathbf{I}_j are the spins of the representative nucleus and j^{th} nucleus, R_j the distance between the two, $|\Delta_{K_F K_F}|$ a constant involving hyperfine splitting constant and K_F the Fermi momentum. H_j' will be time dependent when R_j becomes time dependent due to phonons. Then $R_j(t)$ is written as $R_j^{(0)} + \delta R_j(t)$ where $R_j^{(0)}$ is the equilibrium value. Then the Hamiltonian can be rewritten as,

$$H_j' = \frac{|\Delta_{K_F K_F}|^2 \mathbf{I} \cdot \mathbf{I}_j}{4(2\pi)^3 \hbar^2} \left[F_1(R_j^{(0)}) \delta R_j + F_2(R_j^{(0)}) (\delta R_j)^2 + \dots \right] \quad (2)$$

Now δR_j can be expressed in terms of phonon operators.

The total interaction Hamiltonian when the nucleus interacts with all the other nuclei in the metal, is given by

$$H' = \sum_j H_j' = \frac{|\Delta_{K_F K_F}|^2 \mathbf{I} \cdot \mathbf{I}_j}{4(2\pi)^3 \hbar^2} \sum_j \left[F_1(R_j^{(0)}) \delta R_j + F_2(R_j^{(0)}) (\delta R_j)^2 + \dots \right] \quad (3)$$

In the case of Copper, when restricted to nearest neighbors, j varies over 12 nuclei and $R_j^{(0)}$ is same for all of them. \mathbf{I} and \mathbf{I}_j both have the value $3/2$.

CALCULATION OF α

Since the above Hamiltonian is of exchange type it does not induce any net spin transitions in the spin system if its states are pure Zeeman states. So we have

assumed the existence of a local nondiagonal static magnetic field of the same value H_1 at all the nuclear sites. Then the spin states will be linear combination of Zeeman states. If these are the spin states, H' can induce energy exchange between spins and phonons.

Using the above Hamiltonian with the δR_1 term, transition probabilities are calculated for spin transitions from higher energy state to lower energy state. Then α is calculated using the formula²

$$\alpha = \frac{N}{2\pi\hbar} \left(\frac{\hbar\omega}{kT} \right) \frac{V}{2\pi u} \sum W_{kl} \quad (4)$$

The expression we obtain for α is

$$\alpha = \frac{N}{2\pi\hbar} \left(\frac{\hbar\omega}{kT} \right) \frac{36}{50\pi} \left(\frac{H_1}{H_0} \right)^2 \left[\frac{W_{k_F k_F}^2 m}{4(2\pi)^3 \hbar} \right] \frac{1 - \cos^2 \frac{\omega R_1}{u}}{\omega} \left[F(R_1^{\omega}) \right]^2 g(v) \quad (5)$$

where N is the number of spins per cm^3 , ω the resonance frequency, ρ the density of the sample, u the velocity of sound in metal, H_0 the applied d.c. magnetic field and $g(v)$ the line shape factor.

RESULTS AND DISCUSSION

The absorption coefficient we obtain is of the order of 10^{-20} cm^{-1} . α measured in acoustic magnetic resonance experiments is of the order of 10^{-7} to 10^{-8} cm^{-1} . So the above considered mechanism does not play any appreciable role in spin phonon coupling. In the above treatment it is assumed that phonons are affecting

only the nuclei leaving the electron system undisturbed. But it is suspected that interaction of phonons with nuclei via conduction electrons will be a much stronger mode. To study that kind of mechanisms an approach similar to that of Silverstein³ for antiferromagnetic systems, has to be adapted. Previously a coupling of the nuclear magnetic dipole moment with a self consistent electromagnetic field set up in the metal by the sound wave has been shown⁴ to explain some experiments. If the nucleus possesses quadrupole moment, there can also be a quadrupole coupling with this electro magnetic field. These are being investigated.

ACKNOWLEDGEMENTS

I thank Dr. S. K. Sinha for many valuable discussions and Mr. S. K. Ghatak for clarifying some points.

REFERENCES

1. M.A. Ruderman, C. Kittel; Phys. Rev. 96, 99 (1954).
2. D. I. Bolef; Physical Acoustics Ed. W. P. Mason, Vol. IV, Part A P.130 (1966).
3. S. D. Silverstein; Phys. Rev. 132, 997 (1963).
4. J. Buttel, E. H. Gregory, P. K. Baily; Phys. Rev. Letters, 23, 1030 (1969).

CONTRIBUTIONS OF THE ODD-PARITY VIBRATIONAL MODES TO THE SPIN-LATTICE RELAXATION PROCESSES

Santosh Kumar
Saha Institute of Nuclear Physics, Calcutta-9
' and
D. K. Ray
Universite de Paris, 91-Orsay, France.

I. INTRODUCTION

It has been customary to consider only the even-parity vibrational modes of the molecular complex around the paramagnetic ion in calculating the relaxation rates theoretically⁽¹⁾. This neglect of the contributions of the rotational and odd-parity vibrational modes is not justified for the two-phonon processes particularly at high temperatures. The importance of the rotational modes in such calculations has already been shown⁽²⁾. Here we shall show that the odd-parity modes can also contribute significantly to the relaxation rates. The specific cases with which we deal with are of XY_6 type cubic complexes : Ni^{2+} ($S = 1$) and Cr^{3+} ($S = 3/2$) in MgO crystal.

II. THEORETICAL FORMULATION

The dynamical spin Hamiltonian, \mathcal{H}_{dyn} , for the two-phonon process is given below :

$$\mathcal{H}_{dyn} = \sum_{\alpha, \beta, t, \tau, u} C(\alpha, \beta, t, \tau, u) \sum_{i, j, k} \langle \Gamma_{\alpha}^i | \Gamma_{\beta}^j, \Gamma_{\tau}^k \rangle \\ \times S_z(\Gamma_{\alpha}^i) Q(\Gamma_{\beta}^j) Q(\Gamma_{\tau}^k), \quad (1)$$

where Q 's are the symmetry modes of the molecular complex, and $C(\alpha, \beta, t, \tau, u)$ are the spin-phonon coupling

only the nuclei leaving the electron system undisturbed. But it is suspected that interaction of phonons with nuclei via conduction electrons will be a much stronger mode. To study that kind of mechanisms an approach similar to that of Silverstein³ for antiferromagnetic systems, has to be adapted. Previously a coupling of the nuclear magnetic dipole moment with a self consistent electromagnetic field set up in the metal by the sound wave has been shown⁴ to explain some experiments. If the nucleus possesses quadrupole moment, there can also be a quadrupole coupling with this electro magnetic field. These are being investigated.

ACKNOWLEDGEMENTS

I thank Dr. S. K. Sinha for many valuable discussions and Mr. S. K. Ghatak for clarifying some points

REFERENCES

1. M.A. Ruderman, C. Kittel; Phys. Rev. 96, 99 (1954).
2. D. I. Bolef; Physical Acoustics Ed. W. P. Mason, Vol. IV, Part A P.130 (1966).
3. S. D. Silverstein; Phys. Rev. 132, 997 (1963).
4. J. Buttel, E. H. Gregory, P. K. Baily; Phys. Rev. Letters, 23, 1030 (1969).

CONTRIBUTIONS OF THE ODD-PARITY VIBRATIONAL MODES TO THE SPIN-LATTICE RELAXATION PROCESSES

Santosh Kumar

Saha Institute of Nuclear Physics, Calcutta-9
and

D. K. Ray

Universite de Paris, 91-Orsay, France.

I. INTRODUCTION

It has been customary to consider only the even-parity vibrational modes of the molecular complex around the paramagnetic ion in calculating the relaxation rates theoretically⁽¹⁾. This neglect of the contributions of the rotational and odd-parity vibrational modes is not justified for the two-phonon processes particularly at high temperatures. The importance of the rotational modes in such calculations has already been shown⁽²⁾. Here we shall show that the odd-parity modes can also contribute significantly to the relaxation rates. The specific cases with which we deal with are of XY_6 type cubic complexes : Ni^{2+} ($S = 1$) and Cr^{3+} ($S = 3/2$) in MgO crystal.

II. THEORETICAL FORMULATION

The dynamical spin Hamiltonian, \mathcal{H}_{dyn} , for the two-phonon process is given below :

$$\begin{aligned} \mathcal{H}_{dyn} = \sum_{\alpha, \beta, t, \gamma, u} C(\alpha, \beta, t, \gamma, u) \sum_{i, j, k} \langle \Gamma_{\alpha}^i | \Gamma_{\beta}^j, \Gamma_{\gamma}^k \rangle \\ \times S_z(\Gamma_{\alpha}^i) Q(\Gamma_{\beta}^j) Q(\Gamma_{\gamma}^k), \end{aligned} \quad (1)$$

where Q 's are the symmetry modes of the molecular complex, and $C(\alpha, \beta, t, \gamma, u)$ are the spin-phonon coupling

coefficients. From symmetry arguments we get : $\alpha = 3g$, $5g$; β and γ are both either g-type or u-type representations. The C-coefficients appearing above are evaluated by a perturbation calculation on the ground state singlet with Γ_{1g} symmetry, by using the perturbation Hamiltonian ($\mathcal{H}_{o-L} + \mathcal{H}_{s-o}$) where \mathcal{H}_{o-L} and \mathcal{H}_{s-o} are the orbit-lattice and the spin-orbit interaction terms and their expressions are given by Kumar et al⁽¹⁾. As far as the contributions from the odd-parity modes are concerned, only the quadratic term in \mathcal{H}_{o-L} is of interest to us. This term contributes to the C-coefficients through a third-order perturbation with \mathcal{H}_{o-L} operating once and \mathcal{H}_{s-o} operating twice. The calculated values of these C-coefficients have been given by Ray et al⁽³⁾.

In order to facilitate a comparison of the contributions from the various types of modes we write the expression of the transition probability for the two-phonon processes as :

$$W_1 = W_{M_S+1 \rightarrow M_S} = \frac{1}{\pi} (2M_S+1)^2 (S+M_S+1)(S-M_S) \\ \times \left[(S_{1g} + S_{1u})(1-f) + (S_{2g}+S_{2u})f \right], \quad (2)$$

$$\text{and } W_2 = W_{M_S+2 \rightarrow M_S} = \frac{1}{4\pi} (S+M_S+2)(S+M_S+1)(S-M_S-1) \\ \times (S-M_S) \left[(S_{1g}+S_{1u})(1+f) + (S_{2g}+S_{2u})(3-f) \right] \quad (3)$$

where $f = e^4 + m^4 + n^4$ and e, m, n are the direction

cosines of the applied magnetic field H with respect to the crystal axes. Here S_{1g} , S_{1u} denote the contributions from the even- and odd-parity modes belonging to Γ_{3g} irreducible representation. The corresponding contributions from Γ_{5g} modes are given by S_{2g} , S_{2u} . Expressions for these are given by Ray et al⁽³⁾.

III. RESULTS

We have calculated S_{1g} , S_{1u} , S_{2g} and S_{2u} for temperatures upto 200°K using the Debye model of phonons. Their numerical values are given in Table I for Ni^{2+} case and in Table II for Cr^{3+} case. We find that the odd-mode contribution is negligible at very low temperatures, but it increases sharply with a rise in temperature. The odd-mode and even-mode contributions are equal for the Γ_{3g} and Γ_{5g} modes between 110°-120°K and 70°-80°K, respectively. Thus on the whole we can say that at nearly 90°K the odd-parity modes contribute as much as the even-parity modes. For still higher

TABLE I

The computed values of S_{1g} , S_{1u} , S_{2g} and S_{2u} in sec^{-1} for Ni^{2+} in MgO

Temp. °K	S_{1g}	S_{1u}	S_{2g}	S_{2u}
20	2.591E+1	1.019E-1	3.795E+1	5.004E-1
40	2.283E+2	1.168E+2	3.937E+3	5.782E+2
60	2.412E+4	4.604E+3	3.975E+4	2.305E+4
80	1.081E+5	4.520E+4	1.898E+5	2.287E+5
100	3.099E+5	2.119E+5	5.756E+5	1.081E+6
120	6.814E+5	6.409E+5	1.328E+6	3.289E+6
140	1.260E+6	1.470E+6	2.556E+6	7.571E+6
160	2.068E+6	2.803E+6	4.334E+6	1.448E+7
180	3.113E+6	4.705E+6	6.702E+6	2.436E+7
200	4.399E+6	7.206E+6	9.675E+6	3.736E+7

temperatures the odd-mode contribution dominates more and more over the even-mode contributions. Comparing with the experimental results we find that the temperature dependences are predicted correctly, but the ratio $(1/T_1)_{\text{expt.}}/(1/T_1)_{\text{Debye}}$ is nearly 2 for Ni^{2+} and 16 for Cr^{3+} case.

TABLE II

The computed values of S_{1g} , S_{1u} , S_{2g} and S_{2u} in sec^{-1} for Cr^{3+} in MgO

Temp. °K	S_{1g}	S_{1u}	S_{2g}	S_{2u}
20	1.224E-2	6.370E-5	1.890E-2	2.492E-4
40	1.091E+0	7.300E-2	1.765E+0	2.878E-1
60	1.164E+1	2.878E+0	1.986E+1	1.147E+1
80	5.275E+1	2.825E+1	9.482E+1	1.138E+2
100	1.523E+2	1.324E+2	2.880E+2	5.379E+2
120	3.384E+2	4.005E+2	6.644E+2	1.637E+3
140	6.294E+2	9.184E+2	1.278E+3	3.676E+3
160	1.037E+3	1.752E+3	2.167E+3	7.206E+3
180	1.567E+3	2.940E+3	3.349E+3	1.212E+4
200	2.220E+3	4.503E+3	4.834E+3	1.859E+4

REFERENCES

1. S. Kumar, T. Ray and D. K. Ray; Phys. Rev. 176, 489 (1968).
2. S. Kumar, T. Ray and D. K. Ray; Physica Status Solidi 37, K65 (1970).
3. D. K. Ray, T. Ray, M. J. L. Sangster and S. K. Gupta; Phys. Rev. B 2, 8 (1970).

DISCUSSION

A.K. Pal

Is there any experimental verification of significant contributions towards spin lattice relaxation rate of odd mode vibrations?

Santosh Kumar

Experimental results are available for Fe^{2+} at 123°K and 137°K and for Co^{3+} case for the temperature range of 65°K to 150°K. By a comparison of these results with the theoretical calculations we find that the predicted temperature dependences agree well but not the magnitudes, irrespectives of the inclusion or other wise of the odd-parity modes. However, the agreement in the magnitudes is much improved when we take the odd-parity modes into account which shows that it is essential to take the odd-parity modes into account in carrying out such calculations.

ARTHUR LANA
STILLBORN

[illegible]

Krishnan Mahesh	353
Krishna, N. R.	323
Krishna Kumar, S.	333
Krishnasamy, L.	433
Kulkarni, T. G.	303, 313, 317
Kulkarni, S. R.	703
Kumar, N.	433
Kumar, A. C.	503
Kushwaha, R. P. S.	731
Kushwaha, S. S.	513

Lagn, R. G.	303, 313, 317
Lalithy, Subrata	373
Lala, M. T.	299, 303

Mahajan, M.	453
Mahanty, J.	507
Maitr, S. K.	557
Manchanda, T. C.	253
Manohar, C.	97
Martin, R. L.	599, 633
Marathe, T. R.	603
Mathur, A. E.	151
Mathur, T. K.	253
Mica, R.	431
Mitra, G. B.	591
Mitra, S.	599, 633
Mitra, S. K.	531, 537
Mohan Lal, S. R.	591
Mohan, S.	143
Murthy, G. S. N.	511
Murthy, R. R. N.	239
Murthy, M. R. L. N.	639
Murty, T. S.	165, 583
Murthi, T. T. G. S.	239, 511

Nagarajan, R.	577
Nanda, J. N.	217
Nandwani, S. S.	353
Narayana, P. A.	251, 595
Narlikar, A. T.	201
Natarajan, N. S.	31, 37

Pal, A. K.	549, 555, 561, 629
Pal, D.	555, 561, 629
Palazzi, R. K.	47

Pant, M. M.	57
Paranjpe, S. K.	597
Patil, A. P.	31, 103
Patil, E. K.	77, 81
Paragady, J.	733
Pater, S. H.	271
Pillai, P. R. C.	193
Prash, H.	491
Prasad, R.	423
Puri, S. P.	353, 511, 633, 657

Radhakrishna, S.	231
Radhakrishnan, T. S.	23, 371, 571
Raj, P.	703
Rajm, J. S.	1, 513
Raj, Rerachy, R.	397, 443
Ramakrish, A.	733
Ramakrishna, J.	649, 655
Ramamohan, C. T.	461
Ramamurthy, J.	203
Ramasamy, C.	165, 171, 239, 583

Ramchandani, M. G.	73
Ramesh Chandra	273
Rangarajan, G.	377
Rangarajan, S.	25
Rao, G. M.	595
Rao, L. Madhav	693, 697
Rao, S. Maralicham	177, 233
Rao, B. D. Nagarwara	503, 537, 433

Rao, J. Ramachandra	245
Rao, K. R.	473, 481
Rao, U. R. K.	633
Roy, J. K.	63, 757
Reddy, P. Jayarama	143
Reddy, T. K. Viswanatha	165
Roy, A. K.	549
Roy, Bhimraj	403
Roy, R.	549, 637
Roy, S. C.	121

Sachdev, M.	507
Sahni, T. C.	447
Sai, K. S. K.	231
Saha, A. K.	637
Santosh Kumar	57, 757

Saraf, B. L.	269, 273, 277, 283		
Sarkar, A. K.	423		
Sastry, E. V. R.	211		
Sastry, M. D.	595		
Satya Murthy, N. S.	689, 693, 697		
Satya Pal	525		
Satya Prakash	521		
Saxena, S. P.	747, 751		
Sengupta, S.	423, 637		
Setty, D. L. Radhakrishna	643		
Sharma, B. K.	273		
Sharma, H. N. K.	161, 359		
Sharma, N. D.	363		
Sharma, P. C.	535		
Sharma, R. G.	31, 37		
Sharma, R. P.	713		
Sherwood, R. C.	599		
Shishodia, Y. S.	273, 277, 283		
Singh, K. P.	261, 265		
Singh, R. K.	415, 429		
Singh, Risaal	181		
Singh, V. B.	217		
Singru, R. M.	261, 265		
Singwi, K. S.	81		
Sobhanadri, J.	661		
Srinivasa, K.	435		
Srinivasan, R.	577		
Srinivasan, T. M.	211, 245, 595		
Srivastava, B. P.	359		
Srivastava, G. P.	531		
Srivastava, J. K.	713, 719		
Srivastava, J. P.	251		
Srivastava, K. G.	731		
Srivastava, V. K.	131, 135		
Subramanian, R.		51	
Subramanian, V.		149	
Subramanyam, S. V.		303	
Sundaram, R.		11	
Suryan, G.		155	
Taneja, S. P.		611	
Thaper, C. L.		457	
Thosar, B. V.	309, 315, 317		
Tomar, V. S.		491	
Trevino, S. F.		473, 481	
Tripathi, R. S.		731	
Upadhyaya, U. N.		43, 47	
Upreti, G. C.		591	
Valvoda, V.		385	
Varshneya, N. C.		333	
Venkataraman, G.		447	
Venkateswarlu, P.		245, 595	
Verma, G. S.	531, 535, 539		
Verma, J. K. D.		125	
Verma, P.		45, 409	
Vijaya, M. S.		649, 665	
Vijayaraghavan, P. R.		439	
Vijayaraghavan, R.		567	
Viswamitra, M. A.	373, 379, 385		
Vishwamittar		611, 653	
Viswanathan, B.		293, 299	
Yakhmi, J. V.		683	
Yousesouff, M.		103	

Krishan Mahesh	363	Pant, M. M.	57
Krishna, N. R.	323	Paranjpe, S. K.	697
Krishna Kumar, S.	385	Pathak, A. P.	91, 103
Krishnasamy, L.	435	Pathak, K. N.	77, 81
Kulkarni, V. G.	309, 315, 317	Pasupathy, J.	753
Kulshreshtha, S. K.	703	Pawar, S. H.	201
Kumar, N.	435	Pillai, P. K. C.	193
Kunwar, A. C.	603	Prask, H.	481
Kushwaha, R. P. S.	731	Prasad, R.	423
Kushwaha, S. S.	515	Puri, S. P.	353, 611, 653, 657
Lagu, R. G.	309, 315, 317	Radhakrishna, S.	231
Lahiry, Subrata	573	Radhakrishnan, T. S.	25, 671, 677
Lele, M. V.	299, 303	Raj, P.	703
Mahajan, M.	453	Rajput, J. S.	1, 515
Mahanty, J.	507	Raju, Revathy, R.	397, 463
Malik, S. K.	567	Ramakanth, A.	753
Manchanda, T. C.	255	Ramakrishna, J.	649, 665
Manohar, C.	97	Ramamohan, C. V.	661
Martin, R. L.	599, 633	Ramamurty, J.	205
Marathe, V. R.	603	Ramasasthy, C.	165, 171, 239, 583
Mathur, A. K.	161	Ramchandani, M. G.	73
Mathur, V. K.	255	Ramesh Chandra	273
Mical, R.	481	Rangarajan, G.	577
Mitra, G. B.	393	Rangarajan, S.	25
Mitra, S.	599, 633	Rao, G. N.	595
Mitra, S. K.	333, 337	Rao, L. Madhav	693, 697
Mohan Lai, S. K.	391	Rao, S. Muralidhara	177, 225
Mohan, S.	145	Rao, B. D. Nageswara	323, 327, 453
Murthy, C. S. N.	511	Rao, D. Ramachandra	245
Murthy, K. R. N.	239	Rao, K. R.	473, 481
Murthy, M. R. L. N.	689	Rao, U. R. K.	683
Murty, V. S.	165, 583	Ray, D. K.	63, 767
Murti, Y. V. G. S.	239, 511	Reddy, P. Jayarama	145
Nagarajan, R.	677	Reddy, V. K. Viswanatha	165
Nanda, J. N.	217	Roy, A. K.	549
Nandwani, S. S.	353	Roy, Dhiraanjan	403
Narayana, P. A.	251, 595	Roy, R.	549, 637
Narlikar, A. V.	201	Roy, S. C.	121
Natarajan, N. S.	31, 37	Sachdev, M.	507
Pal, A. K.	549, 555, 561, 629	Sabni, V. C.	447
Pal, D.	555, 561, 629	Sai, K. S. K.	231
Paliwal, R. K.	47	Saha, A. K.	637
		Santosh Kumar	67, 767

Saraf, B L.	269, 273, 277, 283
Sarkar, A K.	423
Sastry, E V R	211
Sastry, M D	595
Satya Murthy, N S	689, 693, 697
Satya Pal	525
Satya Prakash	521
Saxena, S P	747, 751
Sengupta, S	423, 637
Setty, D L Radhakrishna	643
Sharma, B K.	273
Sharma, H N K.	161, 359
Sharma, N D	363
Sharma, P C	535
Sharma, R G	31, 37
Sharma, R P	713
Sherwood, R C	599
Shishodia, Y. S	273, 277, 283
Singh, K. P	261, 265
Singh, R K.	415, 429
Singh Risal	181
Singh, V B	217
Singru, R M	261, 265
Singwi, A. S	81
Sobhanadri, J	661
Srinivasa, K	435
Srinivasan, R	577
Srinivasan, T M.	211, 245, 595
Srivastava, B P	359
Srivastava, C P	531
Srivastava, J K	713, 719
Srivastava, J F	251
Srivastava, K G	731
Srivastava, V K.	131, 135

Subramanian, R.	51
Subramanian, V.	149
Subramanyam, S. V.	303
Sundaram, R.	11
Suryan, G	155

Taneja, S P	611
Thaper, C L	457
Thosar, B V	309, 315, 317
Tomar, V S	491
Trevino, S F	473, 481
Tripathi, R S	731

Upadhyaya, U N	43, 47
Upreti, G C	591

Valvoda, V	385
Varshneya, N C	333
Venkataraman, G	447
Venkateswarlu, P	245, 595
Verma, G S	531, 535, 539
Verma, J K D	125
Verma, P	45, 409
Vijaya, M S	649, 665
Vijayaraghavan, P R	439
Vijayaraghavan, R	567
Viswamitra, M A	373, 379, 385
Vishwamittar	611, 653
Viswanathan, B	293, 299

Yakhmi, J V.	683
Yousouff, M	103

